

UNCLASSIFIED/LIMITED

Technical Report
distributed by



DEFENSE TECHNICAL INFORMATION CENTER

DTIC / Acquiring Information—
Imparting Knowledge

Cameron Station
Alexandria, Virginia 22304-6145

UNCLASSIFIED/LIMITED

UNCLASSIFIED

ZZBZB7

FOR
MICRO-CARD
CONTROL ONLY

1 **OF** **9**

Reproduced by

Armed Services Technical Information Agency

ARLINGTON HALL STATION; ARLINGTON 12 VIRGINIA

"NOTICE: When Government or other drawings, specifications or other data are used for any purpose other than in connection with a definitely related Government procurement operation, the U.S. Government thereby incurs no responsibility, nor any obligation whatsoever, and the fact that the Government may have formulated, furnished, or in any way supplied the said drawings, specifications or other data is not to be regarded by implication or otherwise in any manner licensing the holder or any other person or corporation, or conveying any rights or permission to manufacture, use or sell any patented invention that may in any way be related thereto."

UNCLASSIFIED

AFSWC TR-59-44

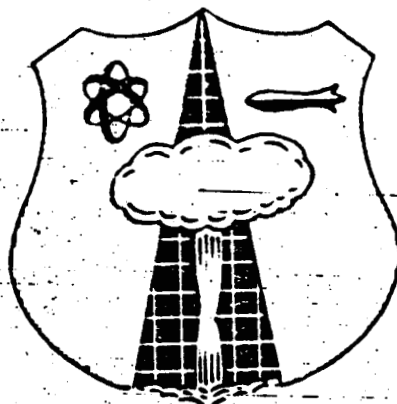
AD No. **228267**
ASTIA FILE COPY

ANP DOC. NO.
NARF-59-32T
FZK-9-140

HEADQUARTERS

AIR FORCE SPECIAL WEAPONS CENTER

AIR RESEARCH AND DEVELOPMENT COMMAND
KIRTLAND AIR FORCE BASE, NEW MEXICO



FC

FILE COPY

ROUTED TO
ASTIA
ARLINGTON HALL STATION
ARLINGTON 12, VIRGINIA
AUG 11 1959

**FISSION PRODUCTS FIELD
RELEASE TEST - I**

ASTIA

NOV 17 1959

TIPDR

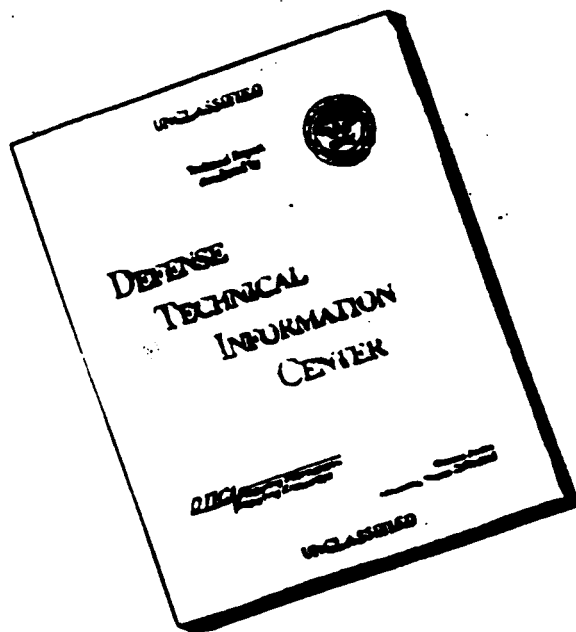
U.S. AIR FORCE
Nuclear Aircraft Research Facility
operated by
CONVAIR

A DIVISION OF GENERAL DYNAMICS CORPORATION
FORT WORTH, TEXAS

SEPTEMBER 1959

ANP DOC. NO.
NARF-59-32T

DISCLAIMER NOTICE



THIS DOCUMENT IS BEST
QUALITY AVAILABLE. THE COPY
FURNISHED TO DTIC CONTAINED
A SIGNIFICANT NUMBER OF
PAGES WHICH DO NOT
REPRODUCE LEGIBLY.

ACKNOWLEDGMENTS

Convair, a Division of General Dynamics Corporation,
acknowledges the participation and cooperation of the following
agencies during Fission Products Field Release Test - I:

General Electric Company

- . fuel element irradiation
- . hot cell processing
- . fuel element radiochemistry

University of Rochester

- . biological tests

U.S. Atomic Energy Commission,
Idaho Operations Office

- . meteorological forecasting
- . health physics control
- . site survey
- . ecological sampling

4925th Test Group Atomic, Air
Force Special Weapons Center

- . field and aerial photography

FISSION PRODUCTS FIELD

RELEASE TEST - 1

U. S. AIR FORCE

Nuclear Aircraft Research Facility

operated by

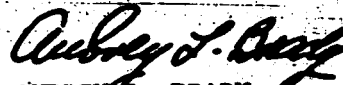
CONVAIR

A DIVISION OF GENERAL DYNAMICS CORPORATION

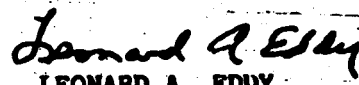
September 1959

Research Directorate
AIR FORCE SPECIAL WEAPONS CENTER
Air Research and Development Command
Kirtland Air Force Base
New Mexico

Approved:



AUBREY L. BRADY
Lt Colonel USAF
Chief, Biophysics Division



LEONARD A. EDDY
Colonel USAF
Director

Project No. 7809
Task No. 78016
Contract No. AF33(600)-32054

TR-59-44

ABSTRACT

~~Fission Products Field Release Test~~ ^{1 test} was performed to check and resolve uncertainties in the currently used methods of safety analysis for nuclear aircraft. Specifically, the test was made to evaluate release percentages, airborne radioactivity, and diffusion and deposition characteristics of fission products from melted aircraft reactor fuel elements. A corollary objective was to determine the retention and distribution of the released fission products in animals located within the release network.

A highly instrumented fan-shaped grid having ~~seven~~ ⁷ concentric arcs with a maximum radius of about ~~five~~ ⁵ miles was used to collect cloud diffusion, meteorological, radiological, radiobiological, and radioactivity deposition data. Release percentages, size of aerosols, deposition velocities, external and internal dose, fluorescent tracer behavior, and atmospheric diffusion parameters were determined.

PUBLICATION REVIEW

This publication has been reviewed and is approved.


CAREY L. O'BRYAN, JR.
Colonel USAP
Deputy Commander

TABLE OF CONTENTS

<u>Topic</u>	<u>Page</u>
ACKNOWLEDGMENT	3
ABSTRACT	5
LIST OF FIGURES	9
LIST OF TABLES	11
I. INTRODUCTION	13
II. CONCLUSIONS	19
III. RECOMMENDATIONS	23
IV. DISCUSSION	25
4.1 Description of Test	26
Test Network	29
Fuel Elements	31
Melting Technique	31
Power Distribution	32
Meteorological Network	32
Release Measurements	33
Release Height	34
Smoke Plume Recording	35
Fluorescent Tracer Measurements	35
Airborne Radioactivity Measurements	35
Particle Size Measurements	36
Activity Deposition Measurements	37
External Dose Measurements	37
Radiochemical Techniques	38
Radiobiological Measurements	38
4.2 Evaluation of Results	38
Fission Product Release Percentages	39
Effluent Characteristics	52
Airborne Radioactivity	58
Deposited Radioactivity	72
Deposition Velocities	78
External Dose	80
Fluorescent Tracer	82
Diffusion Parameters	84
Radiobiology	94
APPENDICES	97
REFERENCES	478

LIST OF FIGURES

<u>No.</u>	<u>Title</u>	<u>Page</u>
1	Instrumentation	27
2	Test Site Location	30
3	Isotope Release with Time (Furnace Sampler Data - Release E)	50
4	Isotope Release Sequence	53
5	Autoradiogram of Andersen-Gelman-Millipore Sampler	57
6	Cesium-137 on Cloud Centerline (Normalized to Unit Inventory)	60
7	Cesium-137 on Cloud Centerline (Normalized to 100-Meter Level)	61
8	Iodine-131 on Cloud Centerline (Normalized to Unit Inventory)	63
9	Iodine-131 on Cloud Centerline (Normalized to 100-Meter Level)	64
10	Ruthenium-103 on Cloud Centerline (Normalized to Unit Inventory)	65
11	Ruthenium-103 on Cloud Centerline (Normalized to 100-Meter Level)	66
12	Zirconium-95 on Cloud Centerline (Normalized to Unit Inventory)	67
13	Zirconium-95 on Cloud Centerline (Normalized to 100-Meter Level)	68
14	Iodine Penetrating Hi-Vol Pleated Filter	71
15	Cesium-137 Deposition on Cloud Centerline (Normalized to Unit Inventory)	73
16	Cesium-137 Deposition on Cloud Centerline (Normalized to 100-Meter Level)	74
17	Iodine-131 Deposition on Cloud Centerline (Normalized to Unit Inventory)	76

LIST OF FIGURES (Con't)

<u>No.</u>		<u>Page</u>
18	Iodine-131 Deposition on Cloud Centerline (Normalized to 100-Meter Level)	77
19	External Dose for Cesium (Releases D and I)	83
20	Isopleth of Air Concentration (Lapse - Release F)	88
21	Isopleth of Air Concentration (Inversion - Release C)	89
22	Airborne Iodine Activity (Comparison with Predictions)	91
23	Airborne Cesium Activity (Comparison with Predictions)	92

LIST OF TABLES

<u>No.</u>	<u>Title</u>	<u>Page</u>
1	Principle Nuclides of Assembly for Releases E, F, and H at End of Irradiation	40
2	Calculated Inventories in Fuel Elements at Release	42
3	Cesium Release Percentages	43
4	ANP Release Model (Meltdown)	44
5	Gross Gamma Release Percentages	45
6	Release Percents of Nuclides Calculated from Network Activity	47
7	Nuclides Recovered from Residue	51
8	Distribution of Material in Andersen Sampler	54
9	Distribution of Nuclides in Andersen Sampler (Release I)	55
10	Distribution of Nuclides in Andersen Sampler (Release E)	55
11	Distribution of Nuclides in Andersen Sampler (Release F)	56
12	Relative Isotopic Diffusion	69
13	Deposition Velocities	78
14	Comparison of Deposition Velocities	80
15	External and Internal Dose Comparison	81
16	"Typical" ANP Atmospheric Diffusion Parameters	85
17	Summary of Diffusion Parameters and Meteorological Conditions	87
18	Median Lower Respiratory Tract and Total Body Deposition Values	96

I. INTRODUCTION

Nuclear aircraft propulsion reactors must operate at high power levels, which result in the production of large quantities of fission products. If a reactor core is destroyed, a portion of the contained radioactivity will escape, become airborne, and diffuse according to the prevailing wind condition. Depending on the amount of activity released, and the position of a would-be receptor, the radioactive cloud may present a serious internal and/or external hazard. It can be shown that the probability of a hazardous release from an aircraft accident is very remote. However, the consequences of such a release must be regarded seriously, since the effects may not necessarily be restricted to a small area.

Reactor cores, or portions thereof, can be destroyed in a variety of ways. The most probable event leading to the release of fission products is a core meltdown, which may take place if after-cooling is halted within several hours following extended operation. A less probable release is a reactor runaway, which may occur if there is a sudden increase in the reactivity of the reactor caused either by a failure of the control system or some crash-induced cause. Only the meltdown case was simulated in this series of experiments.

The problem of hazards prediction is a complex one. Attempts to predict precisely the extent of the hazards have always

been seriously hindered by a lack of quantitative laboratory and field data. There has been incorporated into the Airplane Nuclear Propulsion (ANP) safety analysis program a great deal of conservatism. This is because safety analyses have been based necessarily on meager information and cascading assumptions. Large-scale test data have not been available for predicting with accuracy the amount and physicochemical state of the released fission products, for evaluating the uncertainties of the dispersal characteristics, and for resolving the ultimate biological implications. Experimental tests made to minimize the large safety factors have been only partially successful.

This basis for the various hazard factors used to date are outlined below.

Release Percentages: Some important and related laboratory work has been done by Creek et al. at ORNL (Ref. 1). This laboratory research has established the amounts of fission products released from small specimens. The laboratory work indicated that 50, 1, and 10% respectively of iodine, bone seekers, and cesium could be expected to be released from metallic nuclear aircraft reactor fuel elements. Safety analysis predictions for the ANP program (Ref. 2) have been based on the above percent releases.

Particle Size and Size Distribution: Consideration of the effects of particle size distribution on nuclear aircraft hazard predictions required definition of particle-size distribution and activity distribution.

The ANP model has been based on a log-normal particle size distribution having a geometric median of 7 microns and standard deviation of 2.75. This distribution is based on a study of the effluents released from a variety of industrial processes. It has been assumed that all particles less than 10 microns behave as aerosols. The particle size-activity relationship has been based on bomb data. These are areas of considerable uncertainty (Ref.3).

Atmospheric Diffusion: Air concentrations may be calculated by the Sutton-type, atmospheric diffusion equation if suitable parameters are supplied (Ref. 4). Sutton has given formulas for obtaining these parameters from basic micrometeorological conditions (Ref. 5). Experimental investigations to date have been concerned largely with elevated sources and in most cases the data obtained were for distances less than five miles.

The values of the parameters used in the ANP diffusion model, which are in agreement with AEC and Brookhaven "typical" parameters, are given in Reference 2 and outlined below:

<u>Parameter</u>	<u>"Typical" Lapse</u>	<u>"Typical" Inversion</u>
Stability Parameter (n)	0.25	0.55
Mean Wind Speed (\bar{U} in m/sec)	5.0	3.0
Vertical Diffusion Coefficient (C_z)	0.4	0.05
Crosswind Diffusion Coefficient (C_y)	0.4	0.4

Deposition: The mechanism of cloud depletion by fallout needs to be understood in order to analyze ground contamination hazards. Aerosols and particulates in a radioactive cloud will eventually fallout, washout, or otherwise be removed from the atmosphere. Explaining how the particles are removed requires an understanding of the physicochemical processes involved. Small particles must impact and stick to surfaces if they are to be removed from the cloud. Chamberlain (Ref. 6) has described the advantages of studying deposition in terms of a ratio, i.e., deposited radioactivity to the time integral air concentration. This ratio is defined as the deposition velocity (V_g).

The ANP model attempts to predict deposition (ground contamination) as a factor of air concentration. With the exception of iodine, the entire cloud inventory has been assigned values of V_g (cm/sec) equal to 0.1 and 1.0 for inversion and lapse conditions respectively. Iodine has been assigned the values of 0.25 and 2.5. These values were chosen on the basis of experimental data obtained by Chamberlain.

Biological Effects: In assessing the relative hazards resulting from a reactor accident where fission products are released, the internal dose is much greater than the external dose in cases where the receptor is immersed in the cloud.

The ANP predictions of biological effects are based on the assumption that the person stays in and breaths the cloud during

its full passage. Only gamma rays are considered for external doses, and internal doses are calculated for each isotope using the methods from the International Commission of Radiation Protection (Ref. 7).

OBJECTIVES

With the exception of the fission product inventory, which can be calculated rather accurately, all other major components of a hazards analysis contain assumptions which contribute to the uncertainties of the hazards predictions. The objectives of the Fission Products Field Release Test I (FRT-I) were to reduce the uncertainties of these assumptions and to obtain direct evidence of the downwind hazard resulting from the meltdown of an aircraft reactor fuel element.

Therefore, Convair-Fort Worth, under the direction of Air Force Special Weapons Center of the USAF Air Research and Development Command, performed a series of fission product release experiments in the field at the National Reactor Testing Station, Idaho, during 1958. The series consisted of a total of nine releases in which irradiated metallic fuel-element specimens were melted. Both aged and freshly irradiated (green) specimens were used. All of these releases were conducted on an extensively instrumented sampling network. The basic network extended two miles downwind from the release point, with additional samplers being positioned along an arc approximately five miles from the release point.

II. CONCLUSIONS

The FRT-I experiment demonstrated that the various assumptions used in previous ANP studies of the hazards associated with nuclear-powered aircraft were reasonable for estimating purposes. The test provided information which has helped to refine those parameters previously used. In addition, specific areas of uncertainty have been defined more clearly for further experimentation and analyses.

Within the ranges of the melting temperatures and atmospheric conditions experienced, the following conclusions were reached:

1. Release Percentages Require Adjustment

Fission product release percentages were about as expected, except for cesium and strontium. Whereas 10% (2.3% aerosol and 7.7% particulate) release of cesium was expected, about 30 percent (all aerosol) was released. Network-activity data indicated that approximately one percent of the strontium was released as an aerosol, about a factor of five higher than estimated (0.23% aerosol).

2. Diffusion Model Approximates Centerline Air Concentration

Observed centerline air concentrations of radioiodine during lapse conditions are within a factor of two of the values predicted from ANP "typical lapse" parameters. Cesium concentrations were underpredicted because of an underestimated release percentage. When the cesium data are adjusted to the experimental release percentage, the data for cesium, like iodine, show factor of two agreement with prediction.

Measured centerline concentrations of radioiodine during inversions were an order of magnitude less than predicted using ANP "typical inversion" parameters. The same is true for cesium if the data are normalized to the experimental release percentage. These lower concentrations are attributable to better initial vertical diffusion. An increase in the value of the ANP vertical diffusion coefficient by a factor of ten is indicated.

3. Particle Size Model Requires a Change

Radioactivity in the network was in the form of fine aerosols with most isotopic activities associated with particles less than 5 microns in diameter. Previous ANP studies had assumed a larger aerosol, having a geometric median diameter of 7 microns.

4. Additional Deposition Velocity Data are Required

The average measured proportionality constants between ground and cloud contamination, commonly called the deposition velocity, were nearly the same as those used in previous ANP predictions for lapse releases. However, the measured deposition velocities for inversion and lapse releases were not significantly different from each other. Therefore, ground-to-air contamination ratio predictions were adequate for lapse but an order of magnitude too low for inversion conditions. Cesium deposition rates were unexpectedly an order of magnitude lower than other isotopes.

5. "Lower Respiratory Tract" Deposition Values Appear Valid.

The lower respiratory tract deposition values of 30 and 35% in rats and dogs respectively are not considered to be significantly different from the National Committee on Radiation Protection value of 25% (Ref. 7) because of approximations such as the use of average breathing rates.

6. Inventories Can Be Approximated by Calculations

In general, the fission product inventories as calculated were within average of 19% (maximum variation of 35%) of the values determined radiochemically from pre-melt samples. This is considered to be good agreement.

7. Internal Dose Was As Expected

The internal dose (thyroid) resulting from breathing while submerged in the green release cloud is about three orders of magnitude greater than the external dose. This is in agreement with previous conclusions for aircraft reactors where the relative amounts of iodine are large.

8. External Dose Was Less Than Calculated

The external gamma dose was measured under lapse conditions at 400 meters from the source and was about one-half that predicted using the measured release quantity and "typical lapse" parameters.

9. Radionuclides Were Released at Different Intervals

The sequence of release was iodine, cesium, ruthenium, strontium, zirconium, and cerium. Since the radionuclides were released essentially as separate "puffs" of about two minutes duration, the isotope profiles across the various arcs, because of changing meteorological conditions, also varied.

10. The Fluorescent Tracer and Cesium Aerosol Did Not Interact

No interaction occurred between cesium aerosols and the fluorescent tracer, zinc cadmium sulphide, during simultaneous releases. No large differences in the diffusion patterns were observed.

11. Vertical and Horizontal Stability Parameters Require Adjustment

Adequate description of the dispersal of airborne matter, even over the relatively short distance of this experiment, requires recognition of the anisotropic character of atmospheric diffusion. Values of Sutton's stability parameter "n" obtained from wind profile data do not predict measured FRT-I air concentrations. The radioactivity-data-fit requires both a vertical and horizontal stability parameter.

12. Iodine Aerosols Penetrate High Efficiency Filters

Iodine was the only aerosol which was found to penetrate (>5%) the pleated filter of the Hi-Vol sampler.

III. RECOMMENDATIONS

The results of FRT-I and conclusions reached therefrom have provided important data on the complicated phenomena of release, dispersal, and biological effects of fission products. It is now possible to assess more adequately the hazardous aspects of nuclear-powered aircraft. It is therefore recommended that certain ANP assumptions be modified and experimental work be continued.

Specifically:

1. Modify the existing ANP meltdown parameters to include 30% release of cesium and 1% release of strontium in aerosol form. Leave other isotopic release percentages at present value.
2. Change the value of the existing ANP vertical diffusion coefficient to 0.4 for the inversion case to predict centerline maximum air concentrations for short range diffusion (< 2 mi).
3. Measure, at minimum distances of 20 miles, airborne and deposited radioactivity under strong inversion conditions. Vertical diffusion data should also be collected.
4. Carry out biological studies accompanied by isotopic analyses of sequential blood samples, urine and fecal samples, and body organs. A material balance of radionuclides must be established.

5. Perform contained releases with large segments of ANP fuel elements and collect all of the effluent for isotopic analysis.
6. Perform atmospheric and contained releases at elevated temperatures to determine the dependence of release fraction on temperature.
7. Determine the particle-size distribution of the various airborne and deposited radioisotopes.
8. Conduct extensive deposition velocity studies on grass under inversion and lapse conditions.
9. Investigate the deposition velocity of cesium to determine why it was a factor of ten lower than for other isotopes.
10. Ascertain the behavior of iodine on filters and other surfaces such as vegetation, soil, and gummed paper.
11. Obtain additional data to provide the basis for the selection of typical values for the two components of the stability parameter in anisotropic diffusion.
12. Measure the fission product release characteristics of different types of fuel elements under meltdown conditions.

IV. DISCUSSION

The fission product releases were divided into two series of tests, one series using aged, the other freshly irradiated (green) fuel elements. Nine releases were accomplished and herein referred to as Releases A through I. Five releases were performed with aged fuel elements (A, B, C, D, and I) and four with green fuel elements (E, F, G, and H). Four releases (D, E, F, and I) were performed under moderate lapse conditions and the remainder (A, B, C, G, and H) under moderate inversion conditions. The lapse and inversion cases represented mild and poor diffusion respectively.

The data points representing each release have been assigned a symbol that is used throughout the report. All inversion releases are represented by open symbols and lapse releases by solid symbols.

Pertinent descriptions of the experimental phase and data evaluation are presented in this section. However, detailed descriptions, derivations, test results, calibration information, and operational techniques have been extracted and placed in Appendices A through M. The details and data summaries for each of the nine releases are given in Appendix N. The appendices were prepared in detail because a variety of scientific and engineering disciplines were involved.

4.1 Description of the Test

The experimental effort was generally divided into four phases: preliminary planning, equipping the network, releasing the fission

products, and analysis.

Preliminary planning consisted of selecting a suitable site

from which fission product releases could be made, coordinating

with participating groups and regulatory agencies, and developing

an instrumentation program. Surveys and tests were made to deter-

mine the most appropriate types of air sampling systems, particle

sizing devices, fallout traps, fluorescent tracers and a variety

of other systems to be used. A furnace was designed and built.

Radiochemical techniques were established for processing gaseous

effluent as well as contaminated filter papers, sticky paper, etc.

The instruments were checked and calibrated at Conair-Port Worth

prior to shipping to the site.

The second phase consisted of preparing and equipping the

sampling network. The power was provided from nearby power

sources and motor generator sets. The roads were improved,

meteorological towers and masts erected, and the sampling equip-

ment moved on location. A typical instrument layout is shown

in Figure 1. Animals and deposition trays were put out on the

network just prior to a release. Final adjustments and calibra-

tions were made on the site.

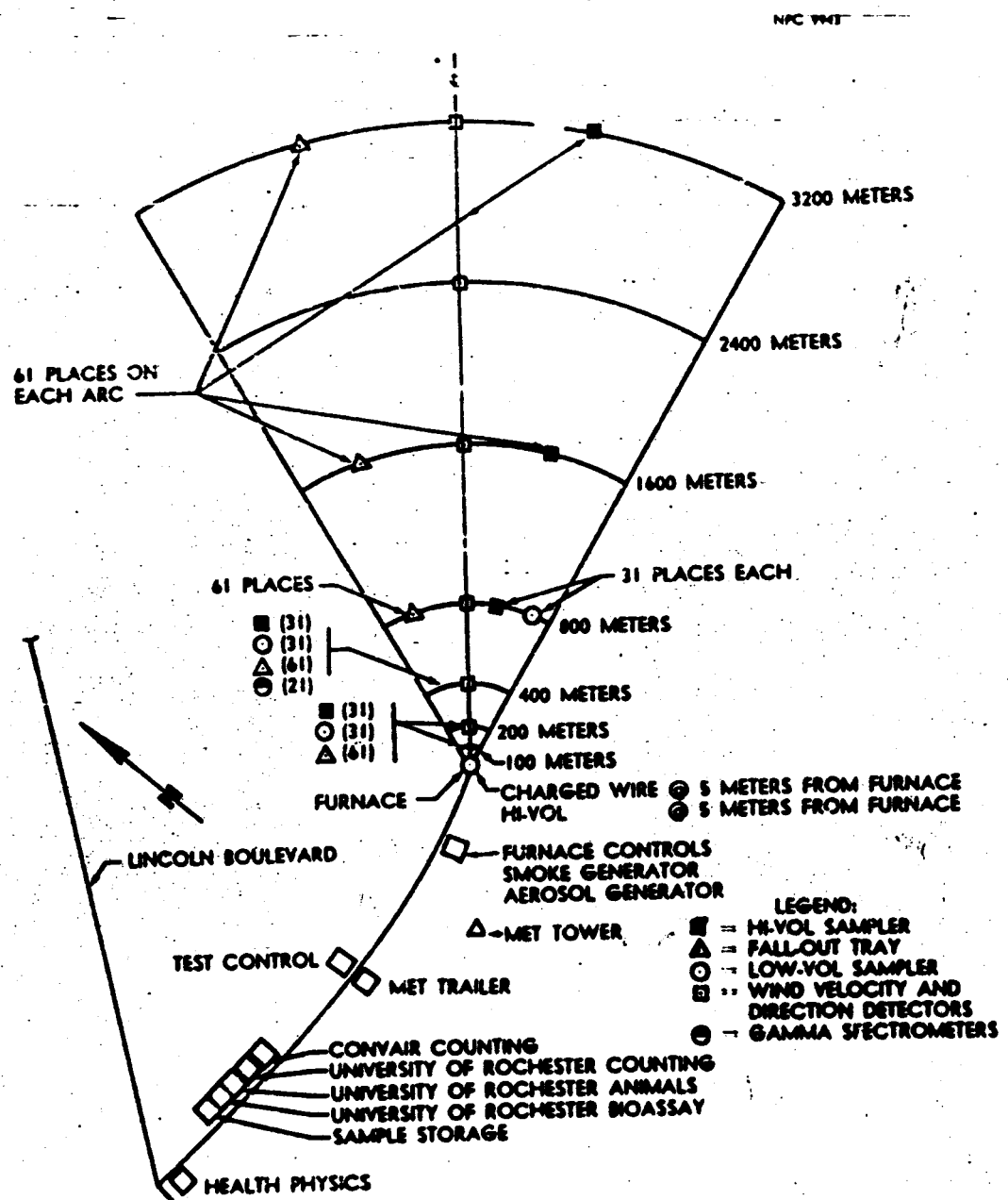


FIGURE 1. INSTRUMENTATION

In the third phase the fuel elements were melted. Furnaces were loaded with irradiated fuel elements, transported to the site, and after appropriate weather and instrument checks were made, the fuel elements were melted. Field operations in general consisted of:

- . Monitoring and recording meteorological data
- . Collecting and monitoring field samples which established cloud-release heights, fission products release percents, external dose, biological exposures, air and ground concentrations of radioactivity, and characteristics of the particulates and aerosols in the effluent.
- . Taking pre- and post-release gamma spectra of the fuel elements.
- . Releasing and measuring the diffusion of smoke plumes and a fluorescent tracer
- . Decontamination and disposal of furnace and preparation of release site for future releases.

The fourth phase consisted of laboratory analysis and data reduction. Samples of the pre- and post-melt fuel elements were analyzed radiochemically for Releases E, G, and H. The network samples, except biological and a few fallout samples, were transported to Convair-Fort Worth for analysis. One or more quantitative gamma spectra measurements were made of each sample and some types of air and deposition samples were analyzed radiochemically.

4.1.1 Test Network

The fission product releases were performed at a site within the National Reactor Testing Station (NRTS). The site was about four miles north of the Central Facilities Area. In general the site was moderately level. Within a radius of 2.5 miles of the release point the area was covered with a generous growth of sagebrush. The soil was of volcanic origin, fine grained and loosely packed. Beyond the 2.5-mile zone the terrain was broken by extensive volcanic rock outcrops so that vehicular entry could be made only on prepared roads. Only a small corner of this lava outcrop extended into the main area of the test site. Since the topsoil was a finely divided windblown material, it was necessary to control the dust by covering most of the road system with an asphaltic emulsion. Figure 2 depicts the location of the test network relative to other facilities at NRTS.

The fan-shaped sampling network subtended an angle of 60° having a center line which coincided with the most probable wind direction, N55 $^{\circ}$ D (Figure 2). On this grid were spaced six instrumented arcs having radii of 100 to 200 meters. An additional "arc" having an approximate radius of five miles was also used during the four green releases. All the fission products were released at the apex of the network.

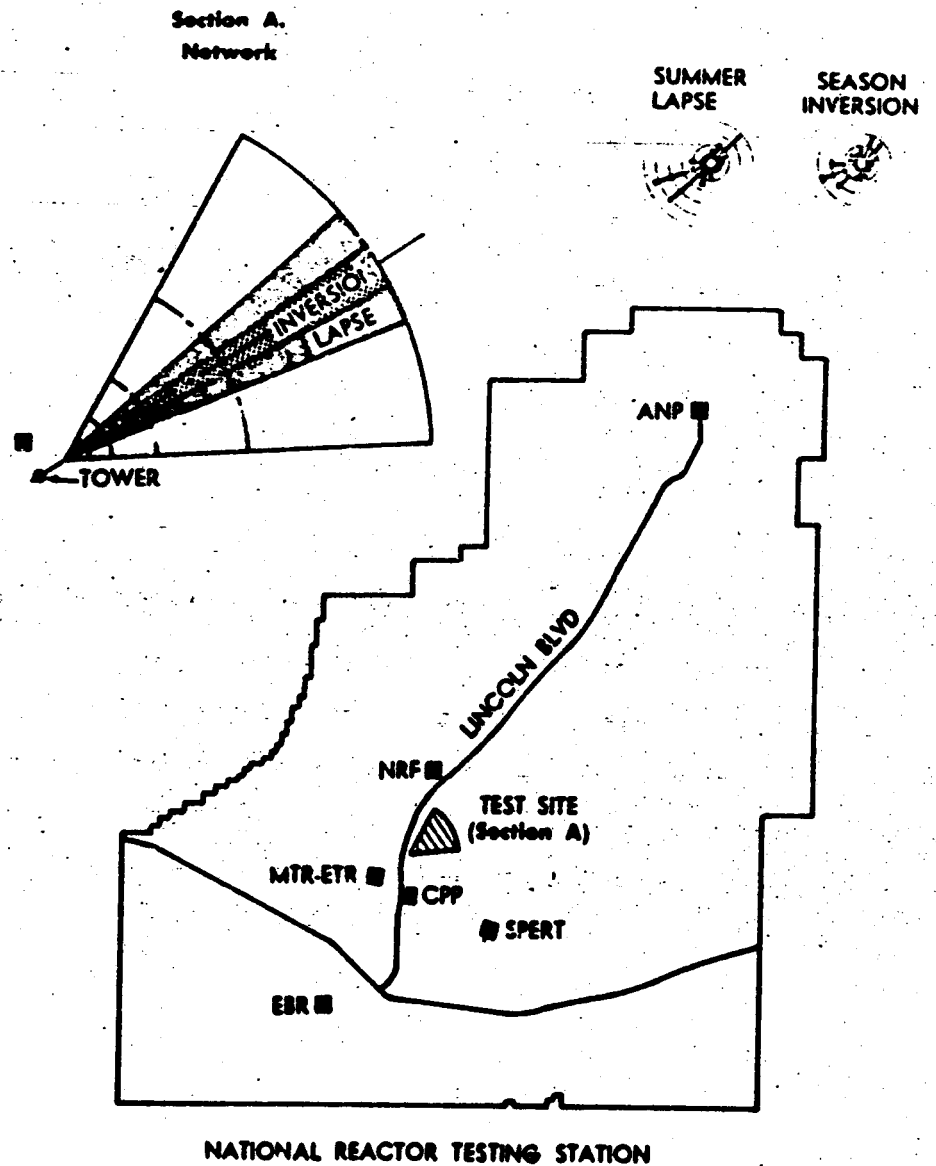


FIGURE 2. TEST SITE LOCATION

4.1.2 Fuel Elements

Specific details of the fuel elements may be found in Reference 8; however, calculated inventories are given in Appendix A. Metallic fuel elements, actually segments of a fuel-element system, were used throughout FRT-1.

The aged releases utilized fuel elements which had been irradiated in the HTR for an in-pile period of 467 hours and cooled for approximately two and one-half years.

The green releases were performed with fuel elements that had been irradiated in the MTR for an in-pile time of 125 hours. These fuel elements were allowed to decay about 6 weeks before the first release.

4.1.3 Melting Technique

Melting of the test samples was accomplished with a specially designed induction furnace (Appendix B). Induction heating was chosen so that fast melting and adequate temperature control could be obtained. The furnace was equipped with sequentially operated effluent samplers, and metered air was introduced to displace the effluent from the furnace crucible. The furnace, power supply, and operating controls were located at or near the apex of the network.

The criteria established for the release operation were as follows:

- . Stage to be melted in air
- . Melt to occur within a few minutes after initial application of power

- . Sustained melt temperature to exist for 10 minutes following initial melting
- . Furnace to be purged with metered air and quantitative samples of the effluent taken throughout the heating cycle
- . Effluent to be released to the environment at five feet above ground level

4.1.4 Power Distribution

Electrical power was supplied by two systems. An overhead power system was designed as a joint effort of the Idaho Operations Office, Atomic Energy Commission, and Convair-Port Worth. This line system supplied power to the release area, control trailer and the equipment on the inner arcs. In addition, generator sets were used on the outermost arcs because of the distances involved. Further details are given in Appendix C.

4.1.5 Meteorological Network

Meteorological data were taken preceding and during each release to characterize the diffusion conditions existing at the time of each test.

To facilitate the collection of the meteorological data, instrumented towers and masts (Appendix D) were erected. The 46-meter-high main apex tower was positioned 200 meters upwind of the release point to provide vertical wind and temperature profiles.

Auxiliary field masts containing wind direction and velocity instrumentation were located on the centerline of the sampling network at distances of 200, 400, 800, 1600, 2400, and 3200 meters downwind of the release point. All data from the auxiliary stations and the main tower were transmitted to recording instruments located in a central control trailer.

Forecasts of general weather conditions, wind direction, and windspeed for the test site were furnished by the United States Weather Bureau Office located at Central Facilities at the NRTS. Each afternoon a general forecast for the following day was provided so that tentative plans could be made for a release. Every morning a detailed synoptic weather forecast was supplied by the Weather Bureau Office. A final forecast for the remainder of the day was made in the early afternoon.

4.1.6 Release Measurements

FRT-1 was not designed to collect all the fission products. Consequently, it was necessary to determine the release percentages by indirect means. In the aged fuel element releases four means were used whereby the release percentages could be obtained, and in the green fuel element releases three methods were used. By using different methods it was possible to cross check the results.

The following methods were used:

Aged Fuel Elements

- . Pre- and post-melt gamma spectra of fuel elements
- . Pre- and post-melt gross gamma dose rates from fuel elements
- . Network sampling of the effluent cloud
- . Fractional sampling of effluent at the furnace

Green Fuel Elements

- . Pre- and post-melt radiochemical analyses
- . Network sampling of the effluent cloud
- . Fractional sampling of effluent at the furnace

4.1.7 Release Height

One of the parameters in the generally used diffusion equations is the effective release height. Since there was no vertical sampling network for the collection of fission products, a charged-wire grid was erected after the fourth release. Vertical wires, Appendix E, were located four feet downwind from the furnace.

After a release the length of the wire was scanned for collected radioactivity. Thus, it was possible to obtain the effective release height from the location of the activity on the wire.

4.1.8 Smoke Plume Recording

Fission product releases were immediately preceded and followed by the release of a visible smoke. The smoke was photographed by both aerial and ground cameras and from these photographs it was possible to observe cloud diffusion characteristics, i.e., the amount of meandering of the cloud and the rate of vertical diffusion. The cloud photography equipment and its use is explained in Appendix F.

4.1.9 Fluorescent Tracer Measurements

The purpose of the fluorescent tracer was to simulate and compare dispersal characteristics of a nonradioactive tracer material with fission products. The tracer employed was zinc cadmium sulphide ($ZnCdS$). This material fluoresces under ultraviolet light and is frequently used in atmospheric diffusion experiments. Tracer tests were made either during or following the fission product releases.

During the fluorescent tracer tests, numerous samples were taken with Andersen type air samplers out to 800 meters downwind of the release point. Appendix G contains details of the fluorescent release and collection procedure.

4.1.10 Airborne Radioactivity Measurements

Airborne radioactivity in the sampling network was collected by Hi-Vol (Staplex) air samplers. A pleated filter, Mine Safety Appliance No. CT77227, was used as the primary filter; however,

for the green releases this pleated filter was backed up by a carbon cartridge, Mine Safety Appliance No. 46727. The pleated filter has a collection efficiency of 99.9% for particles having a mean size of about 0.3 microns. The carbon cartridge was added primarily to collect the iodine that penetrated the pleated filter.

The samplers were kept in operation continuously while the released material was passing over the network. From the amount of radioactivity collected by a sampler, it was possible to establish the time-integral air-concentration of radioactivity at each sampler position.

From these measurements it was possible to establish arc profiles and cloud centerlines. With this information, curve fits for the data were obtained and direct comparisons with other models were made. The derivation of the curve-fit procedure, as well as sampler placement and operation, are given in Appendix H.

4.1.11 Particle Size Measurements

Particle separation was largely accomplished by using Andersen samplers as part of the network sampling scheme. This sampler was used in the collection and sizing of radioactive aerosols as well as fluorescent particles. See Appendix I for details. The sampler is basically a six-stage, Cascade-type impactor. However, some of these samplers were backed-up by two

additional filtering stages, the first incorporating a Gelman molecular membrane filter and the second a Millipore molecular membrane filter. During the green releases a carbon cartridge was also added as the eighth stage of the Andersen sampler system.

4.1.12 Radioactivity Deposition Measurements

Since different types of particles exhibit different tendencies to deposit out on surfaces, several materials were used. Sticky paper, water, sand, and vegetation samples were placed on the network during each release to measure the deposition of radionuclides. Sticky-paper sampling was expected to provide more satisfactory data because better control over exposure conditions could be maintained and a larger number of samples could be taken. The traps containing these sticky papers (Appendix J) were positioned at the same elevation as the Hi-Vol samplers. The traps were designed to provide exposure to direct deposition during cloud passage only. Water and sand trays were located on the ground and around sagebrush. The results of these tests, except sticky paper, have been reported in Reference 9. Sticky paper results are described herein.

4.1.13 External Dose Measurements

To evaluate the present methods of predicting external gamma exposure to personnel from radioactive clouds, twenty recording scintillation gamma detectors were used. These units

were placed at three-degree intervals on the 400-meter arc. See Appendix K for details.

4.1.14 Radiochemical Techniques

The network and furnace effluent analyses were made by Convair-Fort Worth. The pre- and post-melt fuel element samples were assayed by General Electric Vallecitos Laboratory and are reported in Reference 10. General radiochemical techniques are given in Appendix L.

4.1.15 Radiobiological Measurements

Dogs, rats, and rabbits were exposed at several points on the inner arcs to provide biological exposure data. These short-time exposures were conducted to determine:

- . the amount of radionuclides inhaled and ingested
- . the action of body fluids on these nuclides
- . movement of certain of these nuclides (especially I¹³¹) to different parts of the body.

Particle size and airborne radioactivity data were used to facilitate the interpretation of the various biological measurements. The rabbit data are reported in Reference 9. The radiobiological measurements (dogs and rats) were made by the University of Rochester and are described in Reference 11 and Appendix M.

4.2 Evaluation of Results

The field releases provided a substantial amount of data on fission products release percentages, airborne radioactivity, deposited radioactivity, deposition velocities, external dose,

fluorescent tracer, diffusion parameters, and radiobiology. The data in some cases can be compared with what is implied from the existing ANP model, but in other cases, where no model exists, data are presented and discussed in light of the overall hazards analysis.

4.2.1 Fission Products Release Percentages

Since no contained releases were made, several indirect approaches were employed to determine isotopic release percentages. This system provided independent means for determining release percentages and also served as a check on techniques. The methods employed required the following information:

- . The amount of the various radionuclides present in a fuel element before a release
- . The most hazardous radionuclides released to the atmosphere and the sequence of release

The above listing will be discussed in order of presentation.

4.2.1.1 Source Inventories

The principal nuclides in three of the given fuel elements are shown in Table 1. The specimens were part of the fuel element samples used in Releases E, F, and H. Calculated data are compared with data obtained from the Vallecitos radiochemical analyses of the pre-melt sample (Ref. 10). Considering the problem involved in calculating the inventories, the general agreement appears to be good. In the case of iodine, the laboratory and

TABLE 1

Principal Nuclides of Assembly for Releases E, F, and H
at End of Irradiation

Release	Nuclide	Inventory in dpm/gm U235		Ratio: Meas. Value to Calculated Value
		Pre-Melt Sample Analysis	Calculations from Irradiation History	
E	Ru103	2.9×10^{12}	2.9×10^{12}	1.00
	Ce144	1.02×10^{12}	0.77×10^{12}	1.32
	Zr95	2.9×10^{12}	3.9×10^{12}	0.74
	Sr89	5.1×10^{12}	3.78×10^{12}	1.35
	Ba140	2.3×10^{13}	1.8×10^{12}	1.28
	Cs137	0.027×10^{12}	0.020×10^{12}	1.35
	I131	1.4×10^{13}	1.2×10^{13}	1.17
F	Ru103	2.9×10^{12}	2.9×10^{12}	1.00
	Ce144	0.74×10^{12}	0.77×10^{12}	0.96
	Zr95	3.3×10^{12}	3.9×10^{12}	0.85
	Sr89	4.7×10^{12}	3.78×10^{12}	1.25
	Ba140	1.8×10^{13}	1.8×10^{13}	1.00
	Cs137	0.024×10^{12}	0.020×10^{12}	1.20
	I131	1.3×10^{13}	1.2×10^{13}	1.08
H	Ru103	2.3×10^{12}	2.9×10^{12}	0.79
	Ce144	0.78×10^{12}	0.77×10^{12}	1.01
	Zr95	2.8×10^{12}	3.9×10^{12}	0.72
	Sr89	5.4×10^{12}	3.78×10^{12}	1.43
	Ba140	2.3×10^{13}	1.8×10^{13}	1.28
	Cs137	0.028×10^{12}	0.020×10^{12}	1.40
	I131	1.2×10^{13}	1.2×10^{13}	1.00
Ave.	Ru103	2.7×10^{12}	2.9×10^{12}	0.93
	Ce144	0.85×10^{12}	0.77×10^{12}	1.10
	Zr95	3.0×10^{12}	3.9×10^{12}	0.77
	Sr89	5.1×10^{12}	3.78×10^{12}	1.35
	Ba140	2.1×10^{13}	1.8×10^{13}	1.17
	Cs137	0.026×10^{12}	0.020×10^{12}	1.30
	I131	1.3×10^{13}	1.2×10^{13}	1.08

computed data are in good agreement, differing only by about eight percent. The average discrepancy between calculated and measured inventory was about 18%.

These calculated inventories were used as a basis for computing release percentages and network radioactivity. Calculated inventories of those nuclides which were detected in the sampling network are shown for each fuel element at time of release in Table 2. Fuel elements in aged Releases A, B, C, D, and I were estimated to contain 3.4 to 4.7 curies of $\text{Sr}^{90}\text{-Y}^{90}$ and 2.9 to 4.0 curies of $\text{Cs}^{137}\text{-Ba}^{137\text{m}}$. Likewise, calculations showed that fuel elements in the green Releases E, F, G, and H contained considerably lesser amounts of the above named isotopes and considerably more I^{131} , Ce^{141} , $\text{Zr}^{95}\text{-Nb}^{95}$, and $\text{Ru}^{103}\text{-Rh}^{103\text{m}}$.

4.2.1.2 Release Fractions

The amounts of fission products released to the atmosphere were derived through pre- and post-melt gamma spectrum measurements, pre- and post-melt gross gamma dose-rate measurements, release percentages from the network samples, fractional sampling of the effluent at the furnace, and pre- and post-release radiochemical analysis. In the latter two cases, the relative abundance of fission products was obtained indirectly and the results are also expressed as release percentages. The radioactivity in the network was limited to fission products. There was no alpha activity

TABLE 2
Calculated Inventories in Fuel Elements at Release

Nuclide	Curies Prior to Release								
	A Aged	B Aged	C Aged	D Aged	E Green	F Green	G Green	H Green	I Aged
Sr ⁹⁰ -Y ⁹⁰	4.0	3.7	4.7	3.5	0.6	0.6	0.6	0.6	3.4
Zr ⁹⁵ -Nb ⁹⁵	--	--	--	--	64	59	51	51	--
Ce ¹⁴¹	--	--	--	--	74	63	48	48	--
Ru ¹⁰³ -Rh ^{103m}	--	--	--	--	35	31	24	24	--
Cs ¹³⁷ -Ba ^{137m}	3.4	3.1	4.0	2.9	0.5	0.5	0.5	0.5	2.9
I ¹³¹	--	--	--	--	7.8	3.9	1.3	1.2	--

on the several pleated filters assayed for alpha contamination, indicating that the uranium was not released as an aerosol.

Pre- and post-melt gamma spectrum measurements were made with the aged Releases A, B, C, and D, and this technique provided an excellent means of computing cesium release percentages. In these aged releases Cs^{137} was the only isotope that escaped in sufficient quantity so that release percentages could be readily determined from the spectra. Values obtained are shown in Table 3.

TABLE 3
Cesium Release Percentages

Release	Percent
A	43
B	43
C	51
D	83

Roughly 40 to 50 percent of the cesium was released, excepting in Release D. A temperature excursion occurred during Release D, and consequently a greater amount of cesium escaped. These amounts of cesium released are considerably more than that predicted by ANP model. The values for the ANP model are given in Table 4.

The release percentages as measured are about a factor of five greater than those predicted, except in the case of Release D. During this release the measured value was larger than the predicted by a factor of eight. This increase over the estimated values is an important field result. However, this increase does not materially affect the hazards-evaluation results of previous ANP studies because cesium is a muscle seeker, and the muscle dose is several orders of magnitude lower than the controlling organ dose for all organs considered in the ANP studies (Ref. 2).

TABLE 4
ANP Release Model
(Meltdown)

Release % Fraction	Iodine	Noble Gases	Bone Seekers	Cesium
Aerosol	50	100	0.23	2.3
Particulate	0	0	0.77	7.7
Total	50	100	1.00	10.0

The pre- and post-melt gamma dose rate levels from aged fuel elements were measured with an ionization chamber under fixed geometry. This technique also provided very useful information on gross gamma release percentages. The percentage reduction in

gamma dose rate for Releases A, B, and D, shown in Table 5 are interpreted as release percents because changes in geometry of the pre- and post-melt specimens were considered to be negligible. Approximately 20 % of the gamma emitting nuclides were released, except where a temperature excursion occurred in Release D. Based on these gross gamma dose-rate measurements, the higher temperature increased the release percentage by a factor greater than two.

TABLE 5
Gross Gamma Release Percentages

Release	Percent
A	23
B	17
D	54

These measurements were in relative agreement with the pre- and post-melt gamma spectrum measurements. The dose rate measurements provided values which were slightly less than those obtained through gamma spectral procedures because the dose-rate values are weighted by isotopes other than cesium.

Release percentages from network samples provided a means of determining the percent of the initial inventory that was released as an aerosol. By definition in the ANP studies an

aerosol is a particle having a diameter less than 10 microns. The release percentages were computed by comparing simple ratios. For example, the percentages of Sr^{90} released from aged fuel elements were determined from the field air sampler data by equating the dilution factor of the network strontium to the dilution factor of the total cesium release, i.e.,

$$\frac{\text{Sr in filter}}{(\text{Sr release fraction})(\text{Sr Inventory})} = \frac{\text{Cs in filter}}{(\text{Cs release fraction})(\text{Cs Inventory})}$$

In essence, the amount of any nuclide collected in a network air filter divided by the product of its fuel element inventory, release fraction, and filter efficiency gives the furnace-to-filter atmospheric dilution factor for that nuclide. Therefore, it can be reasonably assumed that any material remaining in the cloud at or above the air sampler level at the 100-meter arc and beyond must be aerosol rather than large particulate. Therefore, the dilution factor of this material may be assumed to be the same as that of any other aerosol leaving the furnace at the same time and collected by the filter with the same efficiency. The measured amount of cesium in the filter (normalized to unit inventory) and the cesium release fraction determined from the pre- and post-melt gamma spectrum measurements, Table 3, served to evaluate the right hand side of this equation. Note, however, that the validity of this procedure depends on the assumption that all of the released cesium is in aerosol form and that it is filtered with the same efficiency as the strontium.

The air sampler assays from the green releases were used in a similar manner to evaluate the release percents of Ru^{103} , Ce^{141} , Zr^{95} - Nb^{95} , and Cs^{137} . In these cases the atmospheric dilution factor was evaluated from the I^{131} assay by assuming 50% release of I^{131} . The 50% value is a reasonable value supported by measured results and is also the percentage used in the ANP studies.

The release percents computed by the above method are listed in Table 6. Cesium releases for the green specimens ranged from 24 to 36%. The remaining isotopic releases, except iodine, were less than two percent.

TABLE 6

Release Percents of Nuclides Calculated from Network Activity

Nuclide	Releases*								
	A Aged	B Aged	C Aged	D Aged	E Green	F Green	G Green	H Green	I Aged
Sr^{90}	1.7	0.15	0.17	0.75	--	--	--	--	0.5
Ru^{103}	--	--	--	--	1	0.75	0.8	0.75	--
Ce^{141}	--	--	--	--	0.01	--	0.05	0.3	--
Zr^{95} - Nb^{95}	--	--	--	--	0.03	--	0.25	0.05	--
Cs^{137}	--	--	--	--	30	36	34	24	--

- * Releases A, B, C, D, based on Cesium release percentages from gamma spectrum measurements (Table 3)
- Releases E, F, G, H, based on assumed 50% I^{131} release
- Release I based on assumed 50% Cs^{137} release

The release percents obtained by network sample data were in general agreement with the spectral and dose-rate measurements. The agreement is considered to be good, considering the procedures used in making the comparisons.

The network sample data permitted a broader comparison of isotopes than the previously discussed methods. Table 6 shows a list of isotopes that can be compared with the ANP model shown in Table 4. The measured release percentage of cesium was high by a factor of about 10 to 15 as compared to those used in the ANP studies, based on aerosols only. The measured strontium release percentages were high by a factor of 2 to 3 but the resolution in these calculations is somewhat doubtful.

Fractional sampling of the effluent at the furnace was the final method used in determining release percents. The contents of the eleven evacuated bottles used to sequentially sample the furnace effluent during Release E were analyzed to determine the release percentage of several nuclides and the relative time of their release. Also, an integrating bottle was used to collect effluent throughout the release. The effluent sampling techniques and effluent analysis are described in Appendices B and L, respectively.

Each effluent sampler was separated into three parts for analyses, i.e., (1) the sampling probe tube which extended into the crucible, (2) the glass-wool filter plug through which the gas

sample passed before entering the flask, and (3) the evacuated flask. Of these, the probe tubes were the most radioactive probably because of condensation of fumes onto that portion of the probe extending into the crucible.

The accumulated percent of each radionuclide released during Release E, as based on calculated inventories, is shown in Figure 3. The relative releases in increasing quantities are $\text{Ce}^{141} < \text{Sr}^{89} < \text{Zr}^{95} - \text{Nb}^{95} < \text{Ru}^{103} < \text{Cs}^{137} - \text{Ba}^{137} < \text{I}^{131}$. The iodine release is roughly three orders of magnitude greater than cerium and strontium. Krypton-85 is not shown in Figure 3 because analysis for this isotope was made only from the single integrating sample bottle. It may be seen that some cesium was released shortly after the power was applied to the furnace. However, maximum release occurred about 8 to 10 minutes later, requiring almost two minutes to reach 50% of the peak. Parker, Creek, and Martin (Ref. 1) found that the cesium release percent for "threshold melting" rose from about 9% for small burnup to about 41 % for 25% burnup. Inasmuch as the burnup in the fuel elements used for PRT-1 releases was only 2.3 and 0.33% for aged and green fuel elements respectively, the high release percents observed are probably caused by longer melt durations.

Pre- and post-release radiochemical analyses were made for three green releases (E, G, and H). At the time of the field tests it was deemed necessary to obtain realistic release percentages by performing radiochemical analysis of samples from some of

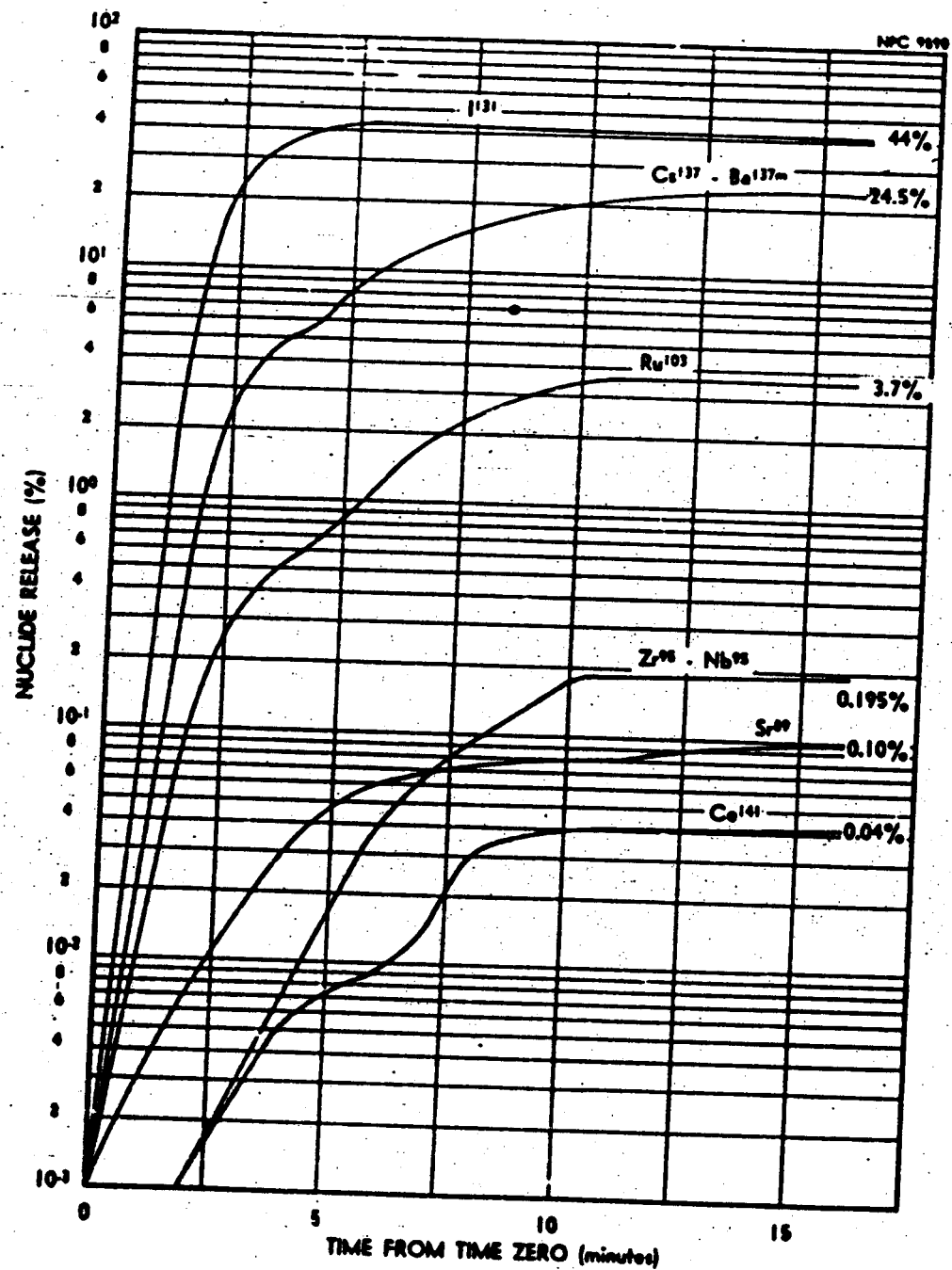


FIGURE 3. ISOTOPE RELEASE WITH TIME (Furnace Sampler Data - Release "B")

the green fuel element specimens and their post-release residues. However, due to difficulties experienced in dissolving some of the residue these analyses can only be used to obtain upper limits to the isotopic release percentages. Consequently, the results presented in this section (Table 7) are not expressed as release percentages but as the percent recovered from the residue. As an example, the field data do not substantiate the high Zr^{95} results reported in the radiochemical analysis (Ref. 10). This may be explained by the fact that Zr^{95} was detected in the undissolved residue. Likewise, there is considerable doubt about the strontium recovery since the undissolved portion of the residue was not checked for beta activity. Some additional details are given in Appendix L.

TABLE 7
Nuclides Recovered from Residue

Nuclide	Percent Recovered		
	Release E	Release O	Release H
Sr^{89}	59	41	36
Zr^{95}	35	34	48
Ru^{103}	91	79	93
I^{131}	0.1	0.04	0.18
Cs^{137}	13	2.9	3.4
Ba^{140}	57	47	26
Ce^{144}	86	102	76

4.2.2 Effluent Characteristics

In order to fully evaluate field results it was desirable to know the release-time behavior of the different isotopes, effective height of the effluent as it left the furnace, and the particle size characteristics.

Sequential fractional sampling of the effluent made it possible to determine the release time of various isotopes. These results are shown in Figure 4. It is apparent that iodine, cesium, strontium, ruthenium, zirconium-niobium, and cerium are released in the order listed. Essentially, all the iodine was released within the first two to three minutes while most of the cesium, ruthenium, and strontium was not released until about eight minutes had elapsed. Zirconium-niobium and cerium were detected about two minutes after the other isotopes began to appear. Essentially all the activity was released within a range of six to eight minutes.

The release height as measured by the charged vertical conductor procedure during Releases E, F, G, H, and I was about 1.7 ± 0.1 meters, i.e., about the same as the height of the top of the furnace.

Particle size measurements were made at five meters downwind from the furnace and on the network. The measurements were made with Andersen samplers and Millipore filters.

Results obtained during Release A at a station five meters downwind from the furnace and samplers located 1.5 meters above

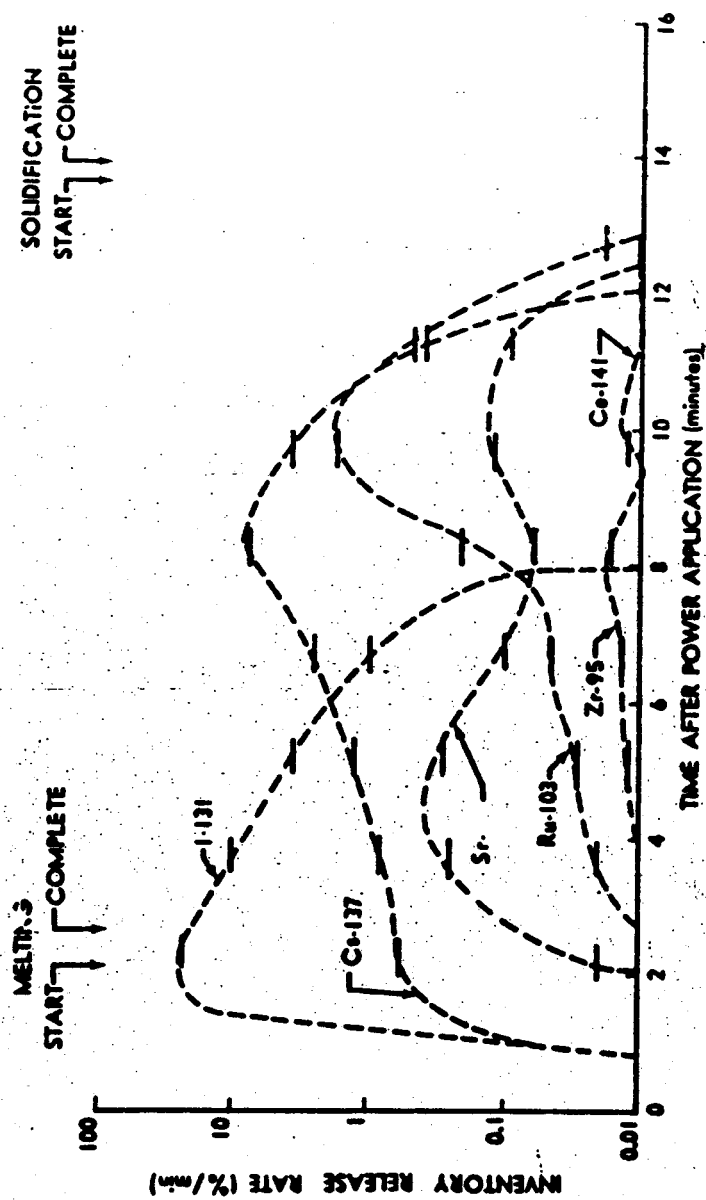


FIGURE 4. ISOTOPE RELEASE SEQUENCE

ground show that roughly half of the zirconium, one-fourth of the ruthenium and cerium and practically none of the strontium and cesium particles were larger than 5 microns. This is shown in the large fractions collected by the first stage of the Andersen sampler, Table 8. The comparison with ZnCdS is also shown in the table where the geometric standard deviation (σ_g) and median sizes (\bar{D}) are shown. It is assumed that the densities are the same.

TABLE 8
Distribution of Material in Andersen Sampler

Stage No.	Stage Activities as Percentages of Sampler Total						
Material	1	2	3	4	5	6	Gelman Filter
Zr ⁹⁵ -Nb ⁹⁵	47	16	18	6	5	2	6
Sr ⁸⁹	3	4	2	3	9	14	65
Ru ¹⁰³ , Ru ¹⁰⁶	21	6	7	6	7	12	41
Cs ¹³⁷ , Ba ^{137m}	1	1	2	2	13	17	64
Ce ¹⁴¹ , Ce ¹⁴⁴	25	10	11	5	9	10	30
Fluorescent Tracer							
\bar{D} (microns)	8.1	3.4	2.3	1.8	1.3	1.0	--
σ_g	1.7	1.5	1.3	1.3	1.3	1.3	--

Samples collected at the 100-meter arc and other positions
(Tables 9, 10, and 11) show that the particle sizes are:

Zirconium-niobium	1 to 5 microns
Cesium	<1 micron
Ruthenium	<1 micron
Iodine	<1 micron
Strontium	<1 micron
Cerium	~half <1 micron
	~half from 1 to 5 microns

TABLE 9

Distribution of Nuclides in Andersen Sampler (Release I)*

Stage No. Nuclide	Stage Activities as Percentages of Sampler Total						
	1	2	3	4	5	6	Gelman Filter
Cs ¹³⁷ -Ba ^{137m}	1	1	1	1	3	5	88

* Mean values from two stations near the cloud centerline on the Arc

TABLE 10

Distribution of Nuclides in Andersen Sampler (Release E)*

Stage No. Nuclide	Stage Activities as Percentages of Sampler Total							
	1	2	3	4	5	6	Gelman Filter	Activated Charcoal
Zr ⁹⁵ -Nb ⁹⁵	9	20	24	21	11	7	7	1
Ru ¹⁰³ , Ru ¹⁰⁶	4	2	1	1	2	2	82	6
I ¹³¹	10	3	3	4	4	3	31	42
Cs ¹³⁷	1	1	1	1	1	1	90	3
Ce ¹⁴¹ , Ce ¹⁴⁴	6	4	7	7	7	11	53	5

* Mean values based on centerline stations from three network arcs

TABLE 11

Distribution of Nuclides in Andersen Sampler (Release F)*

Nuclide \ Stage No.	Stage Activities as Percentages of Sampler Total						
	1	2	3	4	5	6	Gelman Filter
Ru ¹⁰³ , Ru ¹⁰⁶	8	5	--	--	1	1	85
Cs ¹³⁷ -Ba ^{137m}	1	--	--	--	3	5	91

* Mean values based on centerline stations from three network arcs

All the particles measured on the network were within the ANP definition of aerosols, i.e., smaller than 10 microns in diameter. The assumed ANP log normal particle size distribution ($\sigma_g = 2.75$ and $\bar{D} = 7$) was not checked.

The field data show, with the exception of zirconium-niobium, that 50 to 90% of the radionuclides penetrated the Andersen sampler and were deposited on the back-up membrane filter. The percentage of various radionuclides on the membrane filter were fairly uniform for different releases. Also, about 90% of the cesium, iodine, and ruthenium was associated with material that was in the submicron range, i.e., it penetrated the first five stages of the Andersen sampler. No significant change could be detected in the size distribution of the released fission products between the 100- and 800-meter arcs.

Autoradiograms of eight stages taken from an exposed Andersen-Gelman-Millipore sampler system are pictured in Figure 5.

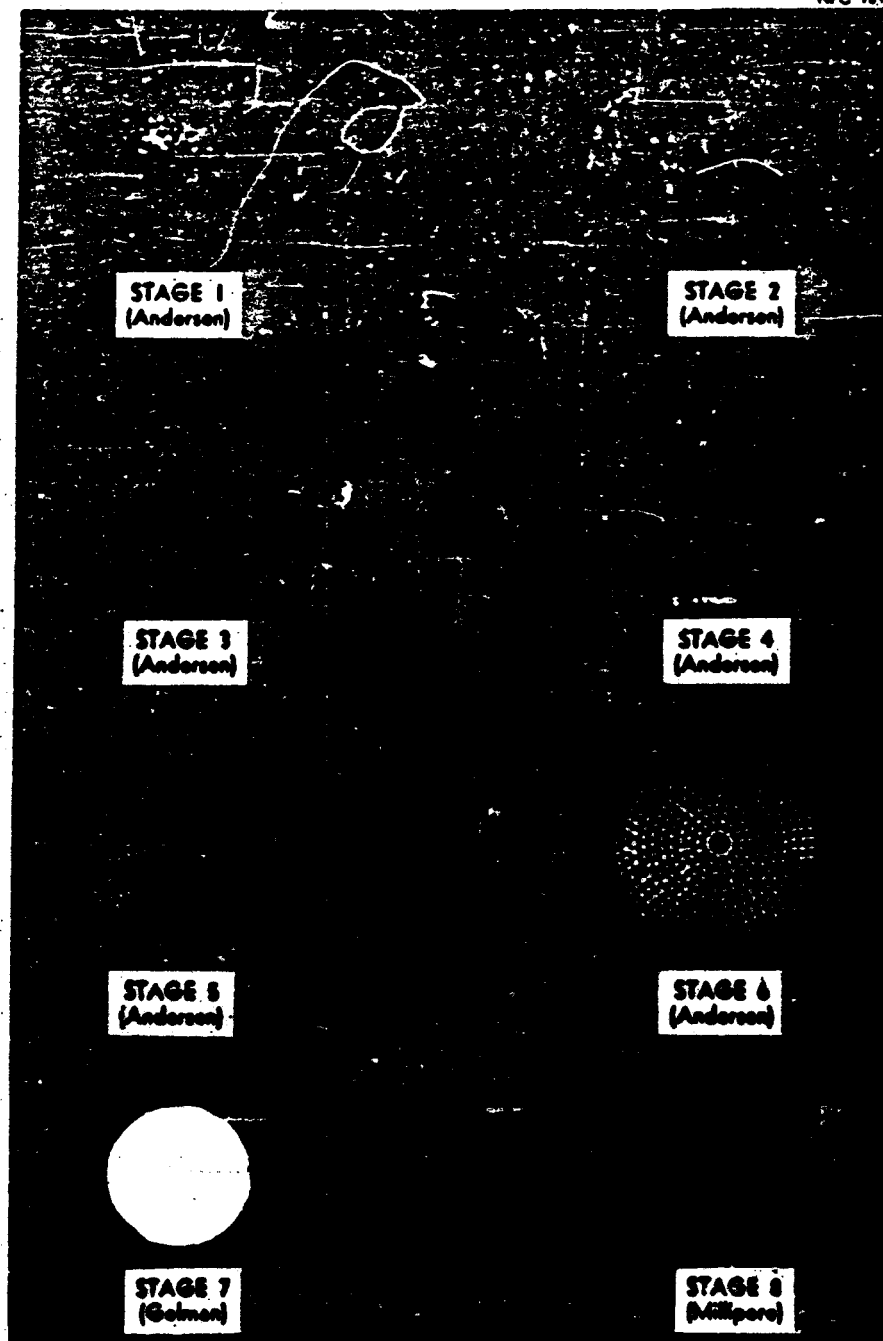


FIGURE 3. AUTORADIOGRAM OF ANDERSON-
GELMAN MILLIPORE SAMPLES

The relative size distribution, predominance of small particles, and effective filtration of the particles by membrane filters is very noticeable in the figure. The greater film exposures in the sixth stage of the Andersen sampler and the Gelman filter are considerably more pronounced as compared to the preceding stages. The lack of radioactivity noted on the second membrane filter (Stage No. 8) is indicative of the high collection efficiency of the membrane filters.

4.2.3 Airborne Radioactivity

The activity in the cloud was measured at various positions on the network. From the data, information was obtained on integral air concentrations, relative isotopic diffusion, and relative retention of nuclides on pleated filters and carbon cartridges.

4.2.3.1 Integral Air Concentration

The data showed that the rates of radioactivity dispersal by atmospheric diffusion varied quite significantly from one release to the next, as measured by Hi-Vol air samplers. Detailed air profile radioactivity data for each release were plotted (Appendix H), and from these plots maximum centerline activity values were obtained. For ease in comparison, the centerline data were normalized to unit inventory in the unmelted fuel element and also to unity at the 100-meter arc. Figure 6 is illustrative of the normalization to unit inventory. In this case the log of the centerline filter activities plotted versus log of

the distance downwind from the release point, are shown with corresponding "least squares" fitted straight lines. The differences in release fractions and in diffusion in the interval 0 to 100 meters result in the curves starting at different values. The curves of Figure 6 were therefore replotted in Figure 7 normalized to unit activity at the 100-meter arc to facilitate the comparison of diffusion rates in the sampling network. The mathematical model which expresses the diffusion of an effluent plume predicts a straight line log-log plot of centerline air concentration. Good diffusion (lapse) results in a steeper slope than does poor diffusion (inversion). The straight line fits the data quite well in most cases. The data from lapse Releases D, E, and F show a significantly greater rate of decrease (better diffusion) than the inversion Releases C, G, and H. Release A was performed under an isothermal condition changing to a very weak inversion condition which probably accounts for the lapse-like behavior.

The ANP predicted lapse and inversion lines for cesium are shown in Figure 8. The predicted activity, according to the lapse curve, is a factor of 10 to 20 lower than the points representing the measured aerosol concentration. However, the predicted inversion concentrations are not materially different from the measured values. It is important to note that the predicted air concentrations are based on a 2.5% cesium release whereas the results show that 10 to 20 times this amount was released.

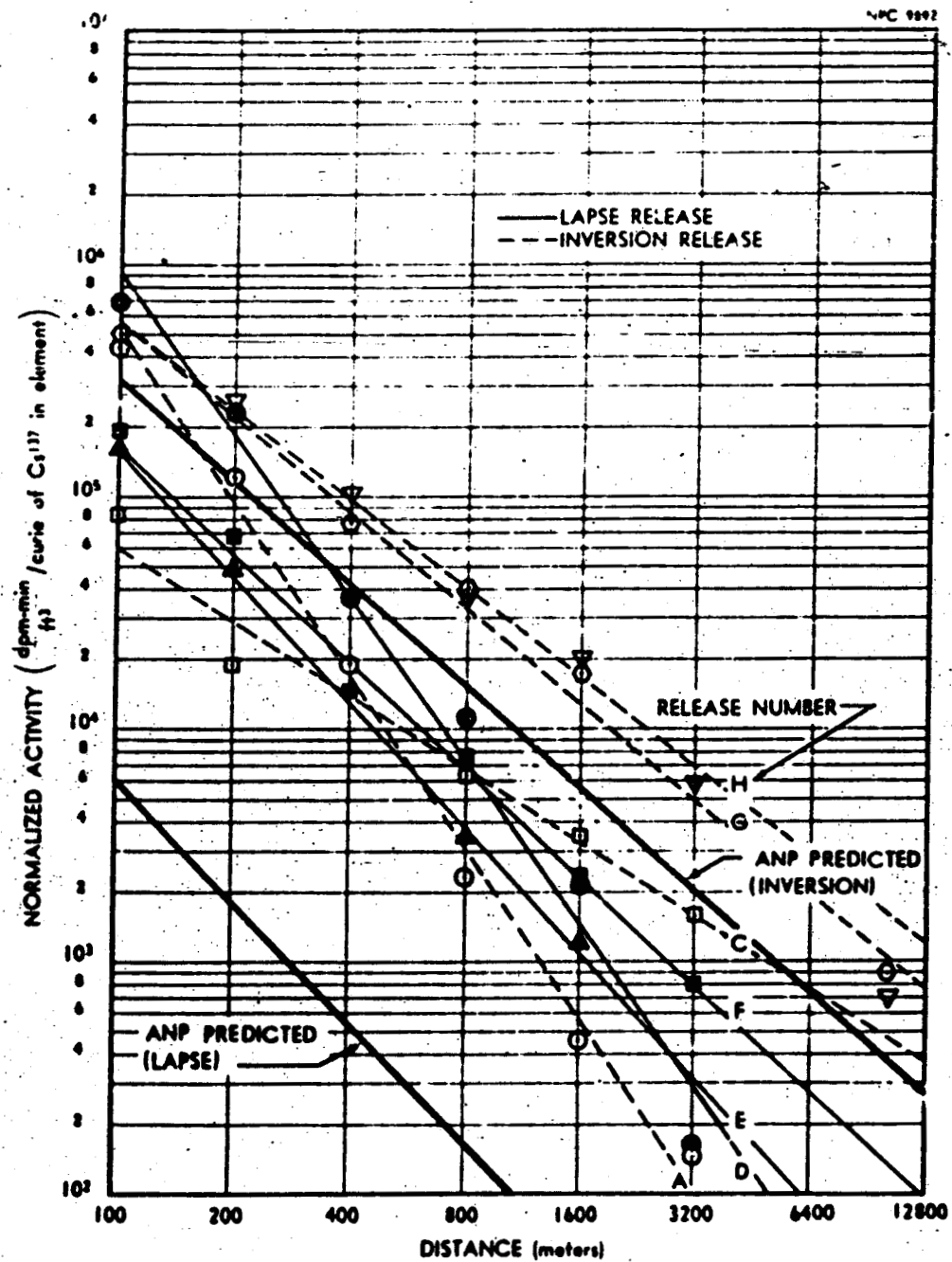


FIGURE 6. CESIUM-137 ON CLOUD CENTERLINE
(Normalized to Unit Inventory)

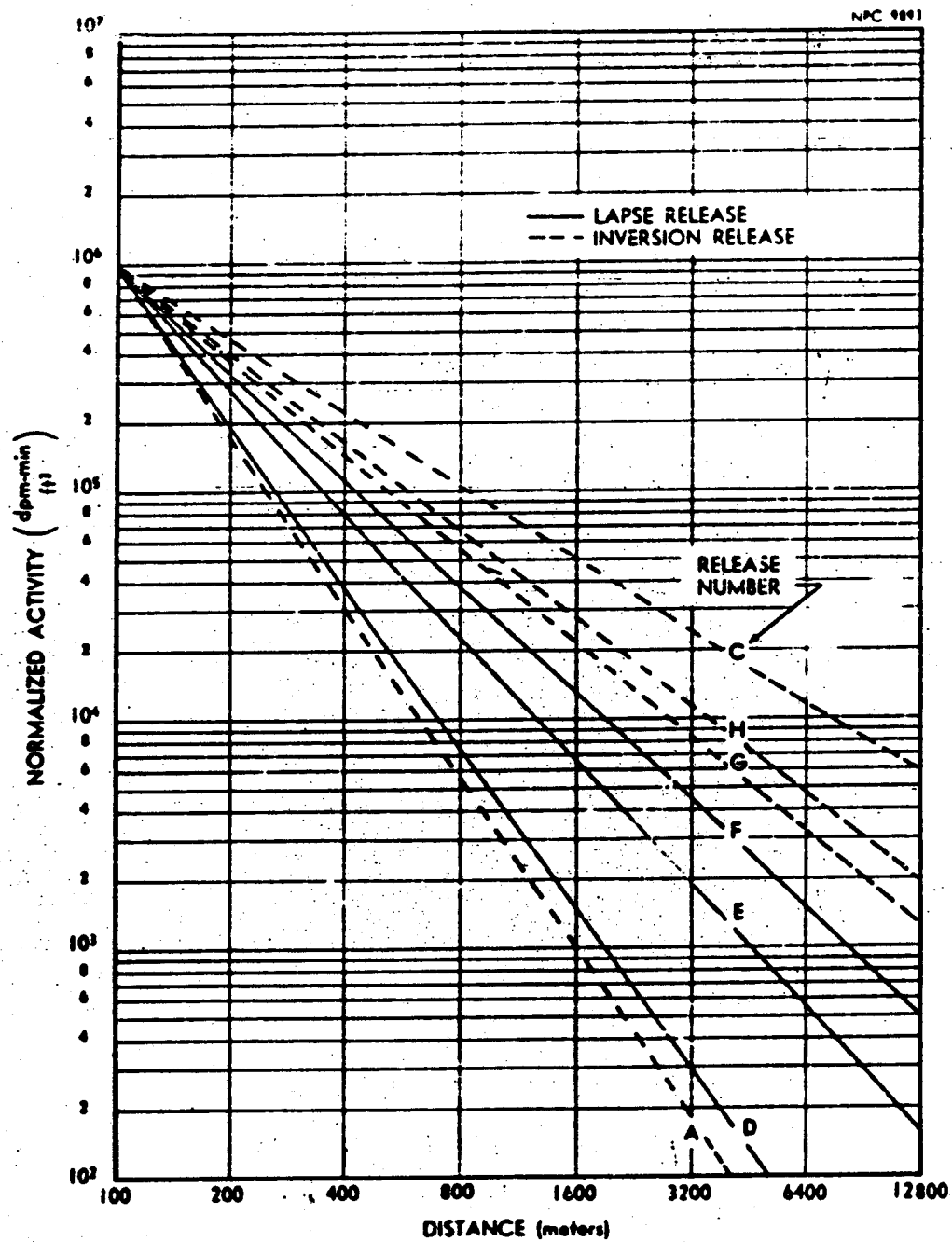


FIGURE 7. CESIUM-137 ON CLOUD CENTERLINE
 (Normalized to 100-Meter Level)

The concentration of iodine along the cloud centerline for lapse Releases F and P and inversion Release H are shown in Figure 8. No significant differences exist between Release F and P. Figure 9 shows that the Release F curve (lapse) is similar to the Release H curve (inversion). This anomaly may be the result of the marginal conditions which existed during Release F, i.e., weak lapse at the tower. As shown in the figure, the ANP predicted lapse concentrations are within a factor of about two of those measured. The predicted inversion levels are a factor of 10 higher than those encountered during the release. These ANP values are based on a 50% iodine release which is consistent with the measured value.

The cloud centerline ruthenium data from inversion Releases G and H and from lapse Releases E and F are shown in Figures 10 and 11. The slopes of the ruthenium curves are essentially the same as those found with cesium.

Zirconium-niobium data are shown in Figures 12 and 13. Here again the slopes of the curves are essentially the same as found for cesium.

4.2.3.2 Relative Isotopic Diffusion

Relative isotopic diffusion is an index of dispersal. A comparison of relative diffusion may be made by forming a concentration ratio $\left(\frac{\text{conc. on 100-meter arc}}{\text{conc. on 3200-meter arc}} \right)$ from the curve fits.

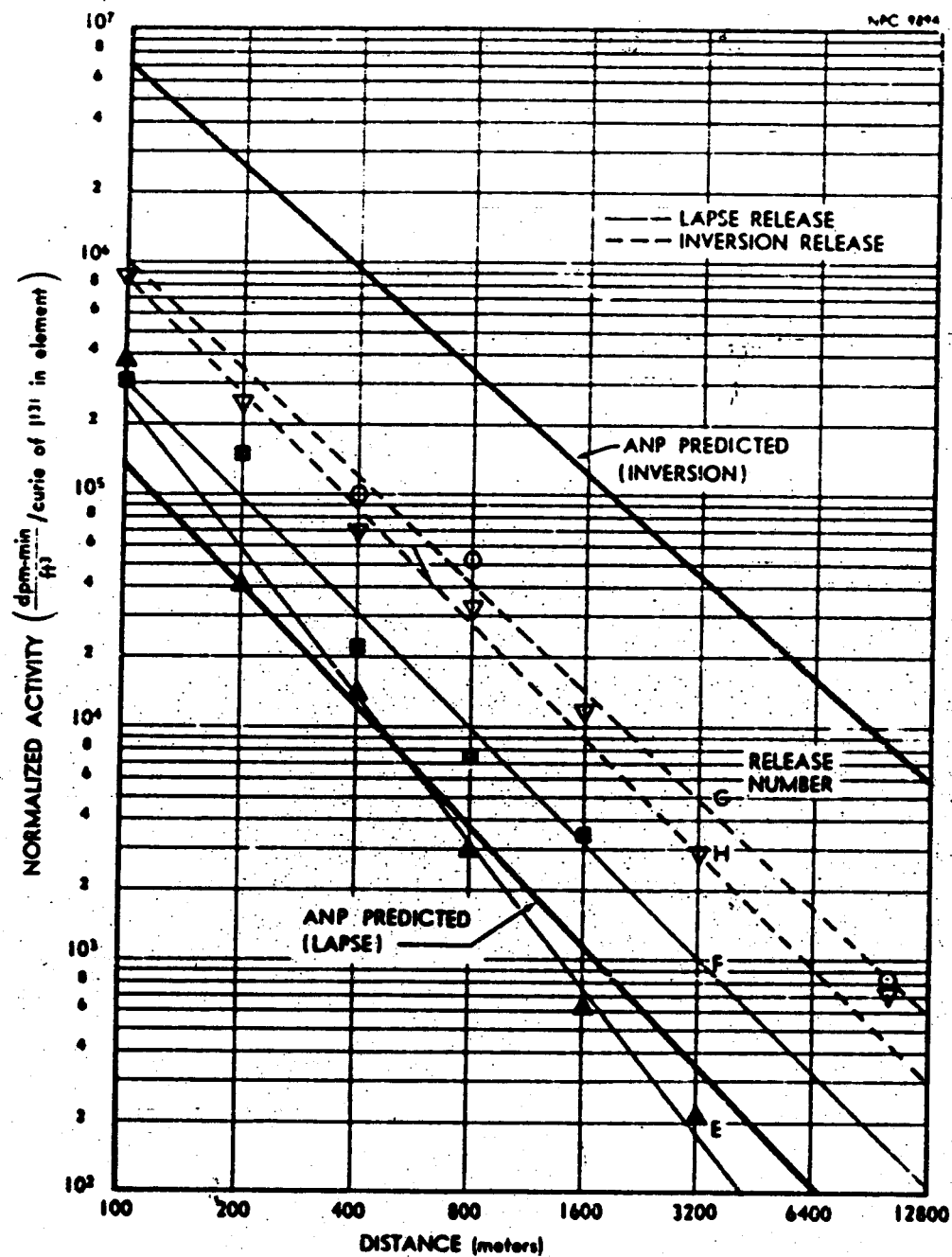


FIGURE 8. IODINE-131 ON CLOUD CENTERLINE
(Normalized to Unit Inventory)

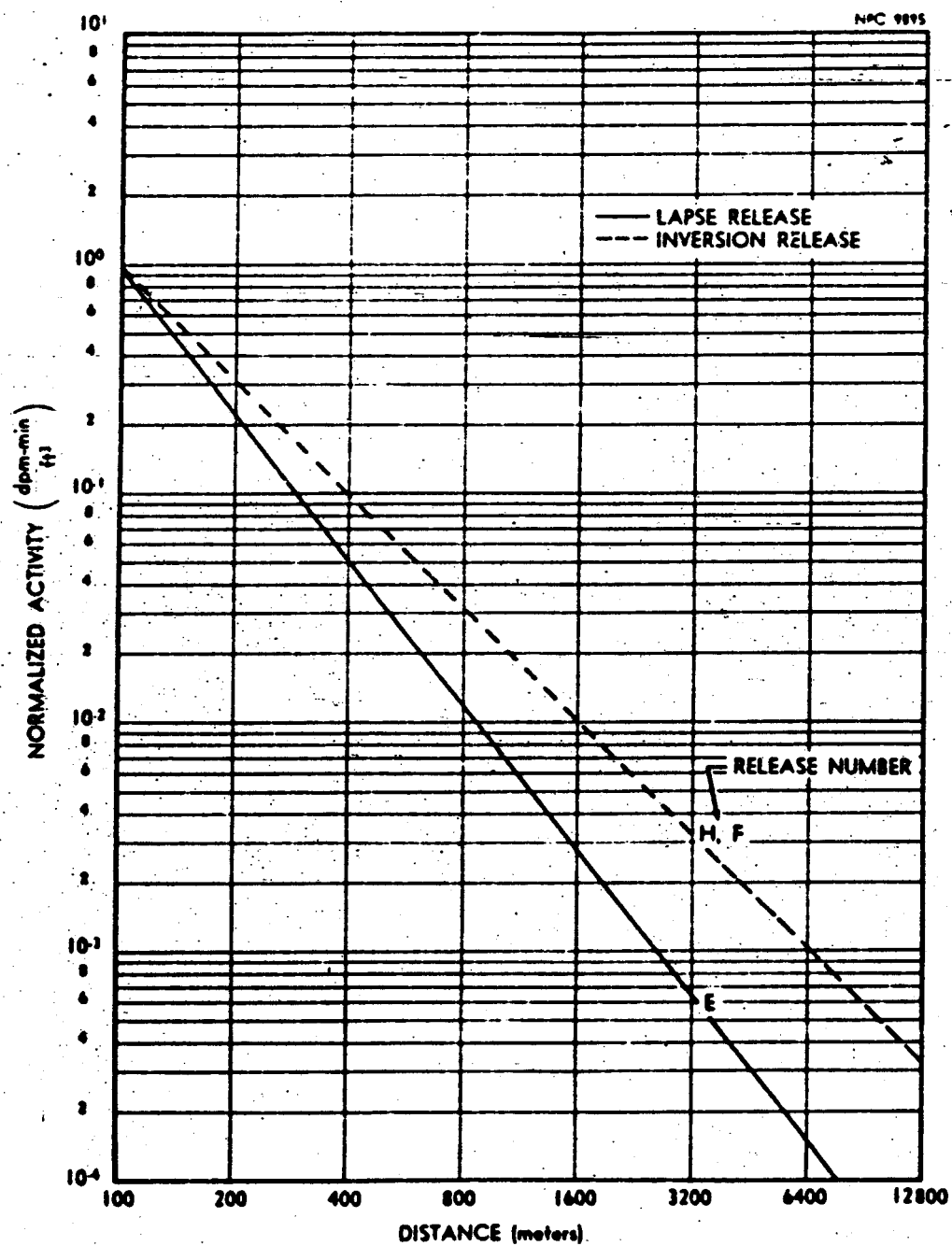


FIGURE 9. IODINE-131 ON CLOUD CENTERLINE
(Normalized to 100-Meter Level)

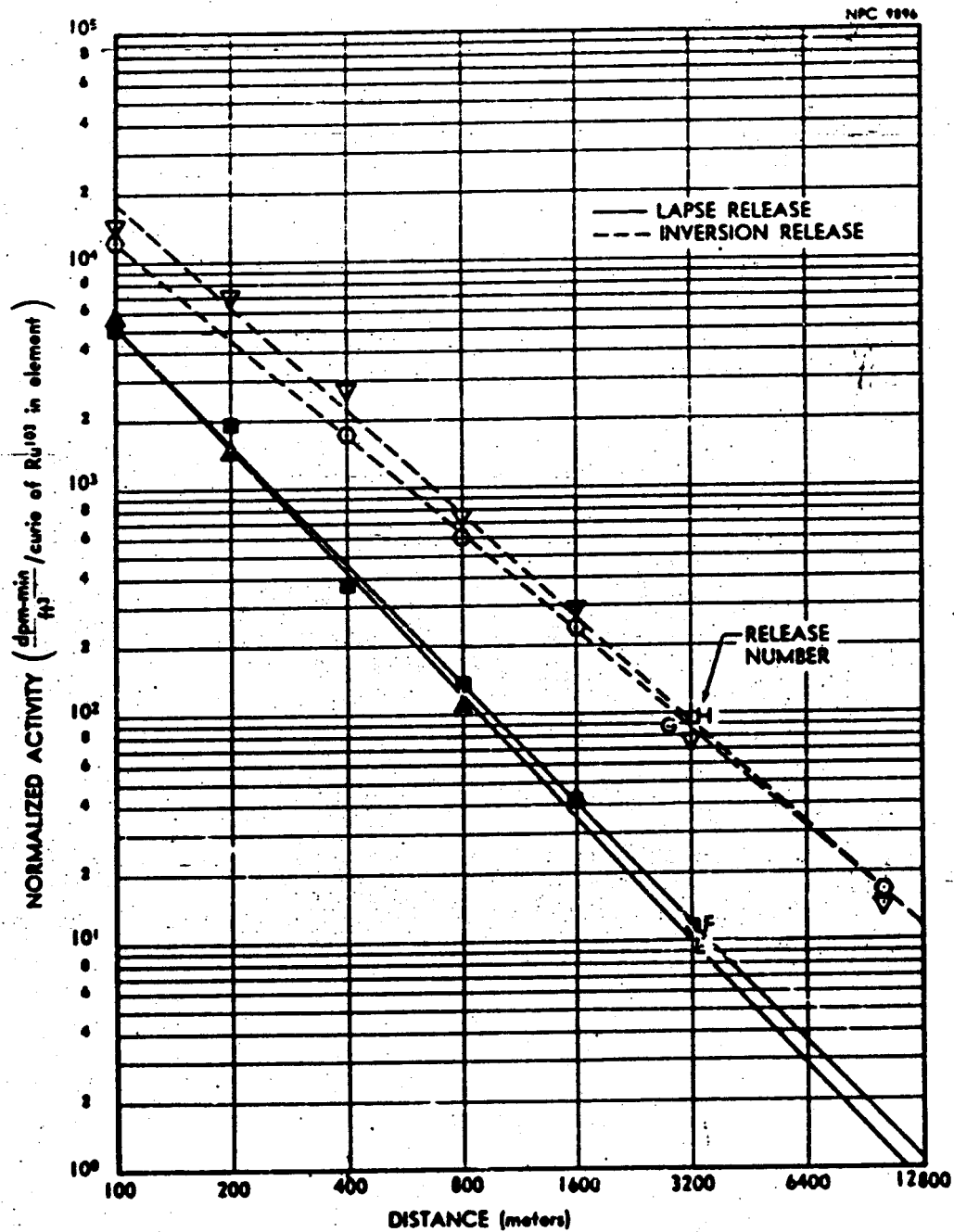


FIGURE 10. RUTHENIUM-103 ON CLOUD CENTERLINE
(Normalized to Unit Inventory)

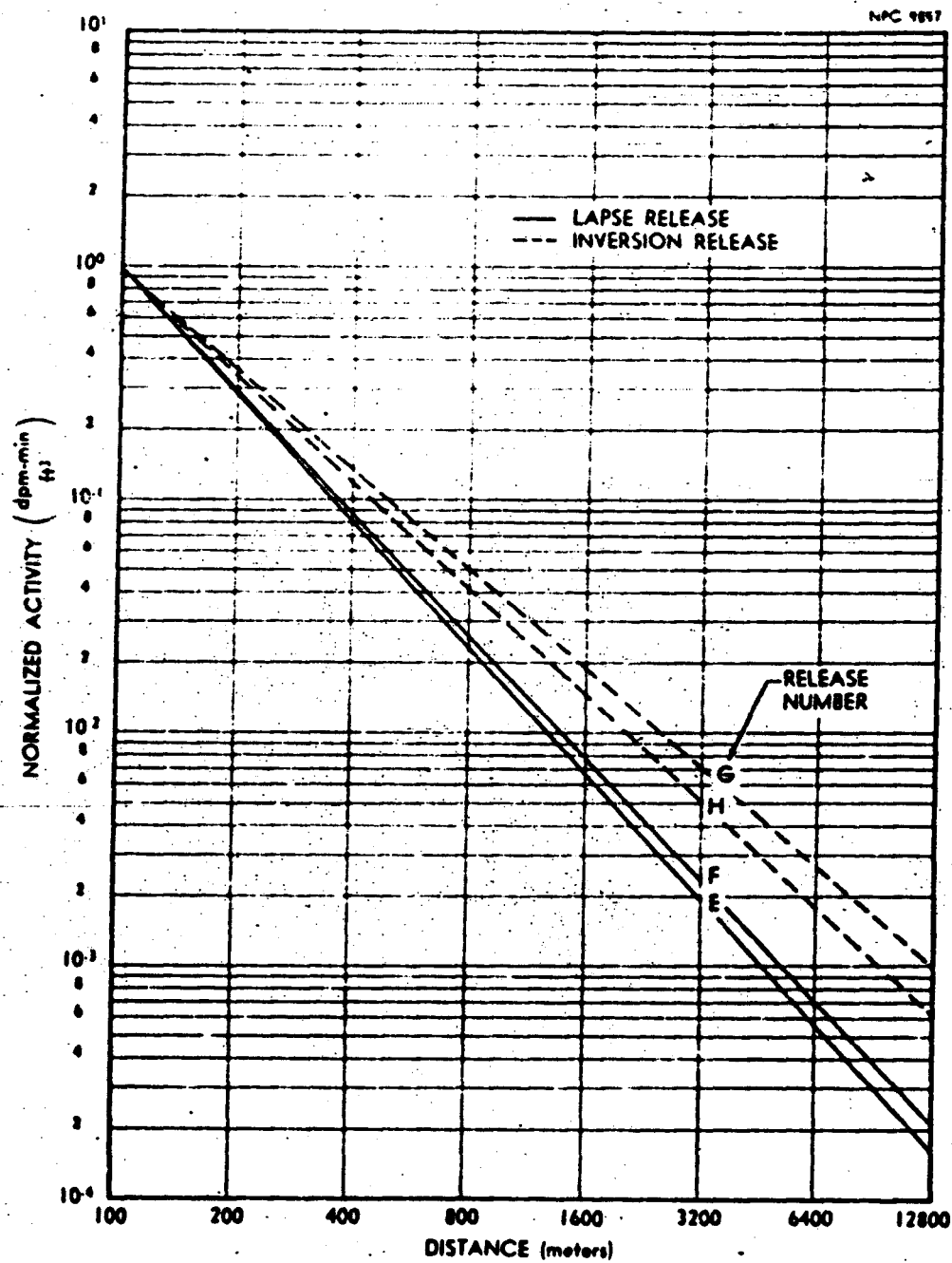


FIGURE 11. RUTHENIUM-103 ON CLOUD CENTERLINE
(Normalized to 100-Meter Level)

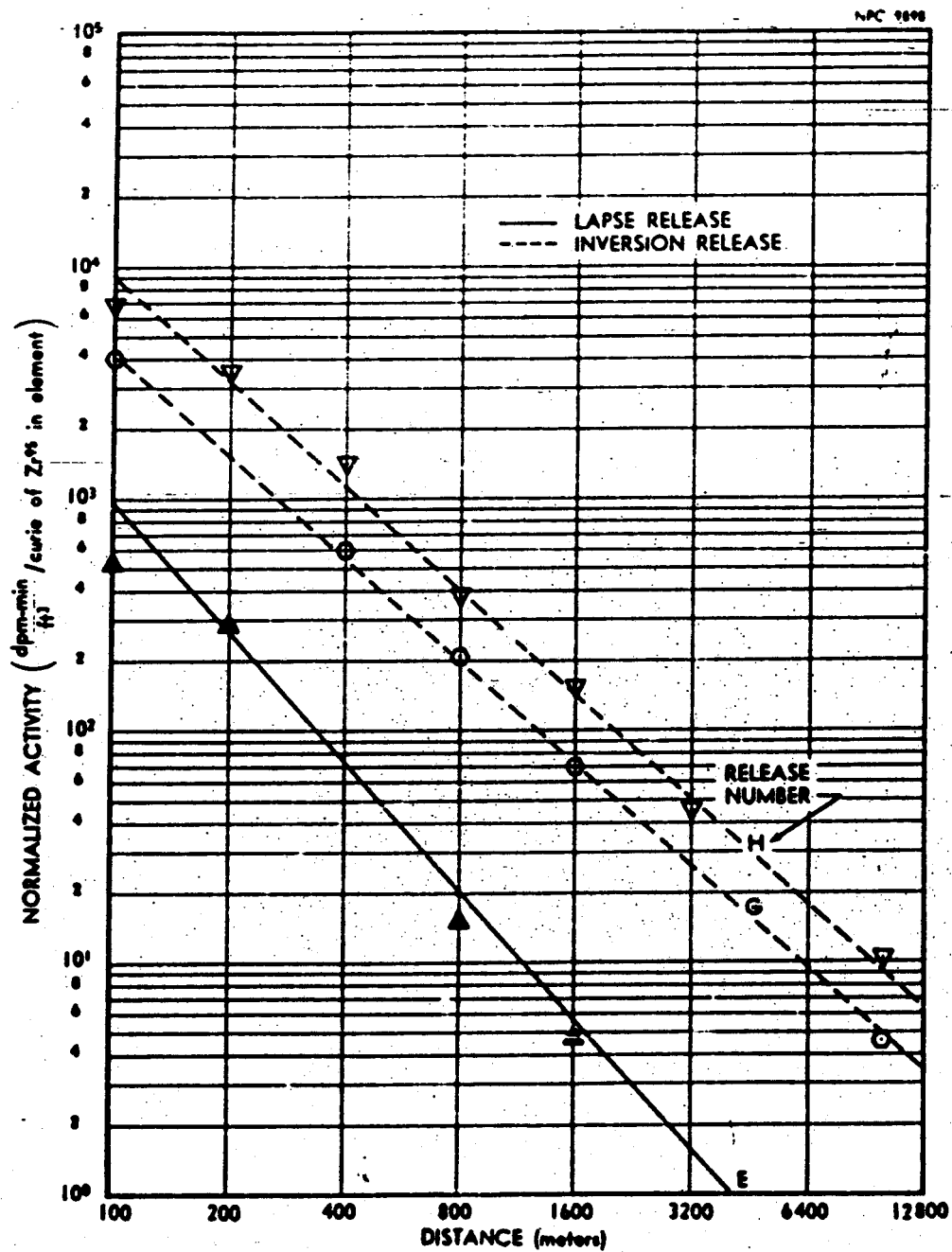
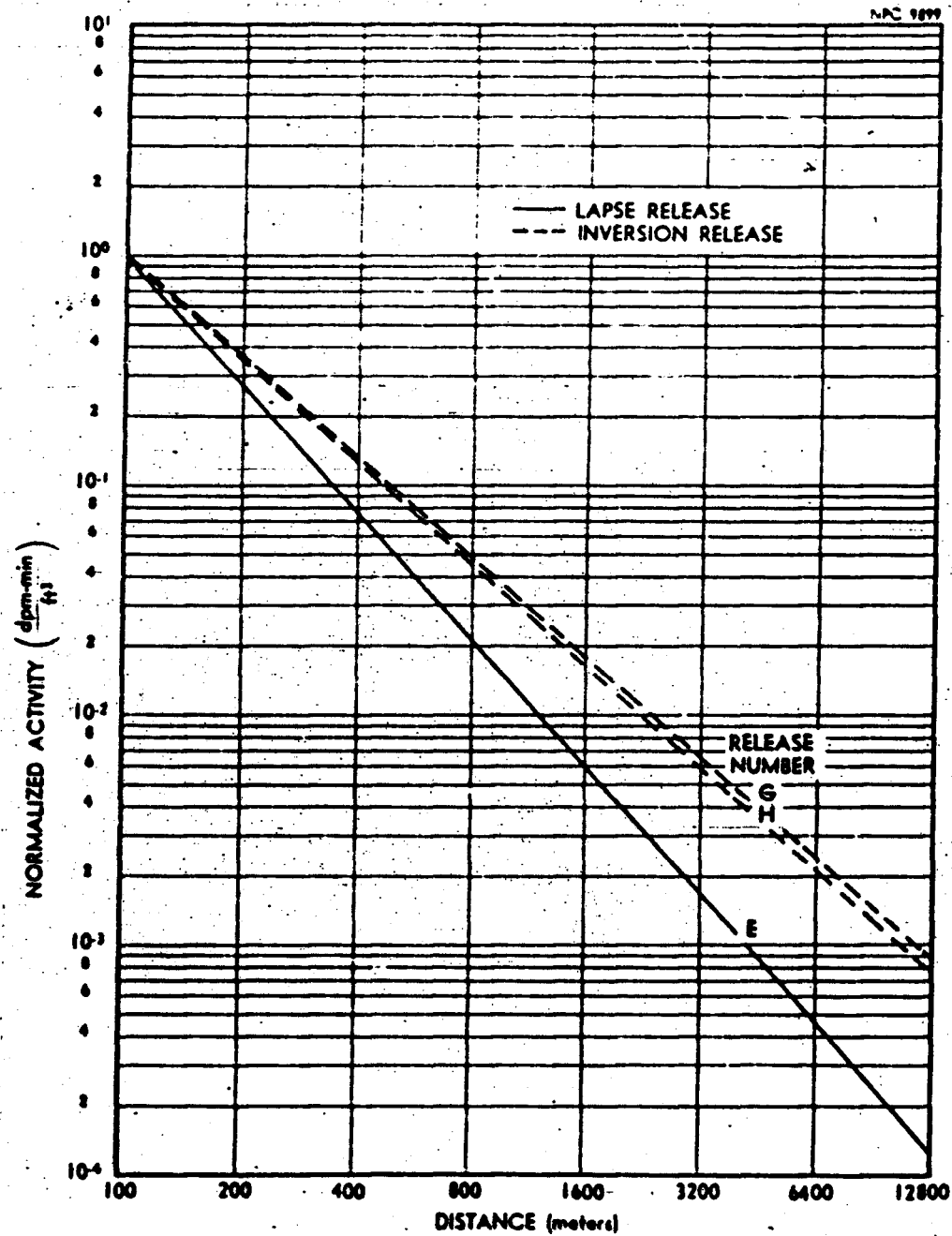


FIGURE 12. ZIRCONIUM-95 ON CLOUD CENTERLINE
(Normalized to Unit Inventory)



**FIGURE 13. ZIRCONIUM-95 ON CLOUD CENTERLINE
(Normalized to 100-Meter Level)**

Table 12 is a listing of these ratios. Generally, the difference in the attenuation factor is more pronounced from one release to another than between nuclides of any given release. The iodine appeared to diffuse more rapidly than other elements. This may have been because iodine was released early in the melting operation when the diffusion condition was usually better than toward the end of the melt.

TABLE 12
Relative Isotopic Diffusion

Nuclide Release				
	Cs ¹³⁷	I ¹³¹	Ru ¹⁰³	Zr ⁹⁵ -Nb ⁹⁵
D-Aged-lapse	3300	--	--	--
E-Green-lapse	567	1530	550	630
F-Green-lapse	210	320	433	--
A-Aged-Weak-inversion	5500	--	--	--
B-Aged-inversion	--	--	--	--
C-Aged-inversion	37.5	--	--	--
G-Green-inversion	120	--	140	150
H-Green-inversion	86	300	200	180
I-Aged-Weak-lapse	--	--	--	--

4.2.3.3 Relative Retention of Nuclides

Relative retention of nuclides on pleated filters and carbon cartridges illustrate the penetrating tendencies of iodine. The results from the various releases are plotted in Figure 12. About 25 to 45% of the iodine, based on total iodine collected by both the pleated filter and back-up carbon cartridge, penetrated the HI-Vol pleated filter. A least-square fit of the percent of iodine penetrating the HI-Vol pleated filter shows that slightly higher percentages are retained on the filters located closer to the release point.

The percentage of iodine collected by the carbon cartridge was dependent upon the concentration of dust in the atmosphere. The interaction of the local dust and iodine was demonstrated during Release G. This release was performed immediately after a dust storm and the percent of iodine collected by the carbon cartridges was greatly reduced. As compared to previous and similar releases the percentage of iodine in the carbon cartridges taken from the 100- to 1600-meter arcs (Release G) was smaller by as much as three orders of magnitude. However, on the five-mile arc, the percent of iodine on the carbon was roughly the same for either dusty or non-dusty conditions, indicating a possible transfer of iodine from the pleated filters to the carbon cartridge. Such a transfer might easily have taken place because the five-mile arc filters remained in operation for some time after the passage of the cloud. Each generator had to be turned off separately and this required some additional time.

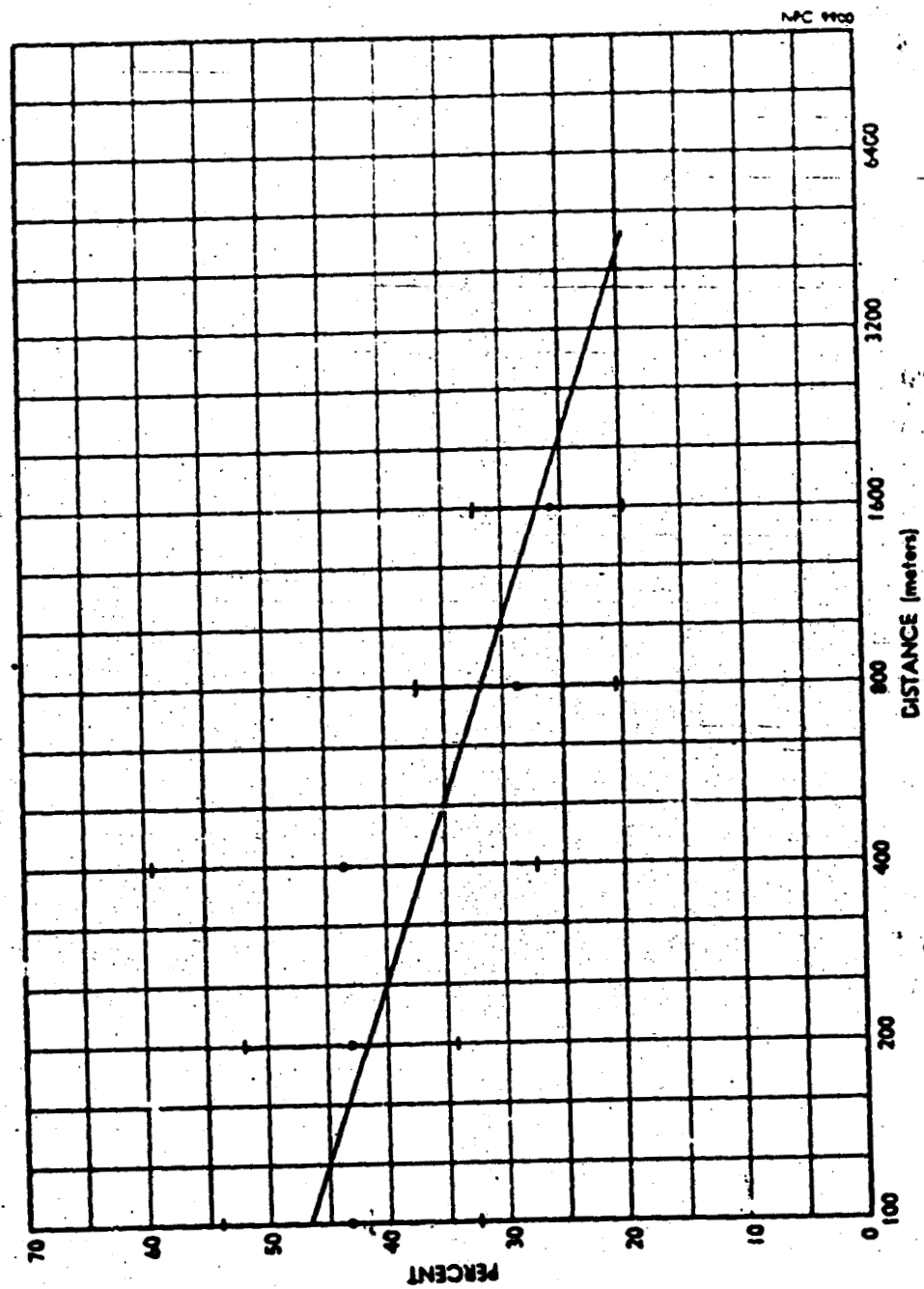


FIGURE 14. IODINE PENETRATING HI-VOL PLEATED FILTER

The percentage of cerium on the carbon cartridge was about one order of magnitude less than iodine, and the percentage for zirconium-niobium, ruthenium and cesium was about two orders of magnitude less than iodine. Unlike iodine these other radionuclides apparently were not influenced by higher concentrations of inert particulates in the atmosphere.

4.2.4 Deposited Radioactivity

Ground contamination decreased with distance similarly to that observed for the air concentration. All deposition data were obtained from sticky paper placed at one-degree intervals on each of the six arcs. The centerline results are normalized and presented as disintegrations per minute per square foot per curie of either Cs^{137} or I^{131} initially in the fuel element. Also, the centerline data were normalized to 1 at the 100-meter arc.

Cesium-137 contamination of sticky paper resulting from lapse Releases D and I and inversion Releases A and C are shown in Figures 15 and 16. Deposition during inversion Release A was more similar to that observed during lapse Releases D and I than inversion Release C. A similar behavior was noted for the air concentrations and this condition was attributed to the transient borderline nature of the inversion existing during Release A.

The ANP predicted curve for deposited cesium activity under lapse conditions is one-half that measured in the field. This difference is caused by the greater cesium release percent and

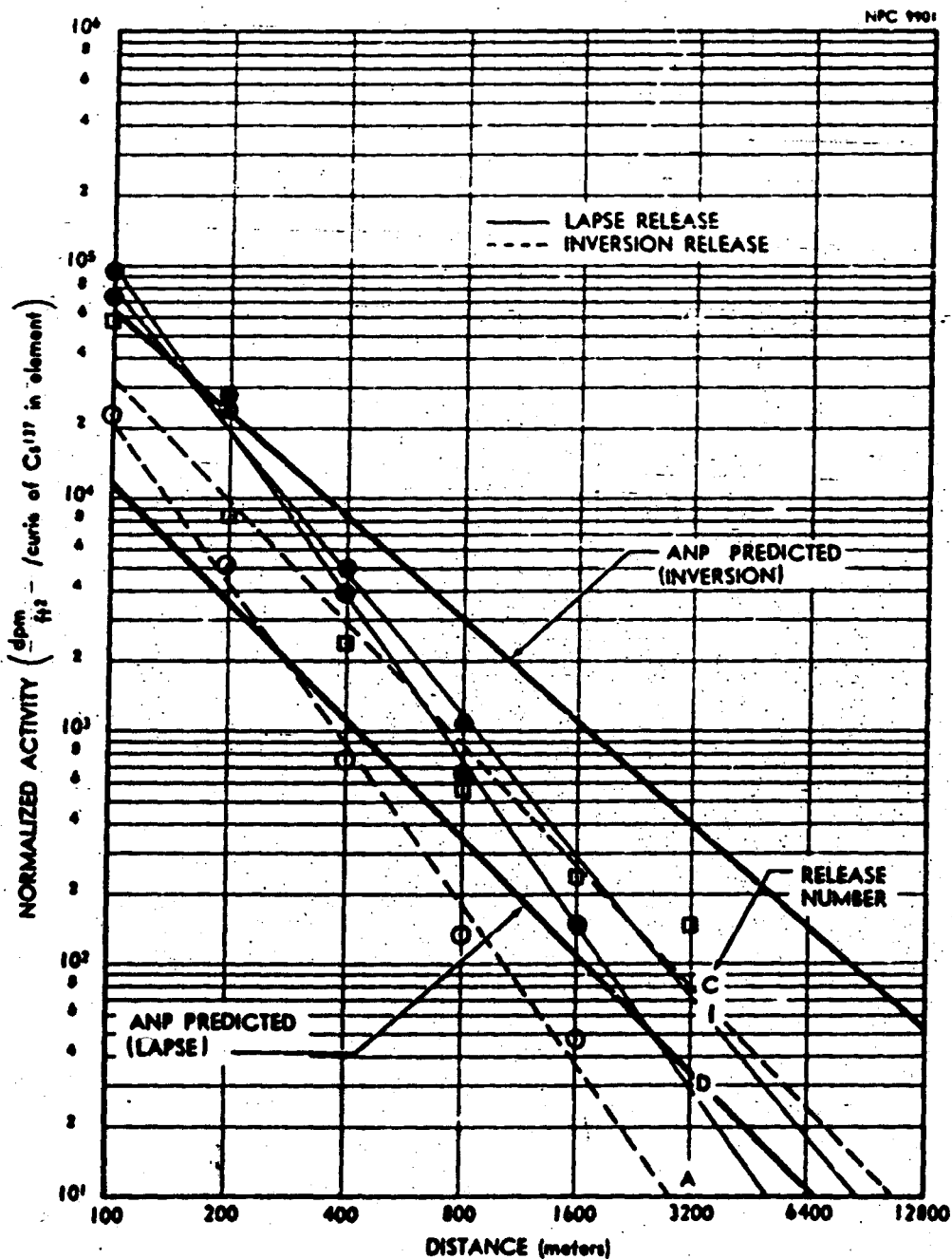


FIGURE 15. CESIUM-137 DEPOSITION ON CLOUD CENTERLINE
(Normalized to Unit Inventory)

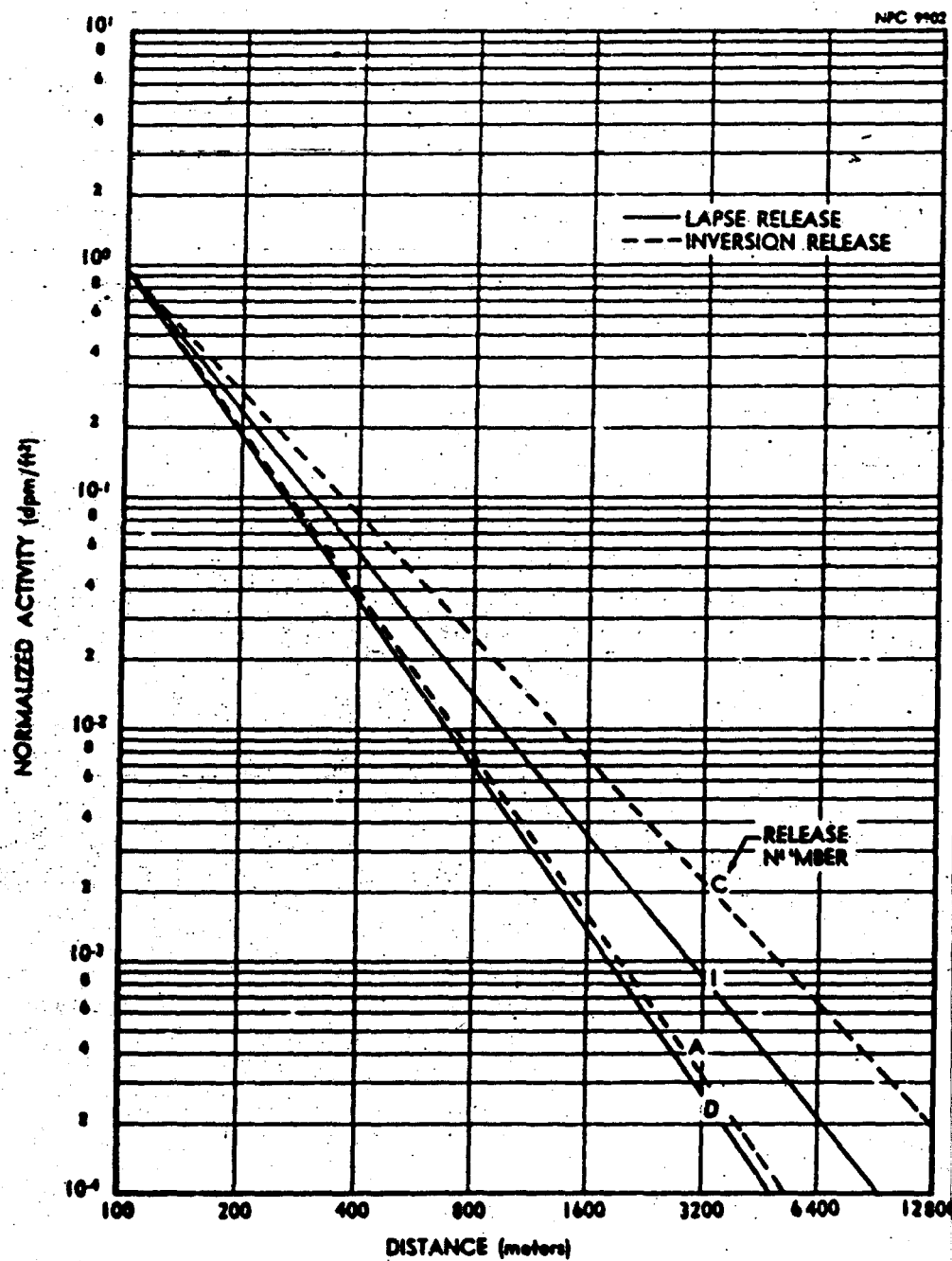


FIGURE 16. CESIUM-137 DEPOSITION ON CLOUD CENTERLINE
(Normalized to 100-Meter Level)

lower deposition velocity measured in FRT-1. However, the ANP predicted curve describing deposition under inversion conditions is larger than the measured deposition by a factor of two. Note that the ANP predicted lapse and inversion ground contamination curves were obtained by multiplying the predicted air concentration curves, Figure 6, by the corresponding settling velocities. In other words, "typical" lapse parameters were very good for predicting air concentrations and ground contamination by one order of magnitude. The over estimation could be compensated for by increasing the "typical" value of C_z by about a factor of ten since better initial vertical diffusion was measured at NRTS.

Similarly, in the case of I^{131} deposition (Figs 17 and 18), the lapse Release F behaved like an inversion release. Iodine-131 air-concentration data (Figs. 8 and 9) showed the same anomaly.

The ground contamination for the lapse condition was overestimated by a factor of two, because the measured deposition velocities were lower by about that factor under the encountered lapse conditions. As a comparison, the predicted iodine ground contamination for the inversion case is higher than that measured. The ANP deposition velocity of 0.25 for iodine is a factor of five smaller than that measured at NRTS. The interrelationships between the iodine ground contamination and airborne activity are similar to the arguments previously presented for cesium; namely,

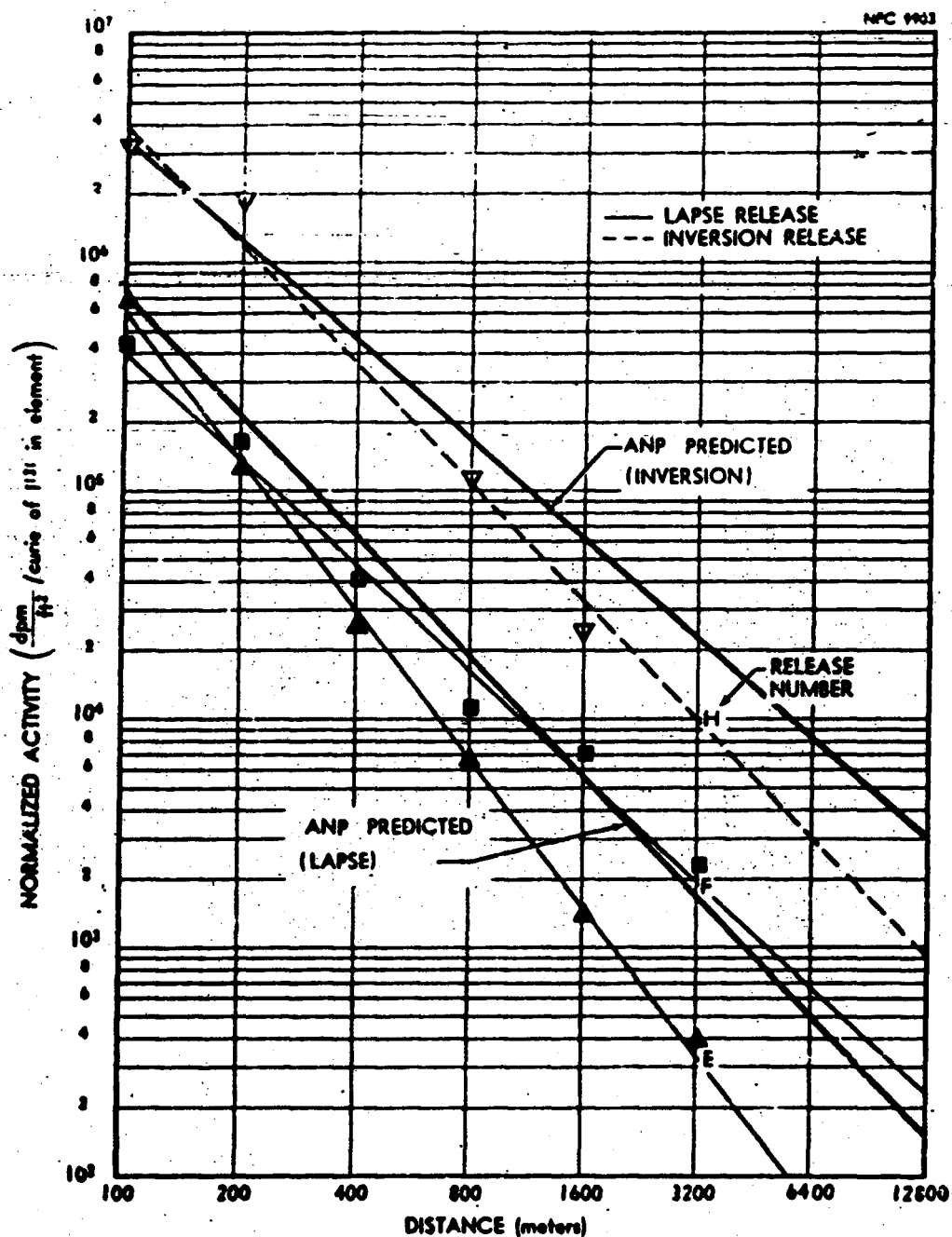


FIGURE 17. IODINE-131 DEPOSITION ON CLOUD CENTERLINE
(Normalized to Unit Inventory)

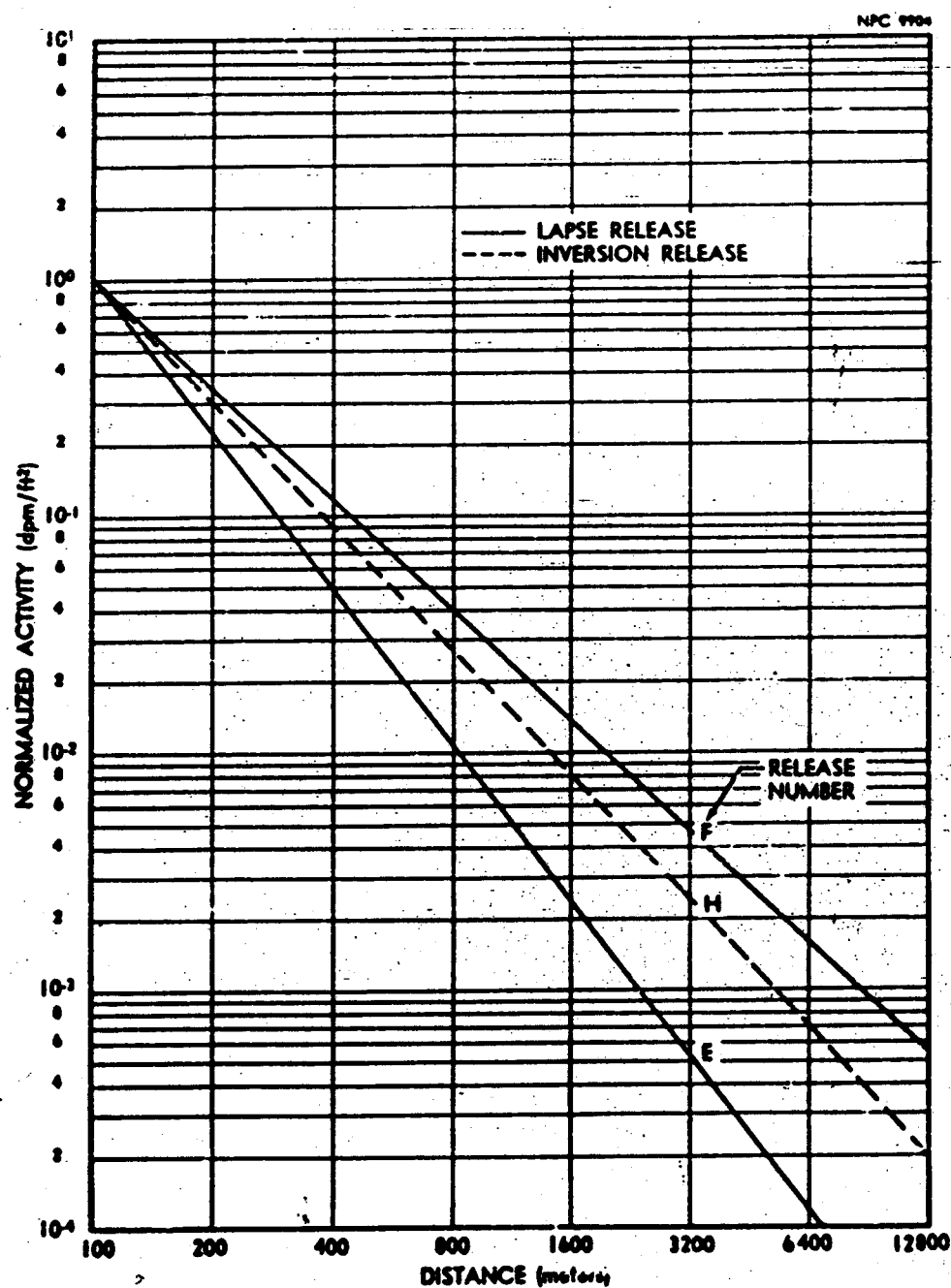


FIGURE 18. IODINE-131 DEPOSITION ON CLOUD CENTERLINE
(Normalized to 100-Meter Level)

the predicted lapse and inversion ground contamination curves were obtained by multiplying the predicted air-concentration curves (Fig. 8) by the corresponding settling velocities.

4.2.5 Deposition Velocity

Deposition velocity V_g (Ref. 6), defined as the ratio of horizontal-surface-deposited activity (curies/sq. meter) to the time integral of air concentration near the surface (curie-seconds/cu. meter), was determined for several nuclides. Average values of V_g obtained from the sticky paper, sand, and water samples for I^{131} , Ru^{103} , Cs^{137} , Zr^{95} - Nb^{95} , and Ce^{141} are shown in Table 13.

TABLE 13
Deposition Velocities

Nuclide	Deposition on Surfaces (cm/sec)		
	Sticky Paper	H ₂ O	Sand
Cs^{137}	0.096 \pm 0.055(38)*	0.088 \pm 0.063(5)	0.041 \pm 0.019(5)
I^{131}	1.1 \pm 0.35(14)	1.6 \pm 0.65(8)	0.74 \pm 0.47
Ru^{103}	2.0 \pm 0.98(11)	2.3 \pm 1.0(9)	0.60 \pm 0.38(9)
Zr^{95} - Nb^{95}	1.4 \pm 0.73(10)	5.7 \pm 3.4(6)	2.9 \pm 2.7(6)
Ce^{141}	0.73 \pm 0.63	--	--

* Number of arc averages from which the average deviation is computed.

The average deposition velocities for sand and water were calculated from ground-level-deposited-activity data reported in Reference 9.

In most cases the amount of radioactivity deposited on water and sticky paper was nearly the same, while that deposited on sand was smaller. Lack of detailed knowledge of the chemical form in which the various nuclides were deposited limits the confidence with which the measured deposition velocities can be extrapolated to other situations. However, it is noted that in general, higher deposition velocities were observed for the sticky paper and water than for the sand.

As a group, the various nuclides exhibited considerable variation in their deposition velocities. Inasmuch as cesium and iodine were found mostly in the submicron particle size range, the large difference between their observed deposition velocities may be attributed to differences in "stickability" or absorptivity rather than to differences in the probability of striking the collecting surface. The ruthenium behaved similarly to the iodine. Zirconium-niobium was apparently affected by the collecting media since sand and water respectively exhibited deposition velocities two and five times that of sticky paper. However, in this case, the difference is not significant because the standard deviations are also very large.

Contrary to the ANP model no differences were noted between lapse and inversion deposition velocities. As shown in Table 14 the average ANP lapse deposition velocities are probably a factor of ten too low, but these are comparisons between sticky paper

deposition velocities and the generalized deposition velocities for surfaces encompassed by the ANP model, presumably grass airfields.

TABLE 14
Comparison of Deposition Velocities
(cm/sec)

Nuclide	ANP Prediction		Experimental*		
	Inv.	Lapse	Inv.	Lapse	Average**
Bone Seekers					
Ce ¹⁴¹	0.1	1.0	0.57	1.2	0.7
Zr ⁹⁵	0.1	1.0	1.7	3.79	1.4
Muscle Seekers					
Cs ¹³⁷	0.1	1.0	0.08	0.104	0.1
Kidney Seekers					
Ru ¹⁰³	0.1	1.0	2.6	1.3	2.0
Thyroid Seekers					
I ¹³¹	0.25	2.5	1.5	0.9	1.1

* Sticky paper

** Weighted average of all measurements

4.2.6 External Dose

The ranges of maximum external doses at the 400-meter arc for FRT-1 were:

Aged	{ 0.0017-0.002 mrem (Lapse)
	{ 0.0004-0.0014 mrem (Inversion)
Green	{ 0.009-0.012 mrem (Lapse)
	{ 0.016-0.024 mrem (Inversion)

These data show that green releases resulted in higher external doses as compared to the aged releases, which was expected. There is, however, insufficient data to compare lapse and inversion cases and to determine which produces the larger doses.

A comparison between external dose and both calculated muscle dose for the aged releases and calculated thyroid dose for the green releases were made (Table 15). Results show that muscle dose from Cs¹³⁷ (aged releases) is 50 to 200 times larger than external dose. The thyroid dose (green releases) is 1100 to 2800 times larger than external dose. Cesium was the predominate isotope in the aged fuel elements while iodine was the most abundant in the green elements. These findings were generally expected.

TABLE 15

External and Internal Dose Comparison

Release	Time After Irradiation	External Dose mrem	Muscle Dose mrem	Thyroid Dose mrem
A-aged	2½ years	0.0014	0.19	--
C-aged	2½ years	0.00037	0.017	--
D-aged	2½ years	0.0017	0.32	--
E-green	43 days	0.012	0.0086	34
F-green	51 days	0.009	0.024	14
G-green	64 days	0.016	0.12	42
H-green	65 days	0.024	0.057	27
I-aged	2½ years	0.0020	0.15	--

An external dose profile for the 400-meter arc, based on average lapse parameters and the measured Cs^{137} release quantity, was determined from existing nomograms (Ref. 14). Figure 19 shows the comparison between the calculated and measured doses for lapse Releases D and I. If the calculated values are used as a basis of prediction, the estimates of external dose will be too large by a factor of two to three.

4.2.7 Fluorescent Tracer

During Releases A and B (aged fuel elements) zinc cadmium sulphide was released for about 10 minutes immediately following fission product release. The release was not made simultaneously because of the uncertainty as to how the fluorescent material might affect the dispersal and deposition of the released fission products. On the basis of these tests, the decision was made to perform Release C simultaneously with a fluorescent tracer release. Since cesium was the only fission product released in a significant quantity, interaction between the fluorescent tracer and cesium fumes or contaminated particles could be observed.

Preliminary data from the Andersen impactors used in Releases A and B indicated a clear particle size differentiation between the tracer and the cesium; that is, the tracer was retained in the upper stages and the cesium was deposited in the lower stages. This proved that if a significant fraction of the cesium should become attached to the tracer particles in a simultaneous

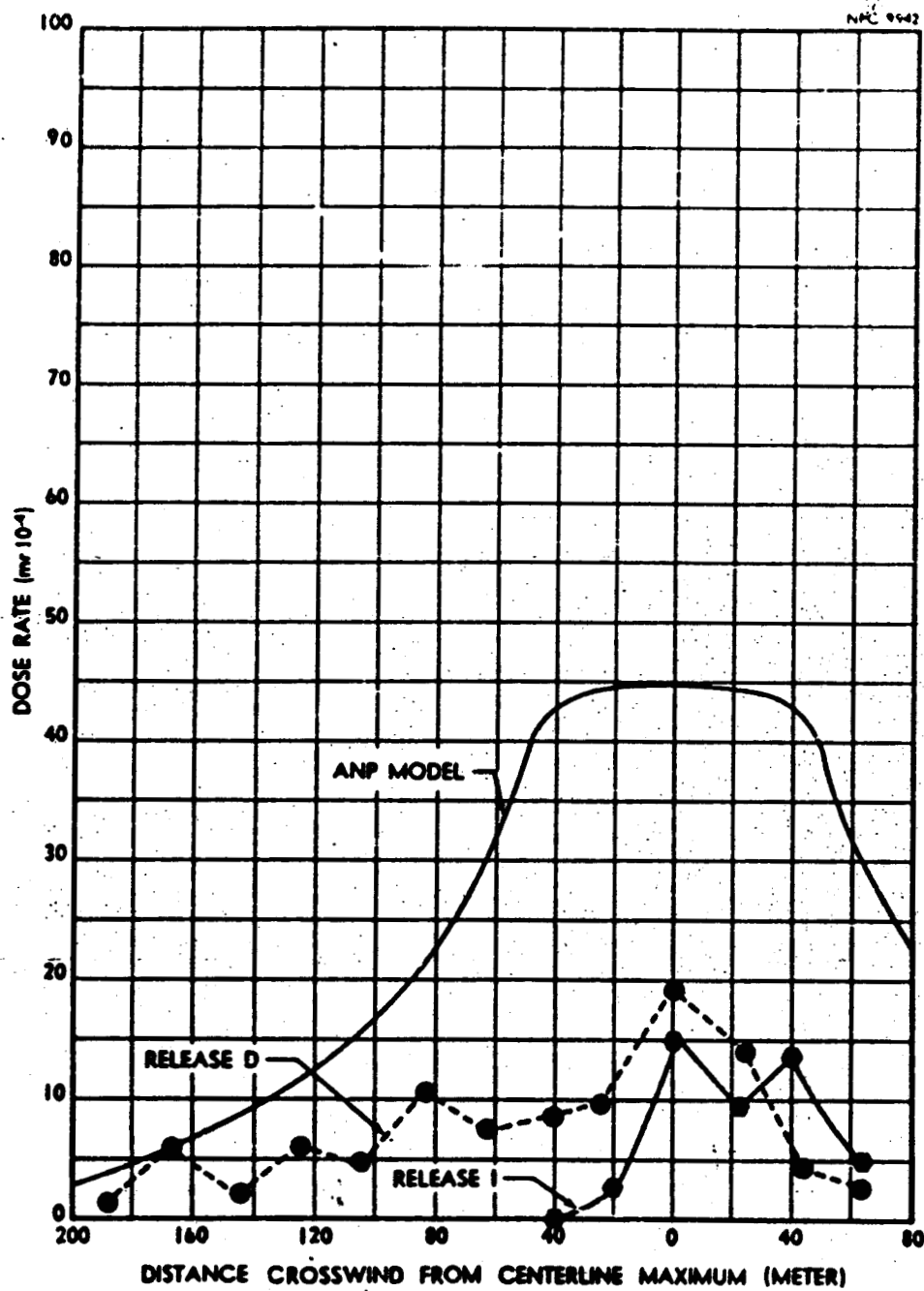


FIGURE 19. EXTERNAL DOSE FOR CESIUM
(Releases D AND I)

release, it could be readily detected. Results of Release C indicated no change in the particle size distribution of the released cesium.

Data adequate for a detailed comparison of fluorescent tracer and fission product dispersal were obtained only during Release C. From these results there appear to be no significant differences between the diffusion characteristics of Cs^{137} and zinc cadmium sulphide. Furthermore, the calculated diffusion parameters indicate that there is no striking difference between the diffusion of gross radioactivity and zinc cadmium sulphide.

4.2.8 Diffusion Parameters

The ability to analytically predict the atmospheric diffusion characteristics of an effluent requires a mathematical model having sufficient "diffusion parameters." These parameters represent the variables of the problem. It is difficult to obtain representative diffusion parameters because they are dependent upon micrometeorological conditions. Lapse rates and vertical variations in wind velocity strongly affect vertical diffusion. Horizontal or vertical velocity components, resulting from spontaneous eddies, affect both horizontal and vertical diffusion. Whenever meteorological conditions change, new diffusion parameters must be used to predict atmospheric mixing. The problem of using one set of parameters for long range diffusion cases is burdened by the natural tendency of meteorological conditions to vary with time.

Many attempts have been made to provide a means for obtaining realistic diffusion parameters. Some are theoretical while others are empirical. Of these, Sutton's formulas are the best known for calculating parameters from micrometeorological data. Sutton's formulas describe the diffusion of a plume from a continuous point source in terms of two diffusion coefficients, C_y (horizontal) and C_z (vertical), and a stability parameter "n".

An empirical set of Sutton-type "typical" lapse and inversion parameters have been suggested as a result of a study by staff members of the Brookhaven National Laboratory and others (Ref. 12). Their findings have strongly influenced the ANP safety analysis studies and their "typical" parameters are herein referred to as the "ANP parameters" (Table 16).

TABLE 16
"Typical" ANP Atmospheric Diffusion Parameters

Parameter	Lapse	Inversion
n	0.25	0.55
C_y	0.40	0.40
C_z	0.40	0.05
\bar{u}	5.0 m/sec	3.0 m/sec
h	0 m	0 m

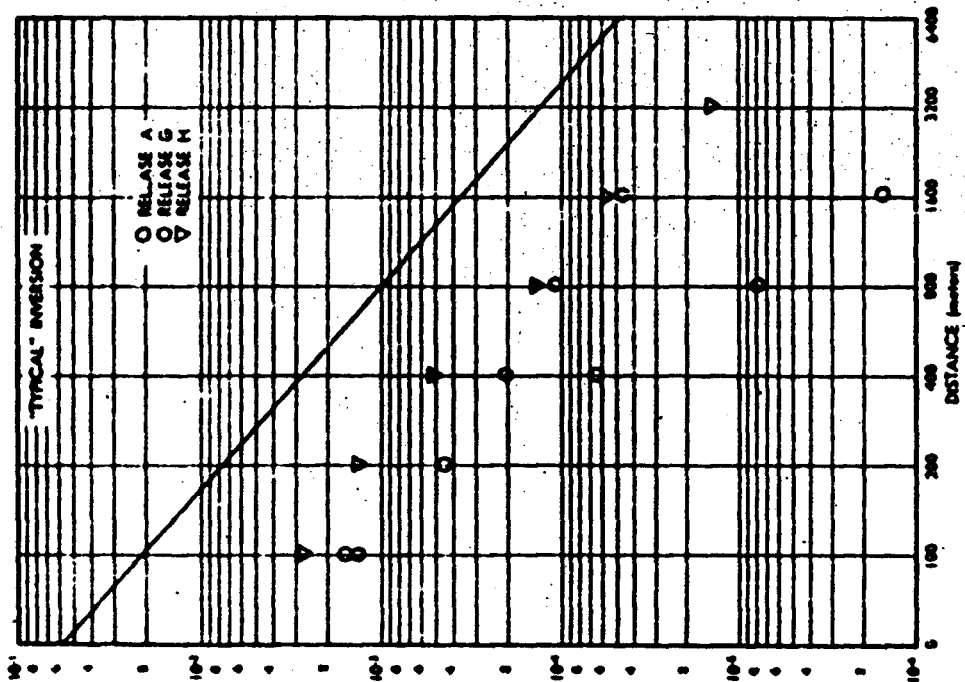
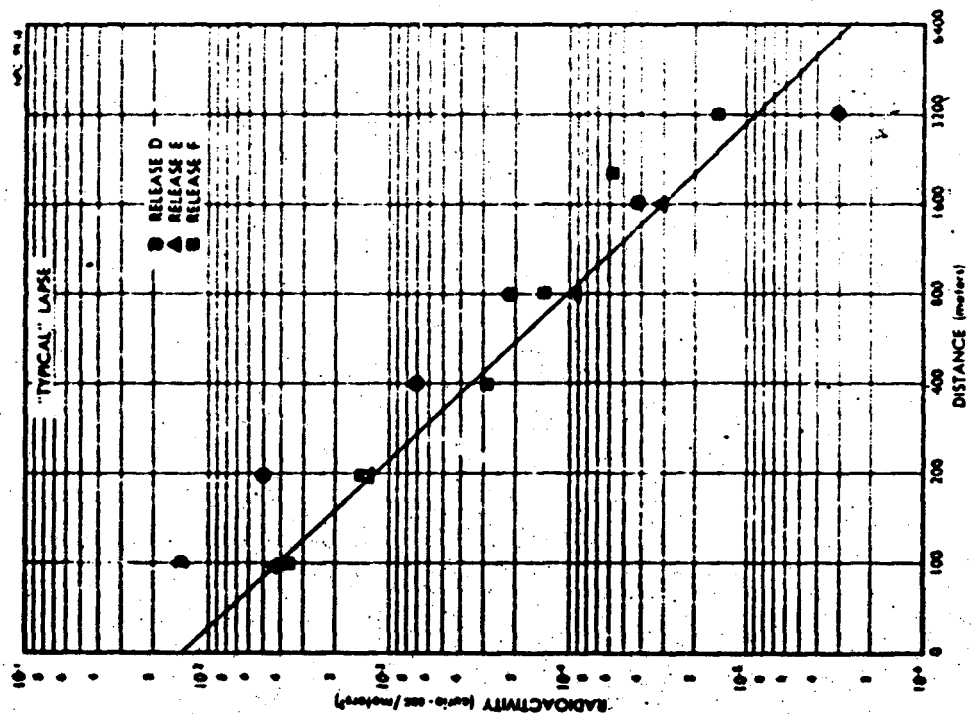


FIGURE 22. AIRBORNE CESIUM ACTIVITY (Comparison with Predictions)

The higher predicted concentrations are due primarily to the larger measured values of C_z as compared to the "typical" value. The more rapid dispersal indicated in Figures 22 and 23 is caused by the parameters $M_y + M_z)^{\frac{2-n}{2}}$. Comparing the values of parameters obtained by fitting the cloud concentration data with those parameters derived from the meteorological measurements reveals several tendencies. These are:

<u>Parameter</u>	<u>Observation</u>
C_y (Horizontal Diffusion)	<ul style="list-style-type: none"> . Shows a tendency to increase with wind velocity . Increases when the bi-vane value of σ_y increases (the crosswind standard deviation of the horizontal velocity components.)
C_z (Vertical Diffusion)	<ul style="list-style-type: none"> . Was larger for the inversion releases and occurred with larger values of "n" than for the lapse releases.
M_y (Horizontal Stability)	<ul style="list-style-type: none"> . Smaller for lapse than for inversion releases . Larger at lower wind velocities
M_z (Vertical Stability)	<ul style="list-style-type: none"> . Lapse values generally higher than are inversion values . Shows a tendency to increase with humidity and temperature . Tends to increase as the bi-vane value of σ_z increases . Tends to decrease as "n" increases

At present these observations lack statistical weight. As more data become available these trends may become more definitive. Calculated parameters may be obtained from experimental results

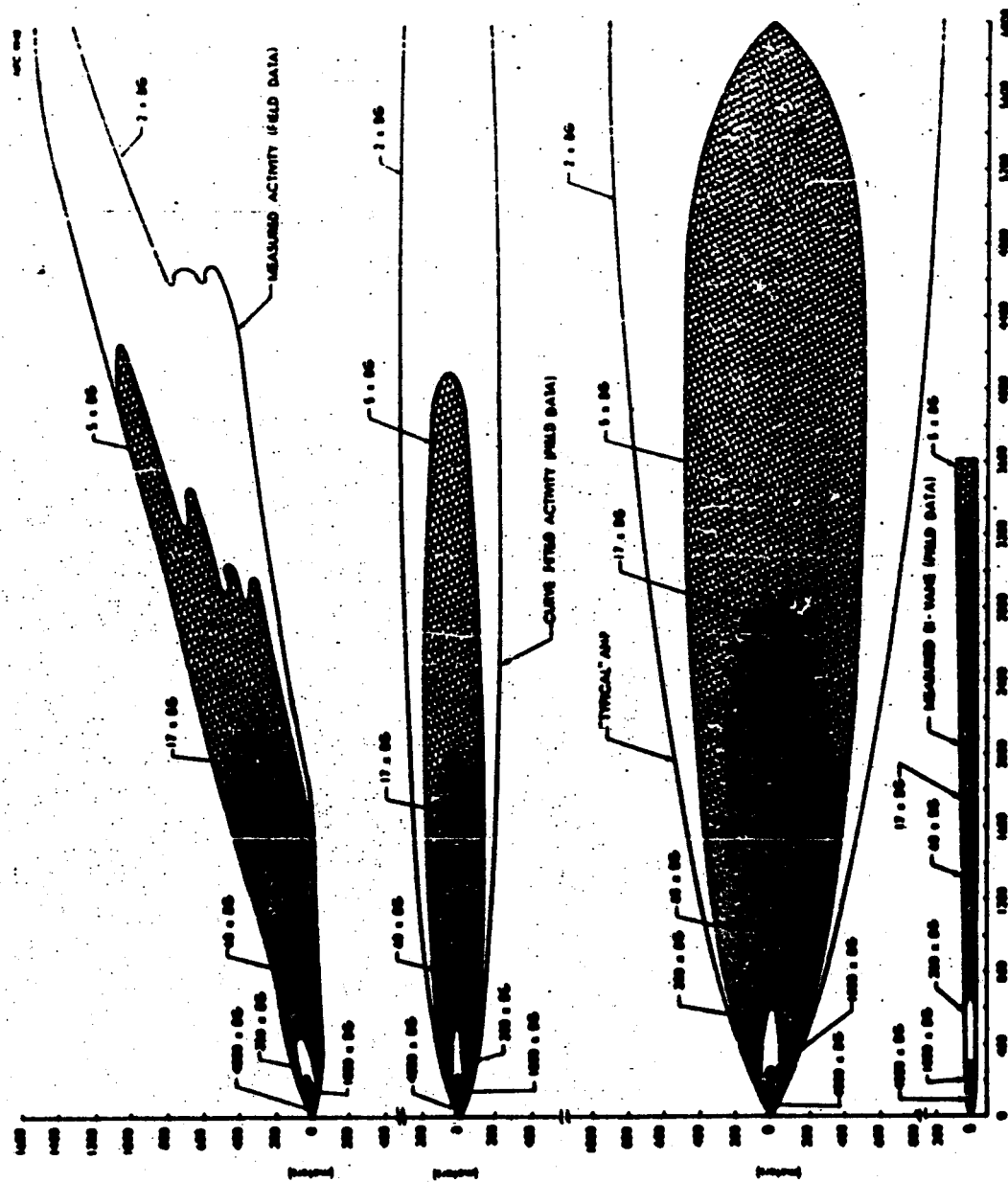
Table 17 summarizes some of the diffusion parameter values, and simultaneous meteorological conditions existing during each release. The techniques used for calculating these parameters may be found in Appendix H. A variety of methods were used to evaluate the parameters including smoke plume photography, fluorescent tracers, gross activity on Hi-Vol air sampler pleated filters, and isotopic radioactivity on pleated filters. Also, a bi-vane, 24 meters above ground on the apex tower, provided data for determination of C_y , C_z , and mean wind deviations in the vertical and horizontal crosswind directions. For comparison purposes the tower wind speed data were used to calculate the stability parameter "n", using the windspeed profile power law. The gross beta-gamma parameters (pleated filter field data) may be considered valid for a continuous release of about ten-minute duration while the isotopic parameters for Cs^{137} , I^{131} , and Ru^{103} are for the component releases of about two-minute duration. The variations in the isotopic parameters for a given release are probably caused by changes in meteorological conditions.

Representative isopleths, normalized to the same centerline value at 100 meters, compare the actual diffusion pattern with that predicted from ANP parameters and that calculated from bi-vane results (Sutton's equations). These are shown in Figures 20 and 21. The "typical" parameters are better than the bi-vane calculated parameters for predicting dispersal of the effluent.

TABLE 17
Summary of Diffusion Parameters and Meteorological Conditions

Item		Release Number										Units	Comments
		A	B	C	D	E	F	G	H	I			
Temperature Pressure Humidity Mean Wind Velocity Lapse Rate (1.5 - 45 m) Lapse Rate (1.5 - 24 m)	M	29	25	27.2	34.6	30.8	22.2	17.5	19.7	20.2	OC	Meteorological Data	
	M	24.99	25.09	25.005	24.97	24.92	25.04	24.94	25.00	25.35	" Hg		
	M	18.5	21.6	12.5	17	12	23	36	22	24	Percent		
	M	-0.37	-2.6	-1.5	0.34	0.6	2.3	4.3	4.0	2.0	m/sec		
	M	-0.05	-2.38	-1.08	0.57	0.51	0.18	-1.0	-1.4	0.32	OC/43.5m		
Bi-vane Mean Dev. Bi-vane Mean Dev. Velocity Power Law Bi-vane Bi-vane	M	9.9	0.308	6.6	1.9	8.6	4.4	4.5	4.6	18	Degrees	Bi-vane at 24 Meters on MFM Meteorological Tower	
	M	4.1	0.679	3.2	2.2	2.2	0.32	2.8	3.0	12	Degrees		
	M	0.26	0.45	0.39	0.28	0.29	0.32	0.37	0.39	0.23			
	M	0.11	0.01	0.05	0.09	0.07	0.04	0.04	0.03	0.15			
	M	0.05	0.02	0.03	0.03	0.07	0.04	0.03	0.03	0.11			
Continuous Plume Photography	M			1.2		1.3			1.0			From Aerial and Ground Photos of Continuous Plume	
	M			0.03		0.02			1.0				
Fluorescent Tracer Pit	M								1.6			Simultaneous Release	
	M			0.85					0.78				
Gross Gamma-Rate Pile Filter Data	M	1.0		0.84	0.68	0.66	0.70	0.57	0.78			Staplex Sampler	
	M	1.7		0.44	1.6	1.4	1.3	0.79	0.64				
Cal37 Pile Filter Pit	M	0.08		0.22	0.61	0.138	0.18	0.22	0.28				
	M	0.02							0.23				
Cal37 Pile Filter Pit	M	0.90		0.76	0.73	0.58	0.50	0.82	0.61				
	M	1.5		0.28	1.6	1.2	1.1	0.53	0.66				
Cal37 Pile Filter Pit	M	0.08		0.37	0.40	1.6	3.0	3.16	0.90				
	M	0.02		50.6	0.007	0.06	0.108	3.5	0.3				
Cal37 Pile Filter Pit	M								0.65				
	M								0.80				
Cal37 Pile Filter Pit	M								0.32				
	M								0.21				
Cal37 Pile Filter Pit	M					0.62	0.57	0.81	0.67				
	M					1.2	1.2	0.53	0.86				
Cal37 Pile Filter Pit	M					1.3	1.9	0.20	0.79				
	M					0.05	0.079	1.0	0.10				

o Based on vertical wire profile (1) meters downwind from the furnace)



is a very early introduction to the subject of the
 book of the world's history

Furthermore, the "typical" ANP parameters fit the crosswind profiles better than the bi-vane parameters. Because of this better fit, the "typical" parameters were further investigated.

Figures 22 and 23 show predicted air-centerline concentrations of iodine and cesium for the lapse and inversion conditions and those air concentrations as measured in the field. The centerline-concentrations were all normalized to the same source strength. The measured centerlines were based on parameters obtained from the diffusion of Cs^{137} and I^{131} . In this comparison the "typical" lapse parameters have proved to be quite good in predicting the measured air concentrations within a factor of two out to 3200 meters. The "typical" inversion ANP parameters were consistently high by about an order of magnitude in predicting downwind air concentrations out to 3200 meters.

Sutton's method of determining values of C_y , C_z , and "n" from meteorological measurements proved unsatisfactory for calculating FRT-1 airborne radioactivity concentration levels. There is the limitation that Sutton's solution of the diffusion equation contains only the single stability parameter "n." Therefore, it cannot be used to describe adequately an anisotropically diffusing cloud. To compensate for the inadequacy of the parameter "n" two parameters, M_y and M_z , were introduced. The general equation defining the various parameters M_y , M_z , C_y , C_z , and "n" are derived in Appendix II.

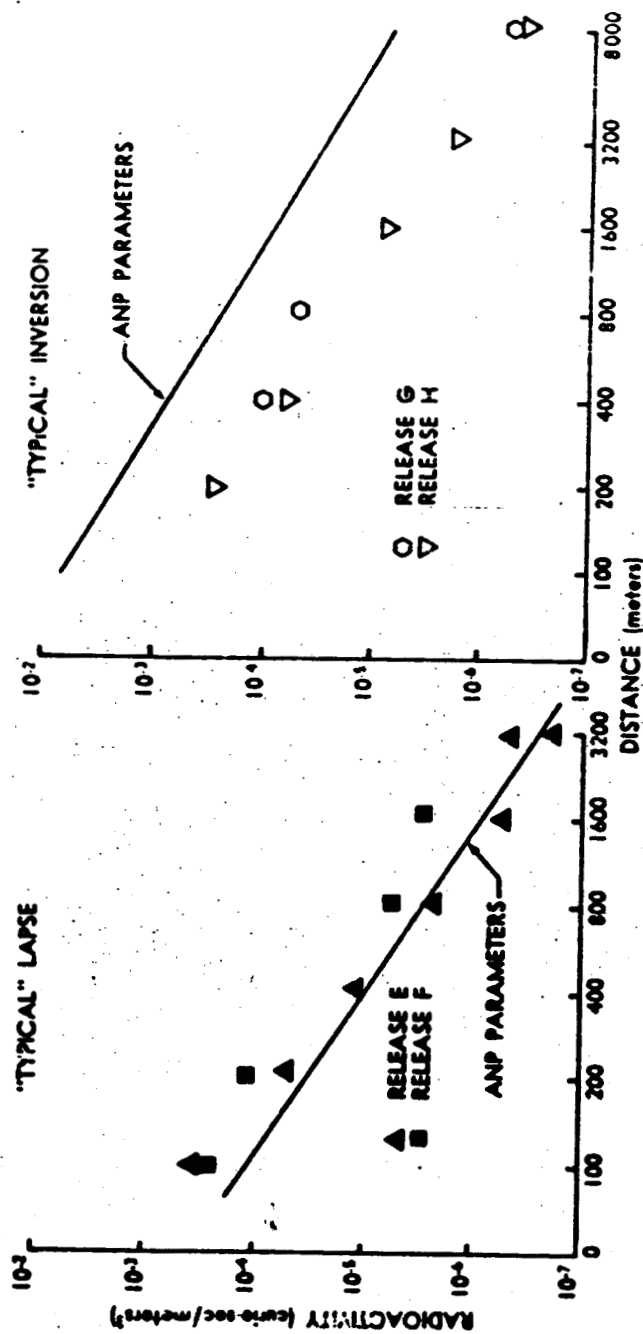


FIGURE 22. AIRBORNE IODINE ACTIVITY (Comparison with Predictions)

that are presented in the literature (Ref. 13) or from future release tests. These may be used to add statistical weight to the general observations. The collection of more information will provide data for:

- . the determination of the dependence of realistic parameters upon basic meteorological measurements
- . an empirical relationship between diffusion parameters and basic meteorological measurements.

4.2.9 Radiobiology

Rats and dogs were exposed to the radioactive cloud under controlled conditions and were sacrificed after the releases to provide data on the fraction of inhaled aerosol deposited in the lung and both lower respiratory tract and upper respiratory tract. The data are summarized in Table 18. Limited data were also obtained on the rates of removal of radioactive particulates from the lung and on the translocation of radioisotopes within the body. During the course of the tests, several of the animal exposure techniques were varied and the effects noted for use in interpretation of these tests and for design of future experiments.

There was a relatively large amount of iodine, as compared to other nuclides, in the stomachs of dogs that were sacrificed within an hour after Releases F, G, and H. This amount of iodine in the gastrointestinal tract was probably caused by temporary entrapment of iodine in the upper respiratory system followed by swallowing.

The lungs were relatively void of iodine as compared to other nuclides, in the stomachs of dogs that were sacrificed within an hour after Releases F, G, and H. This amount of iodine in the gastrointestinal tract was probably caused by temporary entrapment of iodine in the upper respiratory system followed by swallowing.

The lungs were relatively void of iodine as compared with other isotopes, indicating a rapid iodine removal rate. The blood contained about 10% of the total body burden of iodine at the end of an hour. Of the total amount of iodine in the blood about 4% was assimilated by the thyroid.

There was no indication that cesium was localized appreciably in the muscle under the conditions of the tests.

Median LRD (lower respiratory tract deposition) values for rats and dogs were 30 and 35%, respectively, of the total inhaled activity as calculated from the measured air concentrations. These values are somewhat larger than the NBS-HB-52 value of 25%. However, the difference is probably not significant because the breathing rates were not individually measured. A single estimated breathing rate was used for all animals of a given species.

Gastrointestinal (GI) tract and total body internal (TBI) values were used to infer upper respiratory tract deposition (URD). However, the TBI data from Releases D, E, and F were

invalidated as estimates of URD plus LRD because the animals, not being restrained from licking themselves, ingested large amounts of activity in addition to that inhaled. In Releases G, H, and I the animals were restrained and the TBI values were fairly close to the NES-HB-52 value of 75% for URD plus LRD.

TABLE 18

Median Lower Respiratory Tract and "Total Body" Deposition Values

Release	Animal	Number of Animal	Lower Respiratory Deposition (%)		"Total Body"* Internal Disposition (%)	
			Median	Range	Median	Range
D-aged	rat	38	18	8-142		
E-green	rat	54	39	13- 77		
E-green	rat	32				
F-green	rat	20	22	16- 67		
F-green	dog	4	26	18- 36		
G-green	rat	30	45	21-126		
G-green	rat	24			67	28-183
G-green	dog	5	58	40- 88		
H-green	rat	12	28	16- 55	86	64-210
H-green	dog	9	35	11- 99		
I-aged	rat	16	37	17- 38	64	31- 99
I-aged	dog	12	24	8-192		

* The term "Total Body Internal Deposition" represents the summation of fission product concentrations of only those tissues which were analyzed (Ref. 11).

APPENDICES

TABLE OF CONTENTS

(APPENDICES)

<u>Topic</u>	<u>Page</u>
List of Figures	103
List of Tables	109
A. Fuel Element Inventories	113
B. Fuel Element Melting Equipment	117
Induction Furnace	117
Power Supply	122
Effluent Sampling	123
Temperature Measurement	127
Furnace Operation	128
Sampling Flask Adjustments	129
C. Power Distribution System	131
D. Meteorological Measurements	135
Wind Velocity	135
Wind Direction	137
Air Temperature (Dynamic)	138
E. Release Height Determination	139
Equipment	139
Operational Procedure	139
F. Smoke Plume Generation and Data Analysis	143
Equipment	143
Procedure	145
Diffusion Parameters	146
G. Fluorescent Tracer Dispersal and Data Analyses	149
Equipment	149
Data Analyses	149

TABLE OF CONTENTS (Con't)
(APPENDICES)

<u>Topic</u>	<u>Page</u>
H. Airborne Activity Determinations and Data Analyses	153
Equipment	153
Atmospheric Diffusion Parameter Evaluation	157
Activity Diffusion Parameter Evaluation	168
I. Particle Size Measurements	173
Equipment	173
Field Calibration of Flow Rate	176
Laboratory Calibration of Sampler	177
J. Deposition Velocity Determinations	189
Equipment	189
Sticky Paper Analyses	191
Sand and Water Analyses	191
Results	192
K. External Dose Measurements	199
Equipment	199
Calibration	199
Procedure	204
Data Handling	205
L. Radiochemical and Counting Techniques	207
Furnace Effluent Analyses	207
Network Sample Analyses	212
Counting Procedure	213
Spectral Analyses	216
Residue Analyses	228
M. Radiobiology	231
Facilities	231
Procedure	231
Studies Performed	233

TABLE OF CONTENTS (Con't)
(APPENDICES)

<u>Topic</u>	<u>Page</u>
N. Individual Release Data	236
Release A	237
Release B	262
Release C	277
Release D	305
Release E	330
Release F	365
Release G	402
Release H	430
Release I	459

LIST OF FIGURES

(APPENDICES)

<u>No.</u>	<u>Title</u>	<u>Page</u>
B.1	Induction Furnace Assembly	118
B.2	Graphite Crucible	120
B.3	Furnace - Top View	121
B.4	Furnace Assembly	124
B.5	Effluent Sampler - S-Bend (Releases A-E)	125
B.6	Effluent Sampler - Steel Bottle (Releases F-I)	126
D.1	Meteorological Instrument Locations	130
E.1	Charged Wire Collector (Release I)	140
F.1	Location of Ground Cameras	144
H.1	Hi-Vol Air Sampler	154
H.2	Hi-Vol Air Sampler - Assembled	155
I.1	Dismantled Andersen Sampler	174
I.2	Andersen Sampler Assembly	175
J.1	Sticky-Paper Fallout Traps	190
K.1	Portable Scintillation Detector and Recorder	200
K.2	Dosimeter Calibration Curves	202
L.1	Compton Build-up in Cesium Spectrum	222
L.2	Photopeak and Zero Energy Positions	224

Release A

N.A.1	Lapse Rate During Release	239
N.A.2	Pre-Release Smoke Plume	241
N.A.3	Furnace Temperature Profile	243
N.A.4	Sequential-Effluent-Sampler Filter Radioactivities	244
N.A.5	Pre- and Post-Melt Gamma Spectra of Fuel Element	246
N.A.6	Hi-Vol Air Sampler Field Survey (Arc Profiles)	247
N.A.7	Hi-Vol Air Field Survey (Centerline)	248
N.A.8	Hi-Vol Air Sampler Laboratory Assay of Cesium Arc Profiles)	249
N.A.9	Hi-Vol Air Sampler Laboratory Assay of Cesium (Centerline)	251

LIST OF FIGURES (Con't)

(APPENDICES)

<u>No.</u>	<u>Title</u>	<u>Page</u>
N.A.10	Deposited Cesium (Arc Profiles)	252
N.A.11	Deposited Cesium (Centerline)	253
N.A.12	Gamma Dose from Cloud Passage (Arc Profile)	255
N.A.13	Gamma Dose Rate from Cloud Passage (Centerline)	255
N.A.14	Gamma Dose Rate from Cloud Passage (Activity Contours)	256
N.A.15	Gross Radioactivity Isopleth (Field Data)	257
N.A.16	Gross Radioactivity Isopleth (Curve Fit)	257
N.A.17	Contamination of Exposed Rabbits	259
N.A.18	Contamination of Water Samples	261
<u>Release B</u>		
N.B.1	Lapse Rate During Release	265
N.B.2	Furnace Temperature Profile	266
N.B.3	Sequential-Effluent-Sampler Filter Radioactivities	268
N.B.4	Pre- and Post-Melt Gamma Spectra of Fuel Element	269
N.B.5	H1-Vol Air Sampler Field Survey (Arc Profiles)	270
N.B.6	H1-Vol Air Sampler Laboratory Assay of Cesium (Arc Profiles)	271
N.B.7	Deposited Cesium (Arc Profiles)	273
N.B.8	Contamination of Exposed Rabbits	276
<u>Release C</u>		
N.C.1	Lapse Rate During Release	279
N.C.2	Pre-Release Smoke Plume	281
N.C.3	Sequential-Effluent-Sampler Filter Radioactivities	283
N.C.4	Pre- and Post-Melt Gamma Spectra of Fuel Element	284
N.C.5	H1-Vol Air Sampler Field Survey (Arc Profiles)	286
N.C.6	H1-Vol Air Sampler Field Survey (Centerline)	287
N.C.7	H1-Vol Air Sampler Laboratory Assay of Cesium (Arc Profiles)	288
N.C.8	H1-Vol Air Sampler Laboratory Assay of Cesium (Centerline)	289
N.C.9	Deposited Cesium (Arc Profiles)	290
N.C.10	Deposited Cesium (Centerline)	291
N.C.11	Fluorescent Tracer (Arc Profiles)	294
N.C.12	Fluorescent Tracer (Centerline)	295
N.C.13	Gamma Dose from Cloud Passage (Arc Profile)	297
N.C.14	Gamma Dose from Cloud Passage (Centerline)	297
N.C.15	Gamma Dose Rate from Cloud Passage (Activity Contours)	298
N.C.16	Rat Whole-Body Exposure (Arc Profiles)	301
N.C.17	Rat Tissue Exposure	302

LIST OF FIGURES (Con't)

(APPENDICES)

<u>No.</u>	<u>Title</u>	<u>Page</u>
<u>Release D</u>		
N.D.1	Lapse Rate During Release	307
N.D.2	Sequential-Effluent-Sampler Filter Radioactivities	310
N.D.3	Pre- and Post-Melt Gamma Spectra of Fuel Element	311
N.D.4	Hi-Vol Air Sampler Field Survey (Arc Profiles)	313
N.D.5	Hi-Vol Air Sampler Field Survey (Centerline)	314
N.D.6	Hi-Vol Air Sampler Laboratory Assay of Cesium (Arc Profiles)	315
N.D.7	Hi-Vol Air Sampler Laboratory Assays of Cesium (Centerline)	316
N.D.8	Hi-Vol Air Sampler Laboratory Assay of Strontium (Centerline)	317
N.D.9	Deposited Cesium (Arc Profiles)	318
N.D.10	Deposited Cesium (Centerline)	319
N.D.11	Gamma Dose from Cloud Passage (Arc Profile)	322
N.D.12	Gamma Dose Rate from Cloud Passage (Centerline)	322
N.D.13	Gamma Dose Rate from Cloud Passage (Activity Contours)	323
N.D.14	Gross Radioactivity Isopleth (Field Data)	324
N.D.15	Gross Radioactivity Isopleth (Curve Fit)	324
N.D.16	Rat Whole-Body Exposure	326
N.D.17	Rat Tissue Exposure (Non-Restrictive Cages)	327
N.D.18	Rat Tissue Exposure (Restrictive Cages)	328
N.D.19	Contamination of Water Samples	329
<u>Release E</u>		
N.E.1	Lapse Rate During Release	332
N.E.2	Pre-Release Smoke Plume	335
N.E.3	Sequential-Effluent-Sampler Filter Radioactivities	336
N.E.4	Hi-Vol Air Sampler Field Survey (Pleated Filter-Arc Profiles)	339
N.E.5	Hi-Vol Air Sampler Field Survey (Carbon Cartridge-Arc Profiles)	340
N.E.6	Hi-Vol Air Sampler Field Survey (Centerline)	341
N.E.7	Hi-Vol Air Sampler Laboratory Assay (Centerline)	343
N.E.8	Hi-Vol Air Sampler Laboratory Assay of Ruthenium (Arc Profiles)	344
N.E.9	Hi-Vol Air Sampler Laboratory Assay of Cesium (Arc Profiles)	345

LIST OF FIGURES (Con't)

(APPENDICES)

<u>No.</u>	<u>Title</u>	<u>Page</u>
N.E.10	Hi-Vol Air Sampler Laboratory Assay of Zirconium (Arc Profiles)	346
N.E.11	Hi-Vol Air Sampler Laboratory Assay of Cerium (Arc Profiles)	347
N.E.12	Hi-Vol Air Sampler Laboratory Assay of Iodine (Arc Profiles)	348
N.E.13	Deposited Iodine (Arc Profiles)	349
N.E.14	Deposited Iodine (Centerline)	350
N.E.15	Gamma Dose from Cloud Passage (Arc Profile)	354
N.E.16	Gamma Dose Rate from Cloud Passage (Centerline)	354
N.E.17	Gamma Dose Rate from Cloud Passage (Activity Contours)	355
N.E.18	Gross Radioactivity Isopleth (Field Data)	358
N.E.19	Gross Radioactivity Isopleth (Curve Fit)	358
N.E.20	Contamination of Water Samples	359
N.E.21	Rat Whole-Body Exposure	361

Release F

N.F.1	Lapse Rate During Release	369
N.F.2	Furnace Temperature Profile	370
N.F.3	Sequential-Effluent-Sampler-Filter Radioactivities	372
N.F.4	Hi-Vol Air Sampler Field Survey (Pleated Filter-Arc Profiles)	374
N.F.5	Hi-Vol Air Sampler Field Survey (Carbon Cartridge-Arc Profiles)	375
N.F.6	Hi-Vol Air Sampler Field Survey (Centerline)	376
N.F.7	Hi-Vol Air Sampler Laboratory Assay (Centerline)	377
N.F.8	Hi-Vol Air Sampler Laboratory Assay of Iodine (Arc Profiles-Pleated Filter Plus Carbon Cartridge)	378
N.F.9	Hi-Vol Air Sampler Laboratory Assay of Cesium (Arc Profiles)	379
N.F.10	Hi-Vol Air Sampler Laboratory Assay of Ruthenium (Arc Profiles)	380
N.F.11	Deposited Iodine (Arc Profiles)	381
N.F.12	Deposited Iodine (Centerline)	382
N.F.13	Iodine Deposition Velocity	384
N.F.14	Gamma Dose from Cloud Passage (Arc Profile)	387
N.F.15	Gamma Dose Rate from Cloud Passage (Centerline)	387
N.F.16	Gamma Dose Rate from Cloud Passage (Activity Contours)	388
N.F.17	Gross Radioactivity Isopleth (Field Data)	389

LIST OF FIGURES (Con't)

(APPENDICES)

<u>No</u>	<u>Title</u>	<u>Page</u>
N.F.18	Gross Radioactivity Isopleth (Curve Fit)	389
N.F.19	Contamination of Water Samples	391
N.F.20	Contamination of Sand Samples	392
N.F.21	Rat Whole-Body Exposure	394
N.F.22	Rat Tissue Exposure	398
N.F.23	Dog Tissue Exposure	400
 <u>Release G</u>		
N.G.1	Lapse Rate During Release	405
N.G.2	H1-Vol Air Sampler Field Survey (Pleated Filter-Arc Profiles)	408
N.G.3	H1-Vol Air Sampler Field Survey (Carbon Cartridges-Arc Profiles)	409
N.G.4	H1-Vol Air Sampler Field Survey (Centerline)	410
N.G.5	H1-Vol Air Sampler Laboratory Assay (Centerline)	411
N.G.6	H1-Vol Air Sampler Laboratory Assay of Iodine (Arc Profiles)	412
N.G.7	H1-Vol Air Sampler Laboratory Assay of Cesium (Arc Profiles)	413
N.G.8	H1-Vol Air Sampler Laboratory Assay of Ruthenium (Arc Profiles)	414
N.G.9	H1-Vol Air Sampler Laboratory Assay of Zirconium (Arc Profiles)	415
N.G.10	H1-Vol Air Sampler Laboratory Assay of Cerium (Arc Profiles)	416
N.G.11	Gamma Dose from Cloud Passage (Arc Profile)	418
N.G.12	Gamma Dose Rate from Cloud Passage (Centerline)	418
N.G.13	Gamma Dose Rate from Cloud Passage (Activity Contours)	419
N.G.14	Gross Radioactivity Isopleth (Field Data)	420
N.G.15	Gross Radioactivity Isopleth (Curve Fit)	420
N.G.16	Rat Whole-Body Exposure	423
 <u>Release H</u>		
N.H.1	Lapse Rate During Release	433
N.H.2	Pre-Release Smoke Plume	435
N.H.3	Sequential-Effluent-Sampler Filter Radioactivities	437
N.H.4	H1-Vol Air Sampler Field Survey (Pleated Filter-Arc Profiles)	439

LIST OF FIGURES (Cont)

(APPENDICES)

<u>No.</u>	<u>Title</u>	<u>Page</u>
N.H.5	H1-Vol Air Sampler Field Survey (Carbon Cartridge-Arc Profiles)	440
N.H.6	H1-Vol Air Sampler Field Survey (Centerline)	441
N.H.7	H1-Vol Air Sampler Laboratory Assay (Centerline)	442
N.H.8	H1-Vol Air Sampler Laboratory Assay of Iodine (Arc Profiles)	443
N.H.9	H1-Vol Air Sampler Laboratory Assay of Cesium (Arc Profiles)	444
N.H.10	H1-Vol Air Sampler Laboratory Assay of Ruthenium (Arc Profiles)	445
N.H.11	H1-Vol Air Sampler Laboratory Assay of Cerium (Arc Profiles)	446
N.H.12	H1-Vol Air Sampler Laboratory Assay of Zirconium (Arc Profiles)	447
N.H.13	Deposited Iodine (Arc Profiles)	449
N.H.14	Deposited Iodine (Centerline)	450
N.H.15	Gamma Dose from Cloud Passage (Arc Profile)	454
N.H.16	Gamma Dose Rate from Cloud Passage (Centerline)	454
N.H.17	Gamma Dose Rate from Cloud Passage (Activity Contours)	455
N.H.18	Gross Radioactivity Isopleth (Field Data)	456
N.H.19	Gross Radioactivity Isopleth (Curve Fit)	456
N.H.20	Contamination of Water Samples	458

Release I

N.I.1	Lapse Rate During Release	461
N.I.2	Sequential-Effluent-Sampler Filter Radioactivities	463
N.I.3	H1-Vol Air Sampler Field Survey (Arc Profiles)	465
N.I.4	H1-Vol Air Sampler Laboratory Assay of Cesium (Arc Profiles)	466
N.I.5	Deposited Cesium (Arc Profiles)	467
N.I.6	Deposited Cesium (Centerline)	468
N.I.7	Fluorescent Tracer (Arc Profiles)	470
N.I.8	Fluorescent Tracer (Centerline)	471
N.I.9	Gamma Dose from Cloud Passage (Arc Profile)	472
N.I.10	Gamma Dose Rate from Cloud Passage (Centerline)	472
N.I.11	Gamma Dose Rate from Cloud Passage (Activity Contours)	473
N.I.12	Rat Whole-Body Exposure	475
N.I.13	Rat Tissue Exposure	476

LIST OF TABLES

(APPENDICES)

<u>No.</u>	<u>Title</u>	<u>Page</u>
A.1	Calculated Inventory Per Fuel Element	114
H.1	Staplex H1-Vol Sampling Rate for Releases A,B,C,D	158
H.2	Staplex H1-Vol Sampling Rate for Releases E,F,G,H	160
H.3	Staplex H1-Vol Sampling Rate for Release I	162
I.1	Size-Count Medians and Stage Constants	184
I.2	Mass Medians and Stage Constants	186
I.3	ZCDS Distribution in the Andersen Sampler	187
J.1	Release D - Aged Element	193
J.2	Release E - Green Element	194
J.3	Release F - Green Element	194
J.4	Release G - Green Element	195
J.5	Release H - Green Element	195
J.6	Cs ¹³⁷ Deposition Velocity	196
J.7	Ru ¹⁰³ Deposition Velocity	197
J.8	Ce ¹⁴¹ Deposition Velocity	197
J.9	Zr ⁹⁵ -Nb ⁹⁵ Deposition Velocity	198
J.10	I ¹³¹ Deposition Velocity	198
K.1	Dosimeter Calibration	203
L.1	Radioactivity on the Sampling Probe Tubes	209
L.2	Radioactivity in the Sampling Probe Tubes	210
L.3	Radioactivity on the Glass Wool Filters	211
L.4	Spectra Analyses Correction Factors	220
L.5	Compton and Gamma Build-up Correction Factors	221
L.6	Fuel Element Residue Recovery	230
M.1	Animal Locations	232
<u>Release A</u>		
N.A.1	Fission Product Inventory	238
N.A.2	Meteorological Summary	240
N.A.3	Release Percentage	245
N.A.4	Cesium Deposition Velocity	250
N.A.5	Diffusion Parameters	258
N.A.6	Cesium-137 in Sand	260

LIST OF TABLES (Con't)
(APPENDICES)

<u>No.</u>	<u>Title</u>	<u>Page</u>
<u>Release B</u>		
N.B.1	Fission Product Inventory	263
N.B.2	Meteorological Summary	264
N.B.3	Release Percentage	267
N.B.4	Cesium Deposition Velocity	272
N.B.5	Diffusion Parameters	274
<u>Release C</u>		
N.C.1	Fission Product Inventory	278
N.C.2	Meteorological Summary	280
N.C.3	Release Percentage	285
N.C.4	Cesium Deposition Velocity	292
N.C.5	Distribution of Cs ¹³⁷ in the Andersen Sampler	293
N.C.6	Diffusion Parameters	299
N.C.7	Whole-Body Radioactivity in Rats	303
N.C.8	Radioactivity in Rats	304
<u>Release D</u>		
N.D.1	Fission Product Inventory	306
N.D.2	Meteorological Summary	308
N.D.3	Release Percentage	309
N.D.4	Isotopic Deposition Velocities	320
N.D.5	Diffusion Parameters	321
N.D.6	Cesium-137 in Sand	325
<u>Release E</u>		
N.E.1	Fission Product Inventory	331
N.E.2	Meteorological Summary	333
N.E.3	Release Height	337
N.E.4	Release Percentages	338
N.E.5	Isotopic Deposition Velocities	352
N.E.6	Distribution of Isotopes in Andersen Sampler	353
N.E.7	Diffusion Parameters	356
N.E.8	Contamination of Water Samples	357
N.E.9	Radioactivity in Rats	362
N.E.10	Radioactivity of Rats, Residual Carcasses, and Pleated Filters	364

LIST OF TABLES (Con't)
(APPENDICES)

<u>No.</u>	<u>Title</u>	<u>Page</u>
<u>Release F</u>		
N.F.1	Fission Product Inventory	366
N.F.2	Meteorological Summary	367
N.F.3	Release Percentages	371
N.F.4	Isotopic Deposition Velocities	383
N.F.5	Distribution of Isotopes in Andersen Sampler	386
N.F.6	Diffusion Parameters	390
N.F.7	Whole-Body Radioactivity in Rats	393
N.F.8	Radioactivity in Rats	396
N.F.9	Radioactivity in Dogs	399
N.F.10	Decay of Radioactivity in Pleated Filter	401
<u>Release G</u>		
N.G.1	Fission Product Inventory	403
N.G.2	Meteorological Summary	404
N.G.3	Release Percentages	407
N.G.4	Diffusion Parameters	421
N.G.5	Radioactivity in Rats	424
N.G.6	Radioactivity in Dogs	428
N.G.7	Decay of Radioactivity in Pleated Filter	429
<u>Release H</u>		
N.H.1	Fission Product Inventory	431
N.H.2	Meteorological Summary	432
N.H.3	Release Height	436
N.H.4	Release Percentages	436
N.H.5	Isotopic Deposition Velocities	451
N.H.6	Distribution of Isotopes in Andersen Sampler	452
N.H.7	Diffusion Parameters	453
N.H.8	Radioactivity in Sand and Water	457
<u>Release I</u>		
N.I.1	Fission Product Inventory	460
N.I.2	Meteorological Summary	462
N.I.3	Cesium Deposition Velocity	469
N.I.4	Radioactivity in Dogs	477

APPENDIX A

Fuel Element Inventories

The HTRE-type fuel elements used in the field tests were supplied and prepared by the General Electric Idaho Test Station. The elements were designated H-2 type and were taken from HTRE-MTR assemblies 1-T and 1-L-1.

The inventories for the fuel elements were calculated using an IBM-704 code with nuclear input data from the literature. All isotopes presented in a report by T. J. Burnett (Ref.15) were considered. Table A.1 shows the calculated inventory values for the elements in curies and the releases in which they were used. All isotopes are included whose inventories exceed one-tenth curie.

TABLE A.1
Calculated Inventory Per Fuel Element (Curies)

Release Isotope	A (Aged)	B (Aged)	C (Aged)	D (Aged)	E (Green)	F (Green)	G (Green)	H (Green)	I (Aged)	Half- life
⁹⁰ Y	0.0020	0.0016	0.0020	0.0013	54	48	40	40	0.00071	50.6 days
⁹⁰ Y	4.0	3.7	4.7	3.5	0.62	0.62	0.62	0.62	3.4	27.7 yrs.
⁵⁵ Fe	0.035	0.029	0.036	0.025	64	59	51	51	0.016	65 days
⁴¹ Ca	0.000004	0.000003	0.000004	0.000003	74	63	48	47	0.000001	33 days
¹⁴⁴ Pr	16	15	18	13	21	20	20	20	12	282 days
^{103m} 45Rh	0.000048	0.000038	0.000046	0.000029	35	31	24	24	0.000015	39.8 days
¹⁰⁶ 45Rh	1.3	1.2	1.5	1.1	1.0	1.0	1.0	1.0	0.98	1 yr.
^{127m} 52Te	0.057	0.051	0.063	0.044	1.8	1.7	1.6	1.6	0.034	115 days
¹³⁷ 55Ba	3.4	3.1	4.0	2.9	0.52	0.52	0.52	0.52	2.9	33 yrs.

E A.1 (Cont'd.)

D Aged)	E (Green)	F (Green)	G (Green)	H (Green)	I (Aged)	Half- life
0.42	0.085	0.084	0.084	0.084	0.42	10.3 yrs.
-	45	29	14	14	-	12.8 days
-	15	9.2	4.0	3.9	-	11.3 days
-	7.8	3.9	1.3	1.2	-	8.1 days
-	12	10	8	7.9	-	33.5 days
-	3.3	1.2	0.21	0.19	-	5.27 days

TABLE A.1
Calculated Inventory Per Fuel Element (Curies)

Release Nuclide	A (Aged)	B (Aged)	C (Aged)	D (Aged)	E (Green)(Green)	F (Green)(Green)	G (Green)(Green)	H (Green)	I (Aged)	Half- life
^{89}Sr	0.0020	0.0016	0.0020	0.0013	54	48	40	40	0.00071	50.6 days
^{90}Sr	4.0	3.7	4.7	3.5	0.62	0.62	0.62	0.62	3.4	27.7 yrs.
^{95}Zr	0.035	0.029	0.036	0.025	64	59	51	51	0.016	65 days
^{141}Ce	0.000004	0.000003	0.000004	0.000003	74	63	48	47	0.000001	33 days
^{144}Ce	16	15	18	13	21	20	20	20	12	282 days
^{102}Ru	0.0000048	0.0000038	0.0000046	0.0000029	35	31	24	24	0.000013	39.8 days
^{106}Ru	1.3	1.2	1.5	1.1	1.0	1.0	1.0	1.0	0.98	1 yr.
^{127}Te	0.057	0.051	0.063	0.044	1.8	1.7	1.6	1.6	0.034	115 days
^{137}Cs	3.4	3.1	4.0	2.9	0.52	0.52	0.52	0.52	2.9	33 yrs.

APPENDIX B

Fuel Element Melting Equipment

B.1 Induction Furnace

An induction type furnace was selected over a gas-fired or resistance-element furnace on the basis of clean fast heating with good temperature control. The final design was a transportable, shielded furnace capable of heating a fuel element to its melting point in two minutes. Built-in radiation shielding permitted ordinary transportation and handling methods for limited time intervals within the NRTS area.

The cylindrical furnace, which weighed 7,200 pounds, is shown in Figure B.1. It measured 27" O.D. by 32" high, and was comprised of a shield cask (1); lid (2) from which is suspended a cast ceramic cylinder (3) with embedded induction coil (4); cap (5); graphite crucible (6) resting on a ceramic pedestal (7); Pt, Rh-Pt thermocouple (8); 12 effluent sampling tubes (9) connected by glass-wool filled elbows (10), solenoid valves (11), and needle valves (12) to flasks (13); and an air injection tube (14).

The furnace crucible served also as the discharge stack, from which sampling tubes led to an array of 12 fractional-sampling flasks around the vertical face of the furnace. These flasks were installed before each release and removed after the

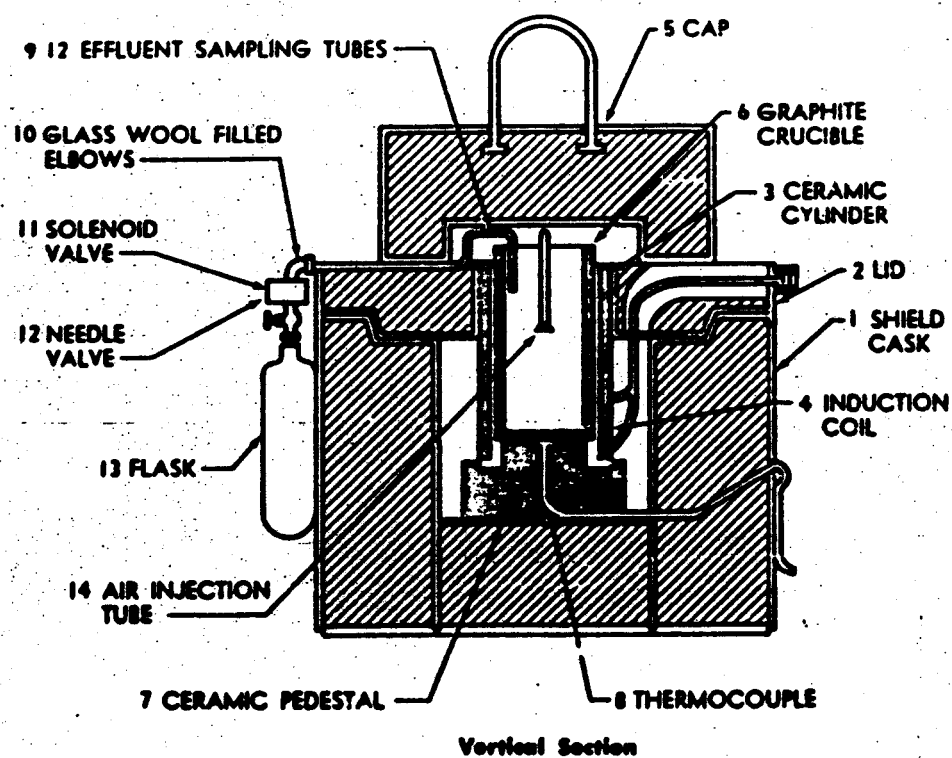


FIGURE B.1 INDUCTION FURNACE ASSEMBLY

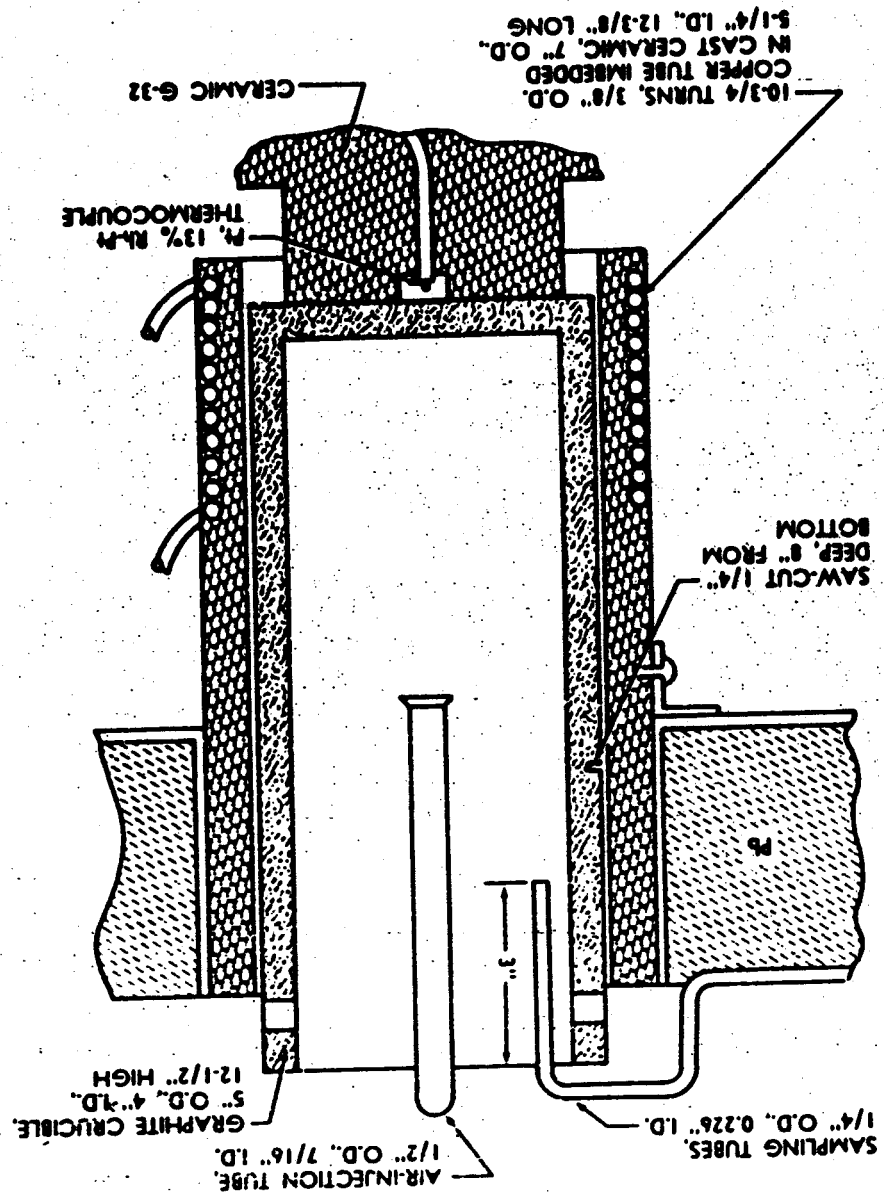
release for subsequent sampling. Metered air was injected into the center of the crucible to remove the effluent from the crucible. The effluent was released to free air at a height of five feet above ground.

The vertical wall of the furnace was a radiation shield having a 6.5-inch thickness of lead cast in-place between the 0.25-inch-thick steel outer and inner shells. The furnace bottom, lid, and cap provided essentially the same shielding thickness and materials excepting where potting compound in the lid insulated the induction coil connections. The calculated dose-rate at the outer face of the furnace was 0.45 R/hr. For the particular fuel elements used, the maximum dose-rate was 0.15 R/hr measured at the cask face mid-plane. A narrow beam of about 5 R/hr was measured at the potting compound in the lid where handling of the furnace was not required. Handling the furnace and sampling flasks at arms length reduced the torso dose-rate to about 0.05 R/hr.

The induction coil, made of $3/8$ " O.D. copper tubing, had $10-3/4$ turns, 7" O.D., and a total length of $5-5/8$ ". The coil was imbedded in a cast ceramic cylinder 7" O.D., $5-1/4$ " I.D., $12-3/8$ " long.

A crucible (Figures B.2, B.3) height of 12.5" was selected from considerations of induction coil size, power loss to nearby shielding, shielding thickness, and the desirability of having the

FIGURE B.2 GRAPHITE CRUCIBLE



NPC 9907
31-3814

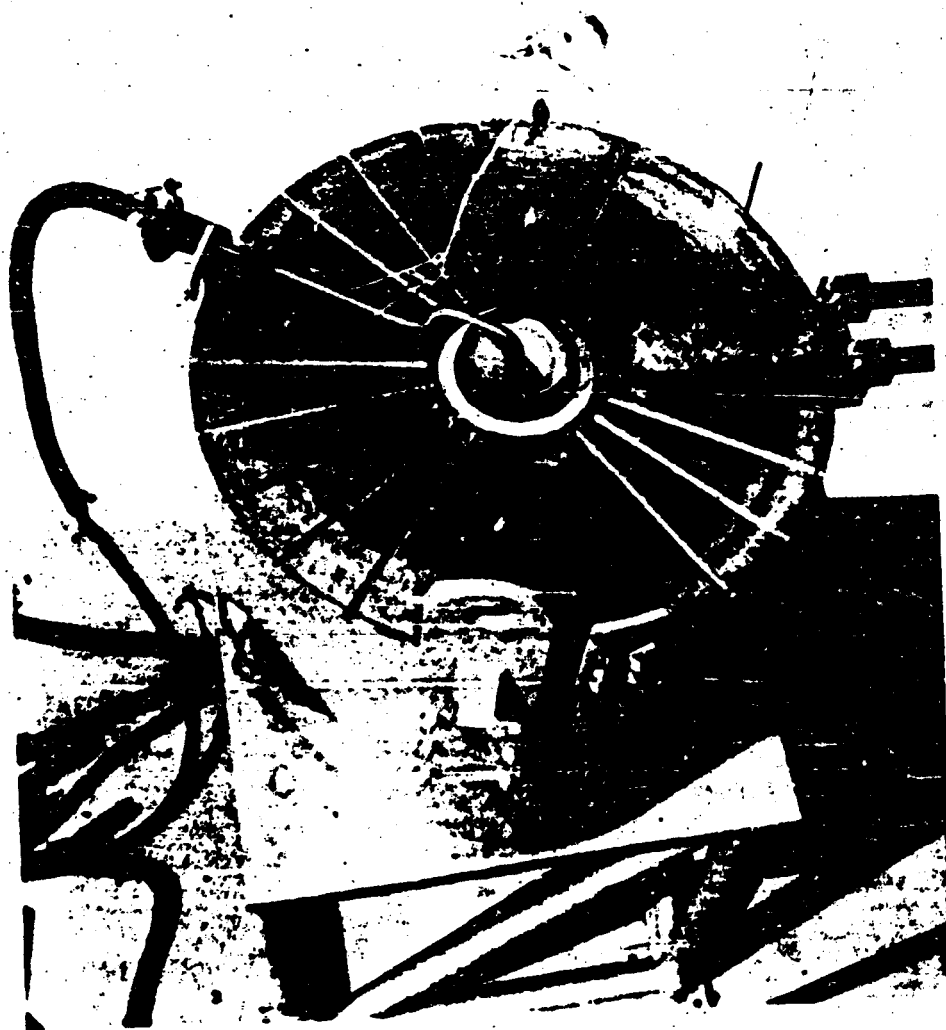


FIGURE B.3 FURNACE - TOP VIEW

rim of the crucible project above the furnace lid. A graphite crucible having a 0.5" wall thickness was an adequate susceptor for 10-kc induction heating, the crucible and fuel element rising in temperature about equally on a fast heat cycle. Two wire-duct holes, 0.625" diameter through the crucible wall near the rim, were provided. A saw-cut, 1/4"-deep around the crucible, 8" from the base, defined a breakage point used after a run to reduce the crucible height to fit within available shipping containers. To minimize the evolution of CO from graphite in air at high temperatures, the crucibles were coated with an alumina wash. The crucible formed the effluent discharge stack which protruded 1/25" above the furnace.

B.2 Power Supply

A 60-kw, air-cooled, motor-generator set with across-the-line starter was mounted on a concrete pad 115 feet upwind from the furnace. The motor-generator set was serviced by 480-volt, 3-phase, 60-cycle power obtained from a transformer and high-line about 200 feet distant. The generator output, 10-kw, single-phase, 440-volt maximum, was adjusted by a continuous variable field supply in the control consoles.

The control console, located 20 feet from the motor-generator set, included a push-button remote-control for the motor-generator starter; a continuously variable generator field supply with panel

ammeter, a main-line contactor for generator to furnace transformer and capacitor bank, panel meters for generator voltage, amperage, and power, a ground detector unit, switches for the two water-coolant pumps, sampling flask controls, and a 110-V service outlet.

A capacitor bank with jumpers provided 7.5- to 303.5-kvar in 7.5-kvar steps to tune the induction coil to resonance. A variable-ratio 10-kw transformer provided impedance-matching between the induction coil and the motor-generator set.

The water-coolant system, Figure B.4, for the capacitor bank, transformer, and induction coil provided water-pressure of about 30 psig at these items. The warm water was returned to a 1,000-gallon tank located 25 feet from the furnace and at the same level as the furnace.

B.3 Effluent Sampling

Effluent from the melted fuel element was purged from the crucible by injecting air at a rate of 1 cfm (local pressure and temperature) at the center of the crucible. The various samplers are depicted in Figures B.5 and B.6. Gas exit velocities from the crucible were not measured; however, calculations indicated the velocity might have been about 0.8 ft-sec^{-1} . Stainless steel tubes 0.25-in.-O.D., 0.226-in.-I.D. sampled the effluent before it reached free air, and a dummy sampling tube having one end sealed was present to provide a measure of effluent condensation at the outer and inner surfaces of the sampling tubes.

NPC 9908
31-3012



FIGURE 1-4 FURNACE ASSEMBLY

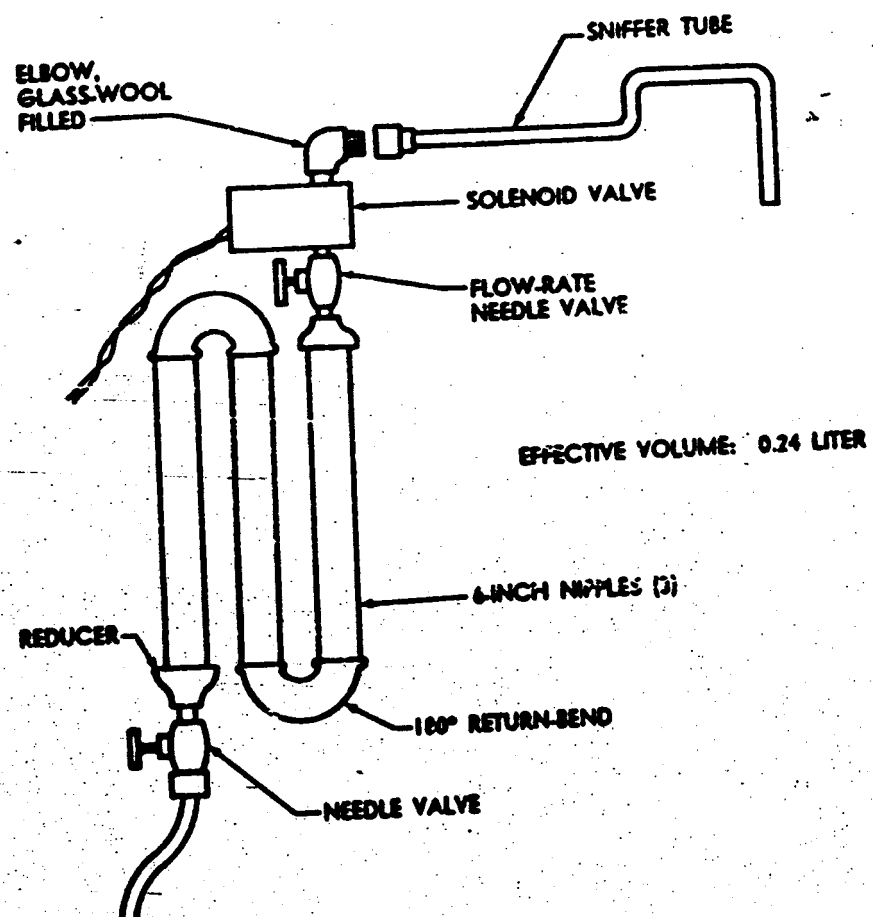
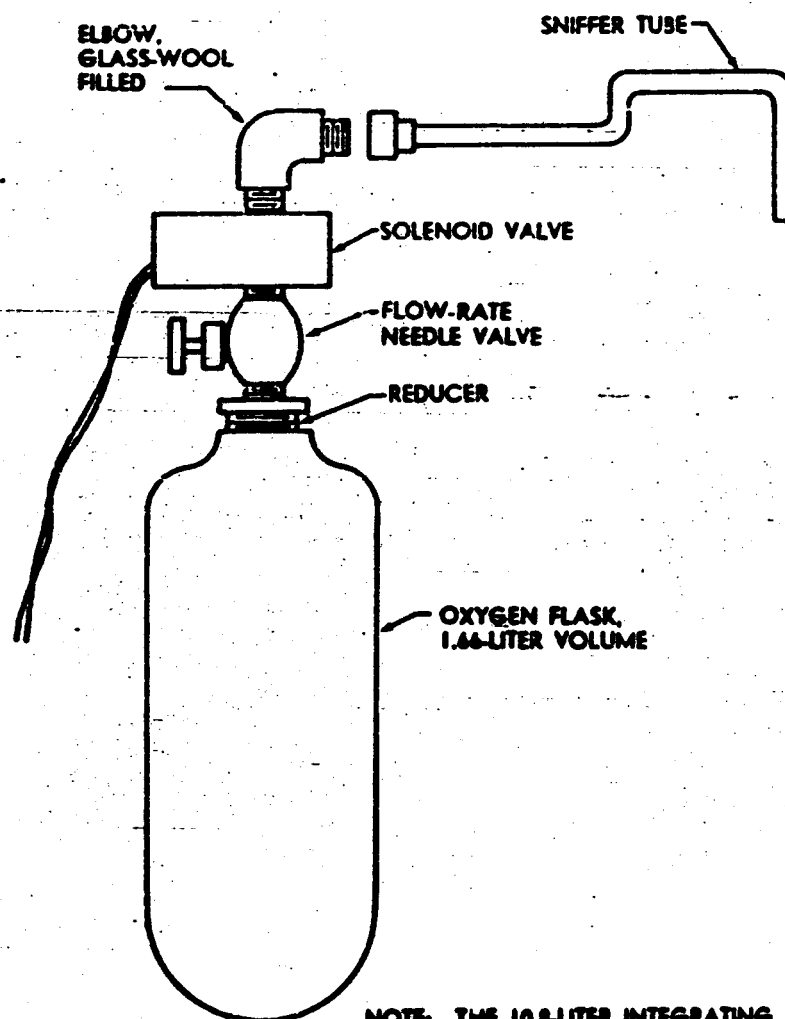


FIGURE 2.5 EFFLUENT SAMPLER - S-BOND
(Release A - 6)



NOTE: THE 10.8-LITER INTEGRATING FLASK ASSEMBLY IS SIMILAR, DIFFERING ONLY IN VOLUME AND LENGTH OF CONNECTION, TO SNIFFER TUBE.

FIGURE B.6 EFFLUENT SAMPLER - STEEL BOTTLE
(Releases P - 1)

Each sampling tube was connected through a solenoid valve and a needle valve to its sampling flask.

Three different sized flasks were used in the nine releases: an S-bend type (Figure B.5) fabricated from three 6-inch nipples and two 180-degree return-bends with an effective volume of 0.24 liter; a steel bottle (Figure B.6) having a volume of 1.66 liter; and a steel bottle having a volume of 10.8 liter, being similar to the one shown in Figure B.6. The S-bend flasks were attached to the vertical face of the furnace by spring-clamps; the 1.66 liter bottles were suspended from the sampling tubes (see Figure B.1) by the glass-wool-filled elbows and were secured by two turns around the furnace with masking tape; and the 10.8 liter bottles were placed in a "bucket-type" receptacle attached to the furnace pedestal.

The 10.8 liter flask was used as an integrating sampler, being turned on shortly after the start of a release and remaining on for about 13 minutes. The S-bend flasks were used for Releases A through E, taking short-time samples periodically throughout the release. The 1.66 liter flasks were used for Releases F through J as short-time samplers.

B.4 Temperature Measurement

A Pt, 13 percent Rh-Pt thermocouple positioned 0.25 in. below the crucible base monitored the temperature in the furnace. With the furnace at thermal equilibrium in the range 1000°C to

1600°C, there was a 150°C temperature difference between the thermocouple and the crucible base. Final calibration was made using dummy fuel elements and observing the start and completion of melting during fast heating cycles for various input wattages. Thermocouple emf was recorded on a 22-mv full-scale strip-chart recorder.

Each release was started at the same energy input to the furnace; variations in the rate of temperature rise of the furnace were observed at the strip-chart recorder and compensated for by suitable adjustments. Panel-meter readings were recorded as needed to assist in the interpretation of the strip-chart recording of the temperature.

B.5 Furnace Operation

A typical furnace operation cycle includes preparation, release, and follow-through:

1. Load furnace with a fuel element at GE-ANP hot cell.
2. Transport furnace to site and place on a pedestal. Establish maximum permissible working time.
3. Wrap vertical face of the furnace with polyethylene sheet. Install previously calibrated sampling flasks on the furnace.
4. Check all connections except the flask solenoid valves.

5. Remove furnace cap about one-half hour before predicted release time; measure sky-shine radiation. Start motor-generator set.
6. Apply power to furnace; melting begins about two minutes later.
7. Start the flow of metered air to crucible at $+ \frac{1}{2}$ minute and begin the sequential triggering of sampling flasks.
8. Reduce the furnace power at about $+3$ minutes and maintain a desired crucible temperature plateau.
9. Turn off furnace power and metered air at $+13$ minutes.
10. Monitor working area for radiation level; replace cap on furnace; monitor for radioactivity; close all needle-valves on the flasks; cover furnace for over-night (all runs were made in the evening).
11. Close water-coolant when crucible temperature drops to about 100°C .
12. Remove sampling flasks from the furnace; measure gamma radiation at the glass-wool filled elbows, and place in plastic containers.
13. Remove furnace connections and wrappings and wash the furnace down until smear tests are acceptable for furnace transportation.
14. Dispose of furnace wrappings and wash-down cloths as hot waste.
15. Wrap furnace and transport to OE-ANP hot cell; remove crucible and melt. Reload furnace with fresh crucible and fuel element.

B.6 Sampling Flask Adjustments

Typical procedures:

1. Evacuate flask to local barometric pressure minus 25 cm Hg.

2. Adjust flow-rate valve at collecting flask such that opening solenoid valve for 30 seconds to atmosphere results in a flask pressure of 15 cm Hg below local atmospheric pressure. The pressure change is 10 cm Hg, and the mass of sample obtained in 30 seconds is equal to $10/76$ times the mass of air which would be in the flask at a pressure of 76 cm Hg.

APPENDIX C
Power Distribution System

The selection of a source-point location near an existing 7.2/12.5 KV 3-phase line made it possible to supply the control trailer area, the source point, and the 100-, 200-, 400- and 800-meter arcs with electric power from an overhead distribution system connected to the existing line. The overhead system was designed as a joint effort of IDO-AEC and Convair and constructed under contract to IDO-AEC. The instrumentation along the above mentioned arcs, and the loads at the control and source points were connected to the overhead system by means of a ground-surface cable system designed by, and constructed under contract to Convair.

The power source for the control area consisted of a 120/208-volt, 3-phase, 45-KVA rating, that supplied lights and power for 10 trailers and the meteorological tower. The power source for the furnace area consisted of a 480-volt, 3-phase, 150-KVA rating, that supplied power to the motor generator and pumps of the induction furnace, the air conditioning unit of the meteorological trailer, and lights and instrumentation for the source area.

The 3-phase, 12.5-KV line was terminated at the 480-volt bank and a single-phase, 7.2-KV line was continued beyond to serve the

first four arcs. The presence of high voltage overhead lines in working areas of the innermost arcs was avoided by running the line along the left boundary of the network and supplying the 100- and 200-meter arcs from transformers located at their left ends. This problem was not considered important beyond the 200-meter arc, therefore, the 400-meter arc was supplied by a transformer at the center and the 800-meter arc was supplied by two transformers, evenly spaced, each supplying half of the arc load.

A study showed that it would be more economical to serve the 1600- and 3200-meter arcs by means of portable gasoline-engine-driven generators and wire and dry type transformers, obtained from U. S. government surplus, than by constructing overhead lines to be connected to the 7.2/12.5-KV line along Lincoln Blvd. The generator plan was therefore adopted and the 1600- and 3200-meter arcs were each supplied electricity from 3 generators of 28 Kw rating at 125-volts, 3-phase. To reduce voltage drop, the generated voltage was stepped up to 250 volts, 3-phase, and this was used as the primary voltage along the arcs. Dry type transformers were used to supply the instrument positions, with one transformer supplying 3 positions with a nominal 120-volt service. This system was designed by and constructed under contract to Convair.

All of the arcs, out to and including the 3200-meter arc, were controlled from a switchboard in the control trailer. After the generators in the 1600- and 3200-meter arcs had been manually started, all power to the 6 arcs could be turned on or off, individually from the control trailer.

The instruments on the 5-mile arc were located so far from each other, and from a power line, that the only practical solution was to use small individual gasoline engine generators for each instrument location. These units, as a matter of availability, averaged about 2.5 Kw in rating but were only loaded to about one-quarter capacity.

APPENDIX D

Meteorological Measurements

Wind Velocity

Velocity detectors were 3-cup Beckman-Whitley type anemometers. Locations of the detectors are shown on Figure D.1.

All wind speed detectors were check-calibrated in the wind tunnel facility at Eglin AFB Weather Section to conform within the manufacturer's tolerances and normalized to calibrations made by NBS (Ref. 10). Break-away or minimum velocity measurements were made.

Prior to installation in the field at NRTS, all wind velocity detectors were dynamically compared on a pulse per unit time basis.

This was done at low, varying, and medium wind speeds. After installation, periodic inspection was accomplished to prevent erroneous readings. These included cup cleaning, minimum drag checks and hi-speed drag checks.

All recording channels were calibrated against a known pulse source, and scales were normalized to a full scale for a low velocity range of 7.5 meters-per-second and a hi-velocity range of 100 meters-per-second. These two ranges best suited the testing parameters desired for the field release test series.

The wind velocity detectors functioned very well and maintenance was confined almost entirely to routine inspection and

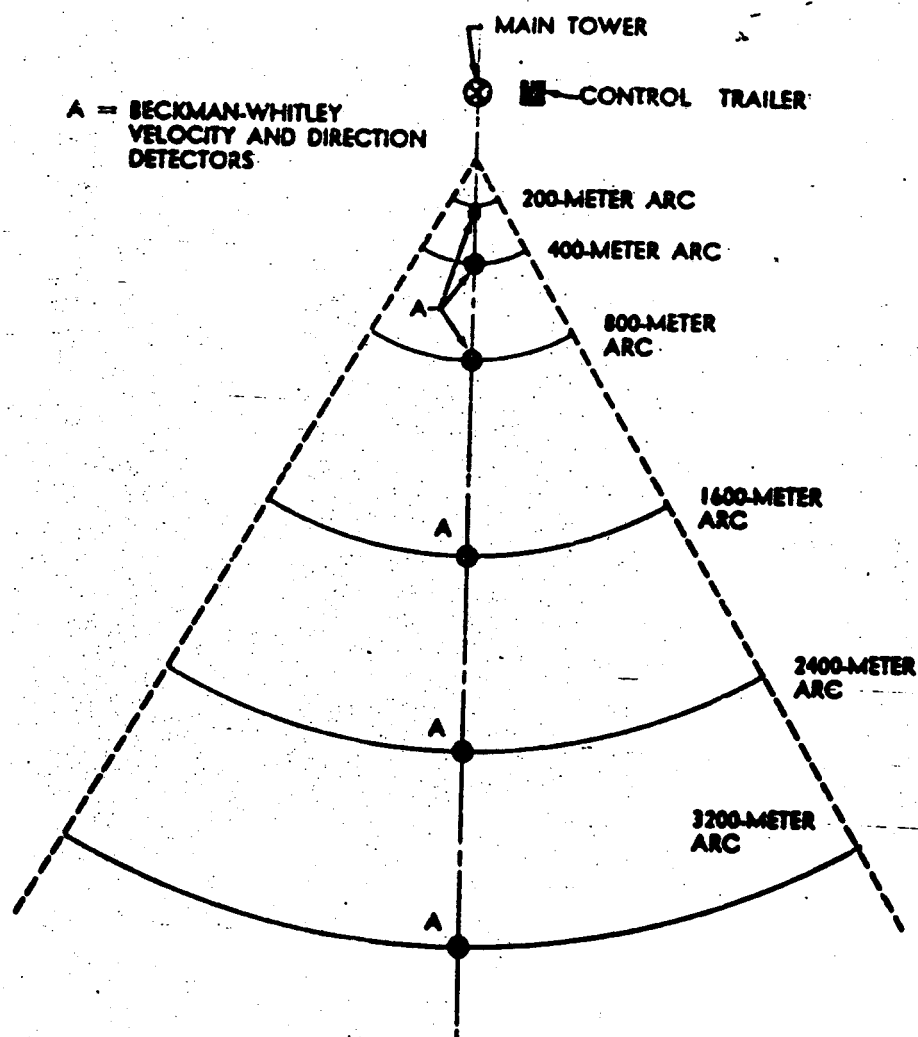


FIGURE B.1 METEOROLOGICAL INSTRUMENT LOCATIONS

cleanup. However, the pulse rate to analog translating medium suffered severe dust damage, and reliability was considered very poor. Test-to-test maintenance of the units consisted of a complete cleanup of relays and other areas that might be subject to damage by dust.

D.2 Wind Direction

Wind Direction detectors were Beckman-Whitley vanes. Locations of the detectors are shown on Figures D.1.

All wind direction detectors were checked for static vane balance, minimum breakaway force, and signal integrity before installation.

All check calibrations were accomplished via chart-pen deflection vs. visual vane alignment on a known backsight reference within the surveyed sampling area. Based on each detector's calibration, an equivalent signal was used to check excitation and full-scale signal deflection prior to any data recording sequence.

Regular pre-data taking checks included chart centerline confirmation, with vane backsighted on a visual reference point full-scale check and adjustment of excitation voltages plus inspection of the mechanical condition of the detector. Mercury cells were used for excitation voltage to insure long-term stability.

Performance of the units was considered satisfactory with the exception of an occasional potentiometer-wiper burnout caused by dead zone switching with a long, large-capacity cable being used for the signal voltages. Adequate suppression was provided to insure against excessive damage.

D.3 Air Temperature (Dynamic)

To determine mean temperatures for inversion and lapse conditions, three shielded copper-constantan thermocouples were installed on the main tower at the 1.5, 24, and 45-meter levels. Recording was accomplished by using a Brown multipoint recorder of 50°C in span.

A separate set of thermocouples was located at the same positions to provide a means of magnifying the difference-temperature variations between positions. Recording was accomplished by stabilized-d.c.-difference amplifiers feeding a 0-1-ma recorder.

APPENDIX E

Release Height Determination

E.1 Equipment

The basic equipment for the release height measurements was a frame structure containing one or more charged vertical wires. The wire or wires were approximately 8 feet in length and were insulated from the supporting frame. The system used during Release I is shown in Figure E.1.

E.2 Operational Procedure

Prior to a release, the framework was placed immediately downwind of the furnace. The high voltage batteries were connected between the wire and ground terminals about 5 minutes before energizing the furnace. Immediately following the release, the batteries were disconnected. After the furnace lid was replaced, the wire was removed from the framework and placed within a box which was constructed so that the wire was supported at the ends. The wire was then transported to the Convair trailer where the collected activity was measured as a function of distance along the wire.

Several types of collection geometries were used during the tests. The geometry is listed for each of the releases:

NPC 912

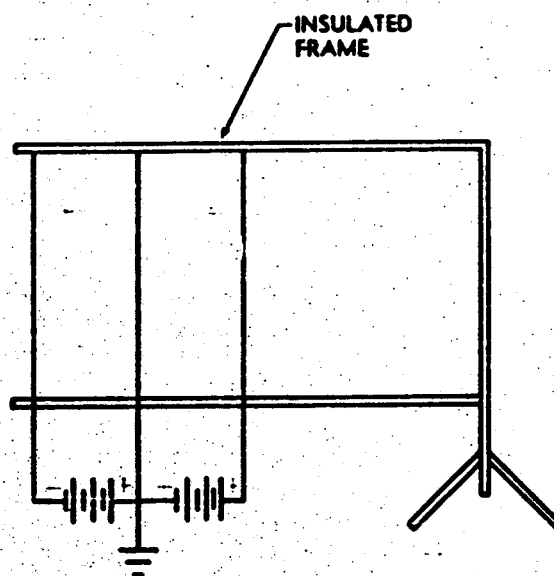


FIGURE E.1 CHARGED WIRE COLLECTOR
(Release 1)

Release E: A single, negatively charged wire, at minus 2450 volts with respect to ground, was placed 42-3/4 inches downwind of the center of the crucible on the network centerline. The furnace top was 43 inches from the top of the wire.

Release F: In an attempt to determine the lateral distribution of the effluent as well as the vertical, three vertical wires, spaced 5 inches apart were placed 48.5 inches downwind of the center of the crucible along the network centerline. All three wires were negatively charged to 2450 volts. Although this geometry gave consistent indications of the source height, the lateral distribution of the activity could not be accurately determined. The electrical field pattern surrounding the wires caused lateral migrations of the ions and misleading results. No further attempts to measure the lateral distribution of the cloud were made during the releases.

Release G: Two wires were installed on the framework 2.75 inches apart, one at a minus 2450 volts and the other at a plus 2450 volts with respect to ground. The frame was positioned so that the two wires were on either side of the centerline 45.5 inches downwind from the center of the crucible.

Release H: The geometry used in Release H was similar to that of Release G. The only difference was that the two wires were 3 inches apart.

Release I: Three vertical wires were spaced 1-1/8 inches apart with the central wire on the grid centerline. The central wire was maintained at ground potential, the left wire was 1225 volts negative and the right wire was 1225 volts positive with respect to the central wire. Figure E.1 illustrates the electrical connections.

APPENDIX F

Smoke Plume Generation and Data Analyses

F.1 Equipment

A U. S. Army Mechanical Smoke Generator, M-3, was used to produce the visible plumes. The M-3 is a pulsejet smoke generator capable of generating a hydrocarbon-base oil smoke at the rate of 25 to 50 GPH. The generator operates satisfactorily with No. 100 Pale Oil. The oil is vaporized and ejected in pulses by means of a pulsating combustion engine. The hot oil vapors condense a short distance after exit from the nozzles, giving a fine oil-aerosol plume.

Conventional K-24 cameras, each fitted with a seven-inch focal length lens and using Kodak Super-XX, Aerial Recon film, were positioned on the ground at previously determined locations to record the passage of the smoke plumes. In order to obtain accurate data from the photographs concerning cloud height, the orientation of the optical axis of each camera had to be known. To accomplish this, each camera was surveyed into position and aligned on precisely placed reference targets. The coverage and position of each ground camera is shown in Figure F.1. All ground cameras were sequenced with intervalometers which were operated from a central control point.

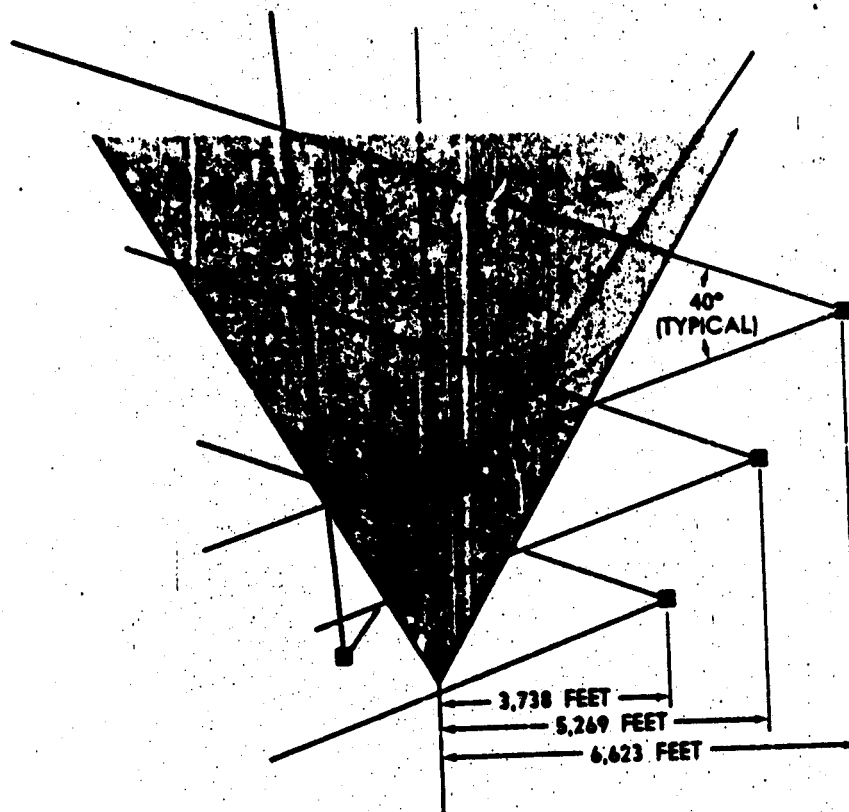


FIGURE F.1 LOCATION OF GROUND CAMERAS

To obtain information concerning cloud path and cloud shape, and to provide the data necessary to correlate angular position data, obtained by the ground cameras, with height measurements, an Air Force L-20 aircraft was fitted with a K-24 camera using a 5.25-inch focal length lens. Sequence photographs, intervalometer controlled for synchronization with ground photography, were taken of the continuous plume and smoke puffs from an altitude of 8500 feet above the terrain along the network centerline. Radio contact between the aircraft and the field test control center permitted simultaneous aerial and ground photography.

F.2 Procedure

Prior to each scheduled fission product release, the oil-fog generator was started in sufficient time to generate a continuous plume extending over as much of the length of the network as possible. After the plume was developed and meteorology was still satisfactory for a release, simultaneous photographs were taken from the air and from the ground. The total time to photograph this plume was approximately ten minutes.

After this series was complete, the oil fog generator was turned off for about two minutes to allow the apex of the plume to move downwind from the release point. At the end of this period, the generator was turned on for one minute to produce a

small cloud approximating a puff. Simultaneous photographs of the "puff" were taken from the air and ground. Photography continued until the puff was no longer visible.

Shortly, one to five minutes, after the "puff" was generated, the furnace was brought to temperature and the fission product release effected. Following the fission product release, which took about thirteen minutes, another "puff" was generated and simultaneously photographed from air and ground cameras until the cloud disappeared.

7.3 Diffusion Parameters

Vertical and horizontal photography accompanied most fission product releases. Diffusion parameters, based on smoke plume analysis, were calculated only for those releases with similar lapse rates.

The derivation of the smoke plume diffusion parameters is based on the assumption that the visible outline of the plume is the same as an isopleth of the cutoff density to transmitted background light which is given by Eq. 1.

$$D_{co} = \frac{2Q}{\sqrt{\pi} C_z \bar{u} x^{3/2}} e^{-\frac{z_{co}^2}{C_z^2 x^{2m_z}}} \quad (1)$$

where

D_{co} = Cutoff density

Q = Source term

C_z = Vertical diffusion coefficient

\bar{u} = Mean wind velocity

x = Distance downwind

m_z = Vertical stability parameter

Z_{co} = Height at which cutoff density occurs

Equation 1 was obtained by integrating Eq. 5 of Appendix H from $-\infty$ to $+\infty$ over y .

Two cases were analyzed:

Case I, the initial rise and the maximum width or height and their associated distances may be estimated. Solving for C_z^2 by substituting (x_1, z_1) and (x_2, z_2) into 1:

$$C_z^2 = \frac{1}{m_z \ln \left(\frac{x_2}{x_1} \right)} \left[\frac{z_1^2}{x_1^{2m_z}} - \frac{z_2^2}{x_2^{2m_z}} \right] \quad (2)$$

where $Z = Z_{co}$ (understood)

Solve Eq. 1 for Z_{co}

$$Z_{co} = C_z x^{m_z} \left[\ln \left[\frac{2Q}{D_{co} \sqrt{\pi} C_z \bar{u}} \right] - m_z \ln x \right]^{\frac{1}{2}} \quad (3)$$

Differentiate Eq. 3 with respect to x and set it equal to 0 to find x when Z_{co} is a maximum.

$$x_{max} = \exp \left[\frac{1}{m_z} \ln \left[\frac{2Q}{D_{co} \sqrt{\pi} C_z \bar{u}} \right] - \frac{1}{2m_z} \right]$$

Substituting into Eq. 3, and solving for C_z^2

$$C_z^2 = \frac{2(Z_{co \max})^2}{(x_{Z_{co} \max})^{2m_z}} \quad (5)$$

Equating Eq. 5 to Eq. 2,

$$2 \ln \left[\frac{x_2}{x_1} \right] - \frac{1}{m_z} \left[\frac{z_1}{z_{\max}} \right]^2 \left[\frac{x_2 \max}{x_1} \right]^{2m_z} + \frac{1}{m_z} \left[\frac{z_2}{z_{\max}} \right]^2 \left[\frac{x_2 \max}{x_2} \right]^{2m_z} = 0 \quad (6)$$

and finally, solve Eq. 6 for m_z and Eq. 5 for C_z .

Case II. All conditions of Case I are met along with the ability to estimate x where $Z_{co} = 0$.

Therefore, it follows that from Eq. 3

$$\ln \left[\frac{2Q}{Q_{co} \sqrt{C_z} u} \right] - m_z \ln (x_{\max}) = 0 \quad (7)$$

Substituting Eq. 7 into Eq. 1,

$$C_z^2 = \left[\frac{z}{x^{m_z}} \right]^2 \frac{1}{m_z \ln \left[\frac{x_{\max}}{x} \right]} \quad (8)$$

and equating Eq. 8 to Eq. 2

$$\frac{z_{\max}^2}{\left[\bar{x}_{z_{\max}} \right]^{2m_z} \ln \left[\frac{x_{\max}}{x_{z_{\max}}} \right]} = \frac{1}{\ln \left[\frac{x_2}{x_1} \right]} \left[\frac{z_1^2}{x_1^{2m_z}} - \frac{z_2^2}{x_2^{2m_z}} \right] \quad (9)$$

It is now possible to solve Eq. 9 for m_z , and Eq. 8 for C_z .

APPENDIX G

Fluorescent Tracer Dispersal and Data Analyses

G.1 Equipment

A Todd Insecticidal Fog Applicator, Model 40-E, was used to disperse the fluorescent tracer.

The two principal functions of the dispersal equipment are to break up the aggregate pigment and release particles at a known and uniform rate. The aerosol generator utilizes the wet dispersal technique, which minimizes reagglomeration of particles.

The outlet nozzle was such that the jet could be directed in any desired direction, but during operation the jet was directed vertically to minimize the immediate deposition of particles. The aqueous spray was visible up to a distance of 10 feet from the nozzle after which droplets evaporated leaving an invisible pigment aerosol.

The quantity of pigment released was measured by noting the decrease in liquid level in the mixing container which contained a known amount of pigment. The fluorescent ZnCdS aerosol was sampled with the Andersen samplers, Appendix I, on the 100-, 300-, 400-, and 800-meter arcs.

G.2 Data Analyses

Zinc cadmium sulfide particles were counted at a magnification of 125X, using a Leitz binocular microscope. An

ultraviolet light was utilized to induce fluorescence, thus enabling the operator to differentiate between zinc cadmium sulfide and atmospheric dust particles.

Stage two of all Andersen samplers was selected for particle-counting analysis. It was determined that stage one collected particles having a large variety of sizes, and stage three required excessive counting times because it contained so few particles. As is typical in Andersen samplers the particles impinged against the collecting media and the resulting collection of particles formed a small circular pattern, hereafter called a colony. Since there were 400 impinging jets per stage, there were an equal number of colonies. This large number of colonies would have required a considerable amount of counting time. Therefore, to determine the average number of particles for the entire stage, all the particles were counted in only eight colonies. The colonies selected for counting were those which happened to be under a set of 90-degree grid lines originating at the center of the stage. Four colonies were counted along one grid line and the remainder of the colonies along the other grid, which meant that eight colonies were counted along a randomly chosen diameter of the stage. In those cases where the average number of particles was small and the standard deviation from the average value was greater than 10, sixteen colonies were counted, i.e., eight colonies per radial distance.

The fluorescent-particle size distribution as found on the various stages of the Andersen sampler was determined by counting the various sized particles with the aid of a microscope. Sizing was accomplished at a magnification of 1250X, dry field, using a Bausch and Lomb graduated reticle. Calibration of the reticle was accomplished with a stage micrometer, resulting in a value of 1.5 microns per division. A total of 200 particles were sized on each stage; they were selected as follows: 50 particles in each of four colonies in the four quadrants of the plate. Whenever possible the 50 particles were selected across the centerline of the colony. Particle size is defined as the extreme diameter of each randomly oriented particle, when all measurements are made on a given axis, i.e., horizontal axis.

APPENDIX H

Airborne Activity Determinations and Data Analyses

H.1 Equipment

High volume (Hi-Vol) air samplers, manufactured by the Staplex Company Company, were used. The units are motor-driven, centrifugal-type air pumps which require 110 volt alternating current for operation. The samplers were connected to a ground power distribution system and operated from a central control point.

The samplers were fitted with a pleated filter, and during the green releases an activated charcoal cartridge was also added. A disassembled and mounted sampler are shown in Figures H.1 and H.2 respectively.

The filter, Mine Safety Appliances Company No. CT77227, was a 4-inch-diameter pleated fiberglass collector, quoted to have a collection efficiency of 99.98 percent for 0.3 micron Di-Octyl Phthalate particles.

The activated charcoal filled cartridge, also obtained from MSA, was fitted to the Staplex air sampler by a minor modification of the filter holder. The cartridges were placed behind the pleated filter during the field tests in which iodine collections were made. This was done to collect those particulates which would not have been intercepted by the pleated filter and to minimize contamination of the cartridge with fission products other than iodine.

NPC 916

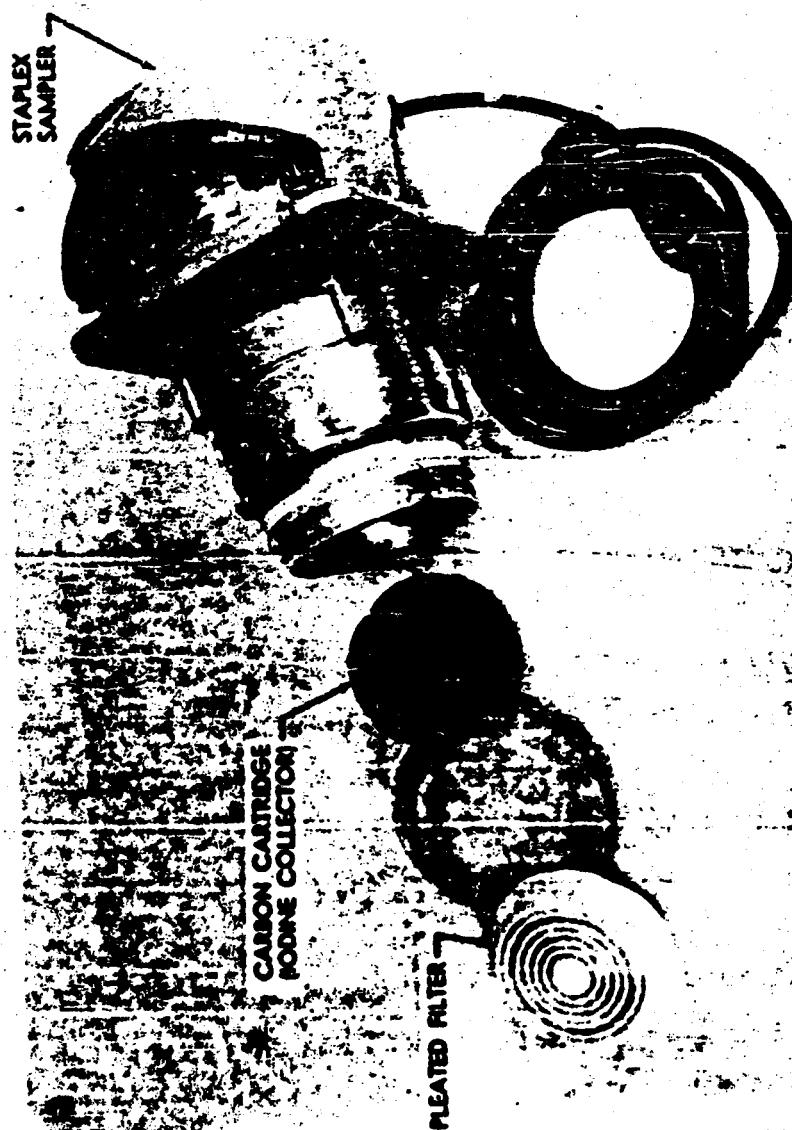


FIGURE M.1 M-VOL AIR SAMPLER

NPC 9917
31-3832



FIGURE N.2 IN-VOL AIR SAMPLER - ASSEMBLED

The iodine collection efficiency of the cartridge is assumed to be 100 percent. This assumption is based on unpublished Convair data which show that all the iodine is absorbed in the carbon cartridge.

The individual units, even when new, showed variation in pumping rate when compared under constant conditions. The exact causes for this non-uniformity are probably caused by one or more of the following factors: (1) variations in bearing friction, (2) rotor or armature unbalance or drag, (3) variation in brush or commutator characteristics, and (4) variation in resistance of filters of the same type.

The above factors apply to samplers running on a constant voltage. The variety of ways in which power was supplied to the various arcs resulted in a whole spectrum of line voltages and voltage drops throughout the network. Variations of ± 5 percent of nominal line voltage were common.

It was impractical to periodically read the small flowmeter on the Hi-Vol instruments and then average the rate as is customarily done because it would involve a prohibitive amount of time in the field.

The only practical solution to the problem seemed to be that of calibrating each sampler against a standard flowmeter under known voltage conditions with pleated filter alone and pleated filter together with carbon cartridge. Tests were run on single samplers to determine a relation between applied

voltage and flowrate with a number of filters to determine the percent variation in flowrate resulting from different filters of the same type. Recording voltmeters were then put on the supply line at the right end of the 100-meter arc, the center of the 400-meter arc, and the left ends of the 800- and 3200-meter arcs. From the resulting data, it was possible to calculate a flowrate for each sampler in the test network. Table H.1 shows a list of calibrated flow rates for each sampler, determined immediately after Release D. These values were used for reducing the field data from the first four releases. The transformer on the 400-meter arc became faulty after Release D, and a calibration could not be performed. This accounts for the average value appearing in the 400-meter arc column.

Table H.2 shows calibrated sampler flow rates determined immediately following Release H. These values were used in reducing the field data for Release E through H. Table H.3 contains sampler calibration data for Release I. Average values only are shown for the 100-, 200-, and 400-meter arcs; this was necessitated by the fact that the calibration was performed with no load on the line except the sampler being calibrated. The absence of voltage drop resulted in higher sampling rates than were obtained during actual test conditions when all samplers were operating. Thus an average value was assigned based on an appropriate loading factor.

H.2 Atmospheric Diffusion Parameter Evaluation

Sutton's well known solution of the Pickian diffusion

TABLE H.1

Staplex Hi-Vol Sampling Rate for Releases A, B, C, D

Station No.	Sampling Rate (grm)					
	100M	200M	400M	800M	1600M	3200M
1	35.8	34.4	36.6	38.4	38.4	35.2
2			↑		41.5	33.1
3	35.4	35.2		37.4	39.6	33.1
4					33.1	36.8
5	35.8	34.9		39.6	39.6	36.2
6					42.1	34.0
7	35.0	34.0		38.1	40.6	36.2
8					40.6	36.2
9	35.8	34.5		40.6	40.6	34.0
10					41.5	36.8
11	34.1	32.6		39.0	41.5	35.8
12					40.6	36.2
13	32.8	34.4		38.4	41.5	37.5
14					40.6	36.2
15	34.8	32.2		39.0	39.0	35.2
16					38.4	35.2
17	35.6	33.8		39.0	40.8	35.2
18					42.2	33.1
19	34.2	31.2		39.0	40.8	30.6
20					38.4	33.7
21	35.6	35.2		39.0	40.0	32.5
22					36.2	33.1
23	32.6	31.8		39.6	37.5	33.7
24					38.4	35.2
25	34.4	35.2		40.0	36.9	34.0
26					38.1	33.8
27	34.4	31.9		38.1	38.4	33.8
28					35.5	33.8
29	35.0	36.0		27.5	36.9	34.0
30					38.1	35.8
31	32.6	32.0		41.5	36.9	35.0
32					40.0	36.2
33	35.8	37.2		35.8	35.2	35.0
34					35.8	35.2
35	33.8	33.5		27.5	38.4	37.5
36					35.4	36.8
37	35.8	33.8		38.1	39.0	35.8
38					39.0	34.0
39	33.8	31.2		40.6	36.2	35.8
40					37.5	34.0
41	36.2	37.9		27.5	38.1	36.2
42					33.1	40.6
43	33.5	33.9		39.6	36.2	38.4
44					35.8	39.0
45	37.0	36.6	36.6	39.0	35.2	39.6
			↓			

TABLE H.1 (Cont'd)

ARC Station No.	Sampling Rate (cfm)					
	100M	200M	400M	800M	1600M	3200M
46			36.6		35.8	41.5
47	33.8	32.8	↑	40.0	35.8	41.5
48					35.8	43.1
49	37.2	36.2		39.6	31.2	42.2
50					37.5	42.5
51	34.1	33.5		40.0	34.0	41.5
52					36.2	42.1
53	35.5	37.7		36.2	37.5	38.4
54					36.2	40.6
55	32.8	33.5		39.6	36.2	40.8
56					36.2	39.0
57	36.5	36.2		36.2	34.0	38.4
58					35.0	27.5
59	33.8	33.8		39.6	35.8	36.2
60			↓		32.5	36.2
61	36.8	36.0	36.6	36.9	33.1	36.2

TABLE H.2

Staplex Hi-Vol Sampling Rate for Releases E, F, G, H


Station	ARC	Sampling Rate (cfm)						5 Mile
		100M	200M	400M	800M	1600M	3200M	
1		19.4		19.4	18.8	19.4	18.1	
2						20.9	18.1	
3			20.4		19.4	19.4	17.8	
4						15.4	18.8	
5		19.4		19.4	20.4	18.8	19.4	
6						20.4	18.1	
7			20.4		20.4	17.1	18.1	
8						20.4	18.8	
9		19.4		17.7	21.5	20.4	18.1	
10						21.9	20.4	
11			17.1		20.9	20.4	18.8	
12						20.4	19.4	
13		20.4		19.8	19.4	20.9	20.4	
14						19.8	18.8	
15			18.1		19.8	18.1	18.8	
16						18.8	18.1	
17		18.8		18.1	19.8	19.4	16.5	
18						20.4	16.5	
19			17.8		19.8	20.4	16.0	
20						19.4	18.1	
21		21.9		18.8	19.8	20.4	16.5	
22						19.4	17.1	
23			17.8		19.8	18.1	17.1	
24						18.1	17.8	
25		20.9		19.4	19.8	20.4	17.8	
26						19.8	16.5	
27			16.5		19.4	18.8	17.1	
28						19.4	18.1	
29		21.5		19.4	19.8	22.5	17.8	
30						19.4	18.8	
31			20.4		20.4	19.4	17.8	
32						20.4	19.8	
33		17.8		18.1	18.8	18.1	18.1	
34						18.1	17.8	
35			19.8		19.4	20.4	19.4	
36						17.8	22.5	
37		20.9		18.1	19.8	20.4	19.4	
38						19.8	16.5	
39			17.1		20.4	18.1	19.4	
40						18.8	18.1	

TABLE H.2 (Cont'd)

Station No.	ARC	Sampling Rate (cfm)						5 Mile
		100M	200M	400M	800M	1600M	3200M	
41		20.4		18.1	19.4	20.9	20.4	20.7
42						18.1	20.4	
43			19.4		20.4	18.8	19.8	
44						21.5	19.8	
45		21.9		20.9	19.8	17.8	19.4	20.7
46						17.8	21.5	
47			17.1		19.4	19.4	22.5	
48						18.1	21.9	
49		21.5		18.8	20.4	16.0	20.9	
50						19.4	20.9	
51			18.8		20.4	18.1	19.4	
52						18.1	19.8	
53		20.9		17.1	19.8	18.1	19.8	
54						18.1	20.4	
55			18.8		19.4	17.8	20.4	
56						19.4	21.5	
57		19.4		17.8	18.1	18.1	20.4	
58						17.8	19.4	
59			16.5		20.4	19.4	17.8	20.7
60						19.4	19.4	
61		19.4		18.1	19.8	17.8	19.4	

TABLE H.3

Staplex Hi-Vol Sampling Rate for Release I

Station No. ARC	Sampling Rate (cfm)				
	100M	200M	400M	800M	1600M
1	34.5	37.1	36.9	37.5	38.4
2	↑	↑	↑		41.5
3				36.9	39.6
4					33.1
5				38.1	39.6
6					42.1
7				36.9	40.6
8					40.6
9				37.5	40.6
10					41.5
11				37.5	41.5
12					40.6
13				37.5	41.5
14					40.6
15				38.1	39.0
16					38.4
17				37.5	40.8
18					42.2
19				36.9	40.8
20					38.4
21				36.2	40.0
22					36.2
23				36.2	37.5
24					38.4
25				35.2	36.9
26					38.1
27				36.2	38.4
28					35.5
29				35.2	36.9
30					38.1
31				40.0	36.9
32					40.0
33				34.0	35.2
34					35.8
35				35.0	38.4
36					35.4
37				35.9	39.0
38					39.0
39				39.6	36.2
40					37.5
41				37.5	38.1
42					33.1
43	34.5	37.1	36.9	38.4	36.2

TABLE 3 (Cont'd)

Station No.	Sample Rate (cfm)				
	100M	200M	300M	800M	1600M
44					35.8
45	34.5	37.1	36.9	38.1	35.2
46					35.8
47	↑	↑	↑	38.1	35.8
48					35.8
49				36.9	31.2
50					37.5
51				39.0	34.0
52					36.2
53				36.2	37.5
54					36.2
55				38.1	36.2
56					36.2
57				35.2	34.0
58					35.0
59				38.4	35.8
60	↓	↓	↓		32.5
61	34.5	37.1	36.9	35.2	33.1

equation (Ref. 5) as applied to eddy diffusion in the atmosphere for continuous point sources has the following form:

$$X(x,y,z) = \frac{Q}{\pi C_y C_z \bar{u} x^{2-n}} \exp \left[-\frac{y^2}{C_y^2 x^{2-n}} \right] \left\{ \exp \left[-\frac{(z-h)^2}{C_z^2 x^{2-n}} \right] + \exp \left[-\frac{(z+h)^2}{C_z^2 x^{2-n}} \right] \right\} \quad (1)$$

where: $X(x,y,z)$ is the concentration at a distance x downwind, y crosswind and z above ground from a release point at $(0,0,h)$.

Q is the rate of release of airborne material at the source point.

\bar{u} is the mean wind speed.

C_y is the horizontal diffusion coefficient.

C_z is the vertical diffusion coefficient.

n is a stability parameter.

h is the height above ground

Practical application of this equation requires that C_y , C_z and n be defined as averaged quantities which may be considered constant over substantial distances and for appreciable periods of time.

Sutton suggested the following methods for obtaining values of C_y , C_z and n from meteorological measurements;

$$C_y^2 = \frac{4N^n}{(1-n)(2-n)\bar{u}^n} \left(\frac{\overline{v^2}}{\bar{u}^2} \right)^{1-n} \quad (2)$$

$$C_z^2 = \frac{4N^n}{(1-n)(2-n)\bar{u}^n} \left(\frac{\overline{w^2}}{\bar{u}^2} \right)^{1-n} \quad (3)$$

$$\frac{\bar{u}(z)}{\bar{u}(z_1)} = \left(\frac{z}{z_1} \right)^{n/2-n} \quad (4)$$

where: N = macroviscosity

$\overline{v^2}$ = mean squared velocity fluctuation in y-direction

$\overline{w^2}$ = mean squared velocity fluctuation in z-direction

Data from the bi-vane at 24 meters above ground on the apex towers have been used to evaluate $\overline{v^2}$ and $\overline{w^2}$. The term n has been evaluated by fitting the above power law (Eq. 4) to the wind speed profiles obtained from the anemometers on the apex tower. Substitution in Eqs. 2 and 3 then yielded values of C_y and C_z respectively. An averaging period of about 30 minutes was used for all meteorological parameters because that was the time interval covered by the release and drift of the cloud through the network. The air samplers were kept running during this period. Therefore, when Eq. 1 is applied to these tests, Q is

interpreted to be the integral of the release rate and $X(x,y,z)$ as the integral of the airborne concentration over this time interval. X is then called the "exposure integral".

There are two ways to compare theory with experimental results. The first method consists of calculating the values at the various sampling stations and comparing them directly with the measured network values of X . This method is useful for showing directly whether or not an existing theory is adequate for prediction purposes. An alternative way to make the comparison is to fit Eq. 1 to the measured network data, i.e., determine those values of C_y , C_z and n which cause Eq. 1 to yield the best approximation to the actual network data and then to compare this set of parameter values with the set obtained from the meteorological data. This method is useful if it is desired to study various theoretical approaches to the calculation of the parameters from meteorological data.

Eq. 1 expresses the inherent anisotropy of the diffusion phenomenon more satisfactorily if separate values of the stability parameter, n , are used for the horizontal and vertical components of the diffusion as follows:

$$X(x,y,z) = \frac{q}{v(C_y x^{ny})(C_z x^{nz})} \exp \left[-\frac{y^2}{C_y^2 x^{2ny}} \right] \left\{ \exp \left[-\frac{z-h}{C_z^2 x^{2nz}} \right] + \exp \left[-\frac{z+h}{C_z^2 x^{2nz}} \right] \right\} \quad (5)$$

where $2 - n = m_y + m_z$ (6)

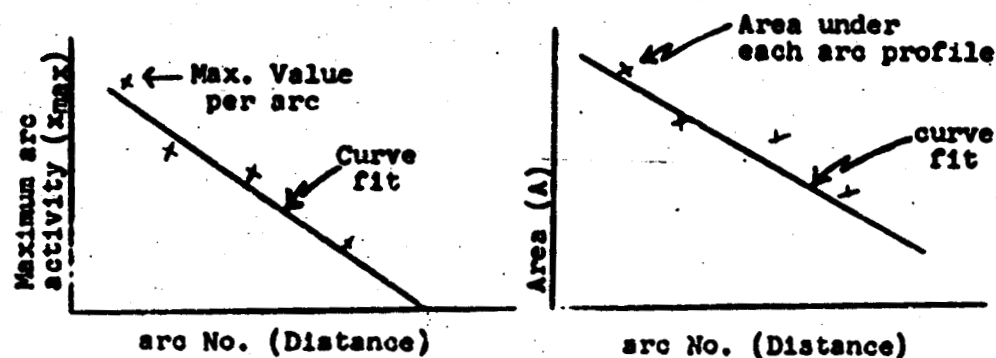
Table 17 (Discussion) shows the values of C_y , C_z , m_y and m_z obtained by fitting the above equation to the network air sampler data. Table 17 also shows the values of C_y , C_z , and n obtained from the meteorological data using Eqs. 2, 3, and 4. No attempt has been made to evaluate separate horizontal and vertical stability parameters m_y and m_z from meteorological data. However, the m_y and m_z parameters evaluated from network data can be combined to give an average value of n (Eq. 6) for comparison with the meteorological value.

H.3 Activity Diffusion Parameter Evaluation

Diffusion parameters were calculated from gross beta-gamma and isotopic pleated filter data (arc profiles) as well as smoke plume photography and meteorological data. Graphical plots of these data from each arc, corrected for sampler flow rate, provide profiles of the integrated cloud concentration. Profiles of this type may be found under each release of Appendix N. From these profiles the maximum value, X_{\max} per arc and the area, A , under each arc profile may be obtained and plotted versus arc numbers (distance). A least squares curve fit to these plots may then be used in conjunction with the equations for a Gaussian profile and the Sutton type diffusion equation to calculate curve fit coefficients, m_y , C_y , m_z , and C_z . A summary of these calculations is shown in Table 17 (Discussion).

The technique for combining the profile data with the diffusion equation is outlined:

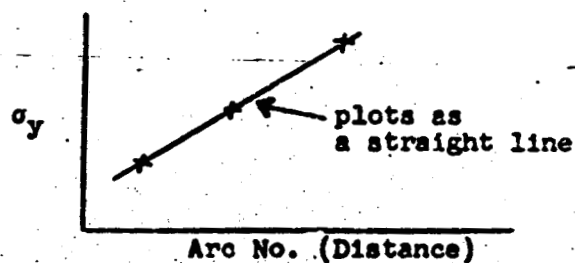
1. Plot the calibration corrected profiles of the cloud activity integrals (See Appendix N).
2. Plot the least squares curve fits of X_{\max} per arc and A per arc



3. Using the Gaussian relationships (Eqs. 7 and 8)

$$x_{\max} = \frac{A}{\sqrt{2\pi} \sigma_y} \quad (7) \quad \text{or} \quad \sigma_y = \frac{A}{\sqrt{2\pi} x_{\max}} \quad (8)$$

where σ_y is the cross wind standard deviation of the forced normal distribution, and x_{\max} is the centerline maximum of the distribution, and choosing values of x_{\max} and A from the curve fits, one can obtain a straight line plot of σ_y vs. arc no.



4. Now, it is possible to calculate the diffusion parameters by substituting values from the above plots into the general Sutton type diffusion equation (Eq. 9).

$$X(x,y) = \frac{Q}{\pi C_y C_z \bar{u} x^{2-n}} \exp - \frac{y^2}{C_y^2 x^{2-n}} \left[\exp - \frac{(z-h)^2}{C_z^2 x^{2-n}} + \exp - \frac{(z+h)^2}{C_z^2 x^{2-n}} \right]$$

Because the top of the furnace and the samplers were at a height (h) of 1.5 meters, and the charged-wire measurements of the effluent a few feet downwind indicated that the release height was also 1.5 meters, $h = z = 0$. Therefore Eq. 9 becomes:

$$X(x,y) = \frac{2C}{\pi C_y C_z \bar{u} x^{2-n}} \exp - \frac{y^2}{C_y^2 x^{2-n}} \quad (10)$$

responding normal profile is

$$N(x,y) = \frac{A}{\bar{u} 2\pi \sigma_y \sigma_z} \exp - \frac{y^2}{2\sigma_y^2} \quad (11)$$

$$X(x,y) = N(x,y)$$

$$\sqrt{2}\sigma_y = C_y x^{\frac{2-n}{2}} \text{ and } \sqrt{2}\sigma_z = C_z x^{\frac{2-n}{2}} \quad (12)$$

is different in the y and z directions the following relationships exist:

$$\sqrt{2}\sigma_y = C_y x^{m_y} \quad (13)$$

$$\sqrt{2}\sigma_z = C_z x^{m_z} \quad (14)$$

m_y and m_z are not necessarily equal.

From the plot of σ_y versus are No. (σ_y as a function of x) possible to pick any two values of x (x_1, x_2) and corresponding values of σ_y thereby solving Eq. 13 for m_y :

$$m_y = \frac{\log\left(\frac{\sigma_y(x_1)}{\sigma_y(x_2)}\right)}{\log\left(\frac{x_1}{x_2}\right)} \quad (15)$$

Then C_y may be determined by using Eq. 13 and calculated values of m_y (Eq. 15):

$$C_y = \frac{\sqrt{2\sigma_y(x_n)}}{x_n^{m_y}} \quad (16)$$

where x_n is equal to any distance.

Then using the relation from Eq. 9 and letting $y = 0$, it is possible to develop Eq. 7.

$$X_{\max}(x) = \frac{2Q}{\tau C_y C_z \bar{u} x^{m_y+m_z}} \quad (17)$$

Next, by using the plot of X_{\max} vs. distance downwind as represented by Eq. 7, two simultaneous equations may be written:

$$X_{\max}(x_1) = \frac{K}{x_1^{m_y+m_z}} \quad \text{and} \quad X_{\max}(x_2) = \frac{K}{x_2^{m_y+m_z}} \quad (18)$$

$$\text{where } K = \frac{2Q}{\tau C_y C_z \bar{u}}$$

which can be solved simultaneously to obtain:

$$\frac{X_{\max}(x_1)}{X_{\max}(x_2)} = \left(\frac{x_2}{x_1} \right)^{m_y+m_z} \quad \text{or} \quad m_y+m_z = \frac{\log \left(\frac{X_{\max}(x_1)}{X_{\max}(x_2)} \right)}{\log \left(\frac{x_1}{x_2} \right)} \quad (19)$$

By solving for m_z , Eq. 20 is obtained:

$$m_z = \frac{\log\left(\frac{x_{\max}(x_1)}{x_{\max}(x_2)}\right)}{\log\left(\frac{x_2}{x_1}\right)} - \frac{\log\left(\frac{\sigma_y(x_1)}{\sigma_y(x_2)}\right)}{\log\left(\frac{x_1}{x_2}\right)} \quad (20)$$

From Eq. 17 one obtains:

$$\frac{Q}{C_z} = \frac{x_{\max}(x_1) C_y \bar{r}^{m_y + m_z}}{2} \quad (21)$$

Thus, C_z may be calculated if one knows the source strength.

APPENDIX I

Particle Size Measurements

I.1 Equipment

Particle separation of released fission products was accomplished by using a multi-stage, sieve-type impactor known as the Andersen sampler. A dismantled sampler and a complete system are shown in Figures I.1 and I.2 respectively. The principle of operation is similar to that of the Casella impactor, but it provides more stages for particle sizing.

Samplers used by Convair in the Release Tests differed from the commonly used models in that each stage contained 400 holes instead of 340. In addition, the use of coated glass plates instead of agar as a collecting medium increased the jet-to-surface spacing from 2.5 to 3.76 mm. The sampler was originally designed for the collection and discrimination of bacterial aerosols.

The Andersen sampler is normally a six-stage fractionator; however, with the addition of a back-up filter, a seventh stage was obtained. During the green releases, an eighth stage, composed of an activated charcoal cartridge, was also added to insure the collection of iodine.

The Andersen sampler was used for two specific investigations during the tests: (1) to determine the activity and particle size distribution of released fission products, and (2) to determine the diffusion characteristics of a fluorescent pigment.

NPC 9918
31-3830

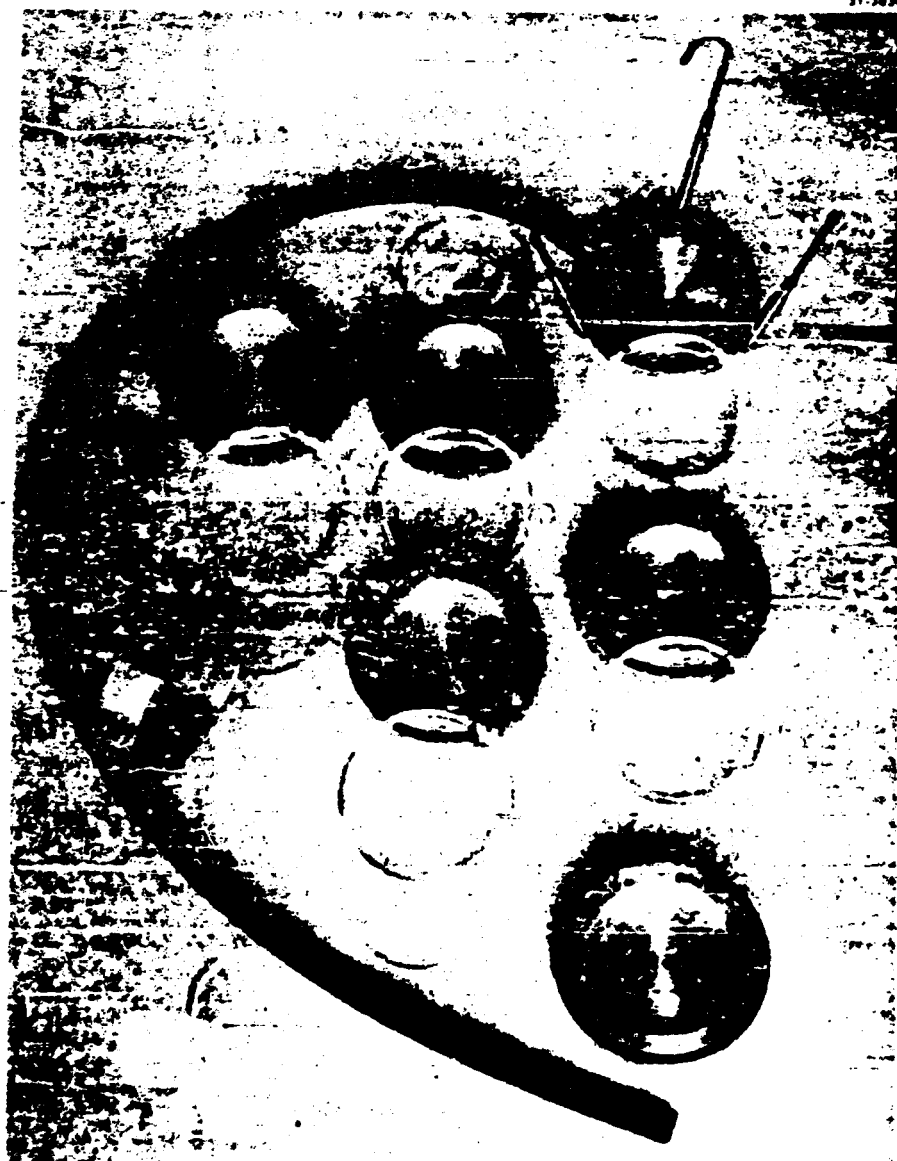


FIGURE 1.1 DISMANTLED ANDERSEN SAMPLER

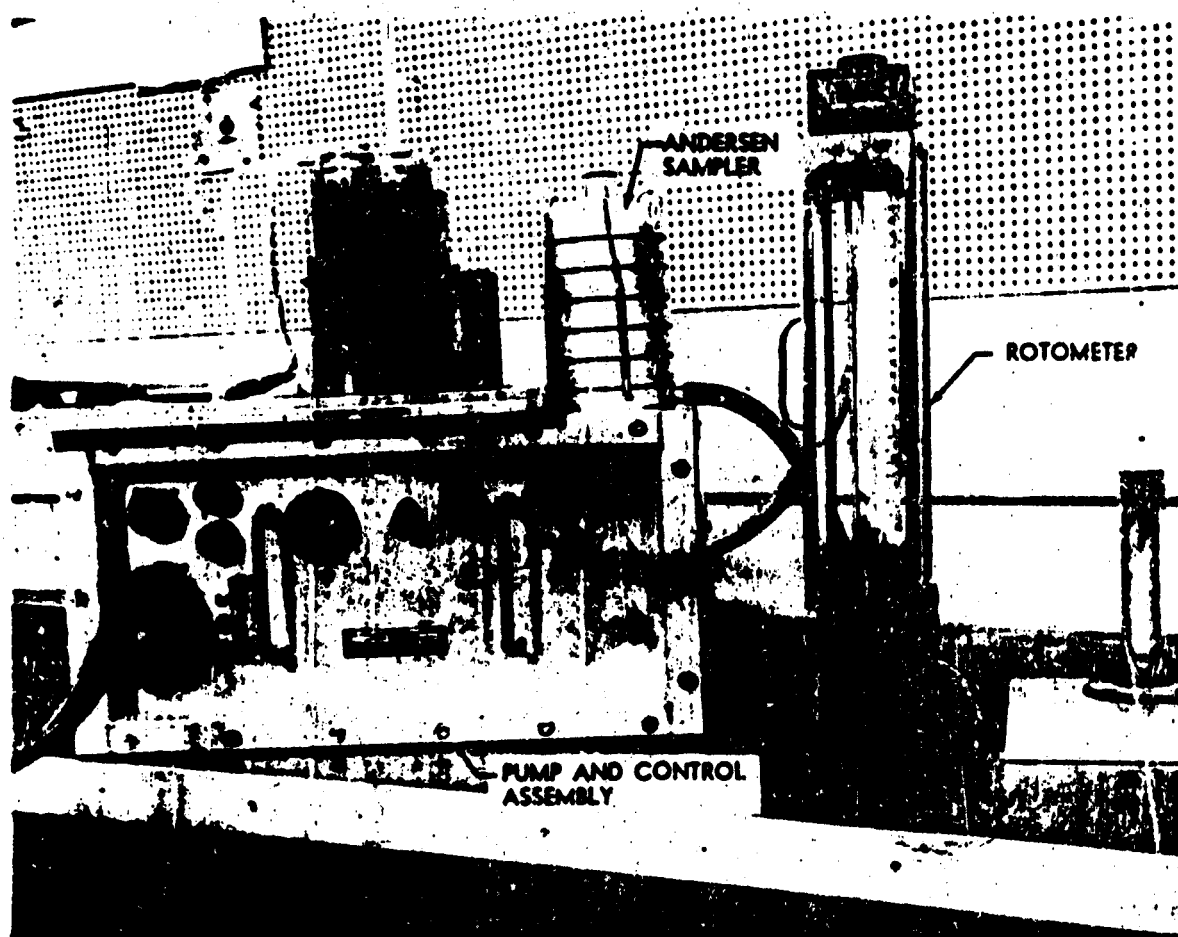


FIGURE 1.2 ANDERSEN SAMPLER

A glass plate, 1/8 inches thick, coated with a silicone-based resin (Dow-Corning 200 Fluid) proved to be a satisfactory particle collecting surface. The resin was placed on each plate by dipping in a solution of xylene containing 1 percent by weight of DC200. The xylene evaporated, leaving a thin uniform coating of resin. The resin was non-drying and maintained an even distribution on the plate through periods of extreme field temperature variations.

I.2 Field Calibration of Flow Rate

The air flow through the Andersen samplers was calibrated five times throughout the test period. During calibration, all of the samplers were turned on simultaneously simulating the field line-load conditions.

A 0-14 SCFM Brooks rotameter was used to calibrate the air flow. The impedance of the rotameter was determined by taking two sets of measurements, one set including one rotameter and the other set two rotameters. The difference between the two readings gave an indication of the rotameter impedance. The rotameter used on the Andersen sampler calibration decreased the flow rate about 5 percent.

The flow rates were affected appreciably by additional sampling equipment attached to the Andersen sampler. Average flow rates with different sampling arrangements are shown:

<u>Sampling Arrangement</u>	<u>SCFM</u>
A	2.00
G	1.75
M	1.75
A + G	1.68
A + M	1.68
A + G + M	1.60
A + G + M + C	1.12

Where A is the Andersen sampler; G, the Gelman filter; M, the Millipore filter, and C, the charcoal trap.

Reproducibility measurements showed the flow rate to be about ± 5 percent.

I.3 Laboratory Calibration of Sampler

Calibration of the original sampler was performed at a flow rate of 1 cfm with particles of unit density. The purpose of this calibration program was threefold: (1) to recalibrate the modified sampler, (2) to extend the calibration range to include higher flow rates and particle densities, and (3) to determine, if possible, the operational limits of the sampler.

The "statistical diameter" was chosen to represent the particle size in a "horizontal" direction, i.e., the length of the projection of the particle on a line across the field of view in the microscope. This method has been shown to give a

representative picture of the size distribution of the sample when the particles are randomly orientated.

Mean vs. Median Size: The difference between the mean and median sizes on a single stage in this study can be neglected on the lower stages due to the narrowness of the distributions obtained on these stages and the relative coarseness (0.75 microns per division) of the measuring instrument. Where sufficient data points existed, a log normal probability plot was drawn and the median noted. Otherwise, the mean size was calculated using the formula:

$$\bar{D} = \sum x f(x)$$

where $f(x)$ = frequency of particles of size x , expressed as a percent.

Size-Count and Mass Medians: A size-count median diameter is obtained directly from the particle size distribution where size is defined as the "statistical" diameter. Frequently, particularly in toxicologic studies, the concentration of a material is more meaningful and the mass median is employed. The size-count distribution is converted to a mass frequency distribution by assuming that the mass of a particle is proportional to the cube of its measured diameter. The size frequency is then weighted by the cube of the average diameter in each class and the resulting frequency plotted against the size. Both size and mass median counts were computed whenever possible.

Impaction Theory: The theory of the Cascade impactor can be applied to the Andersen Sampler. Briefly, for equal impaction efficiency, the equation can be written:

$$I_n = \rho V D_n^2 / \eta l$$

where ρ = particle density

D = particle diameter (if spherical)

V = jet velocity

η = viscosity of air

l = a characteristic length of the system

I_n = constant

Impaction efficiency is the ratio (no. of particles hitting the plate)/(no. of particles entering jet), assuming 100 percent retention by the plate.

With a given air sampler and neglecting any variation in η , the median particle size retained by a stage is given by

$$\bar{D}_m = \frac{C_n}{\rho^{0.5} V^{0.5}}$$

where the subscript, n , refers to the stage number and V is the sampler flow rate.

C_n , the stage constant, can then be obtained experimentally with various density materials and flow rates and used indirectly to indicate the operating range of the sampler.

Procedure: Air flow through the sampler was provided by a Vitro vacuum pump and measured by a Brooks rotameter. Glass discs,

1/8" thick, coated with a 1 percent Dow Corning 200-xylene solution, were used to collect the particles on each stage. Dry powder aerosols of zinc cadmium sulfide ($\rho = 4.1 \text{ gm/cc}$) and Pb_3O_4 ($\rho = 9.1 \text{ gm/cc}$) were generated with a compressed air aspirator. A krylon ($\rho = 1$) aerosol was released using the commercial package generator. Each material was sampled twice at flow rates of 0.9, 1.4, and 2.0 cfm.

A total of 200 particles were sized on each stage from 4 randomly selected colonies. Sizing was accomplished with an eyepiece reticule (calibrated with a stage micrometer) at magnifications of 1250 x, using a 100 x oil immersion objective (1250 x with a 40 x dry objective for krylon sizing on the upper stages). Reticule calibration values were 0.75 microns/division and 1.5 microns/division respectively.

To obtain a measure of the relative amount of material retained by each stage, a radioactive ZnS aerosol was generated, using the aspirator technique in a dry box. Three samples were taken at a flow rate of 1 cfm, and the total Zn^{65} activity on each stage was counted using a 3-inch scintillation crystal and a 256-channel analyzer.

Size-Count Medians and Stage Constants: The average size count median diameter, \bar{D}_g , and the geometric standard deviation, G , are presented in Table I.1 for the various materials and flow rates. For a normal distribution of log-diameters

approximately 68 percent of the particles fall between the median log-diameter $\pm 1 G$. Thus, G is a measure of the dispersion of partical sizes about the mean size.

The constant, C_s was obtained from the formula:

$$\bar{D}_s = \frac{C_s}{\rho^{0.4} V^{0.5}}$$

where \bar{D}_s = median diameter (microns)

ρ = density (gm/cc)

V = sampler flow rate (cfm)

Reduction of the density exponent from 0.5 to 0.4 resulted in a significantly lower average variance in C and was used in all calculations of the size-count stage constants.

Mass Medians and Stage Constants: The average mass median diameters are presented in Table I.2 for krylon and ZnCdS.

Mass median stage constants were calculated from these values using the formula:

$$\bar{D}_m = \frac{C_m}{\rho^{0.4} V^{0.5}}$$

The size-count and mass medians for stages I and VI are at best just good estimates for the true values. The reasons for this are: (1) stage I median is dependent on the upper limit of the sample and (2) Stage VI particles are of a size comparable to the graduations of the reticle which makes accurate size determinations quite difficult. In addition, experiments reported in the

literature have shown that unless improved resolution is obtained, e.g., selenium coating the sample, measurements of particles in the 1-micron range are usually 10-20 percent too high.

Low Flow Data: During the course of the calibration, iron and carbon dust were sampled at a flow rate of 0.3 cfm. Stage constants calculated from these data were approximately twice the value of the constants found at the higher flow rates. These same aerosols sampled at 1.0 cfm yielded the same stage constants as those found in the calibration. This indicates that the constants reported in this calibration are valid only for flow rates greater than 0.7 cfm.

Activity Distribution: The results of the activated zinc sulfide aerosol experiment are presented in Table I.3. A seventh stage millipore filter was added to the Andersen to measure the amount of sub-micron particles present in the aerosol. The activity on the filter consisted of those sub-micron particles plus any slippage of larger particles through the sampler. Comparison with the stage VI results indicated total slippage was probably less than 0.5 percent of the total activity. It appears that if the sampler is to be used with high density material, i.e., $\rho > 4.0 \text{ gm/cc}$, some redesign is indicated to spread the particles more evenly through the device. This may be accomplished in the present sampler by enlarging holes in stage VI to 1.6 mm and placing this stage above the present stage I.

The radioactive zinc sulfide aerosol was sampled with a single stage millipore and sized with the following results:

Size-Count:

Geometric Median = 1.6 microns
Geometric Standard Deviation = 1.9

Mass Median:

Geometric Median = 4.0 microns
Geometric Standard Deviation = 1.6

TABLE I.1
Size-Count Medians and Stage Constants

Stage	Mat'l. Density	Flow Rate (0.9 cfm)			Flow Rate (1.4 cfm)			Flow Rate (2.0 cfm)			Average C _s
		D _g	C _f	C _s	D _g	C _f	C _s	D _g	C _f	C _s	
I	1	12.2	1.3	11.6	10.0	1.4	11.8	9.50	1.5	13.30	10.35 ± 2.19
	4	-	-	-	3.5	1.8	7.2	3.20	1.8	7.85	
	9	-	-	-	-	-	-	-	-	-	
II	1	7.70	1.3	7.3	5.88	1.4	6.94	5.01	1.3	7.06	6.19 ± 0.54
	4	2.97	1.6	4.9	2.76	1.3	5.66	2.35	1.4	5.77	
	9	2.22	1.5	5.06	2.22	1.5	6.29	2.00	1.3	6.77	
III	1	5.65	1.2	5.37	3.86	1.4	4.55	3.46	1.4	4.88	4.68 ± 0.09
	4	2.59	1.4	4.28	2.14	1.3	4.39	1.86	1.4	4.57	
	9	2.06	1.4	4.70	1.59	1.3	4.50	1.44	1.4	4.87	

TABLE I.1 (cont'd.)
Size-Count Medians and Stage Constants

Stage	Mat'l. Density	Flow Rate (0.9 cfm)			Flow Rate (1.4 cfm)			Flow Rate (2.0 cfm)			Average
		\bar{D}_s	\bar{f}_s	C_s	\bar{D}_s	\bar{f}_s	C_s	\bar{D}_s	\bar{f}_s	C_s	
IV	1	2.96	1.4	3.04	2.36	1.4	3.30	2.46	1.5	3.47	3.45 ± 0.22
	4	1.78	1.4	2.94	1.60	1.4	3.29	1.61	1.4	3.95	
	9	1.34	1.3	3.06	1.34	1.3	3.79	1.25	1.3	4.23	
V	1	2.29	1.3	2.31	1.12	1.3	1.32	1.28	1.2	1.80	2.62 ± 0.28
	4	1.35	1.3	2.23	1.32	1.3	2.70	1.40	1.3	3.45	
	9	1.27	1.3	2.50	1.06	1.2	3.00	0.74	-	2.50	
VI	1	1.10	1.4	3.04	0.96	1.2	1.13	0.95	1.4	1.34	1.41 ± 0.25
	4	0.84	1.4	1.38	0.75	1.6	1.54	0.82	1.5	2.01	
	9	-	-	-	-	-	-	-	-	-	

TABLE I.2

Mass Medians and Stage Constants

Stage	Mat'l. Density	Flow Rate (0.9 cfm)			Flow Rate (1.4 cfm)			Flow Rate (2.0 cfm)			Average C _m
		\bar{D}_m	\bar{C}_m	\bar{C}_m	\bar{D}_m	\bar{C}_m	\bar{C}_m	\bar{D}_m	\bar{C}_m	\bar{C}_m	
I	1 5	17	1.3	16.1	14	1.4	16.5	14	1.5	19.7	16.8 ± 0.48
		-	-	-	7.85	1.6	16.1	6.4	1.5	15.7	
II	1 4	8.8	1.4	8.4	7.10	1.4	8.3	5.5	1.6	7.8	7.73 ± 0.44
		4.41	1.4	7.2	3.60	1.4	7.3	3.0	1.5	7.4	
III	1 4	5.8	1.3	5.5	3.5	1.7	4.1	3.3	1.5	4.65	5.01 ± 0.50
		3.71	1.5	6.0	2.3	1.3	4.7	2.1	1.6	5.10	
IV	1 4	2.61	1.5	2.4	2.6	1.8	3.10	2.0	1.4	2.80	3.30 ± 0.48
		2.1	1.5	3.5	1.90	1.3	3.80	1.7	1.5	4.2	
V	1 4	1.8	1.3	1.7	1.5	1.2	1.80	1.2	1.3	1.7	2.27 ± 0.57
		1.3	1.5	2.1	1.3	1.3	2.70	1.5	1.5	3.65	
VI	1 4	1.1	1.5	1.0	1.1	1.3	1.2	1.2	1.2	1.7	1.57 ± 0.26
		1.1	1.3	1.8	0.9	1.6	1.8	0.7	1.7	1.8	

TABLE I.3
ZnCdS Distribution in the Andersen Sampler

Trial No.	Percent of Total Activity on Each Stage						
	I	II	III	IV	V	VI	VII
1	63.5	28.2	6.2	1.1	0.6	0.1	0.3
2	55.5	32.1	8.0	1.9	0.7	0.5	1.3
3	59.1	27.5	8.6	2.6	0.9	0.5	0.7
Average	59.3	29.2	7.6	1.9	0.7	0.5	0.8

APPENDIX J

Deposition Velocity Determination

J.1 Equipment

Deposition collectors were placed at regular intervals downwind of the release point. The units were remotely controlled and could be operated in either the horizontal or vertical position. Each unit consisted of two hinged pieces of 0.25" x 15" x 15" marine plywood. These pieces were spring-loaded and in tension when sandwiched together. A solenoid operated catch was used to maintain the closed position. During a release the solenoid was energized releasing the catch to the plywood cover and exposing the collection surface. Closing of the traps prior to release was necessary to prevent dust contamination of the adhesive. A collector in the closed and opened positions is shown in Figure J.1.

The collecting media used in the fallout units was the standard adhesive coated cellulose acetate sticky paper measuring 0.0015" x 13" x 13". The adhesive was clear, colorless, and pressure sensitive over a temperature range of 0-65°C. The adhesive was protected with a sheet of glassine paper which was removed prior to placement of the plywood boards.

NFC 9729

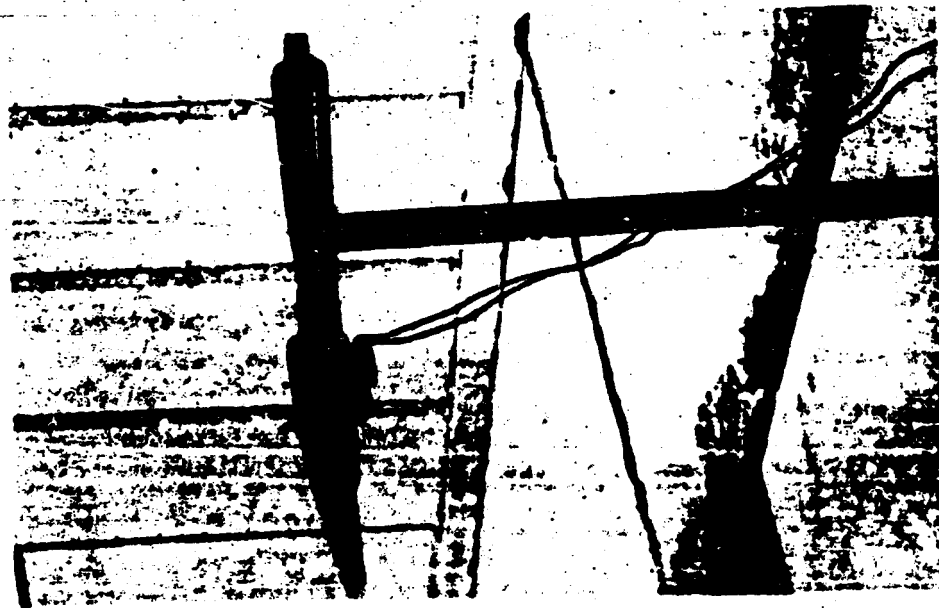
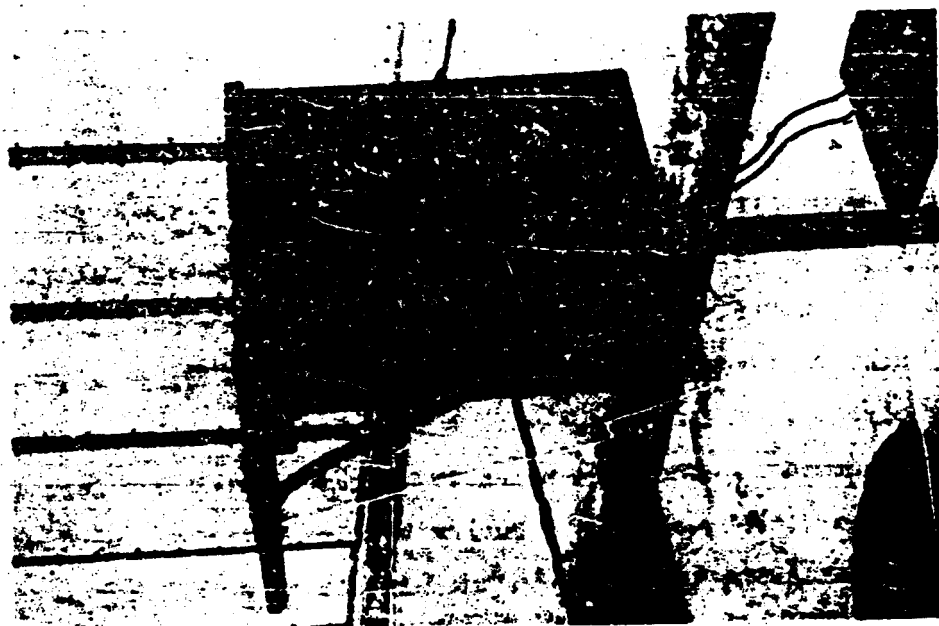


FIGURE 1.1 STICK-PAPEE FALLOUT TRAPS

Following each release, the adhesive coated papers were removed from the fallout units, placed in individual envelopes, and shipped to Fort Worth for analysis.

In addition to the sticky paper collectors, fallout samples were collected in sand and water trays placed at selected grid locations. A liter of water was placed in plastic trays which were 135 square inches in area and 5 inches deep. About 250 ml of acid-washed Ottawa sand was placed in metal trays which were 161 square inches in area and 2 inches deep. The samples were transferred to jars and taken to the laboratory where analyses were performed by the AEC-IDO Health and Safety Group. (Ref. 9).

J.2 Sticky Paper Analyses

Each sample selected for analysis was removed from its envelope in a Blichman hood, rolled and placed in a 1.5" x 7/8" plastic container. After each sample was marked according to health physics requirements, it was removed to the low-level counting laboratory.

J.3 Sand and Water Analyses

Each sample was thoroughly mixed in the jar and a 50 ml aliquot was taken for gross gamma counting, using a thallium activated sodium iodide well counter. The activity of the aliquot was then scaled up to the total sample volume to obtain gross

gamma activity in counts per minute. Following gross gamma counting, gamma spectra were taken of those samples obtained from each arc showing the highest activity.

Gamma spectra of sand and water samples collected during aged Releases A and D showed C_{80}^{137} - B_{80}^{137m} to be present while samples collected during green fuel-element releases showed the presence of I^{131} , Ru^{103} , Cs^{137} , and Zr^{95} .

From these spectra, quantitative estimates were made of the major isotopes in the fallout samples. Stepwise, subtraction of standard spectra for the isotopes in the sample gave the area under the photo peak for the isotope in question. Fallout activities for Releases D, E, F, G, and H corrected for decay are given in Tables J.1 through J.5.

Strontium-90 analyses were also made on water samples obtained during Release F. Each of the samples showed less than the detection limit of 10^{-5} microcuries per square foot. No further Sr^{90} gamma analyses were made.

J.4 Results

Deposition velocities of the various isotopes are given by the ratio of airborne activity concentration to ground contamination level for the same sampling station. Deposition velocities of the major isotopes are tabulated in Tables J.6 through J.10.

TABLE J.1
Release D - Aged Element

Sample	Arc	Station	Fallout, m/c per Sq. Ft.
Water	100	21	(Cs ¹³⁷) 31
		26	41
		31	140
		36	57
		41	95
		48	120
		51	52
		56	1.9
	200	38	4.1
		43	16
		48	32
		53	6.2
	400	36	1.4
		41	1.4
		46	3.6
		56	2.8
Sand	100	46	60
	200	53	1.3
	400	41	1.8

TABLE J.2

Release E - Green Element

Sample	Arc	Station	Fallout, m/c per Sq. Ft.			
			I ¹³¹	Ru ¹⁰³	Cs ¹³⁷	Zr-Nb ⁹⁵
Water	100	26	3000	57		
		31	3200	110		120
		36	3600	86		
		41	1500	390		90
		46	1400	100		
		51	1400	100		
Sand	100	26	720	22	4.8	5.6
		36	760	84	23	48
		46	340	48	9.6	18
	200	23	72	4.0	3.8	
		48	48	3.6	1.9	

TABLE J.3

Release F - Green Element

Sample	Arc	Station	Fallout, m/c per Sq. Ft.	
			I ¹³¹	Ru ¹⁰³
Water	100	11	950	45
		16	620	47
		21	1400	110
		26	1900	110
		36	2200	62
Sand	200	13	260	28
		23	520	52
		28	520	34
	400	26	100	52
	100	16	300	30
		26	120	10
	200	28	110	11

TABLE J.4
Release G - Green Element

Sample	Arc	Station	Fallout, m/c per Sq. Ft.		
			I ¹³¹	Ru ¹⁰³	Zr ⁹⁵ -Nb ⁹⁵
Water	100	6	300	1700	1600
		11	670	710	1000
		16	760	670	670
		21	900	81	150
	200	13	190	57	390
		18	90	290	170
	400	11	57	48	76
	800	13	29	4.8	
Sand	100	16	250	110	160
	200	8	60	19	88
	400	16	19	3.0	2.6

TABLE J.5
Release H - Green Element

Sample	Arc	Station	Fallout, m/c per Sq. Ft.		
			I ¹³¹	Ru ¹⁰³	Zr ⁹⁵ -Nb ⁹⁵
Water	100	6	460	22	
		11	810	520	
		16	460	1300	2600
		21	67	520	260
	200	8	210	95	100
		13	220	460	520
		18	57	470	570
	400	11	140	21	28
		16	40	120	100
	800	13	85	34	27
Sand	100	16	280	160	230
	200	8	100	25	34
	400	16	14	20	22
	800	8	6.4	1.1	1.2

¹³⁷Cs Deposition Velocity

Release	Sample	Velocity Per Location (cm/sec)					
		100m	200m	400m	800m	1600m	3200m
A	SP	0.0278 ± 0.015	0.0215	0.0242	0.0277	0.0658	--
	Sand	0.02 ± 0.012	0.063 ± 0.058	--	--	--	--
	H ₂ O	0.044 ± 0.015	0.025 ± 0.006	--	--	--	--
B	SP	0.0805	0.0888	0.0623	0.0213	0.0178	0.0152
	Sand	--	--	--	--	--	--
	H ₂ O	--	--	--	--	--	--
C	SP	0.2781	0.1021	0.0654	0.0694	0.0437	0.0447
	Sand	--	--	--	--	--	--
	H ₂ O	--	--	--	--	--	--
D	SP	0.0868	0.0935	0.0767	0.0511	0.0466	--
	Sand	0.0363	0.0197	0.0654	--	--	--
	H ₂ O	0.244 ± 0.157	0.0702 ± 0.027	0.0554 ± 0.013	--	--	--
E	SP	0.15 ± 0.06	0.0798	0.110	0.140	0.177	0.442
	Sand	0.25 ± 0.09	0.49 ± 0.24	--	--	--	--
	H ₂ O	--	--	--	--	--	--
F	SP	--	--	--	--	--	--
	Sand	--	--	--	--	--	--
	H ₂ O	--	--	--	--	--	--
G	SP	--	--	--	--	--	--
	Sand	--	--	--	--	--	--
	H ₂ O	--	--	--	--	--	--
H	SP	0.17 ± 0.05	0.14 ± 0.04	0.067 ± 0.034	0.093 ± 0.023	0.19 ± 0.18	0.0473
	Sand	--	--	--	--	--	--
	H ₂ O	--	--	--	--	--	--
I	SP	0.072	0.074	0.108	0.189	--	--
	Sand	--	--	--	--	--	--
	H ₂ O	--	--	--	--	--	--

TABLE J.7

Ru¹⁰³ Deposition Velocities

Release	Sample	Velocity Per Location (cm/sec)					
		100m	200m	400m	800m	1600m	3200m
E	SP Sand H ₂ O	1.3+0.5 0.42+0.05 1.7+0.5	0.68 0.32+0.14 --	0.866 -- --	0.975 -- --	2.88 -- --	-- -- --
F	SP Sand H ₂ O	-- 0.4+0.33 1.58+0.71	-- 0.26 2.24+1.4	-- -- --	-- -- --	-- -- --	-- -- --
G	SP Sand H ₂ O	-- -- --	-- -- --	0.15 1.25 --	-- -- --	-- -- --	-- -- --
H	SP Sand H ₂ O	2.4+0.79 0.68 3.9+2.8	3.1+1.2 0.47 4.97+3.46	1.2+0.79 0.75 2.8+2.14	2.8+1.3 1.92 2.14	4.2+2.5 -- --	1.61 -- --

TABLE J.8

Ce¹⁴¹ Deposition Velocities

Release	Sample	Velocity Per Location (cm/sec)					
		100m	200m	400m	800m	1600m	3200m
E	SP Sand H ₂ O	0.13+0.07 -- --	-- -- --	-- -- --	2.27 -- --	-- -- --	-- -- --
H	SP Sand H ₂ O	0.40+0.29 -- --	0.34+0.13 -- --	0.62+0.67 -- --	1.7+1.7 -- --	0.12+0.026 -- --	0.267 -- --

TABLE J.9
Zr⁹⁵-Nb⁹⁵ Deposition Velocities

Release	Sample	Velocity Per Location (cm/sec)					
		100m	200m	400m	800m	1600m	3200m
E	SP	0.7 ± 0.3	0.72	--	1.25	0.483	--
	Sand	1.2 ± 0.25	--	--	--	--	--
	H ₂ O	4.8 ± 1.9	--	--	--	--	--
F	SP	--	--	--	--	--	--
	Sand	--	--	--	--	--	--
	H ₂ O	--	--	--	--	--	--
G	SP	--	--	--	--	--	--
	Sand	--	--	0.22	--	--	--
	H ₂ O	--	--	3.8	--	--	--
H	SP	1.65 ± 0.53	1.7 ± 0.61	0.69 ± 0.31	3.9 ± 3.4	0.69 ± 0.12	1.85
	Sand	1.02	9.0	0.9	4.8	--	--
	H ₂ O	8.5 ± 3.2	-3.1 ± 8.95	2.4 ± 1.61	1.61	--	--

TABLE J.10
I-131 Deposition Velocities

Release	Sample	Velocity Per Location (cm/sec)					
		100m	200m	400m	800m	1600m	3200m
E	SP	1.1	1.3	0.92	1.15	1.08	--
	Sand	0.43+0.05	0.67+0.24	--	--	--	--
	H ₂ O	1.8+0.05	--	--	--	--	--
F	SP	0.58	0.52	0.80	0.75	0.82	--
	Sand	0.29+0.185	2.6	--	--	--	--
	H ₂ O	3.2+2.3	1.4+0.21	--	--	--	--
G	SP	--	--	--	--	--	--
	Sand	--	--	--	--	--	--
	H ₂ O	--	--	--	0.45	--	--
H	SP	1.35	2.7	--	1.35	0.78	--
	Sand	0.54	0.54	0.32	0.5	--	--
	H ₂ O	0.91	1.2+0.1	1.32+0.5	2.34	--	--

APPENDIX K

External Dose Measurements

K.1 Equipment

The monitoring unit for measuring gamma radiation under conditions encountered in the field was designed by Convair, Fort Worth. A complete unit is shown in Figure K.1. The aluminum can shown on the left of the Figure contains the detector and circuit components.

The detector is a plastic scintillation crystal (NE-102) mounted on a Dumont 6292 photomultiplier tube. The output of the photomultiplier tube provides the input signal for a transistorized pulse integrator-amplifier section, and the output of this section is coupled to the Esterline-Angus recorder which serves as the indicating device. Power for the photomultiplier tube is provided by a 1250 volt battery mounted within the aluminum can.

The monitors were positioned along the 400-meter arc at 3 degree intervals; a total of 21 units were used.

K.2 Calibration

The magnitude of the count rate was established by laboratory calibration of the unit. A pulse-generator signal was applied to the transistor circuit input and adjusted until the selected pulse rate produced full scale reading on the recorder.

Following the initial alignment of the circuits, as described above, each unit was calibrated in the field with a 0.95 mc Cs^{137} - $\text{Ba}^{137\text{m}}$ source. The response of each monitor was determined

NPC 1921
31-3798



1.1 PORTABLE SCINTILLATION DETECTOR AND RECORDER

as a function of the calculated dose rate. The dose rate was computed from the following relationship:

$$D = \frac{6.3 E C}{X^2}$$

where D = dose rate in Roentgens per hour, E = energy of the radiation in Mev., C = source strength in curies, and X = distance from source to detector in feet. Calibration curves of dose-rate vs. recorder reading were obtained for each sensitivity range of all of the monitors. Figure K.2 shows a typical set of curves from the field calibration data.

Extrapolating each range to full scale deflection in Figure K.2 gave the following calibration for that particular unit:

<u>Range</u>	<u>Coverage</u>
Linear I	Bkg. to 0.36 mr/hr
Linear II	Bkg. to 1.3 mr/hr
Linear III	Bkg. to 15 mr/hr
Logarithmic	Bkg. to 40 mr/hr

The maximum dose-rate reading of the most sensitive scale, Linear I, could be adjusted within a wide range of values by proper selection of the voltage that was applied to the photomultiplier tube. This procedure automatically determined the range of the other three scales. The shape of their response curves did not change; the only noticeable effect was that the curves were displaced along the abscissae of Figure K.2, the direction depending on whether the voltage was raised or lowered.

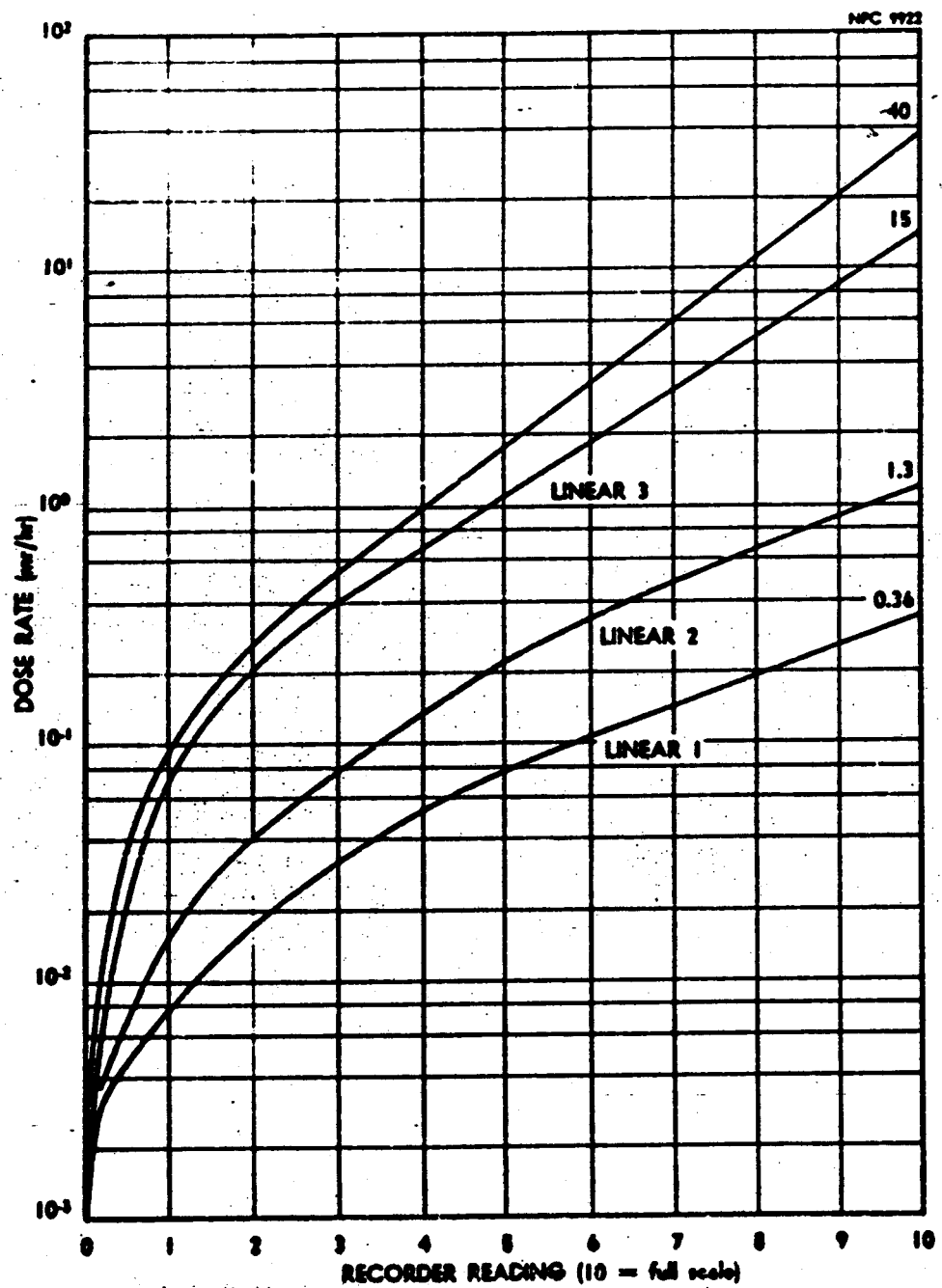


FIGURE K.2 DOSIMETER CALIBRATION CURVES

Consequently, a convenient means of adjustment was available during prerelease calibration of the monitors.

The response curves of Figure K.2 show that the scale sensitivities were not constants. In the ranges selected for use during PRT-1, the monitors could detect a change of 0.002 mr/hr above background on scale Linear I, 0.004 mr/hr above background on scale Linear II, and 0.01 mr/hr above background on scales Linear III and logarithmic. For the nearly linear portions of the curves of Figure K.2 the sensitivity of the units are listed in Table K.1.

TABLE K.1
Dosimeter Calibration

Scale	Sensitivity mr/hr per recorder chart dimension
Linear I	0.026
Linear II	0.034
Linear III	0.045
Logarithmic	0.055

The response of the crystal is relatively constant from energies of about 0.6 Mev and higher but drops off rather sharply for small energies. The monitors were calibrated with a Cs^{137} - $\text{Ba}^{137\text{m}}$ source, and, since the only gamma emitting element present in the effluent of the aged fuel elements was $\text{Ba}^{137\text{m}}$, the external gamma dose rate from these releases was read directly from the recorder chart of the monitor units.

or the green releases a correction was applied to the chart data to compensate for the energy dependence of the scintillation crystal detector.

3 Procedure

Each monitor was placed in an individual, open-end shelter in the field. The three remaining sides and the base of each shelter were constructed of 0.25 in. plywood. The top of the shelter was canvas, providing shade and rain protection for the crystal and photomultiplier tube.

After each release the monitors were removed from the network to the Convair trailer. There, the recorded data could be removed quickly, and the proper maintenance and calibration performed on each monitor. In addition, complete protection from the weather was obtained and radioactive contamination of the units was held to a minimum. The operational procedure consisted of the following steps:

1. Pre-release check-out and calibration of each monitor in the Convair trailer.
2. Transporting the units to the 400-meter arc.
3. Setting the recorder chart speed on "high" and inserting a time reference on the chart.
4. Following the release, the units were collected from the field, calibrated and taken to the Convair trailer.
5. The recorder chart was removed from each unit and properly labeled as to release number and monitor position.
6. Prior to the next release, the units were serviced and any necessary maintenance performed.

K.4 Data Handling

The external dose-rate monitors were included in the experiment primarily to measure the maximum dose-rate and the integrated dose occurring along the 400 meter arc during each release. To extend the usefulness of the monitors, the chart speed of each was determined to an accuracy of 1 part in a 1000. The chart speed used most often was about $3/4$ inch per minute, and by arbitrarily considering $1/16$ inch of chart distance as a lower limit of the resolution of the recorders, the time dependence of the activity was measured to within about 5 seconds. Consequently, a time-activity profile of the effluent could be made at each monitor station for each release. The effluent, as it passed over the 400-meter arc, generated activity indications on the recorders such that when the data from each station was plotted simultaneously on a time axis, a "contour map" of the cloud activity was obtained by connecting areas of equal dose-rates.

APPENDIX L

Radiochemical And Counting Techniques

L.1 Furnace Effluent Analyses

Furnace effluent from Release P was analysed to determine (a) the percent of nuclides released and (b) the time of nuclide release.

Radionuclides from inside and outside the sequential sampling tubes were removed separately. This was achieved by first plugging the tube with Teflon stoppers and removing the outside activity. The plugs were then removed and the inside activity extracted. A combination of chemical action and mechanical agitation was necessary to affect the desired removal of radioactivity from the metal surface. Since most of the deposited radioisotopes were most probably in an oxide form, it was felt that a reducing agent such as oxalic acid would be helpful in the decontamination process. A model T-52 ultrasonic transducer, manufactured by the Branson Ultrasonic Corporation and ultrasonic generator were used to aid the decontamination of the sequential sampling tubes. The tube was placed in a plastic bag containing 300 ml of 5 percent oxalic acid, and the bag and its contents were then put into the water of the ultrasonic transducer. After 20 minutes of agitation, about 50 to 60 percent of the radioactivity was removed. It was necessary to repeat this operation three or four times to obtain an overall removal of 90 percent.

The radioactivity remaining on the tube was measured with an end window counter. Gamma spectrum analyses of the cleaned tubes indicated that the gamma activity retained on the tube had about the same isotopic distribution as that which was removed.

A measured aliquot of the tube washings was placed on a specific quantity of absorbent paper, sealed in a polyethylene bag, and analyzed with a 256-channel spectrometer. A 100-ml aliquot of the washings from the inside of the tube was used for strontium analysis.

The isotopic activities deposited on the outside of the tubes are presented in Table L.1. No strontium analysis was made on the activity outside the tubes. Table L.2 gives the activity retained inside the tubes. No I^{131} could be located in the sampling probe tubes because the tubes were probably too hot for iodine condensation to occur. Tube number 10 was a dummy tube closed at one end. It served to estimate the amount of diffusion taking place in a tube when not open for sampling. The activity deposited inside a tube caused by its operation is equal to the activity inside the tube minus the activity inside tube number 10.

Radioactivity was removed from the glass wool filter by dissolving it in a nitric acid solution. The filter and the elbow were placed in a three-necked flask after which 150 ml of 20-percent HNO_3 were added. The solution was brought to a gentle boil and refluxed for 2 hours. The caustic scrubber served to

TABLE L.1
Radioactivity on the Sampling Probe Tubes

Tube No.	Isotopic Activity, (mc) (corrected to release time)		
	Cs ¹³⁷	Ru ¹⁰³	Ce ¹⁴¹
1	0.21	3.2	No Activity Detected
3	0.28	2.3	" " "
4	0.10	3.7	" " "
5	0.17	3.0	" " "
6	0.15	3.0	" " "
7	0.10	3.7	" " "
8	0.21	2.4	0.006
9	0.15	4.2	0.065
10	0.13	2.9	No Activity Detected
11	0.10	2.8	" " "
12	0.13	2.6	" " "
13	0.08	2.4	" " "
TOTAL	1.81	36.2	0.071

TABLE L.2
Radioactivity in the Sampling Probe Tubes

Tube No.	Isotopic Activity, (mc)(corrected to release time)				
	Zr ⁹⁵ -Nb ⁹⁵	Cs ¹³⁷	Ru ¹⁰³	Ce ¹⁴¹	Sr ⁸⁹
1	0.64	1.1	5.1	0.14	0.060
3	NAD*	0.035	0.51	NAD	0.024
4	0.025	0.055	0.42	0.004	0.021
5	0.11	0.065	0.86	0.012	0.047
6	0.080	0.034	0.68	0.006	0.009
7	0.32	0.043	1.5	0.003	0.012
8	0.064	0.039	0.49	0.040	0.010
9	0.012	0.010	0.18	0.002	0.002
10	0.035	0.008	0.24	0.002	0.015
11	NAD	0.013	0.58	NAD	0.014
12	0.025	0.006	0.21	0.002	0.002
13	NAD	0.004	0.20	NAD	0.003
TOTAL	1.311	1.412	10.97	0.211	0.219

• No Activity Detected

TABLE L.3

Radioactivity on the Glass Wool Filters

Elbow	Isotope Activity, (μ c)(corrected to release time)					
	Zr ⁹⁵ -Nb ⁹⁵	Cs ¹³⁷	Ru ¹⁰³	I ¹³¹	Ce ¹⁴¹	Sr ⁸⁹⁺⁹⁰
1	NAD*	12	2.1	NAD	NAD	
2	"	0.051	0.13	24	"	
3	"	0.24	0.28	6400	"	NAD
4	"	0.11	0.006	1460	"	"
5	"	0.21	0.14	420	"	
6	"	0.48	0.11	73	0.086	
7	9.2	2.9	0.11	NAD	0.18	NAD
8	1.2	31	0.94	NAD	0.092	"
9	1.7	2.4	0.38	3.1	0.007	"
10	NAD	0.20	0.088	7.3	0.002	"
11	0.002	0.13	0.004	1.5	0.001	
12	NAD	0.035	0.001	0.42	NAD	

TOTAL 12.1 49.75 4.289 83.89 0.363

• No Activity Detected

retain the volatile fission products such as iodine and ruthenium tetroxide. Two consecutive extractions with nitric acid were sufficient to remove over 90 percent of the activity. The removal was checked with a Cutie-Pie ionization chamber.

The nitric acid extract and the caustic scrubber solutions were both diluted to a liter, and aliquots from each were taken for gamma spectrum and radiochemical analyses. Aliquots of the solution were filtered; and the filter pads, after being sealed in polyethylene bags, were analyzed by gamma spectroscopy. A 3" NaI crystal was calibrated with Cs^{137} , Ru^{103} , and I^{131} standards, using the appropriate geometry.

The radioactivity deposited on the glass wool filters is shown in Table L.3.

L.2 Network Sample Analyses

Chemical analyses of the pleated filters for strontium and ruthenium were undertaken as follows: (1) the filter was placed in a 10 percent HCl solution, containing 20 mg of Sr and 10 mg of Ru "carrier". (2) After digestion for 30 minutes in HCl, the solution was filtered into a volumetric flask and diluted to 100 ml. (3) For strontium, an aliquot (50 ml) was taken from this flask, evaporated to a small volume, and 10 gm of Sr carrier added. Strontium was precipitated in water. (4) A second Sr precipitation was obtained with fuming nitric acid. Again the precipitate was dissolved in water and contaminating activities

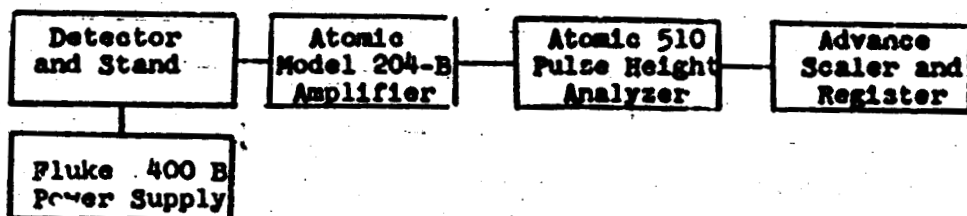
were removed by ferric hydroxide scavenging. Strontium was precipitated as $\text{SrC}_2\text{O}_4 \cdot \text{H}_2\text{O}$. This was filtered, washed, dried, weighed, and counted for beta activity with an end window counter.

For ruthenium, (after step 2 above) a 10-ml aliquot was taken from the flask and 10 mg of Ru carrier added. To this solution NaBiO_3 , H_3PO_4 , and HClO_4 were added. Ruthenium (present as RuCl_3) was oxidized to RuO_4 which was distilled and collected in an NaOH solution. The RuO_4 was reduced by ethyl alcohol, precipitating the Ru as lower valence oxides. These oxides were dissolved in HCl and the resulting RuCl_3 reduced by Mg to metallic Ru. After washing, drying, and weighing, the ruthenium was counted with an end window counter for beta activity.

L.3 Counting Procedure

Samples were delivered to the "hot laboratory", where selected samples were wrapped prior to counting. Fall-out paper samples were sealed in 7/8-inch diameter plastic vials. The pleated-filter and carbon-cartridge samples were sealed in Saran Wrap to prevent contamination of counters and handling areas.

Deposited Activity: The fall-out paper samples were counted on a single channel pulse height analyzer (see block diagram below).



The detector used was an 8F8 well-type NaI(Tl) (1-1/8" x 1-1/2" well) mounted on an RCA 6655 photomultiplier. The detector and pre-amplifier were mounted in a 2-inch lead shield to reduce background. The counter was standardized at the beginning of each day's run and approximately every four hours during the two-shift operation. Cs¹³⁷ or I¹³¹ standards were used for this standardization depending on whether cesium or iodine samples were to be counted. The amplifier gain was adjusted so that the 0.364-Mev and 0.662-Mev photopeaks were arbitrarily set at 21 and 33 divisions (volts) for the I¹³¹ and Cs¹³⁷ samples, respectively. The counter was standardized for Ba¹⁴⁰-La¹⁴⁰ counting by setting the I¹³¹ photopeak (0.364 Mev) at 13 divisions. After standardization the baseline was set at 18 divisions (for I¹³¹ samples) and 30 divisions (for Cs¹³⁷ samples) and in each case the window was set at 6 volts so that the counting interval included the respective photopeaks. The baseline was set at 40 divisions (for Ba¹⁴⁰-La¹⁴⁰ counting) and an integral count was made. Background counting rates were determined for the pulse-height interval of interest prior to the counting of samples.

Airborne Activity: The pleated-filter and carbon-cartridge samples were counted on the RCL Mark 20 Model 2603-2607 (Argonne Type) 256 Channel Spectrometer. The detector used was a 3 x 3-inch NaI(Tl) solid cylinder (Harshaw mounted) on a Dumont 6393 photomultiplier. The phototube, crystal, and pre-amplifier

were mounted in an upright hollow lead cylinder that provided 3 inches of lead shielding on all sides. The 256-channel analyzer was modified so that an integral (gross) counting rate could be made. A pair of Atomic 1090 series multiscalers were ganged for this integral count. The spectrometer was standardized at the beginning of each day's run and approximately every four hours thereafter during the two-shift operation. The standard used was a fall-out paper sample (Cs^{137}). The gain was adjusted so that the photopeak (0.662 Mev) occurred at 7 divisions on the analyzer display scope. An integral count was then made and this value compared to previous values. The gain was then reduced by one-half and the background counting rate determination made prior to counting samples. This reduction in gain resulted in an analysis range of from 0 to approximately 2 Mev for the spectral measurements. A gross counting rate was taken for each sample analyzed, but only representative spectra were taken for most samples. The exception was Release H, in which spectra were taken for all the samples analyzed.

Those samples with activities over approximately 2×10^6 CPM were positioned at 10.2 cm above the crystal. Counting determinations were then made and efficiencies for this position were measured. All other measurements were made with the sample placed on the crystal container.

L.4 Spectral Analyses: Samples that showed sufficient gamma activity were analyzed in an RCL-256 channel analyzer. In general, the spectra of the samples collected during green releases showed the presence of several different peak energies. In conjunction with the energy calibration data and half-life measurements, the parent isotopes were identified. Through the application of several correction procedures, quantitative measurements of the total sample activity, and consequently the total quantity of each isotope present, were obtained.

General: The nature of the 256-channel analyzer "penout" system is such that the area under the photopeak spectral curve is proportional to the total quantity of active material present in the sample. When only a monoenergetic gamma is present, it is an easy matter to measure the area under the curve and convert the result to sample activity using the proper efficiencies and conversion factors. When the sample contains several gamma emitting isotopes, the analysis of the spectrum becomes more involved. Since Compton scattering of the gamma rays occurs in the detector crystal, monoenergetic gamma rays are detected as a distribution of energies. When several such gammas are present, the less energetic photopeaks are superposed on the Compton distribution of the higher energy gammas. This effect must be taken into account when measuring the intensity of each photopeak.

Certain of the photopeaks of interest in these analyses consist of more than a single energy gamma ray. For example,

the $\text{Zr}^{95}\text{-Nb}^{95}$ photopeak is a composite of four energies:

Zr^{95} : 0.768, 0.724 Mev

Nb^{95} : 0.740 Mev

I^{131} : 0.722 Mev

Also, the Cs^{137} photopeak at 0.662 Mev contains contributions from Ru^{103} : 0.610 Mev, and I^{131} : 0.637 Mev. In both cases, the gammas appear as a single but broadened photopeak because the resolution of the NaI detector is not sufficient to separate them into discrete photopeaks. Consequently, in measuring the gamma ray intensity of such photopeaks, a correction must be applied to account for the build-up to the peak height by the interfering gammas. It is to be noted, however, that the composite peak height is used when applying the Compton scattering correction because the detector handles all of the incoming gammas lying in a small energy range very nearly alike.

Unlike ordinary gross counting techniques, a constant background figure can be subtracted from each photopeak height only when the total sample count is much larger than the background at the energy being considered. In cases where the sample activity is nearly equal to or less than the background, account must be taken of the energy distribution of the background radiation

The difficulties listed above apply to the determination of the photopeak height of the photon energy of interest. To

obtain the desired quantitative results, corrections must also be made for the counting time, photo efficiency, crystal detection efficiency factors, detector-sample geometry factor, and percent occurrence of the photon being studied. To convert the corrected

for the length of time the standard was run), and the resolution. Table L.4 indicates the results.

Column f of Table L.4 represents the photon occurrence fraction of the isotope indicated. These values were obtained from the literature (Ref. 17).

The basic method used to resolve complex spectra consist first of determining the shape of the photopeak and Compton distribution of the most energetic gamma present. In order to determine the shape of the Compton scattering portion of the curve, a set of empirical values was established which described the spectral envelope as a function of energy. This was accomplished by taking separate spectra of Cs^{137} , Ru^{103} , I^{131} , Zr^{95} - Nb^{95} standards. In the Compton scattering portion of these spectra, selected points along the envelope were expressed as a percentage of the photopeak height, so that in order to sketch-in the Compton scattering section of the sample curve, it was necessary only to measure the photopeak height and multiply it by the appropriate percentage at a preselected energy value. At low energy photopeak positions, the Compton contribution from higher energy photons can be calculated and subtracted out. This process continues for each photopeak present in the spectrum. Table L.5 lists the values for the pertinent isotopes of FRT-1 samples.

The method used to obtain Compton percentages with respect to photopeak height in Cs^{137} spectrum is shown in Figure L.1. The

TABLE L. 4

Spectra Analyses Correction Factors

Isotope and E_γ (MeV)	Resolution R_s	Photo Fraction P (E)	Detection Efficiency ϵ (E)				Occurrence f
			Carbon Cartridges	Andersen Plates	Gelman or Millipore Filter	Plated Filter	
La^{140} (1.60)	5.2	0.24 ± 0.02	-	-	-	0.090	0.41
$\text{Zr}^{95-\text{Mo}^{95}}$ (0.762)	10.8	0.431 ± 0.04	0.173	0.228	0.220	0.155	0.98
Cs^{137} (0.662)	10.6 ± 0.05	0.479 ± 0.007	0.186	0.247	0.237	0.167	0.92
Ru^{103} (0.498)	11.7 ± 0.15	0.582 ± 0.07	0.207	0.273	0.262	0.185	0.90
I^{131} (0.364)	12.8 ± 0.5	0.684 ± 0.015	0.232	0.306	0.295	0.201	0.80
Ce^{141} (0.145)	18.3 ± 0.1	0.88 ± 0.030	0.274	0.360	0.350	0.221	0.67

TABLE L.5

Compton and Gamma Build-up Correction Factors*

$E_{\text{Mev}} \backslash E_{\text{Mev}}$	$\text{Zr}^{95}\text{-Nb}^{95}$ (0.762) Percent	Cs^{137} (0.662) Percent	Ru^{103} (0.498) Percent	I^{131} (0.364) Percent	Ce^{141} (0.145) Percent
$\text{Zr}^{95}\text{-Nb}^{95}$ (0.762)	-	4.75 ± 0.38	20.0 ± 0.56	19.8 ± 0.20	20.3 ± 0.13
Cs^{137} (0.662)	-	-	6.8 ± 0.48	15.7 ± 0.70	15.6 ± 0.50
Ru^{103} (0.498)	-	10.75	-	3.8 ± 0.30	1.40 ± 0.50
I^{131} (0.364)	0.90 ± 0.1	4.1 ± 0.2	-	-	14.7 ± 0.73

* To use Table, select the isotope from the left hand column whose true peak height (h) is known. The numbers in the columns to the right of this isotope indicate its Compton contribution to the various isotope photopeaks listed. Examples: to correct the Ru^{103} photopeak for Cs^{137} Compton contribution, multiply the measured height (h) of Cs^{137} by 6.8%. Likewise, $h \times 15.7\%$ is the Cs^{137} contribution to the I^{131} (0.364 Mev) photopeak.

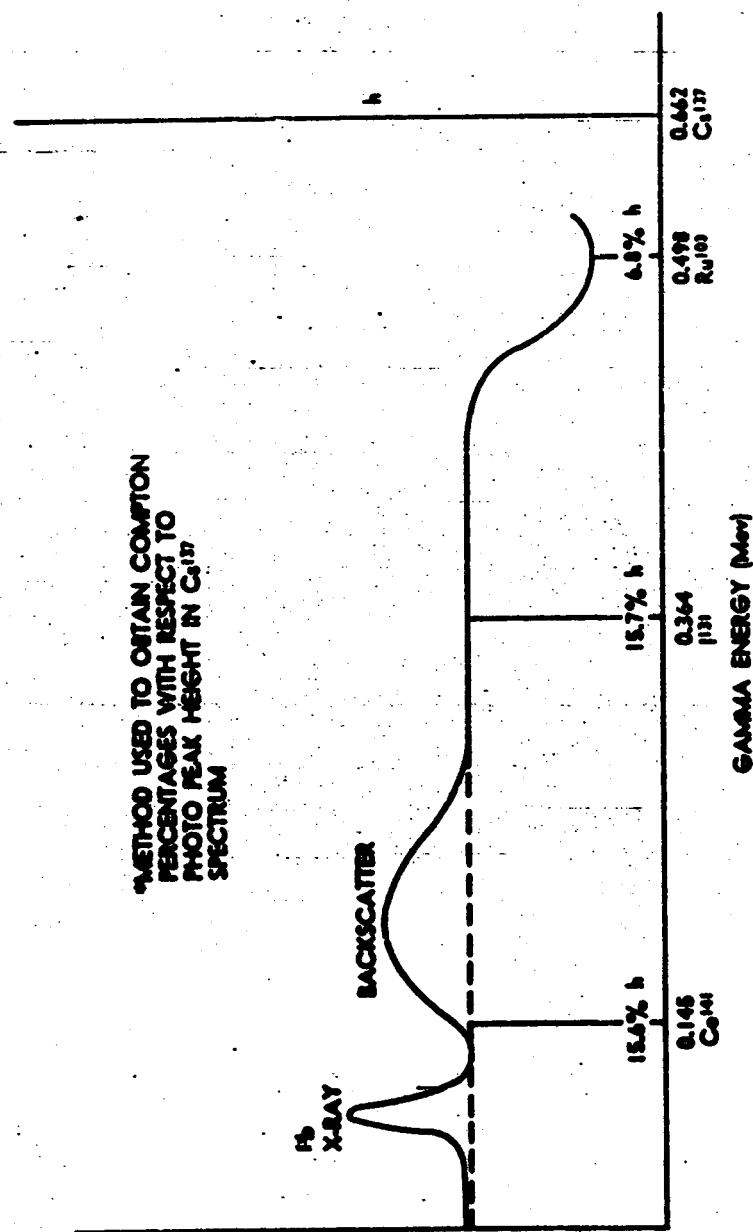


FIGURE L1 COMPTON BUILDUP IN Cs^{137} SPECTRUM

photopeak takes the shape of a Gaussian distribution, and since the area beneath this curve represents sample activity, the area under the curve must be found. It can be shown that the area under a Gaussian distribution curve is equal to 1.0645 times the area of an inscribed isosceles triangle. The area of the isosceles triangle is $h \times \Delta L$, where ΔL is the width of the curve at half maximum. The area under the Gaussian distribution curve becomes:

$$A = 1.0645 \cdot h \cdot \Delta L \quad (1)$$

In practice, it was often impossible to measure ΔL because of interfering photopeaks and Compton contributions. To circumvent this difficulty, the detector resolution:

$$R = \frac{\Delta L}{L} \quad (2)$$

was empirically predetermined for each primary photon energy to be analyzed. L is the measured length from the photopeak centerline to zero energy, Figure L.2. Knowing R , and L being measurable on each spectrum to be analyzed, $\Delta L (=R \times L)$ is easily obtained.

NPC 9724

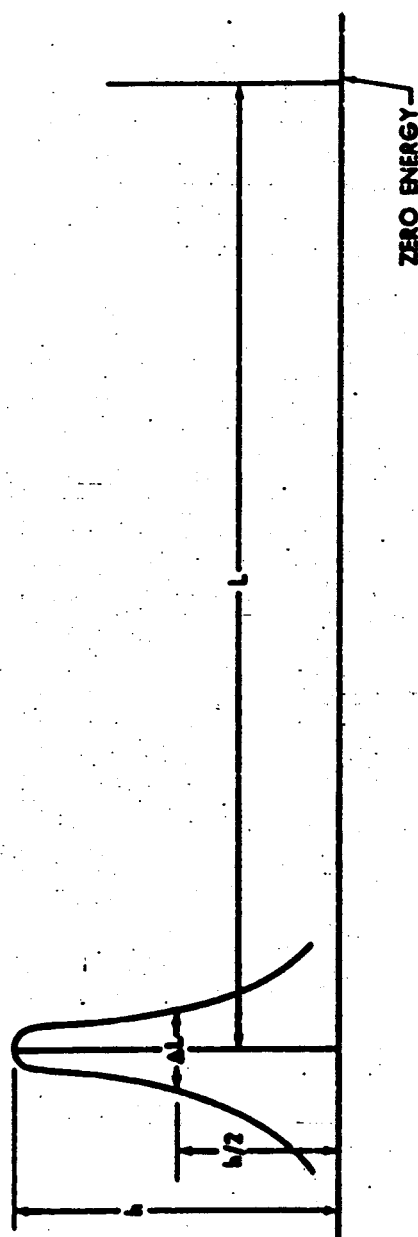


FIGURE L2 PHOTOPEAK AND ZERO ENERGY POSITIONS

Substituting for ΔL , Eq. 1 becomes:

$$A = 1.0645 \cdot h \cdot L \cdot R. \quad (3)$$

Values of R are listed in Table L.4 for the isotopes of interest. It is worth pointing out that R , as defined, is independent of the gain setting in the spectrometer system.

The height, h , can be measured directly from the recorder chart in total counts, and division by the gate-on-time gives the counting rate for the peak energy channel (counts/sec-channel). The length, L , must be converted to channels per unit length, for whatever unit of length is used. This conversion factor can be obtained by dividing the 256 channels by the carefully measured distance required to pen them out on the Brown Recorder chart paper. Note that this conversion figure is dependent on the gain setting of the spectrometer system. Eq. 3 becomes (in units of counts/sec):

$$A = \frac{1.0645 \cdot h \cdot L \cdot R \cdot K}{t} \quad (4)$$

where K is the actual number of channels per unit length, and t is the gate-on-time in seconds. Taking into account the photons which undergo Compton scattering, the total detected counting rate becomes:

$$N' = \frac{A}{P(E)} \quad (5)$$

where $P(E)$ is the photo-fraction as defined above for photons of primary energy E . Equation 5 must also be divided by the detection efficiency, $\epsilon(E)$, to obtain the total 4-pi gamma emission by the sample for the photopeak under analysis. Equation 5 then becomes:

$$N'' = \frac{\Lambda}{P(E) \cdot \epsilon(E)} \quad (6)$$

Since Eq. 6 represents the total sample photon emission rate for a particular photon energy, further division by f , the occurrence fraction for the particular photon, gives the number of sample atoms involved in the decay process:

$$N''_T = \frac{\Lambda}{P(E) \cdot f(E) \cdot T} \quad (7)$$

A further refinement can be made by taking into account the time lapse from release to spectral analysis by multiplying Eq. 7 by $e^{\lambda_1 T}$, where T is the time lapse from field release to spectral analysis and λ_1 is the decay constant of the isotope. This gives:

$$C = \frac{1.0645 \cdot h \cdot L \cdot R \cdot K \cdot \lambda_1 T}{\lambda_1 \cdot f \cdot t \cdot P(E) \cdot F \cdot \epsilon(E)} = \frac{\text{DPM-Min}}{ft^3} \quad (8)$$

where C is the effluent activity at the time of release of the i th isotope collected during the sampling period. In Eq. 8, F is the flow rate through the sampler in ft^3/Min .

Equation 8 provided the working basis from which fission product activities of the effluent were obtained using spectrometer data.

Application: The step by step analysis of a spectral chart from the analyzer is outlined below. The procedure is that which was followed in analyzing FRT-1 samples using the values listed in Tables L.4 and L.5. The method is completely general, however, and may be adapted to any isotope provided the appropriate values of the quantities listed in the Tables have been previously obtained:

1. Sketch in the photopeak shapes.
2. Draw in photopeak centerlines and locate the zero energy point.
3. Identify the photopeaks (Energy and isotope).
4. Measure and record the distance from the zero energy point to the centerline of each photopeak.
5. Draw in the average background level as established by background runs. (Take account of scale changes.)
6. Begin the analysis with the highest energy photopeak displayed.
7. Measure the height of this peak in counts above the background level.
8. Multiply the height of the peak by the appropriate percentage listed in Table L.5 to determine the Compton contribution under the lower energy photopeaks. Construct a table so that each photopeak height may be listed and from which background and Compton contributions can be deducted.
9. Measure the height of the second most energetic photopeak above the background plus the Compton contribution from the first peak analyzed.
10. Multiply the height of the second peak by the appropriate percentages in Table L.5 to determine the Compton correction to be applied to the succeeding peaks. The

I^{131} and Ce^{141} peaks are to be treated similarly. Enter the values found in table constructed in step 8 above and deduct them from the background-corrected height of step 7.

11. Continue this process until the lowest energy photopeak is measured. If there is not a definite peak where Ce^{141} or I^{131} should be found, yet the sum of the background and the Compton contributions from higher energy gammas is less than the value of the curve in that region, one is not justified in assuming that the difference is due to the isotope sought. Background contributions may fluctuate considerably, particularly for long gate-on-times or for sample activities close to the level of background activity.
12. After the photopeak height of I^{131} (0.364 Mev) has been obtained, refer to Table K.5 for the empirical value of the contribution to the $Zr^{95}-Nb^{95}$ by I^{131} (0.722 Mev). Also, determine the contribution of Ru^{103} to the Cs^{137} peak. These contributions must be subtracted in order to get the true photopeak height of Cs^{137} and $Zr^{95}-Nb^{95}$.
13. Substitute the net values found in step 11 and the proper quantities from Table L.4 into Eq. 8. Substitute also for K, λ , T, and F to obtain the activity of the i th isotope in the effluent at release time.

L.5 Residue Analyses

Post-melt portions of the radioactive fuel elements were analyzed for the quantities of isotopic activity by the General Electric Vallecitos Atomic Laboratory. No analysis of the aged fuel elements were made. Techniques for analyzing green fuel elements were as follows: (1) the can containing the crucible was

at the time of transfer from the dissolver pot to the 5 liter storage vessel. The solution was diluted to volume and aliquots taken for radiochemical analysis. (2) The residue in the dissolver pot was heated to dryness and KHSO_4 added. Temperature was maintained at 230°C for 8 hours. After cooling, the fusion mixture was dissolved and the aliquot analyzed.

A gamma analysis was run on all unleached crucible pieces and sample residue by means of a 256-channel analyzer using a special scanning plug in the radiation lock of the hot cell. Both Cs^{137} and Co^{60} standards were used for calibration. Table L.6 shows the results of the chemical analysis for three green releases. The values shown are the percentages of the various isotopes retained in the residue and the crucible. A detailed description of the radiochemical analysis is presented in Reference 10.

TABLE L.6

Fuel Element Residue Recovery

Nuclide	Percent Retention		
	Release E	Release G	Release H
Ru ¹⁰³	91	79	93
Ce ¹⁴⁴	86	102	76
Zr ⁹⁵	35	34	48
Sr ⁸⁹	59	41	36
Ba ¹⁴⁰	57	47	26
Cs ¹³⁷	13	2.9	3.4
I ¹³¹	0.10	0.04	0.18
Xe ¹³³	0.16	0	0

APPENDIX M

Radiobiology

Radiobiological tests were performed during the last seven releases by personnel from the University of Rochester (Ref. 11). Detailed biological results are presented under each release in Appendix N. Therefore, only a brief outline of facilities, procedures, and studies performed are outlined in this appendix.

M.1 Facilities

1. An air-conditioned, mobile laboratory was used at the site for dissecting and counting biological specimens.
2. The laboratory was equipped with a 5" x 6" NaI(Tl) crystals which had a 3" x 5" well.
3. Albino rats of the Wistar strain of both sexes weighing between 150 and 200 grams were kept in the laboratory until exposure time.
4. Beagle-type mongrel dogs of both sexes weighing between 7 and 14 kilograms were kept near the laboratory in two trailers specifically designed for housing animals.

M.2 Procedure

1. Animals were placed at various stations on the network grid at least 15 minutes before each release. Table M.1 shows where animals were placed during each release. At least two rats were placed at each station before each of the Releases C, D, E, F, G, and H; before Release I

four rats were placed at each station. Some animals were anesthetized prior to Releases F and G.

TABLE M.1
Animal Locations

Location Release	100-meter	200-meter	400-meter	800-meter
C (aged)	Rats*	Rats*	Rats*	Rats*
D (aged)	Rats*,**	Rats*,**		
E (green)	Rats**	Rats**	Rats**	
F (green)	Rats** Dogs*	Rats*		
G (green)	Rats** Dogs**	Rats** Dogs**		
H (green)	Rats** Dogs**	Rats** Dogs**		
I (aged)	Rats** Dogs**	Dogs**	Dogs**	

* Unrestrained

** Restrained to prevent nose or pelt licking

2. Early post-release recovery of exposed animals was desired.
3. After Releases C, D, E, and F rats were sacrificed in mass by suffocation with CO₂. After Releases G, H, and I, dogs were anesthetized by intravenous injection of sodium pentothal followed by maximal bleeding from the carotid artery.

M.3 Studies Performed

Restraining Cages: During the course of Releases C and D, the effect of restraining cages on GI (gastrointestinal tract) and total-body-internal deposition in rats was investigated. It was discovered that unrestrained rats showed extremely high GI activity presumably because they had licked their noses and fur. In subsequent releases all rats were restrained. A similar effect was noted with unrestrained dogs in Release F. Therefore, the dogs were muzzled for Releases G, H, and I.

Effects of Anesthetization: One-third of the rats in Release F and one-half those in Release G were anesthetized prior to exposure. In the GI tract median activities were reduced by a factor of 4 and 3 respectively for anesthetized and unanesthetized rats. The lower-respiratory-tract deposition (LRD) values were reduced by about 1.5 in each case. However, the LRD reduction is placed in doubt by anomalous total-body-internal deposition (TBI) values.

Lower-Respiratory-Tract Deposition: Radioactivity that was retained in the lungs was correlated with air concentration results to obtain LRD percentages. The median values thus obtained for inhaled activity deposited in the lower respiratory-tract (lung) ranged from 30-35 percent.

Total Body Deposition: Radioactivity was summed for all body organs analyzed and correlated with measured air concentrations to obtain TBI (total body internal deposition) values which had a mean near 70 percent of the inhaled radioactivity.

Sacrifice Times: After Release C there was a delay of 45 minutes before the rats were sacrificed, which resulted in appreciable transference of radioactivity from the lungs to the bloodstream and even to the kidney. Shortening of this time delay to 15 minutes resulted in increasing the ratio of whole body to kidney activity from about 50 to almost 350.

Metabolism Studies: Two exposed dogs from Release G were kept for metabolism studies. Urine and fecal excretion rates and body organ retention times were investigated. Excretion studies indicate:

- . Large portion of activity has a total effective half-life (T_{eff}) of about 10 days.
- . Remainder has a rather long T_{eff} of approximately 100 days.

Dogs' lungs lost about 90 percent of activity in 50 and most of the activity was removed shortly after exposure. The remaining radioactive material was apparently quite stable. Spectral analyses indicated the persistence of Ru^{103} , Cs^{137} and Zr^{95} in decreasing abundance.

Isotope Identification: Decay curves for body organs were plotted for isotopic identification. In a few instances, channel gamma spectroscopy was used to give relative isotope abundances.

APPENDIX N

This appendix contains detailed data on each of the nine Releases A through I.

APPENDIX N-A

(Release A)

A.1 Summary

Type of Sample ----- Aged Fuel Element
Date and Release Time ----- 25 July 1958; 6:09 PM
Lapse Rate (1.5 - 45 m) ----- -0.37°C
Lapse Rate (1.5 - 24 m) ----- -0.05°C
Mean Wind Speed ----- 3.6 meters/sec
Wind Direction ----- Network Centerline
Cloud Photography ----- Both aerial and ground
Fluorescent Tracer ----- Released for 10 minutes
immediately following
fission product release
Animals ----- Rabbits on inner arcs(Ref.9)
Network Radioactivity ----- Detected out to 1600 meters;
maximum reading of pleated
filters on 100-meter arc,
140 mr/hr, using Cutie Pie
External Dose ----- Maximum dose rate on 400-
meter arc, 0.052 mr/hr,
using scintillation detector
described in Appendix K.

A.2 Fuel Element

The fuel element had been irradiated to generate 7×10^4 watts for a total of 467 hours and had decayed for 922 days. The predominant nuclides present at the time of release are shown in Table N.A.1.

TABLE N.A.1

Fission Product Inventory

<u>Nuclide</u>	<u>Curies Calculated</u>
Sr ⁹⁰	4
Ce ¹⁴⁴ - Pr ¹⁴⁴	16
Pm ¹⁴⁷	10
Ru ¹⁰⁶ - Rh ¹⁰⁶	1.3
Cs ¹³⁷ - Ba ^{137m}	3.4

A.3 Meteorological Conditions

The wind directions and velocities prevailing during this release are shown in Table N.A.2

Lapse rates existing at the apex tower during the release, between the 1.5-meter level and both the 24- and 45-meter levels, are shown in Figure N.A.1. It indicates that at the time the furnace was energized, i.e., time zero, a weak lapse condition existed. However, at two minutes after time zero, the estimated time of melting, an inversion condition is evident and continued, except for a short neutral condition, during the remainder of the test.

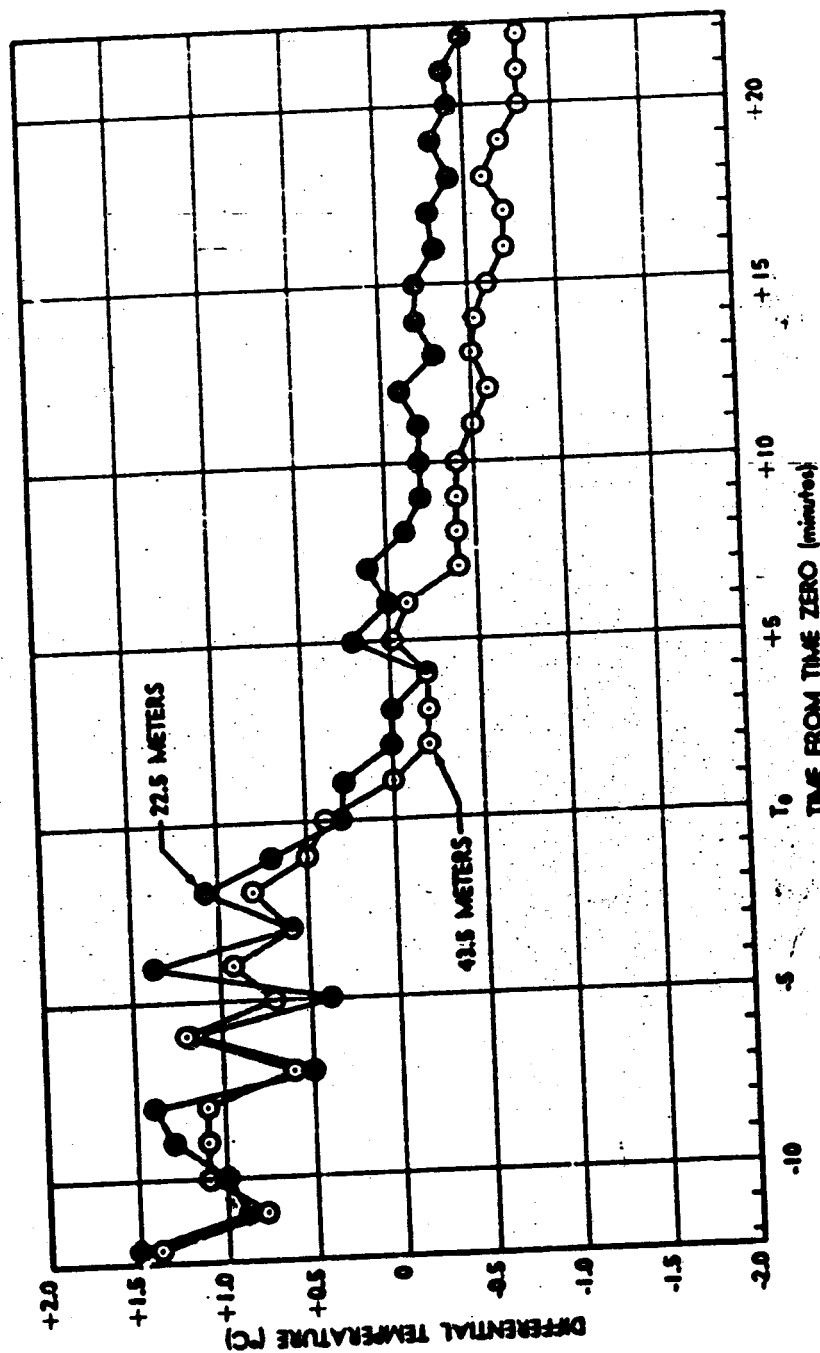


FIGURE N.A.1 LAPSE RATE DURING RELEASE

TABLE N.A.2
Meteorological Summary

APEX TOWER

Height (meters)	Wind Direction			Wind Velocity (meters/sec)		
	Max.	Min.	Ave.	Max.	Min.	Ave.
1.5	0	0	244°			3.6
3.0						4.2
6.0						4.7
12.0						5.1
24.0						5.5
45.0						6.0

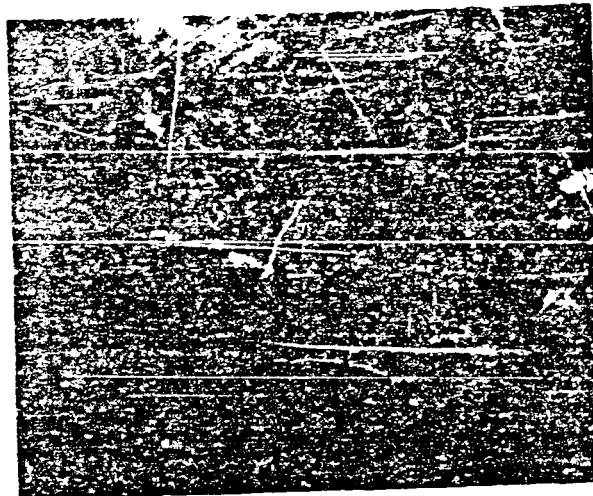
FIELD MASTS

Location (Arc)	Wind Direction			Wind Velocity (meters/sec)		
	Max.	Min.	Ave.	Max.	Min.	Ave.
200-meter	279°	214°	244°	6.5	1.8	4.0
400 "	267	198	232	6.5	2.0	4.0
800 "			242			3.8
1600 "			242			3.8
2400 "			240			4.3
3200 "	265	202	228	7.8	1.8	4.3

A.4 Smoke Plume Photography

Photographic documentation of the visible smoke cloud was accomplished during this test. Aerial and ground photographs were taken of the pre-release continuous plume at 23 minutes prior to the fission product release and are shown in Figure N.A.2. However, since the smoke was released under lapse conditions, while the fission products were dispersed under inversion conditions, a correlation would not be possible; thus no photographic analyses were performed.

NPC 9718



Aerial View



Ground View

FIGURE N.A.2 PRE-RELEASE SMOKE PLUME

A.5 Furnace Conditions

The furnace operating program established for all releases is summarized as follows: the furnace was energized at time zero with a sufficient initial power input so that the time to melt the fuel element was approximately two minutes. This time was established by numerous melts of non-loaded fuel elements. Following melting of the element, the furnace power was controlled so that the crucible temperature was kept at approximately 100 degrees centigrade above the stage melting point. This level was maintained for a ten-minute period, at which time the power was shut off. The temperature as a function of time during this release is shown in Figure N.A.3.

A.6 Effluent Samplers

Data obtained from sequential samplers located at the top of the furnace crucible, indicated that the fission product release was increasing for approximately 3.4 minutes after time zero (Figure N.A.4). Additional samples were obtained at seven and twelve minutes. The close interval sampling, i.e., eight samples during the initial 3.4 minutes, was established prior to release because it was believed that the release would take place during the first few minutes after melting. Since this apparently was not the case, the timing was set in all subsequent releases to spread the effluent sampling over the entire melt interval.

A.7 Release Percentages

The percent release of Cs^{137} was determined from the pre- and post-melt gamma spectra of the fuel element. These spectra are

NPC 9848

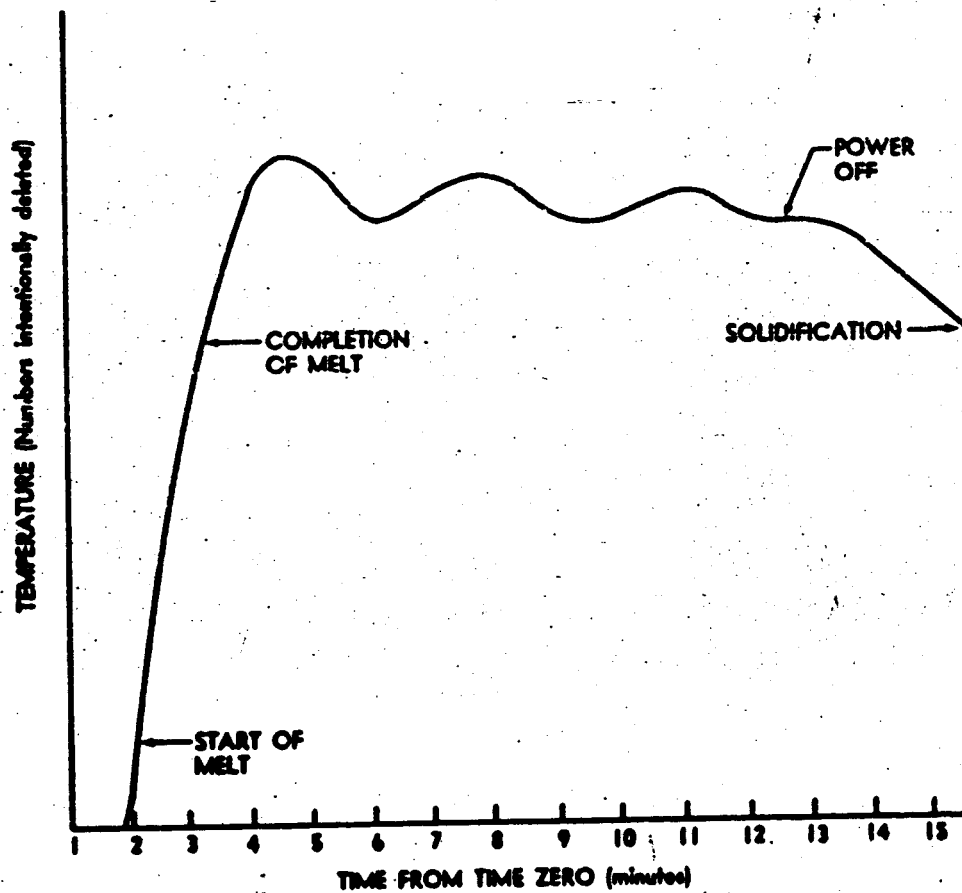


FIGURE N.A.3 FURNACE TEMPERATURE PROFILE

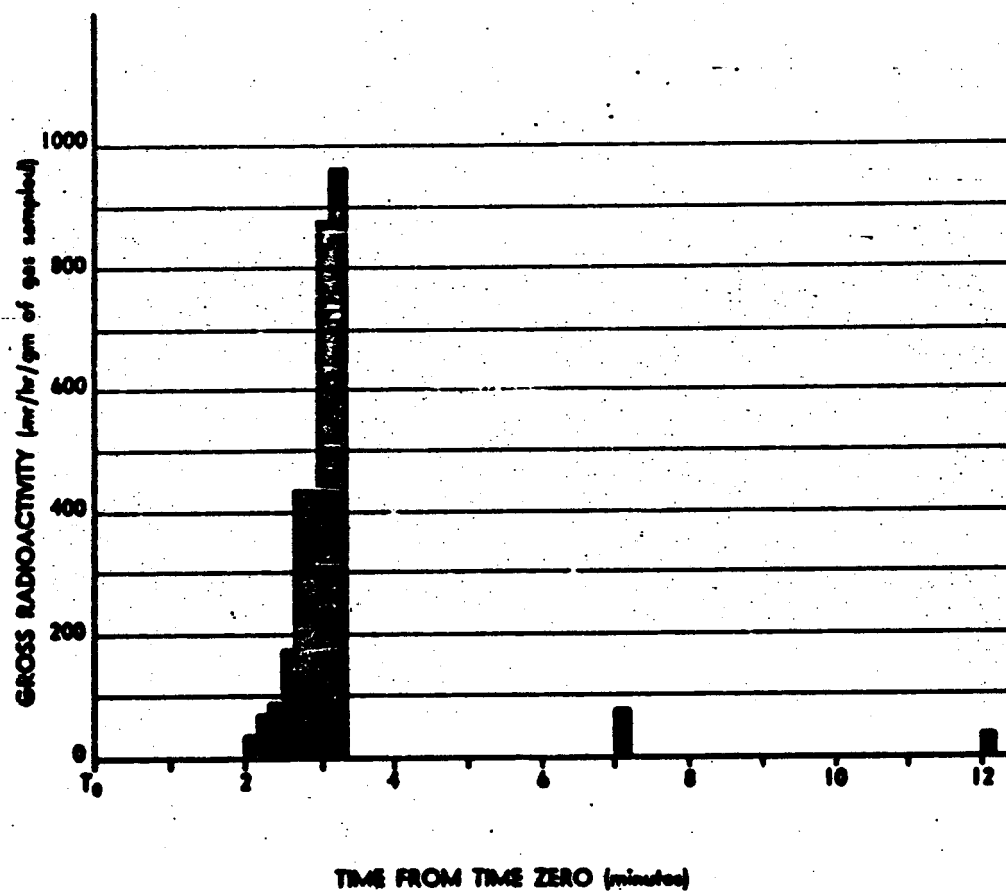


FIGURE N.A.4 SEQUENTIAL-EFFLUENT-SAMPLER FILTER RADIOACTIVITIES

shown in Figure N.A.5. The percentage of the Sr^{90} released was calculated from the results of Sr^{90} field sample radiochemical analysis, the fuel element inventory Sr^{90} to Cs^{137} ratio, and the measured Cs^{137} release percent. Table N.A.3 lists the release percents obtained.

TABLE N.A.3
Release Percentage

Nuclide	Percent
Cs^{137}	43
Sr^{90}	1.7

A.8 Air Sampler Field Survey

The term "field survey" refers to contact measurements which were taken on the H1-Vol pleated filters immediately following the test with a beta-gamma survey meter (with Cutie Pie when over 20 mr/hr). Figure N.A.6 shows the arc profiles of the filter readings in mr/hr, corrected for sampler flow rate and background. Figure N.A.7 shows a least-squares fit to the filter readings of the cloud centerline stations as a function of distance from the release point.

A.9 Airborne Radioactivity

Airborne Cs^{137} as determined by laboratory counting of the H1-Vol pleated filters is shown on Figure N.A.8. The data have

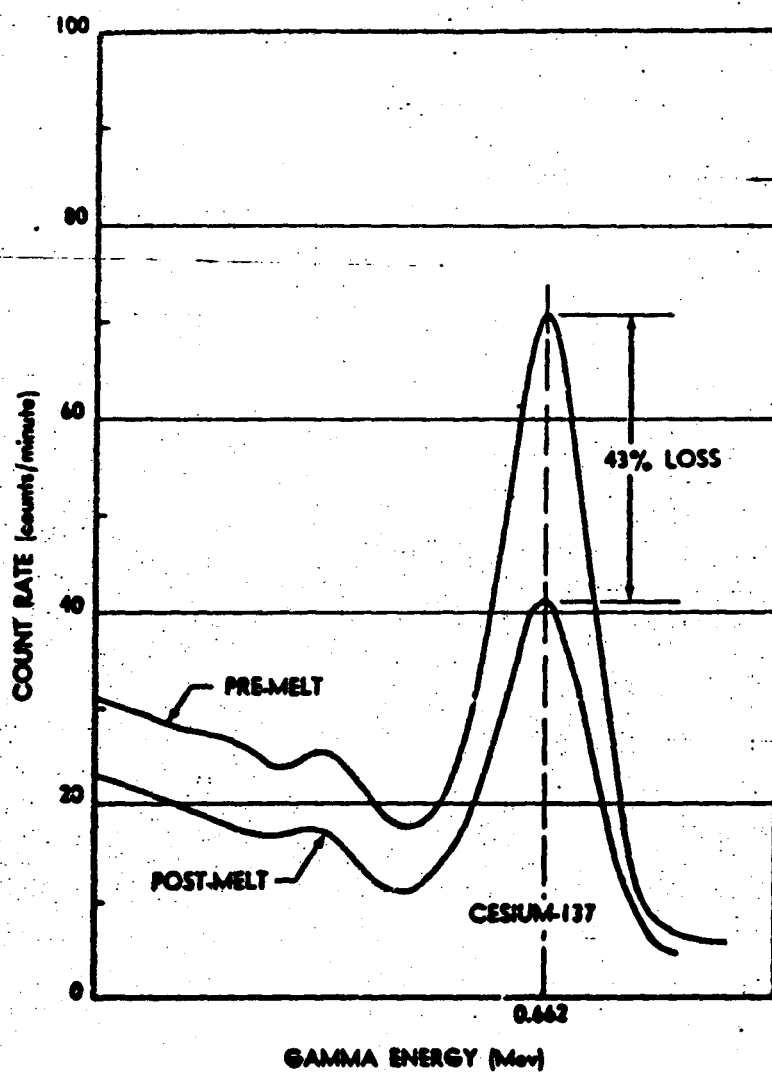


FIGURE N.A.5 PRE- AND POST-MELT GAMMA SPECTRA OF FUEL ELEMENT

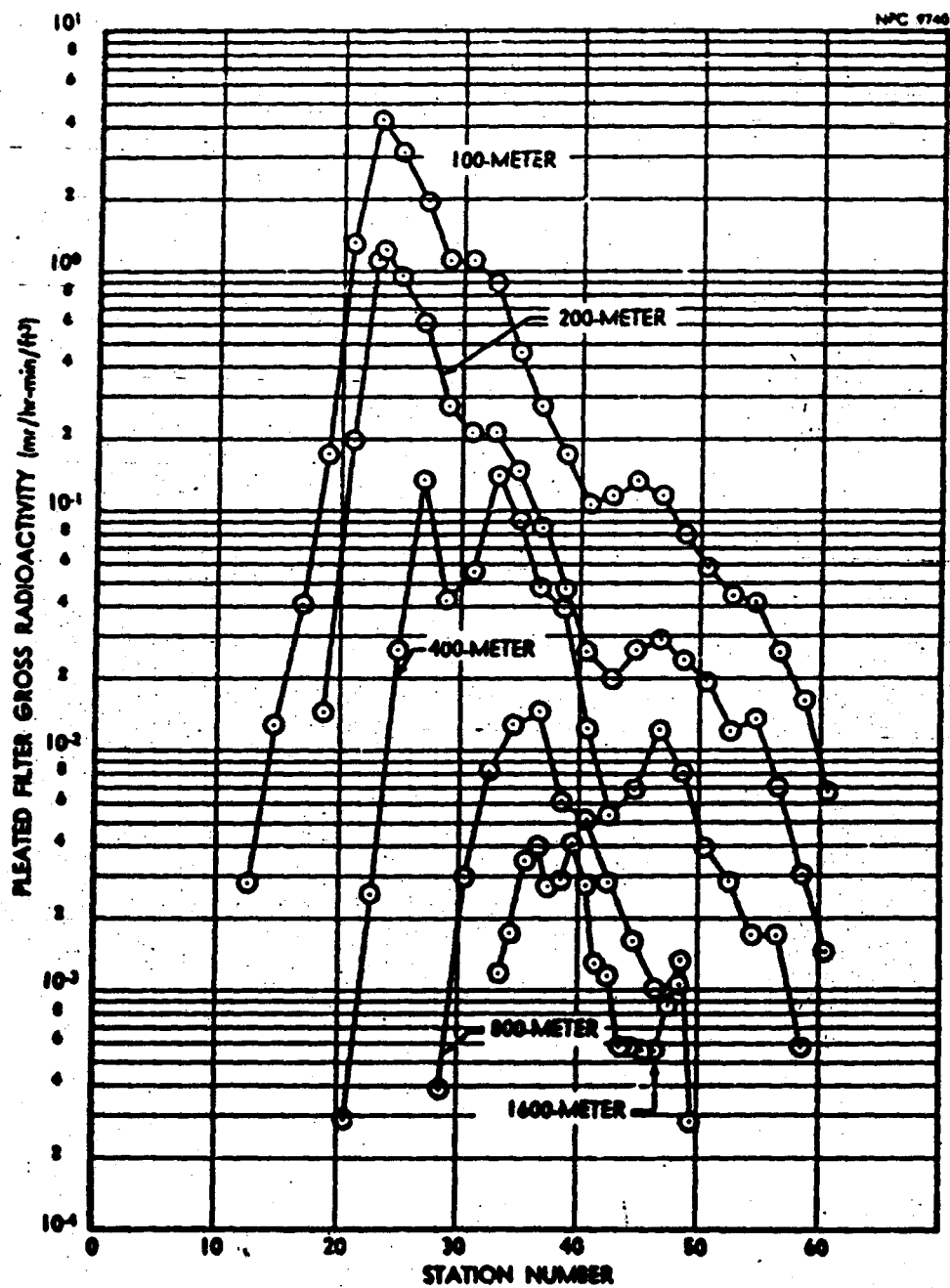


FIGURE N.A.6 HI-VOL AIR SAMPLER FIELD SURVEY
(Arc Profiles)

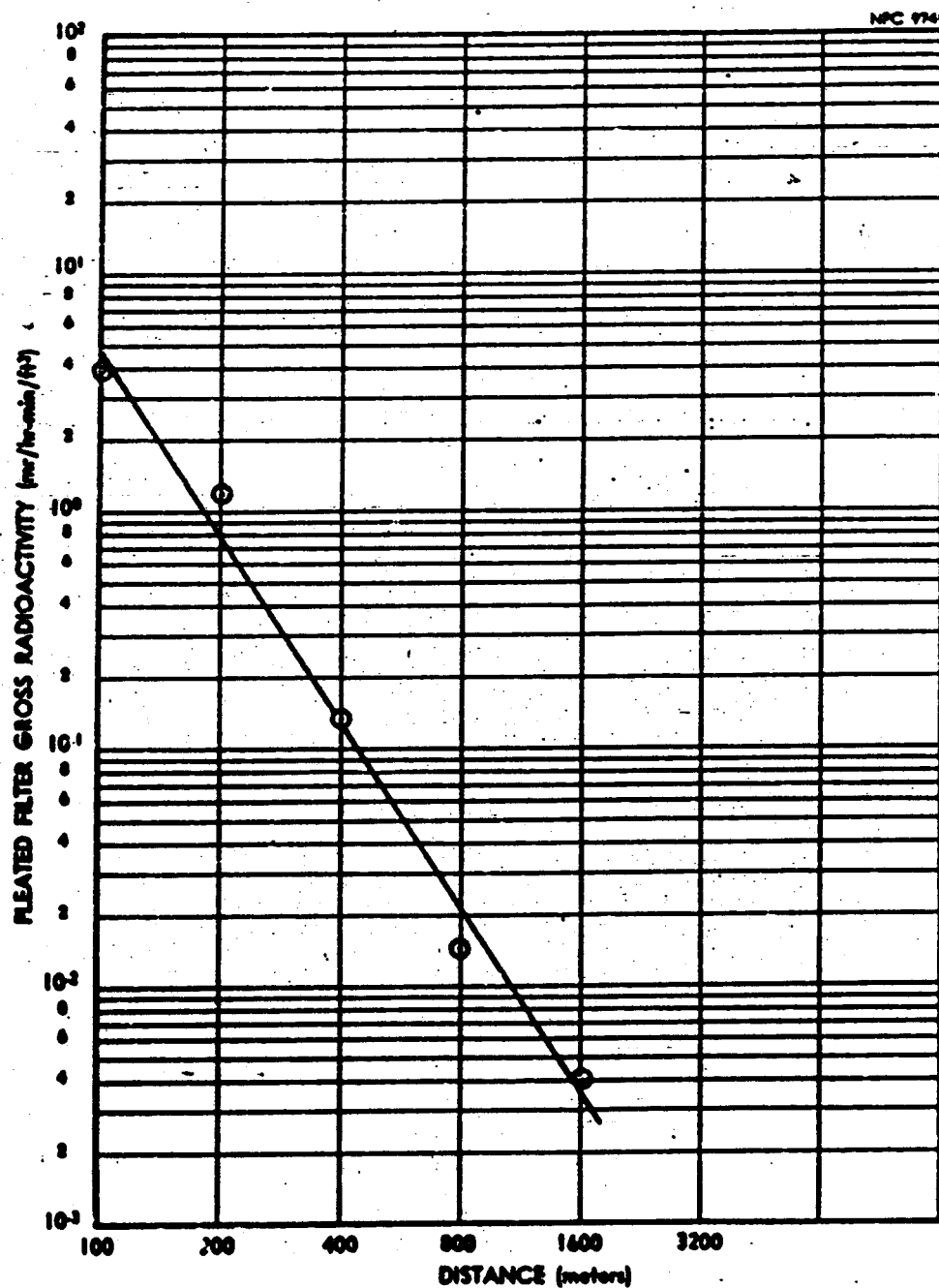


FIGURE N.A.7 HI-VOL AIR SAMPLER FIELD SURVEY (Centerline)

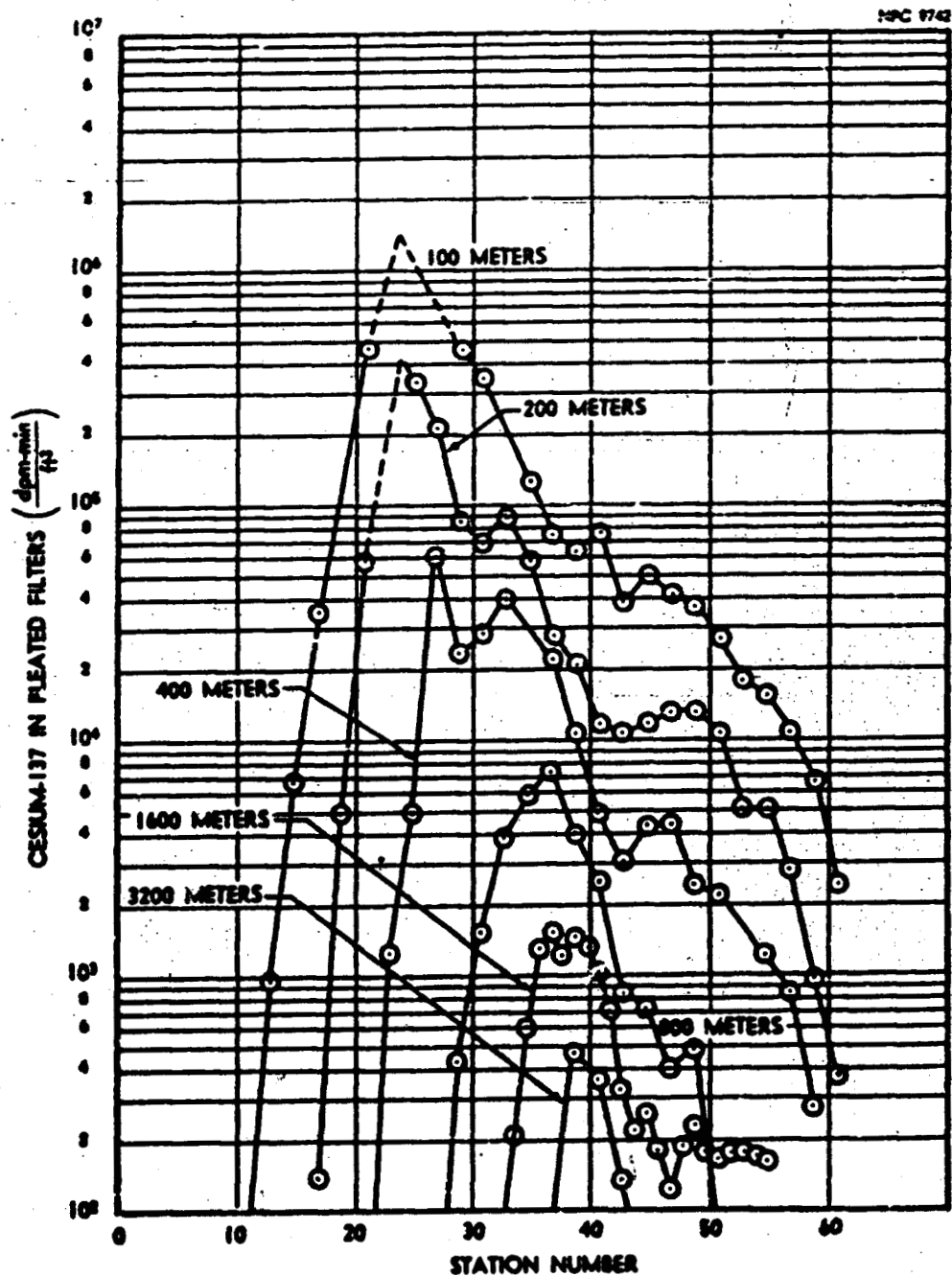


FIGURE N.A.8 HI-VOL AIR SAMPLER LABORATORY ASSAY OF CESIUM (Arc Profiles)

been corrected for sampler flow rate and are reported in terms of DPM-MIN. Figure N.A.9 is a plot of the Cs^{137} centerline data with a straight-line least-squares fit. Note that the slope of the line is essentially the same as that obtained from the air sampler field survey.

A.10 Deposited Radioactivity

The cesium deposited on the gummed fallout papers is shown in Figures N.A.10 and N.A.11. Figure N.A.11 shows the maximum value from each arc of Figure N.A.10 plotted versus distance from the release point. A straight line has been fitted to the points.

A.11 Deposited Velocity

The average deposition velocity for cesium, as a function of distance from the release point, is shown in Table N.A.4. The values for this parameter are the ratios of the areas under the sticky-paper activity arc profiles to the areas under the air sampler arc profiles. Little change is evident in this parameter as a function of downwind distance.

TABLE N.A.4

Cesium Deposition Velocity (cm/sec)

Arc (meters)	Sticky-Paper	Water	Sand
100	.0278	.044 ± .015	.02 ± .002
200	.0215	.025 ± .006	.063 ± .058
400	.0242		
800	.0277		
1600	.0658		

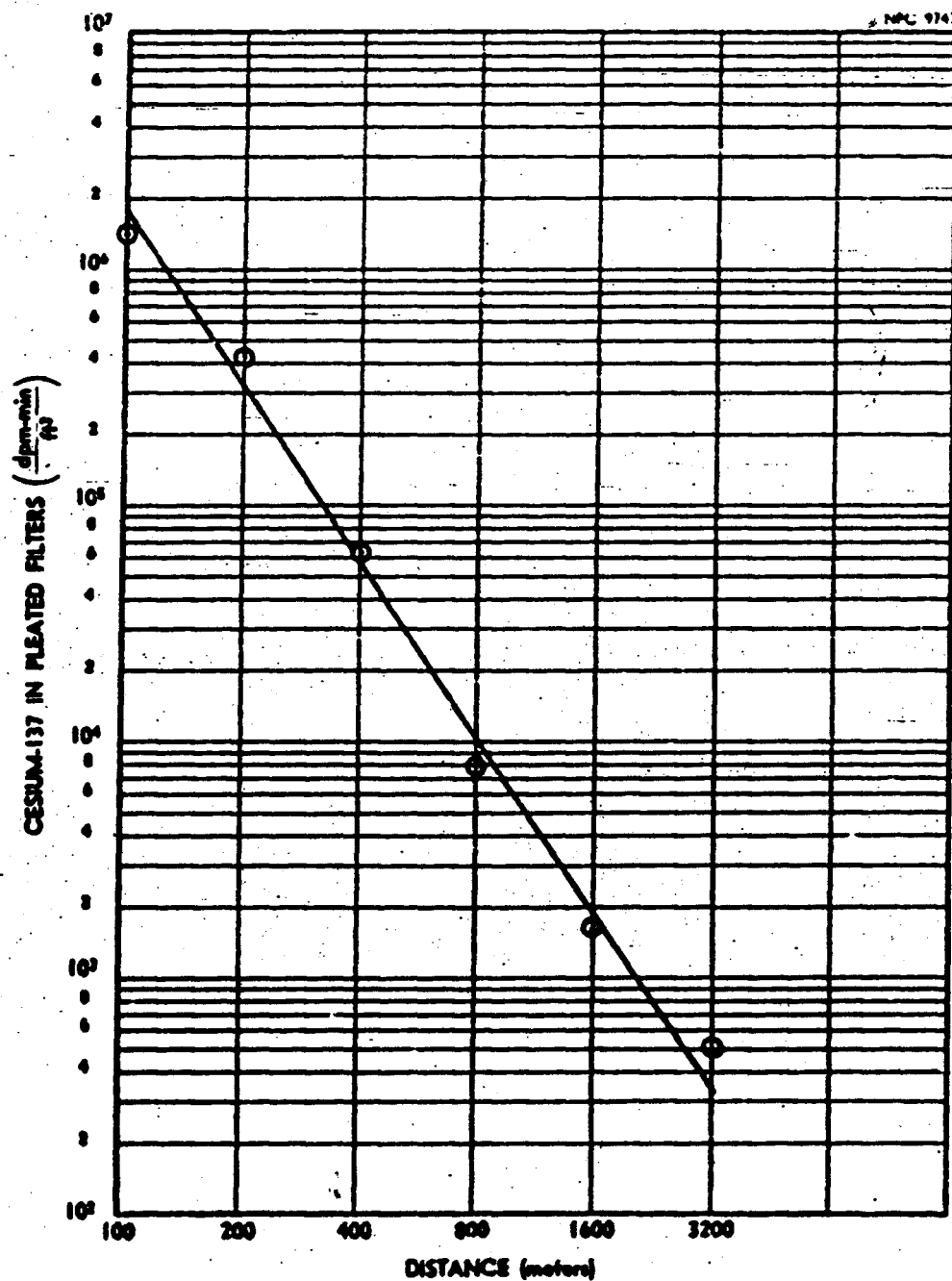


FIGURE N.A.9 HI-VOL AIR SAMPLER LABORATORY ASSAY OF CESIUM (Centerline)

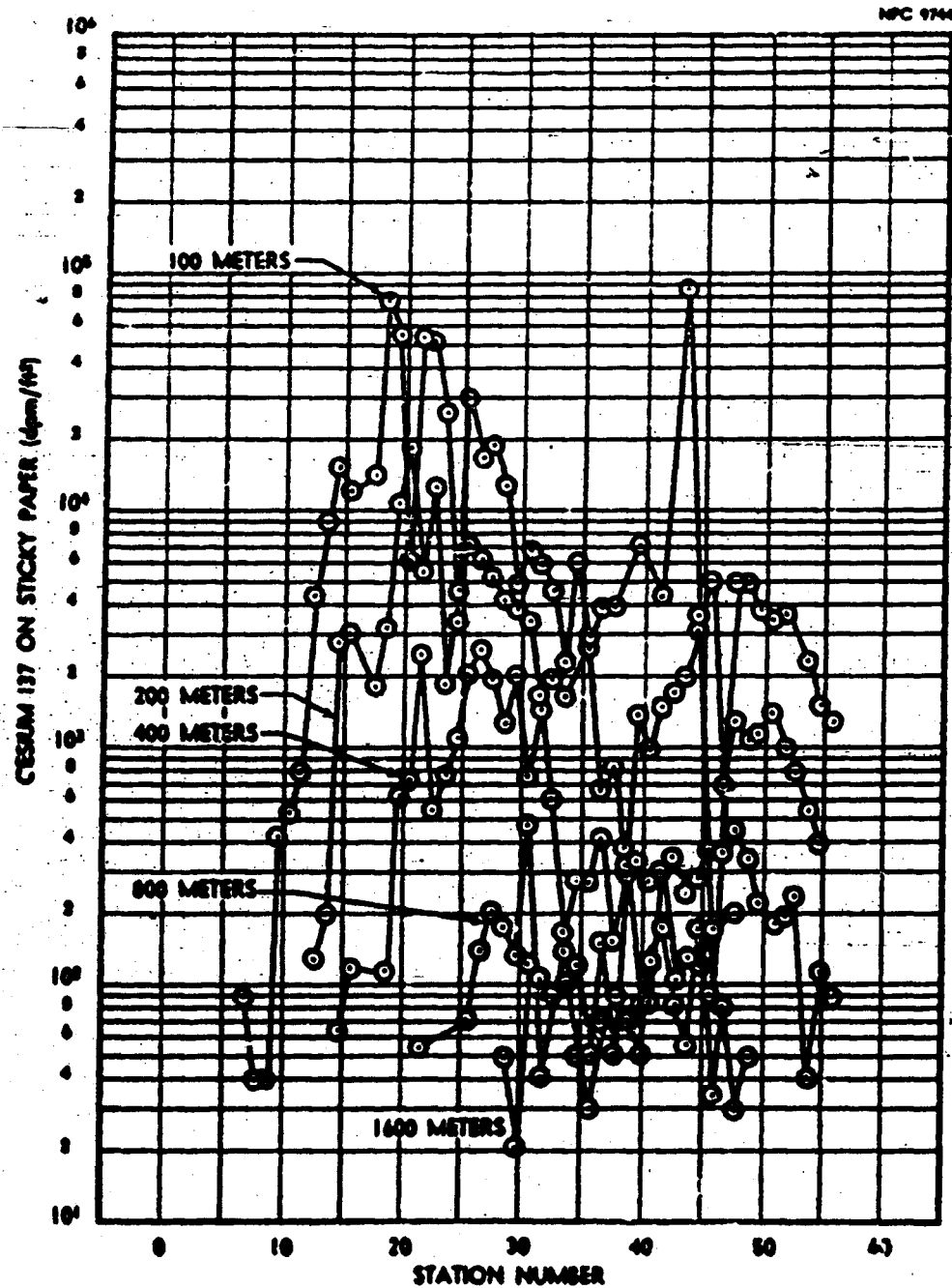


FIGURE NLA.10 DEPOSITED CESIUM (Arc Profiler)

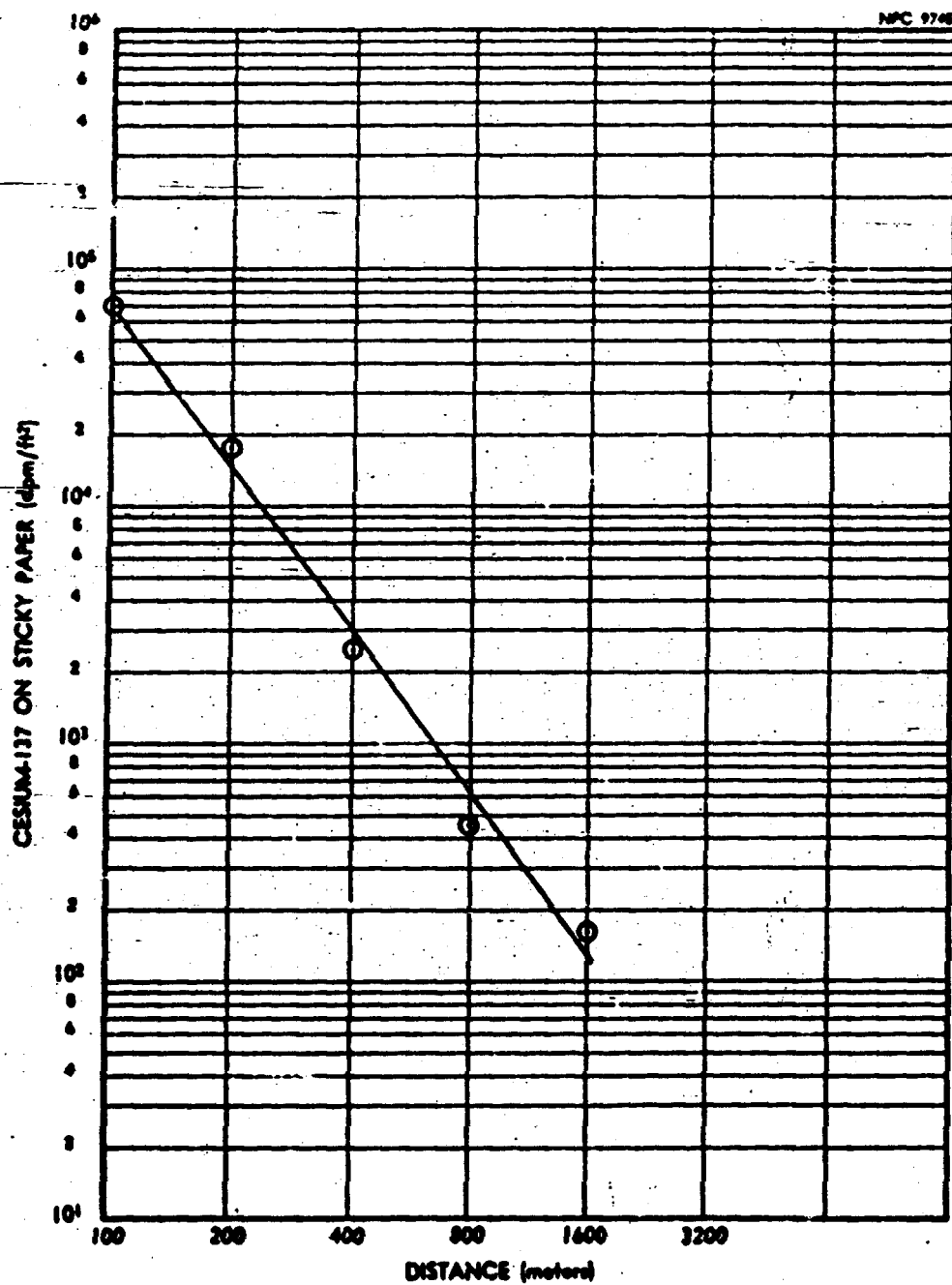


FIGURE N.A.11 DEPOSITED CESIUM (Centerline)

A.12 Fluorescent Tracer Distribution

Because of a shift in wind direction coincident with the release of fluorescent tracer, no fluorescent tracer data were obtained. The tracer cloud centerline did not appear on the network but moved an undeterminate distance off the right side of the grid.

A.13 External Dose

The gamma dose rate from cloud passage was measured and recorded at every three degrees on the 400-meter arc using the gamma scintillation detectors described in Appendix K.

The integrated gamma dose received at each station on the 400-meter arc during passage of the cloud is shown in Figure N.A.12. The gamma dose rate as a function of distance, taken from the detector station nearest the centerline of the effluent cloud, is shown in Figure N.A.13.

An approximate reconstruction of the gamma activity release sequence is shown in Figure N.A.14. The figure is a plot of the dose rate levels as a function of time and position, across the 400-meter arc.

A.14 Diffusion Parameters

The diffusion parameters obtained from this test are shown in Table N.A.5. The actual gross activity isopleth and its curve fit isopleth, normalized to the maximum filter reading on the 100-meter arc, are shown in Figures N.A.15 and N.A.16 respectively.

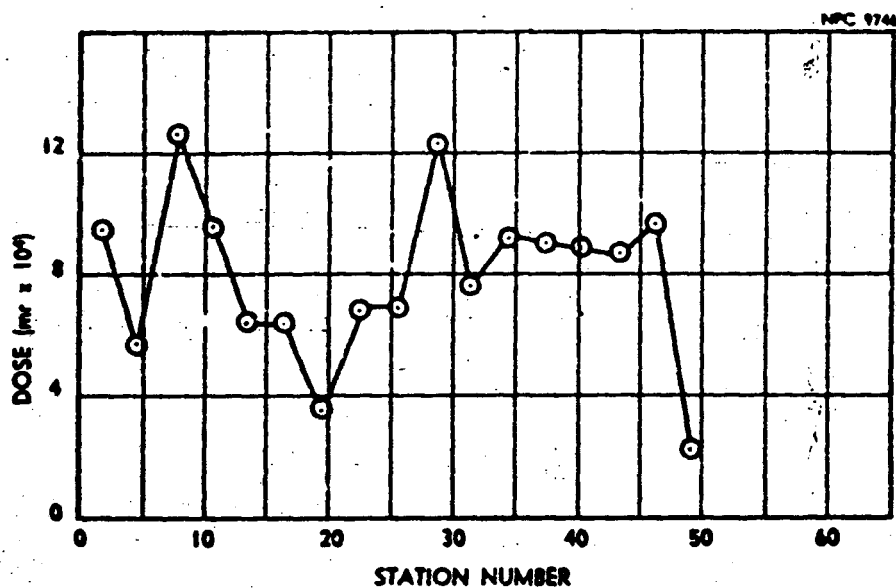


FIGURE N.A.12 GAMMA DOSE FROM CLOUD PASSAGE (Arc Profile)

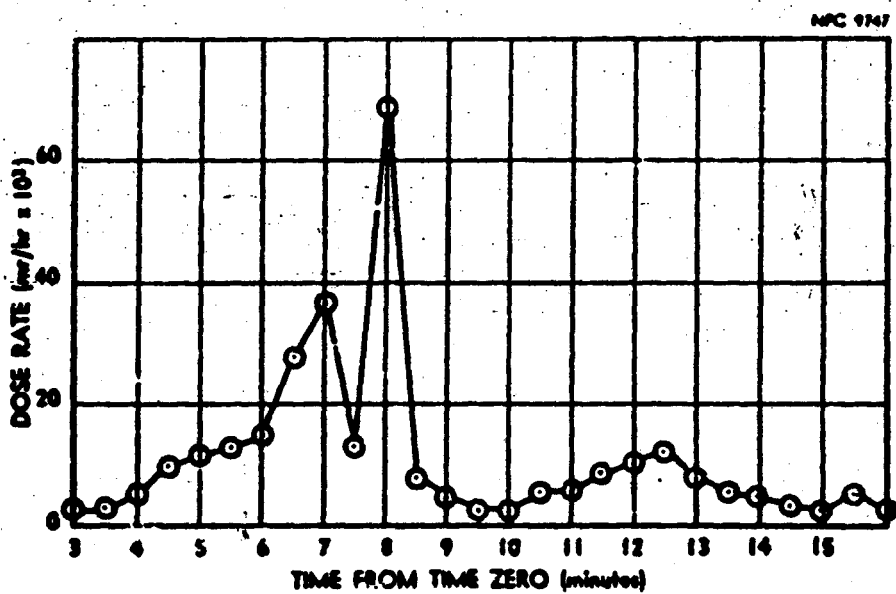


FIGURE N.A.13 GAMMA DOSE RATE FROM CLOUD PASSAGE (Centerline)

NPC 1740

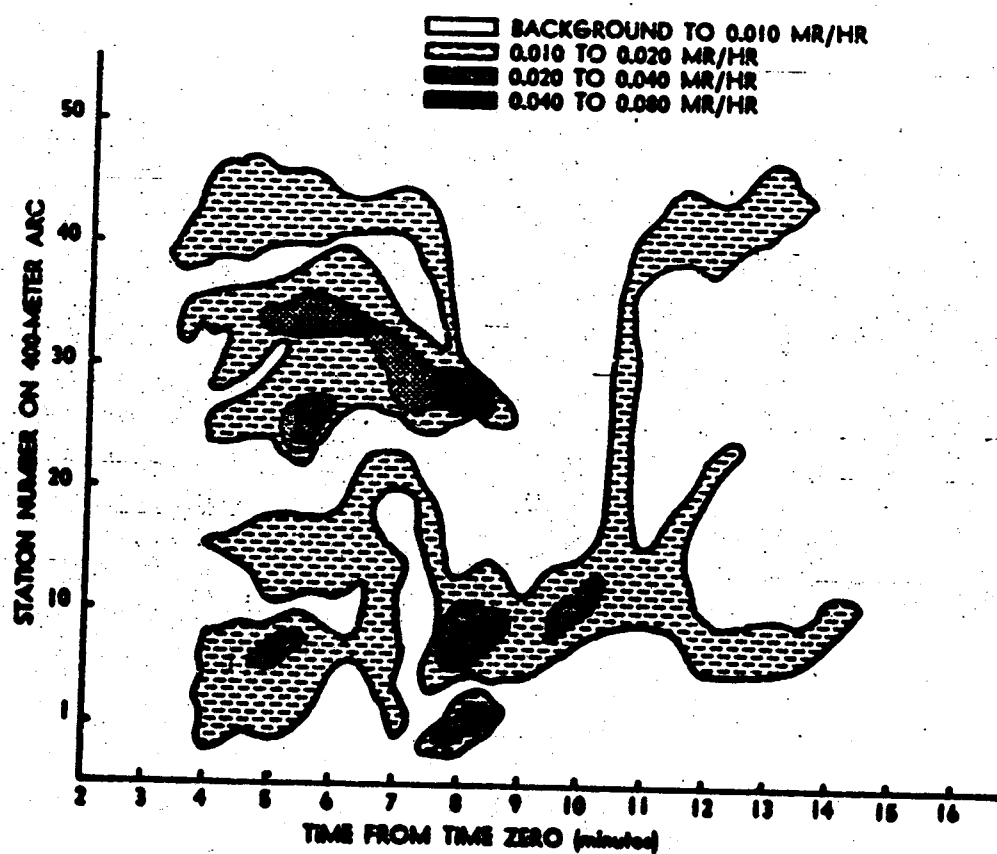


FIGURE N.A.14 GAMMA DOSE RATE FROM CLOUD PASSAGE
(Activity Contours)

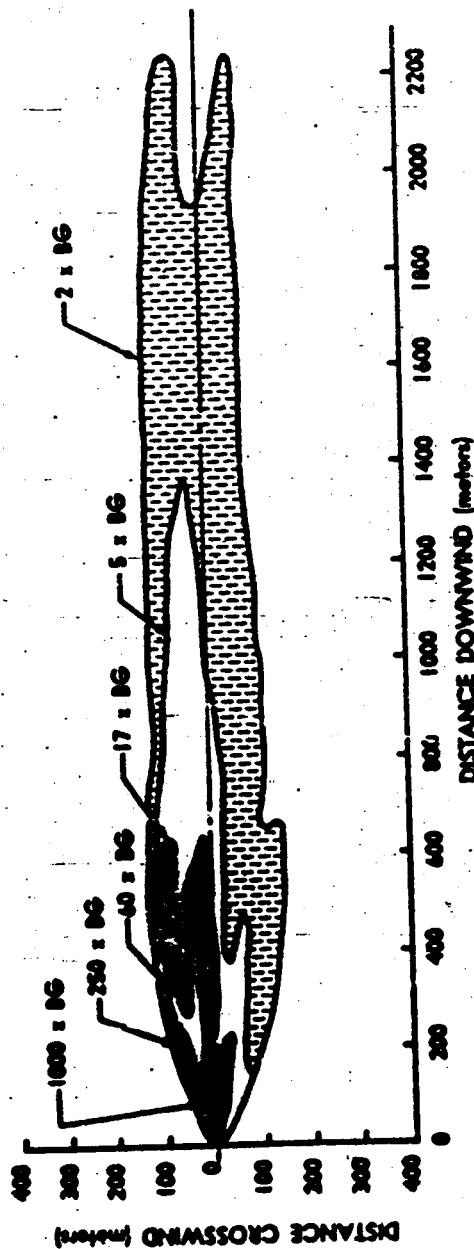


FIGURE N.A.15 GROSS RADIOACTIVITY ISOPLETH (Field Data)

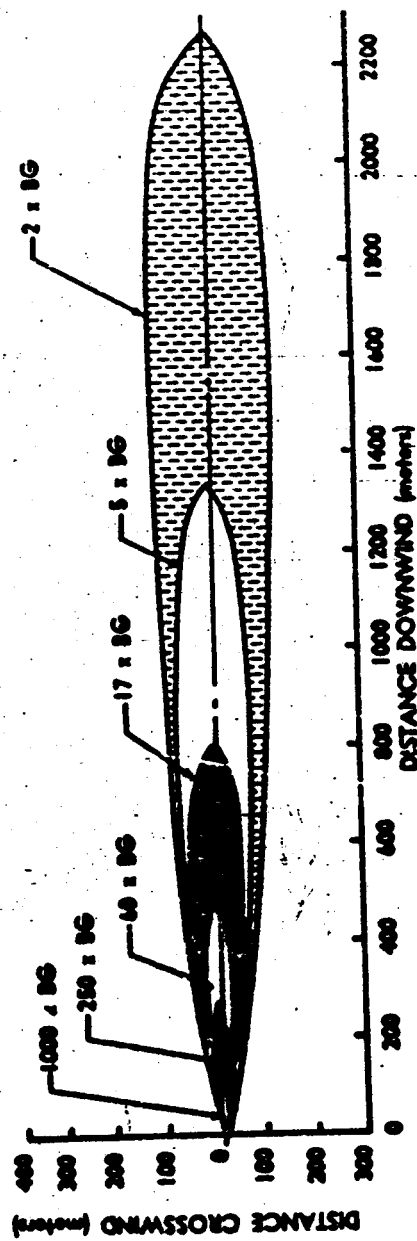


FIGURE N.A.16 GROSS RADIOACTIVITY ISOPLETH (Curve PH)

TABLE N.A.5
Diffusion Parameters

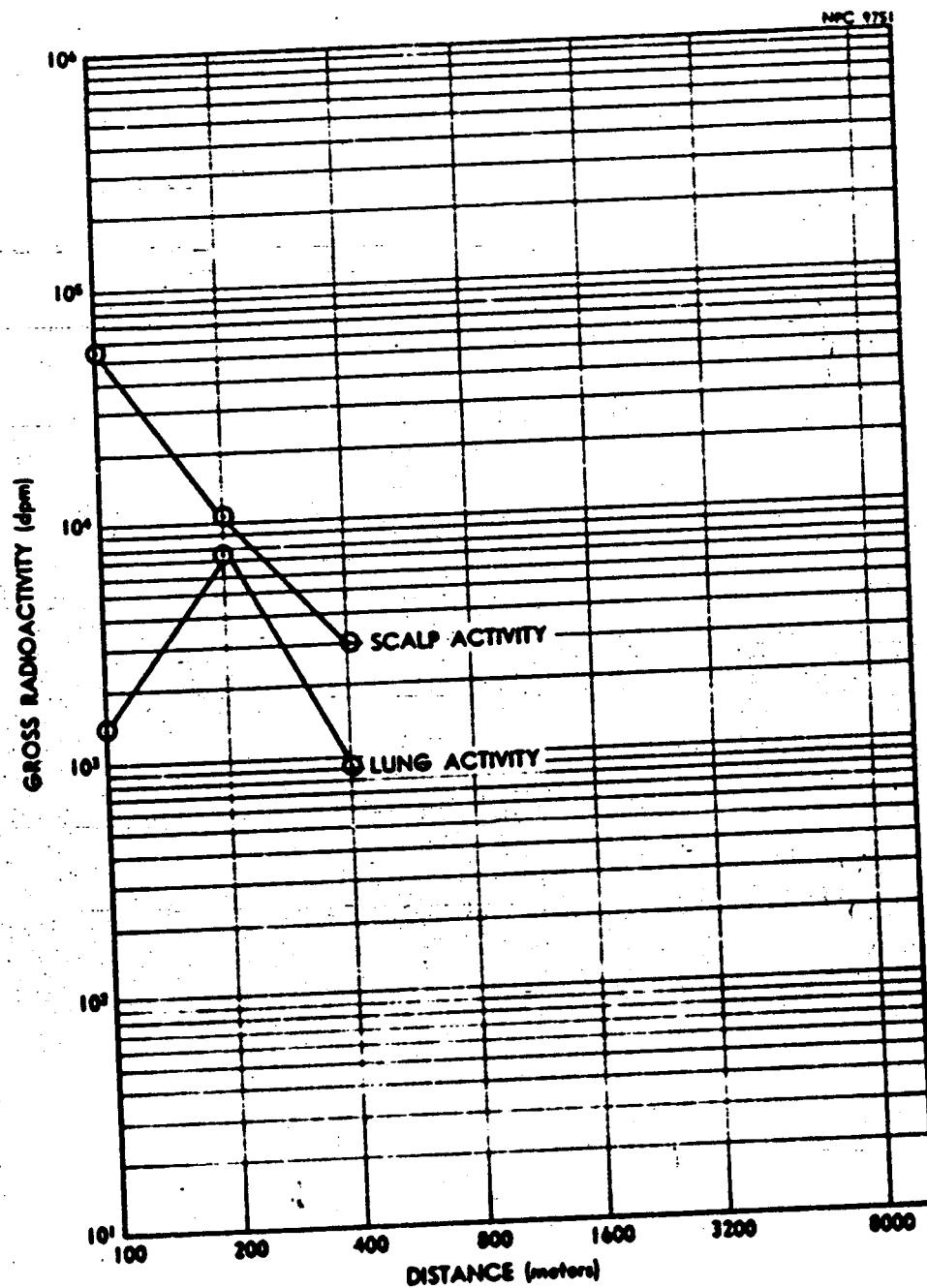
Parameters	Field-Survey Data-Fit	Cs137 Fit	Bivane
Horizontal Stability Parameter (M_y)	1.0	0.98	--
Vertical Stability Parameter (M_z)	1.7	1.5	--
Horizontal Diffusion Coefficient (C_y)	0.08	0.08	0.11
Vertical Diffusion Coefficient (C_z)	--	0.02	0.05
Sutton's Stability Parameter (n)	--	--	0.26

A.15 Radiobiology

During this release Dutch rabbits were exposed in restraining cages (Ref 9). Thirty animals were used with only the head and ears of each rabbit exposed. After release, the scalp and ears were counted to give an indication of external contamination and the lungs and trachea for internal contamination. These results are shown on Figure N.A.17.

A.16 Sand and Water Collection

During this release, fallout samples were collected in water and sand traps. The water samples were selected on the basis of the centerline of the cloud as determined in the field survey of air



sampler activities, evaporated to 50 ml, and gamma counted. Sand samples were selected in the same manner, leached for 30 minutes with boiling 6 N HCl, the leachate concentrated to 50 ml, and gamma counted. Results are shown in Figure N.A.18 and Table N.A.6, respectively.

TABLE N.A.6
Cesium-137 in Sand

Location	Curies
100 meter arc	
Station 26	18 x 10 ⁻⁹
Station 36	1.8 x 10 ⁻⁹
200 meter arc	
Station 8	0.32 x 10 ⁻⁹
Station 23	4.8 x 10 ⁻⁹
Station 38	0.56 x 10 ⁻⁹
Station 53	0.72 x 10 ⁻⁹

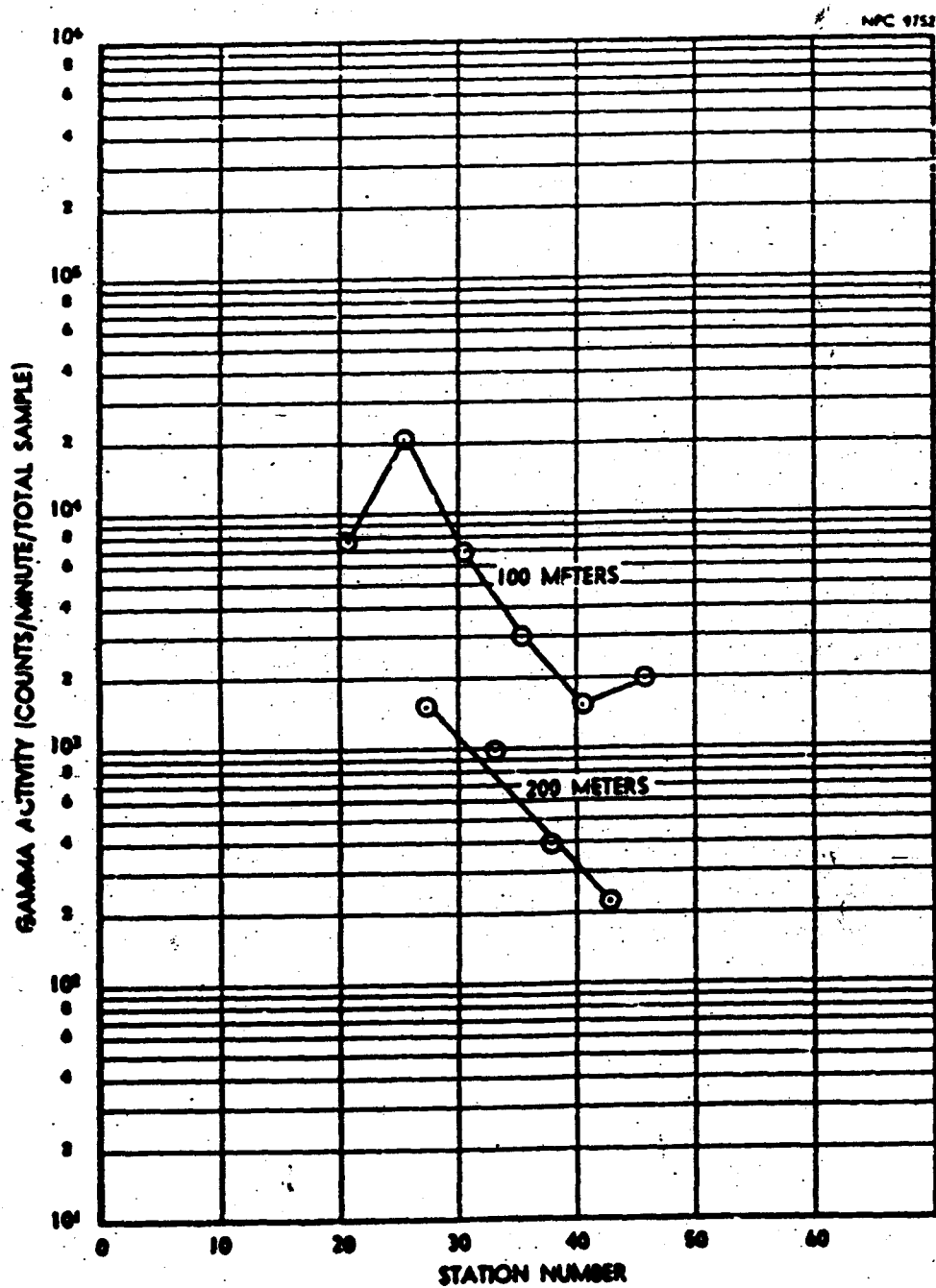


FIGURE N.A.18 CONTAMINATION OF WATER SAMPLES

APPENDIX N-B

(Release B)

B.1 Summary

Type of Sample -----	Aged Fuel Element
Date and Release Time -----	4 August 1958; 8:16 PM
Lapse Rate (1.5 - 45 m) -----	-3.6°C
Lapse Rate (1.5 - 24m) -----	-2.4°C
Mean Wind Speed -----	2.5 meters/sec
Wind Direction -----	Right edge of network
Cloud Photography -----	No photograph
Fluorescent Tracer -----	Released for 10 minutes immediately following fission product release
Animals -----	Rabbits on inner arcs (Ref. 9)
Network Radioactivity -----	Detected out to 3200 meters; maximum reading of pleated filters on 100-meter arc, 160 mr/hr, using Cutie Pie
External Dose -----	Maximum dose rate on 400-meter arc, 0.0057 mr/hr, using scin- tillation detector described in Appendix K.

B.2 Fuel Element

The fuel element had been irradiated to generate 6.6×10^4 watts for a total of 457 hours and had decayed for 932 days. The predominant nuclides present at the time of release are shown in Table N.B.1.

TABLE N.B.1
Fission Product Inventory

Nuclide	Curies Calculated
Sr ⁹⁰	3.7
Ce ¹⁴⁴ - Pr ¹⁴⁴	15
Pm ¹⁴⁷	9.3
Ru ¹⁰⁶ - Rh ¹⁰⁶	1.2
Cs ¹³⁷ - Ba ¹³⁷	3.1

B.3 Meteorological Conditions

The wind directions and velocities prevailing during this release are shown in Table N.B.2. The direction data shows that the fission product cloud centerline was along the right hand edge of the sampling network. At approximately the 800-meter arc the centerline swung back to the grid and remained just within the grid past the 3,200-meter arc.

Lapse rates, existing at the apex tower during the release, between the 1.5-meter level and both the 24- and 45-meter levels,

are shown in Figure N.B.1. An inversion condition existed during dispersal of the fission products.

TABLE N.B.2
Meteorological Summary

APPEX TOWER

Height (meters)	Wind Direction			Wind Velocity		(meters/sec)
	Max.	Min.	Ave.	Max.	Min.	Ave.
1.5						2.64
3.0						2.89
6.0						4.16
12.0						5.18
24.0						5.90
45.0						--

B.4 Furnace Conditions

The furnace operating schedule for this test closely followed the established procedure (App. N-A, Sec. A.5). The furnace was taken to temperature and held there for ten minutes. The temperature as a function of time during this release is shown in Figure N.B.2.

B.5 Effluent Samplers

Reduction of the data obtained by the sequentially operated effluent samplers show that the major release of activity occurred

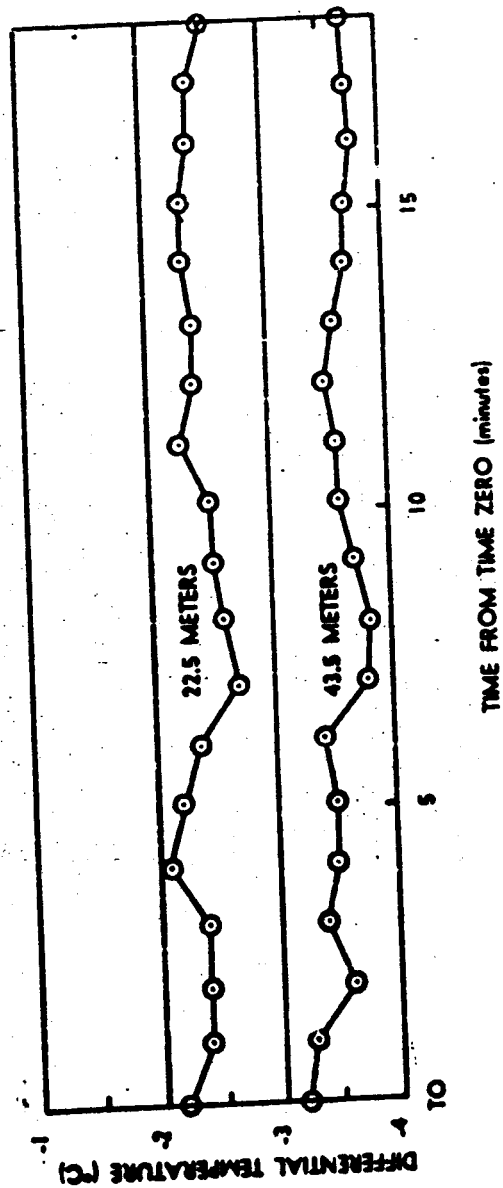


FIGURE N.B.1 LAPSE RATE DURING RELEASE

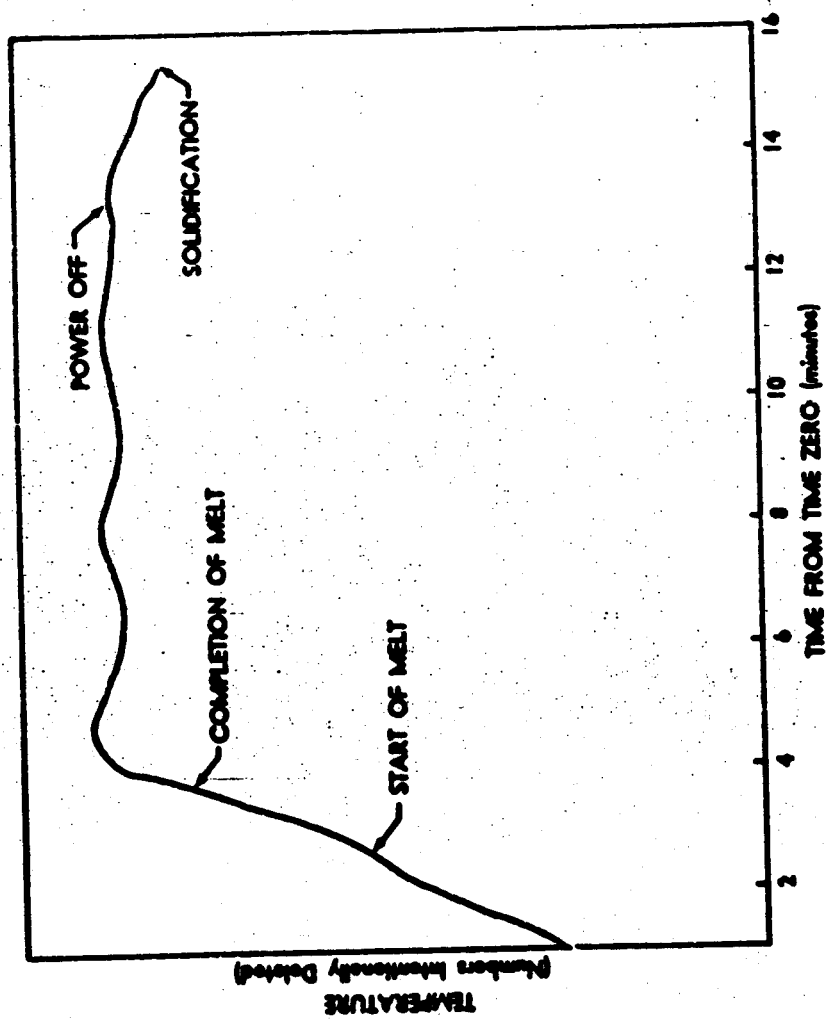


FIGURE 12.2 FURNACE TEMPERATURE PROFILE

at approximately three minutes after time zero. These data are shown in Figure N.B.3.

B.6 Release Percentages

The percent release of cesium as determined by pre- and post-melt gamma spectrometry is shown in Table N.B.3. The gamma spectra from which the Cs^{137} release fraction was determined are shown in Figure N.B.4. Percent release of Sr^{90} was not determined because the cloud centerline pleated filter data was not available.

TABLE N.B.3

Release Percentage

Nuclide	Percent
Cs^{137}	43

B.7 Air Sampler Field Survey

The term "field survey" refers to contact measurements which were taken on the Hi-Vol pleated filters immediately following the test with a beta-gamma survey meter. Figure N.B.5 shows the are profiles of the filter readings in mr/hr , corrected for sampler flow rate background. The profiles are incomplete because part of the cloud was off the network.

B.8 Airborne Radioactivity

Airborne Cs^{137} activity as determined by laboratory counting of the Hi-Vol pleated filters is shown on Figure N.B.6. These dat

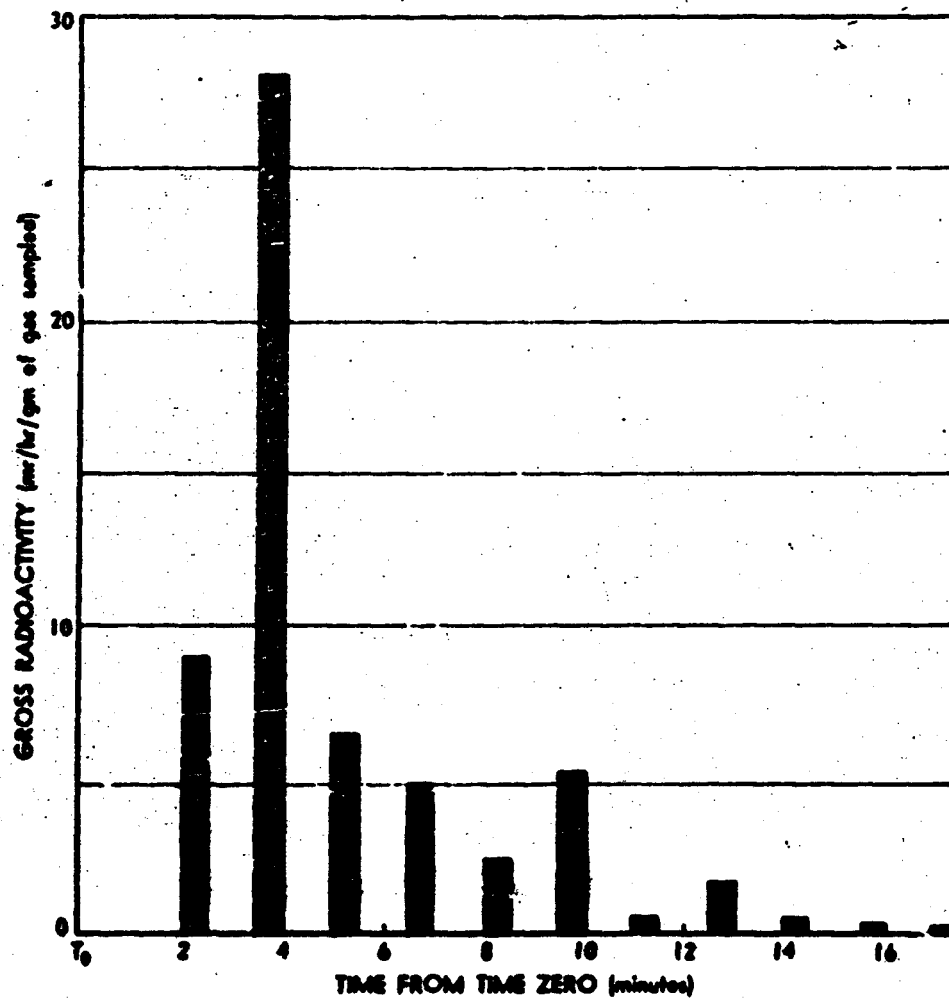


FIGURE N.B.3 SEQUENTIAL-EFFLUENT-SAMPLER FILTER

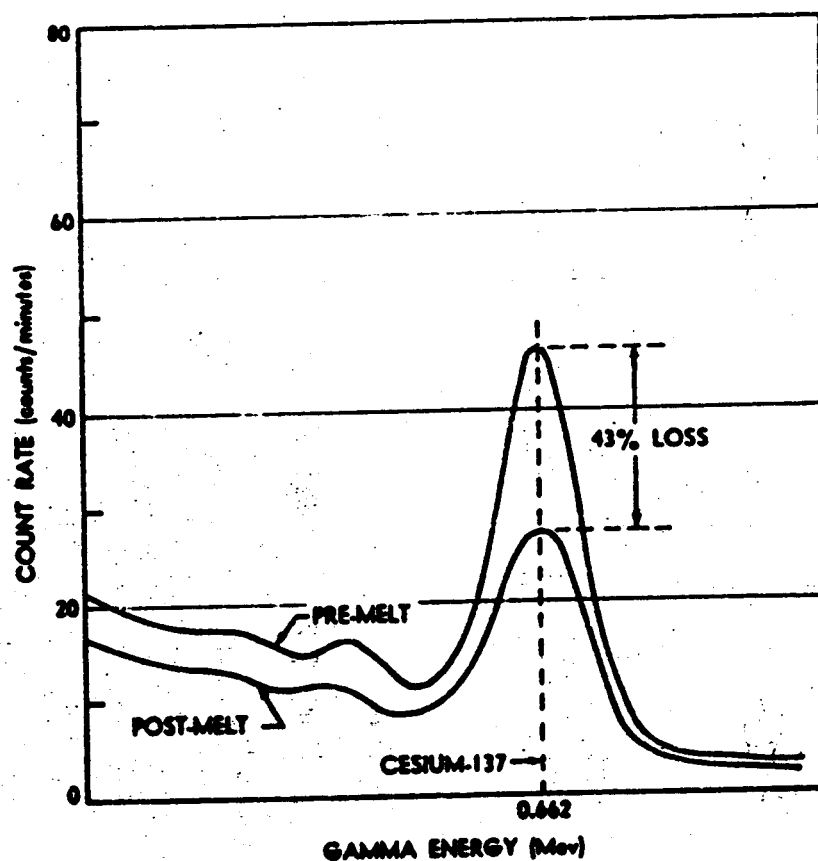


FIGURE N.E.4 PRE- AND POST-MELT GAMMA SPECTRA OF FUEL ELEMENT

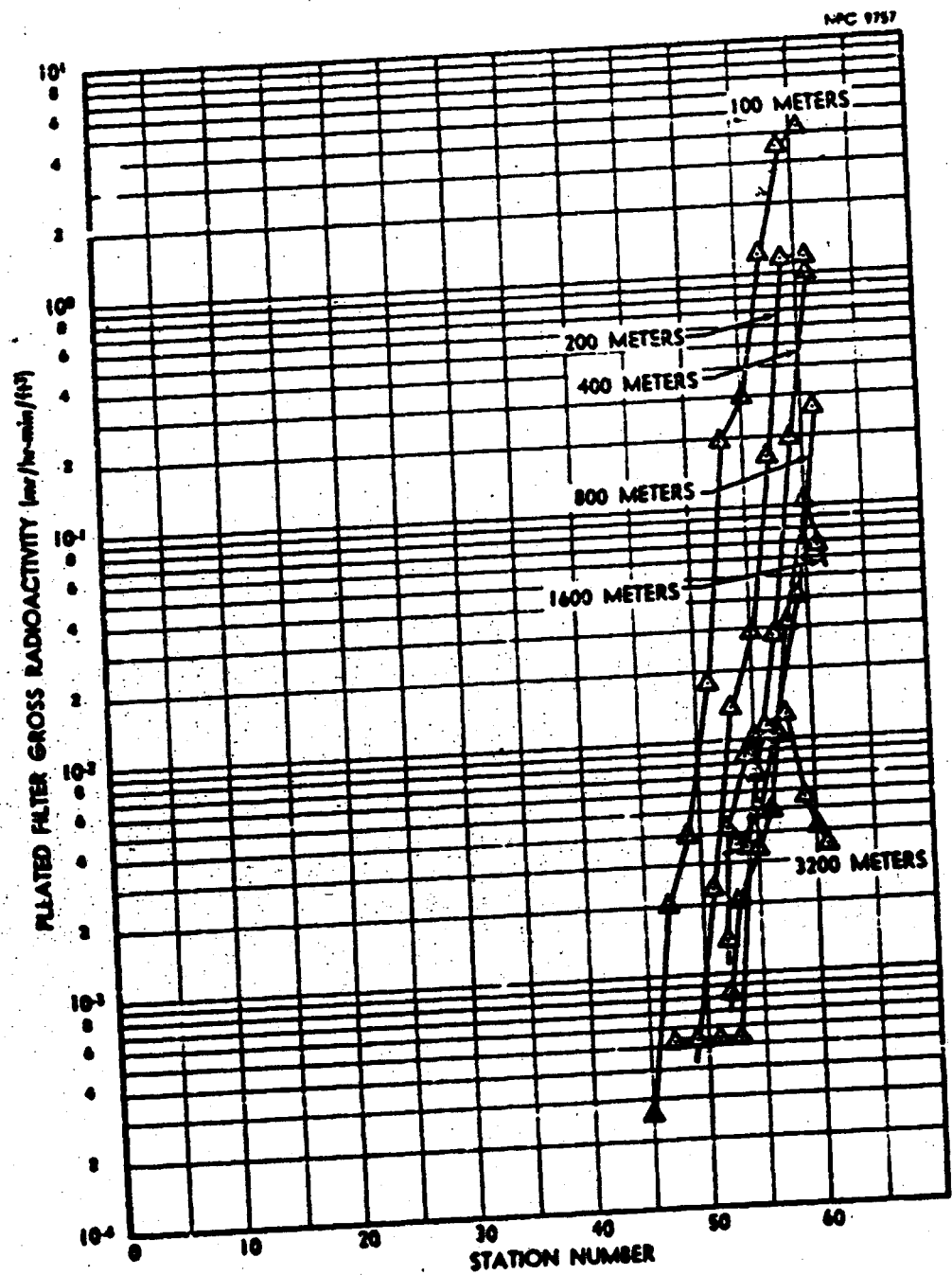


FIGURE N.E.5 H₂VO₄ AIR SAMPLER FIELD SURVEY
(Arc Profiles)

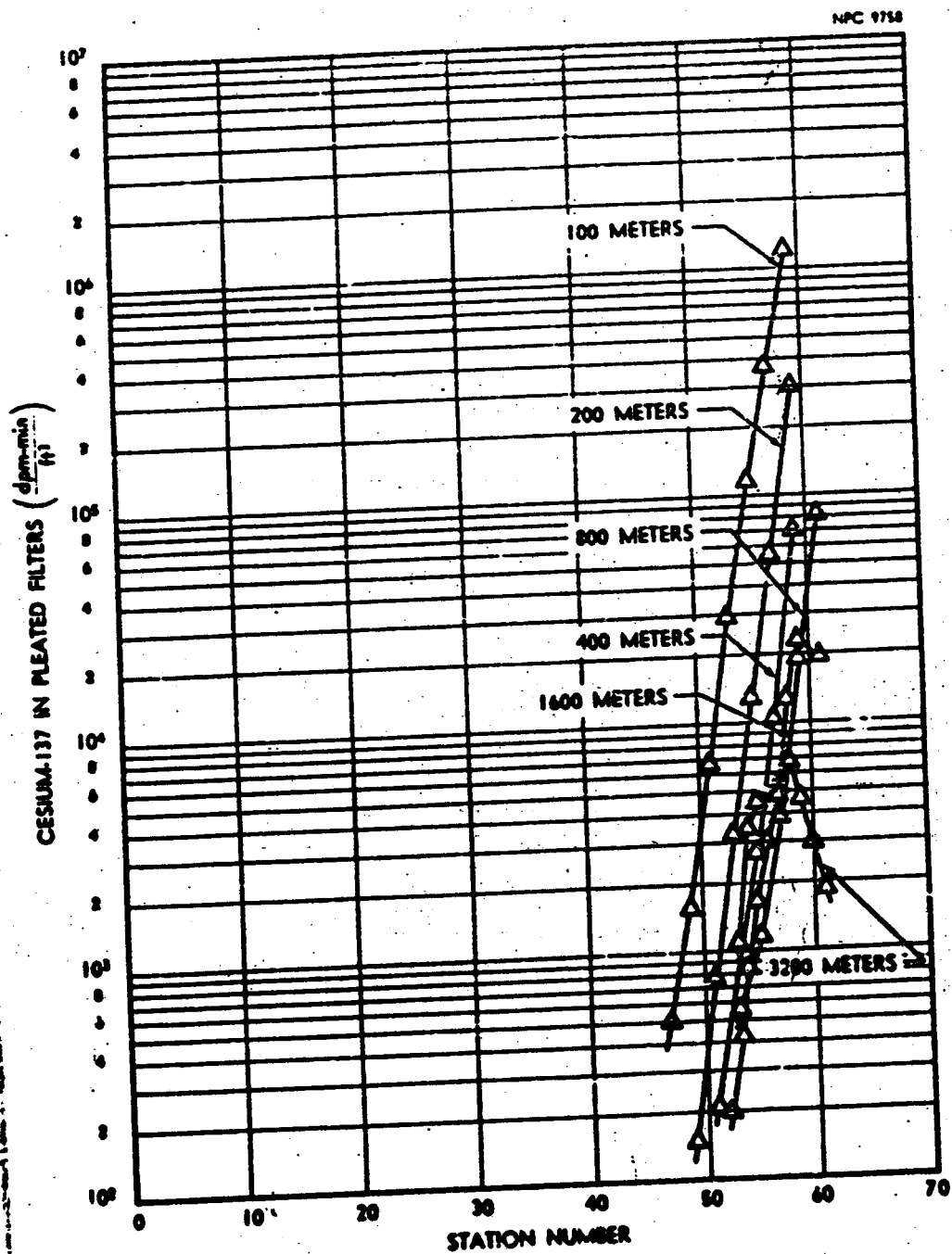


FIGURE N.8.6 HI-VOL AIR SAMPLER LABORATORY ASSAY OF CESIUM (Arc Profiles)

have been corrected for sampler flow rate and are reported in terms of DPH-Min . Because of the cloud drift off the network, the profiles are ^{ft³} incomplete.

B.9 Deposited Radioactivity

The cesium deposited on the fallout papers is shown in Figure N.B.7. The arc profiles are incomplete as the cloud centerline was off the right hand side of the network.

B.10 Deposition Velocity

The average deposition velocity for cesium as a function of distance from the release point is shown in Table N.B.4. The values for this parameter were determined by ratioing the areas under the sticky paper activity arc profiles to the areas under the air sampler activity arc profiles.

TABLE N.B.4
Cesium Deposition Velocity

Arc (meters)	Velocity (cm/sec)
100	0.081
200	0.089
400	0.062
800	0.021
1600	0.018
3200	0.015

B.11 Fluorescent Tracer Distribution

No tracer data were obtained during this release because the cloud centerline was off the sampling network.

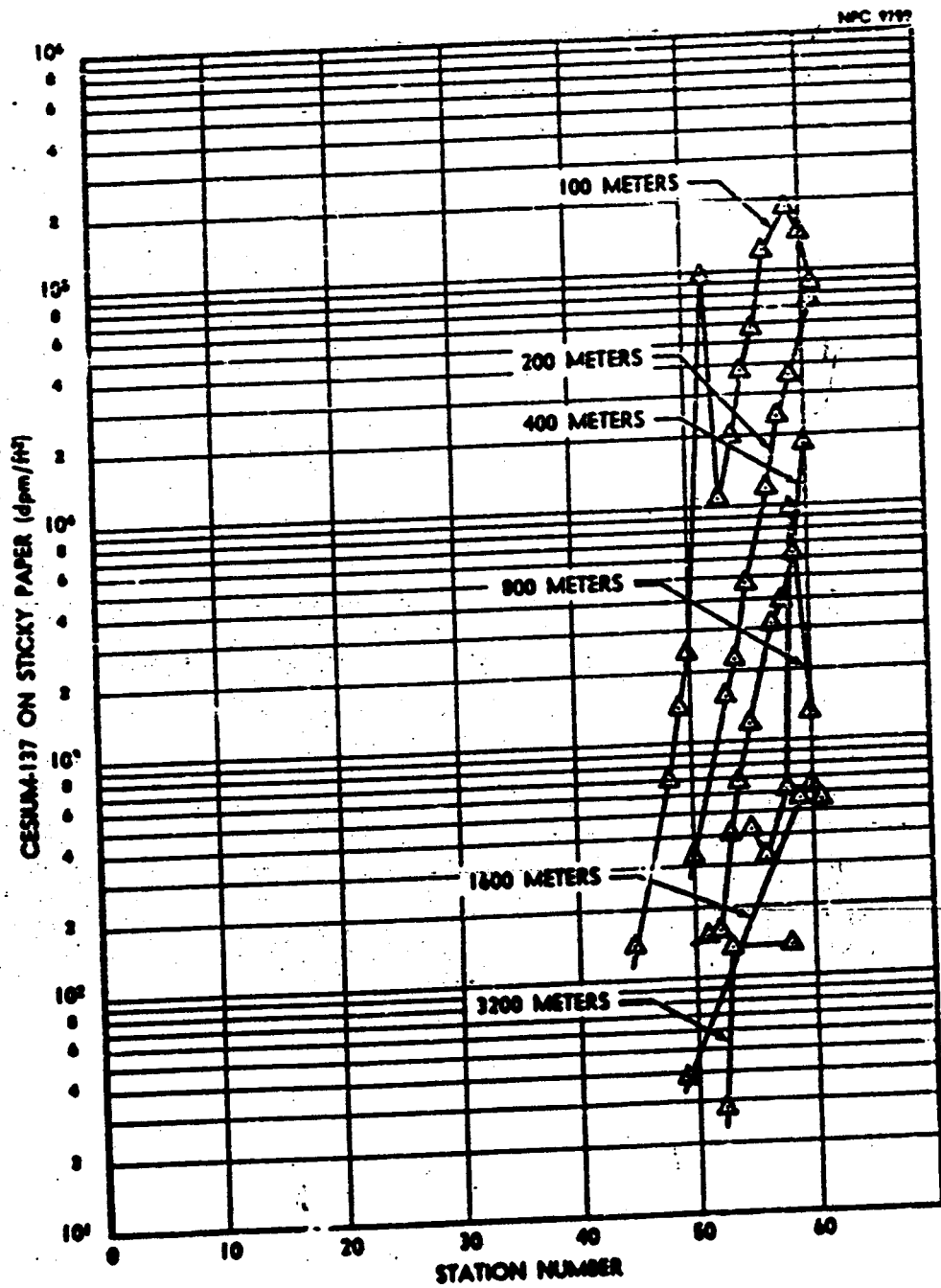


FIGURE N.B.7 DEPOSITED CESIUM (Arc Profiles)

B.12 External Dose

No external dose data are available from this release because of the direction of the cloud path.

B.13 Diffusion Parameters

The diffusion parameters obtained from this test are shown in Table N.B.5. The field-survey-data fit and Cs¹³⁷ fit were not calculated because the cloud was only partially on the network.

TABLE N.B.5
Diffusion Parameters

Parameters	Field-Survey-Data Fit	Cs ¹³⁷ Fit	Bivariate
Horizontal Stability Parameter (M_y)	--	--	--
Vertical Stability Parameter (M_z)	--	--	--
Horizontal Diffusion Coefficient (C_y)	--	--	0.02
Vertical Diffusion Coefficient (C_z)	--	--	0.02
Sutton's Stability Parameter (n)	--	--	0.45

B.14 Radiobiology

Dutch rabbits were used with only the head and ears of each rabbit exposed. After release, the scalp and ears were counted

D' to give an indication of external contamination, and the lungs and trachea were counted to show the extent of internal contamination. These results are shown on Figure N.B.8.

B.15 Sand and Water Collection

No samples were collected because the fallout missed the major part of the water-sand sampling grid.

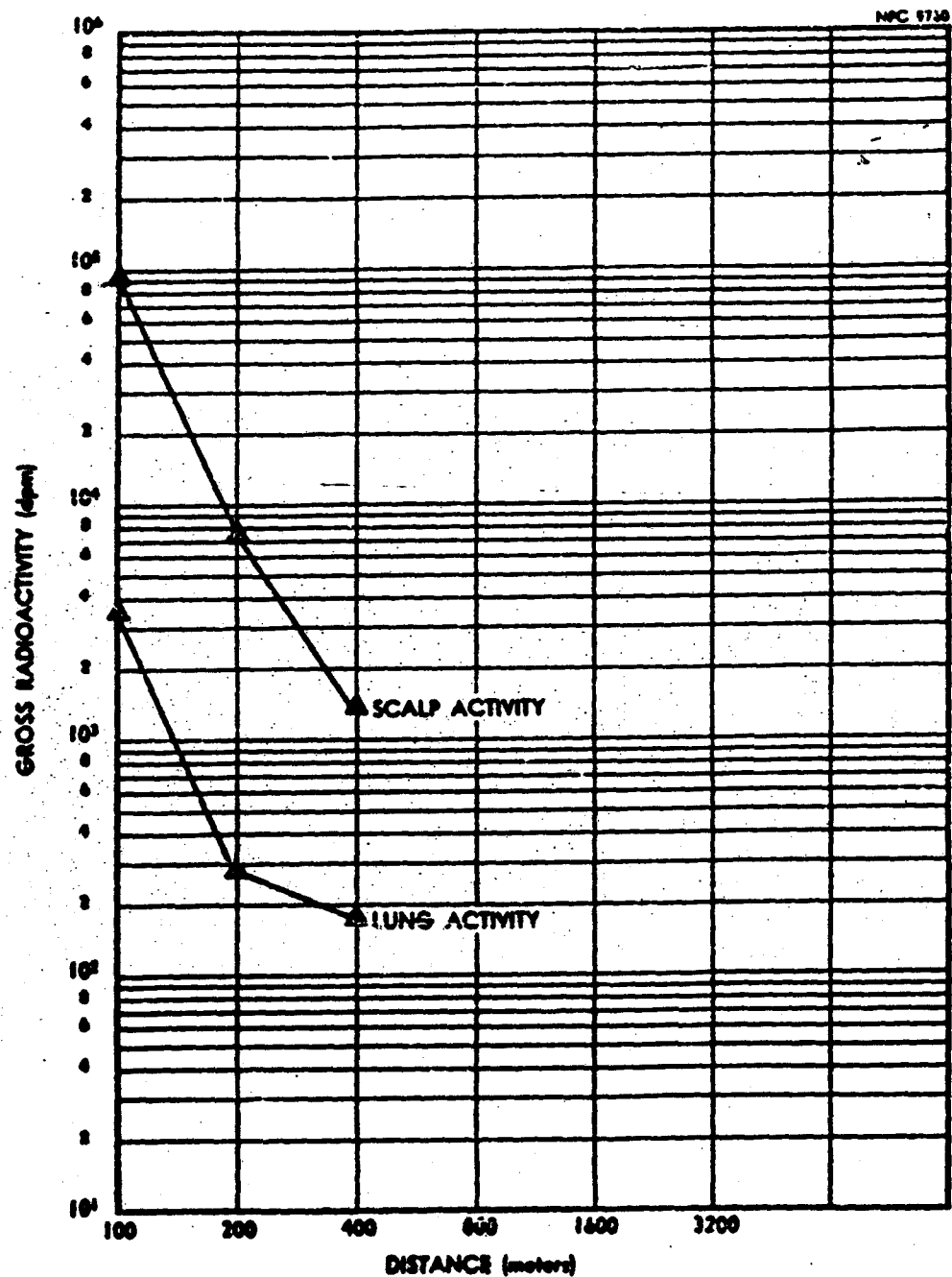


FIGURE N.E.8 CONTAMINATION OF EXPOSED RABBITS

APPENDIX N-C

(Release C)

C.1 Summary

Type of Sample -----	Aged Fuel Element
Date and Release Time -----	6 Aug. 1958; 7:14 PM
Lapse Rate (1.5 - 45 m) -----	-1.5°C
Lapse Rate (1.5 - 24 m) -----	-1.08°C
Mean Wind Speed -----	2.3 meters/sec
Wind Direction -----	Network Centerline
Cloud Photography -----	Ground only
Fluorescent Tracer -----	Released simultaneously, with fission product release
Animals -----	Rats on 100- and 200-meter arcs (Ref. 11) Rabbits on 100, 200, and 400-meter arcs (Ref. 9)
Network Radioactivity -----	Detected out to 3200 meters; maximum reading of pleated filters on 100-meter arc, 42 mr/hr using Cutie Pie.
External Dose -----	Maximum dose rate on 400- meter arc, 0.028 mr/hr using scintillation detector described in Appendix K.

C.2 Fuel Element

The fuel element had been irradiated to generate 7×10^4 watts for a total of 467 hours and had decayed for 934 days. The predominant nuclides present at the time of release are shown in Table N.C.1.

TABLE N.C.1

Fission Product Inventory

Nuclide	Curies Calculated
Sr ⁹⁰	4.7
Ce ¹⁴⁴ - Pr ¹⁴⁴	18
Pm ¹⁴⁷	12
Ru ¹⁰⁶ - Rh ¹⁰⁶	1.5
Cs ¹³⁷ - Ba ^{137m}	4

C.3 Meteorological Conditions

The wind directions and velocities prevailing during this release are shown in Table N.C.2. Variations in wind direction were experienced, but they were of such short duration that the effluent path was only slightly displaced from centerline.

Lapse rates, existing at the apex tower during the release, between the 1.5-meter level and both the 24- and 45-meter levels, are shown in Figure N.C.1. It shows that an inversion existed for an appreciable time before the release and continued to deepen following the release.

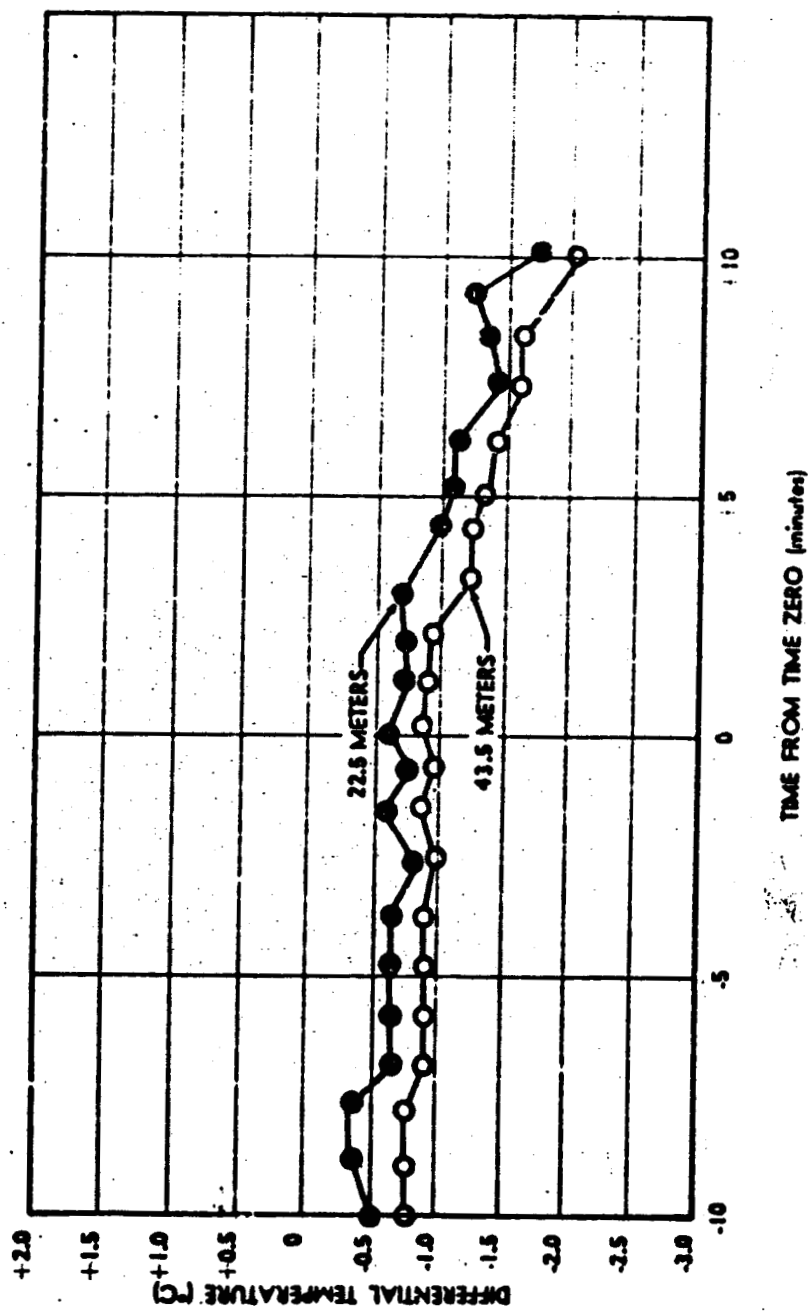


FIGURE NLC.1 LAPSE RATE DURING RELEASE

TABLE N.C.2
Meteorological Summary

APEX TOWER

Height (meters)	Wind Direction			Wind Velocity (meters/sec)		
	Max.	Min.	Ave.	Max.	Min.	Ave.
1.5	264°	201°	239°	4.4	1.1	2.3
2.0			233	4.4	--	2.9
6.0			--	5.4	1.7	3.5
12.0			--	5.9	7.3	4.2
24.0			245	6.4	3.0	4.9
45.0			256	7.0	3.0	5.2

FIELD MASTS

Location (arc)	Wind Direction			Wind Velocity (meters/sec)		
	Max.	Min.	Ave.	Max.	Min.	Ave.
200-meter	260°	195°	232°	5.6	1.4	2.8
400	259	202	231	4.4	1.0	2.3
800	276	214	242	3.9	1.2	2.2
1600	270	209	234	2.9	1.3	2.0
2400	271	208	235	--	--	--
3200	271	208	230	3.5	0.9	1.8

C.4 Smoke Plume Photography

Photographic documentation of the visible smoke plume was accomplished at only one station during this release. The photograph from which the parameters M_z and C_z were obtained is shown in Figure N.C.2.

NPC 1762



Figure N.C.2 PRE-RELEASE SMOKE PLUME

C.5 Furnace Conditions

During previous releases, the furnace required approximately two minutes at maximum power input to begin melting the fuel element. During this release it was estimated that a period of approximately five minutes was required to reach the melting point because of furnace malfunction. Also, the normal furnace program required a thirteen minute furnace operation time, but, because of the slow melt, the time during which the sample was held molten was increased. However, it is not evident from the data that this deviation affected the fission product release.

C.6 Effluent Samplers

The results of the sequential sampler data indicate that the major release of activity, as shown in Figure N.C.3, occurred between 5 and 5.5 minutes after time zero. The sampling intervals for this release were spaced over a 14.5-minute period.

C.7 Release Percentages

The percent release of Cs^{137} , as determined from the pre- and post-melt gamma spectra analyses, is shown in Table N.C.3. The gamma spectra from which those data were derived is shown in Figure N.C.4. The release percent of Sr^{90} , also shown in Table N.C.3, was determined by comparing the results of Sr^{90} field sample radiochemical analysis with the fuel element inventory Sr^{90} - Cs^{137} ratio and the measured Cs^{137} release percent.

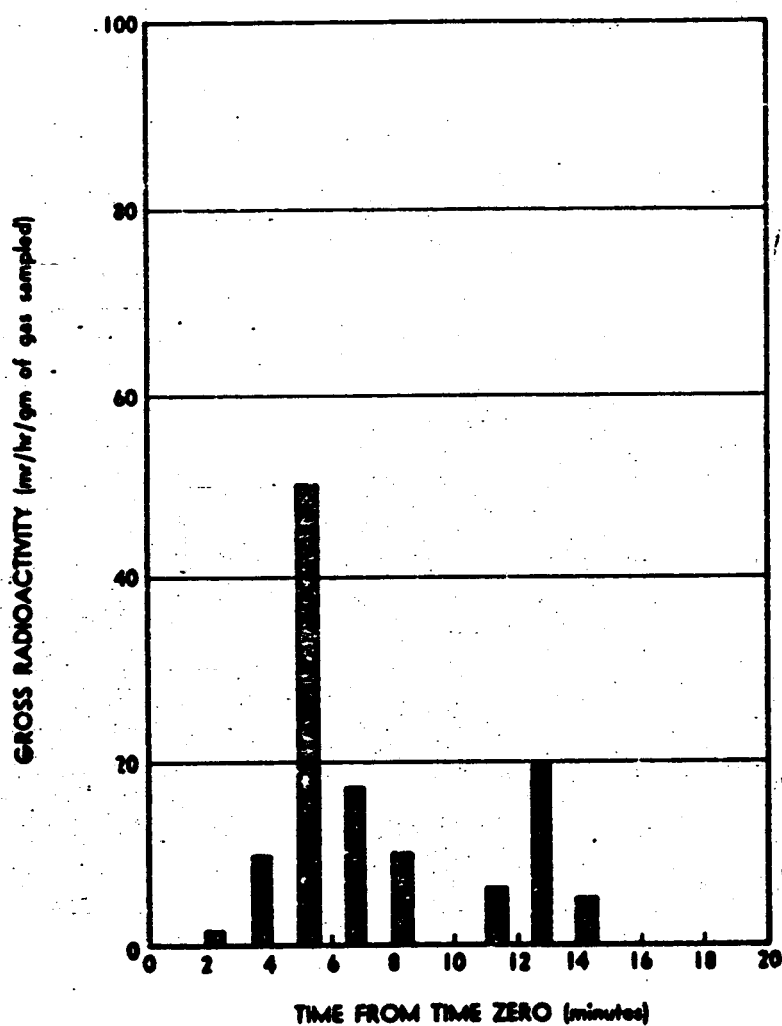


FIGURE N.C.3 SEQUENTIAL-EFFLUENT-SAMPLER FILTER RADIOACTIVITIES.

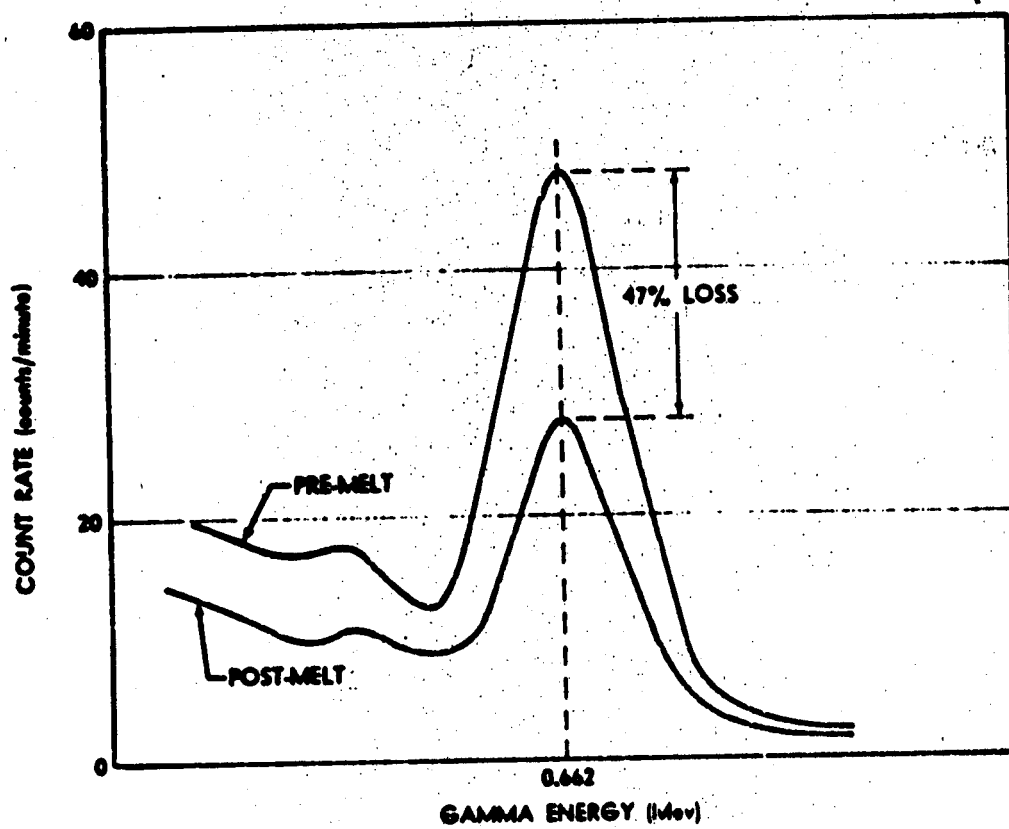


FIGURE H.C.4 PRE- AND POST-MELT GAMMA SPECTRA OF FUEL ELEMENT

TABLE N.C.3
Release Percentage

Nuclide	Percent
Cs ¹³⁷	47
Sr ⁹⁰	0.03

C.8 Air Sampler Field Survey

The gross gamma activity on the pleated filters is shown in Figures N.C.5 and N.C.6. Figure N.C.5 shows the arc profiles of the filter readings corrected for flow rate and background. Figure N.C.6 shows the pleated filter readings of the cloud centerline stations as a function of distance from the release point. Also shown is the least-squares fit to all the data points.

C.9 Airborne Radioactivity

The network cesium data are shown in Figures N.C.7 and N.C.8. Figure N.C.7 shows the cesium profiles on each arc corrected for sampler flow rate. Figure N.C.8 is a plot of the Cs¹³⁷ centerline activity with a least-squares curve fit. Note that the slope of the line is very nearly the same as that obtained from the curve fit of the air sampler field survey.

C.10 Deposited Radioactivity

The cesium collected on the gummed fallout papers is shown in Figures N.C.9 and N.C.10. Figure N.C.10 shows the maximum

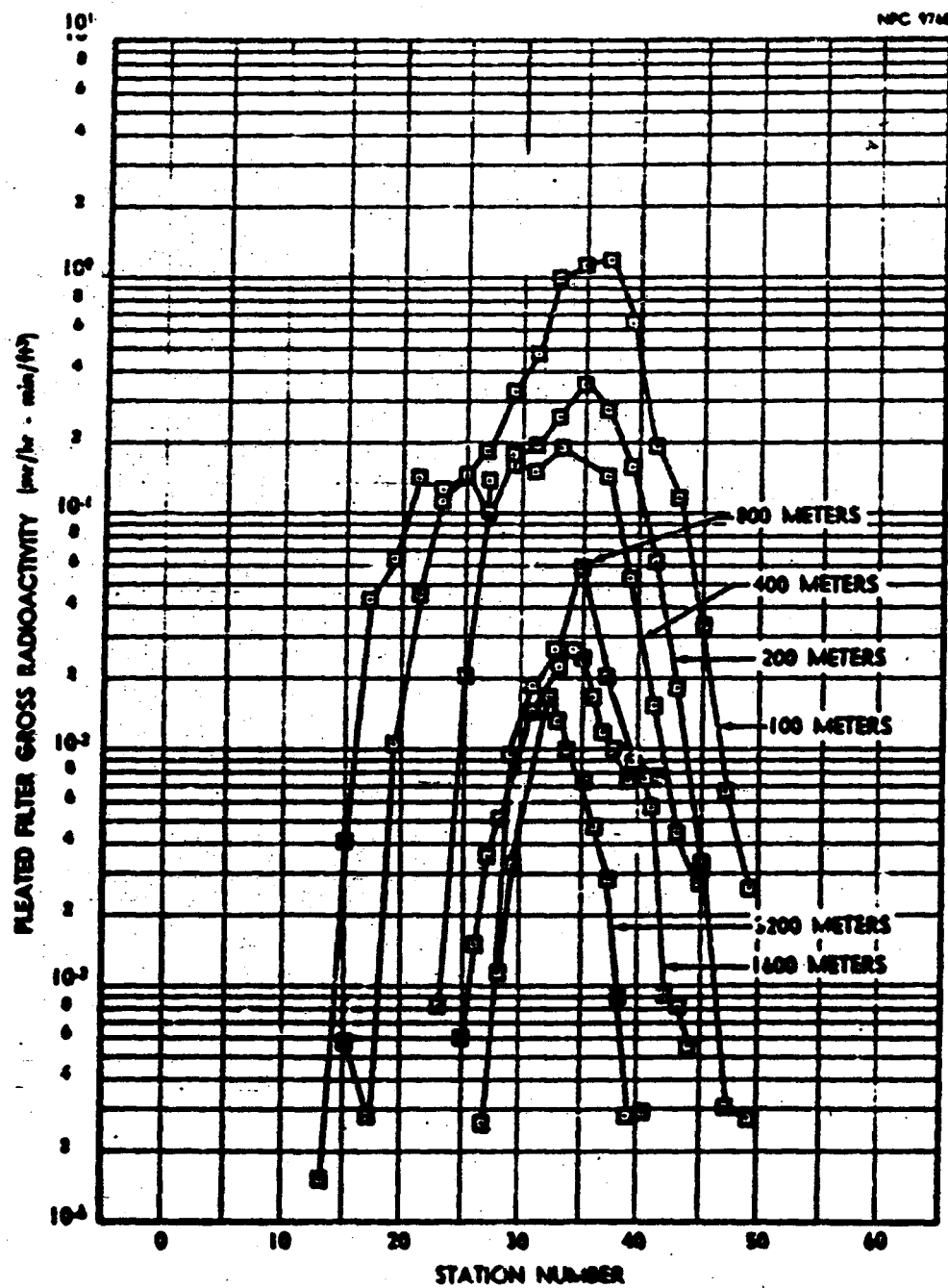


FIGURE H.C.5 H-VOL AIR SAMPLER FIELD SURVEY

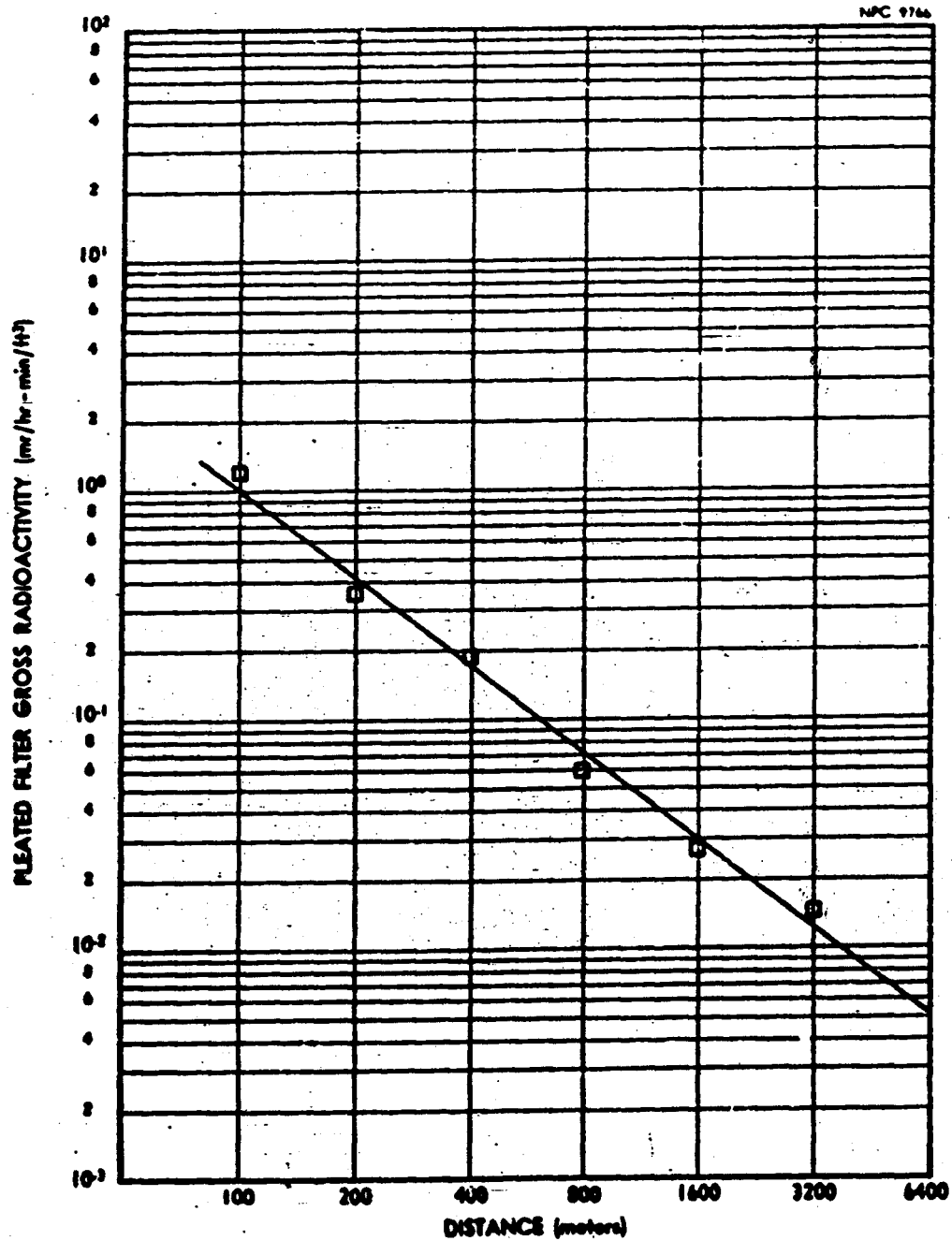
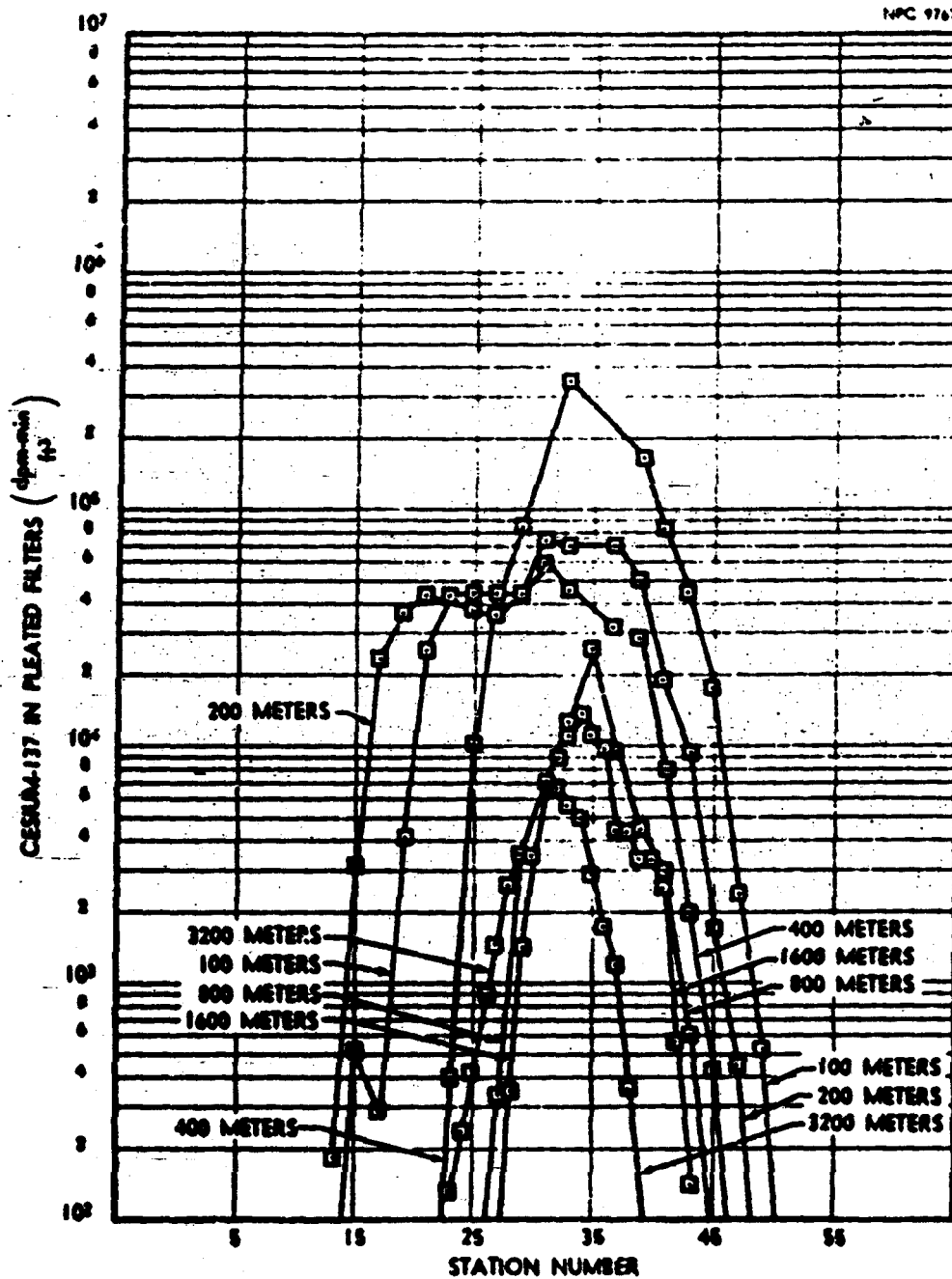


FIGURE H.C.6 H5-VOL AIR SAMPLER FIELD SURVEY
(Centerline)



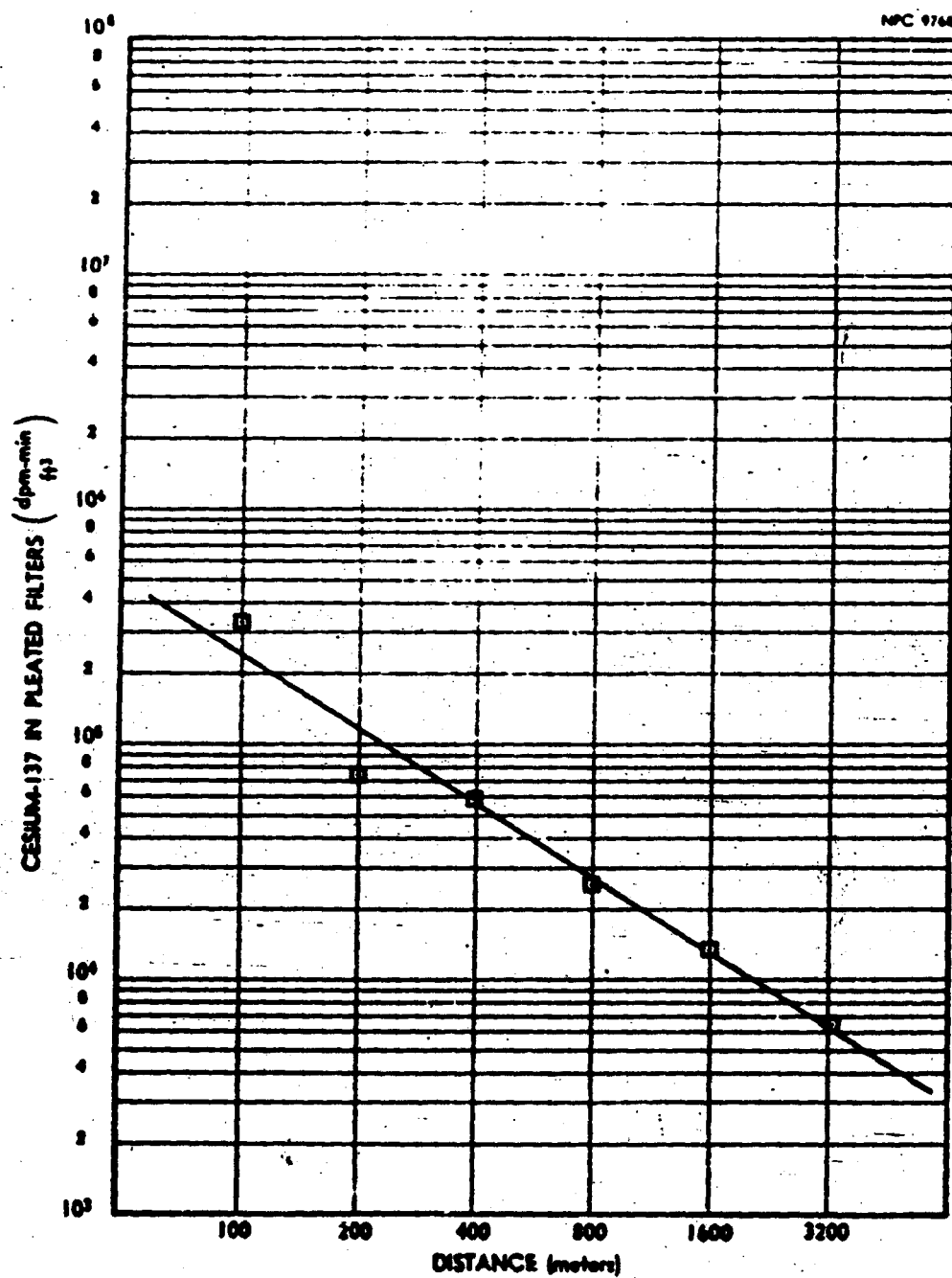
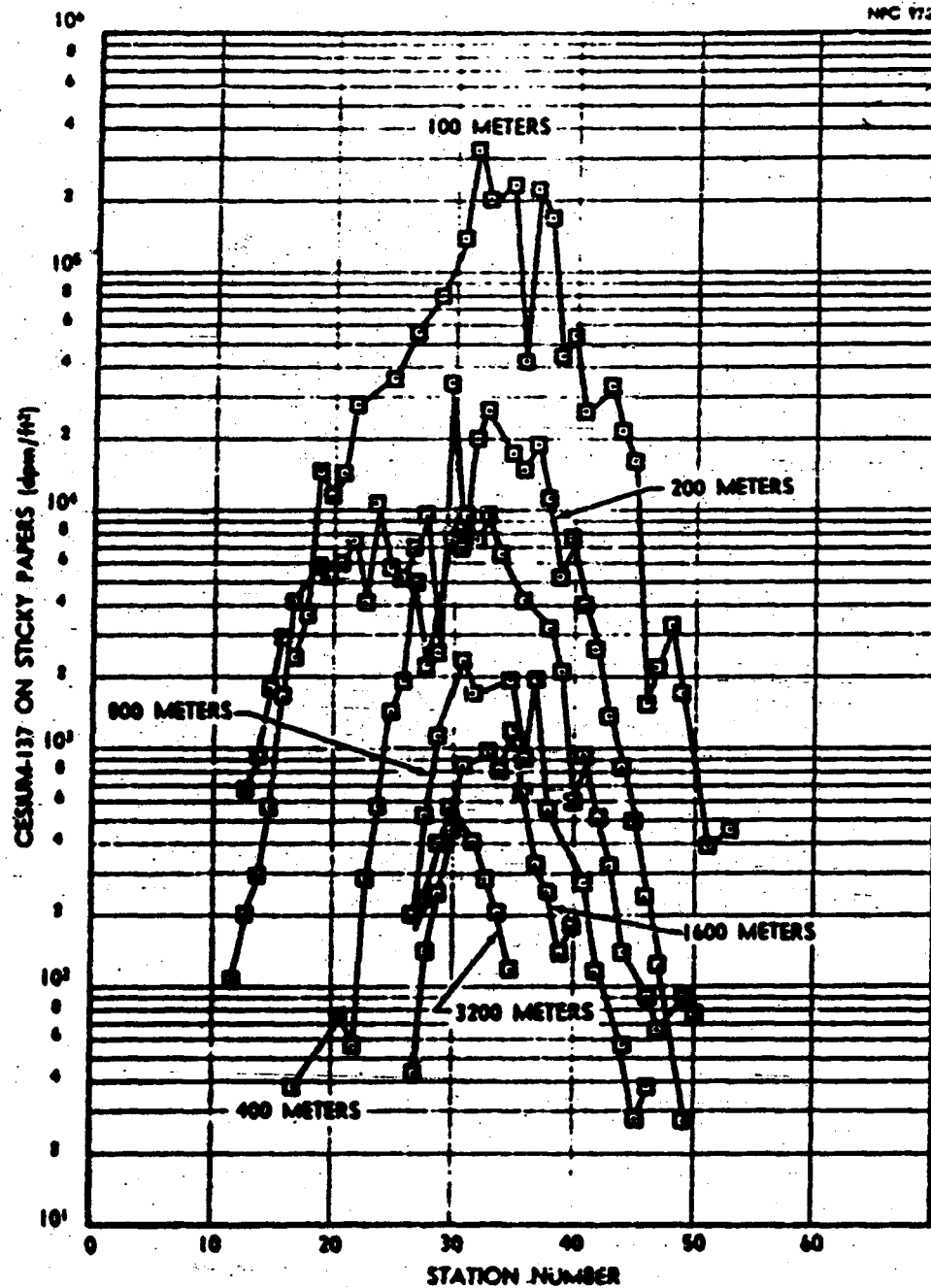


FIGURE N.C.8 HI-VOL AIR SAMPLER LABORATORY ASSAY
OF CESIUM (Centerline)

NPC 9759



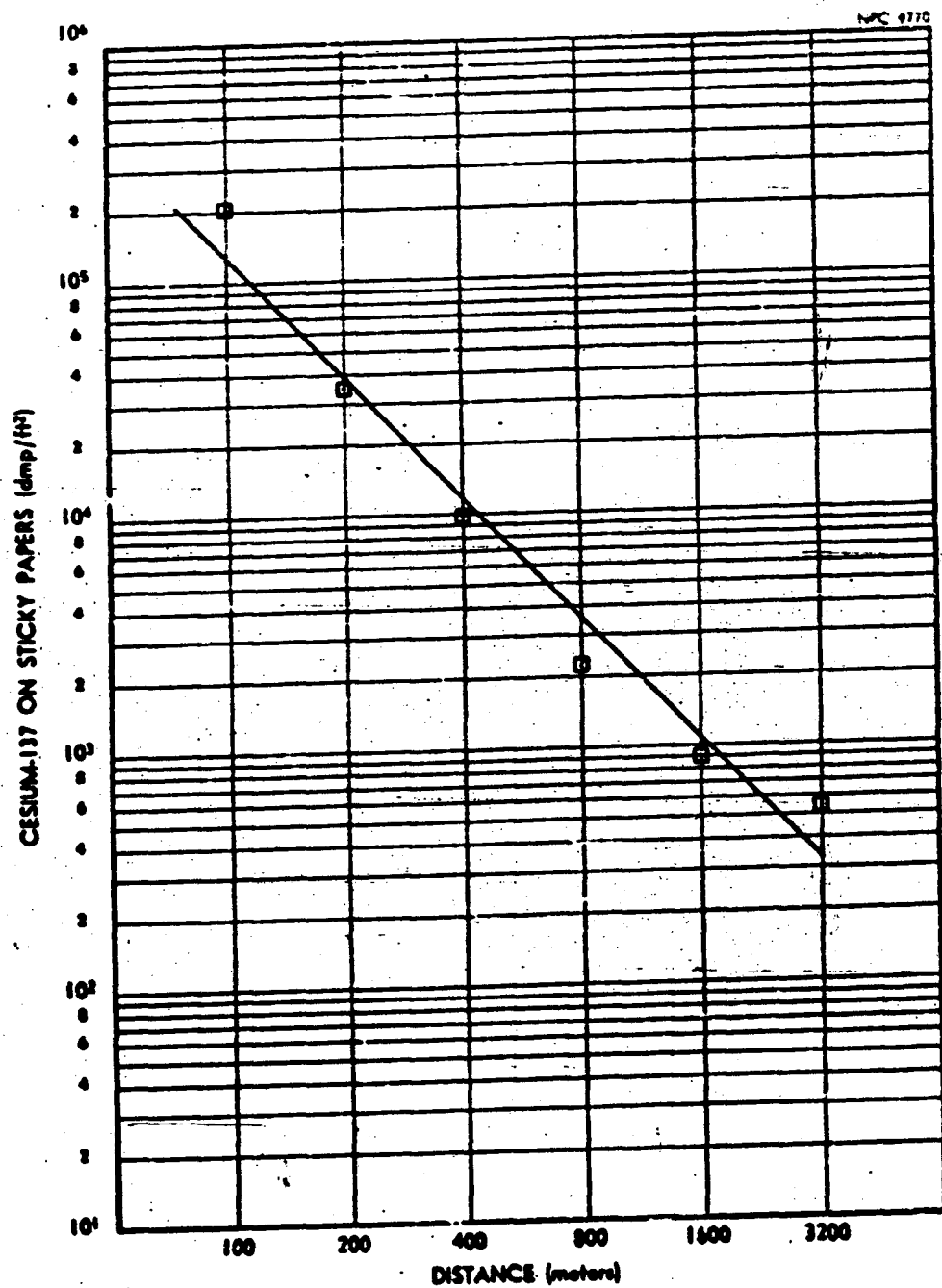


FIGURE N.C.10 DEPOSITED CESIUM (Centerline)

radioactivity values per arc in dpm/ft² as a function of distance. Figure N.C.9 shows the gummed-paper cesium activity profile for each arc from which the cloud centerline values were estimated.

C.11 Deposition Velocity

The average deposition velocity for cesium as a function of distance downwind from the release point is shown in Table N.C.4. This parameter is derived from the ratio of gummed paper activity to pleated filter activity.

TABLE N.C.4

Cesium Deposition Velocity

Arc (meters)	Velocity (cm/sec)
100	0.28
200	0.10
400	0.06
800	0.07
1600	0.04
3200	0.04

C.12 Particle Size

Particle size studies were made during Releases C, E, F, and H. The quantities of radioactive cesium collected during Release C on the 100-meter arc by three Andersen samplers with millipore backup filters are shown in Table N.C.5. About 85 percent of the cesium was collected by the millipore filter, indicating a predominance of submicron particles.

TABLE N.C.5
Distribution of Cs¹³⁷ In The Andersen Sampler

Stage	Activity (DPM _{min}) ft ³	
	Station 28 100-meter arc	Station 32 100-meter arc
1	870	880
2	860	1170
3	875	1300
4	1220	1630
5	3880	4550
6	7700	5500
7*	93500	132000

* No. 7 Stage - Millipore Filter

C.13 Fluorescent Tracer

The assay of the airborne fluorescent particle concentration was made by counting particles on the Andersen plates with a microscope using ultraviolet illumination (Appendix G). The fluorescent tracer network data are shown in Figures N.C.11 and N.C.12.

Figure N.C.11 shows the arc profiles from which centerline values were taken. Figure N.C.12 shows arc centerline values plotted as a function of distance.

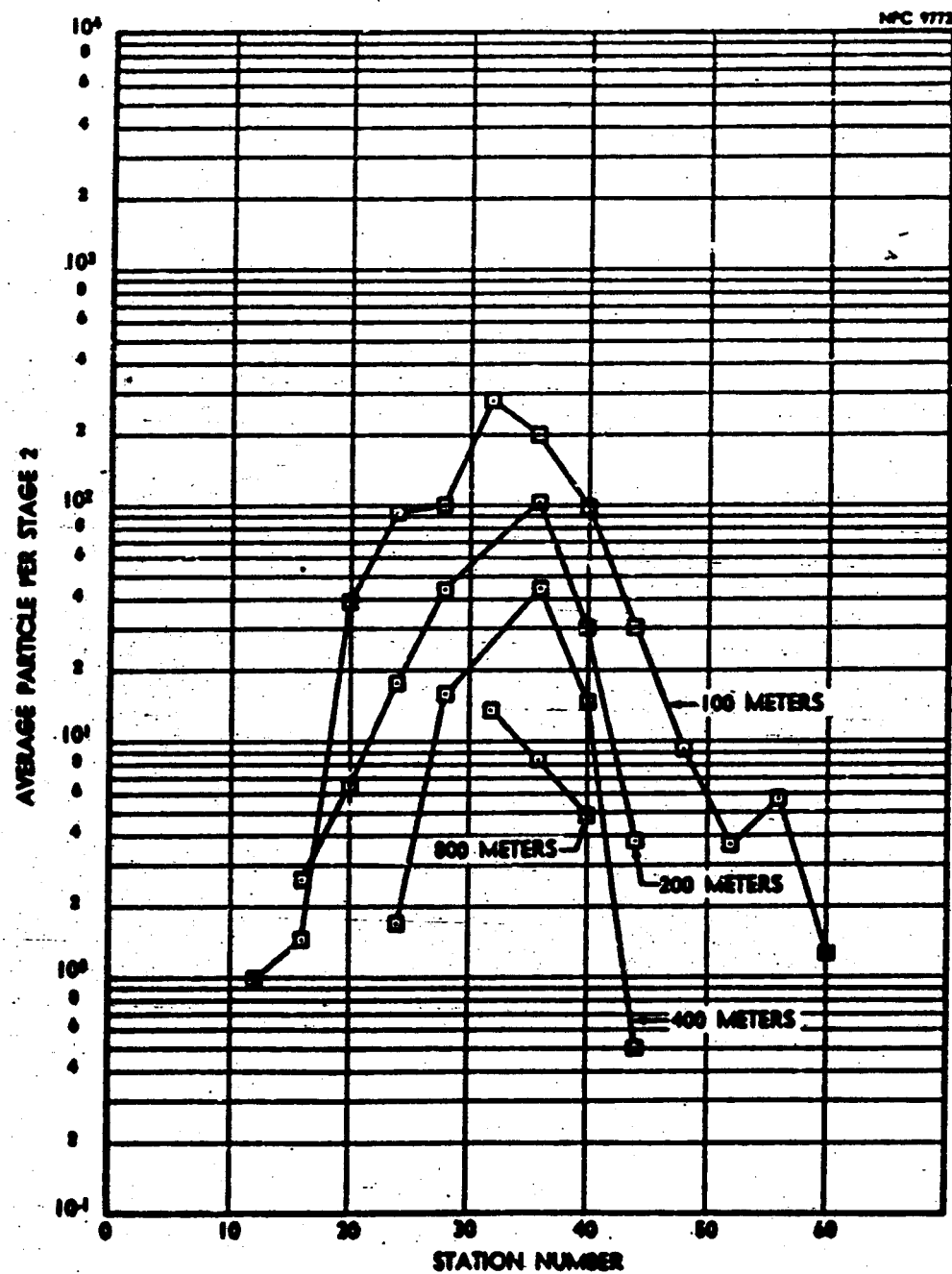


FIGURE N.C.11 FLUORESCENT TRACER (Arc Profiles)

NPC 9771

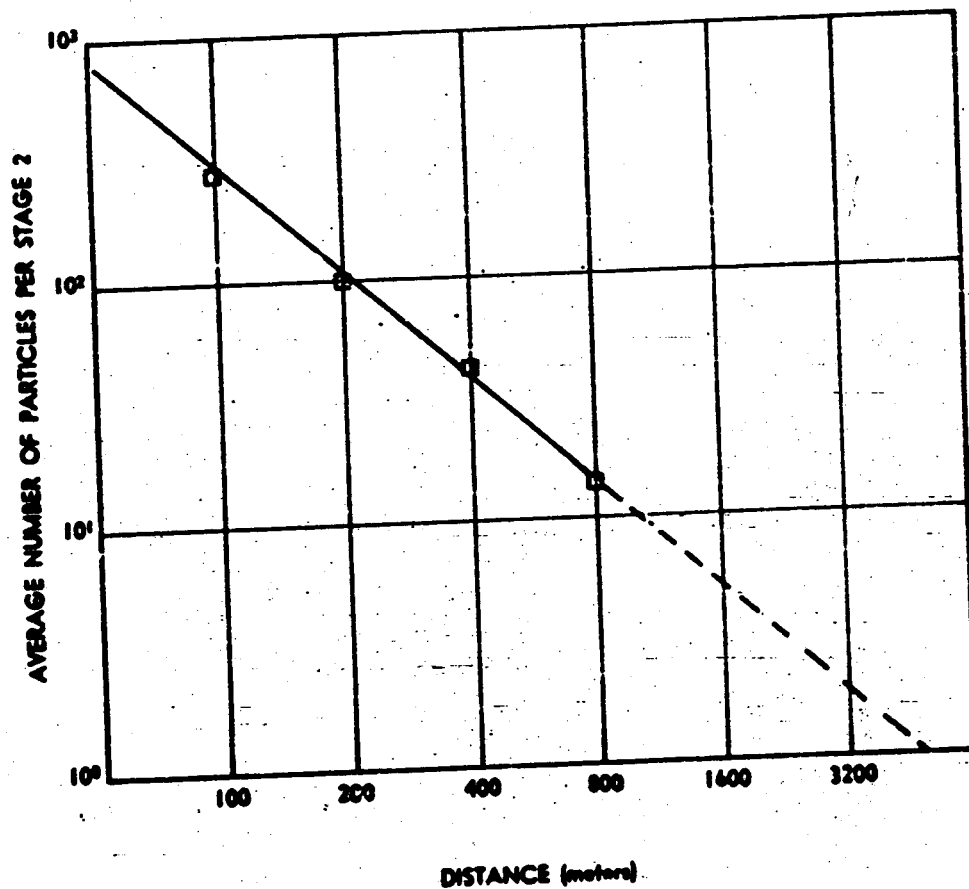


FIGURE N.C.12 FLUORESCENT TRACER (Centerline)

C.14 External Dose

The gamma dose rate was measured and recorded every three degrees on the 400-meter arc. The integrated dose received at each station during passage of the effluent cloud is shown in Figure N.C.13. The trace of the variation of the dose rate with time at the detector station nearest the centerline of the cloud, Station 34, is shown in Figure N.C.14.

An approximate reconstruction of the passage sequence of the gamma activity is shown in Figure N.C.15.

C.15 Diffusion Parameters

Release C was a simultaneous fission product-fluorescent tracer release. Here the relative behavior of the two effluents is of particular interest because of the prospect of simulating a radioactive effluent with a nonradioactive tracer.

The diffusion parameters obtained by fitting Hi-Vol air sampler field survey data to a modified Sutton-type solution of the diffusion equation (see Appendix H) are shown in Table N.C.6. Included in the table are parameter values obtained by the same method of the Hi-Vol air sample assays of cesium¹³⁷, fluorescent particle assays of Andersen sampler plates, and smoke plume photography results (see Appendix F). General agreement is observed between the parameters, with the exception of the smoke plume M_2 and the C_g 's from cesium and smoke.

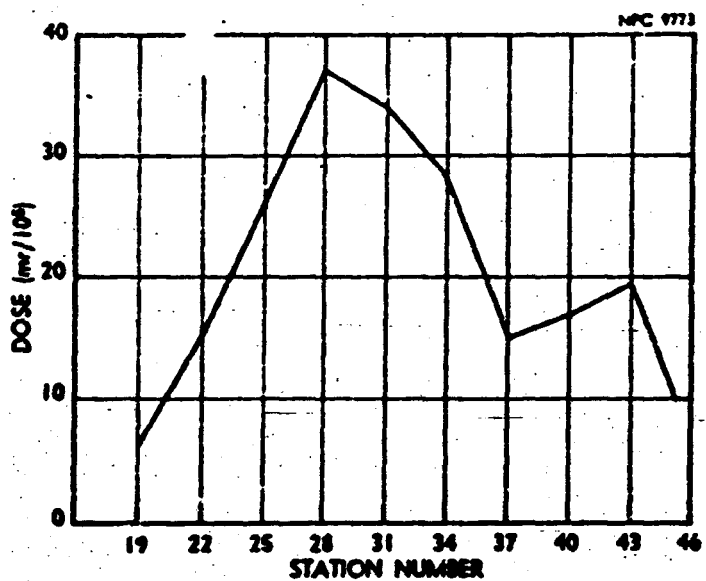


FIGURE N.C.13 GAMMA DOSE FROM CLOUD PASSAGE (Arc Profile)

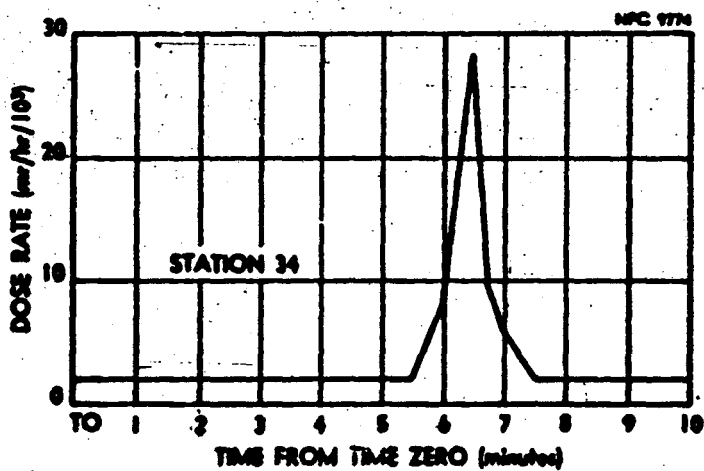
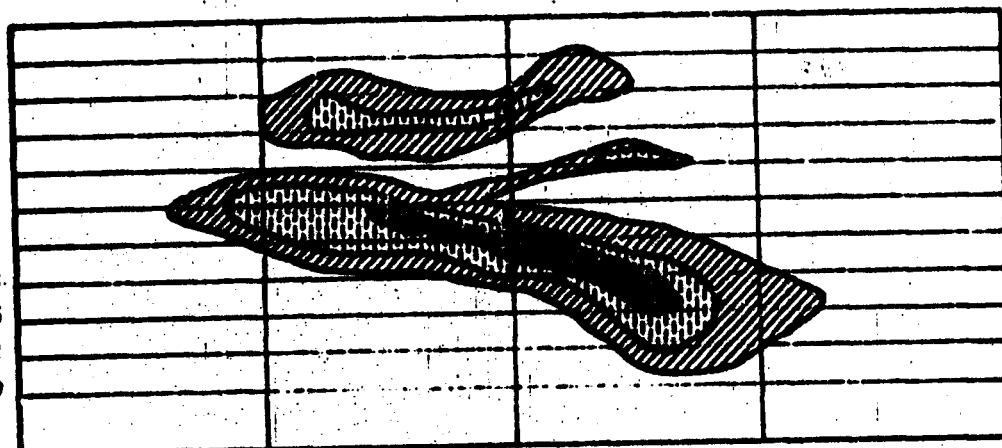


FIGURE N.C.14 GAMMA DOSE RATE FROM CLOUD PASSAGE (Centerline)

STATION NUMBER ON 400-METER ARC

3
4
5
6
7
8
9
10
11
12
13
14
15
16
17
18
19
20
21
22
23
24
25
26
27
28
29
30
31
32
33
34
35
36
37
38
39
40
41
42
43
44
45
46
47
48
49
50
51
52
53
54
55
56
57
58
59
60
61
62
63
64
65
66
67
68
69
70
71
72
73
74
75
76
77
78
79
80
81
82
83
84
85
86
87
88
89
90
91
92
93
94
95
96
97
98
99
100



TIME FROM TIME ZERO (minutes)

- BACKGROUND TO 0.006 MR/HR
- 0.006 - 0.010 MR/HR
- 0.010 - 0.020 MR/HR
- 0.020 - 0.040 MR/HR

The smoke data were obtained approximately 20 minutes before the start of the fission product release, during which time a near isothermal condition existed. This difference in lapse rate may account for the elevated M_z value.

The C_z value obtained from the cesium-data fit appears quite different from the smoke data and values obtained from other releases. No adequate reason for this high value can be offered; however, there are two factors which may have contributed to the discrepancy. First, the inner arcs were inoperative during the initial minutes of melting. Some activity may have passed these arcs without being detected. This theory, however, is not substantiated by air sampler activities or deposition samples. Secondly, a portion of the effluent cloud may have become separated and carried off the network. This would account for the elevated C_z value. Because of the above differences no isopleths were constructed.

TABLE N.C.6
Diffusion Parameters

Parameters	Field Survey Data Fit	Cs ¹³⁷ Fit	Tracer Fit	Plume Fit
M_y	0.84	0.76	0.85	--
M_z	0.44	0.28	0.59	1.2
C_y	0.22	0.37	0.25	--
C_z	--	56.0	--	0.03
n	--	--	--	--

C.16 Radiobiology

For Release C, two rats were placed at each two-degree interval on the 100-, 200-, 400-, and 800-meter arcs. Exposure cages were constructed of 1/2-inch wire mesh, each animal having freedom of movement. Recovery began 45 minutes after the release and was completed in 30 minutes. Those animals known to be in the cloud were sacrificed and placed in plastic bags for whole body counting. The animals which indicated a significant accumulation of radioactivity were sacrificed and lung, trachea, kidney and GI tract were removed and fission product content determined. Tissues from the two rats at each station were counted together, yielding an average value.

Whole body counts are presented in Table N.C.7 as disintegrations per minute per rat. Figure N.C.16 shows these data plotted to give arc profiles.

In like manner, tissue data are presented in Table N.C.8 and plotted in Figure N.C.17. Because the release consisted almost entirely of Cs^{137} , the counting efficiency for Ba^{137m} , approximately 50 per cent, was used to express the data in terms of disintegrations per minute.

C.17 Sand and Water Collections

The water and sand sampling program was not used during this release.

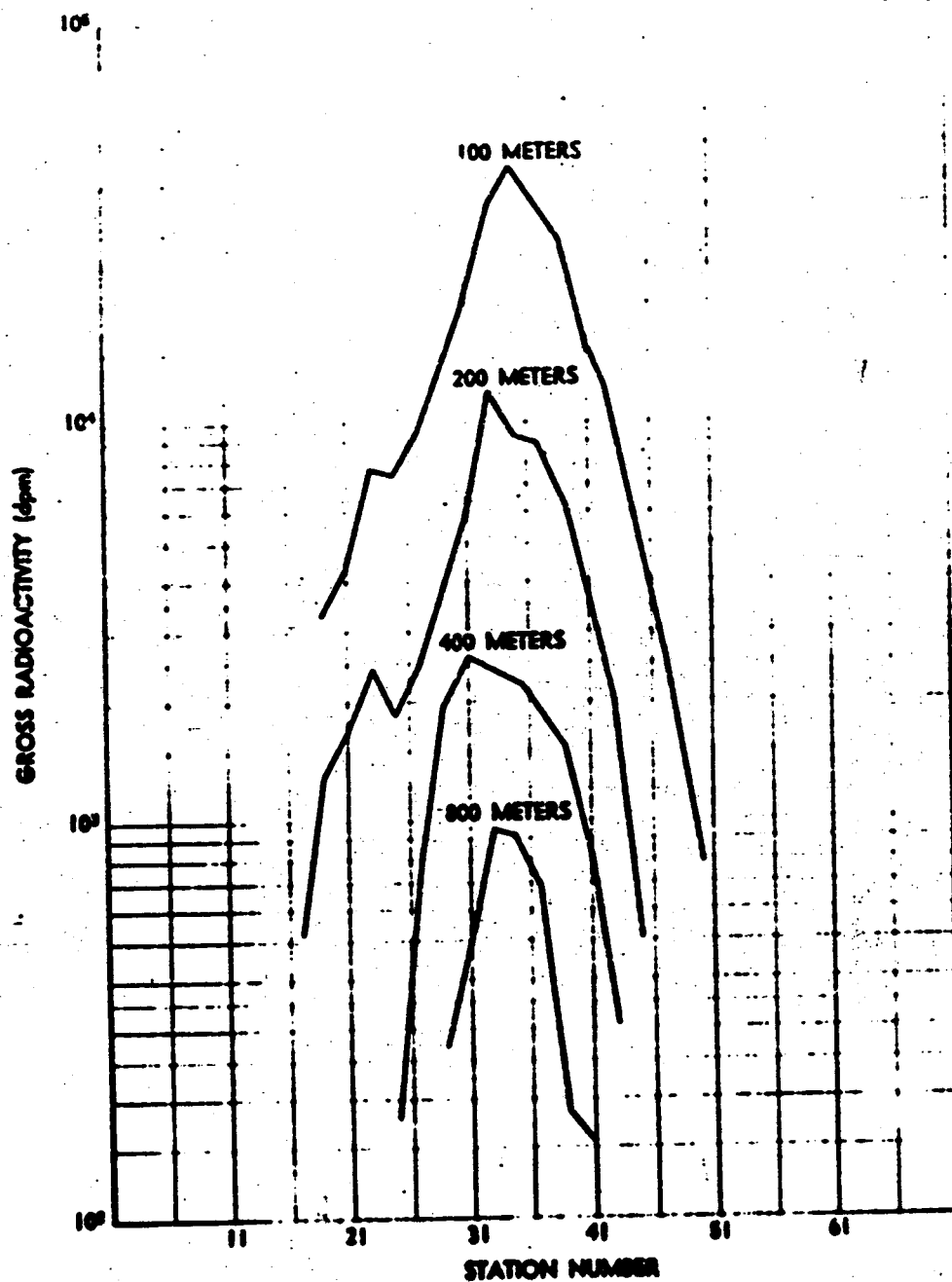


FIGURE N.C.16 RAT WHOLE-BODY EXPOSURE (Arc Profiles)

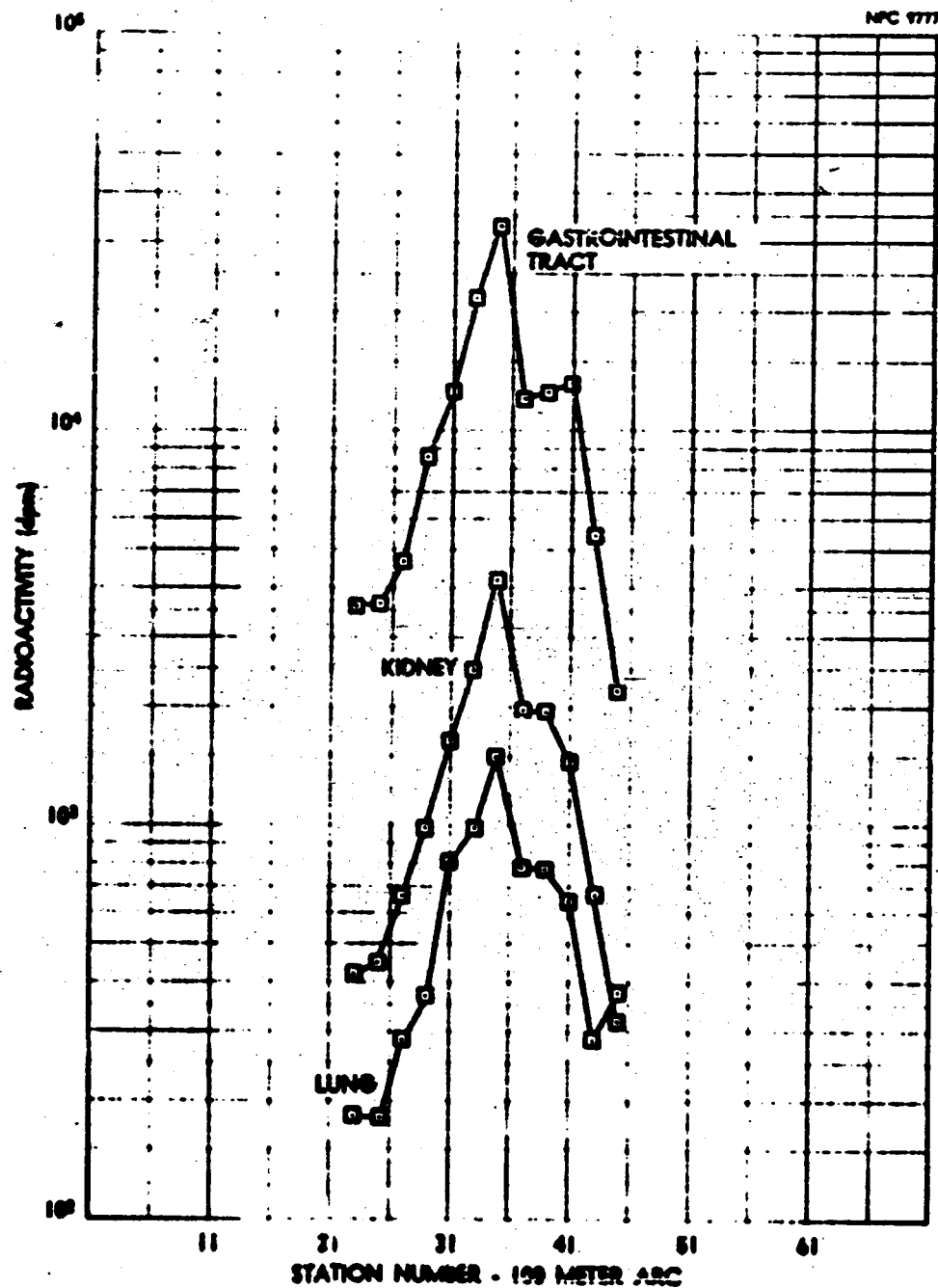


FIGURE NL-17 RAT TISSUE EXPOSURE

TABLE N.C.7
Whole-Body Radioactivity in Rats

Arc and Station	Disintegration/min.			Arc and Station	Disintegration/min.		
	Rat #1	Rat #2	Ave.		Rat #1	Rat #2	Ave.
100-19	3360	3360	3360	200-39	6260	n.s.	6260
-21	4770	3760	4270	-41	3610	3530	3570
-23	8890	5970	7430	-43	1690	2220	1950
-25	6750	7720	7230	-45	624	396	510
-27	10100	8470	9270	-47	107	68	88
-29	14300	12100	13200	-49	77	32	54
-31	18100	22300	20200	400-25	190	178	184
-33	34000	31900	33000	-27	858	608	733
-35	37800	47700	42700	-29	1830	2090	1960
-37	34400	n.s.	34400	-31	2140	2910	2520
-29	22900	33600	28000	-33	2240	2510	2370
-41	16900	14300	15600	-35	2190	2410	2300
-43	9780	12300	11000	-37	1700	2110	1900
-45	5220	n.s.	5220	-39	1540	1440	1490
-47	2510	2550	2530	-41	857	753	605
-49	788	878	833	-43	302	376	319
200-16	60	56	58	-45	218	168	193
-17	444	569	506	-47	114	126	120
-19	1390	1190	1290	800-29	221	233	227
-21	1990	1360	1670	-31	514	420	467
-23	2310	2540	2430	-33	1060	853	956
-25	1970	1740	1860	-35	797	1080	937
-27	2910	2030	2470	-37	732	607	670
-29	3290	4060	3760	-39	186	---	93
-31	5720	5850	5780	-41	275	236	256
-33	10900	12200	11600	-43	139	101	120
-36	12100	7340	9700	-45	---	38	19
-38	8800	8030	8410				

n.s. = no sample

--- Background

TABLE N.C.8
Radioactivity in Rats

Arc and Station	Disintegrations/min/ organ-			
	Trachea	Lung	Kidney	G.I. Tract
100-23	all	187	422	3560
-25	back-	181	447	3650
-27	ground	289	685	4610
-29		366	985	4450
-31		810	1620	12350
-33		975	2490	21400
-35		1500	4220	32350
-37		775	1930	11900
-39		775	1940	12400
-41		640	1435	12950
-43		285	665	5400
-45		372	315	2185
200-31	all	215	429	5050
-33	back-	275	320	8600
-35	ground	472	1020	9600
-37		319	1150	8200
-39		---	278	27750
-41		---	505	3400

*---Background

APPENDIX N-D

(Release D)

D.1 Summary

Type of Sample ----- Aged Fuel Elements
Date and Release Time ----- 14 August 1958; 6:16 PM
Lapse Rate (1.5 - 45 m) ----- $/0.54^{\circ}\text{C}$
Lapse Rate (1.5 - 24 m) ----- $/0.57^{\circ}\text{C}$
Mean Wind Speed ----- 4.3 meters/sec
Wind Direction ----- Network Centerline
Cloud Photography ----- No photography
Fluorescent Tracer ----- Released for 10 minutes
immediately following
fission product release
Animals ----- Rats on 100- and 200-
meter arcs (Ref. 11)
Network Radioactivity ----- Detected out to 3200
meters; maximum reading
of pleated filters on
100-meter arc, 240mr/hr,
using Cutie Pie.
External Dose ----- Maximum dose rate on
400-meter arc, 0.072
mr/hr, using scintilla-
tion detector described
in Appendix K

D.2 Fuel Element

The fuel element had been irradiated to generate 6.1×10^4 watts for a total of 467 hours and had decayed for 942 days. The predominant nuclides present at the time of release are shown in Table N.D.1.

TABLE N.D.1
Fission Product Inventory

Nuclide	Curies Calculated
Sr ⁹⁰	3.5
Ce ¹⁴⁴ - Pr ¹⁴⁴	13
Pm ¹⁴⁷	8.6
Ru ¹⁰⁶ - Rh ¹⁰⁶	1.1
Cs ¹³⁷ - Ba ^{137m}	2.9

D.3 Meteorological Conditions

The wind directions and velocities prevailing during this release are shown in Table N.D.2.

Lapse rates as a function of time after release, existing between the 1.5-meter and both the 24- and 45-meter levels at the apex tower, are shown in Figure N.D.1.

NPIC 9778

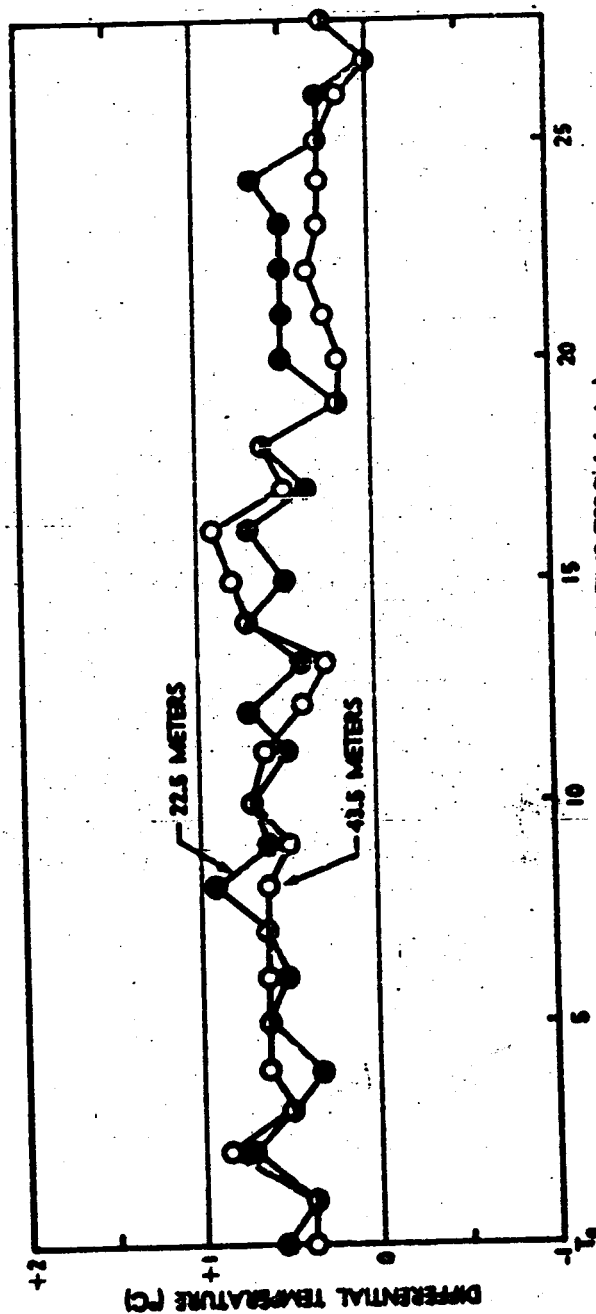


FIGURE 14.5.1 LAPSE RATE DURING RELEASE

D.4 Furnace Conditions

At 2.5 minutes after energizing the induction furnace the temperature thermocouple broke resulting in the loss of temperature readings. From that point on, control of the furnace temperature was attempted according to previous release furnace power programs. Duplication was not accomplished and an excessive melt temperature resulted. It is estimated that the furnace temperature exceeded the planned temperature plateau by 300 to 400°C at approximately five minutes after initiating the melt.

D.5 Effluent Samplers

The data obtained from the sequentially operated effluent samplers show that the major release of radioactivity occurred at approximately five minutes after initiating the melt. These data are shown in Figure N.D.2.

D.6 Release Percentages

The release percentages of Cs^{137} and Sr^{90} as determined by pre- and post-melt gamma spectrometry and Hi-Vol air sampler data respectively are shown in Table N.D.3. The gamma spectra from which the percent release of Cs^{137} was determined are shown in Figure N.D.3.

TABLE N.D.3
Release Percentage

Nuclide	Percent
Cs^{137}	83
Sr^{90}	0.68

TABLE N.D.2

Meteorological Summary

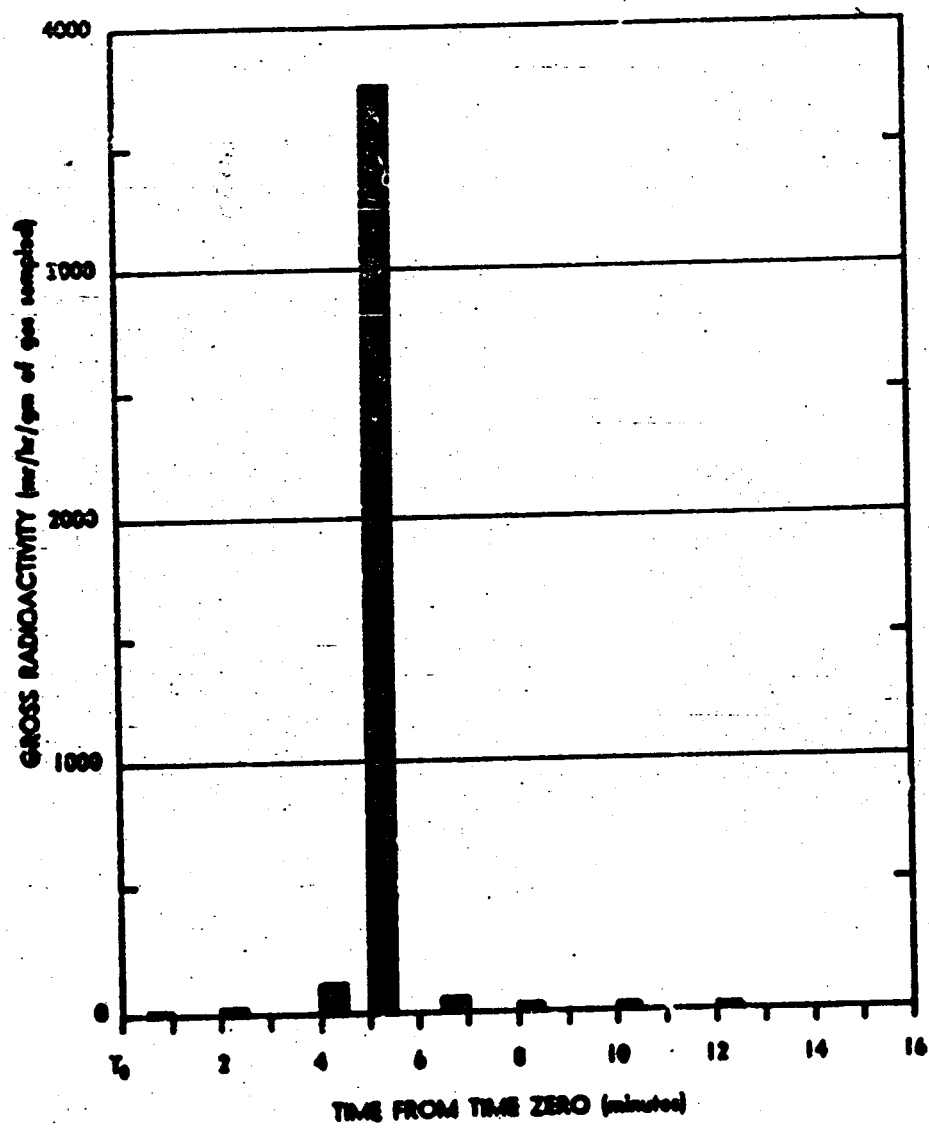
APEX TOWER

Height (meters)	Wind Direction			Wind Velocity (meters/sec)		
	Max.	Min.	Ave.	Max.	Min.	Ave.
1.5	272°	192°	233°	8.0	2.0	4.26
3.0	270	194	234	8.5	2.1	4.99
6.0	--	--	--	8.4	2.6	5.54
12.0	--	--	--	9.1	3.3	6.18
24.0	265	201	234	10.2	1.8	6.69
45.0	275	217	244	10.3	4.8	7.34

FIELD MASTS

Location (Arc)	Wind Direction			Wind Velocity (meters/sec)		
	Max.	Min.	Ave.	Max.	Min.	Ave.
200 meter	277°	201°	234°	8.0	2.8	5.10
400	265	198	229	8.6	2.0	4.98
800	279	205	237	8.7	2.0	5.12
1600	274	190	230	8.0	2.7	5.12
2400	271	177	233	8.3	1.9	4.77
3200	310	162	227	7.3	1.0	4.31

NYC 9779



NPC 1710

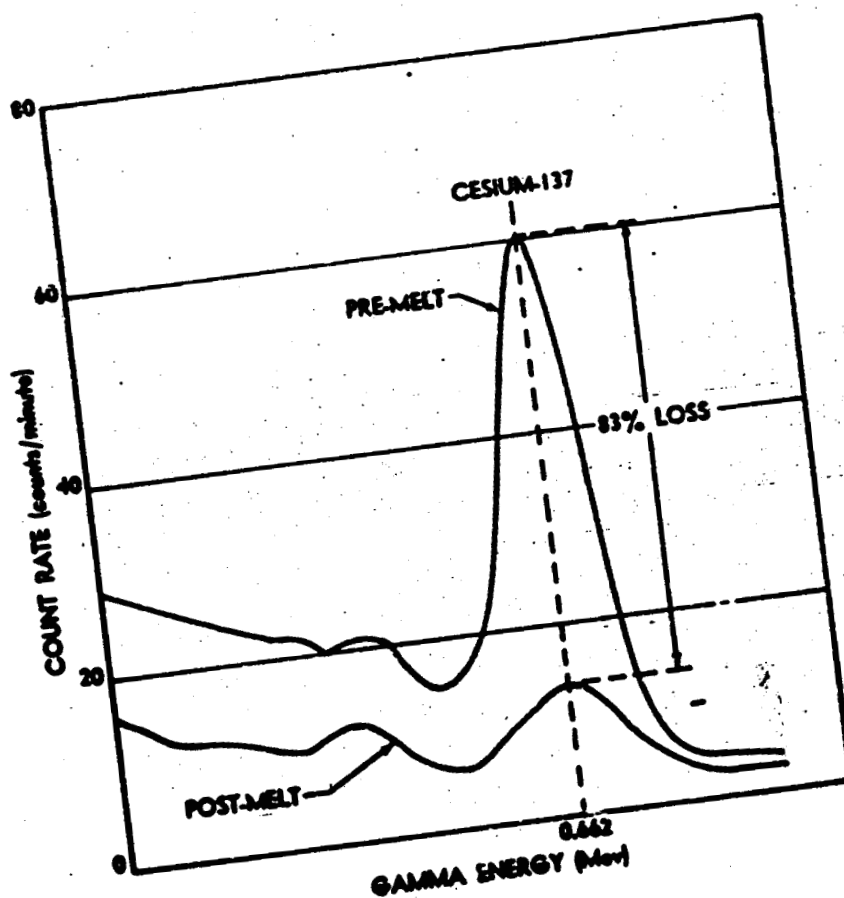


FIGURE N.D.3 PRE- AND POST-MELT GAMMA SPECTRA OF FUEL ELEMENT

D.7 Air Sampler Field Survey

The term "field survey" refers to contact measurements which were taken with a beta-gamma survey meter on the Hi-Vol, pleated filters immediately following the test. Figure N.D.4 shows the arc profiles of the filter readings corrected for sampler flow rate and background. Figure N.D.5 shows the pleated filter readings of the cloud centerline stations as a function of distance from the release point. Also shown is the least-squares fit to the data points.

D.8 Airborne Radioactivity

Airborne radioactivity of Cs^{137} , as determined by laboratory counting of the filters, is shown on Figure N.D.6. These data have been corrected for sampler flow rate. Figure N.D.7 is the centerline plot of Figure N.D.6 with a least-squares fit to the data points.

Radiochemical analysis of the centerline stations on all arcs was performed for this release. The data for Sr^{90} and a least-squares curve fit are shown on Figure N.D.8.

D.9 Deposited Radioactivity

The cesium deposited on the gummed fallout papers is shown in Figure N.D.9 and N.D.10. Figure N.D.9 presents the deposited activity arc profiles from which the centerline data (Figure N.D.10) were taken.

NPC 9781

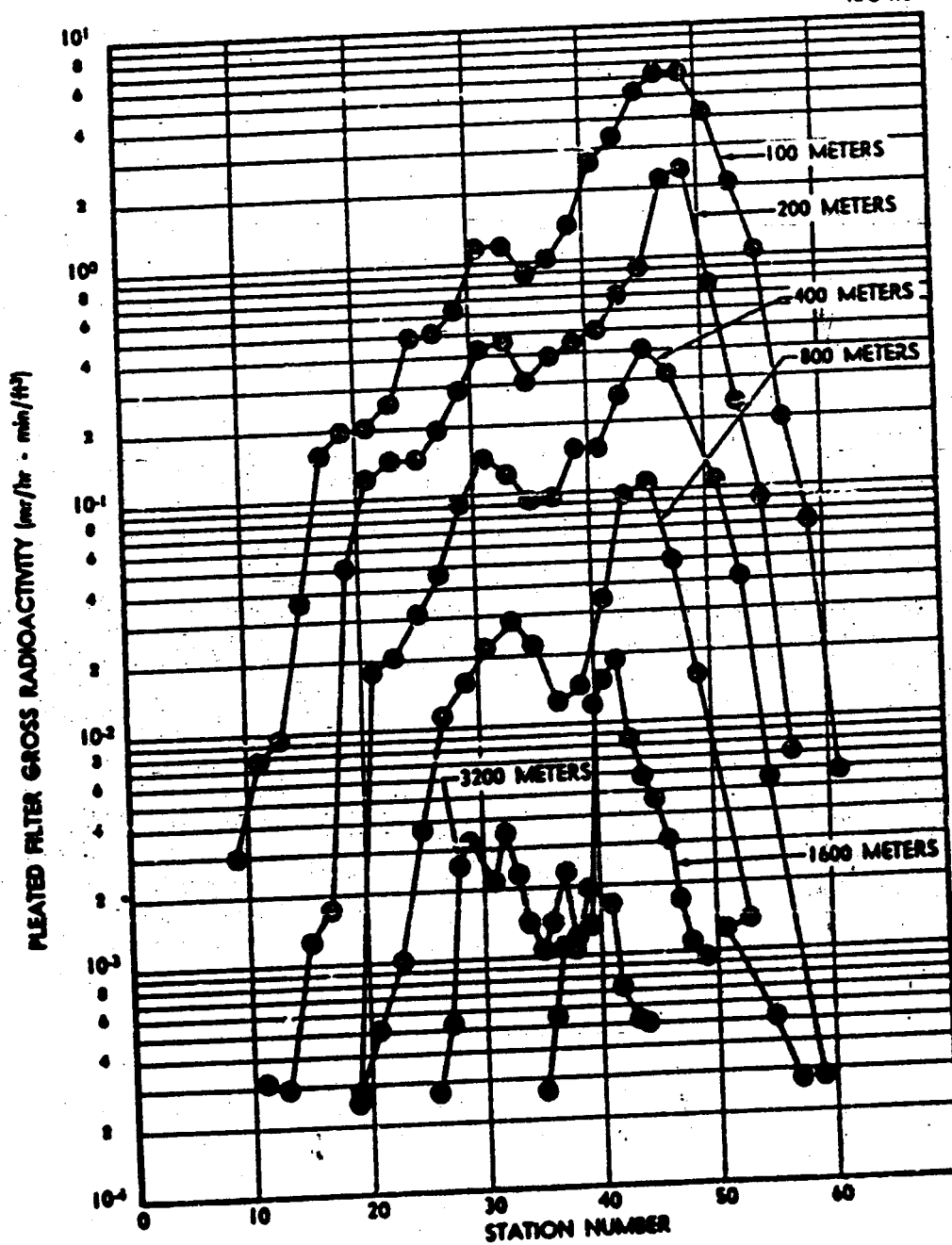


FIGURE N.D.4 HI-VOL AIR SAMPLER FIELD SURVEY
(Arc Profiles)

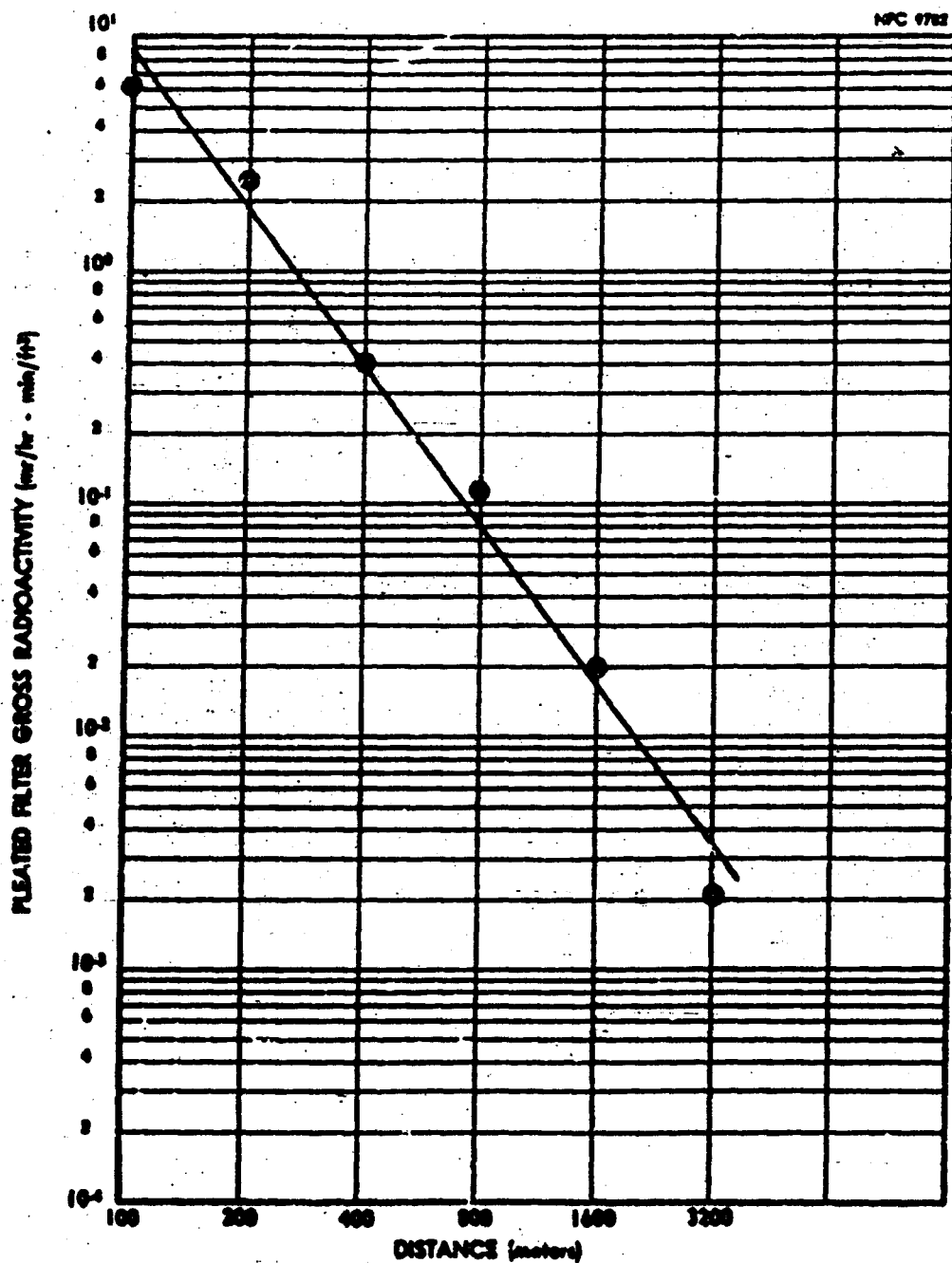


FIGURE M.D.5 M-VOL AIR SAMPLER FIELD SURVEY
(Continued)

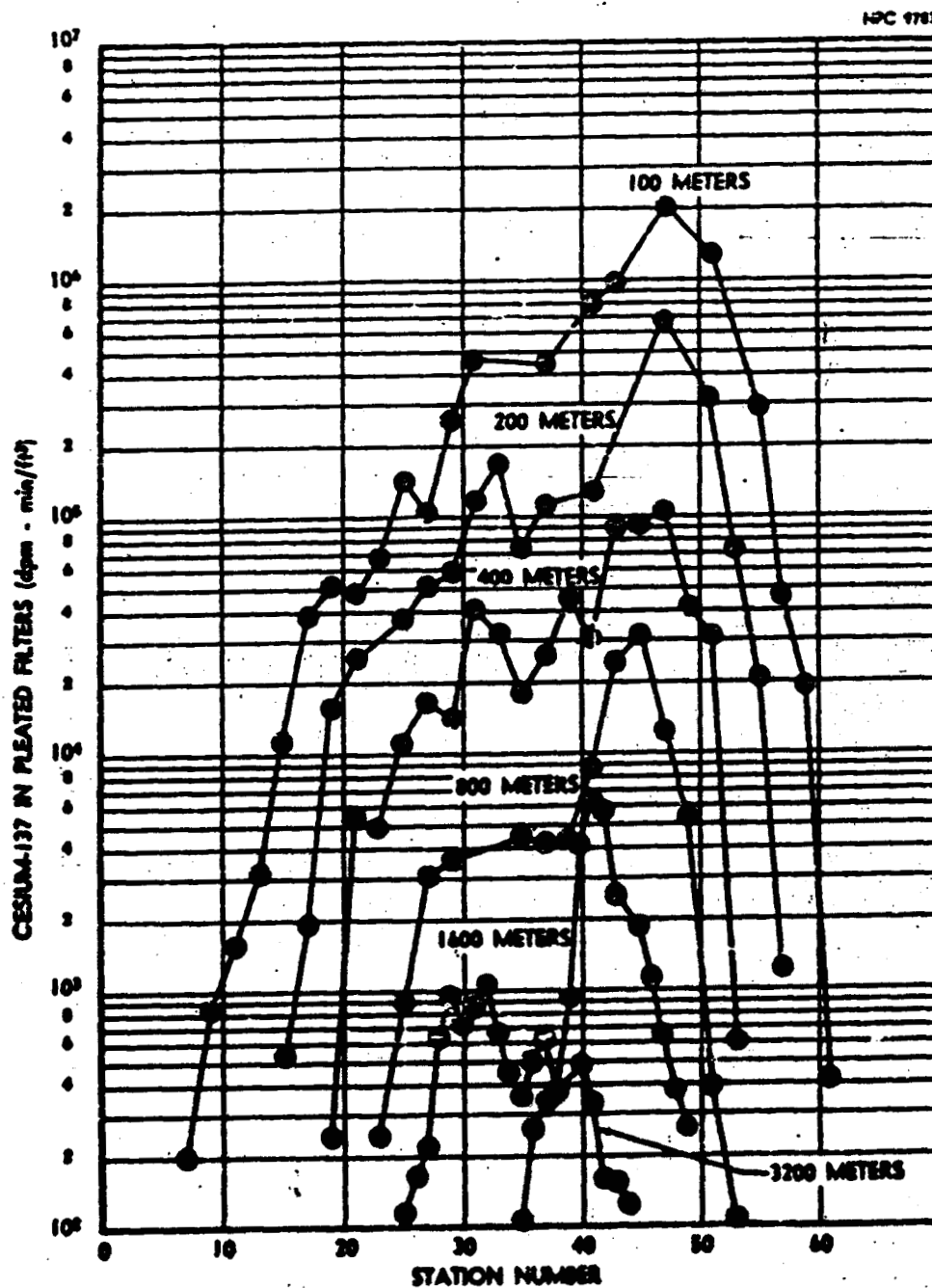


FIGURE N.B.6 HI-VOL AIR SAMPLER LABORATORY ASSAY OF CESIUM (Arc Profiles)

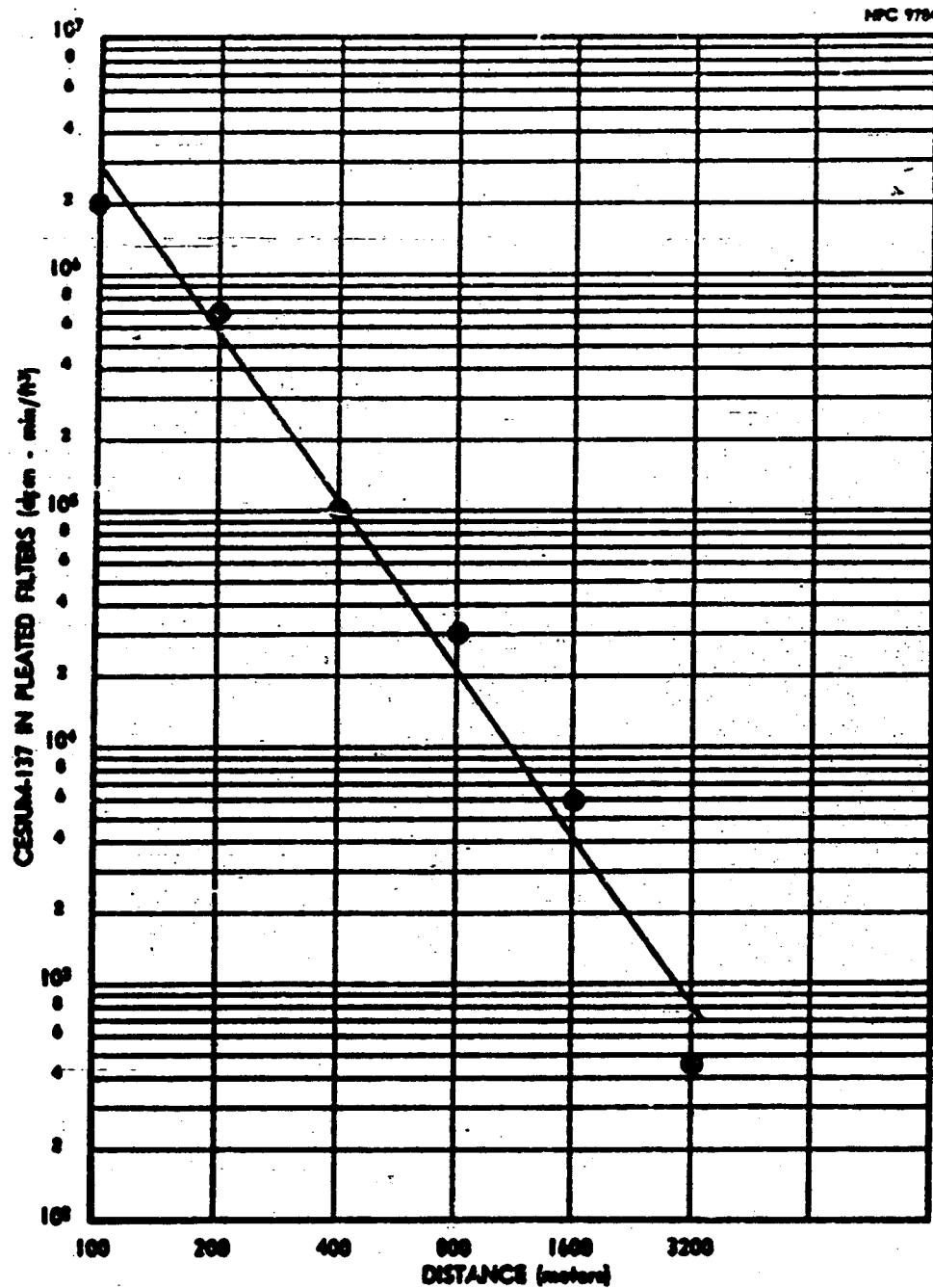


FIGURE N.B.7 IN-VOL AIR SAMPLER LABORATORY ASSAY
OF CESIUM (Centerline)

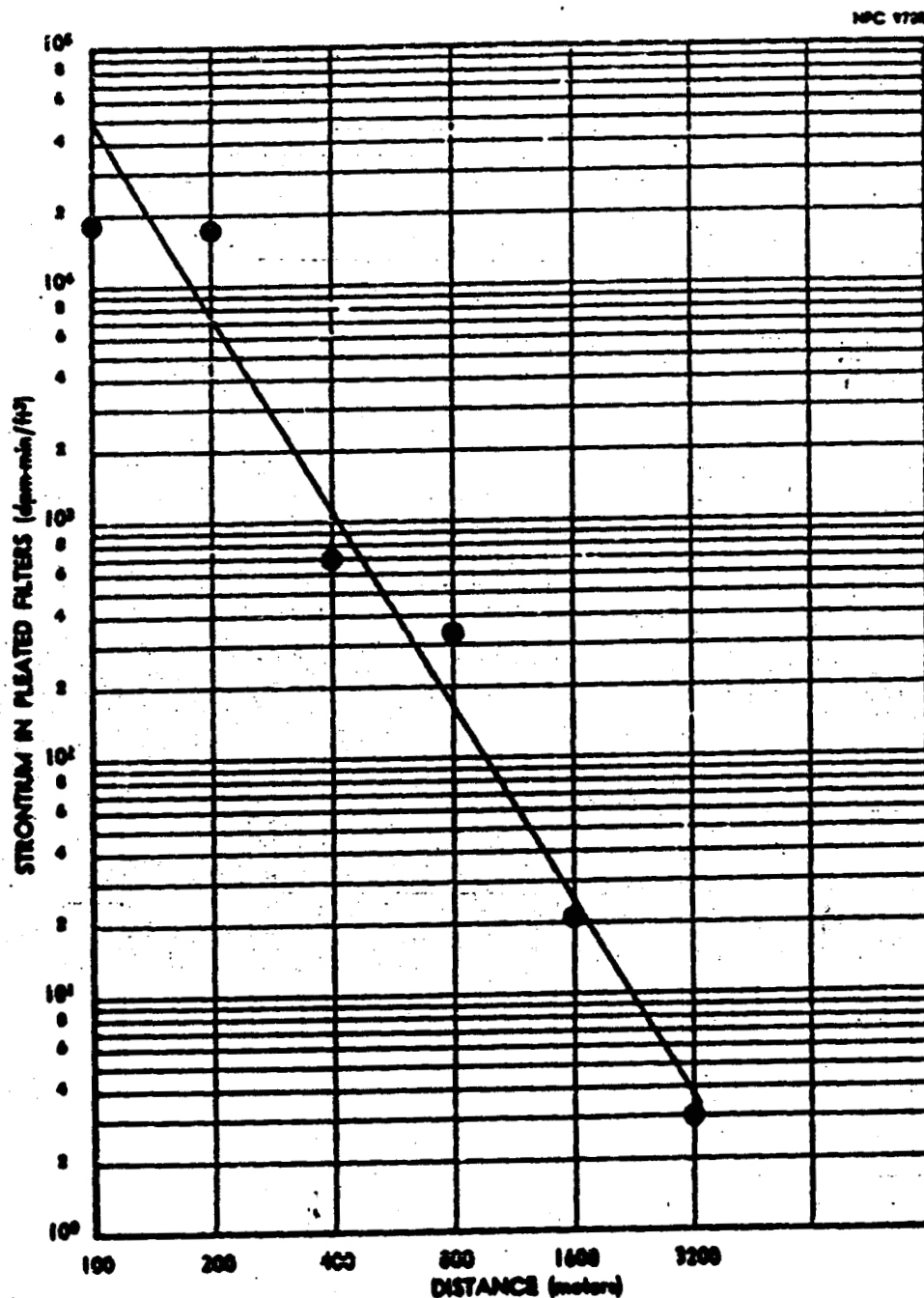


FIGURE N.B.S. HI-VOL AIR SAMPLER LABORATORY ASSAY
OF STRONTIUM (Centerline)

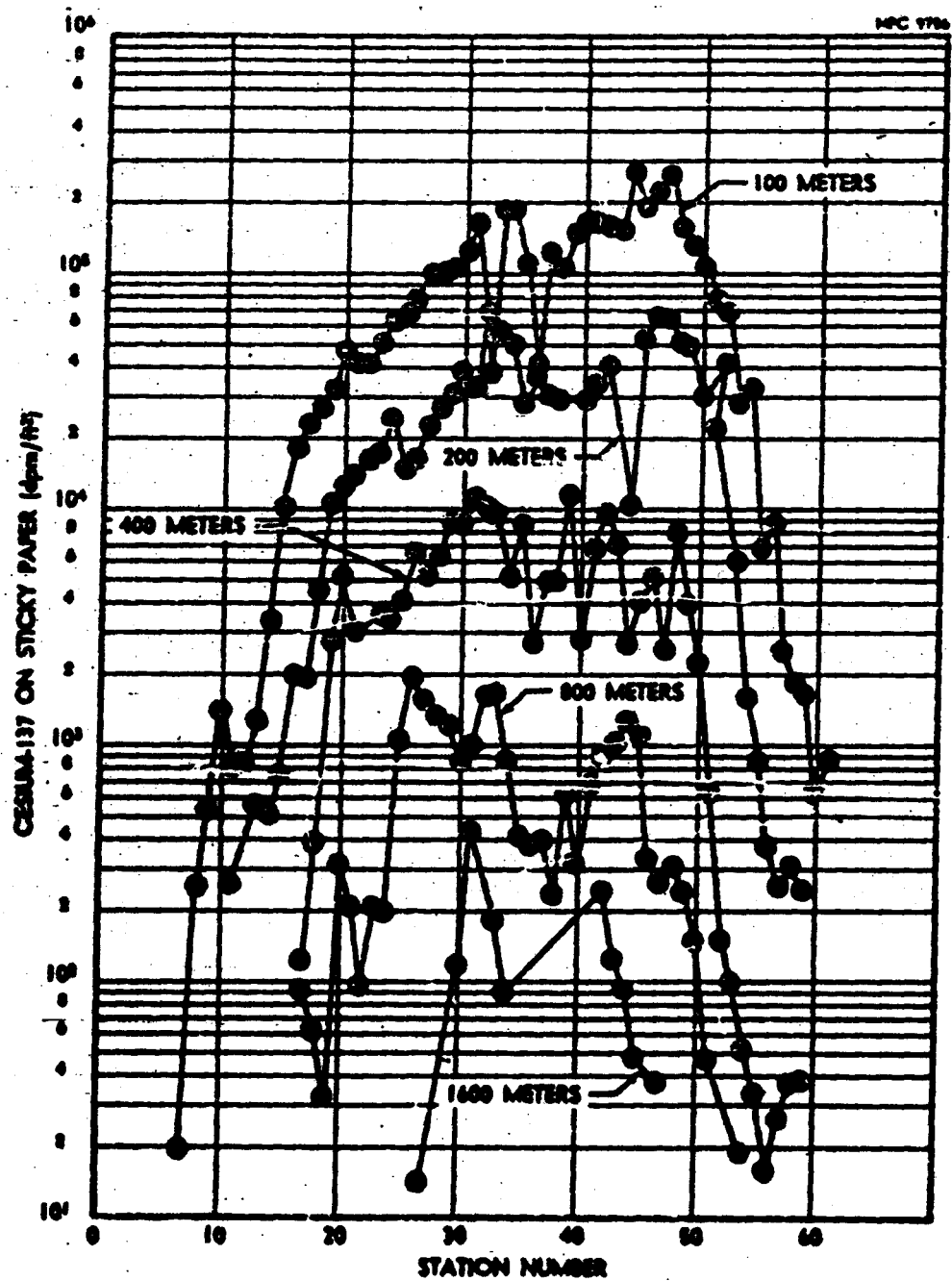


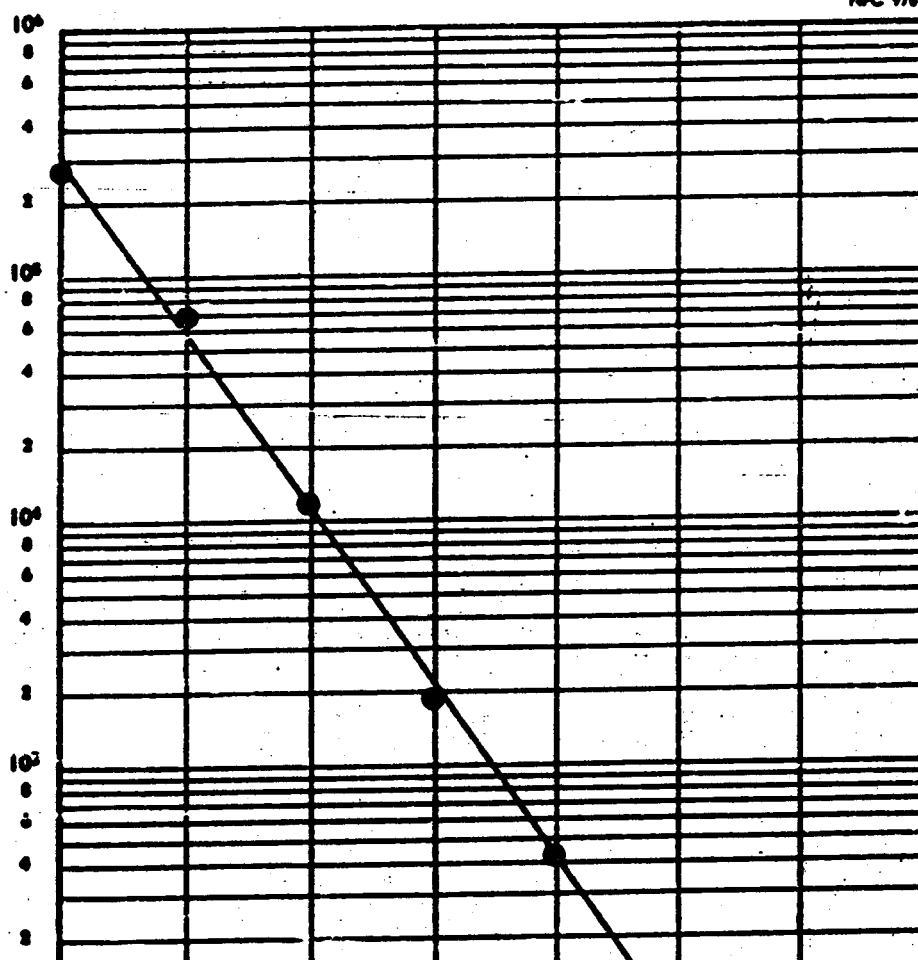
FIGURE N.B.9 DEPOSITED CESIUM ACTIVITY
(Are Profiles)

2)

5)

CELLULOSE ON STICKY PAPER (dpm/IN)

NPC 9787



D.10 Deposition Velocity

The average deposition velocity for cesium as a function of distance from the release point is shown in Table N.D.4. The values for this parameter were determined by raticing the areas under the sticky paper activity arc profiles to those under the sampler activity arc profiles.

TABLE N.D.4
Isotopic Deposition Velocities (cm/sec)

Arc (meters)	Sticky-Paper		Water	Sand
	Cs ¹³⁷	Sr ⁹⁰	Cs ¹³⁷	Cs ¹³⁷
100	0.087	.97±.58	.244±.157	.0363
200	0.094	1.4±.3	.0702±.027	.0197
400	0.077	1.77	.0554±.013	.0654
800	0.051			
1600	0.047			

D.11 Fluorescent Tracer Distribution

Counting of fluorescent particles was not done because the release was not simultaneous with fission product release; and, therefore, diffusion conditions were not the same.

D.12 External Dose

Gamma dose rates were measured and recorded at every three degrees on the 400-meter arc using the gamma scintillation detectors.

The integrated dose received at each station during passage of the effluent cloud is shown in Figure N.D.11. The trace of the dose rates taken at the detector stations nearest the centerline of the cloud is shown in Figure N.D.12.

An approximate reconstruction of the gamma activity passage sequence is shown in Figure N.D.13.

D.13 Diffusion Parameters

The diffusion parameters obtained from this test are shown in Table N.D.5. The actual gross activity isopleth and its curve fit isopleth, normalized to the maximum filter reading on the 100-meter arc, are shown in Figures N.D.14 and N.D.15.

TABLE N.D.5
Diffusion Parameters

Parameters	Field-Survey Data Fit	Cs137 Fit	Bivane Fit
Horizontal Stability Parameter (M_y)	0.68	0.73	--
Vertical Stability Parameter (M_z)	1.6	1.6	--
Horizontal Diffusion Coefficient (C_y)	0.61	0.40	0.09
Vertical Diffusion Coefficient (C_z)	--	0.007	0.03
Sutton's Stability Parameter (n)	--	--	0.28

NPC 9708

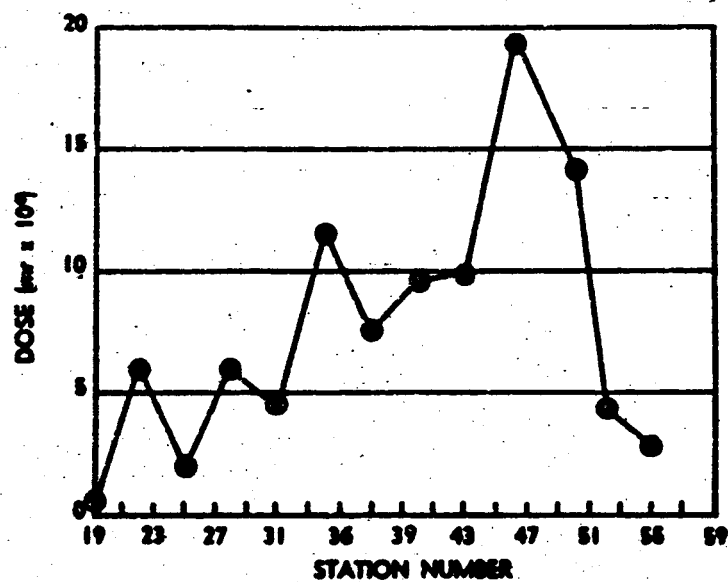


FIGURE N.B.11. GAMMA DOSE FROM CLOUD PASSAGE
(Arc Profile)

NPC 9709

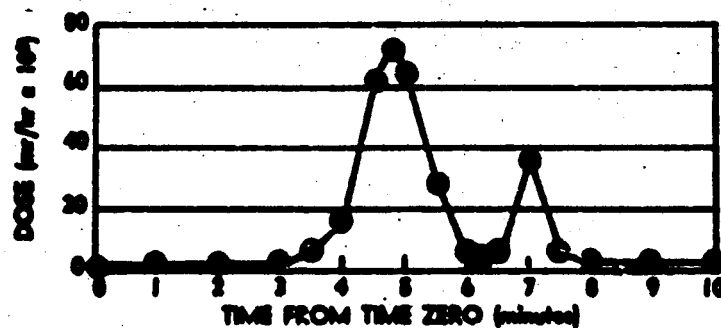


FIGURE N.B.12. GAMMA DOSE RATE FROM CLOUD PASSAGE
(Centerline)

MPC 9790

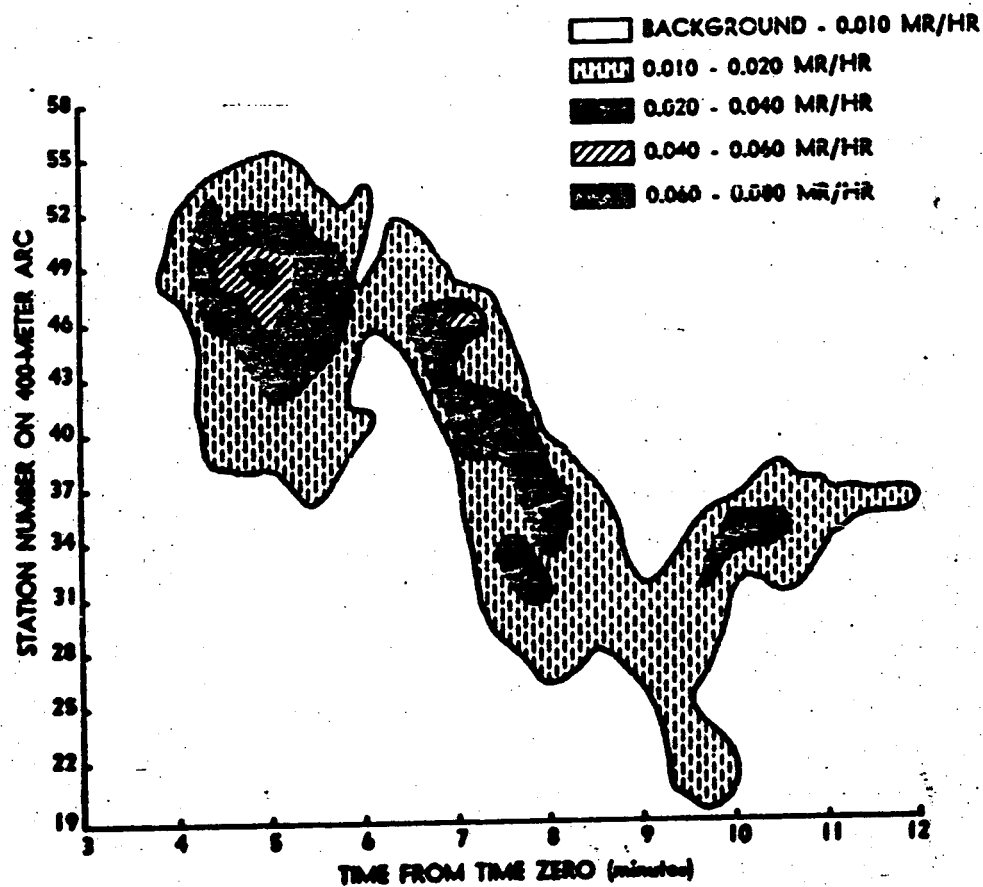
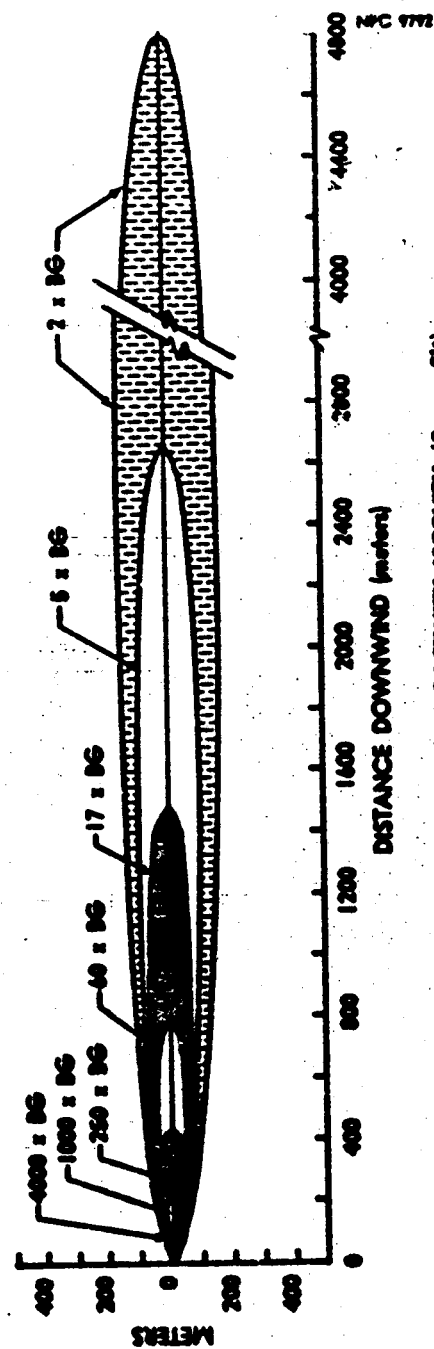
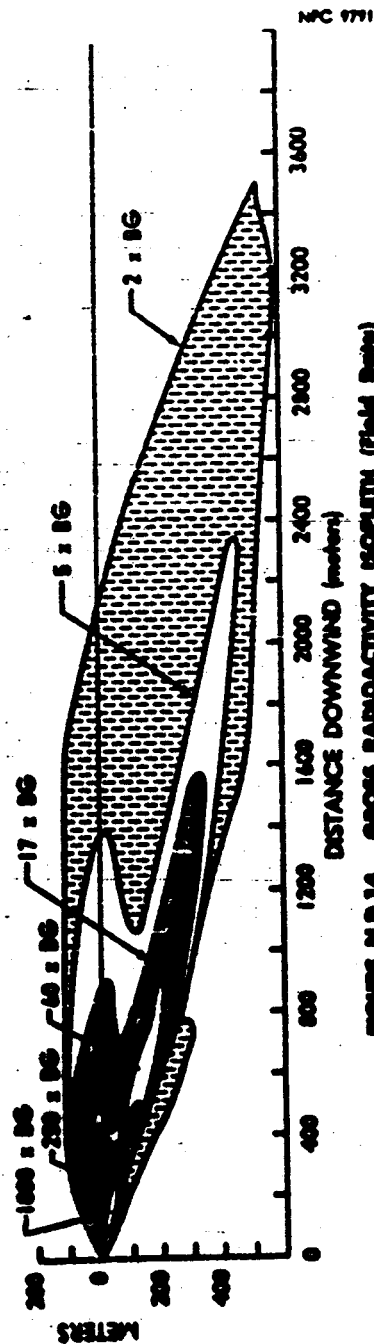


FIGURE N.B.13 GAMMA DOSE RATE FROM CLOUD PASSAGE
(Activity Contour)



D.14 Radiobiology

Rats were placed every two degrees on the 100- and 200-meter arcs. Because of an unrealistic increase in the gastrointestinal tract burdens caused by licking during release C, a new type exposure cage was used at one-half of the stations during release D. This cage consisted of a cone made of 1/4-inch mesh hardware cloth. Whole body and tissue determinations for fission products were the same as in Release C.

Data from whole body counting are plotted in Figure N.D.16. Data from tissue analysis are plotted in Figures N.D.17 and N.D.18.

D.16 Sand and Water Collection

Fallout samples were collected in water and sand traps. The sand and water samples were not radioactive enough to allow direct gamma counting of a 50-ml aliquot. Therefore, the water samples were selected on the basis of the cloud path as determined by the field survey of air samplers and were evaporated to 50 ml and gamma counted. Sand samples were selected in the same manner (see Appendix N-A, Section A.5). Results for the water and sand samples are shown in Figure N.D.19 and Table N.D.6 respectively.

TABLE N.D.6
Cesium-137 in Sand

Location	Curies/ft ²
100-meter arc Station 46	60×10^{-9}
200-meter arc Station 53	1.3×10^{-9}
400-meter arc Station 41	1.8×10^{-9}

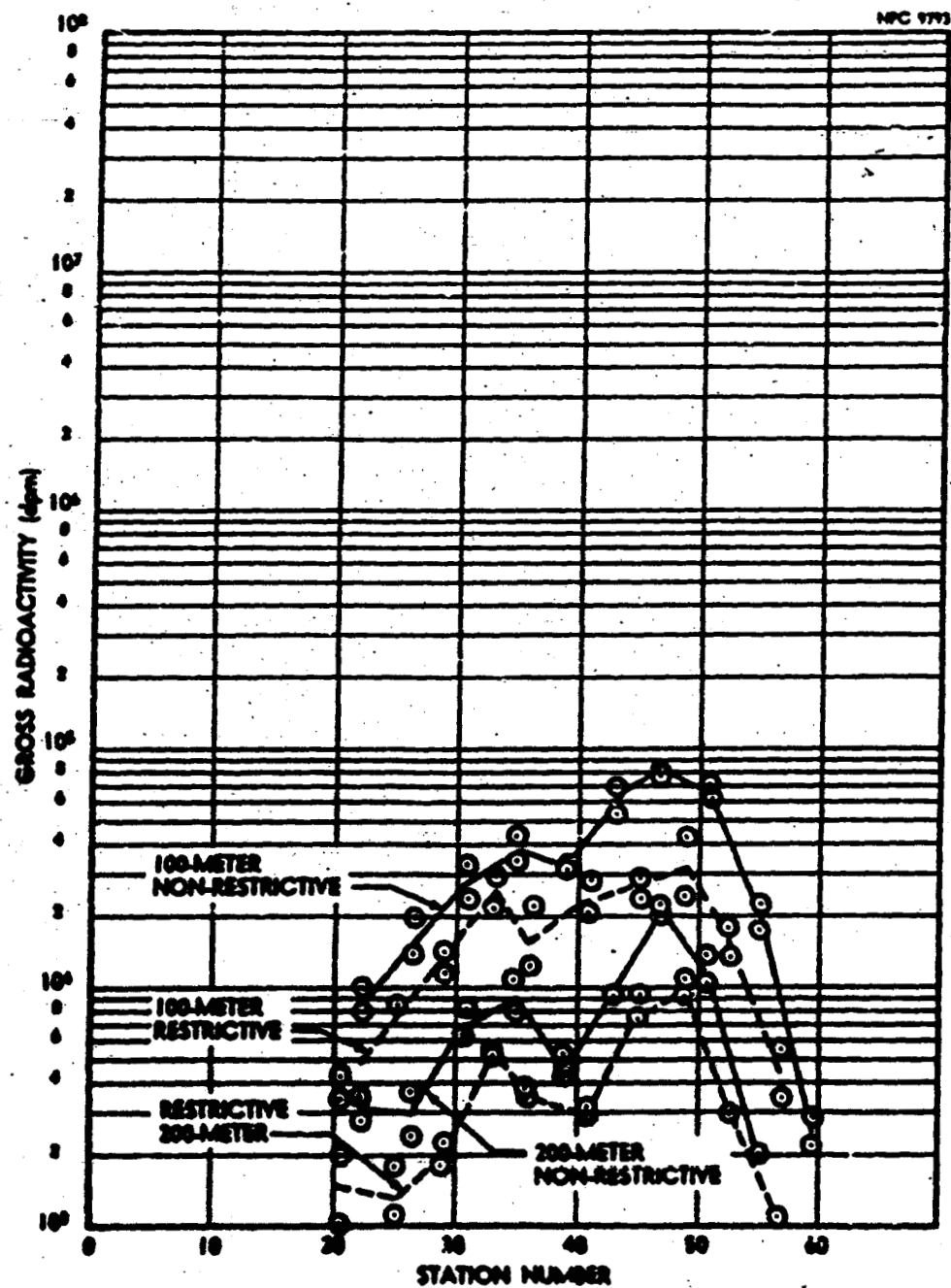


FIGURE N.B.16 RAT WHOLE-BODY EXPOSURE (Are Profiles)

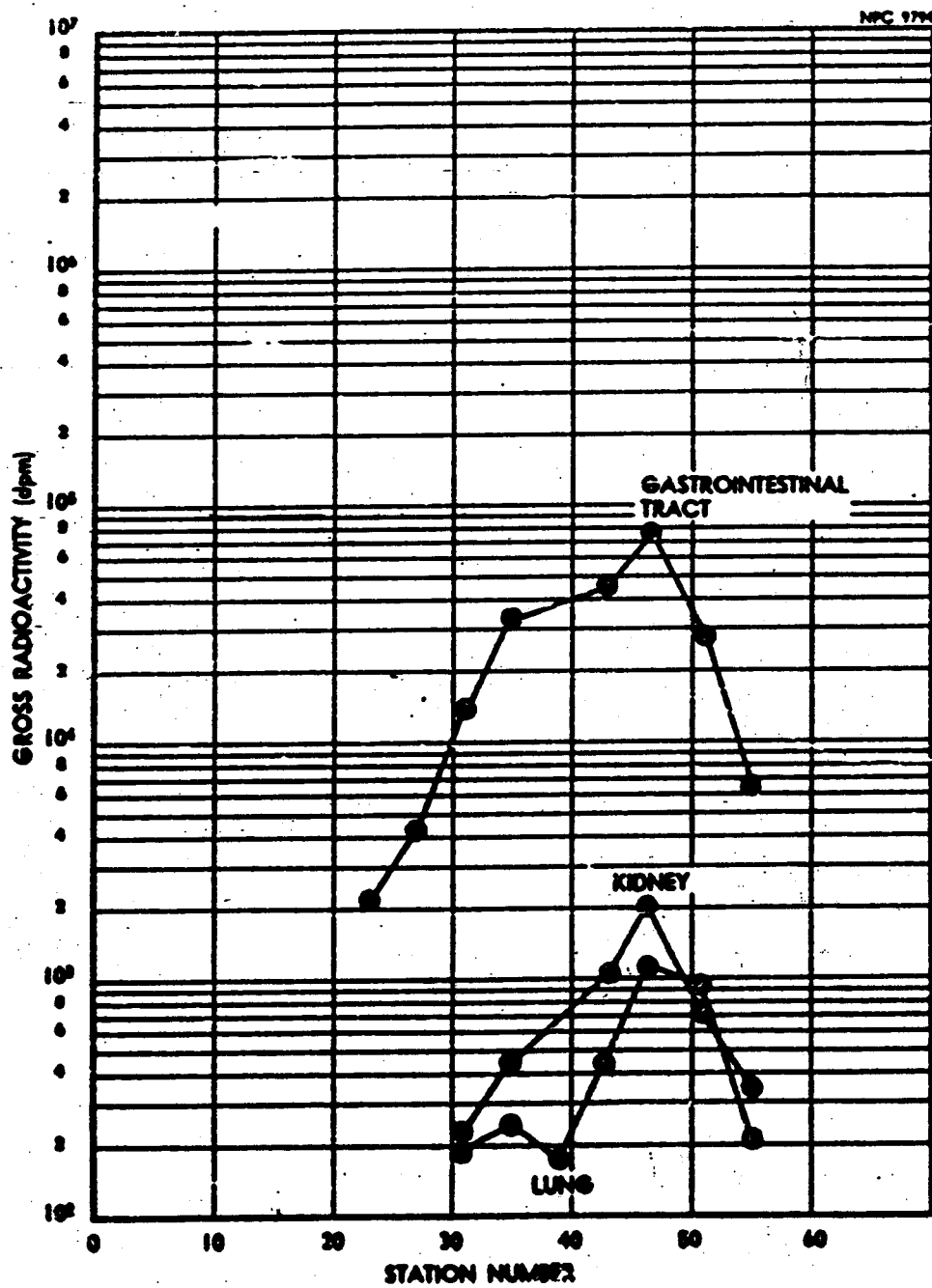


FIGURE N.B.17 RAT TISSUE EXPOSURE (Non-Restrictive Cages)

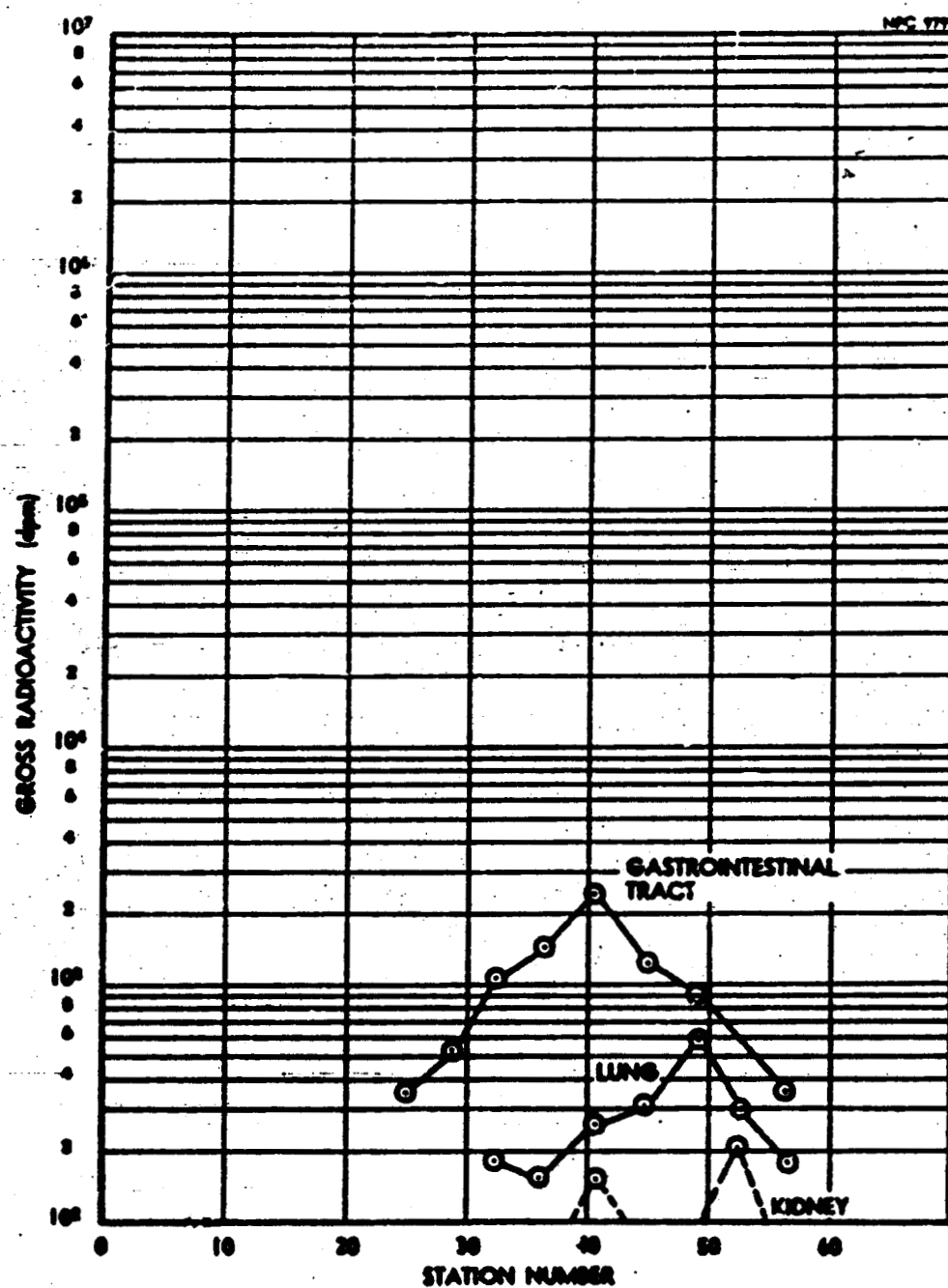


FIGURE N.R.16 RAT TISSUE EXPOSURE (Restrictive Cages)

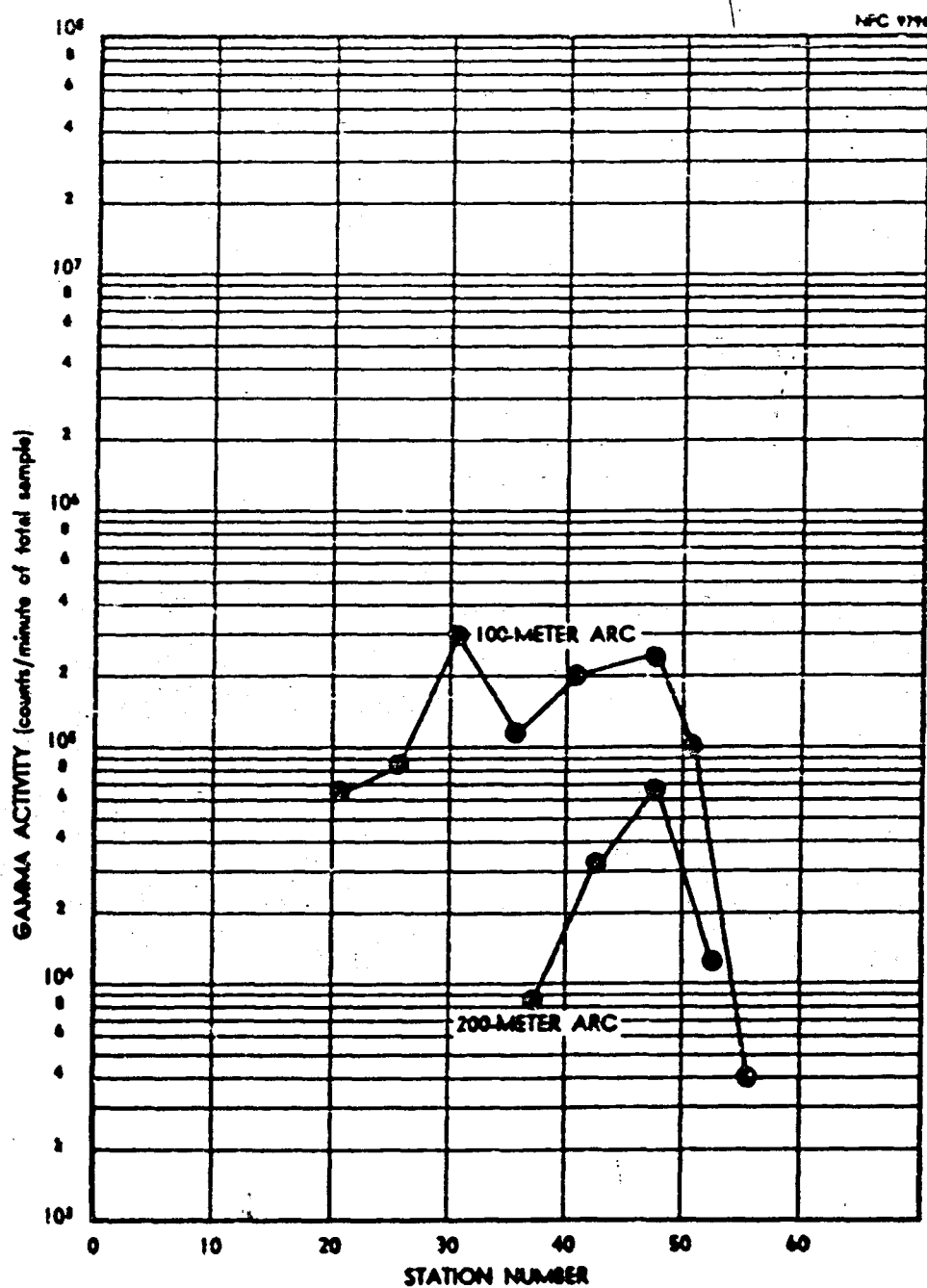


FIGURE L.D.19 CONTAMINATION OF WATER SAMPLES

APPENDIX N-E

(Release E)

E.1 Summary

Type of Sample ----- Green Fuel Element
Date and Release Time ----- 27 Aug 1958; 5:19 PM
Lapse Rate (1.5 - 45 m) ----- $\nearrow 0.65^{\circ}\text{C}$
Lapse Rate (1.5 - 24.5 m) ----- $\nearrow 0.51^{\circ}\text{C}$
Mean Wind Speed ----- 6.8 meters/sec
Wind Direction ----- Network Centerline
Cloud Photography ----- Both aerial and ground
Fluorescent Tracer ----- Released for 10 minutes
immediately following
fission product release
Animals ----- Rats on three inner arcs(Ref.11)
Network Radioactivity ----- Detected out to 3200 meters;
maximum reading of pleated
filters on 100-meter arc,
220 mr/hr, using Cutie Pie
External Dose ----- Maximum dose rate on 400-
meter arc, 0.35 mr/hr, using
scintillation detector
described in Appendix K.

B.2 Fuel Element

The fuel element had been irradiated to generate 3.4×10^4 watts for a total of 125 hours 6 minutes and had decayed for 42 days and 22 hours. The predominant nuclides present at the time of release are shown in Table N.E.1.

TABLE N.E.1
Fission Product Inventory

Nuclide	Curies Calculated
Sr ⁸⁹	54
Y ⁹¹	63
Zr ⁹⁵	64
Nb ⁹⁵	79
Ce ¹⁴¹	74
Ce ¹⁴⁴ - Pr ¹⁴⁴	21
Pm ¹⁴⁷	2.8
Ru ¹⁰³ - Rh ^{103m}	35
Cs ¹³⁷ - Ba ^{137m}	0.5
Ba ¹⁴⁰ - La ¹⁴⁰	45
Pr ¹⁴³	48
Nd ¹⁴⁷	15
I ¹³¹	7.8
Te ^{129m} - Ge ¹²⁹	12

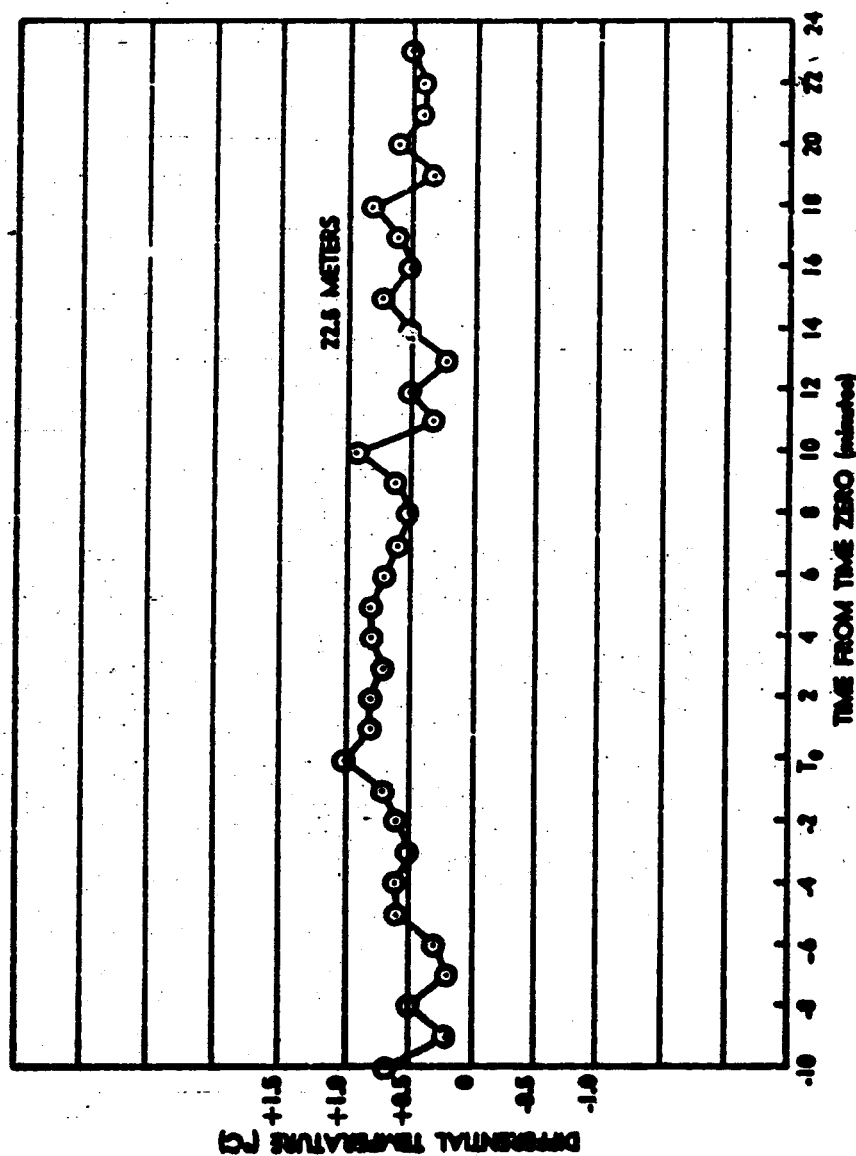


FIGURE 11.1 LAPSE RATE DURING RELEASE

E.3 Meteorological Conditions

The wind directions and velocities prevailing during this release are shown in Table N.E.2. The average wind velocity for the release was determined by averaging the data from the 1.5-meter level on the main tower over the release time. The average wind velocity was 6.8 meters per second. Fluctuations in wind direction were observed; however, the deviations did not move the effluent significantly from the network-centerline path.

Lapse rates, existing at the apex tower during the release, between the 1.5-meter level and both the 24- and 45-meter levels, are shown in Figure N.E.1.

TABLE N.E.2
Meteorological Summary
APEX TOWER

Height (meters)	Wind Direction			Wind Velocity (meters/sec)		
	Max.	Min.	Ave.	Max.	Min.	Ave.
1.5	272°	206°	237°	13	3.0	6.8
3.0	268	199	233	13	3.4	7.5
6.0	--	--	--	14	4.2	8.8
12.0	--	--	--	14	4.7	9.0
23.0	273	217	238	14	6.0	10.9
45.0	276	229	249	15	6.4	12.0

TABLE N.E.2 (Cont'd)
Meteorological Summary

FIELD MASTS

Location (Arc)	Wind Direction			Wind Velocity (meters/sec)		
	Max.	Min.	Ave.	Max.	Min.	Ave.
200 meter	279°	212°	242°	13	1.7	6.4
400	274	207	233	13	3.5	8.1
800	276	211	239	11	2.8	7.4
1600	268	208	237	12	3.8	7.7
2400	269	204	236	12	3.4	8.0
3200	263	195	226	11	4.4	8.5

E.4 Smoke Plume Photography

Photographic documentation of the smoke cloud was accomplished with ground and aerial photography. The photograph from which the diffusion parameters were calculated is shown in Figure N.E.2

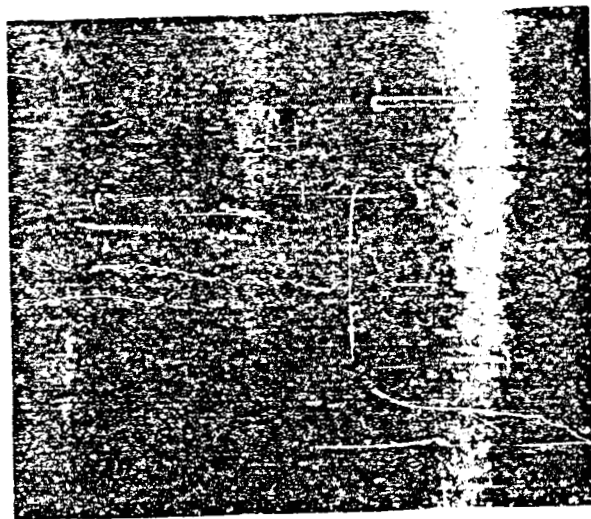
E.5 Furnace Conditions

The operation of the furnace for this release was normal and similar to Release A (Appendix N-A, Section A.5).

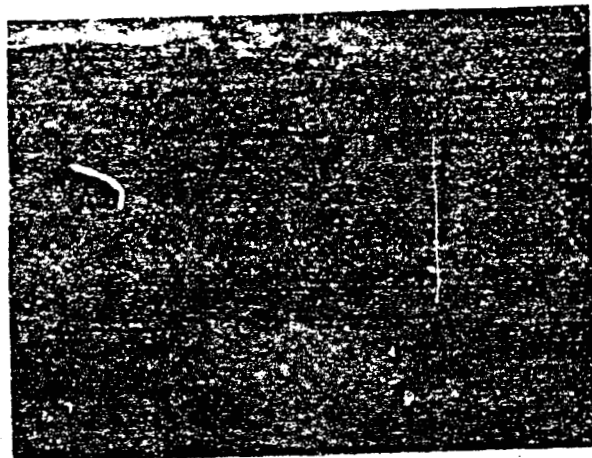
E.6 Release Height

During this release a single negatively charged wire was placed on the network centerline 42-3/4 inches downwind from the center of the crucible. The furnace top was four feet below the top of the wire. The wire was scanned with a collimated-G.M. instrument, and the resulting data are shown in Table N.E.3.

NPC 9798



Aerial View



Ground View

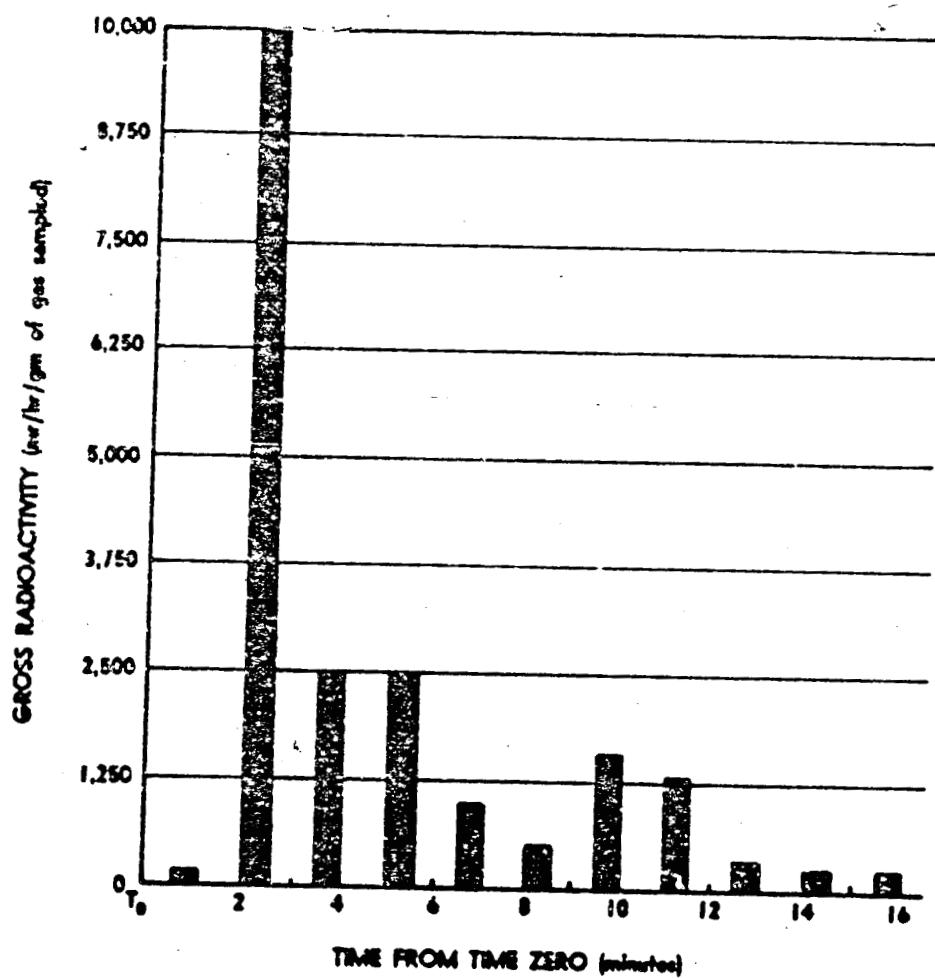


FIGURE N.E.3 SEQUENTIAL-EFFLUENT-SAMPLER FILTER RADIOACTIVITIES

The effective release height is assumed to be that level on the charged wire indicated by the most contamination. In this instance, the release height corresponds to the top of the furnace.

Spectral analyses of the activity on the wire indicated the presence of a number of isotopes, with I^{131} , Ru^{103} - Rh^{103m} , and Cs^{137} - Ba^{137m} the most prominent.

TABLE N.E.3
Release Height

Distance from Top of Wire (ft)	Dose Rate (mr/hr)
2.0	1
3.0	2
3.5	13
3.75	20
4.0	40
4.25	36
4.5	23
5.0	10

E.7 Effluent Samplers

The effluent sampler filter plug activity as a function of time from time zero is shown in Figure N.E.3. The escape of isotopes from the melt appears quite selective and the release of each isotope was completed at approximately 3 minutes from time zero.

E.8 Release Percentages

The percent release of specific isotopes as determined by pre- and post-melt radiochemistry, and network activity is shown in Table N.E.4. Also shown is the release percentage as determined from the effluent samplers. Pre- and post-melt gamma spectral analyses were not performed on the green elements because the spectra were too complex.

TABLE N.E.4

Release Percentages

Nuclide	Effluent		Pre- and Post-Radiochemistry (%)	Network Data (%)
	Sequential	Integral		
Sr ⁸⁹	1.1	--	41	--
Zr ⁹⁵	0.05	0.04	65	0.03
Ce ¹⁴¹	0.04	0.01	14	0.01
Ru ¹⁰³	4	0.5	9	1
Cs ¹³⁷	26	12	87	30
Ba ¹⁴⁰	--	--	43	--
I ¹³¹	50	--	100	50

E.9 Air Sampler Field Survey

Figures N.E.4 and N.E.5 show the pleated-filter and carbon-cartridge activity are profiles corrected for background and sampler flow rate. Figure N.E.6 shows the cloud centerline

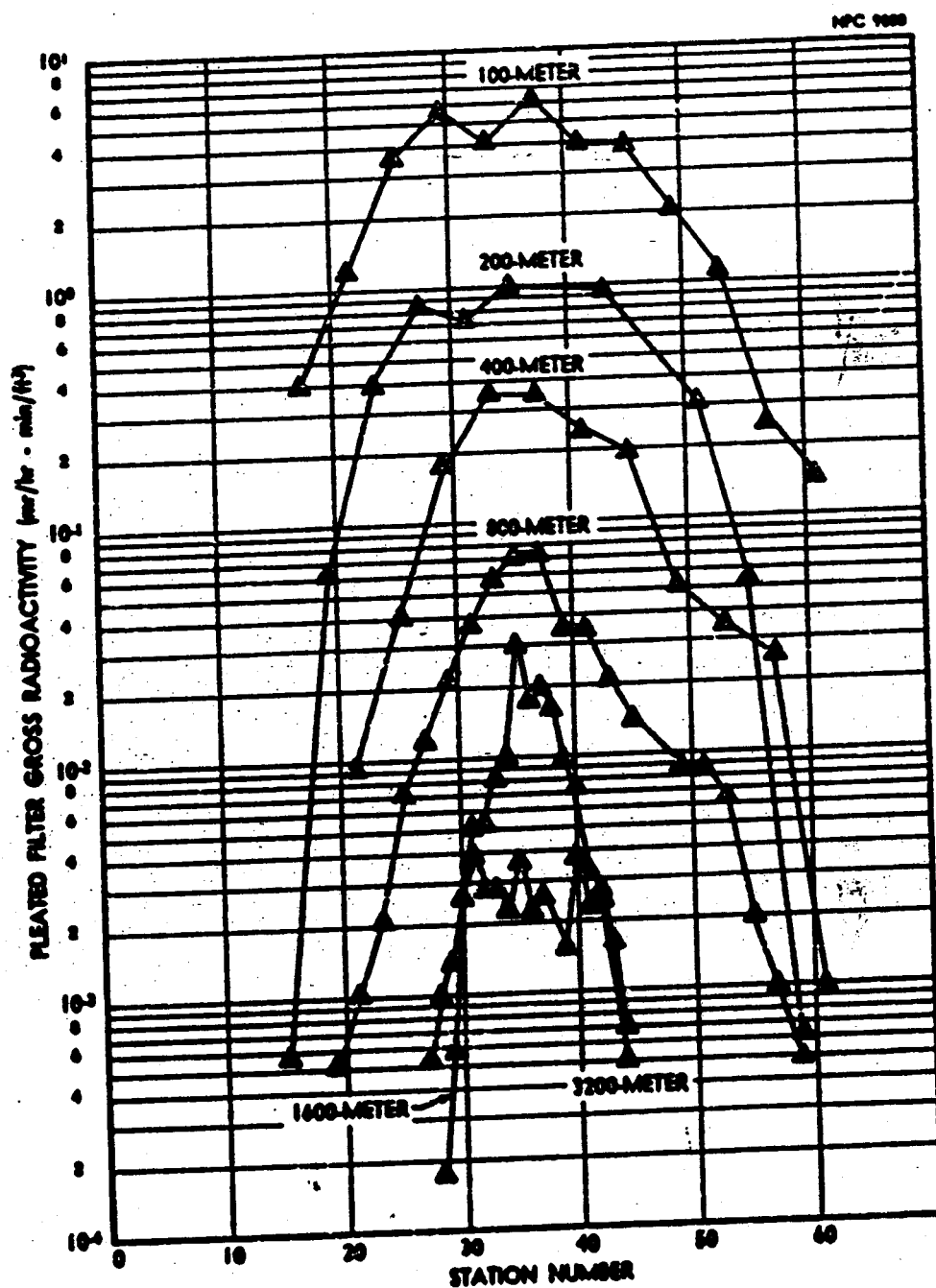


FIGURE H.1.4 H₂VO₄ AIR SAMPLER FIELD SURVEY
(Pleated Filter - Air Profiles)

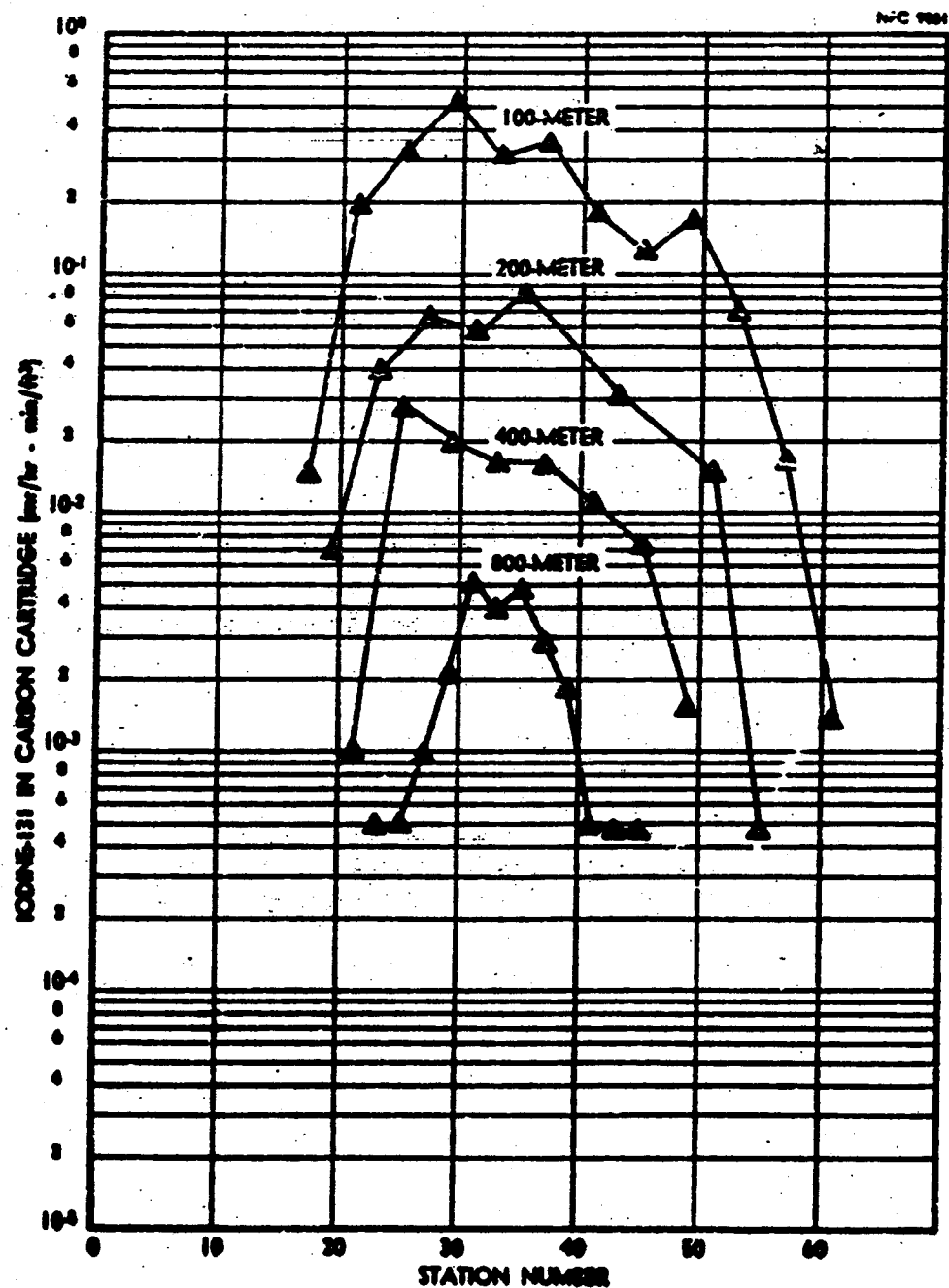


FIGURE M.E.3 HI-VOL AIR SAMPLER FIELD SURVEY
(Carbon Cartridge - Air Profile)

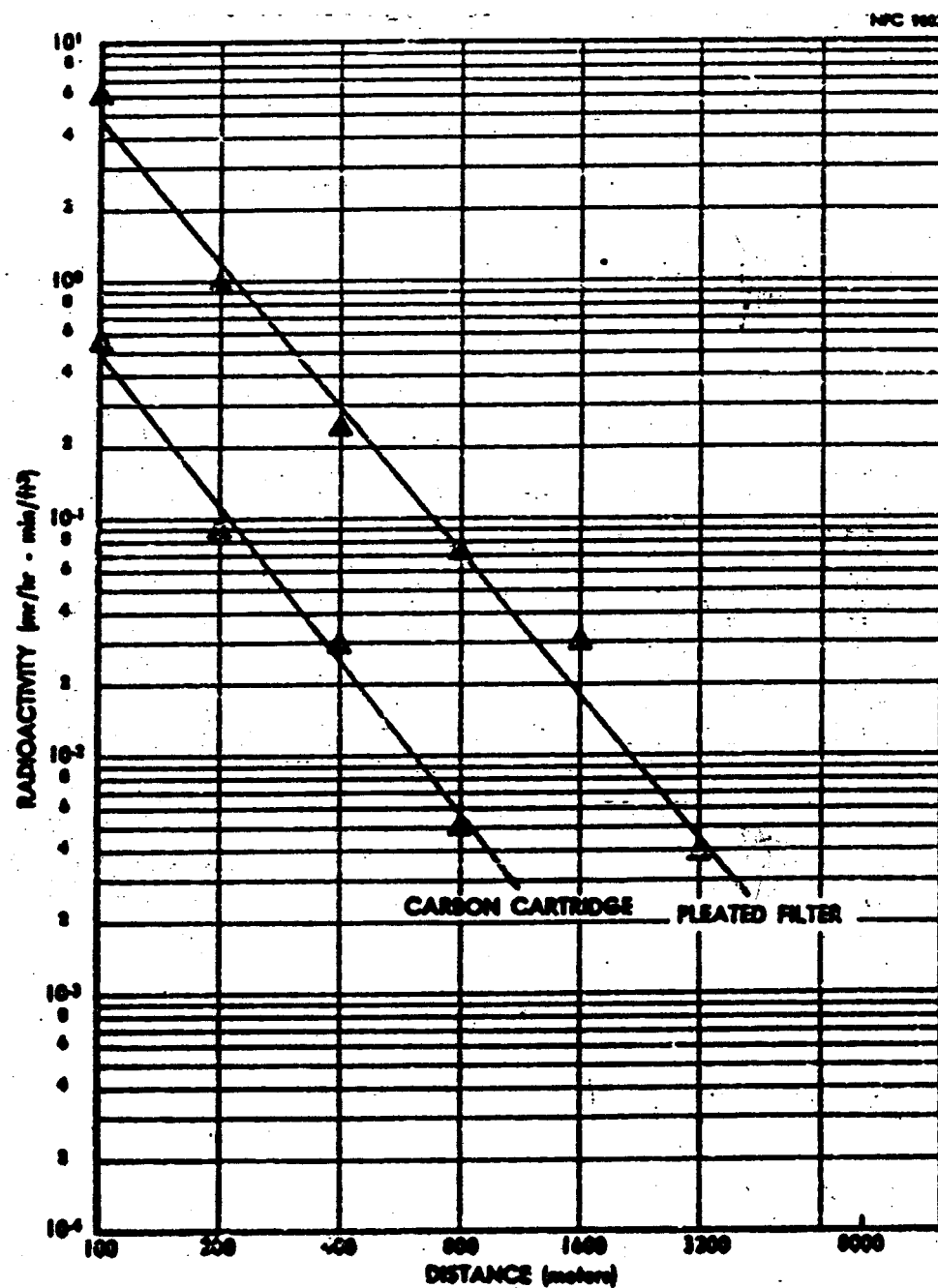


FIGURE H.2.4 DE-VOL AIR SAMPLER FIELD SURVEY (Sancti Spiritus)

readings as a function of distance from the release point. Also shown is a straight line least-squares fit to the data points.

E.10 Airborne Radioactivity

The radioactivity along the cloud centerline at each arc for iodine, ruthenium, cesium, zirconium, and cerium, plotted as a function of distance from the release point, are shown in Figure N.E.7. It was necessary to include the iodine activity collected on both the pleated-filter and carbon-cartridge of the Hi-Vol sampler, since a significant fraction of the iodine was retained by the filter. The remaining isotope data were obtained from the pleated filter only. The radioactive iodine ratios of pleated-filter to carbon-cartridge will be presented later.

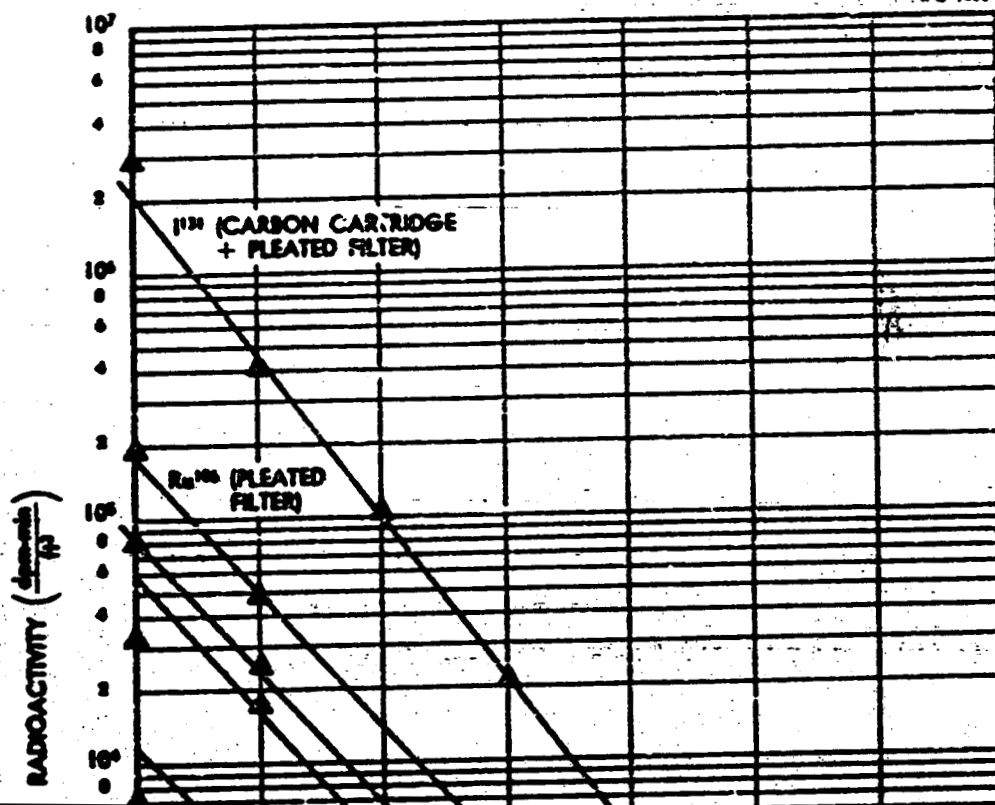
The arc profiles, corrected for sampler flow rate, for ruthenium, cesium, zirconium, cerium, and iodine are shown in Figures N.E.8, N.E.9, N.E.10, N.E.11, and N.E.12 respectively.

E.11 Deposited Radioactivity

The iodine profiles for each arc are shown in Figure N.E.13. The deposition of iodine as a function of distance along the centerline from the release point is shown in Figure N.E.14.

On the 200- and 300-meter arcs, only centerline sticky papers were analyzed for iodine. This procedure was followed for most of the green releases. Because of the large number of samples, it was necessary to select only certain samples from the cloud centerline on the intermediate arcs, thereby emphasizing the deposited radioactivity on the inner and outer arcs.

PAC 1005



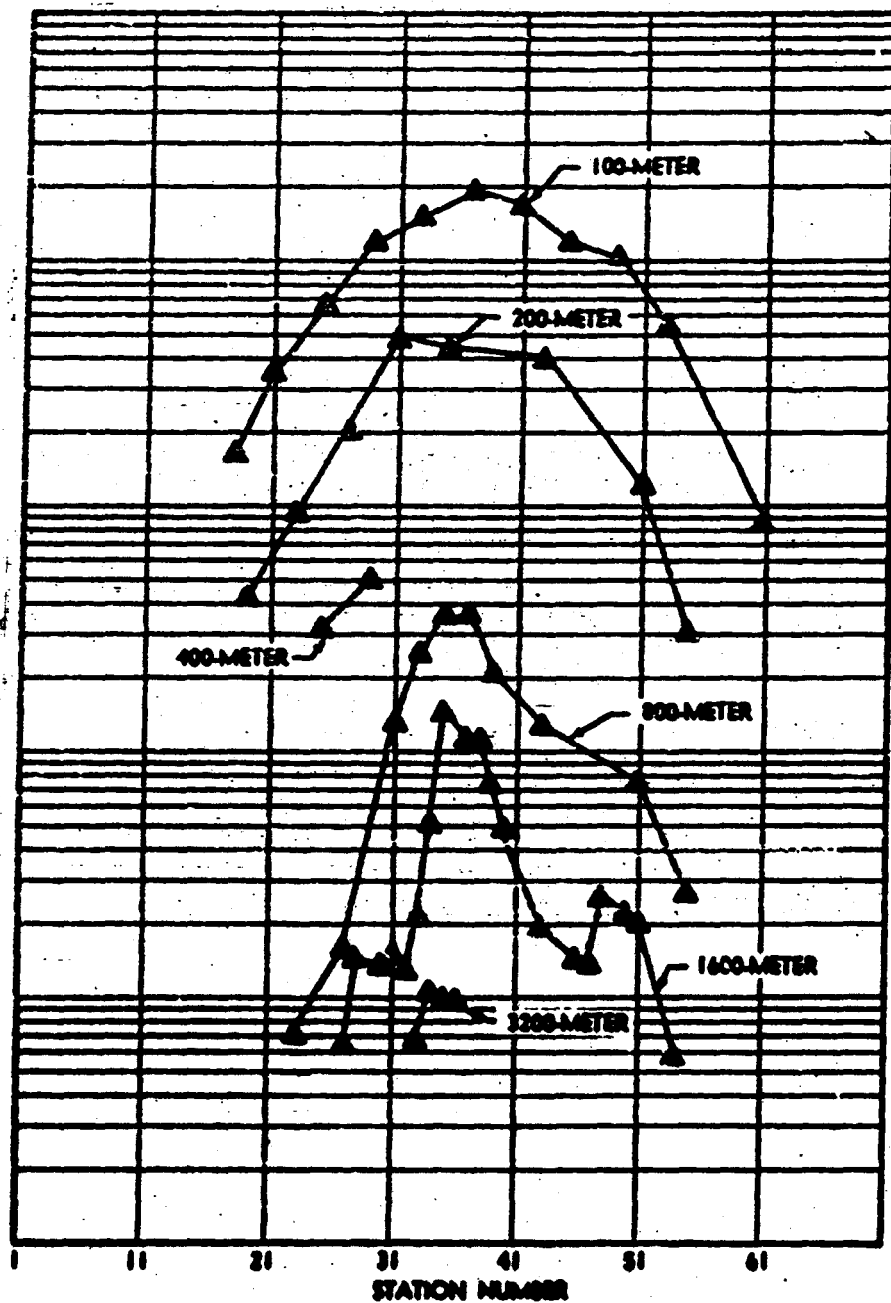


FIGURE 11.5 NE-VOL AIR SAMPLER LABORATORY ASSAY OF
SAMPLERS (Are Profiles)

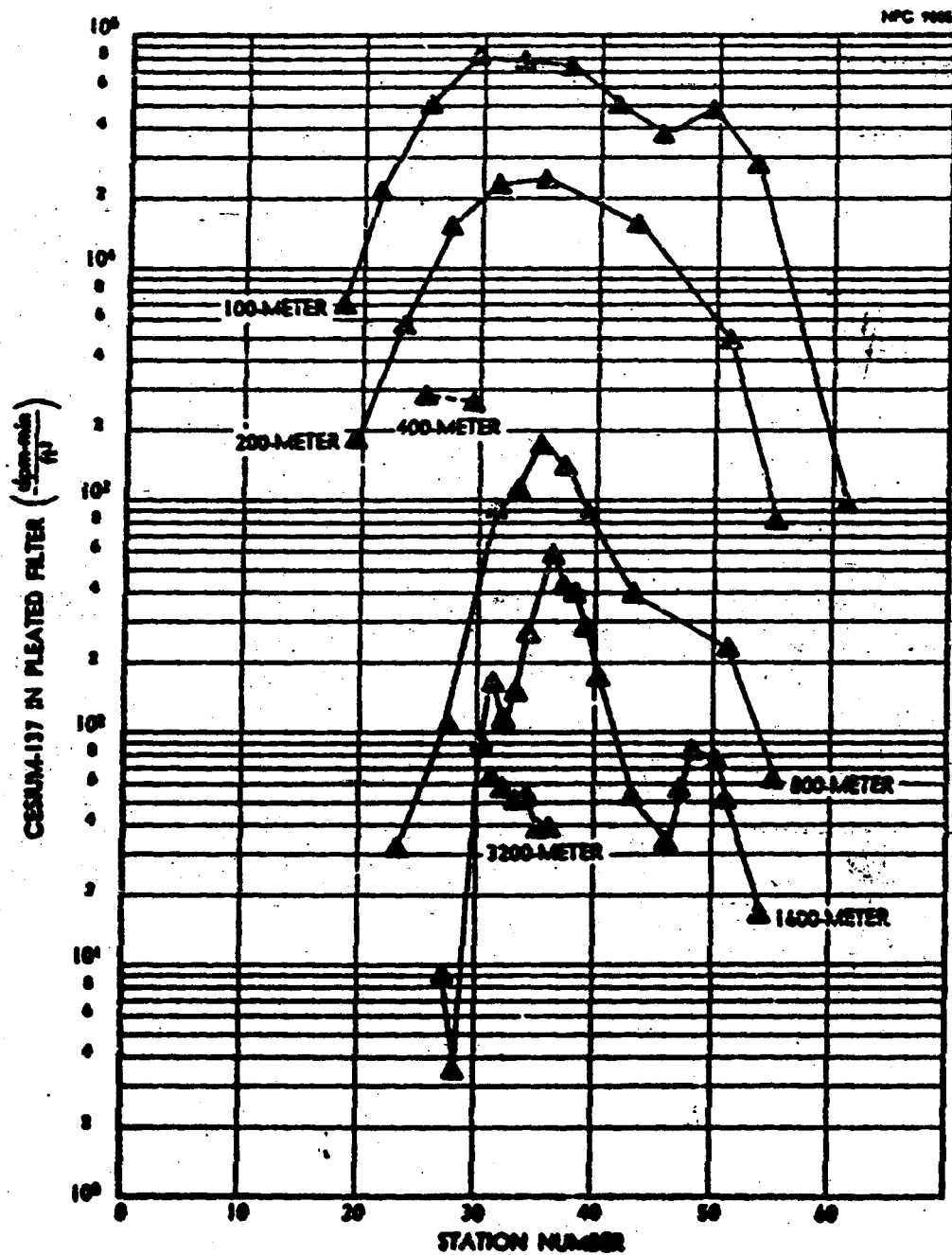


FIGURE N.E.9 H2-VOL AIR SAMPLER LABORATORY ASSAY OF CESIUM (Are Profiles)

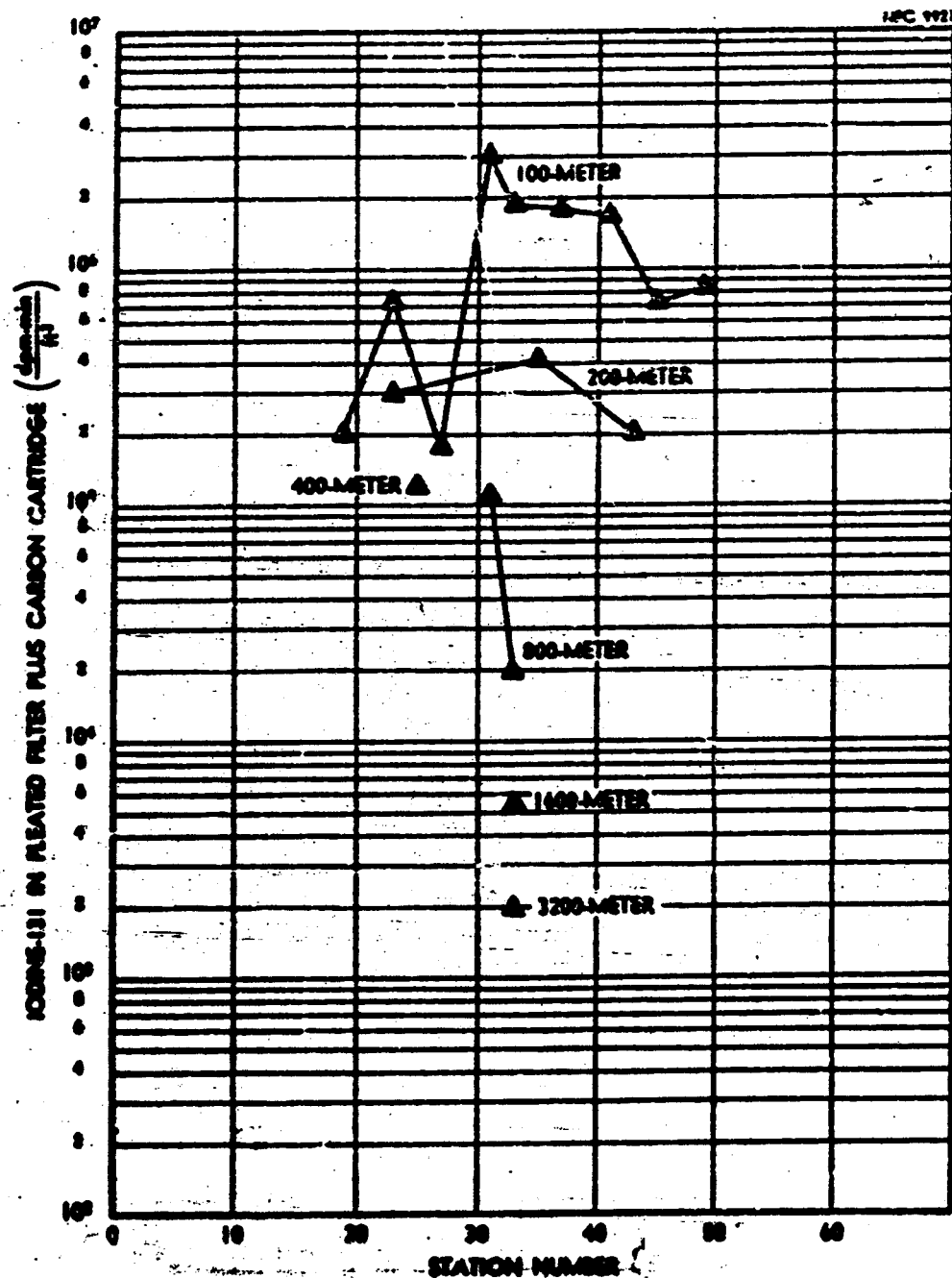


FIGURE 16.2.12 NUCLEAR AIR SAMPLER LABORATORY ARRAY
OF 60000 (400 Profiles)

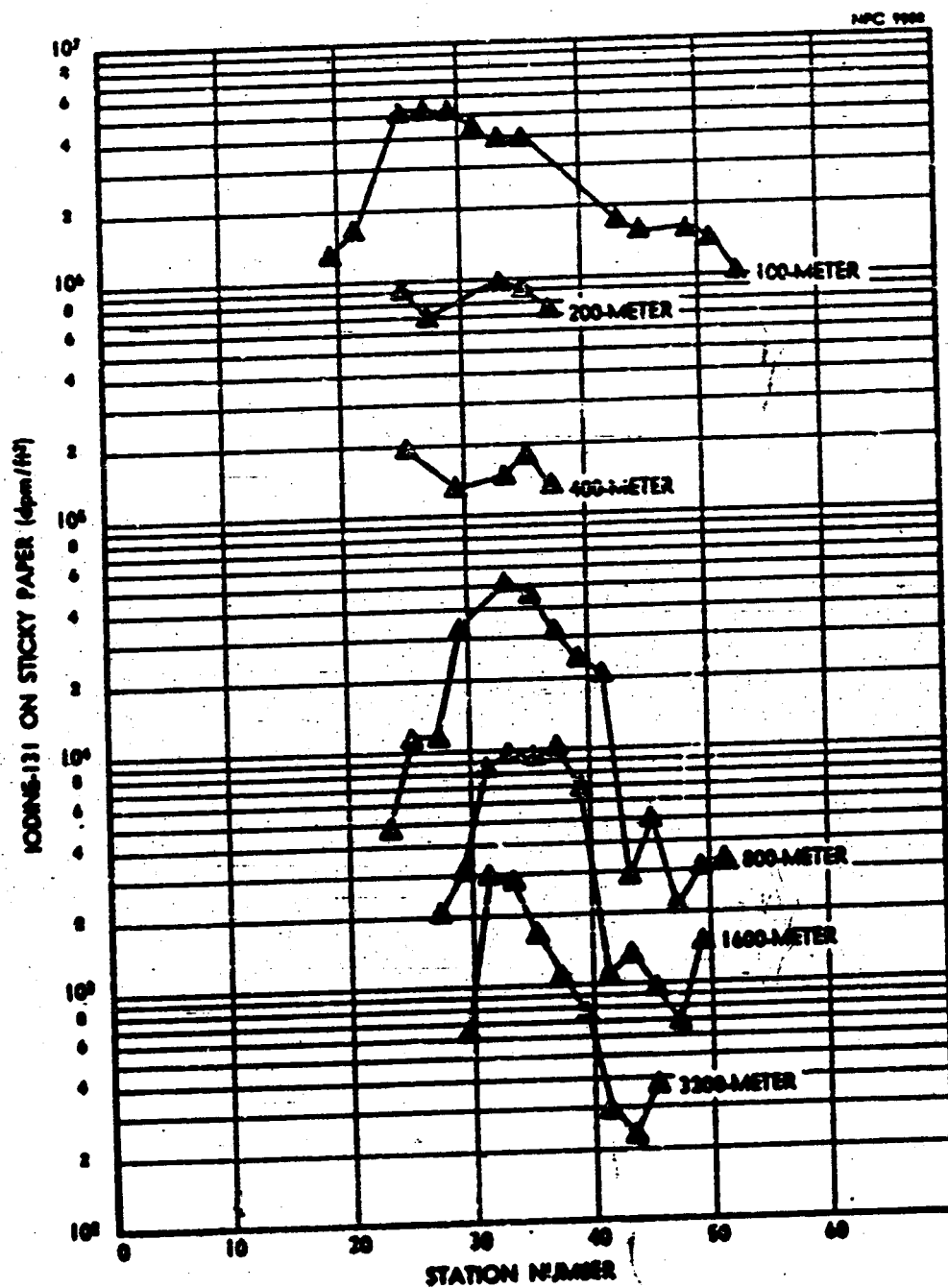


FIGURE M.L.13 DEPOSITED IODINE (Are Profiles)

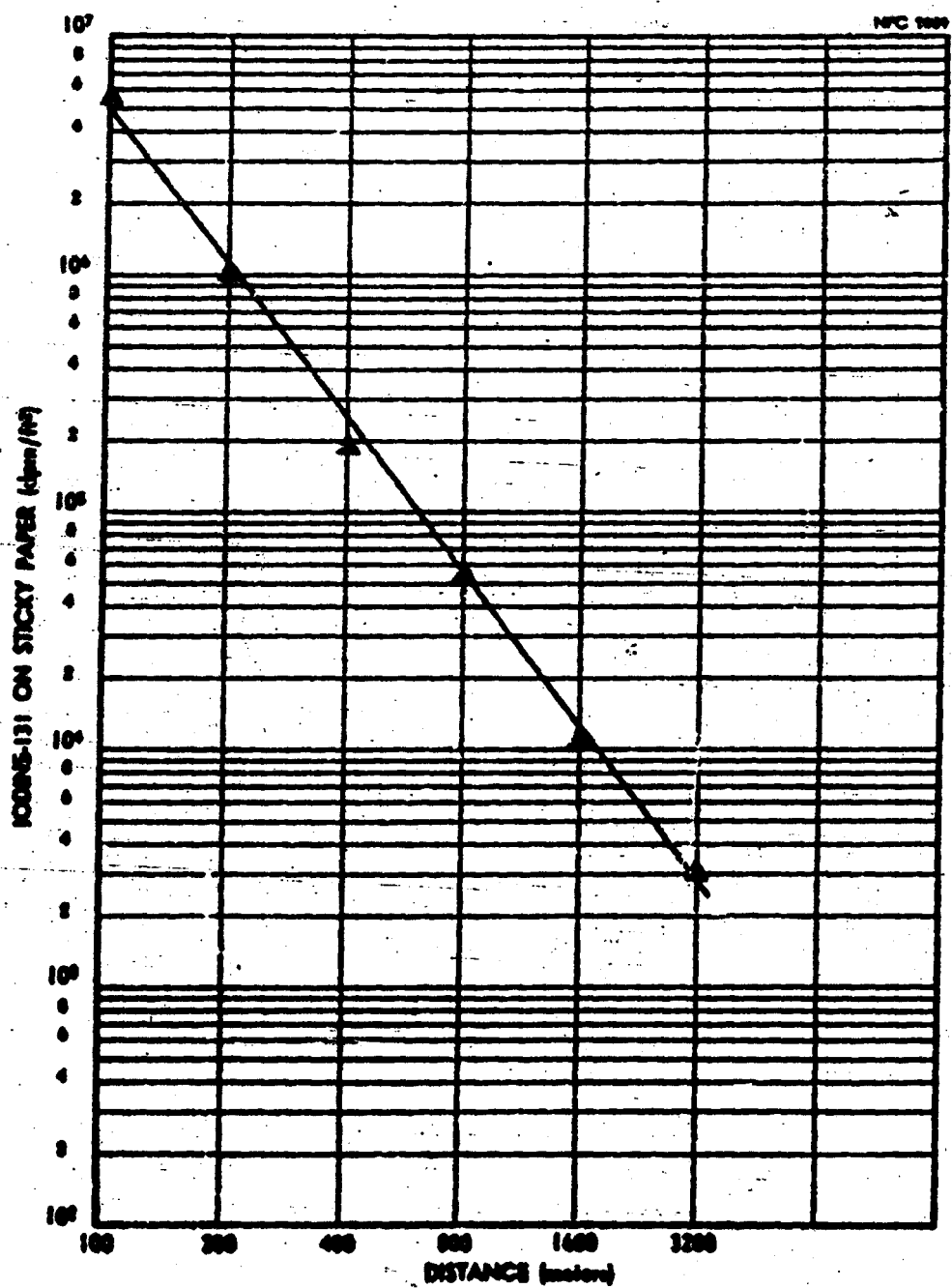


FIGURE D.L.14 REPORTED 10005 (Centerline)

E.12 Deposition Velocity

The average deposition velocity for iodine, as a function of distance from the release point, is shown in Table N.E.5. Each value was determined from the ratio of the area under the sticky paper arc profiles to the area under the air sampler arc profiles.

E.13 Particle Size

The quantities of radioactivities of specific isotopes in the various stages and back-up collectors of three Andersen samplers on the 100-, 200-, and 400-meter arcs are shown in Table N.E.6.

E.14 Fluorescent Tracer

No tracer data were obtained during this test.

E.15 External Dose

Gamma dose rates resulting from cloud passage were measured and recorded on the 400-meter arc. The integrated dose at each detector station along the arc is shown in Figure N.E.15.

Figure N.E.16 shows the dose rate versus time of cloud passage recorded by the detector nearest to the cloud centerline.

Figure N.E.17 shows the dose rate levels along the 400-meter arc versus time of cloud passage. This figure is an approximate reconstruction of the gamma image of the cloud as seen by the detectors.

E.16 Diffusion Parameters

The diffusion parameters obtained during this release are shown in Table N.E.7. For comparison, actual gross activity

74418 K-65

[illegible]

TABLE N.E.6

Distribution of Isotopes in Andersen Sampler

Location and Stage	Activity (DPM $\frac{\text{Min}}{\text{ft}^3}$)				
	Zr ⁹⁵ -Nb ⁹⁵	Cs ¹³⁷	Ru ¹⁰³	I ¹³¹	Ce ¹⁴¹
Arc 1 (Station 36)					
1	1151	200	5670	50000	350
2	5844	174	4380	8650	1172
3	5850	533	2310	9360	1250
4	3375	480	1650	8200	1012
5	1515	1500	1980	8180	727
6	847	4550	2945	5180	1045
Gelman Filter	850	180000	267000	200000	5500
Activated Charcoal	-	87	3670	205000	720
Arc 2 (Station 44)					
1	2510	166	4100	13850	392
2	600	180	1610	10450	300
3	2820	190	841	3370	590
4	1330	150	963	2020	425
5	1035	375	894	2160	284
6	650	1580	1314	1910	292
Gelman Filter	330	18000	33500	13200	1950
Arc 4 (Station 40)					
1	90	56	472	4680	50
2	100	73	175	2150	32
3	142	73	185	8500	99
4	191	36	218	2810	87
5	112	85	336	3010	85
6	69	107	132	2630	85
Gelman Filter	80	3950	6150	10500	785
Activated Charcoal	25	300	800	20500	78

MFC 16-8

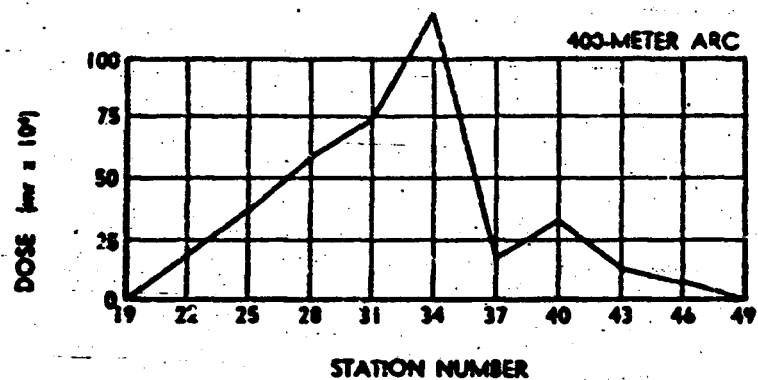


FIGURE N.E.15 - GAMMA DOSE FROM CLOUD PASSAGE
(Arc Profile)

MFC 16-11

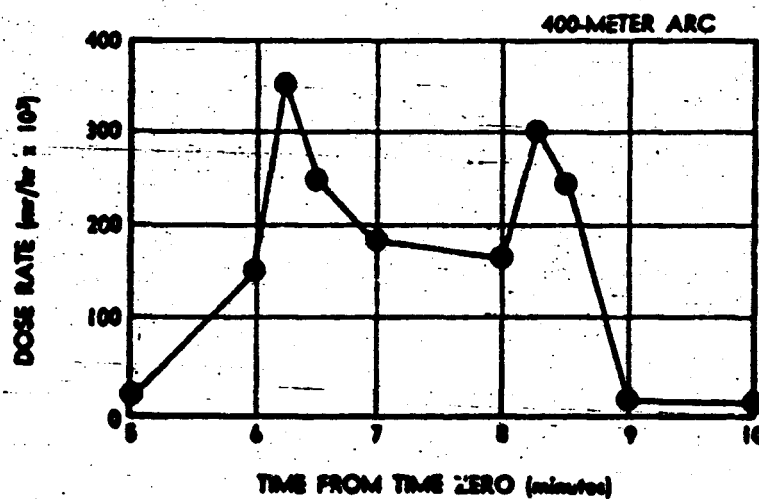


FIGURE N.E.16 - GAMMA DOSE RATE FROM CLOUD PASSAGE
(Centerline)

NPC 9812

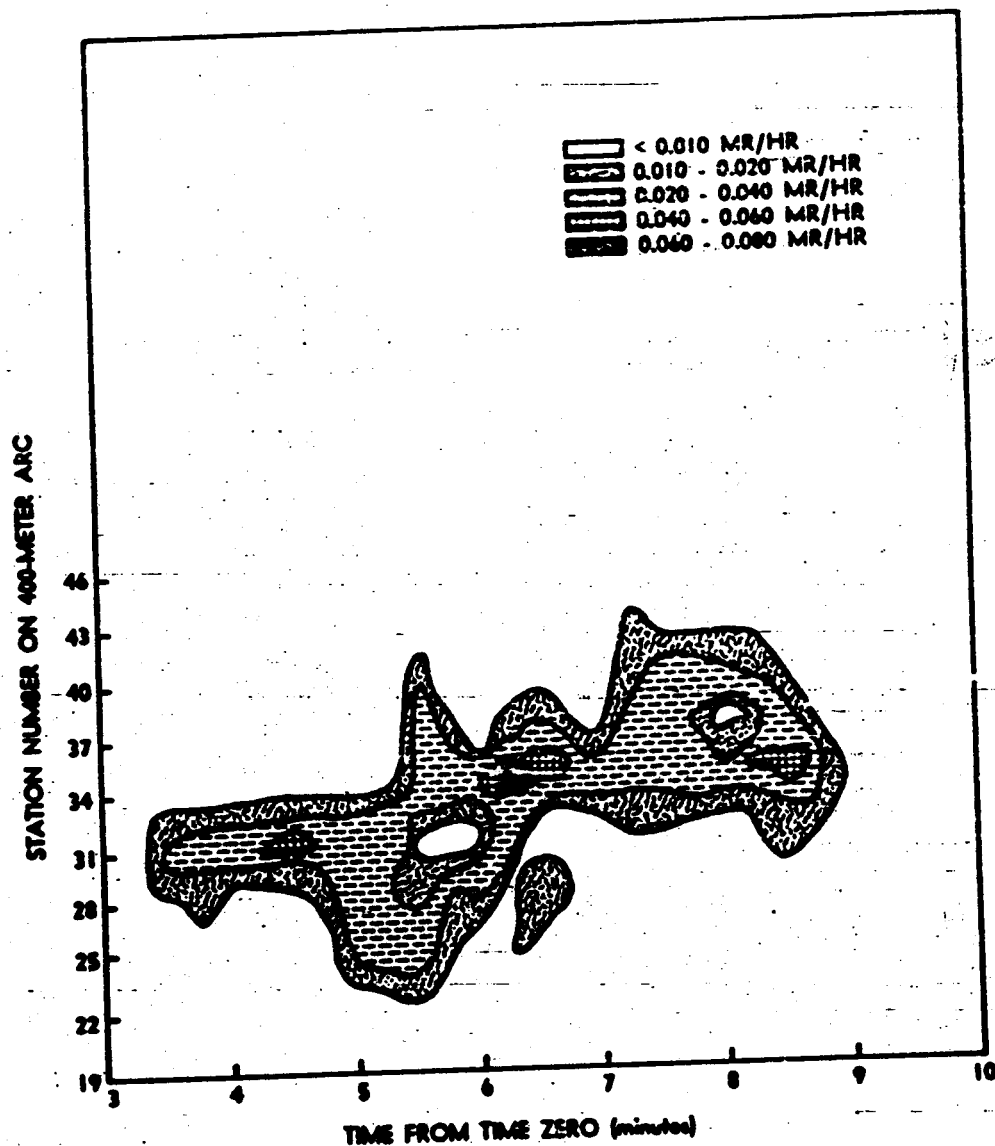


FIGURE N.E.17 GAMMA DOSE RATE FROM CLOUD PASSAGE
(Activity Contours)

TABLE K.E.7

Diffusion Parameters

Parameters Data Fit	M_y	M_z	C_y	C_z	n
Field Survey Data	0.66	1.4	1.1	0.15*	--
Cs ¹³⁷	0.58	1.2	1.6	--	--
Ru ¹⁰⁶	0.62	1.2	1.3	--	--
Ce ¹⁴¹	0.81	0.71	0.34	--	--
Zr ⁹⁵ -Nb ⁹⁵	0.47	0.70	0.66	--	--
Bi-vane Data (24 meters)	--	--	0.07	--	0.29
Bi-vane (1.5 meters)	--	--	0.09	--	0.29
Smoke Plume	--	1.32	--	0.02	--

* Vertical Wire

isopleths are presented in Figure N.E.18. The curve fit isopleths are presented in Figure N.E.19. Both graphs are normalized to the maximum pleated-filter value on the 100-meter arc.

E.17 Sand and Water Traps

For this release, water and sand deposition samples were obtained on the 100-, 200-, 400-, and 800-meter arcs. Figure N.E.20 shows the gross gamma activity profiles for the water samples. Gamma spectrum analysis indicated the activity was caused primarily by I^{131} and Ru^{103} . The results of the analysis are presented in Table N.E.8.

TABLE N.E.8
Contamination of Water Samples

Station (100-meter arc)	I^{131} muc/ft ²	Ru^{103} muc/ft ²
26	3000	57
31	3200	110
36	3600	86
41	1500	390
46	1400	100
51	1400	100

E.18 Radiobiology

Rats were placed two at a station, every two degrees on the 100-, 200-, and 400-meter arcs. Each was housed in a cone-type restrictive exposure cage five feet above terrain. Entry to the

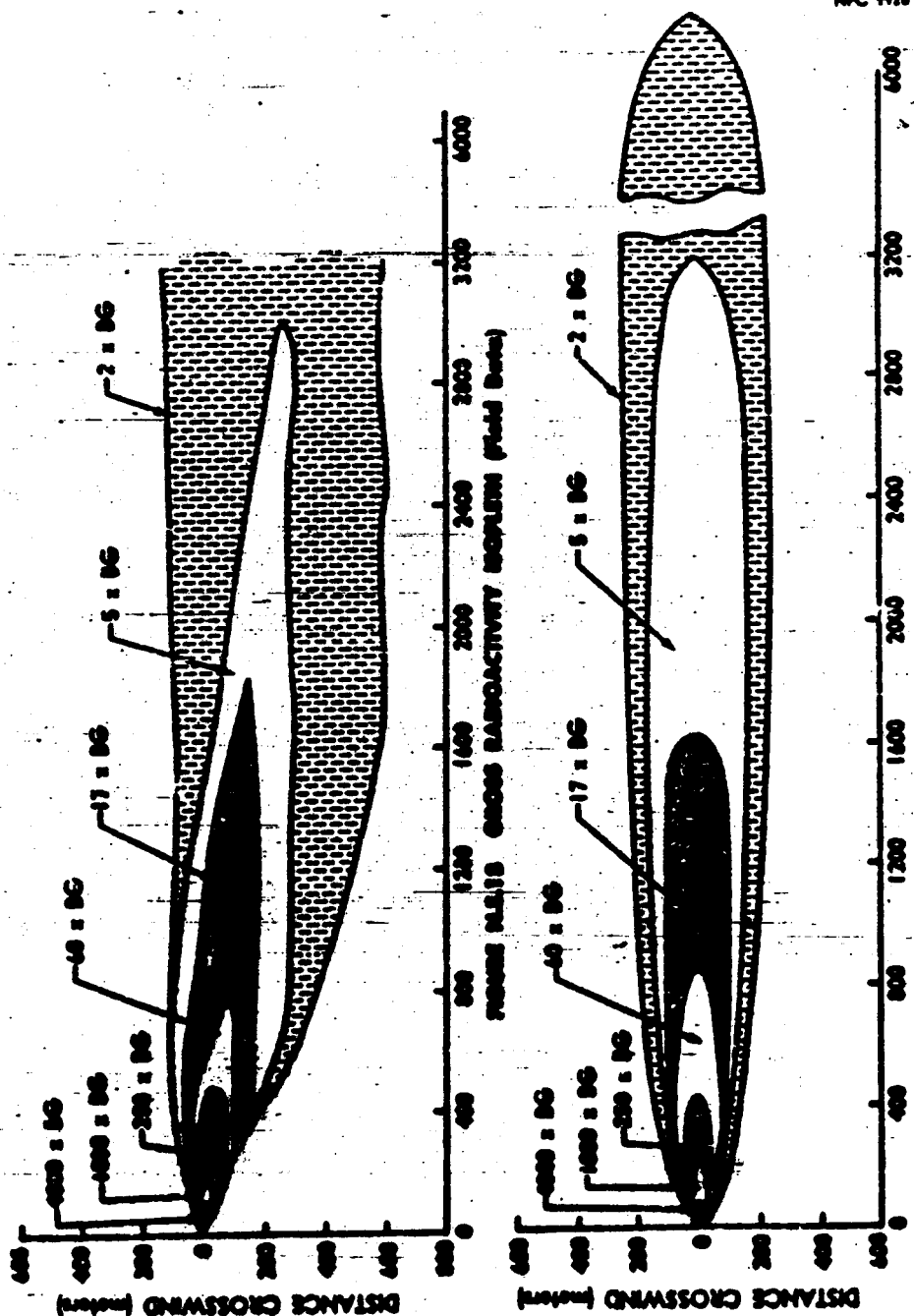


FIGURE NL119 CROSS RADIOACTIVITY ISOPLETH (Curve Fit)

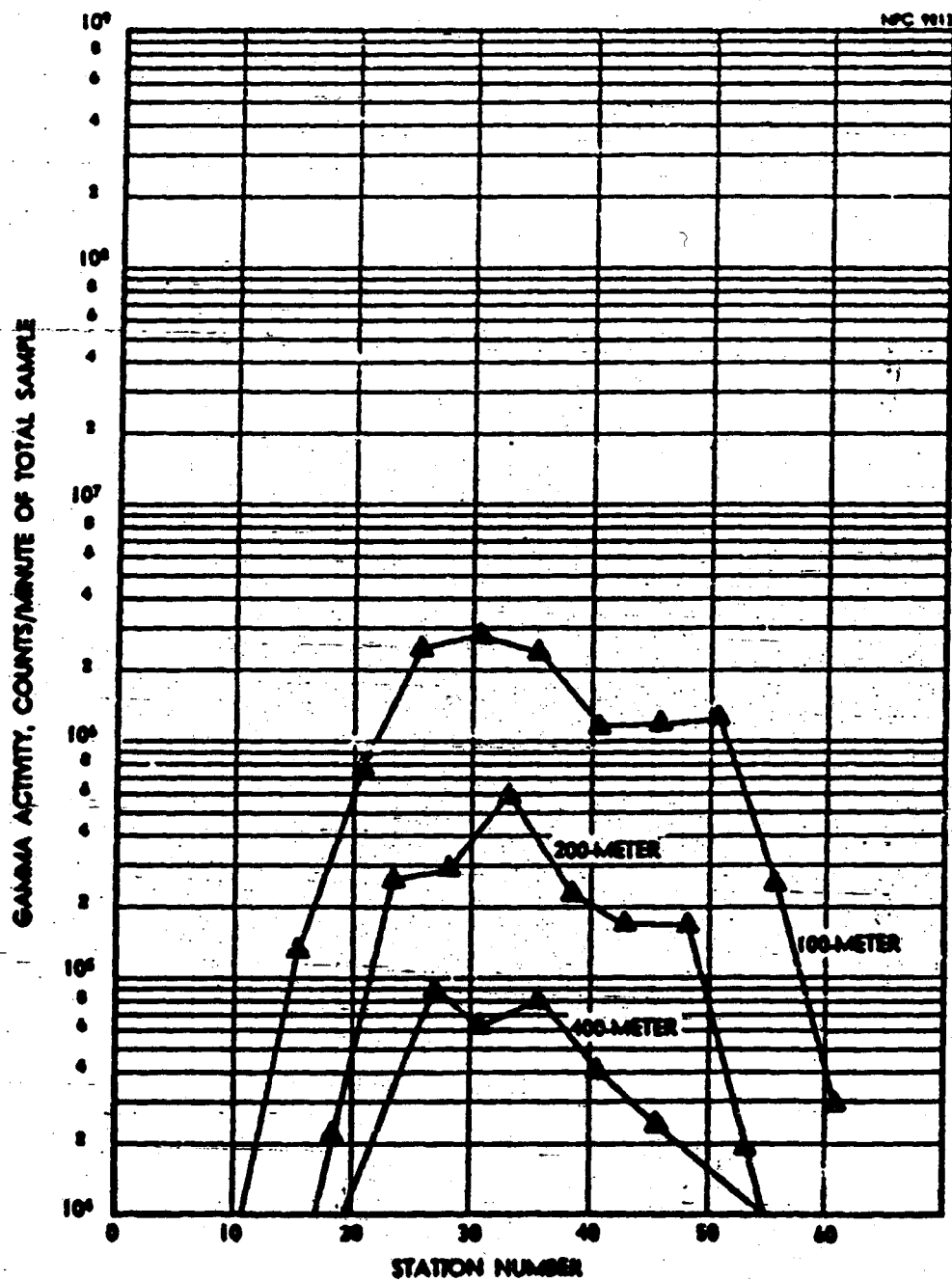


FIGURE N.L. 30 CONTAMINATION OF WATER SAMPLES

network for recovery was no later than 45 minutes after the release. Animals were sacrificed, counted, and autopsied immediately after collection. A filter from a HI-Vol air sampler was counted 3 hours after the release, and at intervals thereafter, for a comparison with biological samples counted on the same counter. Decay schemes were determined on two whole rats (Station 2-34) and on two residual carcasses after autopsy (Station 1-30).

Whole body data from these rats are plotted as profiles in Figure N.E.21. Tissue data are presented in Table N.E.9 in counts per minute per organ. The data from green releases cannot be expressed in absolute radioactivity units because of the variety of energies involved and the different counting efficiency for each. The data for the whole rats (Station 2-34) and the residual carcasses (Station 1-30), along with counts obtained from the HI-Vol filters (Station 1-31), are presented in Table N.E.10. Here also, the data are expressed in counts per minute instead of absolute units.

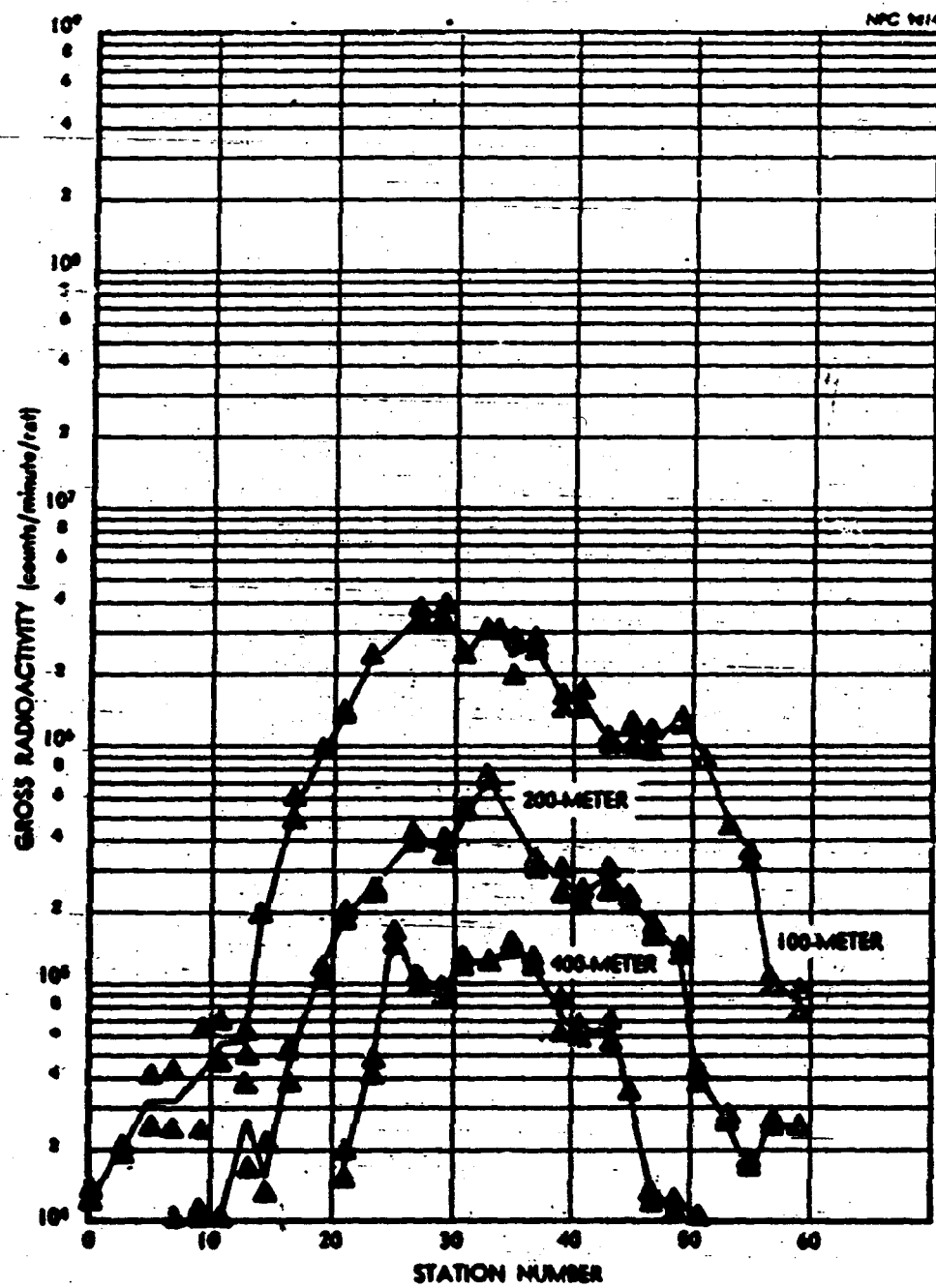


FIGURE N.E.21 RAT WHOLE-BODY EXPOSURE

TABLE N.E.9
Radioactivity in Rats

Arc and Station	Counts/min/Organ				
	Lung	G.I. Tract	Thyroid	Trachea	Kidney
AT 6 HOURS					
1-24	2860	53300	1659	277	1657
28	3330	80500	3374	32	1659
36	1180	13966	654	49	440
40	1020	5569	614	---	98
AT 1 DAY					
1-24	2610	50050	1495	330	1556
28	3197	76980	3188	374	2065
36	1018	13512	711	95	437
40	855	5445	190	79	294
AT 2 DAYS					
1-24	2473	46343	1455	282	1428
28	2971	72027	2873	461	1927
36	991	12476	513	73	411
40	745	5069	1720	201	251
AT 5 DAYS					
1-24	1957	36972	1121	273	1160
28	2295	57471	2166	149	1434
36	893	10069	385	48	295
40	764	3952	128	63	195
AT 12 DAYS					
1-24	1172	20304	575	152	716
28	1435	32473	1160	232	854
36	646	5947	254	48	248
40	612	2481	118	119	123

TABLE N.E.9 (Con't)

Arc and Station	Counts/min/Organ				
	Lung	G.I. Tract	Thyroid	Trachea	Kidney
AT 24 DAYS					
1-24	493	9011	195		272
28	690	14961	465		383
36	454	2965	87		112
40	410	1256	24		107
AT 35 DAYS					
1-24	187	4536	99		74
28	314	8027	180		130
36	226	1726	---		---
40	295	764	---		---
AT 54 DAYS					
1-24		2207	---		
28	199	4304	---		
36		990			
40	241	465			

TABLE N.E.10

Radioactivity of Rats, Residual Carcasses, and Pleated Filters

Days After Release	(Counts/min.)				Filter Paper (Station 1-13)
	Whole Rats (Station 2-34)		Residual Carcasses (Station 1-30)		
	#1	#2	#1	#2	
0.25	711403	786821	2624306	2395005	116,000
0.50					113,267
1					103,832
2	620794	726891	2394897	2177224	99,943
5	500221	586093	1995618	1792226	81,070
6					74,163
10					56,372
12	297780	346140	741120	859190	52,352
14					43,989
22					27,311
26					23,546
27	105146	129836	434780	393264	
32					18,750
53					11,430
63					10,220
125					7,240
160					6,502
188					5,718
193	7202	939	21200	21032	

APPENDIX N-F

(Release F)

P.1 Summary

Type of Sample -----	Green Fuel Element
Date and Release Time -----	4 Sept. 1958; 5:12 P.M.
Lapse Rate (1.5 - 45m) -----	+0.38°C
Lapse Rate (1.5 - 24.5m) -----	+0.18°C
Mean Wind Speed -----	5.3 meters/sec
Wind Direction -----	Network Centerline
Cloud Photography -----	Aerial only
Fluorescent Tracer -----	Released for 10 minutes immediately following fission products release
Animals -----	Rats on 100- and 200-meter arcs. Dogs on 100-meter arc. (Ref. 11)
Network Radioactivity -----	Detected out to 5 miles; maximum reading of plated filter on 100-meter arc, 135 mr/hr, using Cuite Pie.
External Dose -----	Maximum dose rate on 400- meter arc, 0.009 mr/hr, using scintillation detector described in Appendix K.

F.2 Fuel Element

The fuel element had been irradiated to generate 3.4×10^4 Watts for a total of 125 hours and 6 minutes and had decayed for 50 days and 22 hours. The predominant nuclides present at the time of release are shown in Table N-F.1.

TABLE N-F.1

Fission Product Inventory

Nuclide	Curies Calculated
Sr ⁸⁹	48
Y ⁹¹	57
Zr ⁹⁵	59
Nb ⁹⁵	67
Ce ¹⁴¹	63
Ce ¹⁴⁴	20
Pm ¹⁴⁷	2.8
Ru ¹⁰³ -Rh ^{103m}	31
Cs ¹³⁷ -Ba ^{137m}	0.52
Ba ¹⁴⁰ -La ¹⁴⁰	29
Pr ¹⁴³	32
Nd ¹⁴⁷	9.2
I ¹³¹	3.9
Te ^{129m} -Te ¹²⁹	10

P.3 Meteorological Conditions

The wind directions and velocities prevailing during this release are shown in Table N.F.2. The average wind velocity for the release was determined by averaging the data from the 1.5 meter level on the apex tower over the release time. The velocity average was 5.3 meters per second. Fluctuations in the wind directions were observed; however, the deviations did not move the effluent significantly from a network-centerline path.

Lapse rates, existing at the apex tower during the release, between the 1.5 meter level and both the 24- and 45-meter levels, are shown in Figure N.F.1.

TABLE N.F.2
Meteorological Summary

APEX TOWER

Height (meters)	Wind Direction			Wind Velocity (meters/sec)		
	Max.	Min.	Ave.	Max.	Min.	Ave.
1.5	260°	205°	231°	9.7	1.6	5.23
3.0	250	194	229	10.0	2.6	6.05
6.0	-	-	-	-	-	-
12.0	-	-	-	11.9	4.3	7.98
24.0	238	204	222	12.5	4.7	8.91
45.0	257	228	241	12.9	6.4	10.02

TABLE N.F.2 (Continued)

Meteorological Summary

FIELD MASTS

Location (arc)	Wind Direction			Wind Velocity (meters/sec)		
	Max.	Min.	Ave.	Max.	Min.	Ave.
200-meters	264°	205°	234°	8.2	2.4	5.45
400	247	205	226	10.4	3.1	6.64
800	254	204	228	10.0	2.5	6.05
1600	253	201	226	9.8	3.3	6.56
2400	254	204	226	11.2	3.5	7.10
3200	244	205	216	10.6	4.2	7.64

F.4 Smoke Plume Photography

No analysis was made of the visible smoke photographs because the photography was performed under inversion conditions and the fission products released under lapse conditions.

F.5 Furnace Conditions

The operation of the furnace for this release was normal (App. N-A, Sec. A.5).

F.6 Release Height

During this release, three vertical wires spaced 5 inches apart, were placed 48.5 inches downwind from the center of the

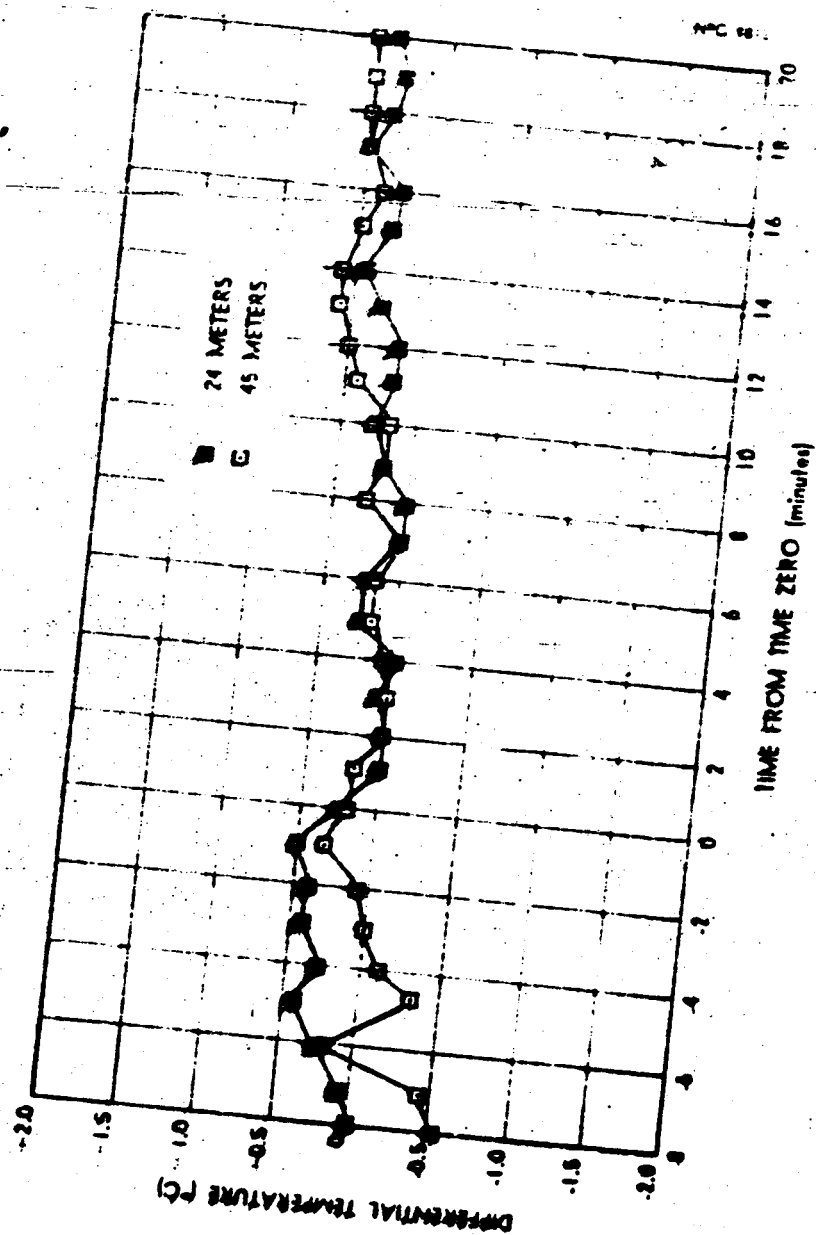


FIGURE M.2.1 LASSO DATA DURING RELEASE

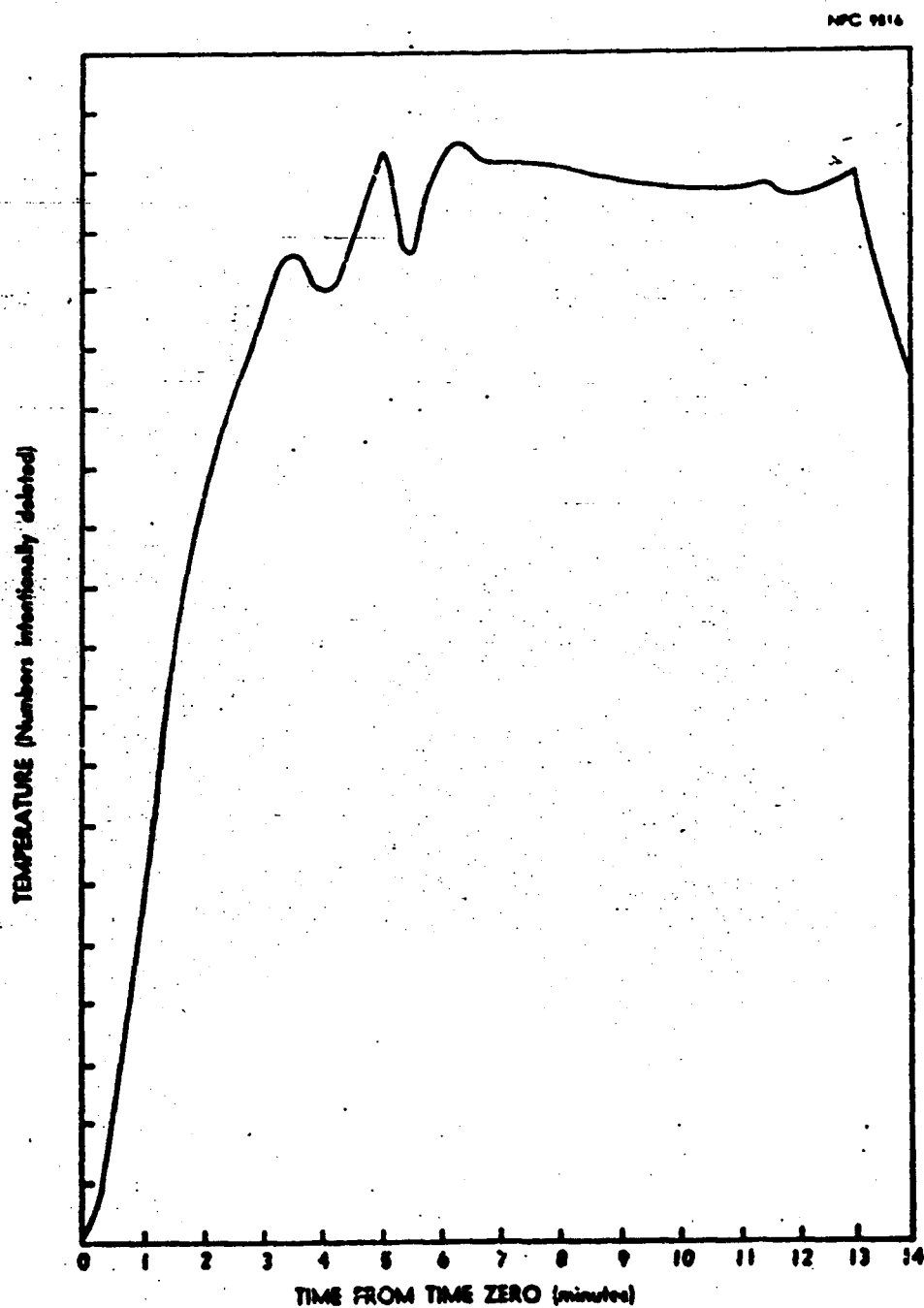


FIGURE N.J.2 FURNACE TEMPERATURE PROFILE

that the effective release height was approximately 4 inches below the top of the furnace.

F.7 Effluent Samplers at Furnace

The effluent sampler filter plug radioactivity as a function of time is shown in Figure N.F.3. The data show that the maximum activity release occurred two minutes after time zero. This time corresponds to the theoretical melt time as established by pre-release furnace calibrations.

F.8 Release Percentages

The release percentages of specific isotopes as determined by pre- and post-melt radiochemistry and network centerline activity are shown in Table N.F.3.

TABLE N.F.3
Release Percentages

Nuclide	Network*Data (%)
Ru ¹⁰³	.75
I ¹³¹	50
Cs ¹³⁷	36

* These data were determined assuming 50 percent release of iodine.

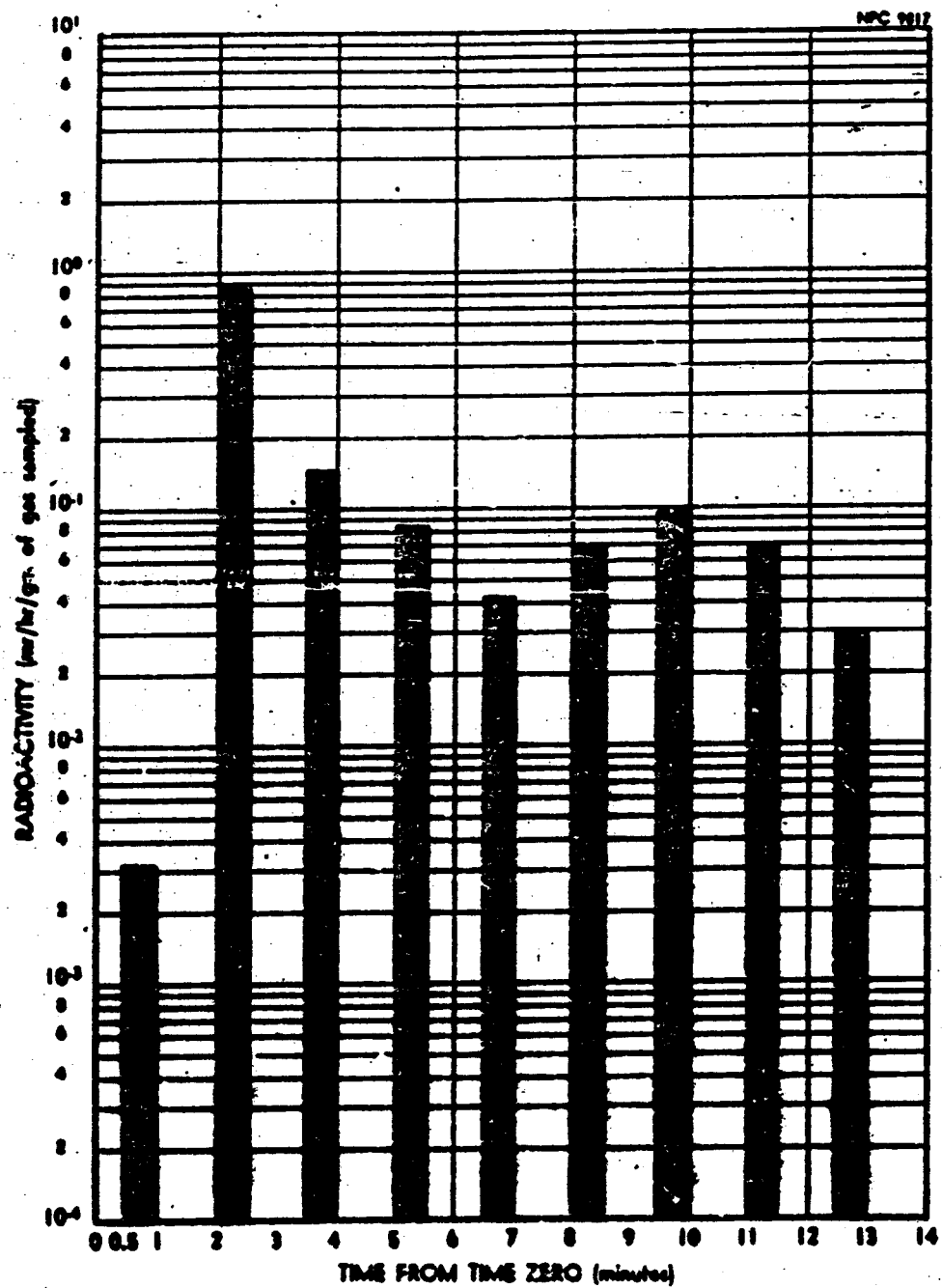


FIGURE M.7.3 SEQUENTIAL EFFLUENT-SAMPLER FILTER

F.9 Air Sampler Field Survey

The gross radioactivity measurements of the pleated filters and carbon cartridges, corrected for background and sampler flow rate, are shown in Figures N.F.4, N.F.5, N.F.6. Figures N.F.4 and N.F.5 present filter and cartridge arc profiles from which centerline values were taken. Figure N.F.6 shows the reading nearest the center of the arcs as a function of distance from the release point. Also shown is a straight line least-squares fit to the data points.

F.10 Airborne Radioactivity

The cloud centerline values for iodine, cesium and ruthenium, plotted as a function of distance from the release point are shown in Figure N.F.7. The iodine curve represents the total iodine collected by the filters and cartridges, whereas the remaining isotope data were taken from the filters only. Little activity other than iodine was present on the carbon cartridges.

The arc profiles for iodine, cesium, and ruthenium are shown in Figures N.F.8, N.F.9, and N.F.10 respectively. They represent the laboratory assays of the Hi-Vol air sampler data. All the measurements were corrected for sampler flow rate.

F.11 Deposited Radioactivity

The profiles of the deposited iodine on the network sampling arcs are shown in Figure N.F.11. The cloud centerline deposition of iodine, as a function of distance from the release point, is shown in Figure N.F.12.

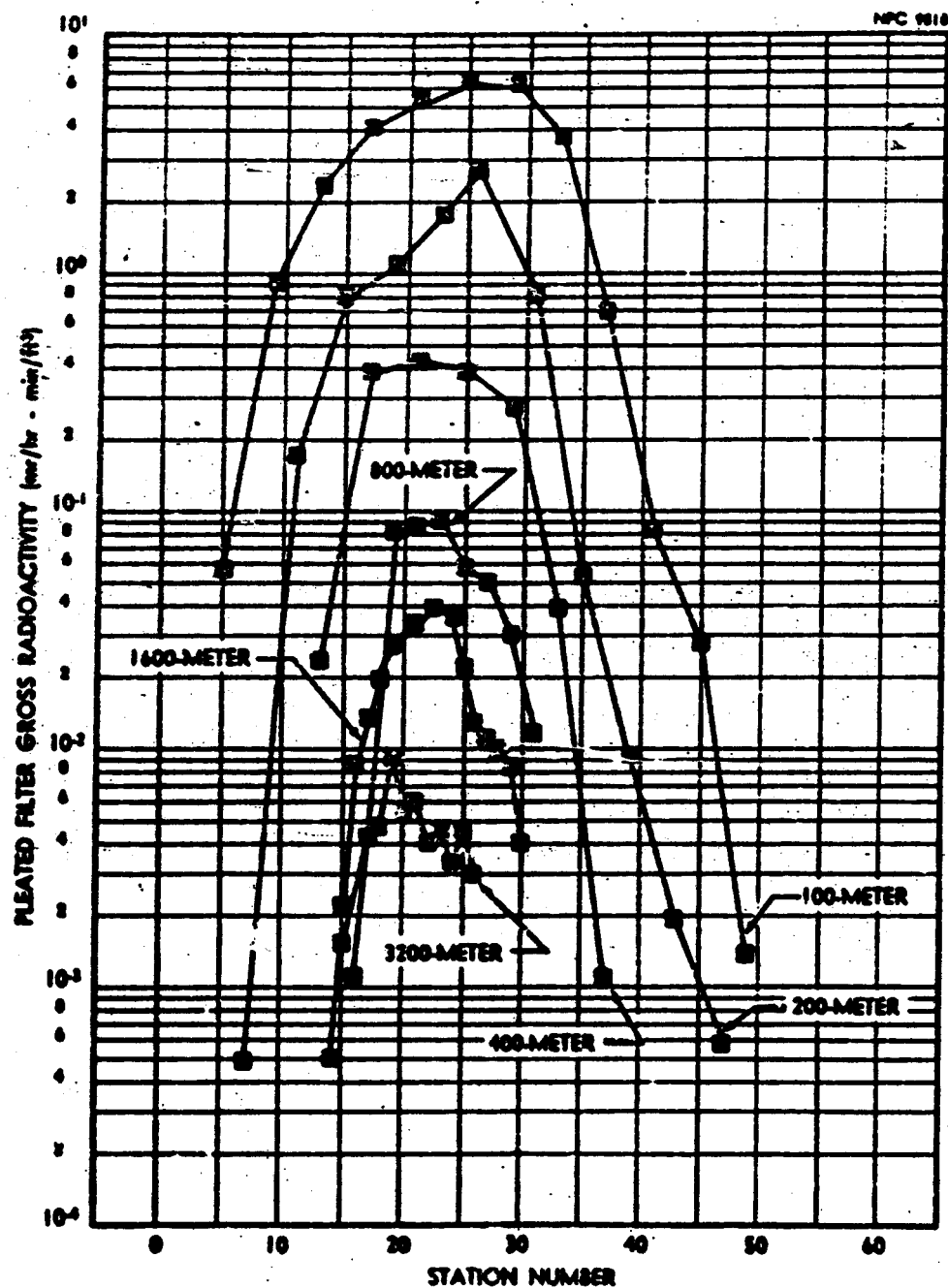


FIGURE N.7.4 NE-VOL AIR SAMPLER FIELD SURVEY
(Pleated Filter - Arc Profile)

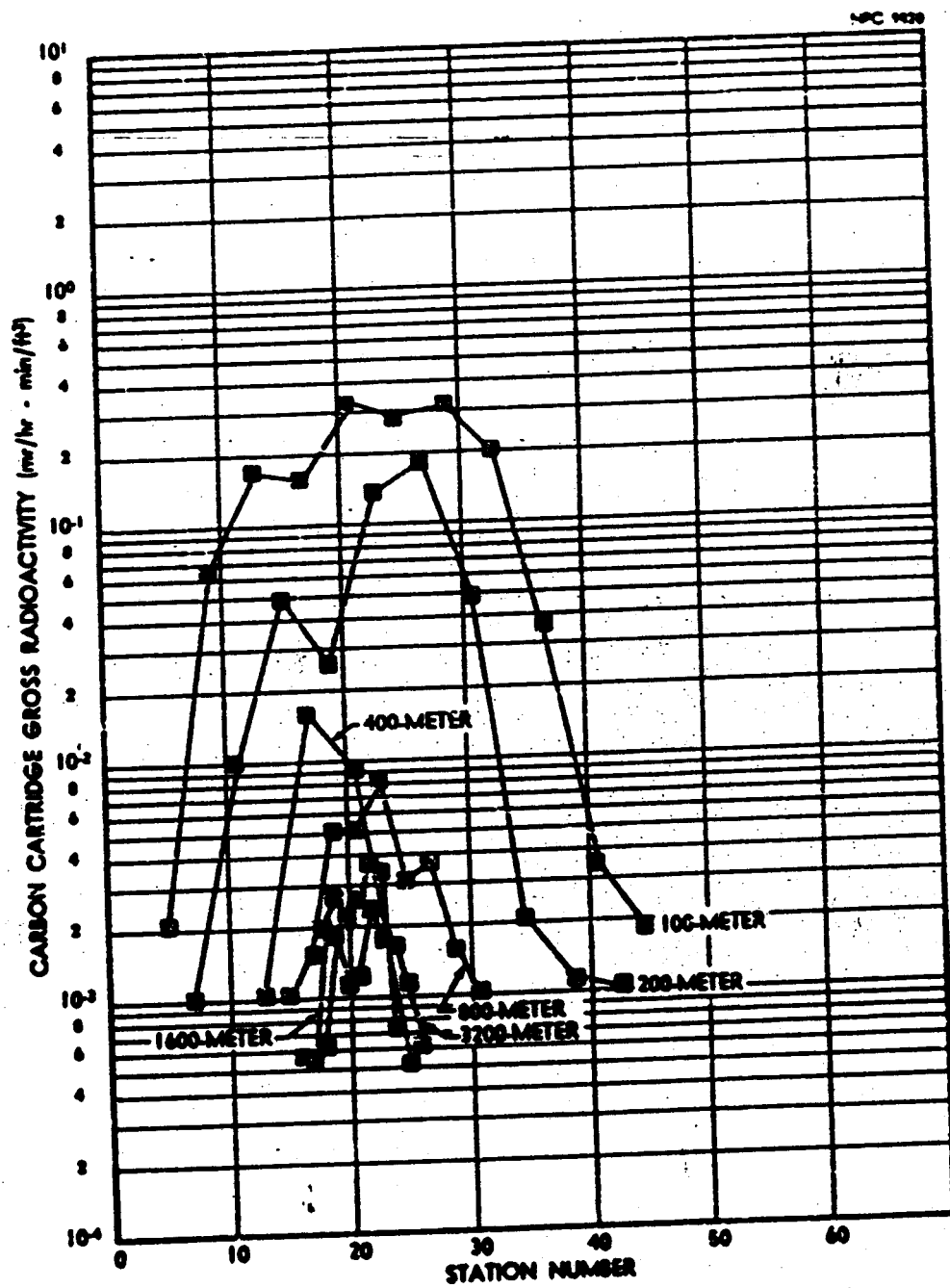


FIGURE N.7.5 HI-VOL AIR SAMPLER FIELD SURVEY
(Carbon Cartridge - Arc Profiles)

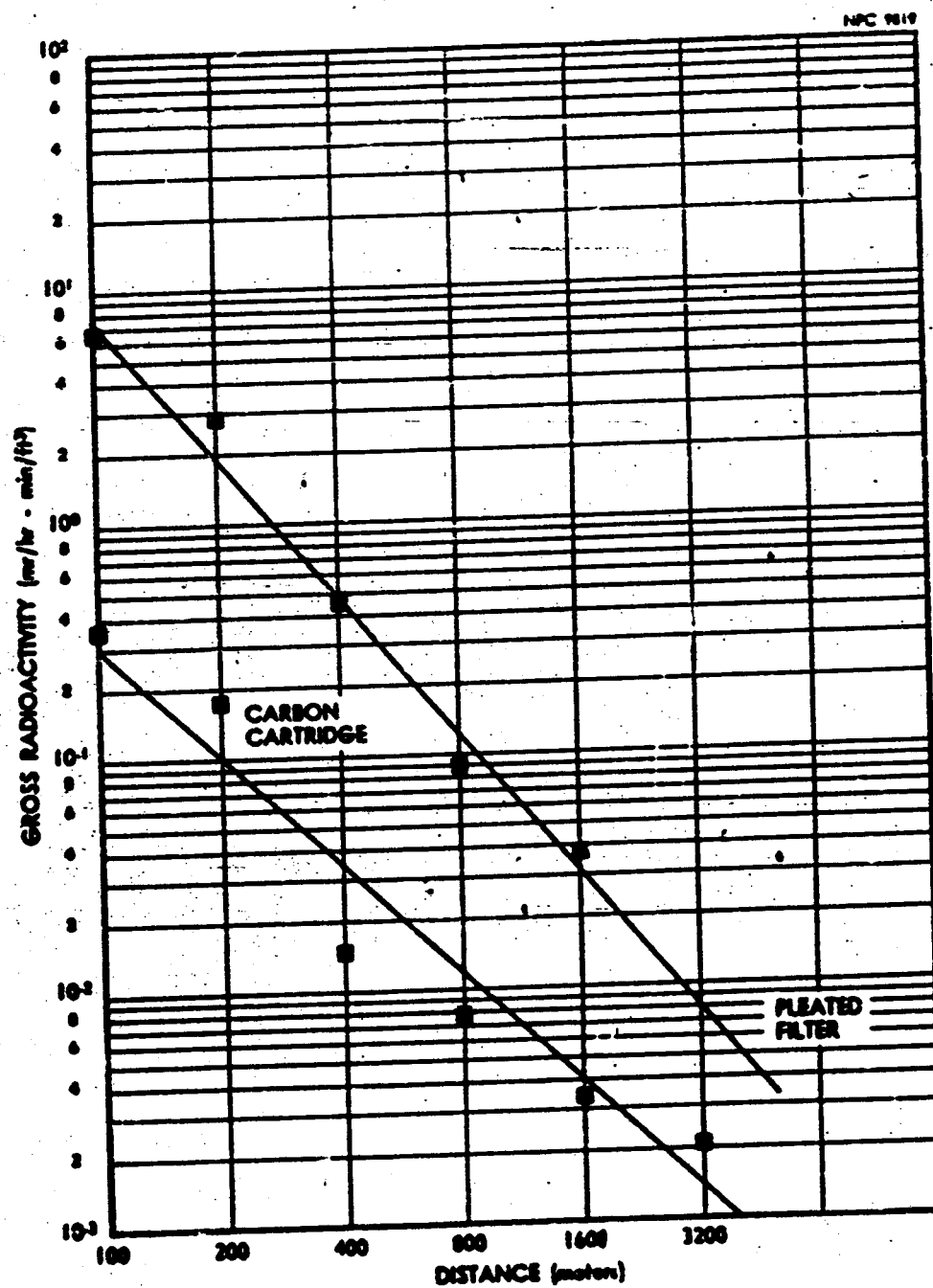


FIGURE N.F.6 HI-VOL AIR SAMPLER FIELD SURVEY
(Centerline)

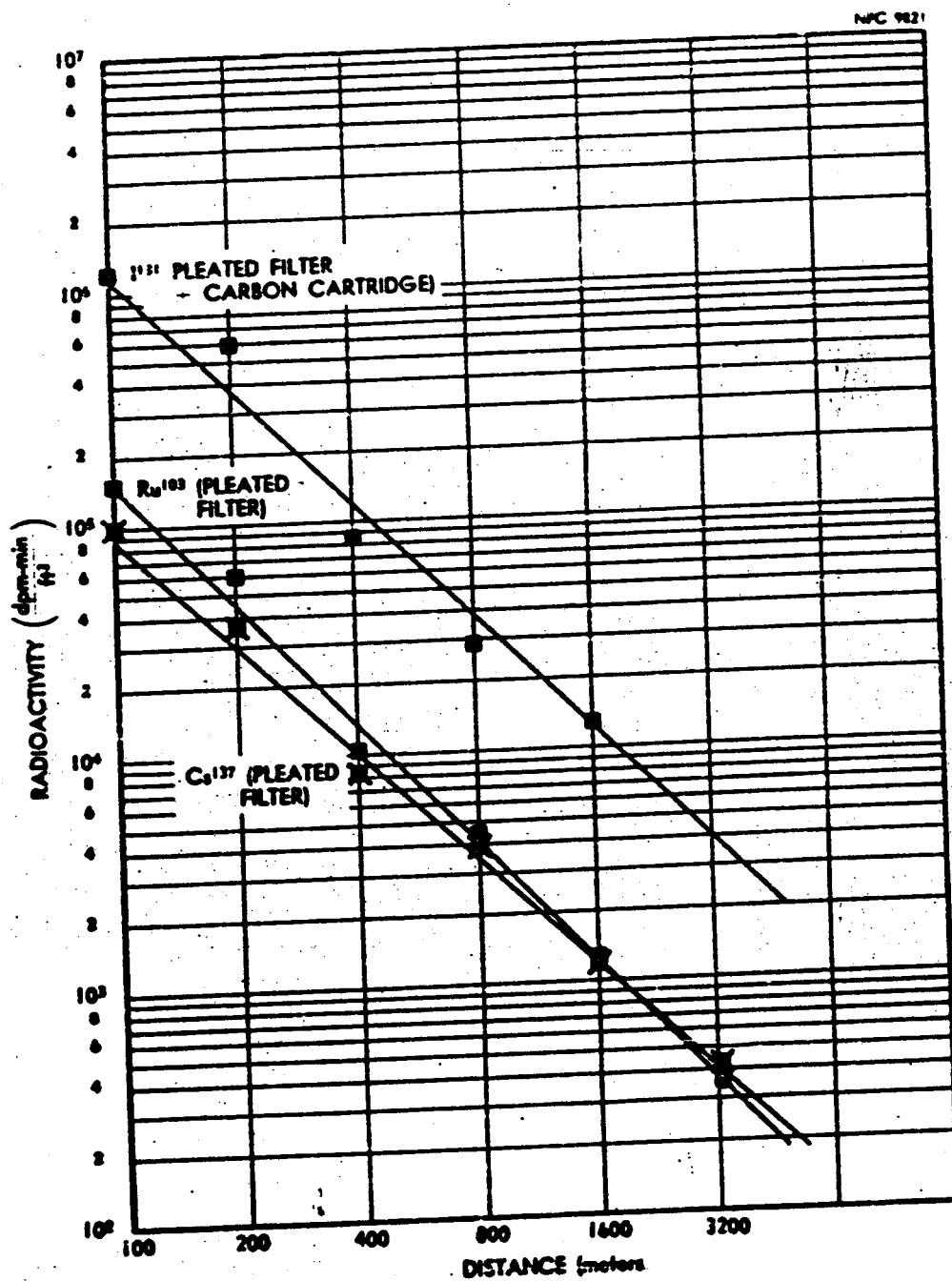


FIGURE N.F.7 HI-VOL AIR SAMPLER LABORATORY ASSAY
(Centerline)

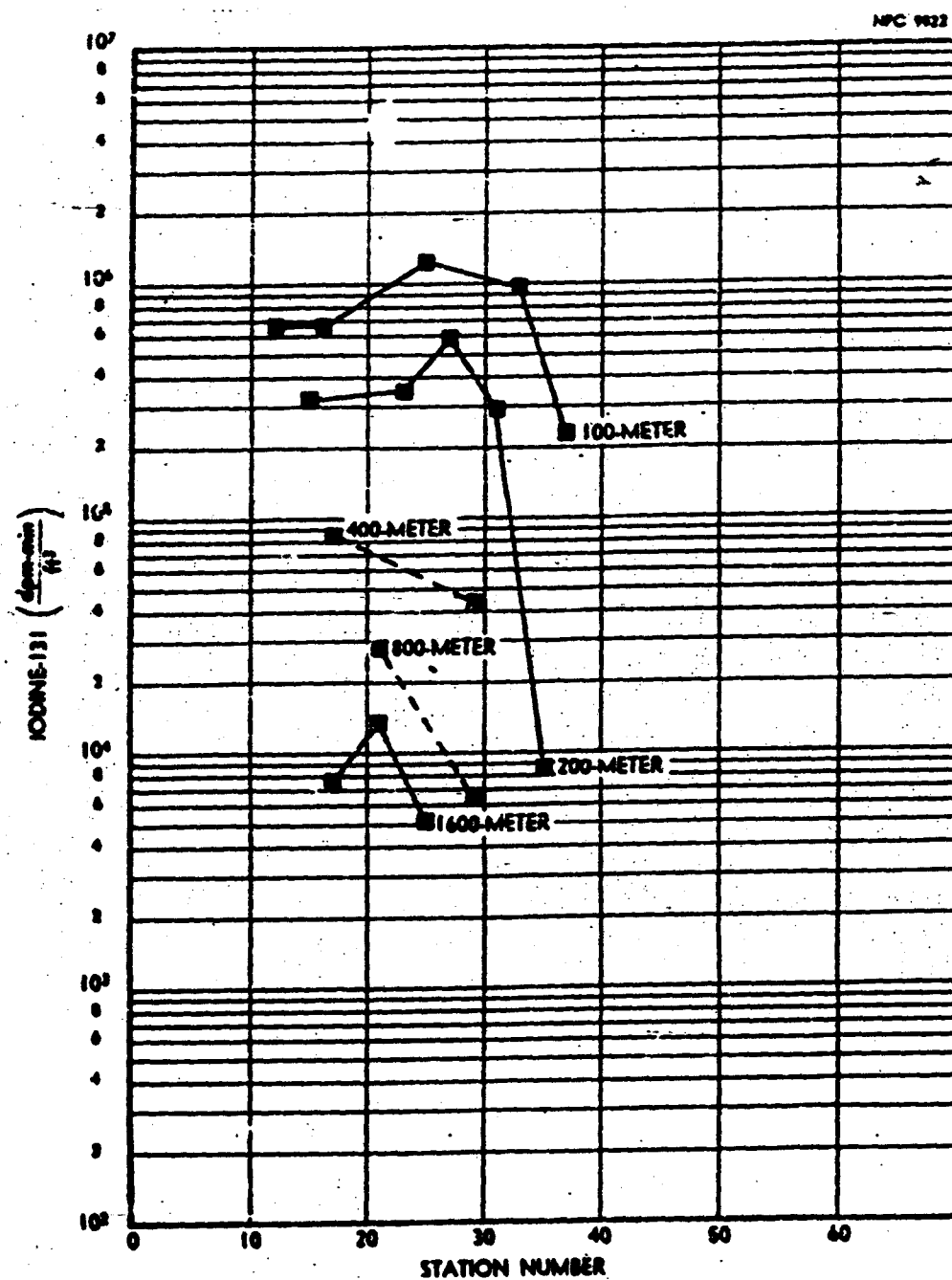


FIGURE N.F.3 15-VOL AIR SAMPLER LABORATORY ASSAY OF IODINE
(Arc Profiles - Plotted Filter Plus Carbon Cartridge)

NPC 9823

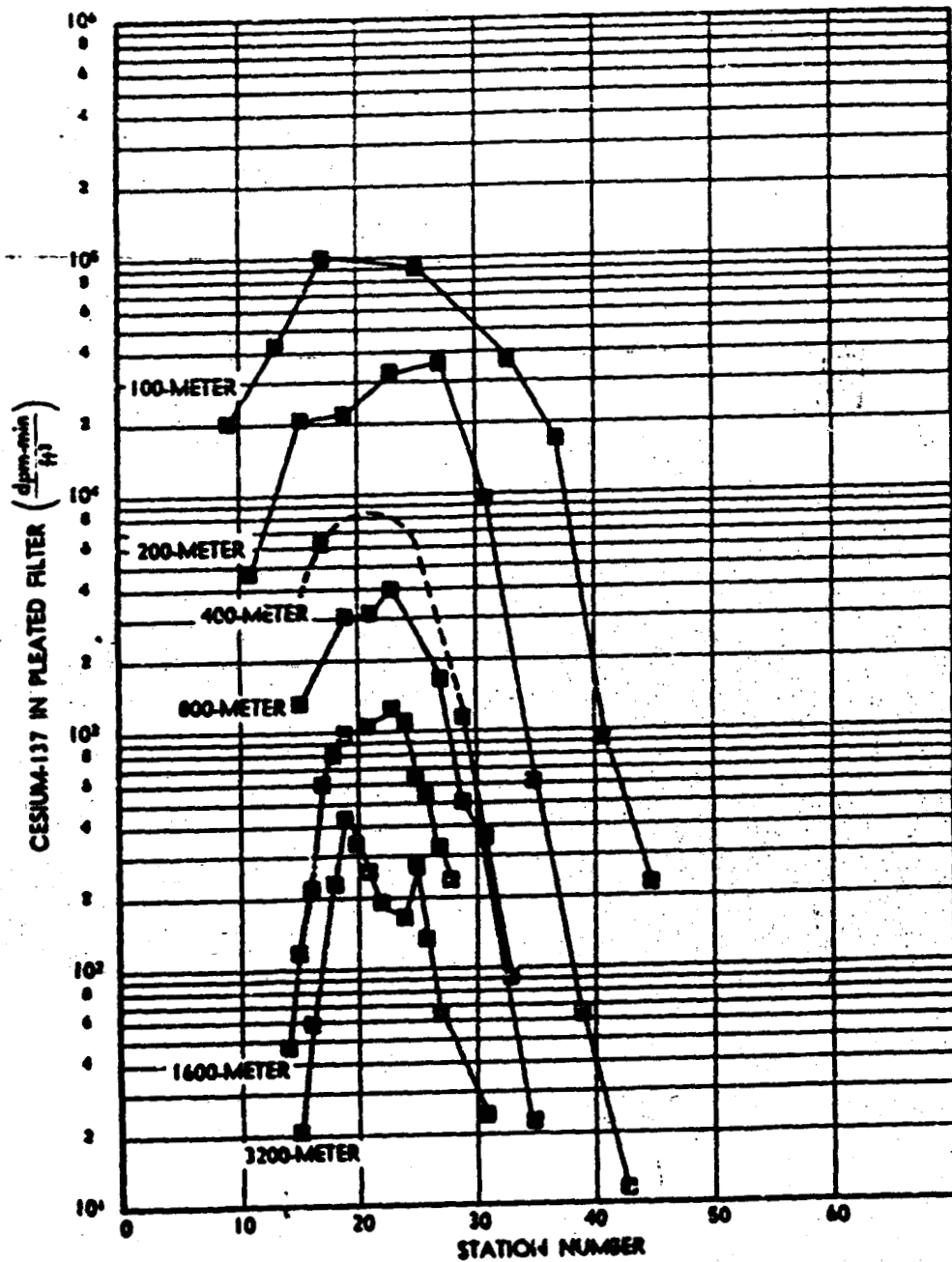


FIGURE N.J.9. HI-VOL AIR SAMPLER LABORATORY ASSAY OF CESIUM (Arc Profiles)

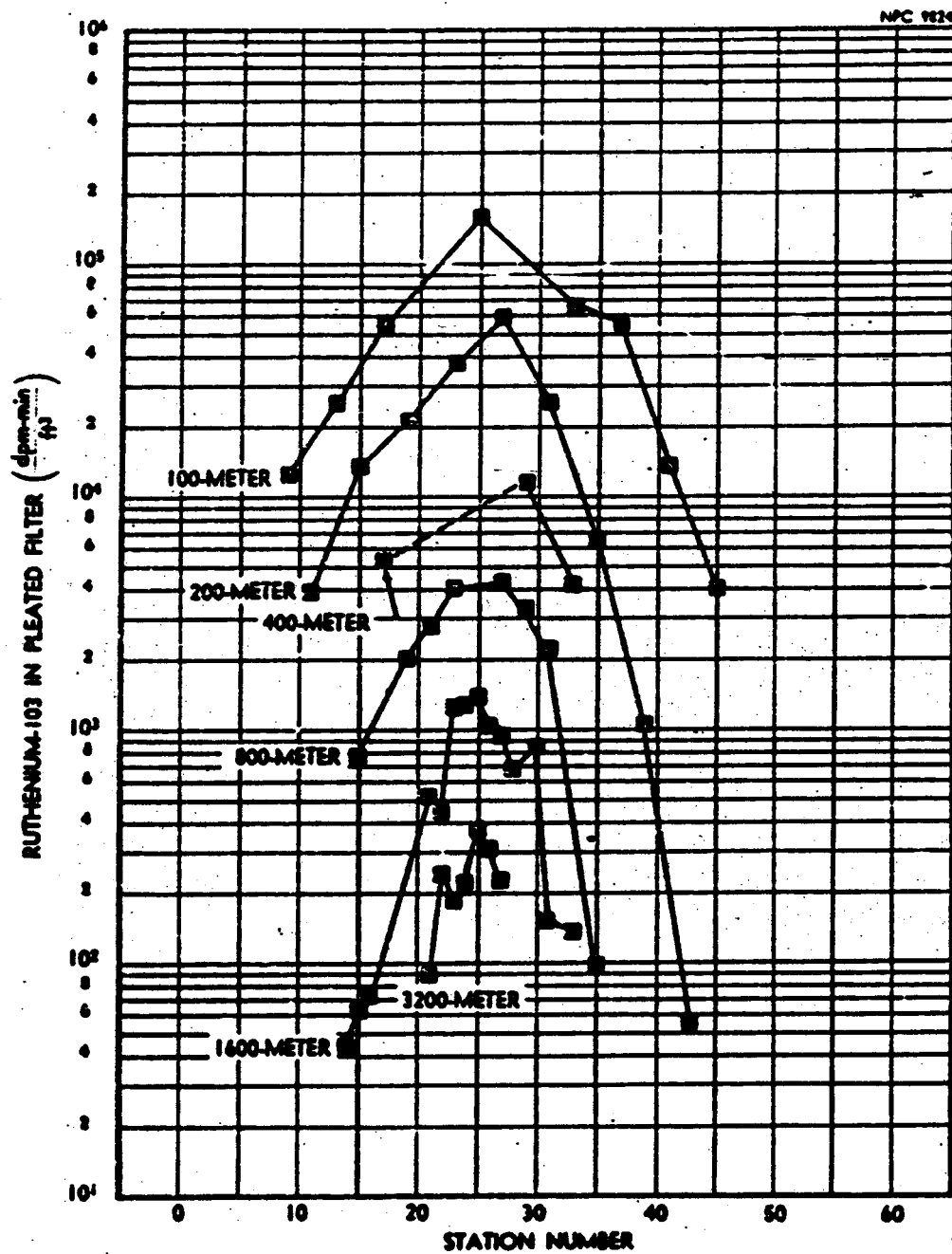


FIGURE N.F.10 NE-VOL /JE SAMPLER LABORATORY ASSAY OF RUTHENIUM (Arc Profiles)

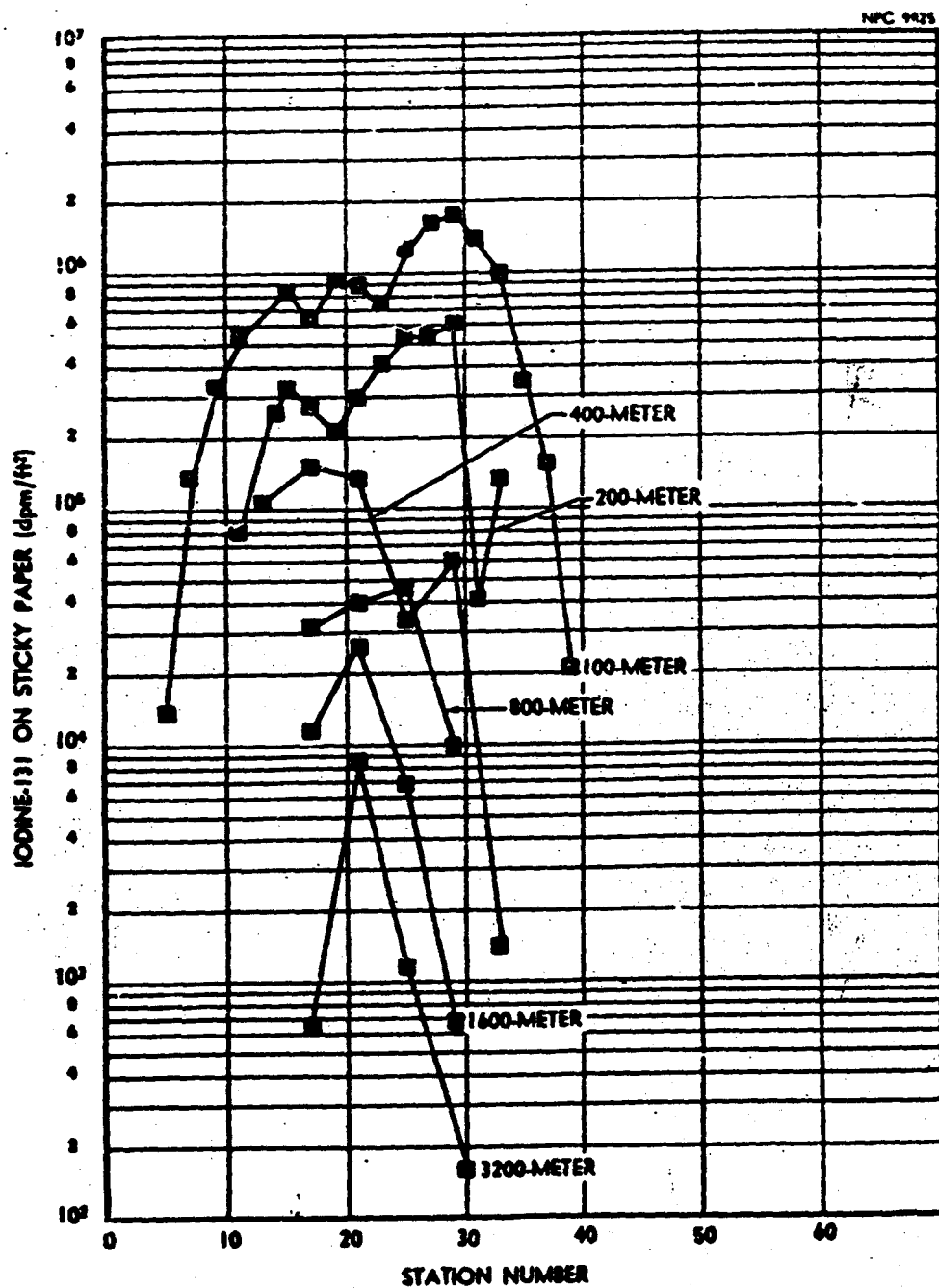


FIGURE N.J.11 DEPOSITED IODINE (Arc Profiles)

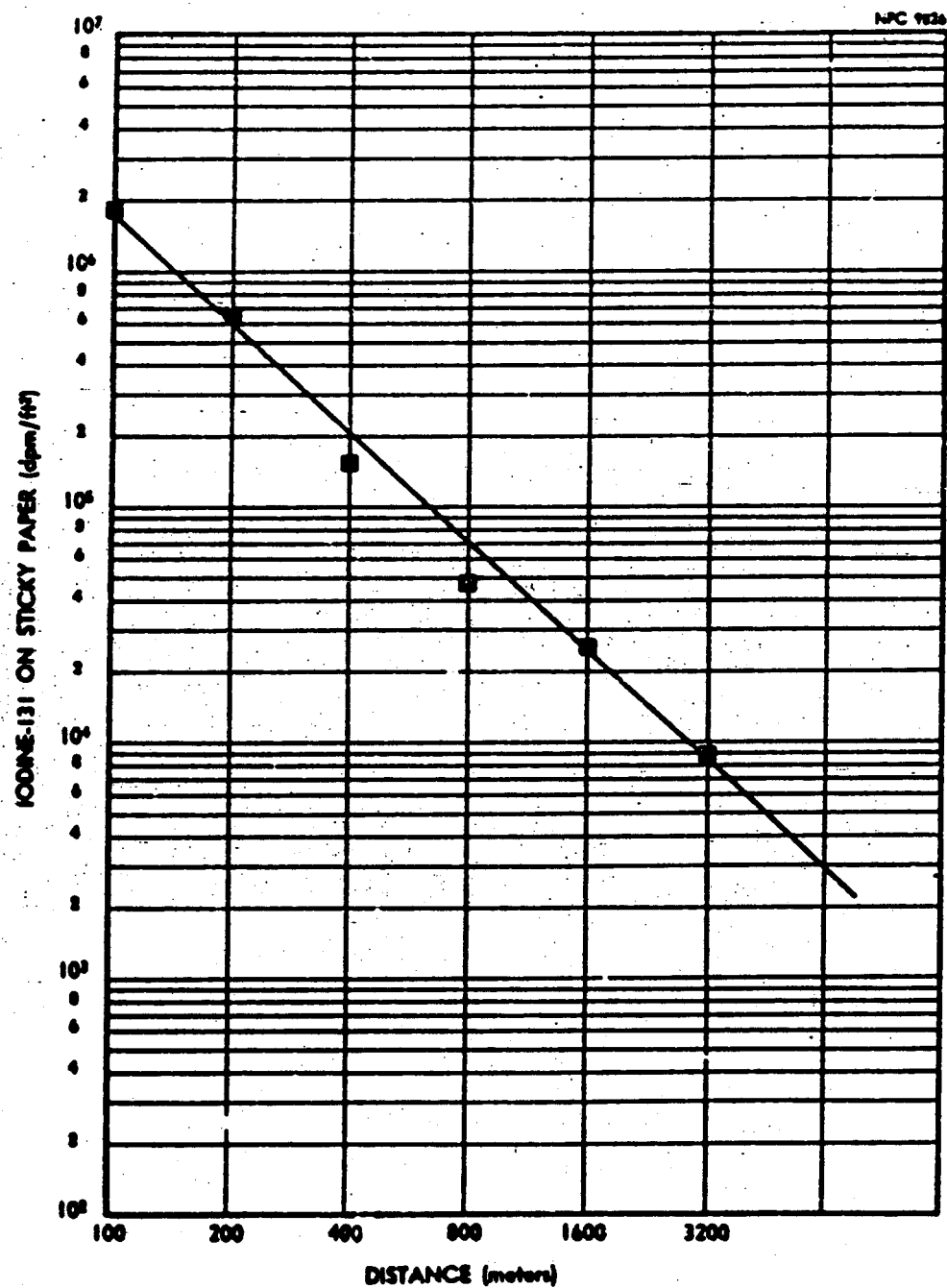


FIGURE N.7.12 DEPOSITED IODINE (Centerline)

F.12 Deposition Velocity

The isotopic deposition velocities are shown in Table N.F.4. The deposition velocity for iodine, as a function of distance from the release point, is shown in Figure N.F.13. The values for the 100-, 200-, and 1600-meter arcs are based on the pleated filter and carbon cartridge profiles, while the values for the 400- and 800-meter arcs are based on two stations only. The deposition velocities were determined from the ratio of the areas under the sticky-paper arc profiles to the area under the air sampler profiles.

TABLE N.F.4
Isotopic Deposition Velocities (cm/sec)

Arcs (Meters)	Sticky Paper	Water		Sand	
	I ¹³¹	I ¹³¹	Ru ¹⁰³	I ¹³¹	Ru ¹⁰³
100	.58	3.2-2.3	1.58-.71	.29-.185	.4-.33
200	.52	1.4-.21	2.2-1.42	2.6	.26
400	.80	-	-	-	-
800	.75	-	-	-	-
1600	.82	-	-	-	-

F.13 Particle Size

The radioactivities of specific isotopes contained in the six stages of three Andersen samplers and their back-up filter assemblies on the 100-, 200- and 400-meter arc centerline are shown in Table

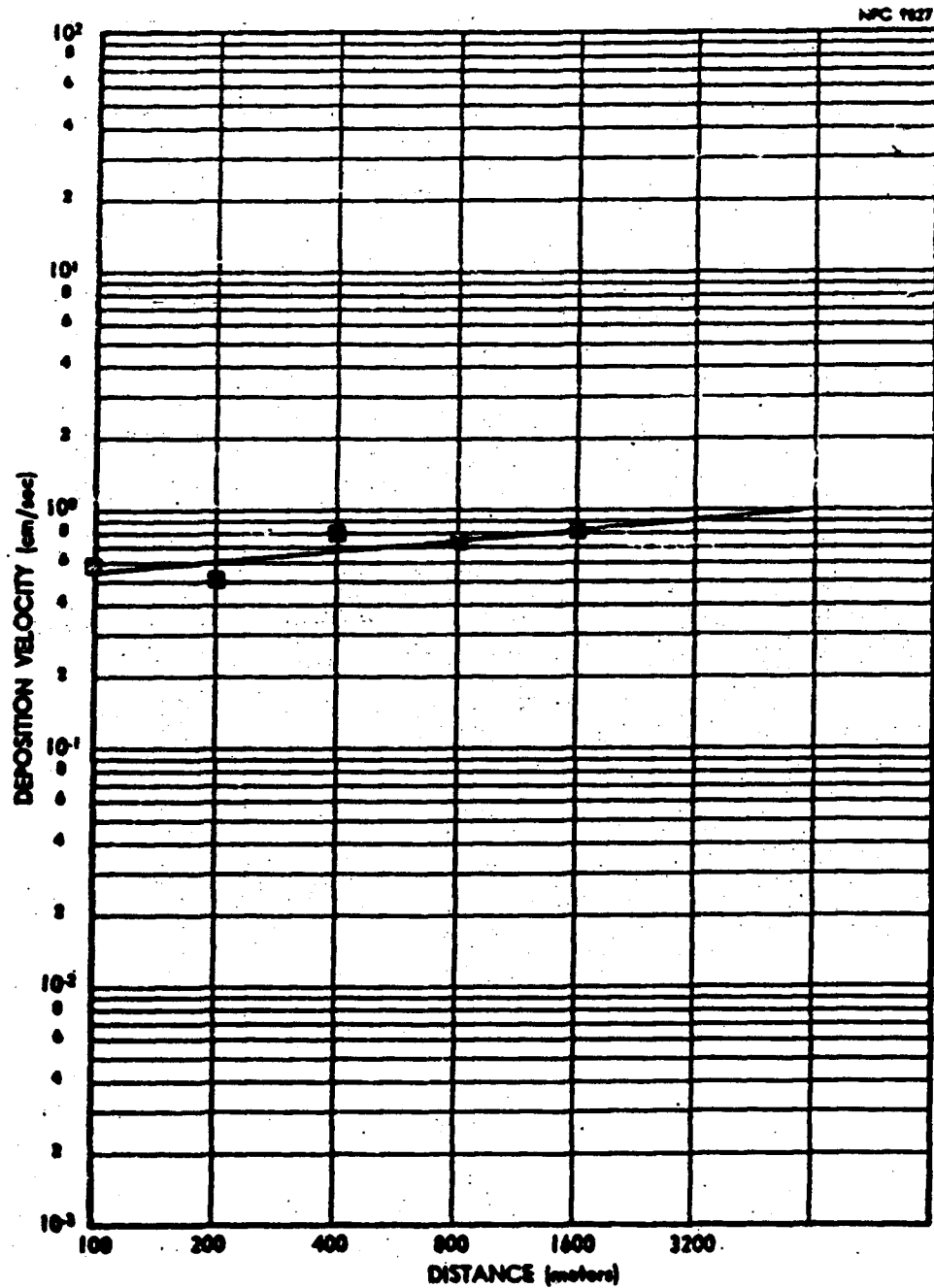


FIGURE N.F.13 IODINE DEPOSITION VELOCITY

N.P.5.

From 80 to 95 percent of the cesium and ruthenium activities were observed on the back-up filter indicating the activity was associated with particles in the submicron size range.

F.14 Fluorescent Tracer Distribution

Sufficient tracer data were not obtained beyond the 400-meter arc to permit reliable determinations of the diffusion characteristics for this material.

F.15 External Dose

Gamma dose measurements were made at a distance of 400 meters downwind from the release point. The integrated dose at each detector station is shown in Figure N.F.14. Figure N.F. 15 shows the time versus dose rate recording from the dosimeter nearest the cloud centerline. The approximate reconstruction of the effluent cloud, as measured by the detectors, is shown in Figure N.F.16. This latter figure shows the isodose rate levels at positions along the 400-meter arc versus time.

The actual gross radioactivity isopleths are presented in Figure N.F.17. The curve fit isopleths are shown in Figure N.F.18. Both graphs are normalized to the maximum pleated filter value on the 100-meter arc.

TABLE N.F.5

Distribution of Isotopes in Andersen Sampler

Location and Stage	Activity (DPM $\frac{\text{min}}{\text{ft}^3}$)	
	Cs-137	Ru-103
Station 24* (100 meter)		
1	530	5385
2	242	559
3	280	294
4	347	257
5	710	371
6	2645	574
7	63500	45500
Station 24** (200 meter)		
1	272	2080
2	175	3210
3	143	146
4	164	127
5	696	228
6	1573	196
7	24000	19500
Station 24*** (400 meter)		
1	44	276
2	30	63
3	25	42
4	32	44
5	57	45
6	198	59
7	4650	3620

* Centerline - Station 26

** Centerline - Station 26

*** Centerline - Station 21

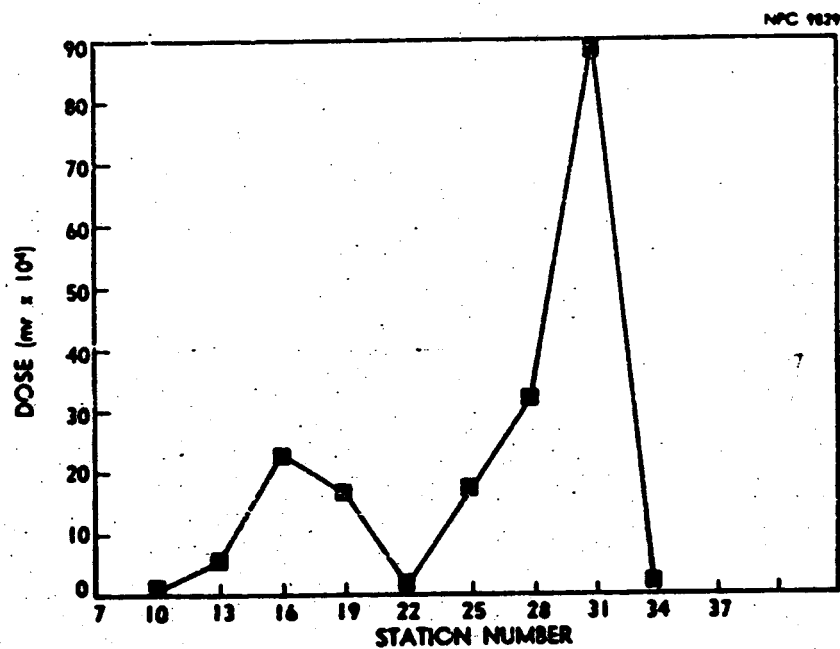


FIGURE N.F.14 GAMMA DOSE FROM CLOUD PASSAGE
(Arc Profile)

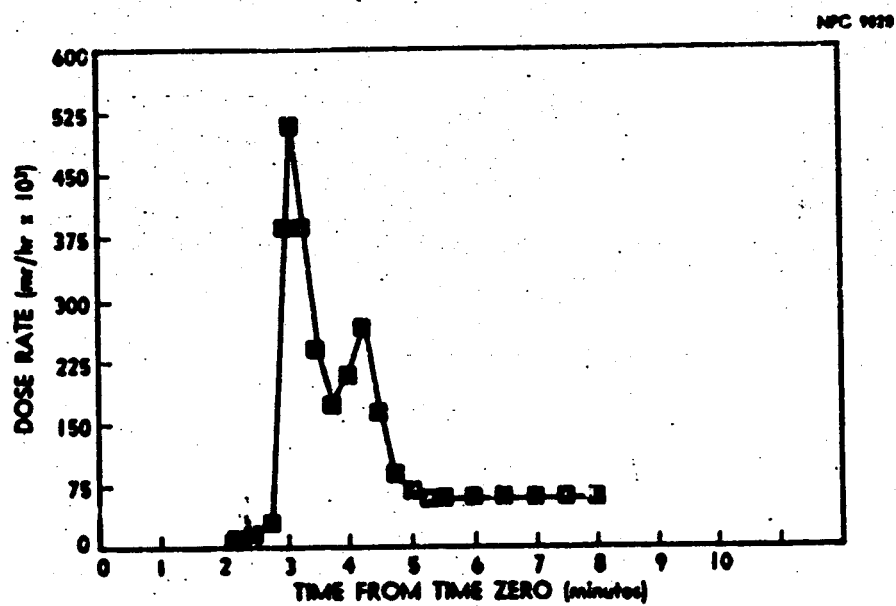


FIGURE N.F.15 GAMMA DOSE RATE FROM CLOUD PASSAGE
(Centerline)

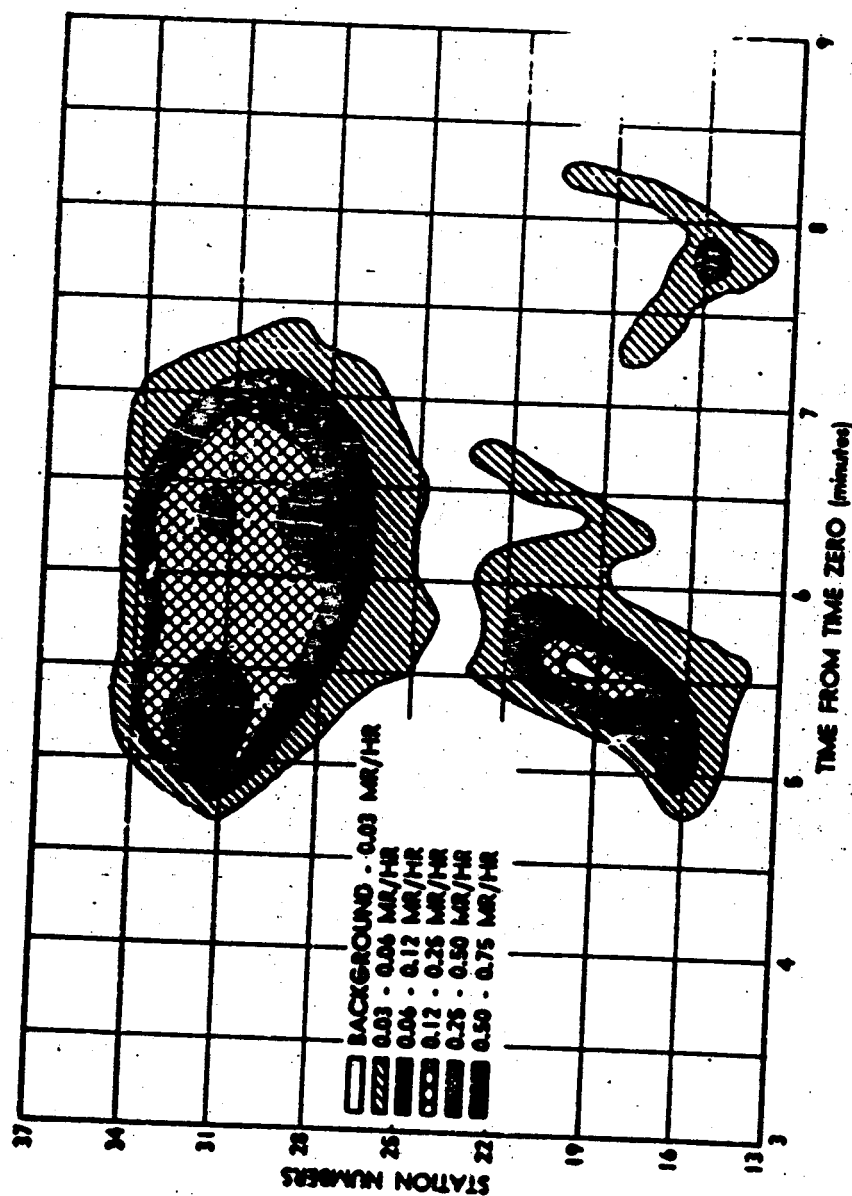


FIGURE NJ.16 GAMMA DOSE RATE FROM CLOUD PASSAGE
(Activity Centers)

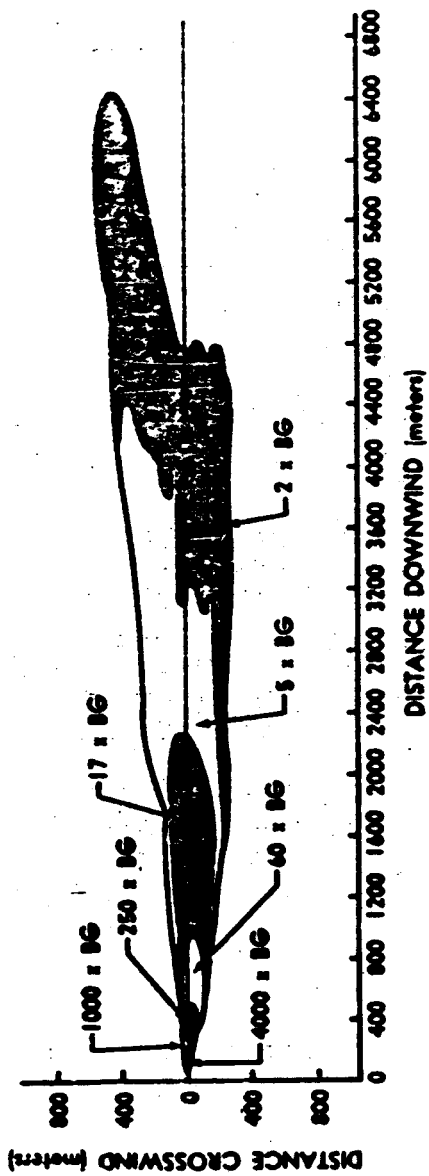


FIGURE N.J.17 GROSS RADIOACTIVITY ISOPLETH
(Field Data)

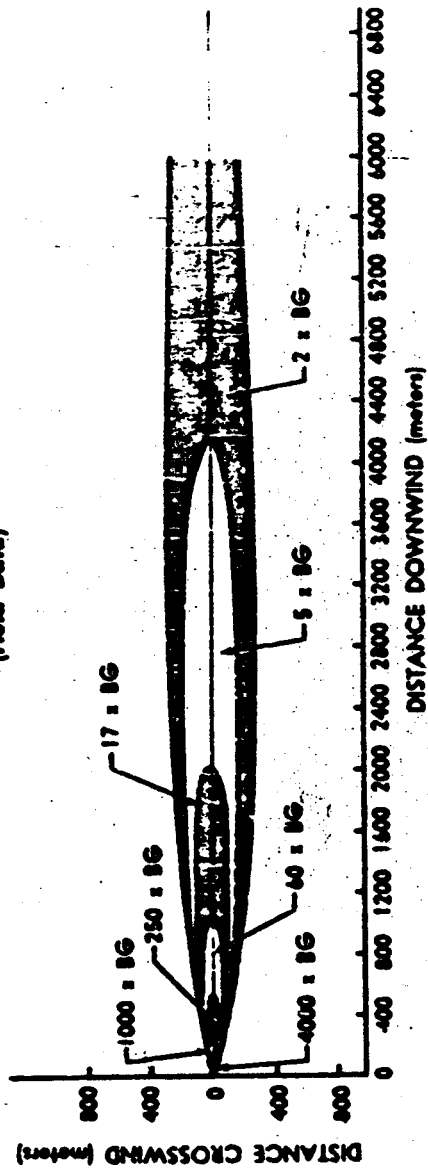


FIGURE N.J.18 GROSS RADIOACTIVITY ISOPLETH
(Curve Fit)

F.16 Diffusion Parameters

The diffusion Parameters obtained during this release are shown in Table N.F.6.

TABLE N.F.6
Diffusion Parameters

Parameter	Field Survey Data Fit	Bivane Data (24 meters)
M_y	0.70	--
M_z	1.3	--
C_y	0.70	0.04
C_z	0.18*	--
n	--	0.32

* Vertical Wire

F.17 Sand and Water Traps

Arc profiles of the gross gamma activity found in water and sand samples are shown in Figures N.F.19 and N.F.20. The data were reduced as explained in Appendix N-A, Sec. A.15.

F.18 Radiobiology

Rats were placed two at a station every two degrees on the 100- and 200-meter arcs. Each was housed in a restrictive, cone-shaped exposure cage placed five feet above ground. Recovery from the arcs was completed no later than 45 minutes after a release. Whole body count data are presented in Table N.F.7 as counts per minute per rat. Figure N.F.21 shows the average values plotted to give relative fallout profiles. Tissue count data obtained for

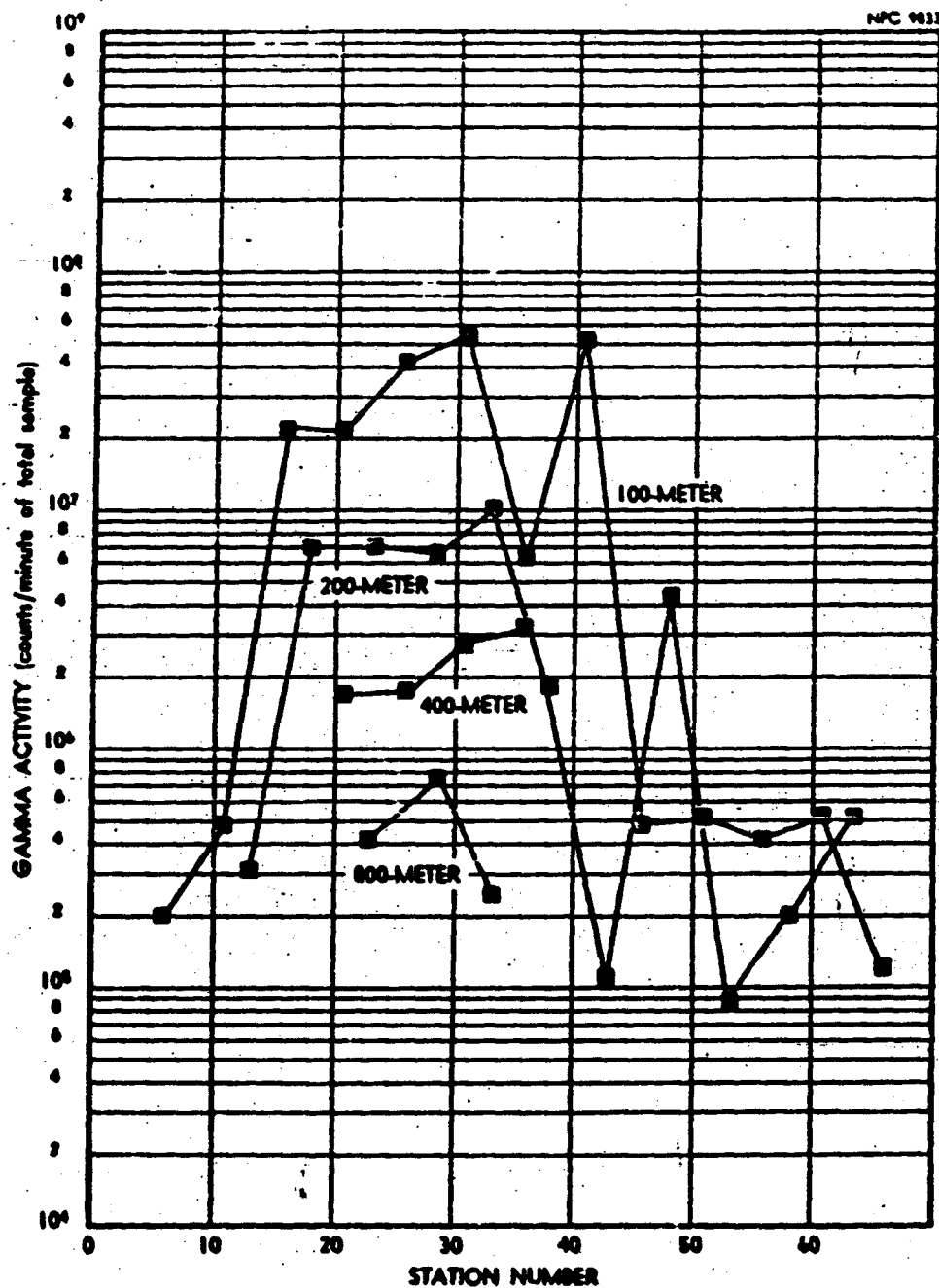


FIGURE N.J.19 CONTAMINATION OF WATER SAMPLES

NPC 9834

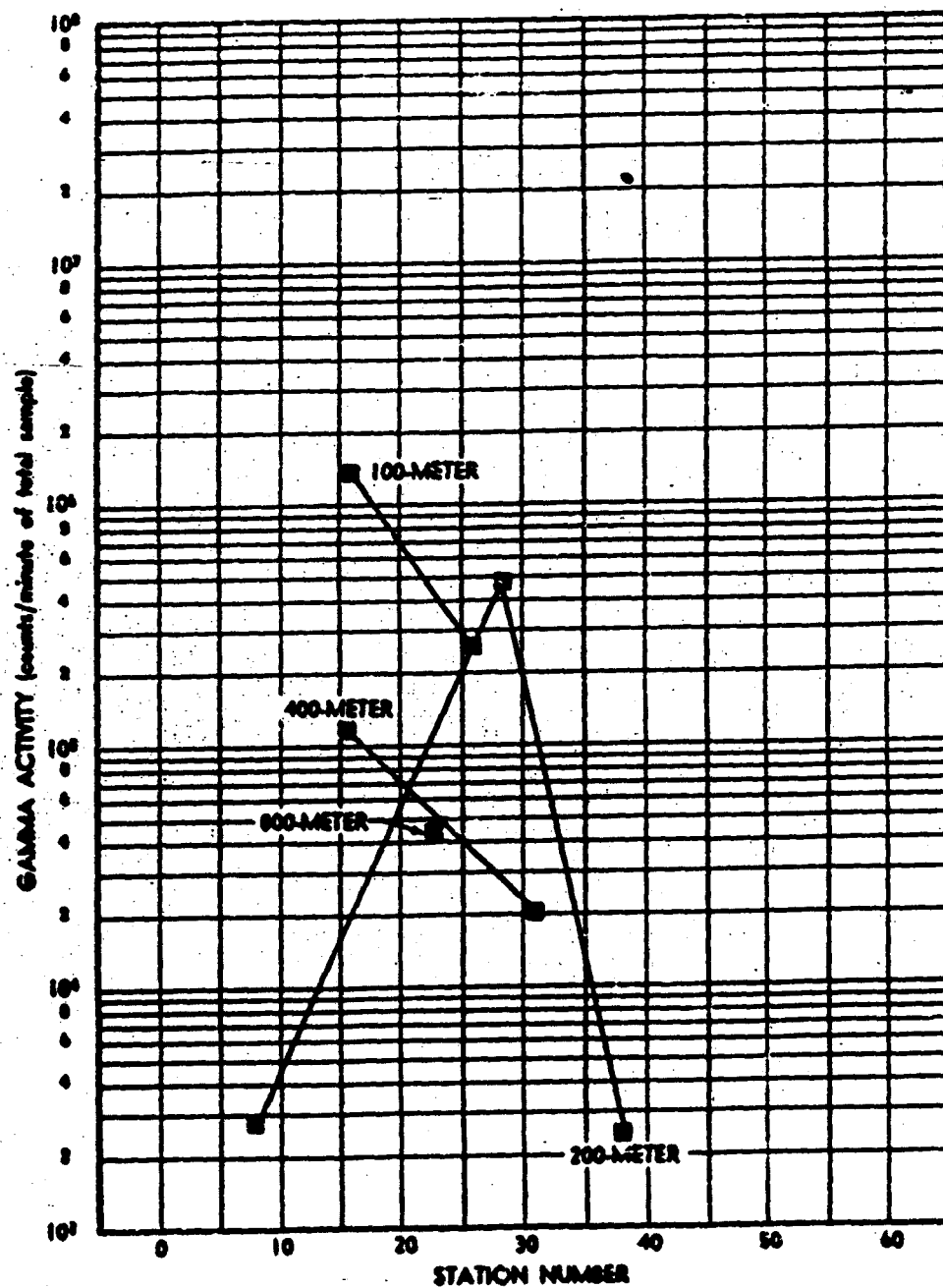


TABLE N.P.7

Whole-Body Radioactivity in Rats

Arc and Station	Count/Min			Arc and Station	Count/Min		
	Rat #1	Rat #2	Average		Rat #1	Rat #2	Ave. age
100- 5	19500	35200	27400	200- 3	10200	10700	10500
7	60300	58500	59400	5	19200	14300	16700
9	295000	314000	305000	7	37000	12400	24700
11	648000	577000	613000	9	13100	8300	10700
13	788000	790000	789000	11	69100	31400	50000
15	791000	801000	796000	13	177000	189000	183000
17	888000	828000	858000	15	376000	380000	378000
19	1220000	1410000	1320000	17	383000	368000	376000
21	1430000	1770000	1600000	19	309000	325000	317000
23	1360000	1480000	1420000	21	327000	322000	325000
25	1580000	2060000	1820000	23	337000	405000	371000
27	2360000	2400000	2380000	25	624000	621000	623000
29	2080000	2110000	2100000	27	616000	603111	610000
31	2040000	1550000	1800000	29	516000	486000	501000
33	1650000	1330000	1490000	31	490000	494000	492000
35	718000	712000	715000	33	193000	244000	218000
37	315000	323000	319000	35	54900	62300	58600
39	154000	164000	159000	37	23200	17600	20400
41	66000	109000	87000	39	11800	12800	12400
43	24700	21600	23200	41	40900	29500	35200
45	29900	13200	21600	43	9000	14400	11700
47	31900	30600	31300	45	13000	9300	11200
49	38800	10200	20000	47	8200	6900	7600
51	8800	11000	9900	49	16000	6700	8700
53	32500	17000	17000	51	8300	9600	9000
55	9100	19100	14100	53	7400	6500	7000
57	8200	8200	8200	55	10400	7700	9100
59	10800	12000	11400	57	6300	4300	5300
61	7700	9700	8700	59	11300	12000	11600
				61	16000	2400	9200

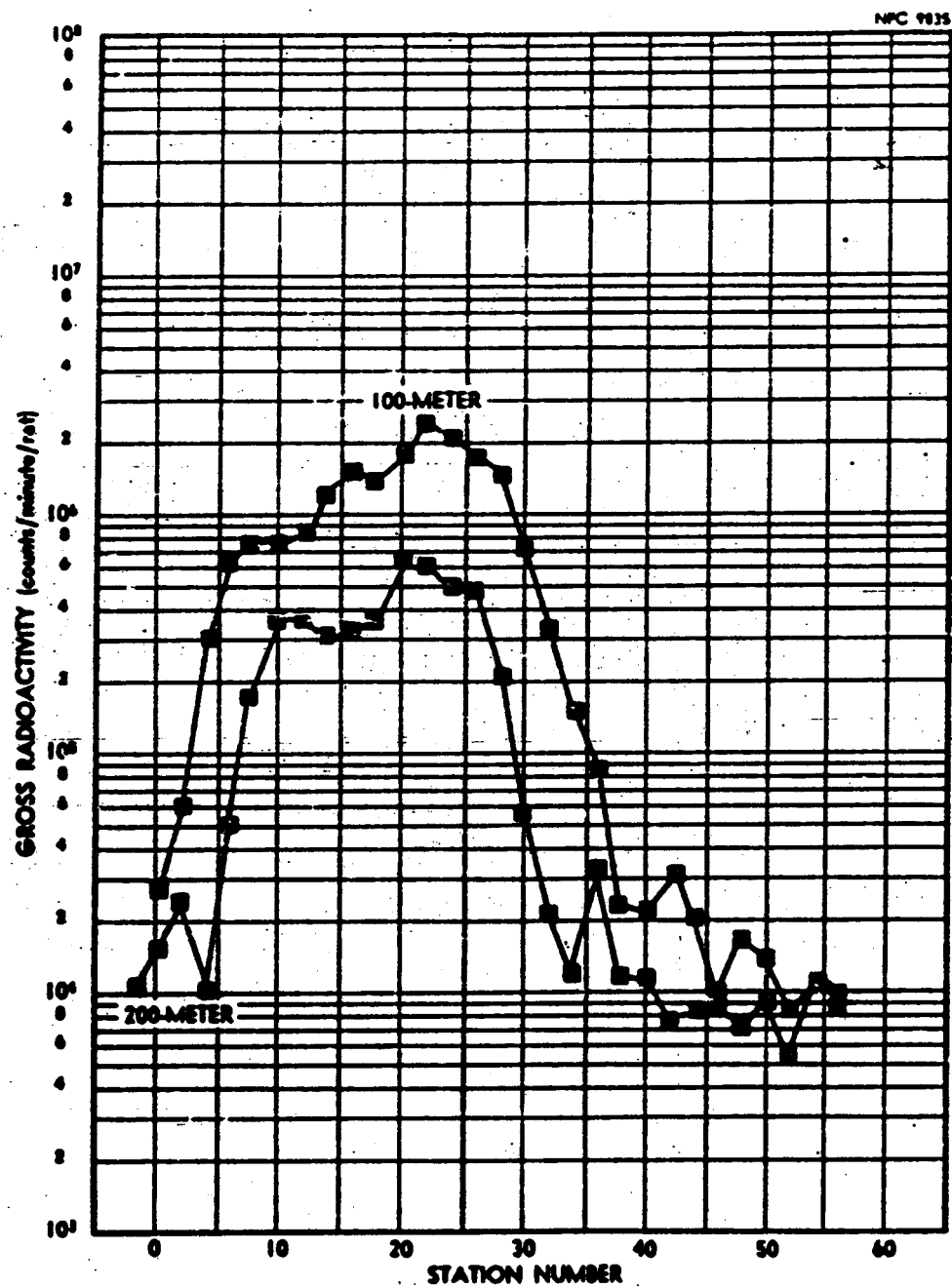


FIGURE N.J.21 RAT WHOLE-BODY EXPOSURE

various post-release times are presented in Table N.F.8. Figure N.F.22 shows relative radioactivity measured at various organs one day after release.

Five dogs were placed on the 100-meter arc. Recovery commenced at approximately 45 minutes after release. Data on tissue radioactivity are presented in Table N.F.9. The results are shown in counts per minute per organ at various post-release times. Figure N.F.23 shows relative radioactivity measured at various organs from 100-meter arc after one day.

The decay of the gross radioactivity as determined by measurements made at one of the Hi-Vol-Air-Sampler pleated filters is shown in Table N.F.10. The filter was from the 100-meter arc, station 6.

TABLE
Radioactive Rats

Arc and Station	Counts/organ				
	Lung	G.I. Tract	Heart	Trachea	Kidney
103-13	159	492		157	167
-15	921	2769		532	753
-19	49	815		148	788
-21	---	3574		235	---
-25	325	986		86	94
-27	1336	10183		48	467
-31	222	1339		56	139
200-25	317	1224		58	148
-27	---	1622		---	---
31	---	1024		---	---
100-13	201	751		94	110
-15	372	3040		63	182
-19	318	749		157	127
-21	528	3334		92	216
-25	363	1009		63	82
-27	1310	9471		36	453
-31	292	1197		789	1236
200-25	379	1106		45	71
-27	195	1752		44	125
-31	180	795		63	77

TABLE N.F.8
(Cont'd)

At 6 Days

Arc and Station	Counts/min/organ				
	Lung	G.I. Tract	Thyroid	Trachea	Kidney
100-13	166	506	73	87	60
-15	257	2072	80	49	124
-19	256	537	28	91	91
-21	462	2326	40	74	172
-25	326	692	29	12	75
-27	1083	6511	141	---	295
-31	248	825	35	---	124
200-25	278	833	26	41	52
-27	142	1179	33	31	55
-31	169	534	132	169	89

At 17 Days

100-21	338	1099	730	---	96
-27	685	2899	---	139	---

At 27 Days

100-21	336	611	---	---	64
-27	535	1546	---	---	94

At 45 Days

100-27	351	581	---	---	---
--------	-----	-----	-----	-----	-----

At 117 Days

100-27	172	242	---	---	---
--------	-----	-----	-----	-----	-----

At 185 Days

100-27	167	176	---	---	---
--------	-----	-----	-----	-----	-----

NPC 1034

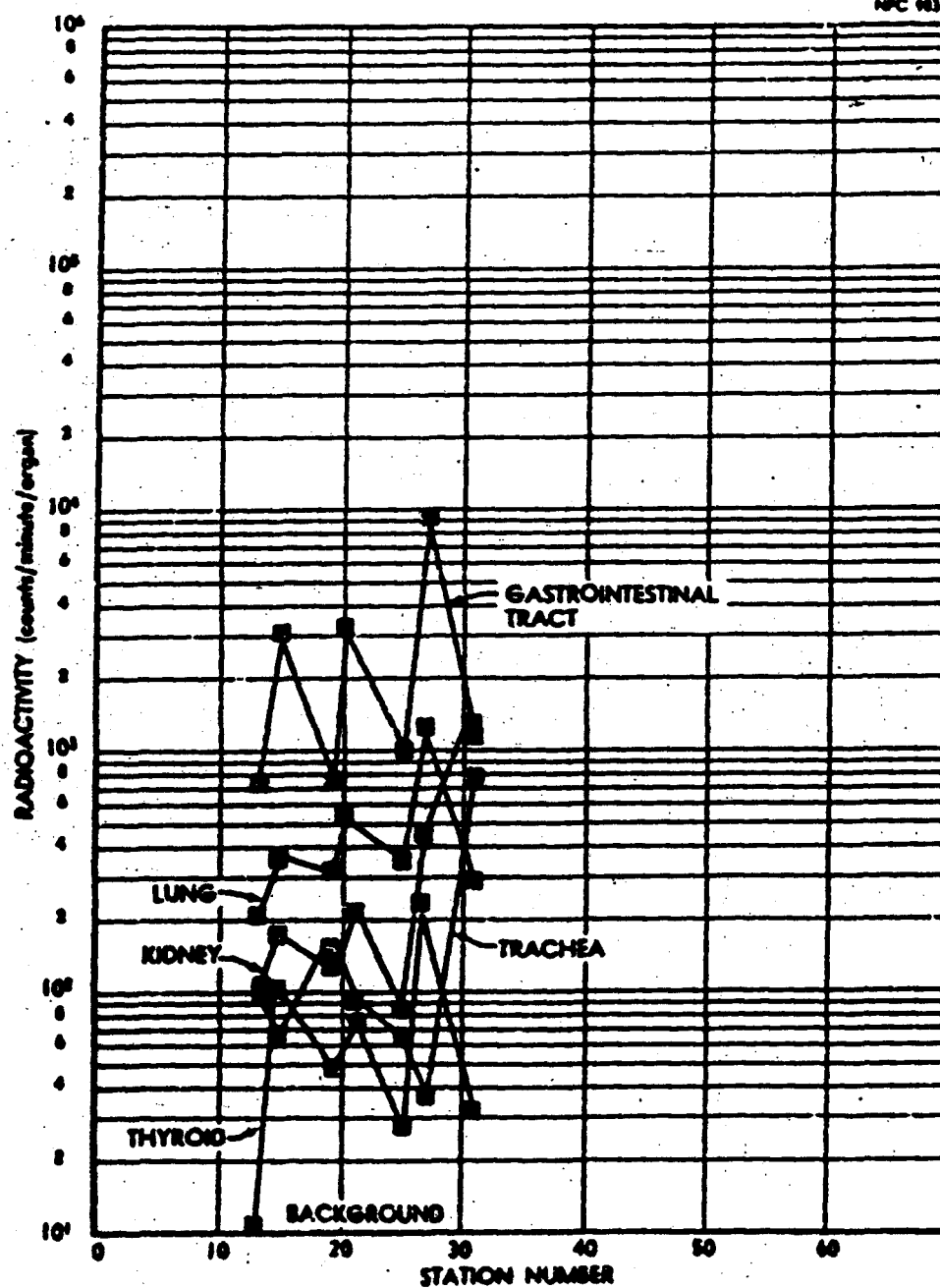


TABLE N.F.9
Radioactivity in Dogs
(Counts per Minute)

Tissue	100-11			100-21			100-31			100-41		
	100-11	100-21	100-31	100-41	100-11	100-21	100-31	100-41	100-11	100-21	100-31	100-41
Kidney	2910	3326	3472	142	1992	2406	2354	326				
Large Intestine	1044	1606	1750	240	740	1042	1252	350				
Small Intestine (1)*	6726	5974	11754	2348	4708	4040	8136	1910				
Small Intestine (2)	3964	4432	1974	474	1984	3120	1254	468				
Stomach	182682	400110	87776	7952	124386	281224	60482	5828				
Esophagus	16342	11514	3824	1804	11184	7816	2692	1420				
Lung	8890	22000	13672	1570	6240	15864	10152	1282				
Trachea	1160	2286	966	262	884	1678	676	260				
Thyroid	1360	3790	2254	118	992	2502	1498	236				
Bladder Urine	768	1570	1892	76	510	972	1314	180				

*Intestine counted in two parts

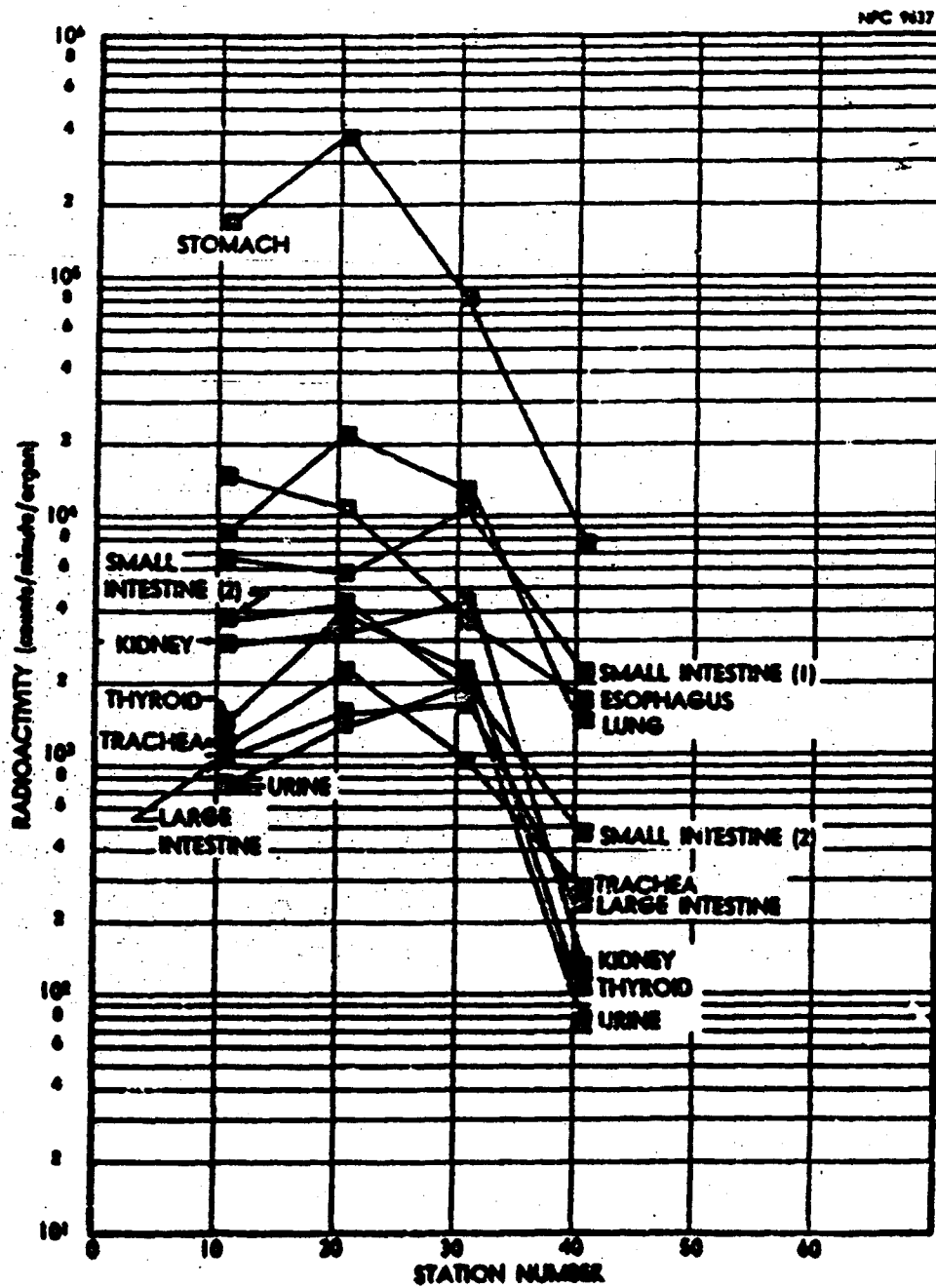


FIGURE M.F.25 DOG TISSUE EXPOSURE

TABLE N.F.10

Decay of Radioactivity in Pleated Filter

Decay Time (Days)	Filter Activity (Counts/Minute)
0.25	386986
0.5	380953
1	363542
2	335116
4	286374
6	265014
9	228650
14	155913
17	134270
24	112618
45	55922
55	52150
117	37427
152	34665
180	31630

APPENDIX N-G

(Release G)

G.1 Summary

Type of Sample ----- Green Fuel Element
Date and Release Time ----- 17 September 1958; 7:04 PM
Lapse Rate (1.5-45 m) ----- -1.0°C
Lapse Rate (1.5-24 m) ----- -0.71°C
Mean Wind Speed ----- 4.3 meters/sec
Wind Direction ----- Left Side of Network
Cloud Photography ----- No photography
Fluorescent Tracer ----- Inoperative
Animals ----- Rats and dogs on inner arcs
(Ref. 11)
Network Radioactivity ----- Detected out to approximately
6 miles; maximum reading of
pleated filters on 100-meter
arc, 270 mr/hr, using Cutie
Pie
External Dose ----- Maximum dose rate on 400-meter
arc, 0.080 mr/hr, using
scintillation detector des-
cribed in Appendix K

G.2 Fuel Element

The fuel element had been irradiated to generate 3.4×10^4 watts for a total of 125 hours 6 minutes and had decayed for 64

days. The pre-dominant isotopes present at the time of release are shown in Table N.G.1.

TABLE N.G.1
Fission Product Inventory

Nuclide	Curies Calculated
Sr ⁸⁹	40
Y ⁹¹	49
Zr ⁹⁵	51
Nb ⁹⁵	52
Ce ¹⁴¹	48
Ce ¹⁴⁴ Pr ¹⁴⁴	20
Pm ¹⁴⁷	2.8
Ru ¹⁰³ Rh ^{103m}	24
Ru ¹⁰⁶ Rh ¹⁰⁶	1
Te ^{127m} Te ¹²⁷	1.6
Ba ¹⁴⁰ La ¹⁴⁰	14
Pr ¹⁴³	16
Nd ¹⁴⁷	4
I ¹³¹	1.3
Te ^{129m} Te ¹²⁹	8

G.3 Meteorological Conditions

The wind directions and velocities prevailing during this release are shown in Table N.G.2.

The lapse rates existing between the 1.5- and both the 24- and 45-meter levels at the apex tower, plotted as a function of time after beginning of the release, are shown in Figure N.G.1.

TABLE N.G.2

Meteorological Summary

APEX TOWER

Height (meters)	Wind Direction			Wind Velocity (meters/sec)		
	Max.	Min.	Ave.	Max.	Min.	Ave.
1.5	244°	197°	218°	7.17	1.83	4.30
3.0	237	194	214	7.80	2.58	4.91
6.0	-	-	-	7.71	3.81	5.99
12.0	-	-	-	7.86	4.14	6.82
24.0	225	193	307	11.1	6.0	8.23
45.0	243.	217	228	11.9	6.9	9.36

FIELD MASTS

Location (arc)	Wind Direction			Wind Velocity (meters/sec)		
	Max.	Min.	Ave.	Max.	Min.	Ave.
200-meter	242°	202°	221°	7.65	3.03	5.33
400	-	-	214	-	-	5.67
800	-	-	219	-	-	5.48
1600	-	-	-	-	-	6.18
2400	-	-	222	-	-	6.14
3200	-	-	226	-	-	6.42

G.4 Smoke Plume Photography

No smoke photography was completed during this release.

G.5 Furnace Conditions

The furnace operation during this test closely followed the established criteria previously described (App. N-A, Sec. A.5).

G.6 Release Height

For estimation of the effective effluent release height and to obtain information regarding the charge of the released particulates, two wires of opposite charges were vertically positioned, 2.75 inches apart, 46 inches downwind of the furnace crucible.

Following the test, the wires were scanned with a collimated OM-survey meter. From these data, the effective release height is estimated to be five feet above ground.

G.7 Release Percentages

Release percentages were determined by using the pleated filter data from the 100-meter arc and establishing ratios between the cesium, ruthenium, cerium and zirconium content of the pleated filter and the iodine content. It was assumed that 50 percent of the iodine was released from the fuel element. These data are shown in Table N.G.3.

TABLE N.G.3
Release Percentages

Nuclide	Network Data (%)
Cs ¹³⁷	34
Ru ¹⁰³	0.8
Ce ¹⁴¹	0.05
Zr ⁹⁵	0.25
I ¹³¹	50

G.8 Air Sampler Field Survey

The gross radioactivity measurements of the pleated filters and carbon cartridges corrected for sampler flow rates and background, are shown in Figures N.G.2, N.G.3 and N.G.4. The arc profiles are shown in Figures N.G.2 and N.G.3. The values nearest the cloud centerline at each arc are shown in Figure N.G.4 plotted as a function of distance from the release point. Also shown is a straight line least-squares fit to the data points.

G.9 Airborne Radioactivity

The cloud centerline values for iodine, cesium, ruthenium, zirconium and cerium, as a function of distance from the release point, are shown in Figure N.G.5. The arc profiles for these isotopes are shown in Figures N.G.6, N.G.7, N.G.8, N.G.9, and N.G.10. All the measurements were determined by laboratory assay of the Hi-Vol air sampler pleated-filters and carbon cartridges corrected for sampler flow rate.

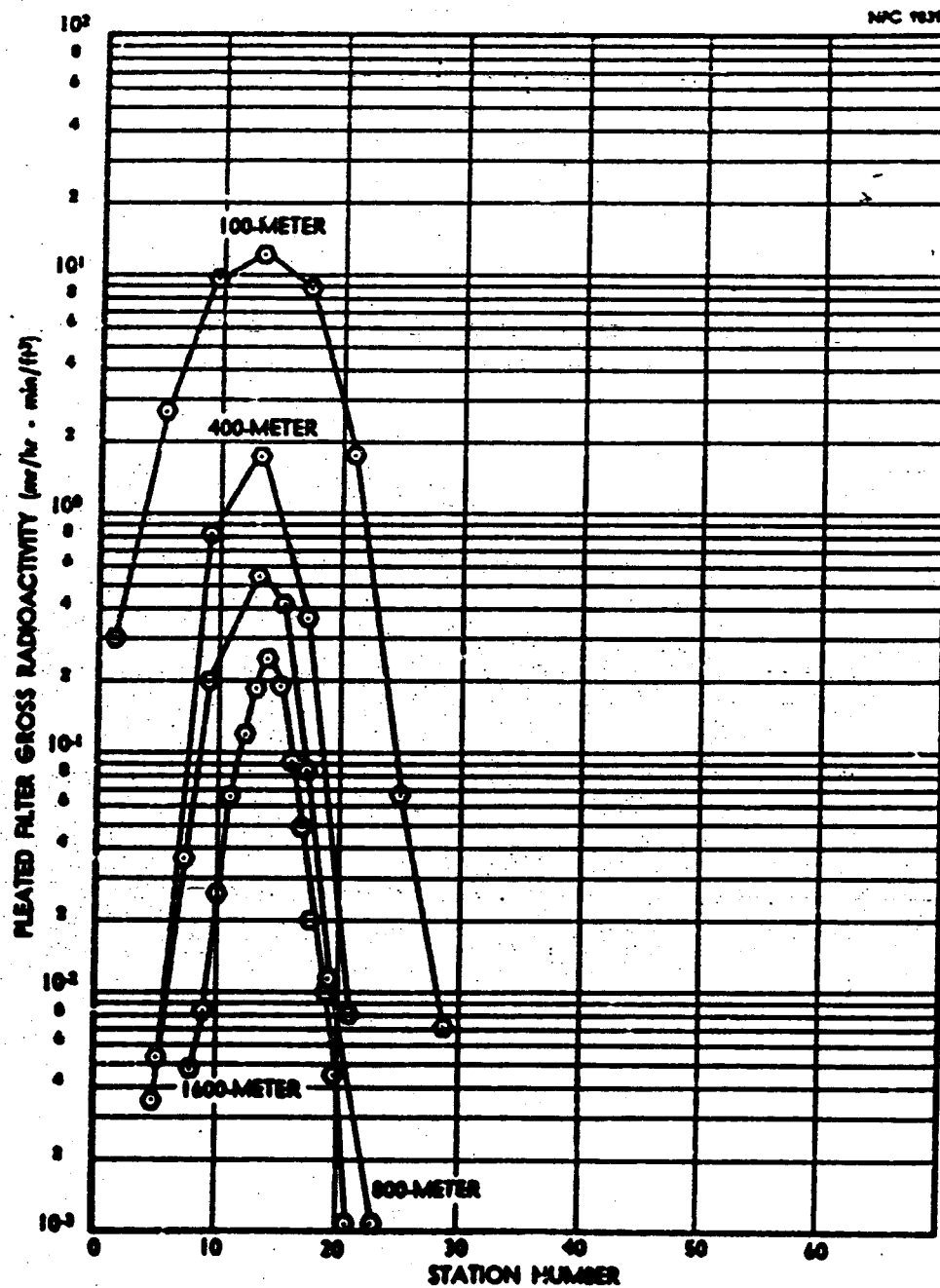


FIGURE H.6.2 H₂-VOL AIR SAMPLER FIELD SURVEY
(Pleated Filter - Arc Profiles)

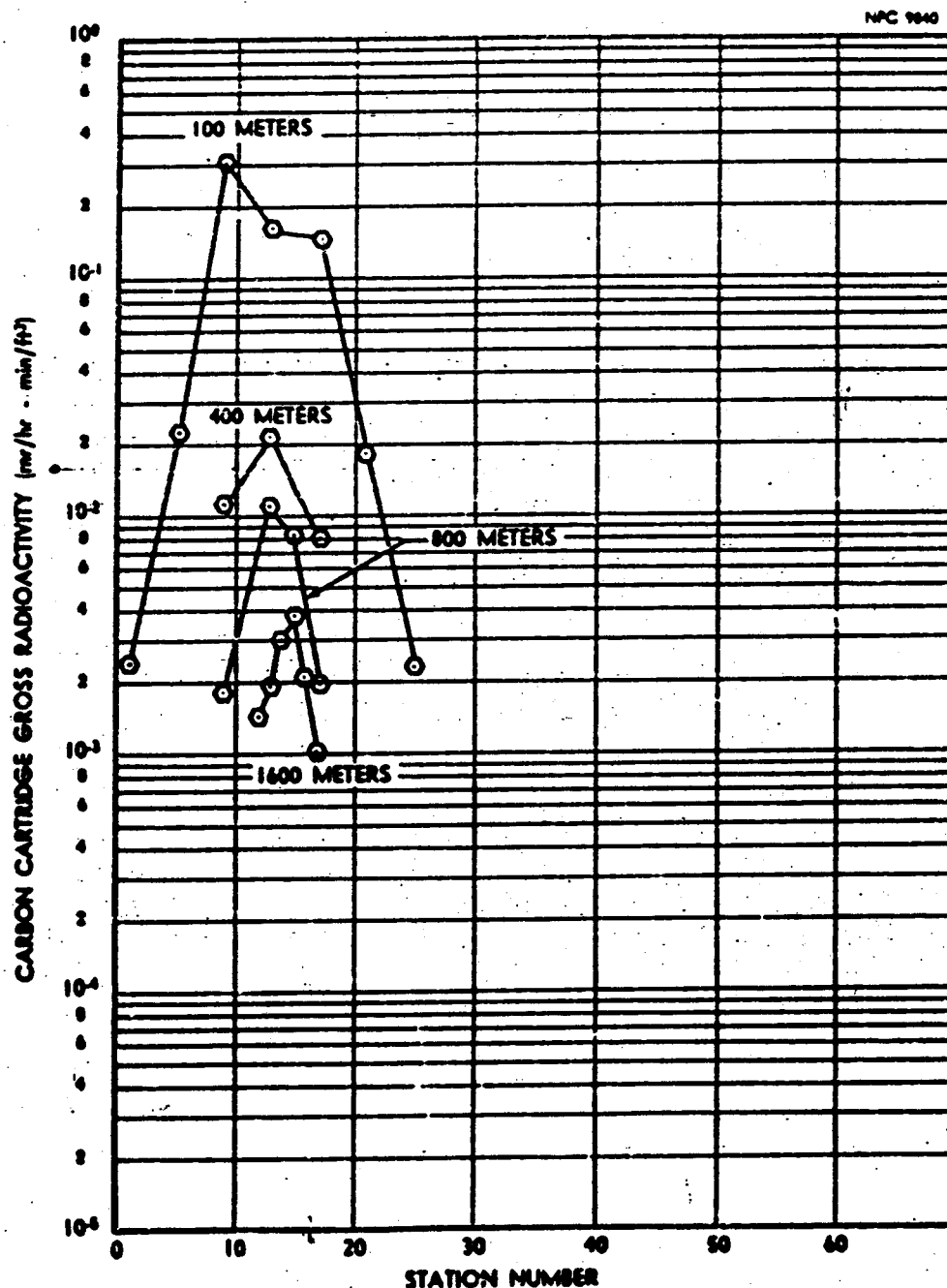


FIGURE N.G.3 H₂-VOL AIR SAMPLER FIELD SURVEY
(Carbon Cartridge - Are Profiles)

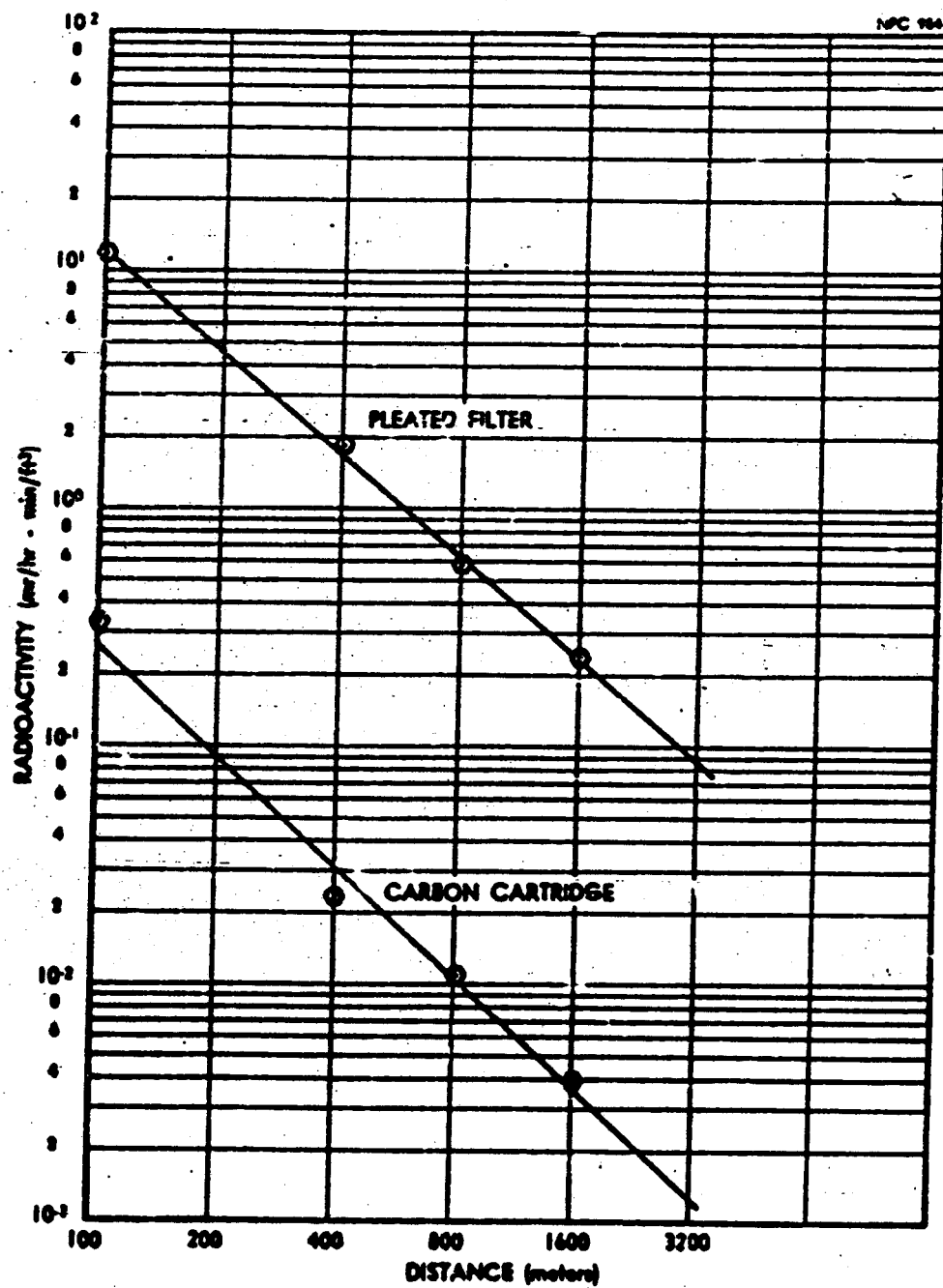


FIGURE N.G.4 H₂VO₄ AIR SAMPLER FIELD SURVEY
(Centerline)

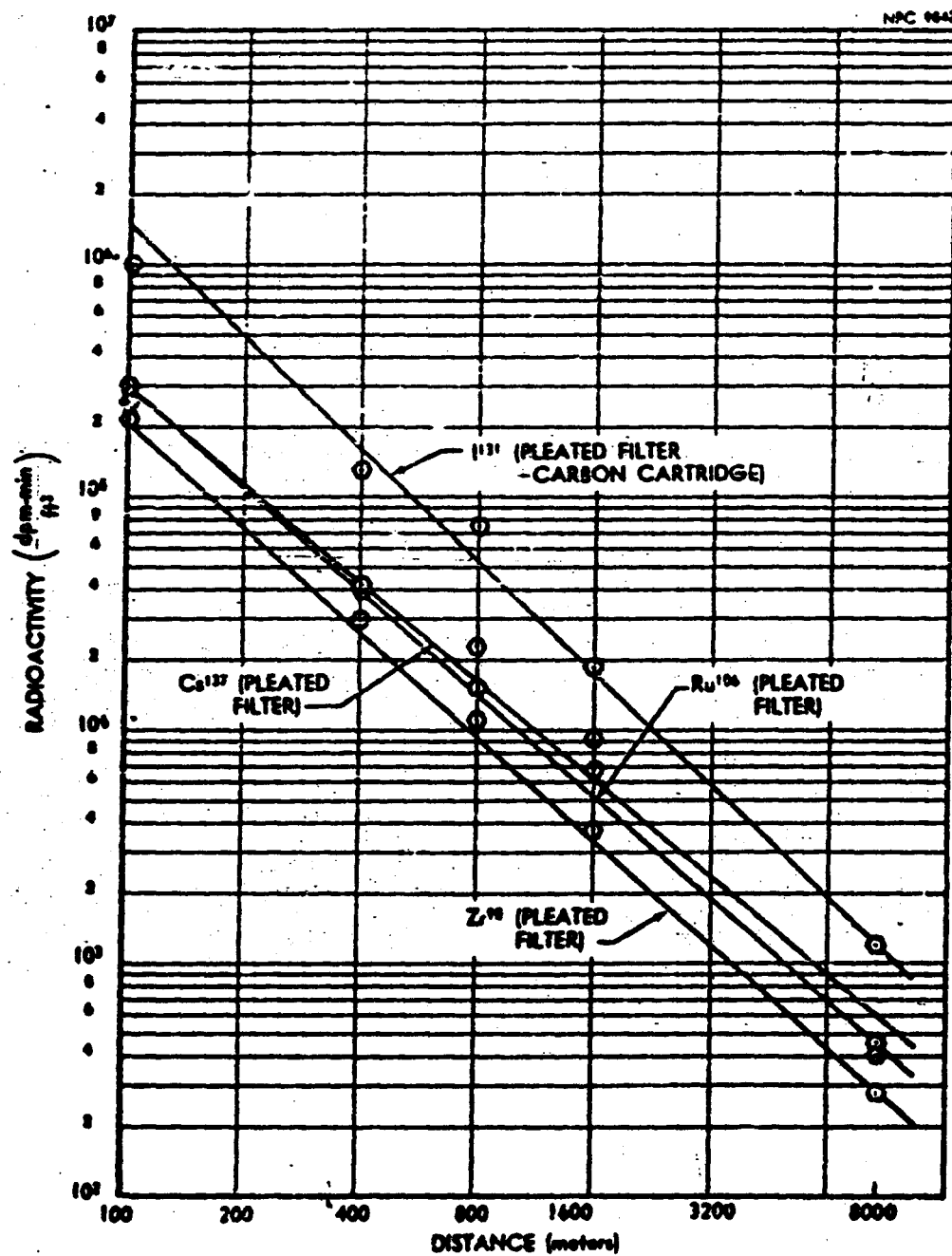


FIGURE N.G.5 H₂-VOL AIR SAMPLER LABORATORY ASSAY
(Centerline)

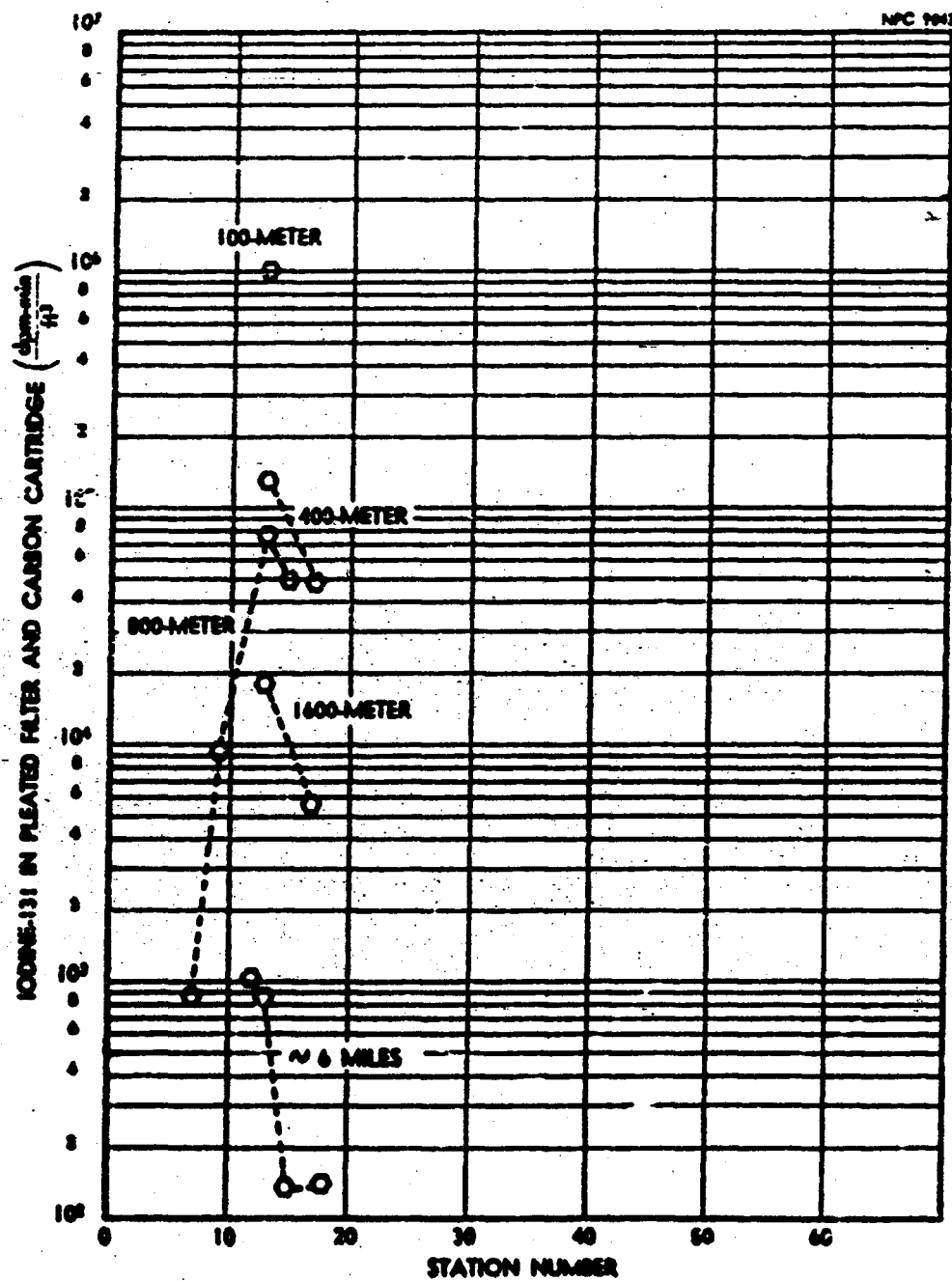


FIGURE N.3.4 HI-VOL AIR SAMPLE LABORATORY ASSAY OF IODINE (Arc Profiles)

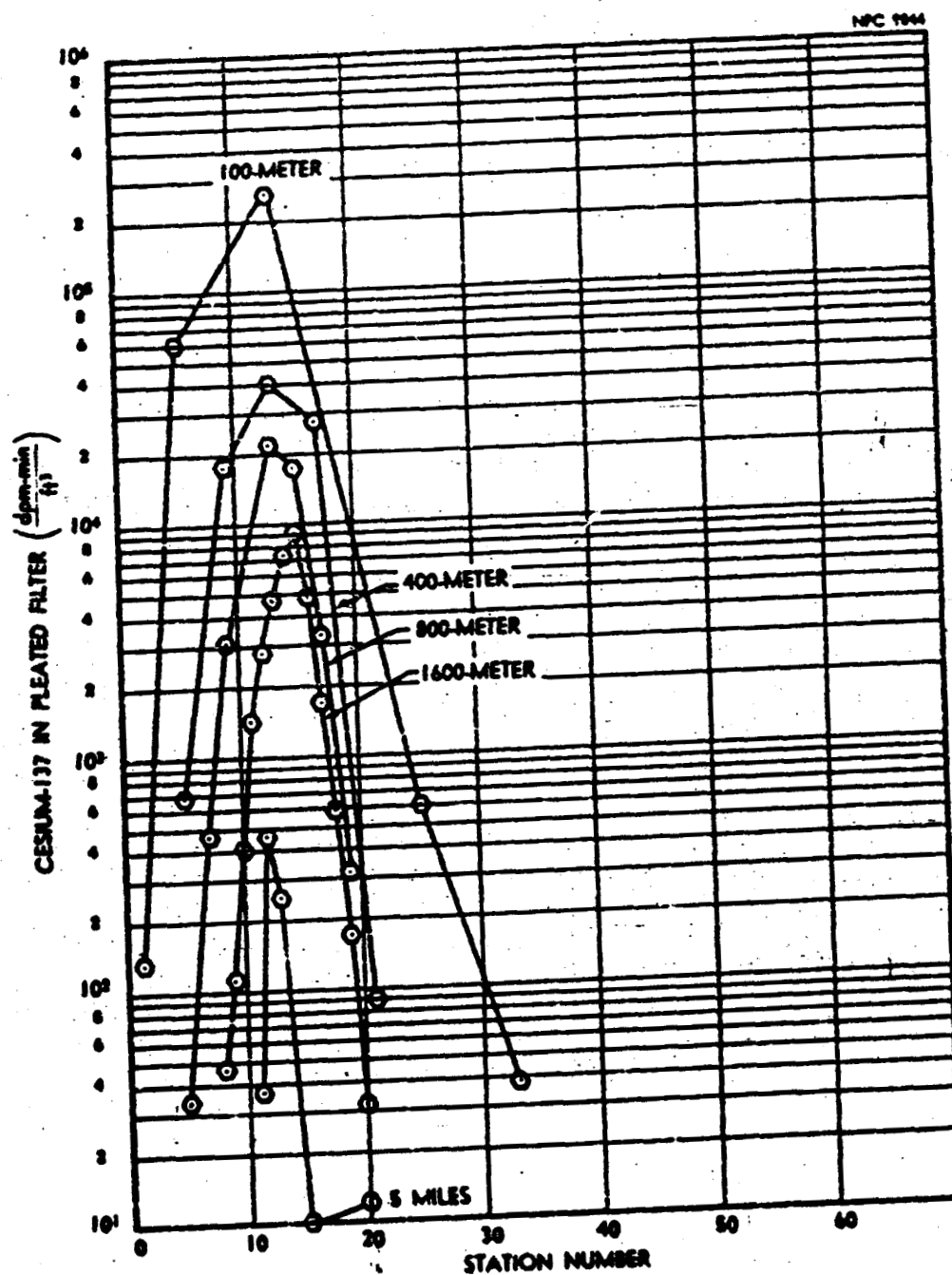


FIGURE N.S.7 IN-VOL AIR SAMPLER LABORATORY ASSAY OF CESIUM (Are Profiles)

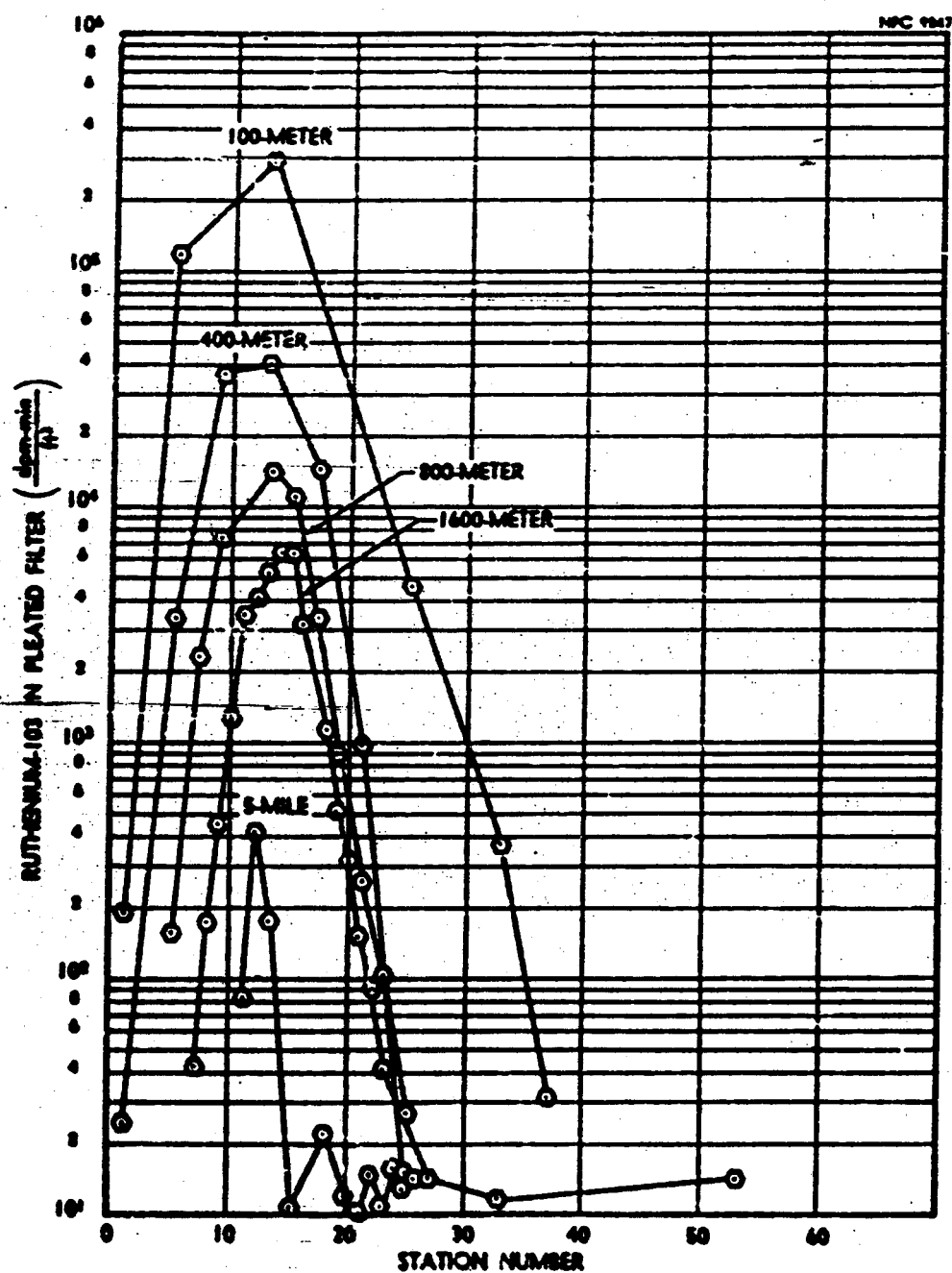


FIGURE N.6.8 HI-VOL AIR SAMPLER LABORATORY ASSAY OF RUTHENIUM (Are Profile)

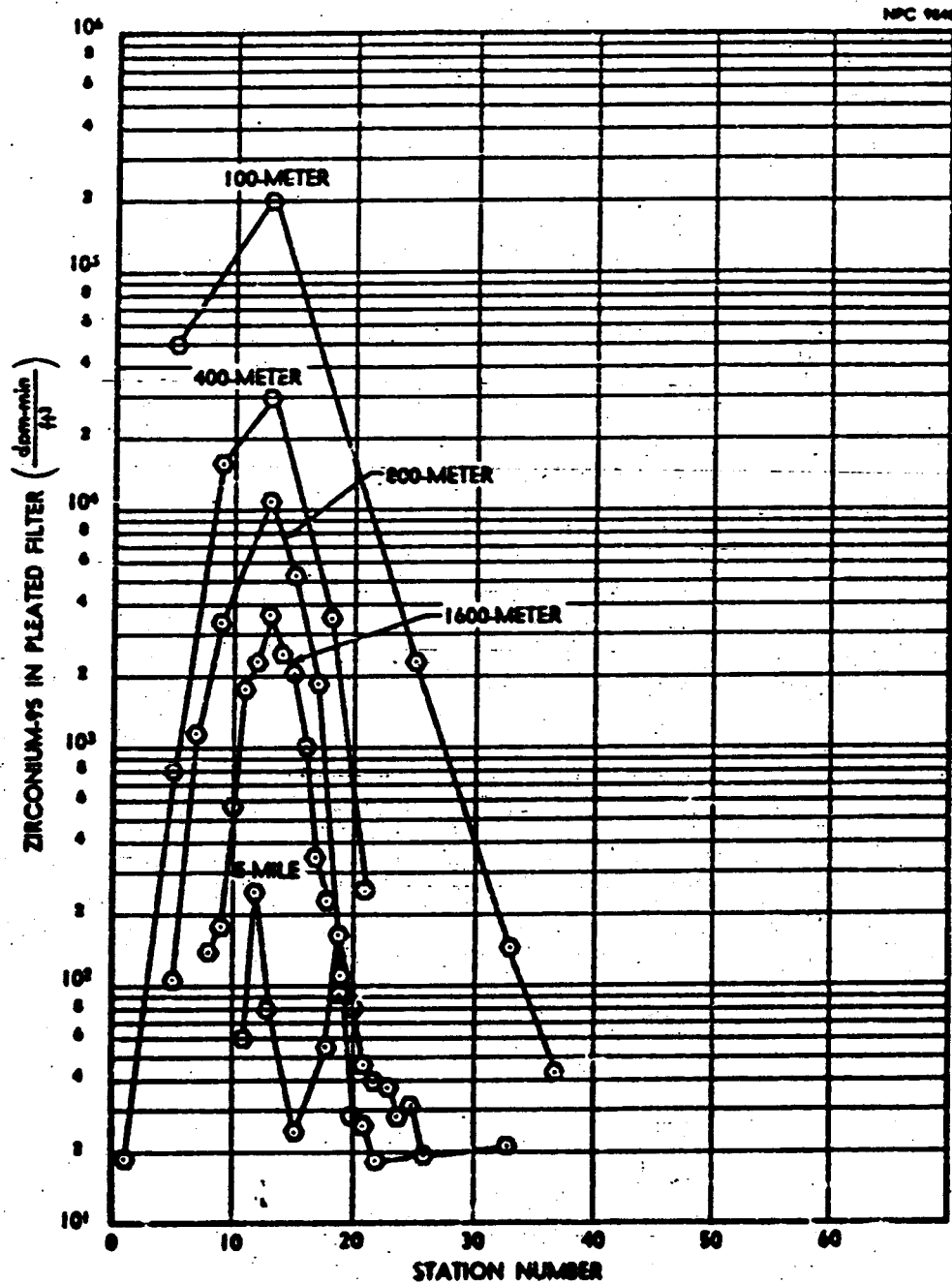


FIGURE N.S. 9 NO-104 AIR SAMPLER LABORATORY ASSAY OF ZIRCONIUM (Arc Profiles)

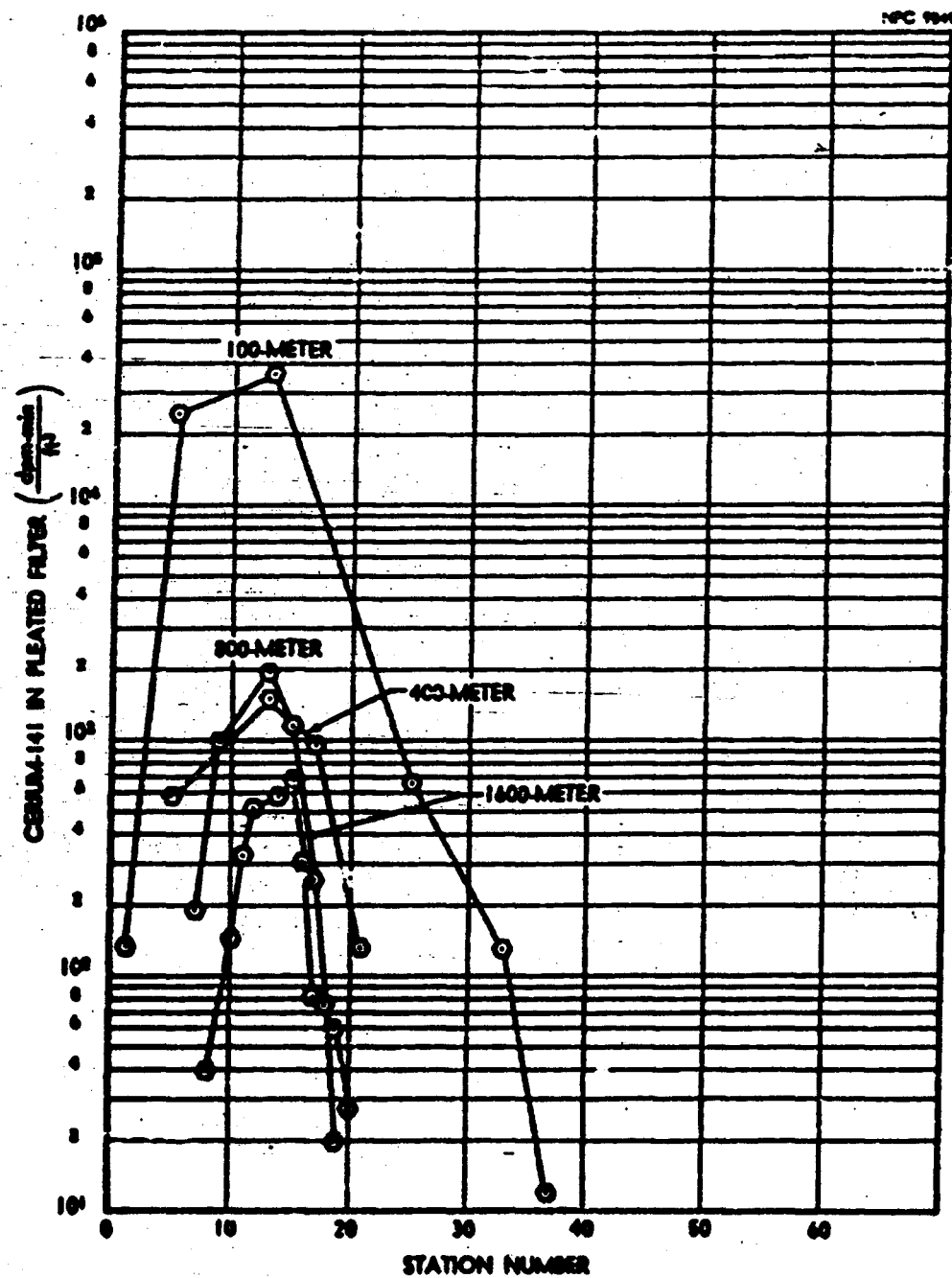


FIGURE N-6.10 NE-VOL AIR SAMPLER LABORATORY ASSAY OF CERIU-141 (Are Predicted)

G.10 Deposited Radioactivity

Deposited radioactivity was not measured during this release because the hinged fallout collectors were not energized at the proper time. When finally energized, the cloud had drifted off of the network.

G.11 Deposition Velocity

Because of the absence of deposited radioactivity data, no deposition velocities have been calculated for this release.

G.12 Fluorescent Tracer

Because of inactivation of the 200-meter arc and lack of sufficient particle concentration past the 400-meter arc, no fluorescent tracer data are available from this experiment.

G.13 External Dose

The gamma dose data obtained on the 400-meter arc are shown in Figures N.G.11, N.G.12 and N.G.13. The dose accumulated during the cloud passage at each station across the arc is presented in Figure N.G.11. Figure N.G.12 shows the gamma dose rate, as recorded by the detector nearest the cloud centerline. Figure N.G.13 shows a reconstruction of the effluent cloud that was required to produce the dose rate plotted against the time measurements and recorded by the 400-meter arc detectors.

G.14 Diffusion Parameters

The diffusion parameters obtained during this release are shown in Table N.G.4. For comparison, the measured isopleths and their curve fit counterparts are shown in Figures N.G.14 and N.G.15 respectively.

NPC 9550

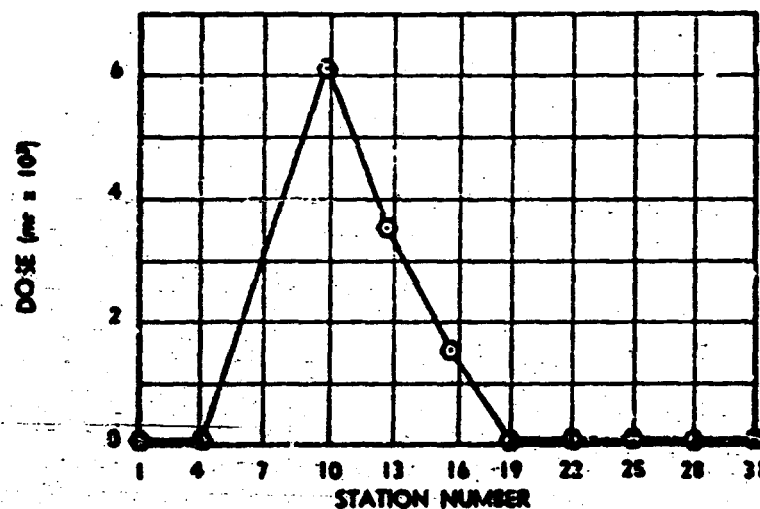


FIGURE N.G.11 GAMMA DOSE FROM CLOUD PASSAGE (Arc Profile)

NPC 9561

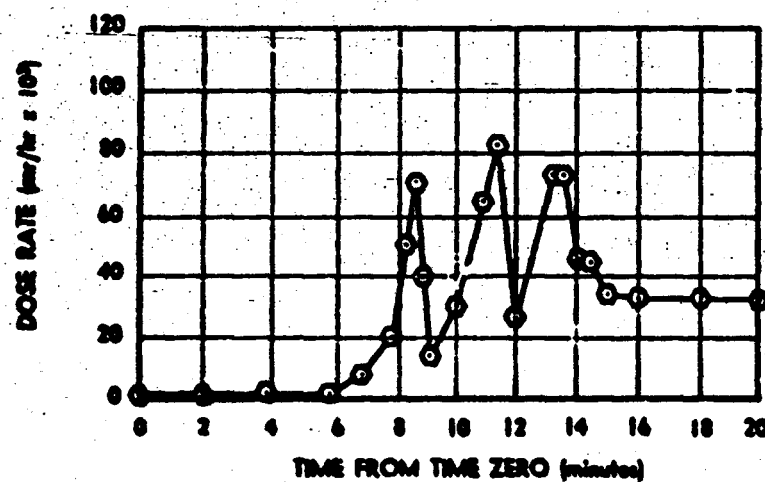


FIGURE N.G.12 GAMMA DOSE RATE FROM CLOUD PASSAGE (Centerline)

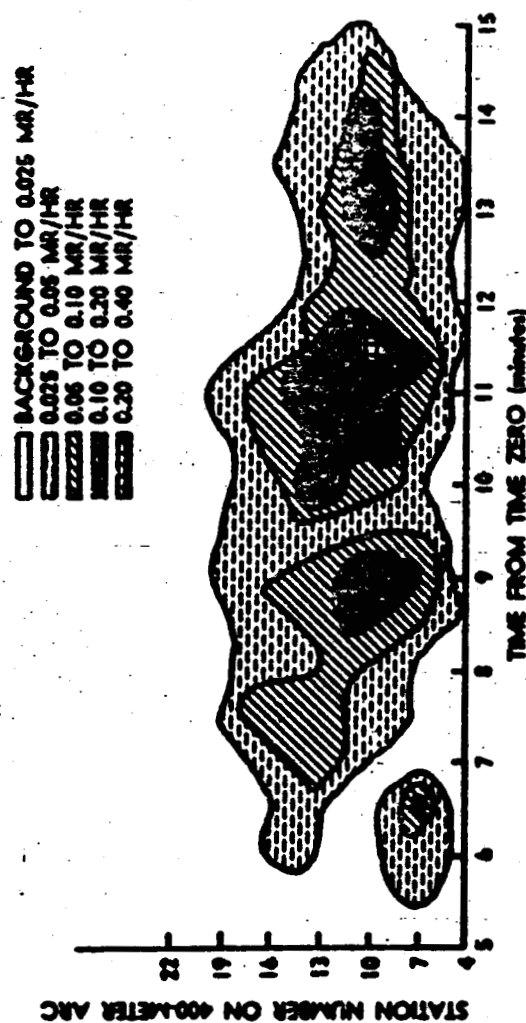


FIGURE N.B.13 GAMMA DOSE RATE FROM CLOUD PASSAGE
(Activity Contours)

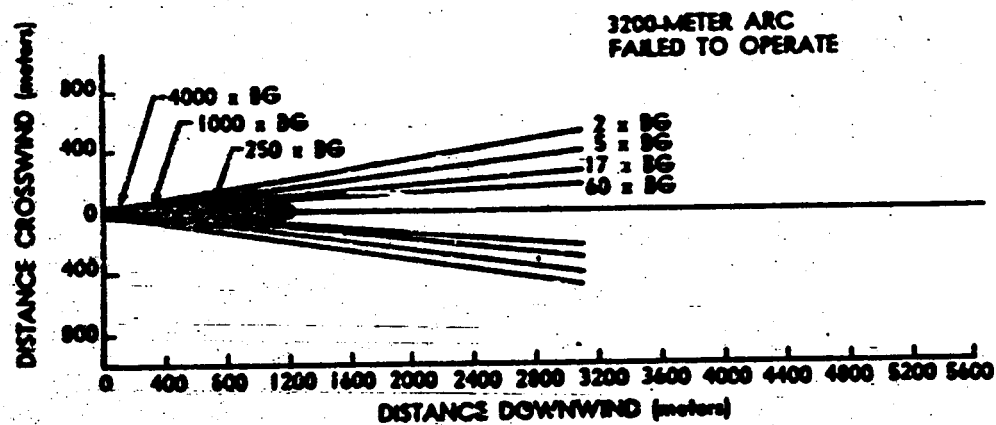


FIGURE H.6.14 CROSS RADIOACTIVE ISOPLITHS
(Field Data)

NPC 1004

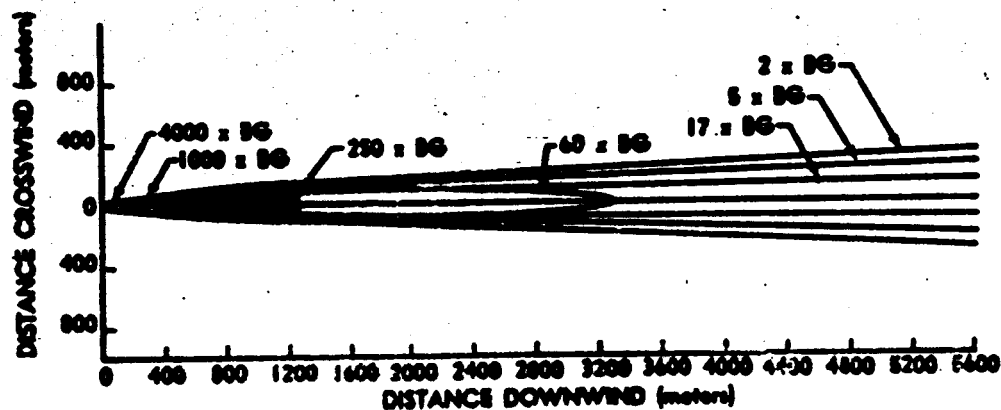


FIGURE H.6.15 CROSS RADIOACTIVITY ISOPLITHS

TABLE N.G.4

Diffusion Parameters

Parameters	Field Survey Data Fit	Cs ¹³⁷ Fit	Ru ¹⁰³ Fit	Bivane Data (24 meters)
M_y	0.67	0.82	0.83	-
M_z	0.79	0.43	0.63	-
C_y	0.52	0.16	0.20	0.04
C_z	0.22*	3.5	1.3	0.03
"n"	-	-	-	0.37

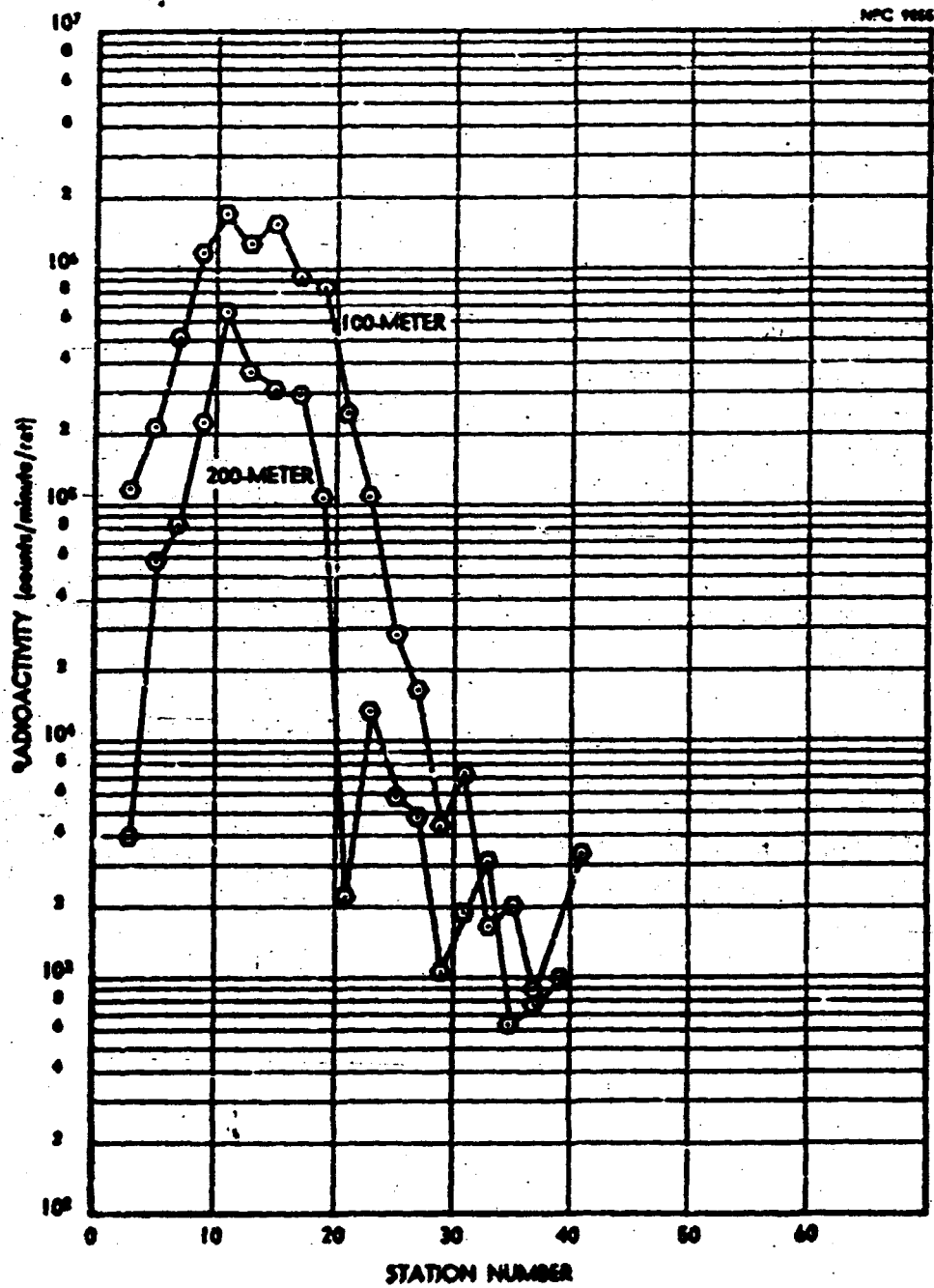
* Vertical wire

G.15 Radiobiology

Rats were placed two at a station at alternate stations (every two degrees) on the 100- and 200-meter arcs. All animals were exposed in restrictive cages; those placed at station numbers divisible by 4 were anesthetized with intraperitoneal sodium pentothal prior to placement in the field. The sacrifice procedure was changed from the suffocation by CO₂ used in previous releases to an injection of sodium pentothal through the exposure cages as they were suspended in the field. Sacrifice was complete by no later than 60 minutes post-release. Whole body counts were obtained on all rats (through 40 degrees on each arc) and autopsies were performed as in previous releases. Tissues were counted at various times to enable isotopic separation of the fission products. These data are given in Table N.G.5. Each value is the average of

two rats at each station. Data from the whole body counting are presented in Figure N.G.16.

Dogs were placed singly every four degrees on the 100-meter arc and every six degrees on the 200-meter arc. Each dog was muzzled in an attempt to reduce licking and mouth breathing. Entrance to the area for pickup was approximately 30 minutes post-release at which time the "hottest" stations were selected by survey meter reading on the face of the high volume filter. Dogs from these stations were anesthetized in the field by intravenous injection of sodium pentothal. They were then removed from the area and scrubbed with warm water and detergent to remove as much external contamination as possible. Two dogs, from stations 100-5 and 100-13 were placed into metabolism cages for daily collection of urine and feces. These animals were studied until their excretion contained very little radioactivity. The remainder of the "hot" dogs were bled maximally (after decontamination) by severing the carotid artery. They were then bagged in polyethylene to await autopsy. The tissues removed for analysis were the same as in Release P. However, for this release, urine samples of approximately 120 ml each also were analyzed. The tissue distribution data for various counting times after the release are presented in Table N.G.6, as counts per minute per organ, except for blood and bladder urine for which they are reported on a per sample basis.



AT 6 DAYS

Arc and Station	Counts/min/Organ				
	Lung	G.I. Tract	Thyroid	Trachea	Kidney
100- 5	201	174	n.s.	n.s.	n.s.
7	327	238	---	142	---
9	758	265	---	---	82
11	1230	2770	51	92	131
13	476	202	---	36	---
15	920	685	---	---	---
17	465	231	---	---	---
19	416	498	---	---	33
21	149	131	n.s.	n.s.	n.s.
200- 9	239	n.s.	n.s.	n.s.	n.s.
11	453	378	n.s.	n.s.	n.s.
13	290	157	n.s.	n.s.	n.s.
15	228	276	n.s.	n.s.	n.s.
17	202	n.s.	n.s.	n.s.	n.s.
19	225	n.s.	n.s.	n.s.	n.s.

AT 12 DAYS

100- 5	210	45	n.s.	n.s.	n.s.
7	288	201	---	129	111
9	668	239	---	---	85
11	1100	1860	58	59	101
13	477	---	51	42	---
15	813	379	51	---	72
17	454	74	44	40	47
19	315	241	352	40	126
21	142	---	n.s.	n.s.	n.s.
200- 9	174	n.s.	n.s.	n.s.	n.s.
11	404	169	n.s.	n.s.	n.s.
13	233	---	n.s.	n.s.	n.s.
15	175	283	n.s.	n.s.	n.s.
17	136	n.s.	n.s.	n.s.	n.s.
19	176	n.s.	n.s.	n.s.	n.s.

AT 15 DAYS

Arc and Station	Counts/min/Organ	
	Lung	G.I. Tract
100- 5	163	54
7	263	145
9	622	136
11	954	1900
13	356	187
15	805	406
17	451	117
19	329	288
21	138	
200- 9	169	
11	406	197
13	237	111
15	202	287
17	146	
19	204	

AT 32 DAYS

100- 5	84	---
7	135	52
9	379	---
11	621	930
13	245	---
15	511	116
17	293	71
19	262	121
21	96	69
200- 9	130	
11	258	94
13	174	57
15	112	181
17	67	
19	73	

AT 104 DAYS

Arc and Station	Counts/min/Organ	
	Lung	G.I. Tract
100- 5	48	75
7	36	22
9	117	---
11	317	406
13	100	138
15	354	99
17	124	113
19	124	---
21	75	---
200- 9	---	---
11	55	142
13	---	91
15	119	---
17	56	---
19	83	---

AT 172 DAYS

100- 9	144	
11	278	207
13		62
15	233	
17	127	41
19	77	
200- 11		59
15	79	

TABLE N.O.6
Radioactivity in Dogs

	Counts/min/Organ -- Arc and Station Location								
	100m-9°	100m-17°	100m-21°	100m-25°	200m-7°	200m-13°	200m-19°	200m-25°	200m-31°

AT D - 2 DAYS

Blood	4830	7780	n.s.	753	684	1850	1050	440	245
-------	------	------	------	-----	-----	------	------	-----	-----

AT D - 4 DAYS

Kidney	2020	3670	--	--	182	664	358	74	612
Large Intestine	874	1950	--	242	---	324	122	108	420
Small Intestine (1)	2540	7940	64	272	5960	964	1670	232	1330
Small Intestine (2)	1990	4330	--	126	2230	790	290	108	860
Stomach	20700	39100	82	928	4620	17100	11500	182	11100
Esophagus	2070	2800	--	94	268	2550	608	---	230
Lung	35900	59300	154	388	4010	17300	996	184	12500
Trachea	564	806	60	---	40	514	68	---	56
Thyroid	1060	3010	88	178	324	994	1010	88	1730
Bladder									
Urine	406	556	188	122	232	1500	592	112	746

AT D - 10 DAYS

Blood	2430	3460	n.s.	242	257	539	396	156	---
-------	------	------	------	-----	-----	-----	-----	-----	-----

AT D - 12 DAYS

Kidney	1370	2160			102	392	244		542
Large Intestine	532	1204			---	284	105		224
Small Intestine (1)	1670	5310			5070	632	1310		948
Small Intestine (2)	1170	3010			1970	586	196		444

TABLE N.2.7

Decay of Radioactivity in Pleated Filter

Decay Time (Days)	Filter Activity (Counts/Minute)
0.5	57900
3	57600
4	57900
5	55500
7	51200
11	47500
12	41900
32	30300
42	25400
104	11200
139	7710
167	5840

APPENDIX N-H

(Release H)

H.1 Summary

Type of Sample -----	Green Fuel Element
Date and Release Time -----	18 Sept. 1958 - 6:32 PM
Lapse Rate (1.5-45m) -----	-1.5°C
Lapse Rate (1.5-24.5m) -----	-1.0°C
Mean Wind Speed -----	4.0 meters/sec
Wind Direction -----	Left of Network Centerline
Cloud Photography -----	Both aerial and ground
Fluorescent Tracer -----	Release for 10 minutes immediately following fission product release
Animals -----	Rats and dogs on inner arcs (Ref. 11)
Network Radioactivity -----	Detected out to approxi- mately 6 miles; maximum reading of pleated filters on 100-meter arc, 370 mr/hr, using Cutie Pi
External Dose -----	Maximum dose rate on 400-meter arc, 0.16 mr/hr, using scintillation detector described in Appendix K

H.2 Fuel Element

The fuel element had been irradiated to generate 3.4×10^4 watts for a total of 125 hours 6 minutes and had decayed for 65 days. The predominant nuclides present at the time of release are shown in Table N.H.1.

TABLE N.H.1
Fission Product Inventory

Nuclides	Curies Calculated
Sr ⁸⁹	40
Y ⁹¹	49
Zr ⁹⁵	51
Nb ⁹⁵	52
Ce ¹⁴¹	47
Ce ¹⁴⁴ Pr ¹⁴⁴	20
Pm ¹⁴⁷	2.8
Ru ¹⁰³ Rh ^{103m}	24
Ru ¹⁰⁶ Rh ¹⁰⁶	1.0
Te ^{127m} Te ¹²⁷	1.6
Sa ¹⁴⁰ La ¹⁴⁰	14
Pr ¹⁴³	16
Nd ¹⁴⁷	3.9
I ¹³¹	1.2
Te ^{129m} Te ¹²⁹	7.9

N.3 Meteorological Conditions

The wind data under which this test was performed are shown in Table N.H.2. The lapse rates existing during the release between the 1.5-meter and both the 24- and 45-meter levels at the apex tower are shown in Figure N.H.1.

TABLE N.H.2
Meteorological Summary

APEX TOWER

Height (meters)	Wind Direction			Wind Velocity (meter/sec)		
	Max.	Min.	Ave.	Max.	Min.	Ave.
1.5	-	-	215°	-	-	4.0
3.0	-	-	211	-	-	4.7
6.0	-	-	-	-	-	5.7
12.0	-	-	-	-	-	6.5
24.0	-	-	-	-	-	8.0
45.0	-	-	224	-	-	9.2

FIELD MASTS

Location (Ave)	Wind Direction			Wind Velocity		
	Max.	Min.	Ave.	Max.	Min.	Ave.
200 meter	-	-	218°	-	-	5.1
400	-	-	210	-	-	5.1
800	-	-	214	-	-	4.7
1600	-	-	219	-	-	4.9
2400	-	-	215	-	-	4.6
3200	-	-	210	-	-	4.9

NPC 1984

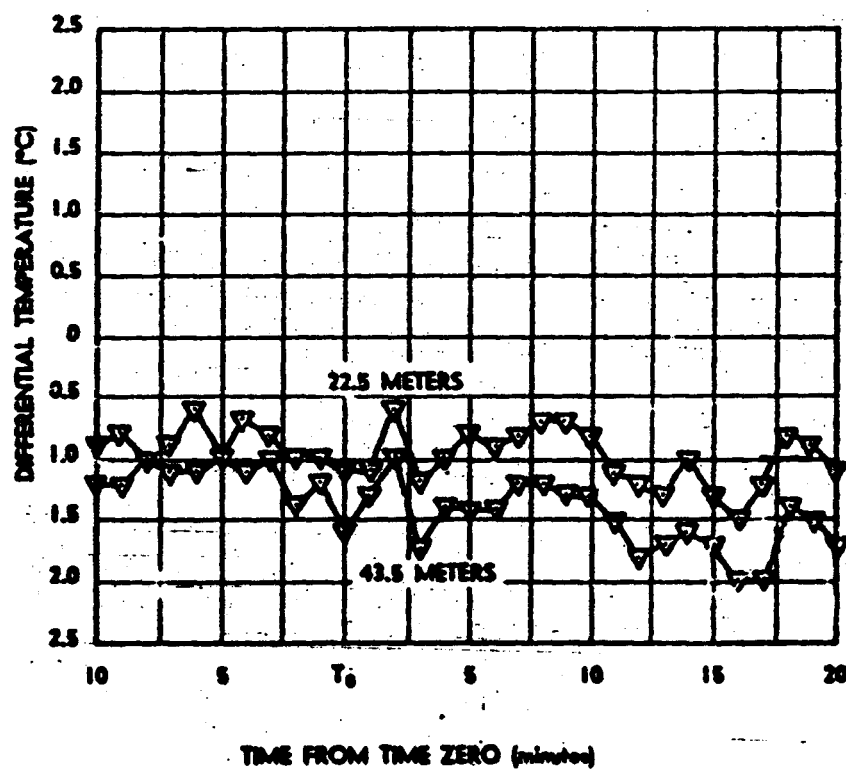


FIGURE N.H.1 LAPSE RATE DURING RELEASE

H.4 Smoke Plume Photography

Photographic documentation of the smoke cloud was accomplished with both aerial and ground photography. The photographs used in the determination of the diffusion parameters are shown in Figure N.H.2. The aerial photograph shows that a visible plume was developed which extended past the 800-meter arc.

H.5 Furnace Conditions

Excessively high temperatures were developed during this release, being similar to those of Release D. Estimates based on the post-melt condition of the crucible and on the furnace power program show that a temperature of 500-800°C above the melting point of the fuel element was reached. This temperature was from 400-700°C above that planned.

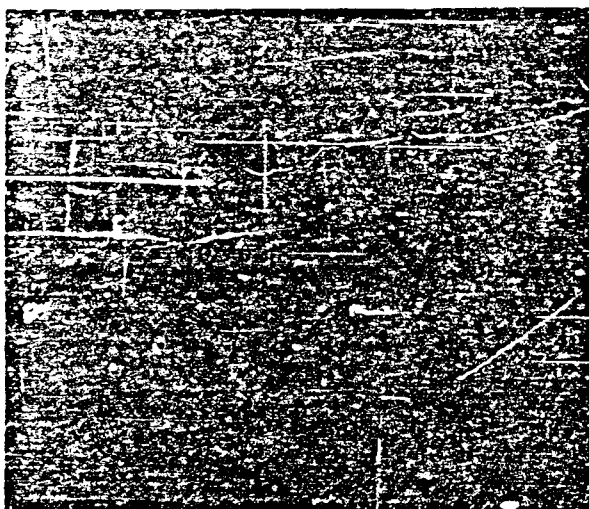
H.6 Release Height

Two vertical, oppositely charged wires were positioned 46 inches downwind of the furnace crucible. The distribution of radioactive material collected on these wires is shown in Table N.H.3.

H.7 Effluent Samplers

The sequential sampler filter radioactivities, shown in Figure N.H.3, indicate that the maximum release of nuclides occurred at approximately 3.5 minutes after the power was applied to the furnace. Also, the figure shows that activity was released at a fairly uniform rate, with an increase beginning at five minutes after time zero. This second rise corresponds with the

NPC 9957



Aerial View



Ground View

FIGURE N.H.2 PRE-RELEASE SMOKE PLUME

TABLE N.H.3
Release Height

Distance From Top of Wire (ft)	Radioactivity (mr/hr)	
	Negative Wire	Positive Wire
1	< 1	< 1
2	< 2	< 1
3	50	30
3.5	85	80
Top of Furnace (3.7)	83	75
4	65	65
5	10	10
6	< 5	< 5

TABLE N.H.4
Release Percentages

Nuclide	Network Data (%)
Ru ¹⁰³	0.75
Cs ¹³⁷	24.0
Cs ¹⁴¹	0.3
Zr ⁹⁵	0.05
I ¹³¹	50.0

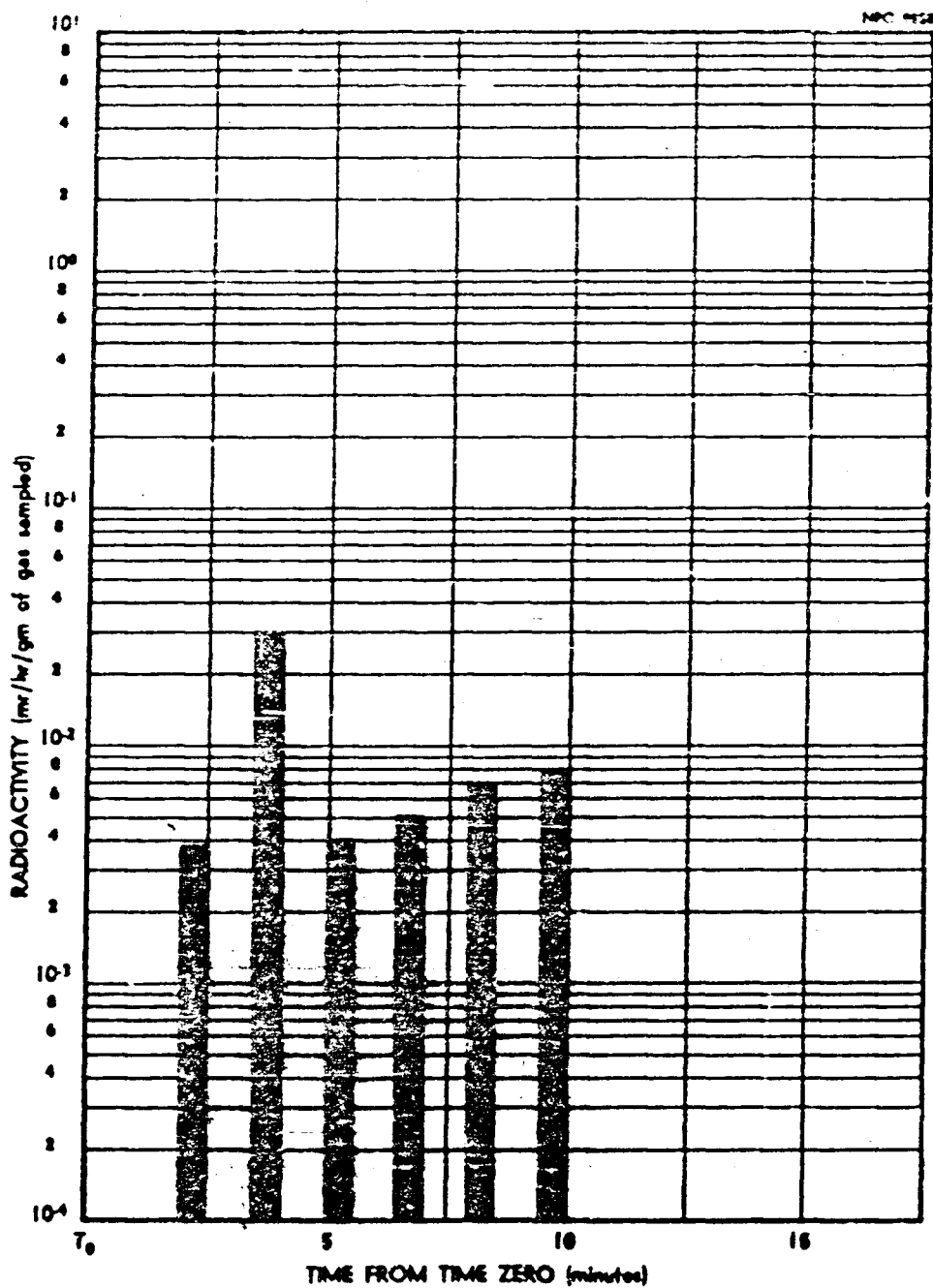


FIGURE N.H.3 SEQUENTIAL-EFFLUENT-SAMPLER FILTER RADIOACTIVITIES

estimated time of occurrence of the furnace temperature excursion.

H.8 Release Percentages

The release percentages of ruthenium, cesium, cerium and zirconium were determined from the 100-meter arc pleated-filter isotopic data. The percentages were obtained by ratioing the amounts of the above listed nuclides in the centerline pleated filters to the iodine content of these filters and assuming 50 percent release of the latter from the melt. These data are shown in Table N.H.4.

H.9 Air Sampler Field Survey

The gross radioactivity measurements of the pleated-filter and carbon-cartridges, corrected for sampler flow rate and background, are shown in Figure N.H.4, N.H.5 and N.H.6. The arc profiles for these collectors are shown in Figures N.H.4 and N.H.5. Figure N.H.6 shows the values at each arc along the centerline plotted as a function of distance from the release point. A straight line least-squares fit is shown through the data points.

H.10 Airborne Radioactivity

The cloud centerline values for iodine, cerium, zirconium, ruthenium, and cesium, as determined by lab assay of the Hi-Vol air sampler pleated filters and carbon cartridges are shown in Figure N.H.7. There is little difference in the change in concentration with distance between these isotopes. The arc profiles from which the centerline values were taken are shown in Figures N.H.8, N.H.9, N.H.10, N.H.11 and N.H.12.

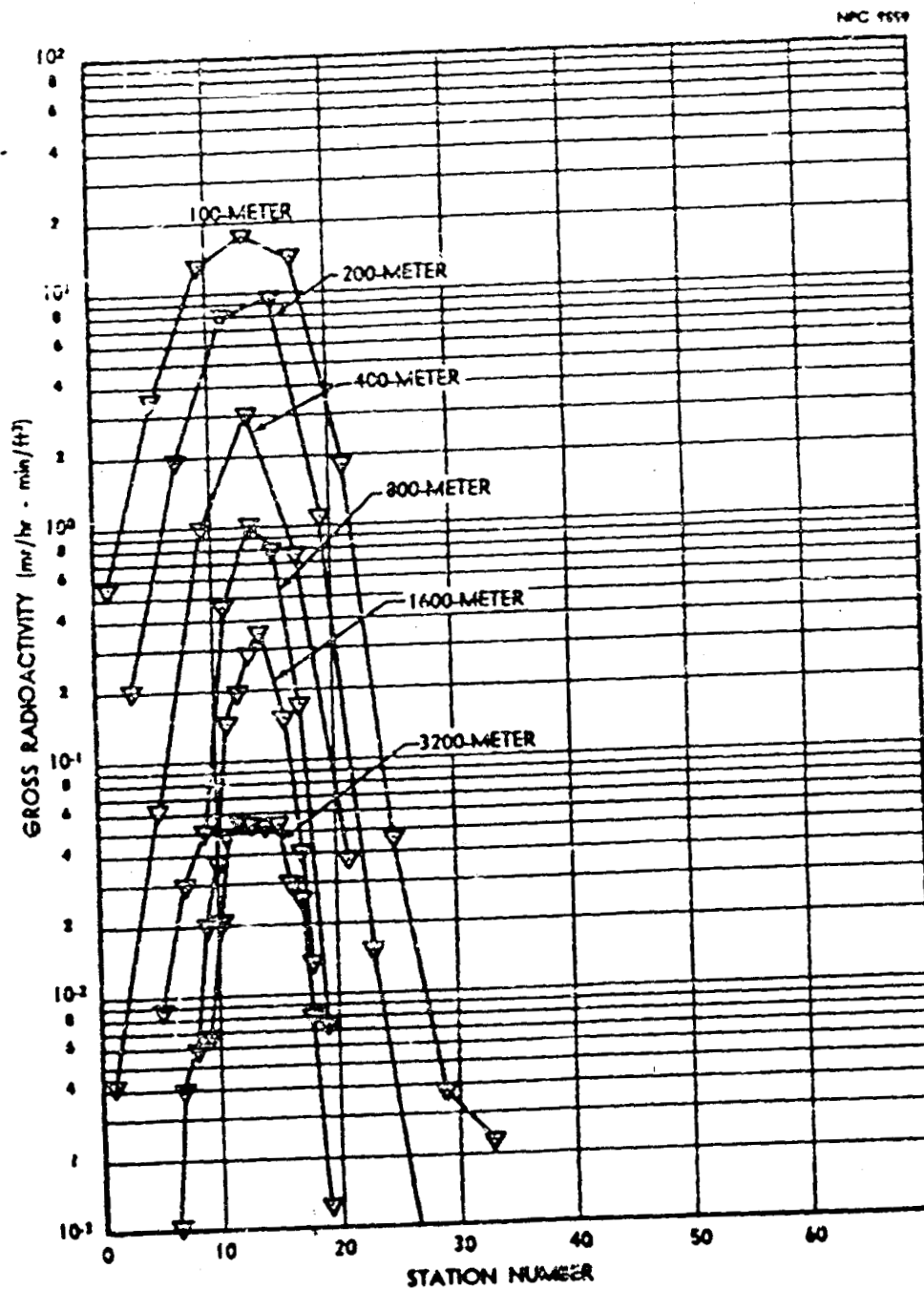


FIGURE N.M.4 HI-VOL AIR SAMPLER FIELD SURVEY
(Plotted Filter - Arc Profiles)

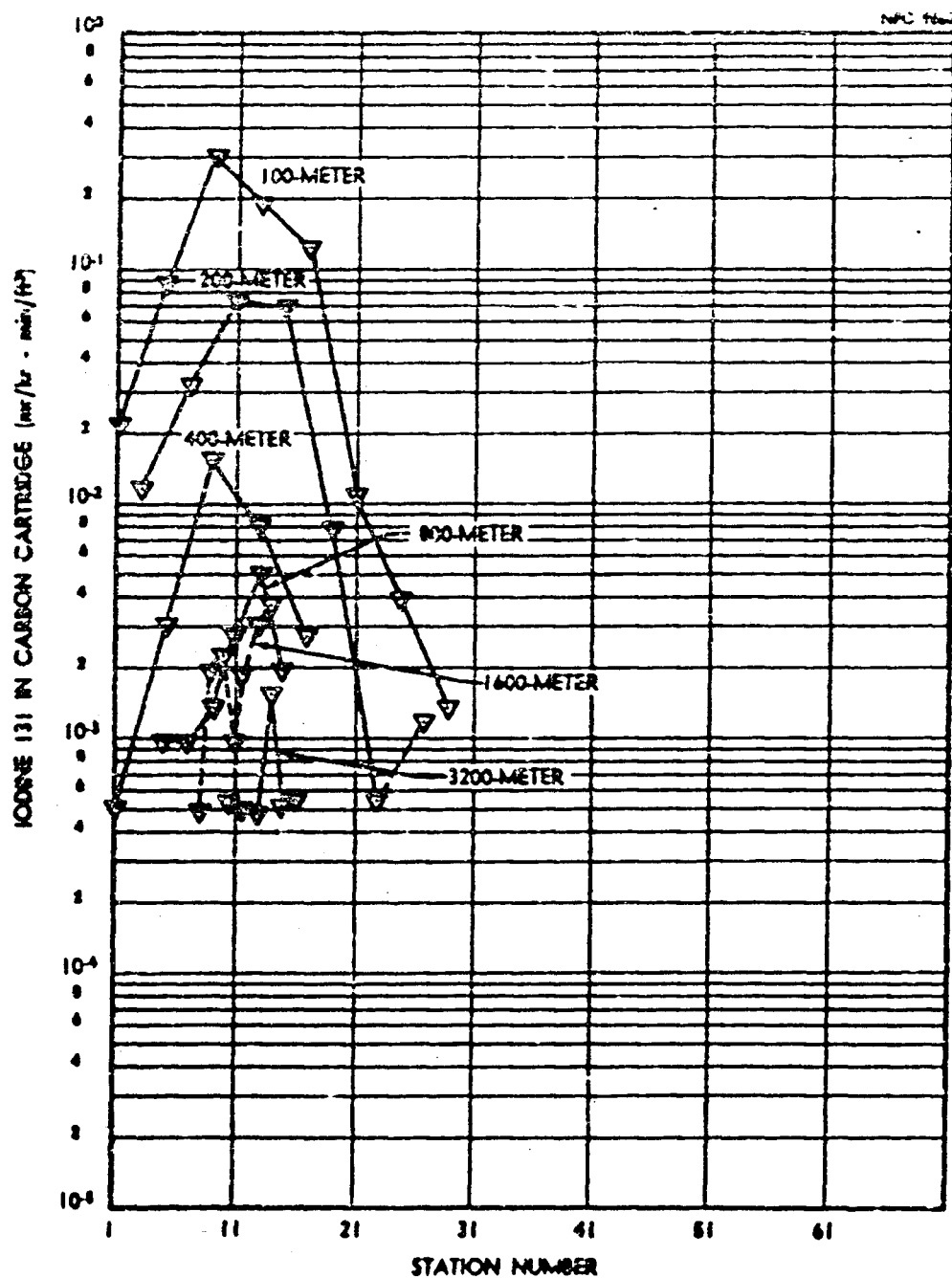


FIGURE M.M.3 NEVOC AIR SAMPLER FIELD SURVEY
(Carbon Cartridge - Air Provinces)

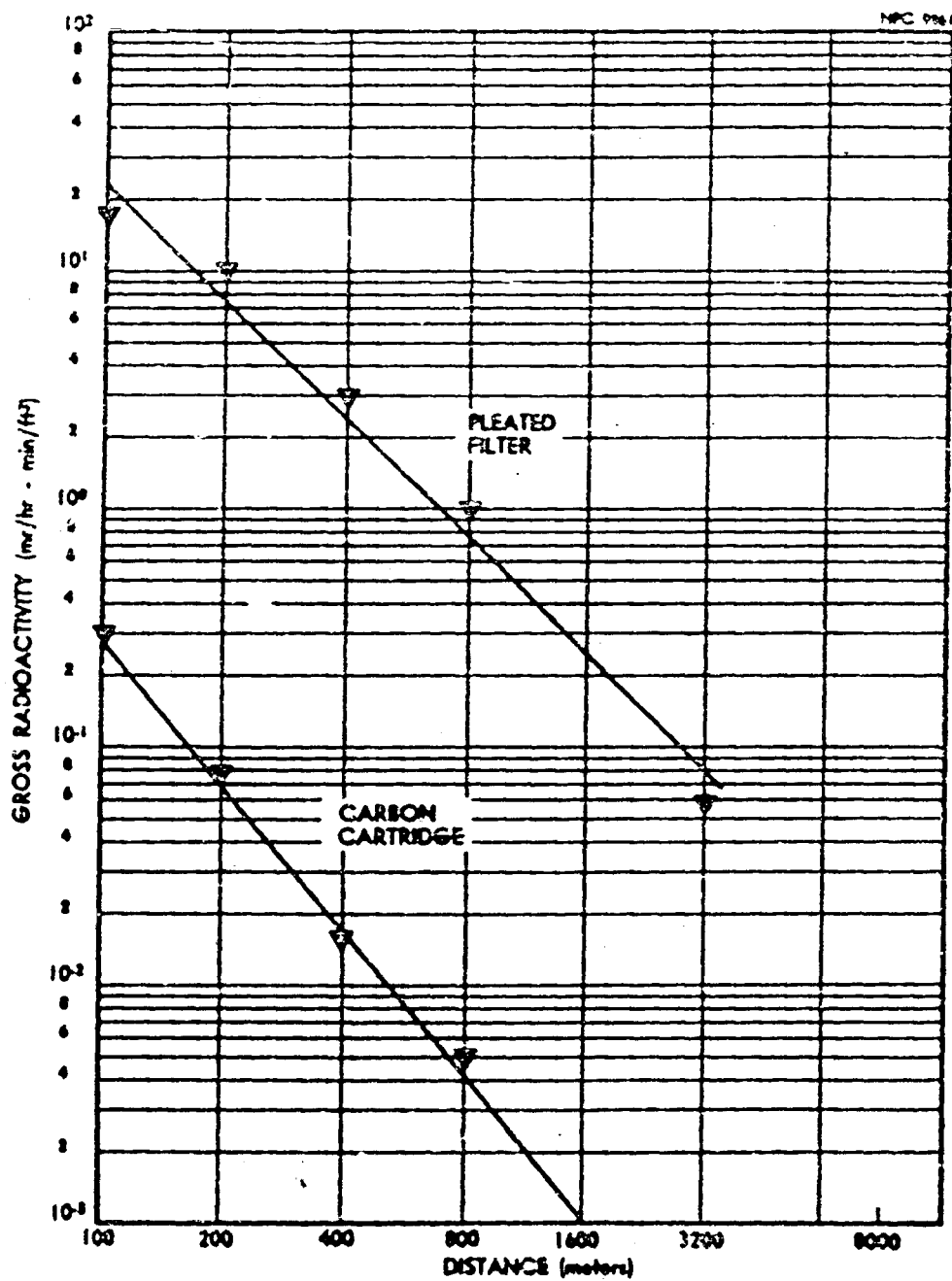


FIGURE PL-1.5 HI-VOL AIR SAMPLER FIELD SURVEY (Continued)

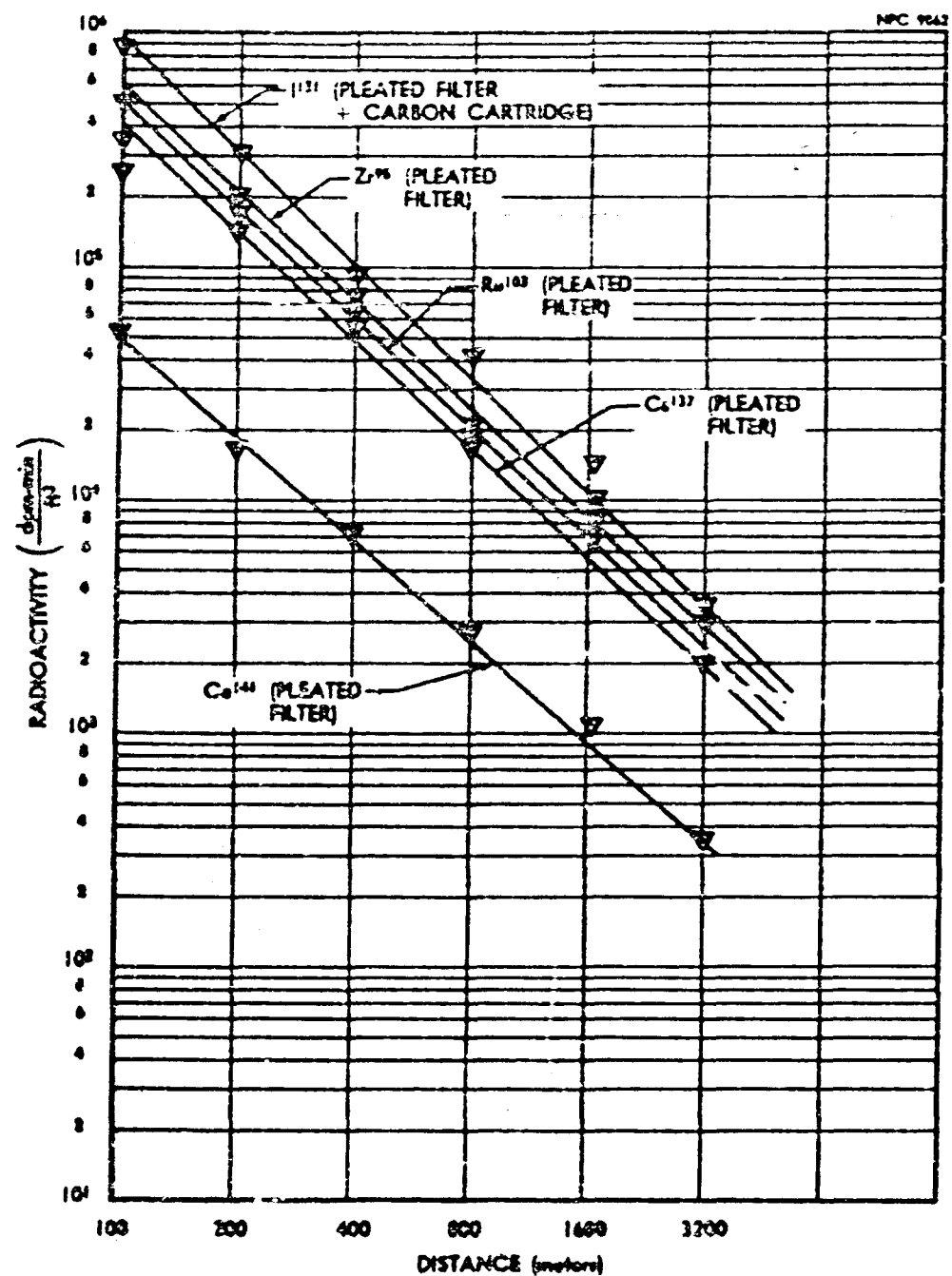


FIGURE N.M.7 HI-VOL AIR SAMPLER LABORATORY ASSAY
(Continued)

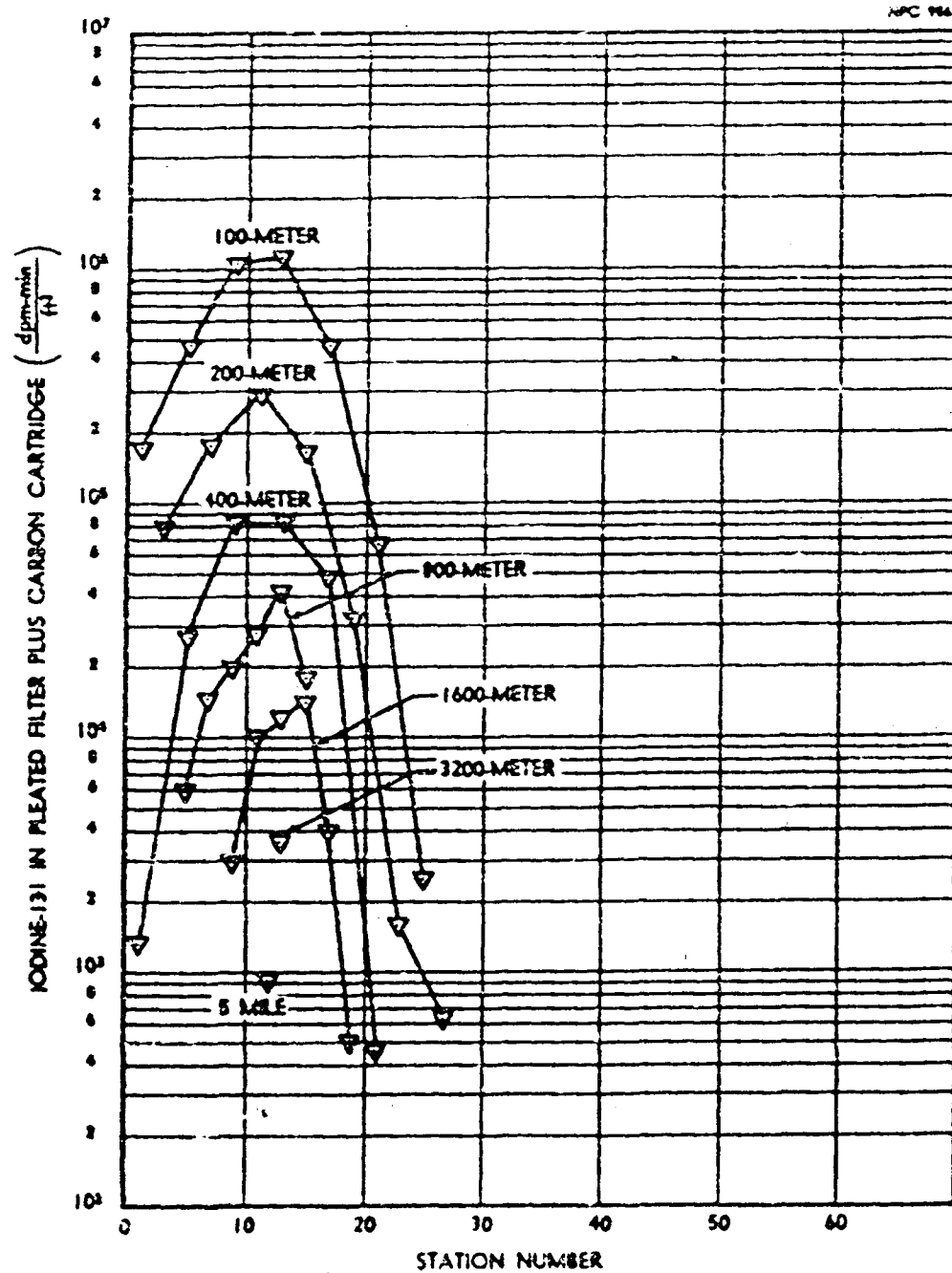


FIGURE N.M.3 MI-VOL AIR SAMPLER LABORATORY ASSAY OF IODINE (Are Prefiles)

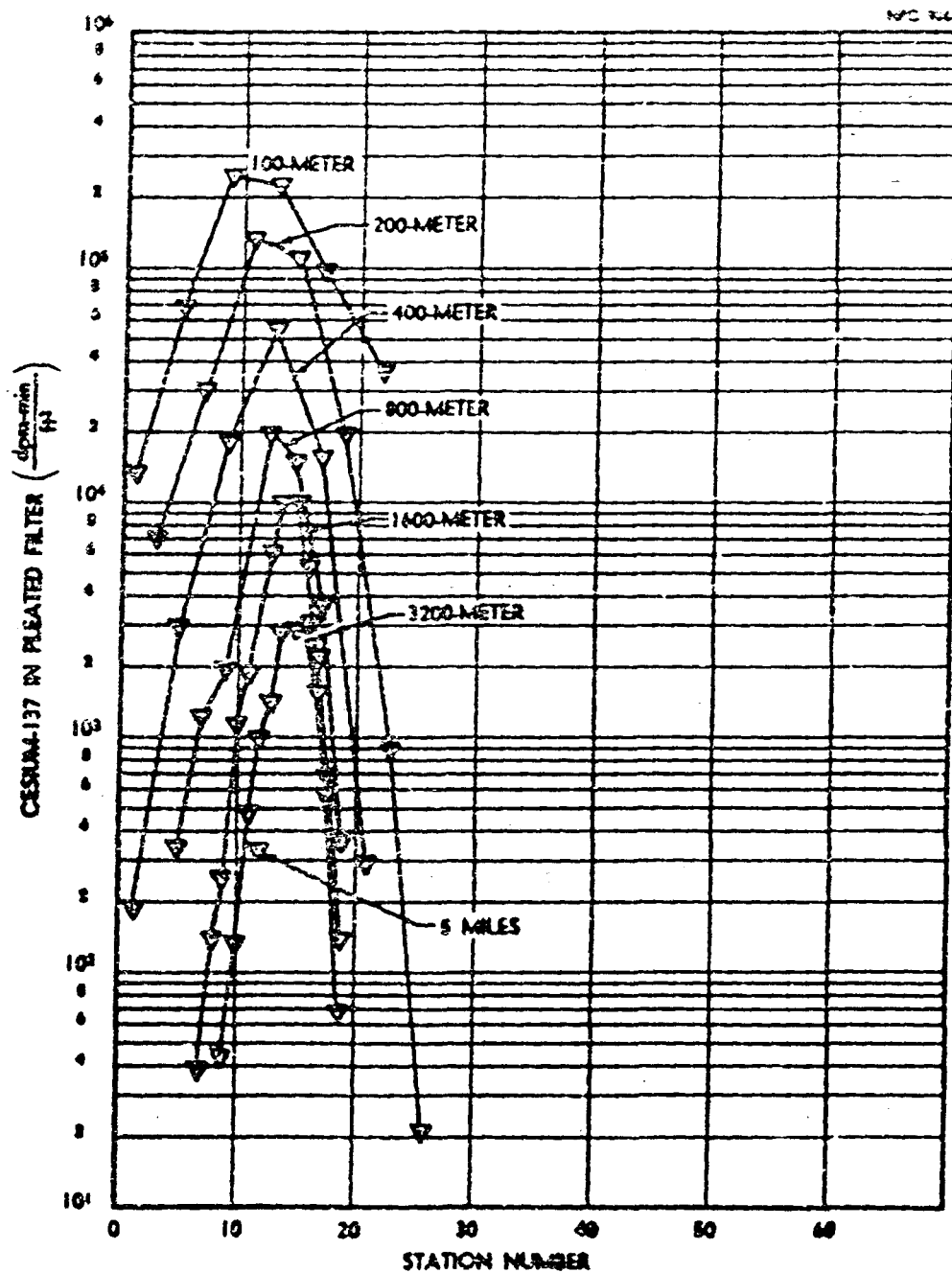


FIGURE M.N.9 MS-404 AIR SAMPLER LABORATORY ASSAY OF CESIUM (Are Probes)

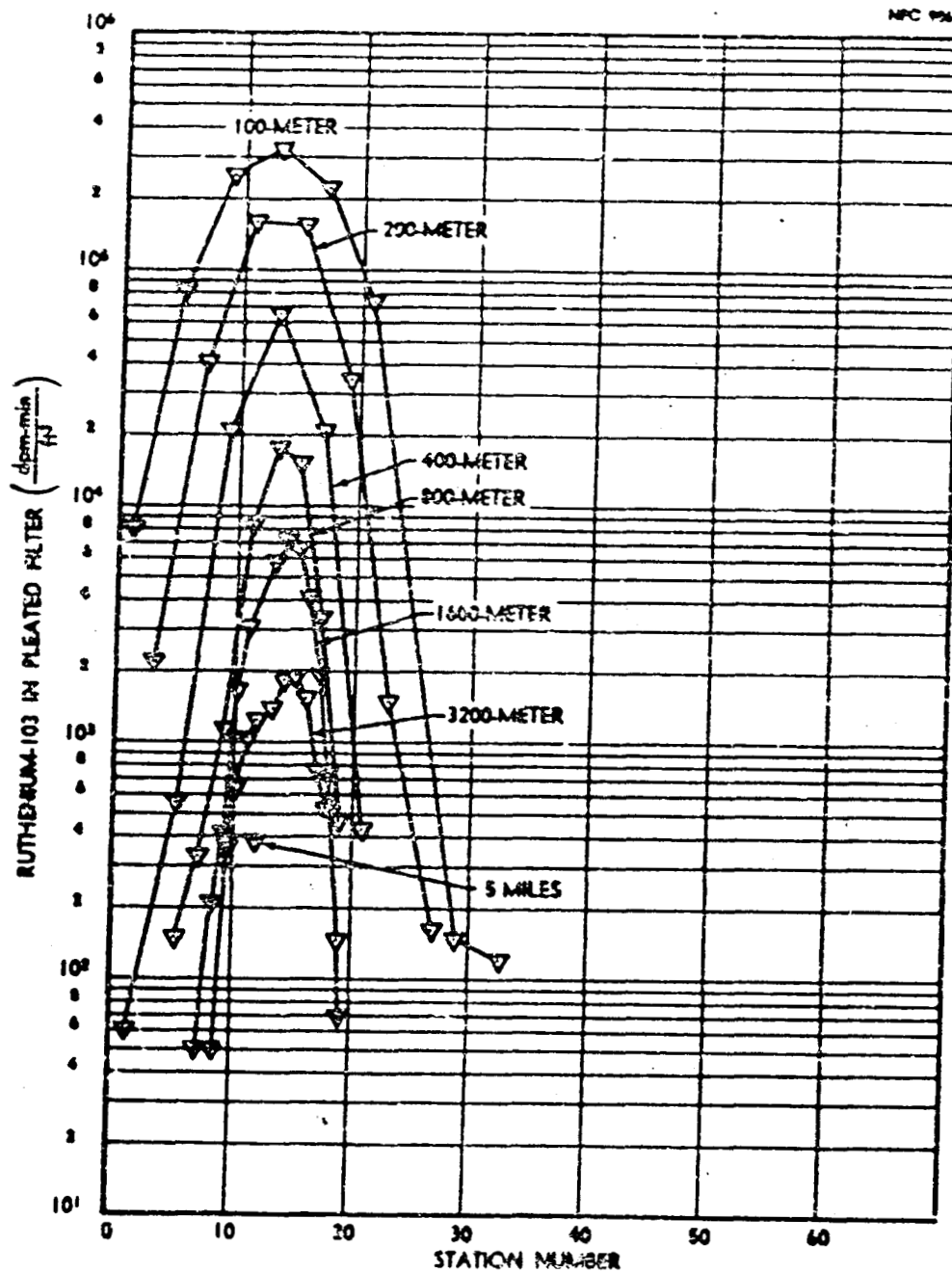


FIGURE N.M.10 NE-VOL AIR SAMPLER LABORATORY ASSAY OF

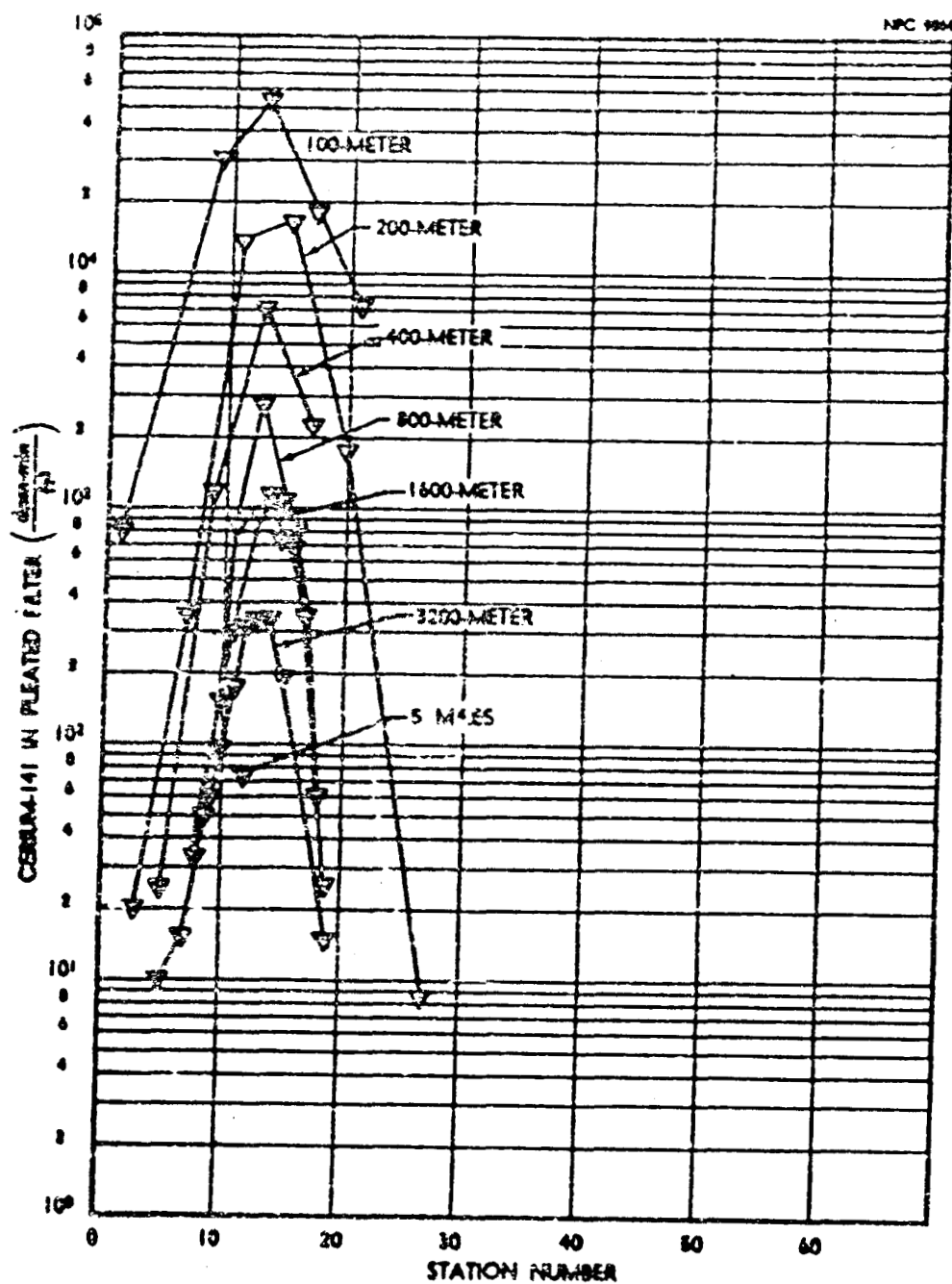


FIGURE N-11.11 DEPTH AND STATION LABORATORY ASSAY OF CERIUM (Are Profile)

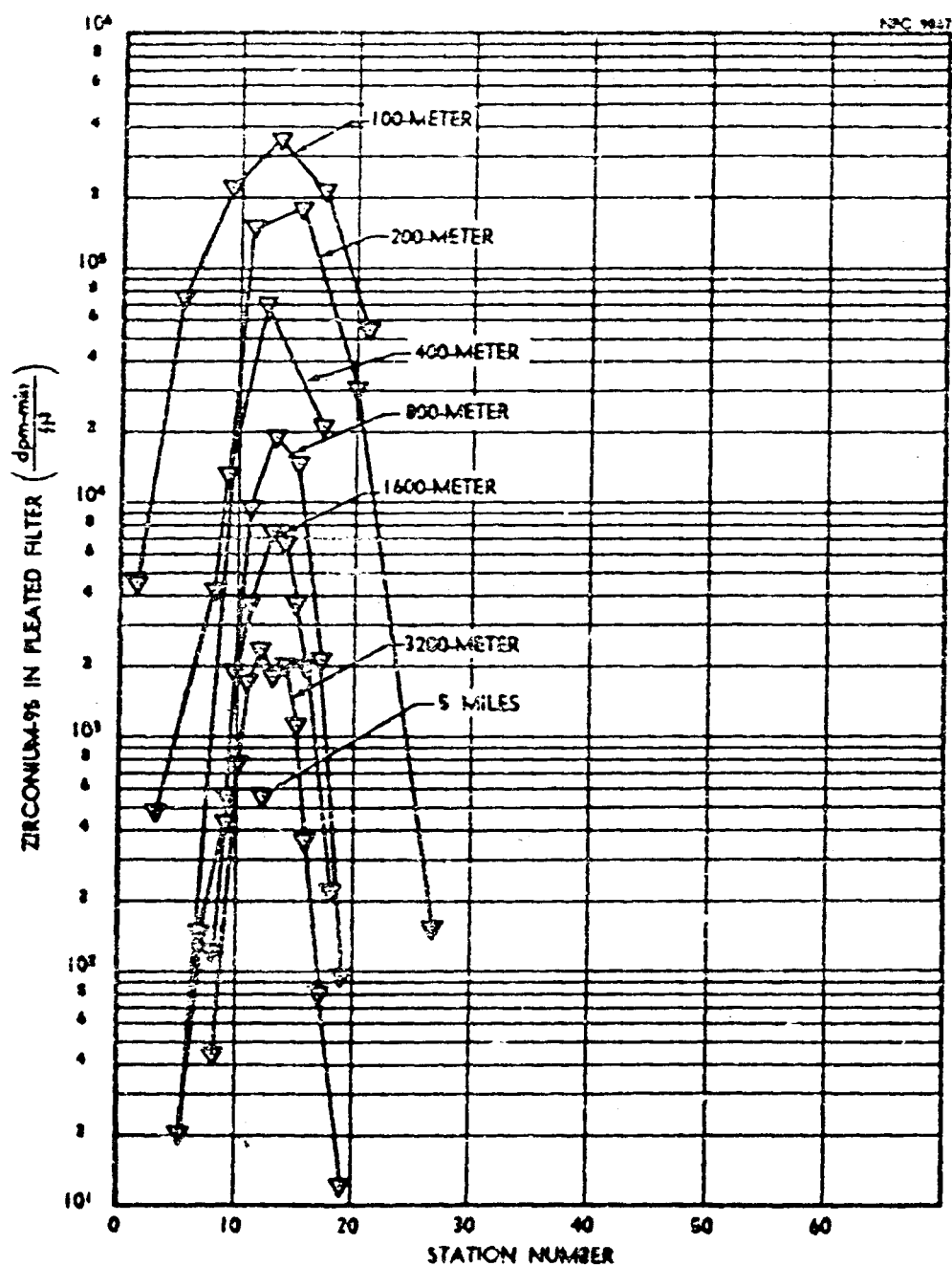


FIGURE N.M.12 HI-VOL AIR SAMPLER LABORATORY ASSAY OF ZIRCONIUM (Arc Profiles)

H.11 Deposited Radioactivity

The cloud deposition of iodine along each arc is shown in Figure N.H.13. These values are also shown in Figure N.H.14. plotted along the centerline as a function of distance from the release point.

H.12 Deposition Velocity

The deposition velocity for iodine as a function of distance as determined by the ratio of the area under the deposited iodine profiles to the area under the iodine air concentration profiles is shown in Table N.H.5.

H.13 Particle Size

A study was made of the particle size distribution and relative abundance of specific nuclides sampled by an Andersen Sampler with a molecular membrane back-up filter at a point five meters on centerline downwind from the furnace and at a height of 1.5 meters. The activities of the isotopes collected on each of the seven stages of this sampler are given in Table N.H.6. Based on the removal characteristics of the No.7 stage molecular membrane filter, which was predominantly in the sub-micron range when preceded by the Andersen sampler, more than 50 percent of each nuclide was in the sub-micron range, excepting zirconium.

H.14 Fluorescent Tracer

No tracer data are available during this release because of a wind shift.

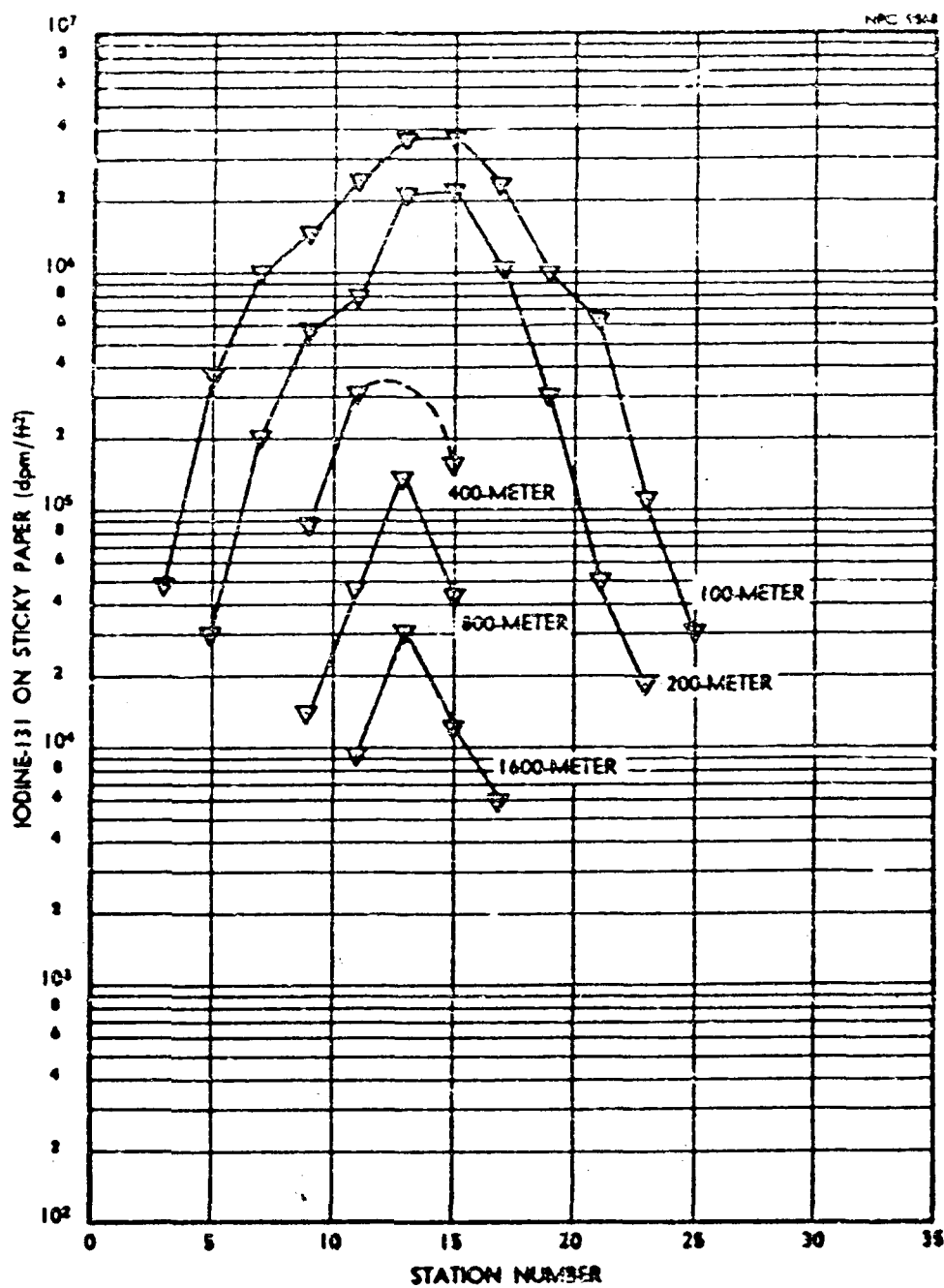


FIGURE N.M.13 DEPOSITED IODINE (Are Profiles)

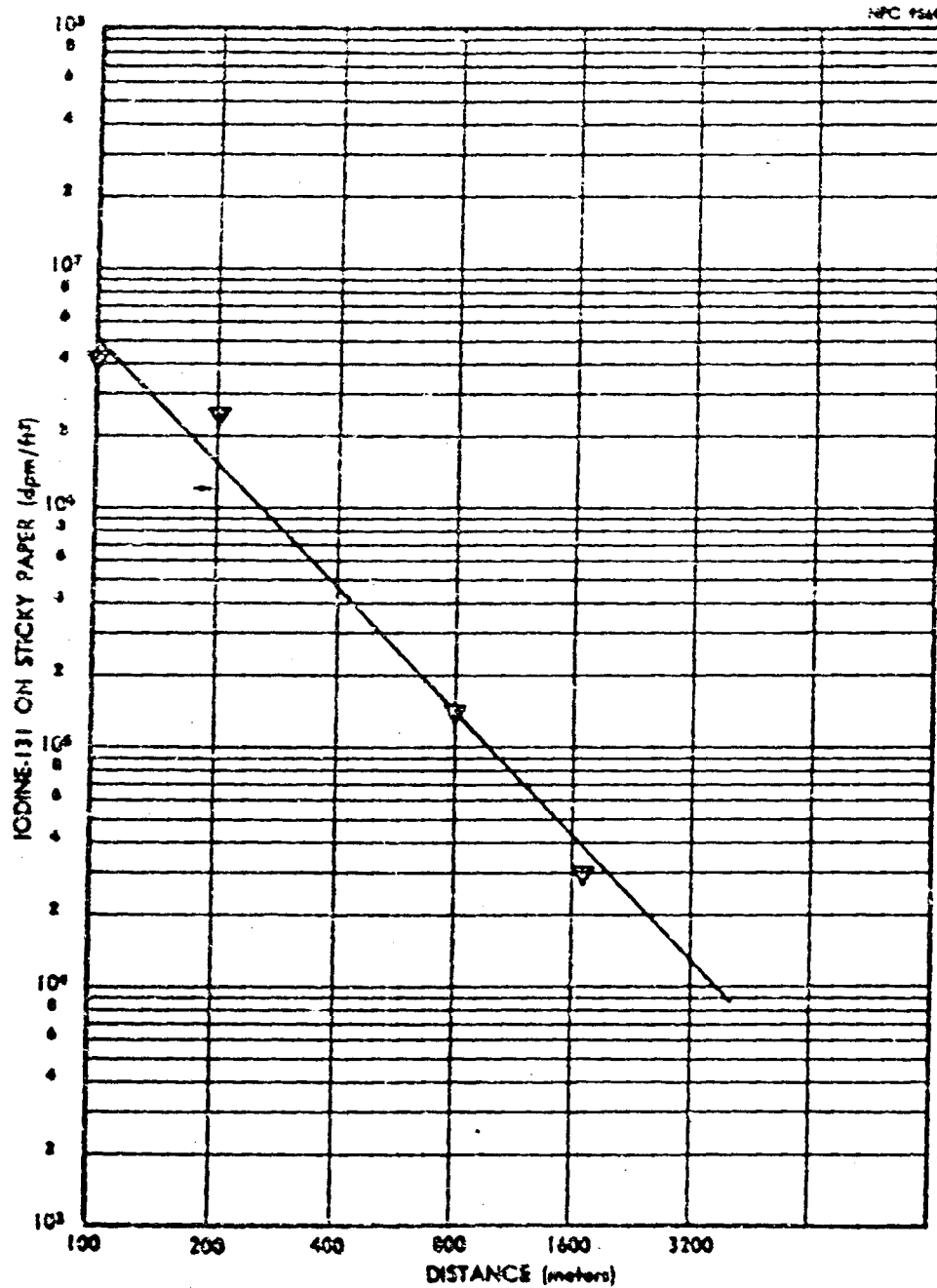


FIGURE N.H.14 DEPOSITED IODINE (Csarvtime)

TABLE H.H.5
Isotopic Deposition Velocities (cm/sec)

Arc (meters)	Sticky Paper					Water			Sand		
	I131	Cs137	Ru103	Zr95-Nb95	Cs141	I131	Ru103	Zr95-Nb95	I131	Ru103	Zr95-Nb95
100	1.35	.17±.05	2.4±.79	1.65±.53	.40±.29	0.91	3.9±2.8	8.5±3.2	0.54	0.60	1.02
200	2.7	.14±.04	3.1±1.2	1.7±.01	.34±.13	1.2±.1	4.9±3.4	13.1±8.95	0.54	0.47	9.0
400		.067±.034	1.2±.79	.69±.31	.62±.67	1.32±.5	2.8±2.1	2.4±1.6	0.32	0.75	0.9
800	1.35	.093±.023	2.8±1.3	3.9±3.4	1.7±1.7	2.34	2.14	1.61	0.5	1.92	4.8
1600	0.78	.19±.18	4.2±2.5	.69±.12	.12±.026						
3200		.0473	1.61	1.85	.267						

TABLE N.H.6

Distribution of Isotopes in Andersen Sampler

Stage	Nuclide Activity $\frac{\text{DPM-Min}}{\text{ft}^3}$				
	Zr ⁹⁵ -Nb ⁹⁵	Cs ¹³⁷	Ru ¹⁰³ , Ru ¹⁰⁶	Sr ⁸⁹	Ce ¹⁴¹ , Ce ¹⁴⁴
1	260,000	14,000	128,000	25,300	27,500
2	91,000	9,200	40,000	31,600	11,000
3	104,000	17,500	46,000	17,400	11,800
4	36,000	26,000	36,000	25,300	5,300
5	27,000	158,000	41,000	91,600	10,100
6	6,500	195,000	71,000	135,800	11,300
7	35,000	750,000	250,000	644,800	32,500

H.15 External Dose

The gamma dose from the effluent cloud, as determined by the detectors along the 400-meter arc, is shown in Figure N.H.15. The dose rate, as a function of elapsed time as recorded by the detector nearest the cloud centerline, is shown in Figure N.H.16. The gamma image of the cloud, or the isodose rate levels at detector positions versus time is shown in Figure N.H.17.

H.16 Diffusion Parameters

The diffusion parameters obtained during the release are shown in Table N.H.7. For comparison, Figures N.H.18 and N.H.19 show the actual activity isopleth and the curve-fit isopleths respectively.

TABLE N.H.7
Diffusion Parameters

Parameters	Field Survey Data Fit	Cs ¹³⁷ Fit	Ru ¹⁰³ Fit	I ¹³¹ Fit	Bivane Data (24 meters)	Smoke Plume Fit
M _y	0.78	0.61	0.67	0.85	-	1.0
M _z	0.34	0.68	0.86	0.80	-	1.0
C _y	0.28	0.96	0.79	0.32	0.03	1.8
C _z	0.23*	0.30	0.10	0.21	0.03	0.78
n	-	-	-	-	0.39	-

* Vertical wire

NPC 1573

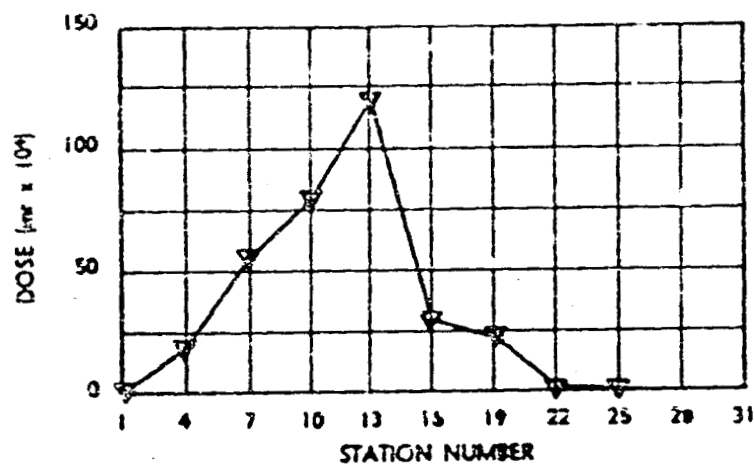


FIGURE N.H.15 GAMMA DOSE FROM CLOUD PASSAGE (Arc Profile)

NPC 1571

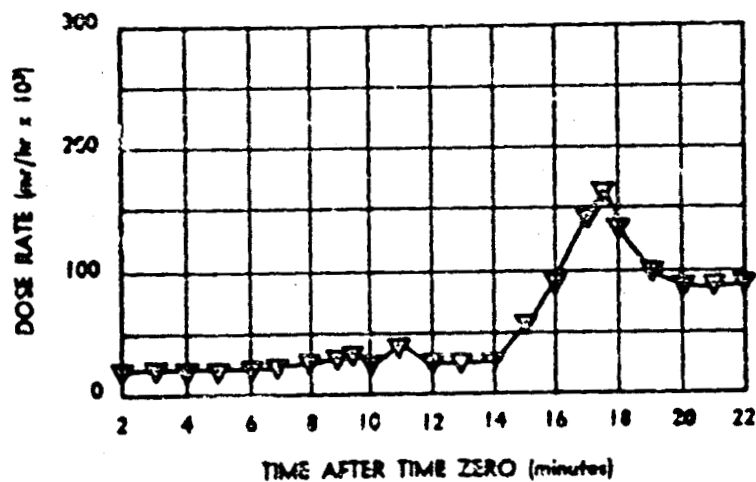


FIGURE N.H.16 GAMMA DOSE RATE FROM CLOUD PASSAGE (Centerline)

NPC 9972

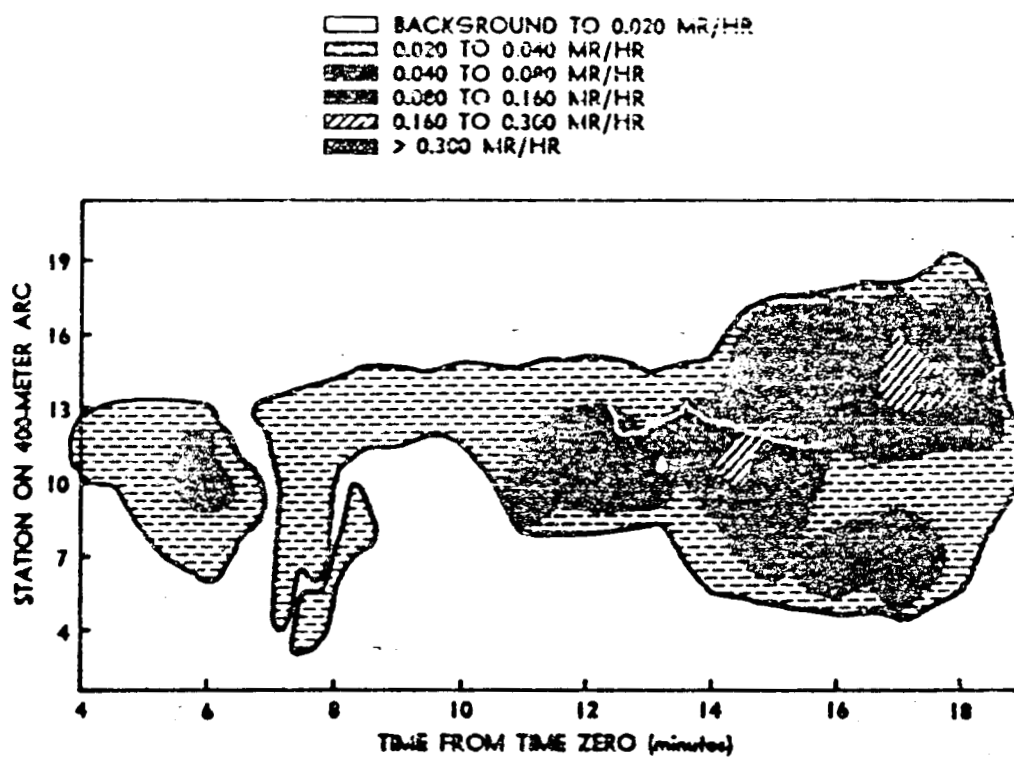


FIGURE NLX.17 GAMMA DOSE RATE FROM CLOUD PASSAGE
(Activity Centroids)

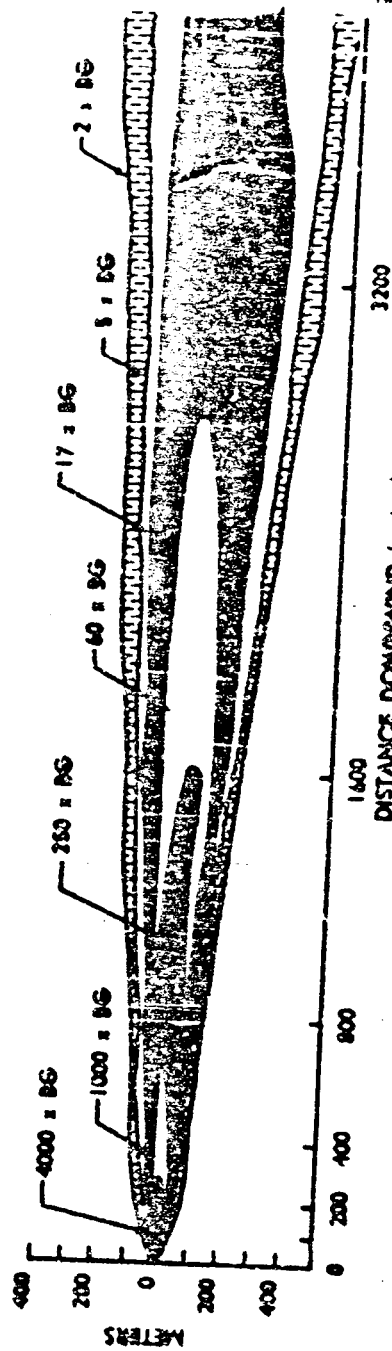


FIGURE N.H.18 GROSS RADIOACTIVITY ISOLITH
(Field Data)

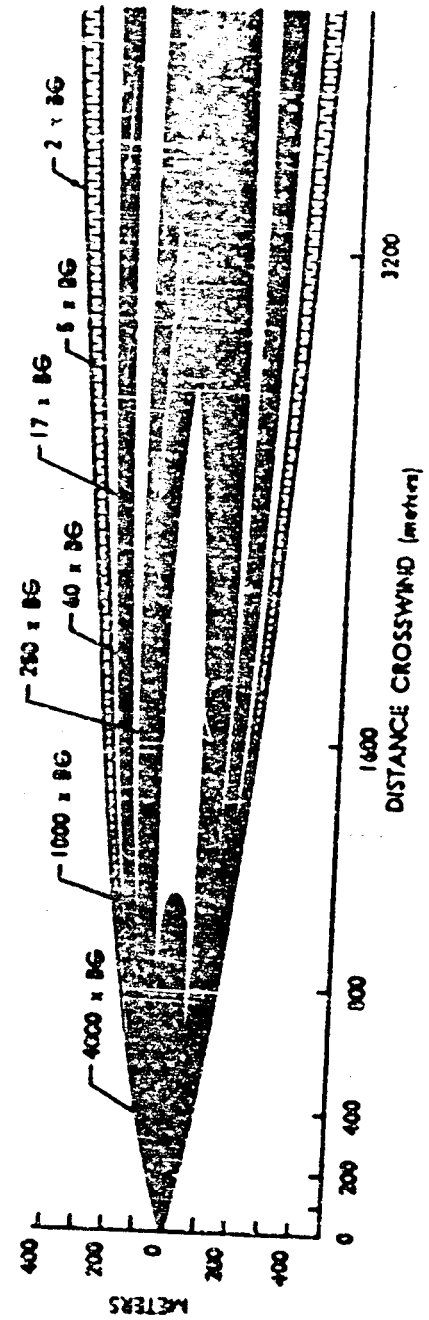


FIGURE N.H.19 GROSS RADIOACTIVITY ISOLITH
(Curve Fit)

H.17 Sand and Water Traps

Spectral analysis of sand and water samples from this release indicated the presence of I^{131} , Ru^{103} , and $Zr^{95}-Nb^{95}$ in significant amounts. Figure N.H.20 shows the gross gamma activity of the water samples across the various arcs. Table N.H.8 shows the isotopic contamination for both sand and water samples.

TABLE N.H.8
Radioactivity in Sand and Water

Sample	(Arc Location - Station)	Activity (m curies/ft ²)		
		I^{131}	Ru^{103}	$Zr^{95}-Nb^{95}$
Water	100 meter - 6	460	22	--
	- 11	810	520	--
	- 16	460	1300	2600
	- 21	67	520	260
	200 meter - 8	210	95	120
	- 13	220	460	520
	- 18	57	470	570
	400 meter - 11	140	21	28
	- 16	40	120	100
Sand	100 meter - 16	280	160	230
	200 meter - 8	100	25	34
	400 meter - 16	14	20	22
	800 meter - 8	6	1	1

NPC 9175

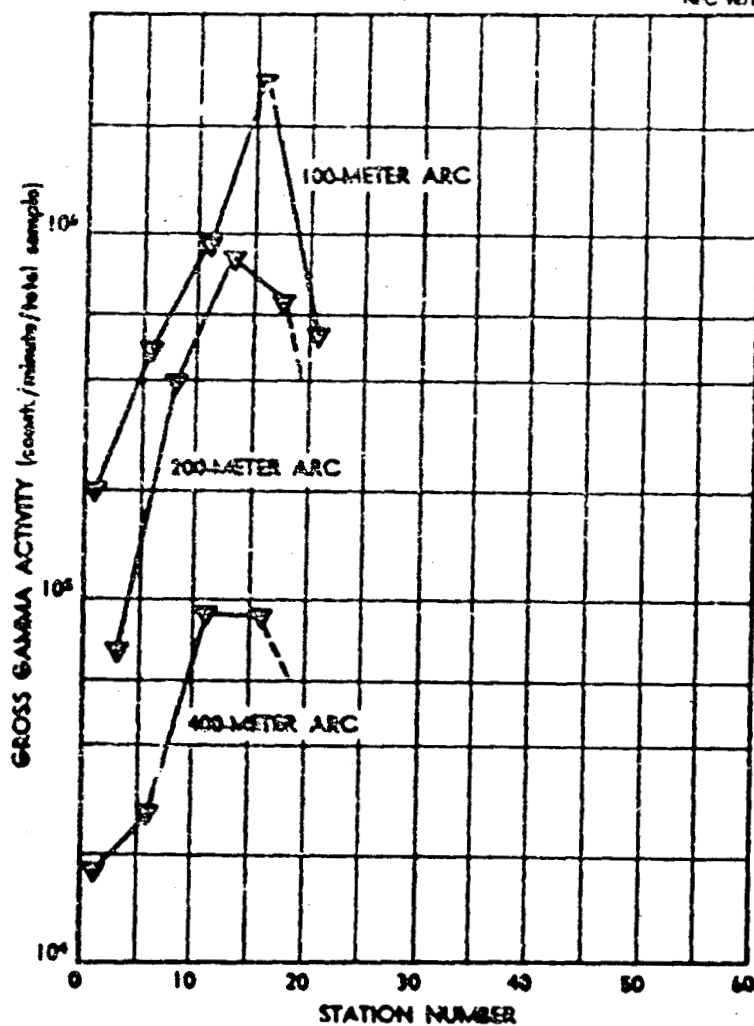


FIGURE N.K.30 CONTAMINATION OF WATER SAMPLES

APPENDIX N-I

(Release I)

I.1 Summary

Type of Sample -----	Aged Fuel Element
Date and Release Time -----	26 Sept. 1958; 4:22 PM
Lapse Rate (1.5-45m) -----	+0.32°C
Lapse Rate (1.5-24m) -----	+0.55°C
Mean Wind Speed -----	2 meters/sec
Wind Direction -----	Left edge of network
Cloud Photography -----	No photography
Fluorescent Tracer -----	Released simultaneously with fission product release
Animals -----	Rats and dogs on inner arcs (Ref. 11)
Network Radioactivity -----	Detected out to 1600 meters; maximum reading of pleated filters on 100-meter arc, 80 mr/hr, using Cutie P1
External Dose -----	Maximum dose rate on 400- meter arc, 0.072 mr/hr using scintillation detec- tor described in Appendix F

I.2 Fuel Element

The fuel element had been irradiated to generate 7.7×10^4 watts for a total of 467 hours and had decayed for 985 days. The predominant nuclides present at the time of release are shown in Table N.I.1.

TABLE N.I.1
Fission Product Inventory

Nuclide	Curies Calculated
Sr ⁹⁰	3.4
Ce ¹⁴⁴ -Pr ¹⁴⁴	12
Pm ¹⁴⁷	8.3
Ru ¹⁰⁶ -Rh ¹⁰⁶	0.98
Cs ¹³⁷ -Ba ^{137m}	2.9

I.3 Meteorological Conditions

The wind directions and velocities prevailing during this release are shown in Table N.I.2.

Lapse rates, existing at the apex tower during the release, between the 1.5-meter level and both the 24-meter and 45-meter levels, are shown in Figure N.I.1.

I.4 Furnace Conditions

Furnace operation for this test closely followed the normal power input program established during Release A (App. N-A, Sec. A.5).



FOUR H.I. LATE RATE DURING RELEASE

TABLE N.I.2

Meteorological Summary

APEX TOWER

Height (meters)	Wind Direction Ave.	Wind Velocity (meters/sec) Ave.
1.5	212 ^o	2.00
3.0	209	1.95
6.0	-	2.33
12.0	-	2.73
24.0	193	2.95
45.0	225	3.14

FIELD MASTS

Location (Arc)	Wind Direction Ave.	Wind Velocity (meters/sec) Ave.
200 meter	216 ^o	2.20
400	221	2.27
800	221	2.76
1600	234	2.94
2400	222	2.85
3200	206	3.06

I.5 Effluent Samplers

The radioactivity collected by the effluent samplers is shown in Figure N.I.2. A maximum release of activity at approximately 3.5 minutes from time zero is indicated.

I.6 Release Percentages

No pre- and post-melt gamma spectrometry was accomplished during this release. The release percent for strontium was obtained in the same manner as previously explained (App. N-A, Sec. A.7) except that a 50 percent cesium release was used in the

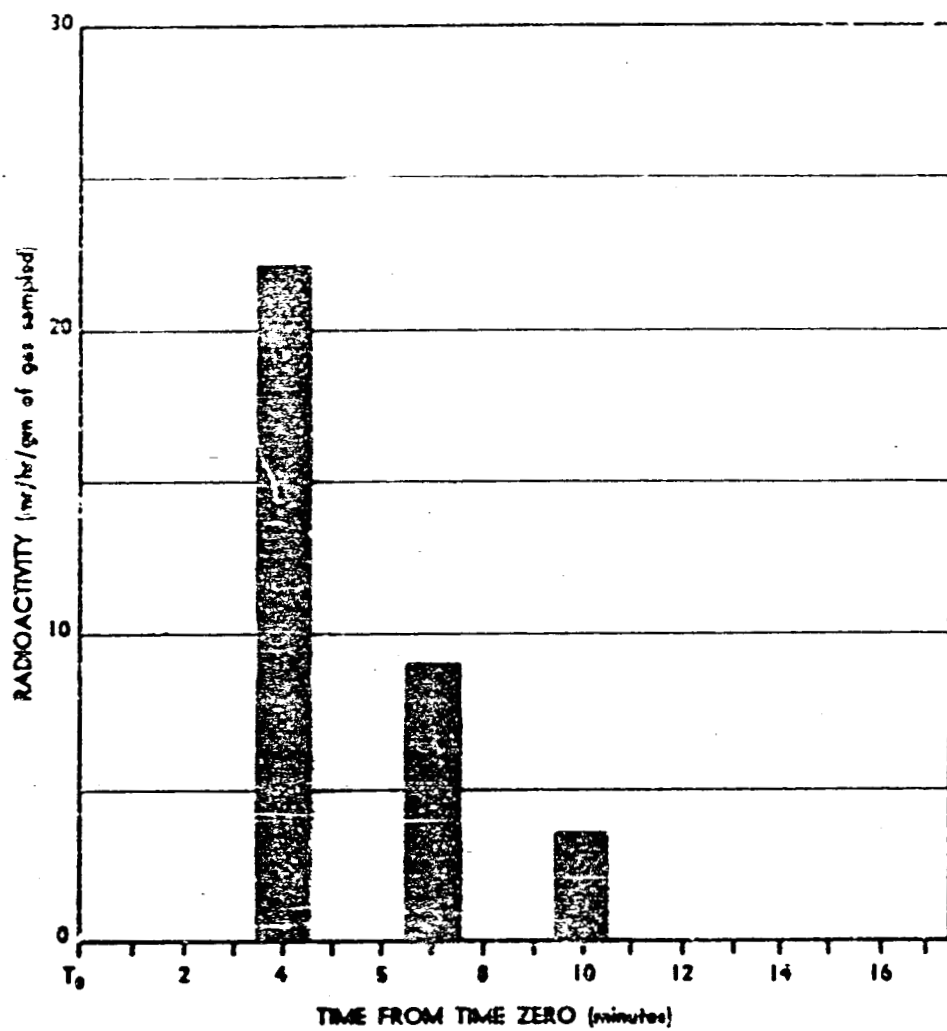


FIGURE N.1.2 SEQUENTIAL-EFFLUENT-SAMPLER FILTER RADIOACTIVITIES

in the calculation (the average cesium released from other aged releases). This procedure gave a strontium release percent of 0.53 ± 0.25 .

I.7 Air Sampler Field Survey

The term "field survey" refers to contact measurements which were taken on the Hi-Vol pleated filters immediately following the test with a beta-gamma survey meter (Cutie Pie for readings > 20 mr/hr). Figure N.I.3 shows the arc profiles of the filter readings corrected for sampler flow rate and background.

I.8 Airborne Radioactivity

Airborne Ce^{137} radioactivity as determined by laboratory counting of the filters is shown in Figure N.I.4. A centerline curve was not constructed because of loss of a part of the cloud from the network.

I.9 Deposited Radioactivity

The cesium deposited on the gummed fallout papers placed around the arcs is shown in Figure N.I.5. Figure N.I.6 shows a plot of the maximum value of each arc (centerline) as a function of distance from the release point.

I.10 Deposition Velocity

The deposition velocity for cesium as a function of distance from the release point is shown in Table N.I.3. Each value was determined by establishing the ratio of the area under the sticky paper activity arc profile to the corresponding area under the Hi-Vol air sampler activity arc profile.

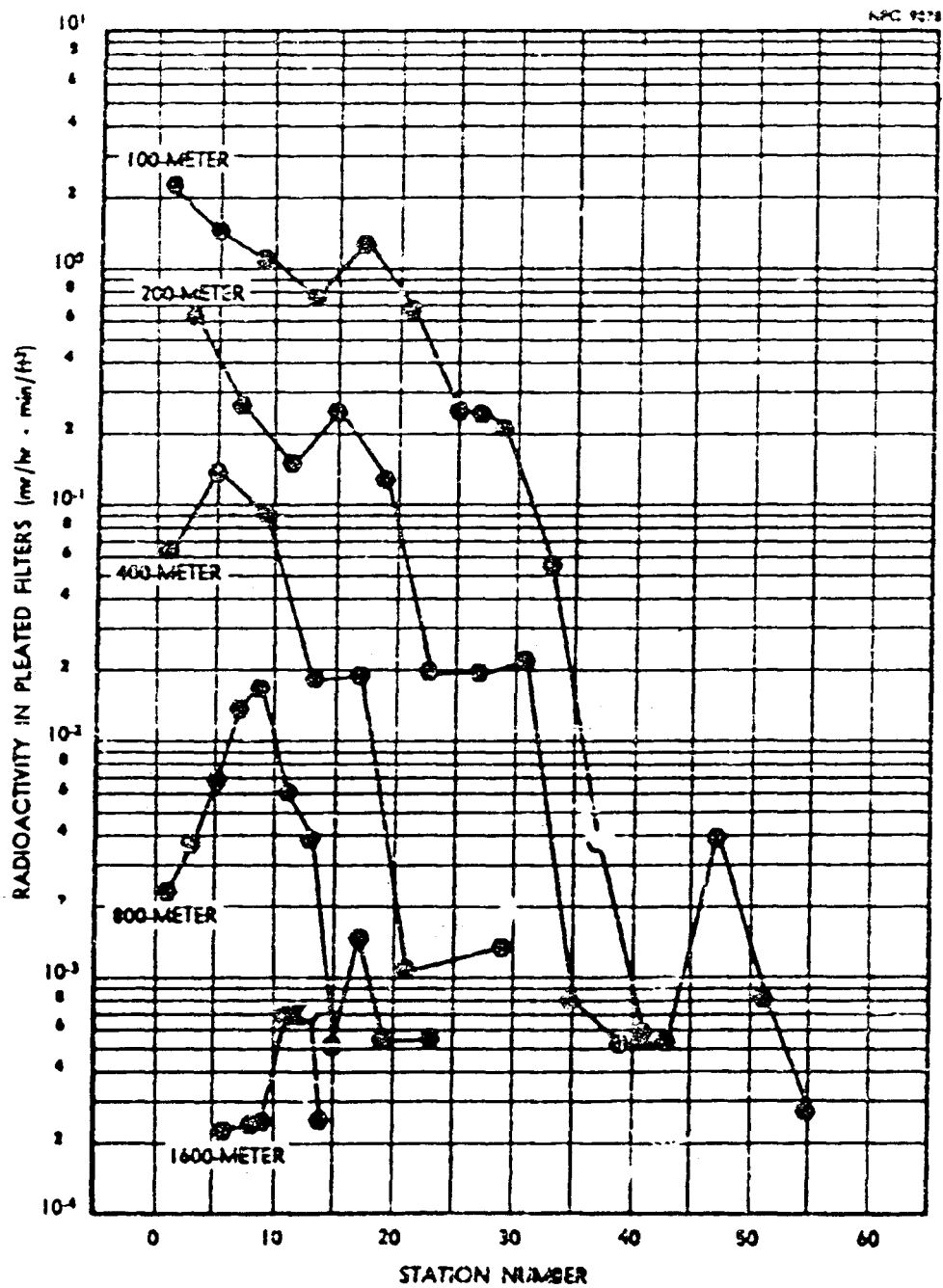


FIGURE M.1.3 H₂VO₄ SAMPLER FIELD SURVEY
(Arc Profiles)

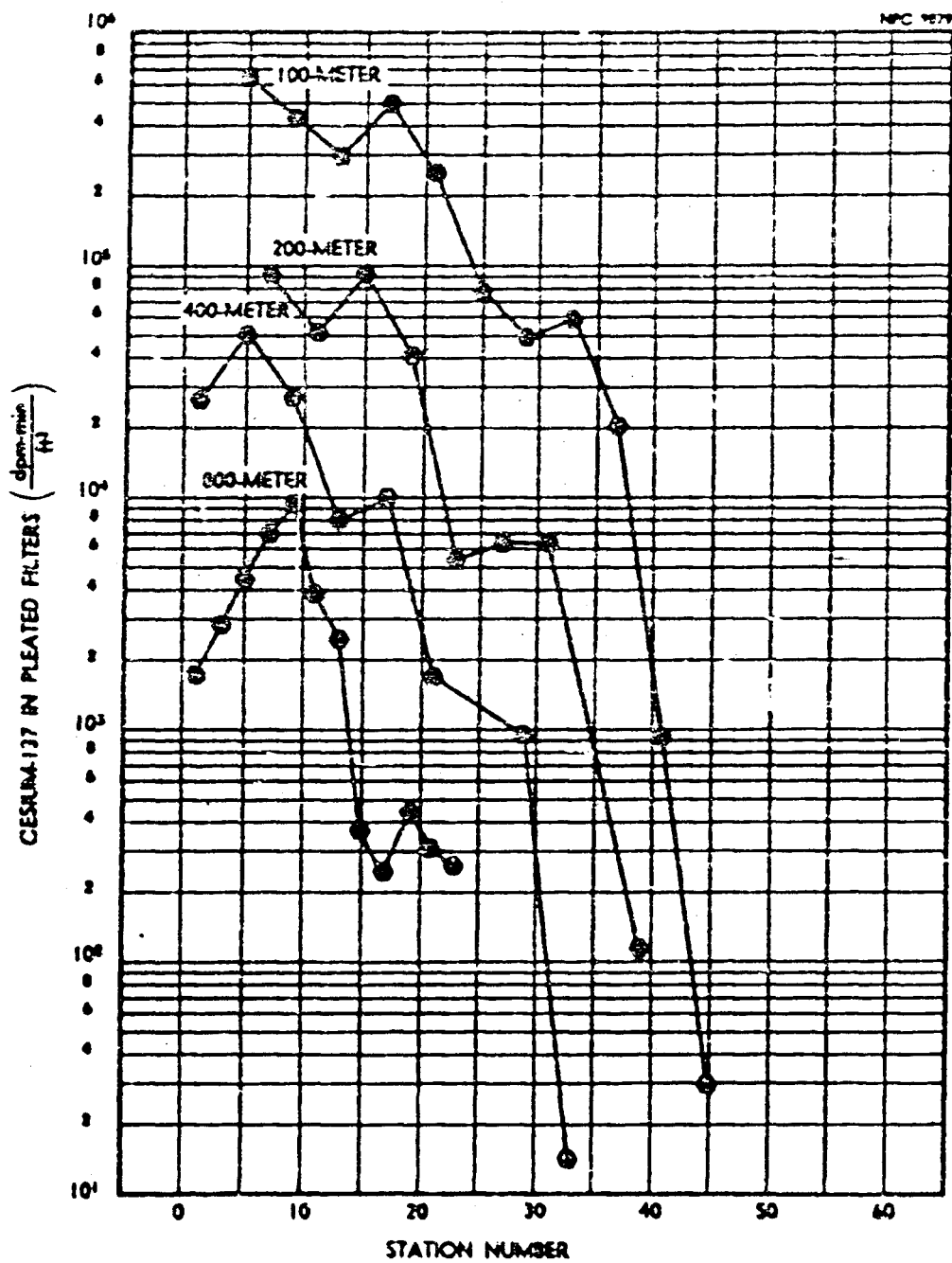


FIGURE N-14 NEVADA SAMPLE LABORATORY ASSAY OF CESRA-137 (Are Profile)

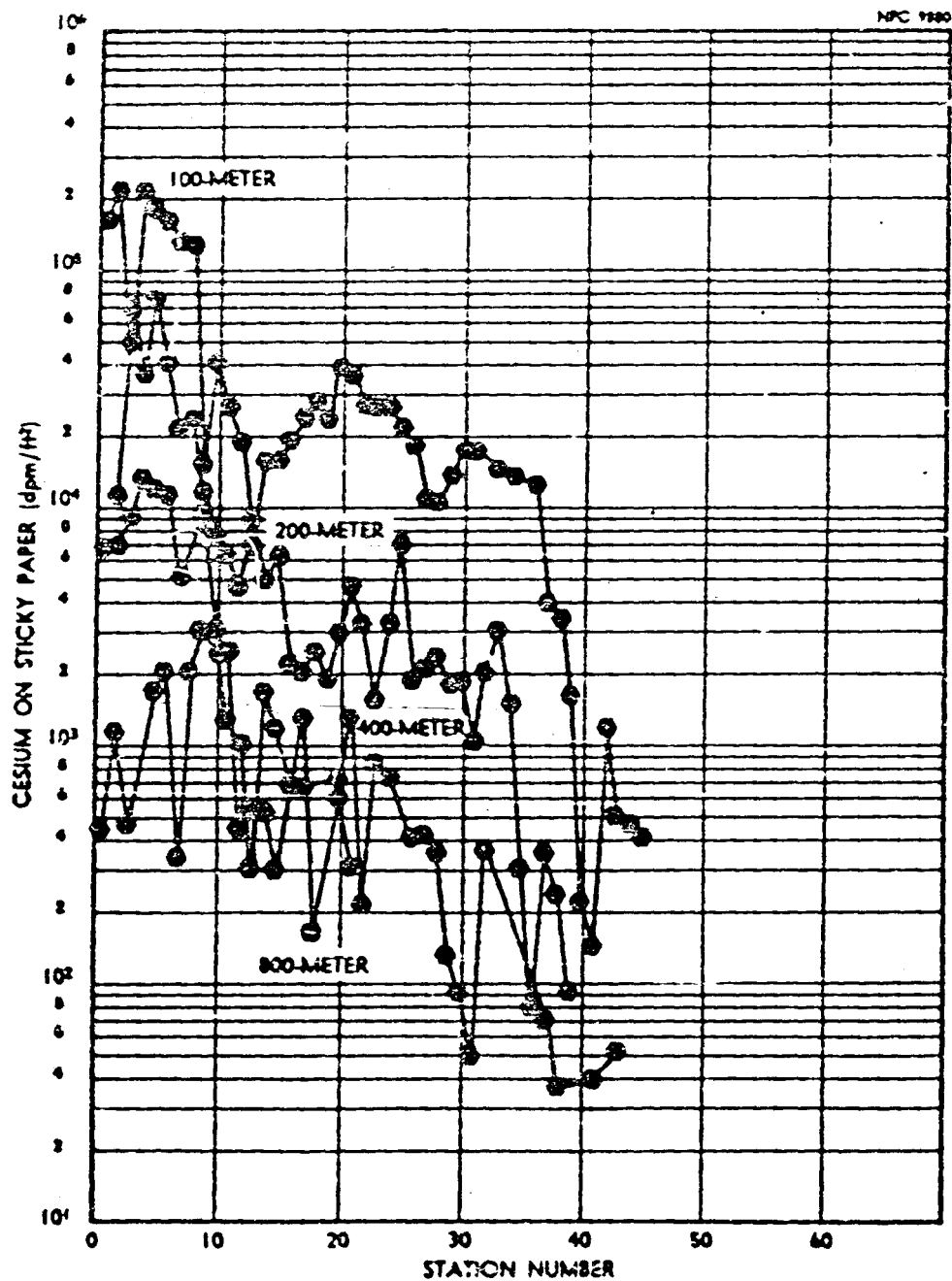


FIGURE N.1.5 DEPOSITED CESIUM (Arc Profiles)

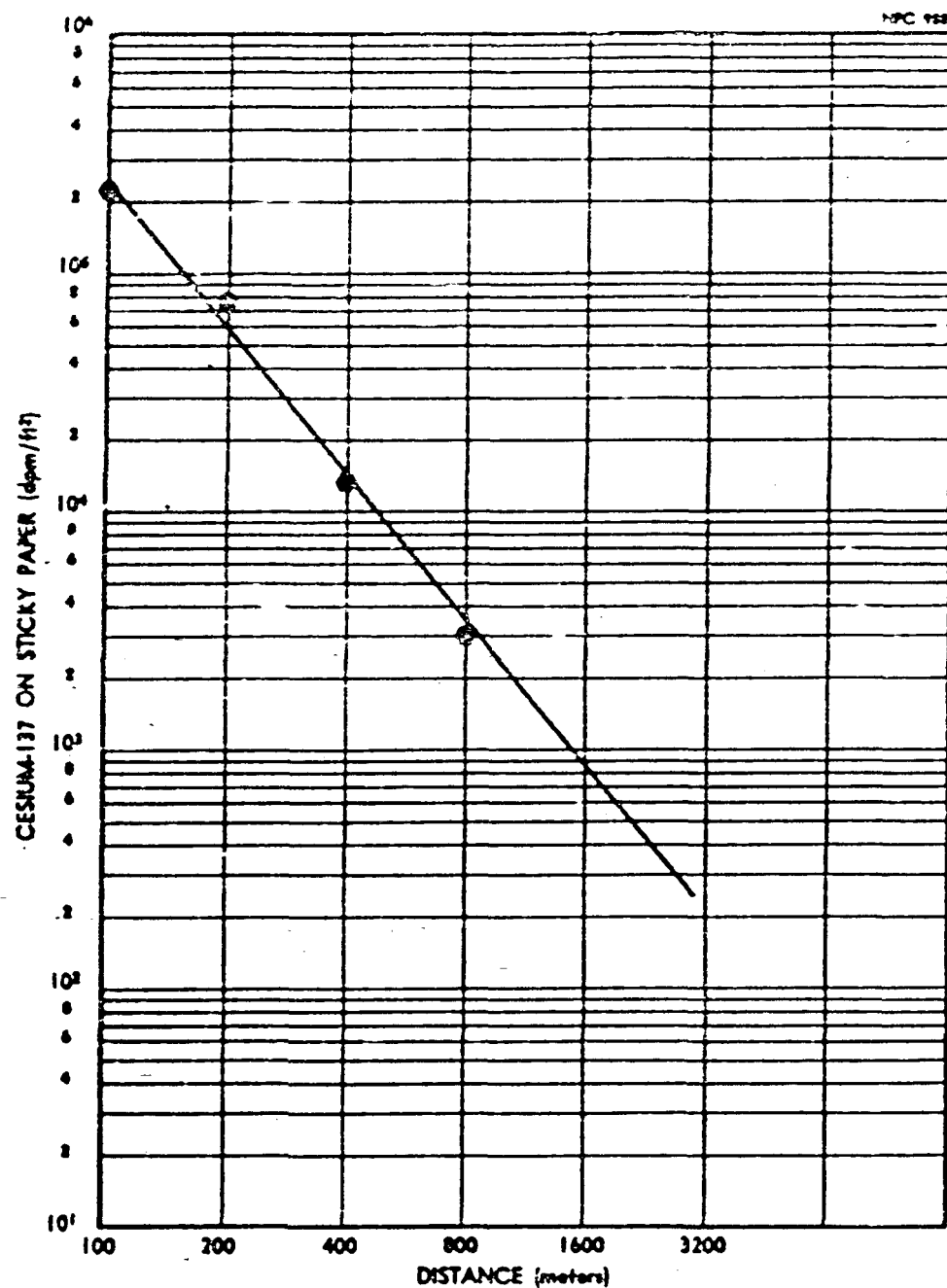


FIGURE N.1.6 DEPOSITED CESIUM (Concorline)

TABLE N.I.3
Cesium Deposition Velocity

Arc (meters)	Velocity (cm/sec)
100	0.072
200	0.074
400	0.108
800	0.137

I.11 Fluorescent Tracer Distribution

The fluorescent tracer data are presented in Figures N.I.7 and N.I.8. The profiles for the inner arcs are shown in Figure N.I.7. Figure N.I.8 shows the cloud centerline particle concentrations as a function of distance from the release point.

I.12 External Dose

The external dose data are shown in Figures N.I.9, N.I.10, and N.I.11. The integrated dose at each detector station across the 400-meter arc is shown in Figure N.I.9. Figure N.I.10 shows the dose rate recorded by the detector located nearest the fission product cloud centerline plotted against elapsed time. The iso-dose rate levels, shown as time versus position across the 400-meter arc, appear in Figure N.I.11.

I.13 Diffusion Parameters

Because of the loss of a significant portion of the fission product cloud off the network, diffusion parameters were not obtained from this test.

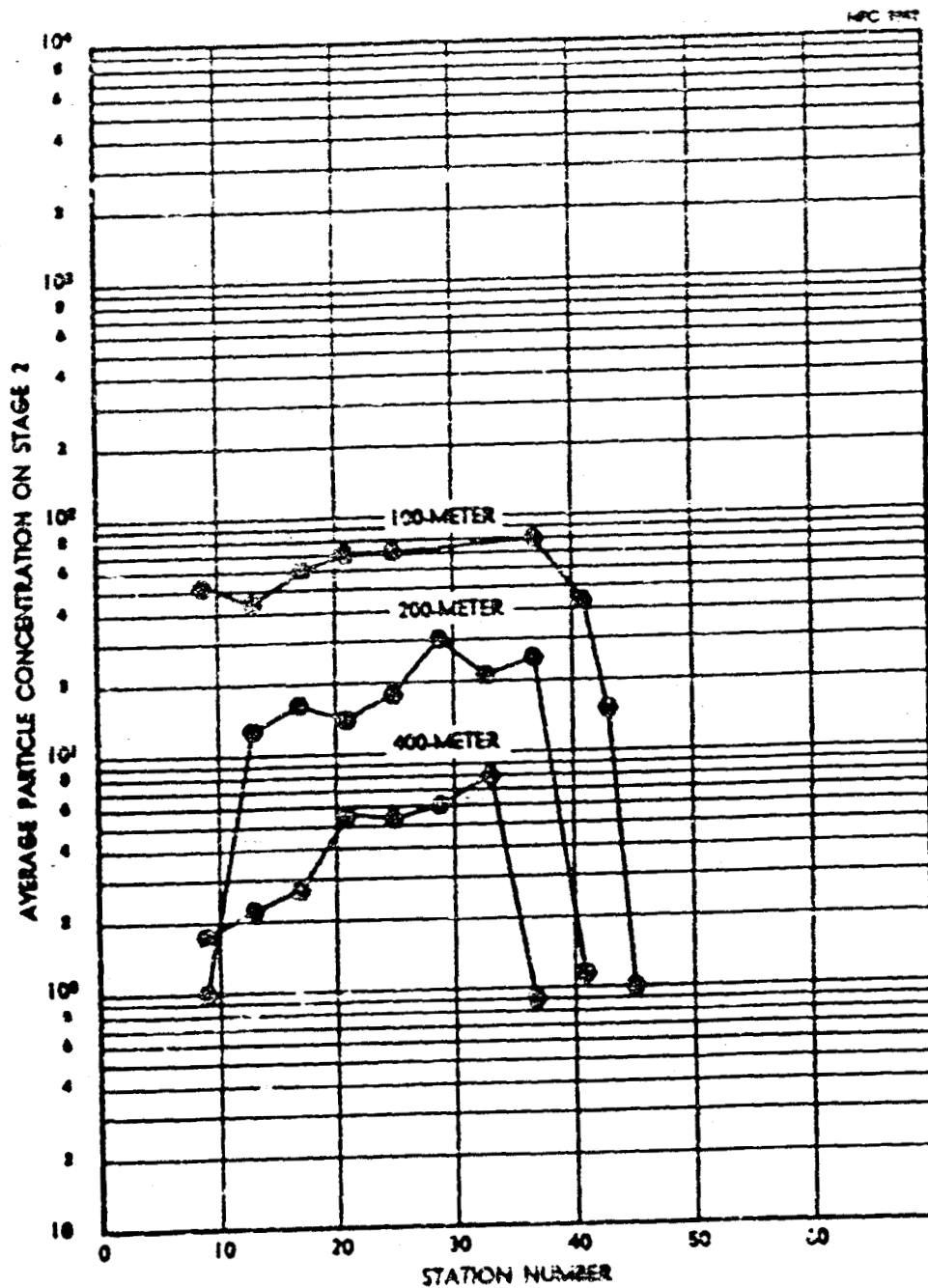


FIGURE N.1.7 FLUORESCENT TRACER (Arc Profiles)

NPC 0083

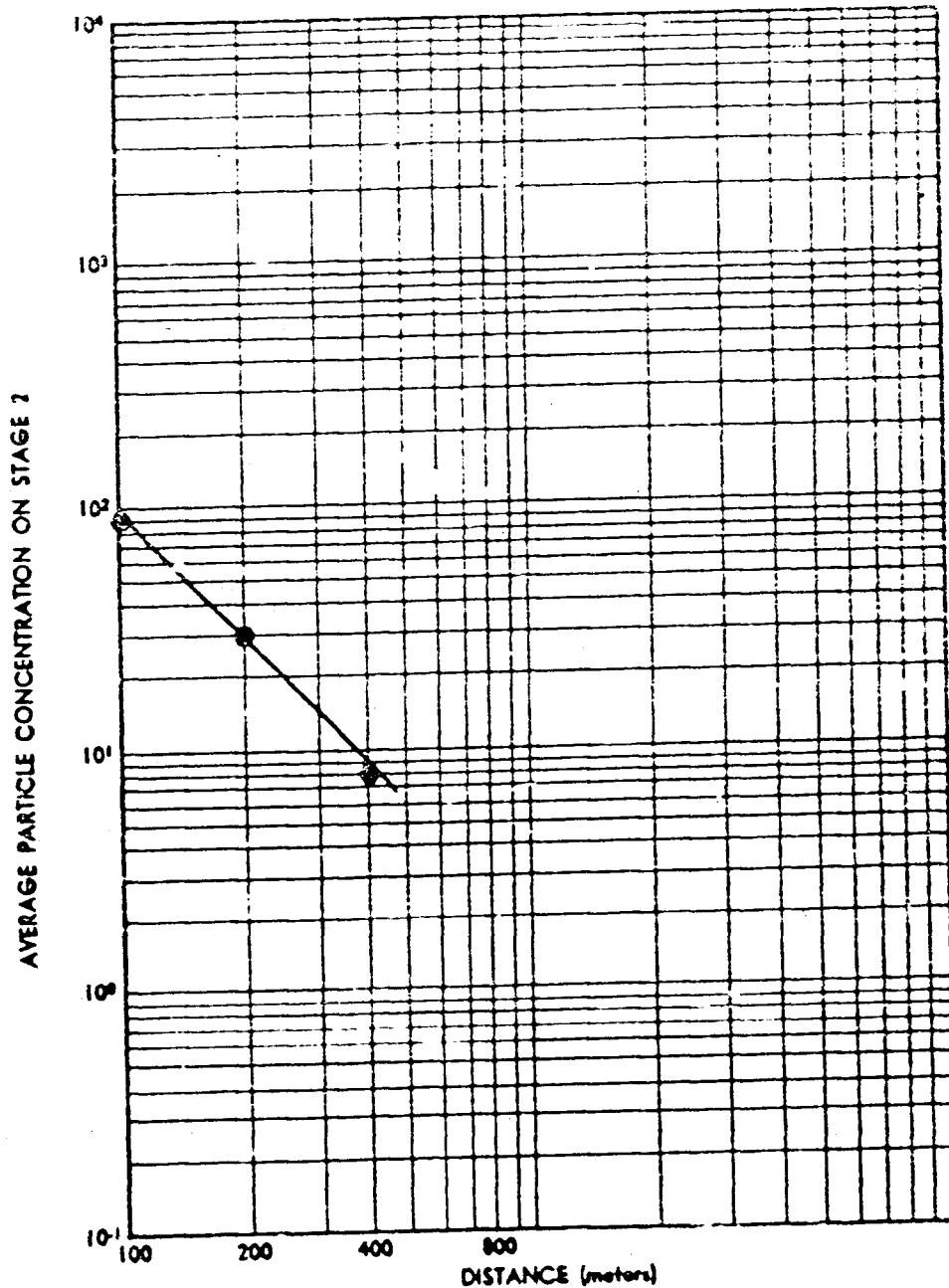


FIGURE M.1.8 FLUORESCENT TRACE (Centerline)

NPC 1004

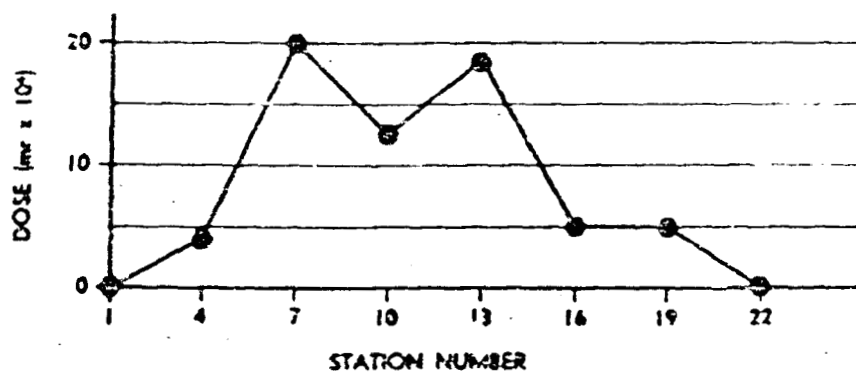


FIGURE N1.9 GAMMA DOSE FROM CLOUD PASSAGE
(Arc Profile)

NPC 1005

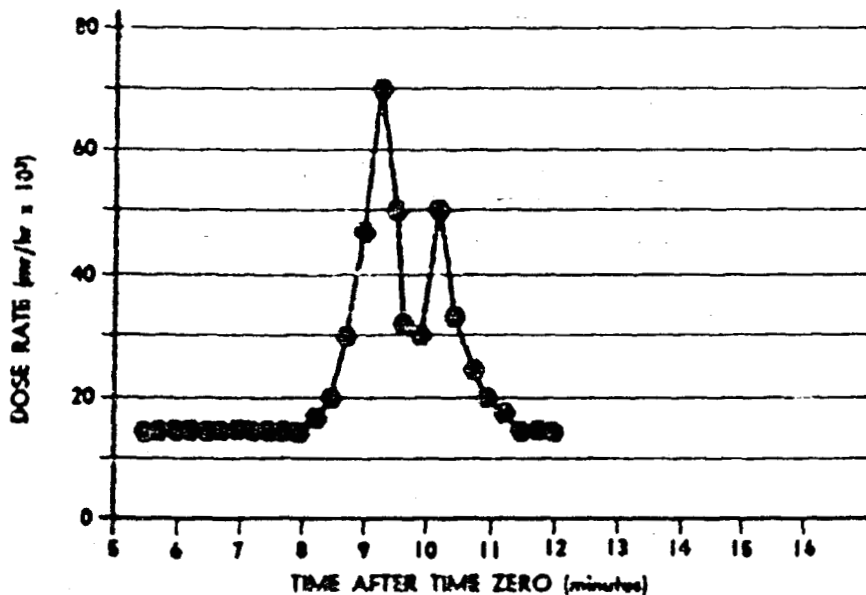


FIGURE N1.10 GAMMA DOSE RATE FROM CLOUD PASSAGE
(Centerline)

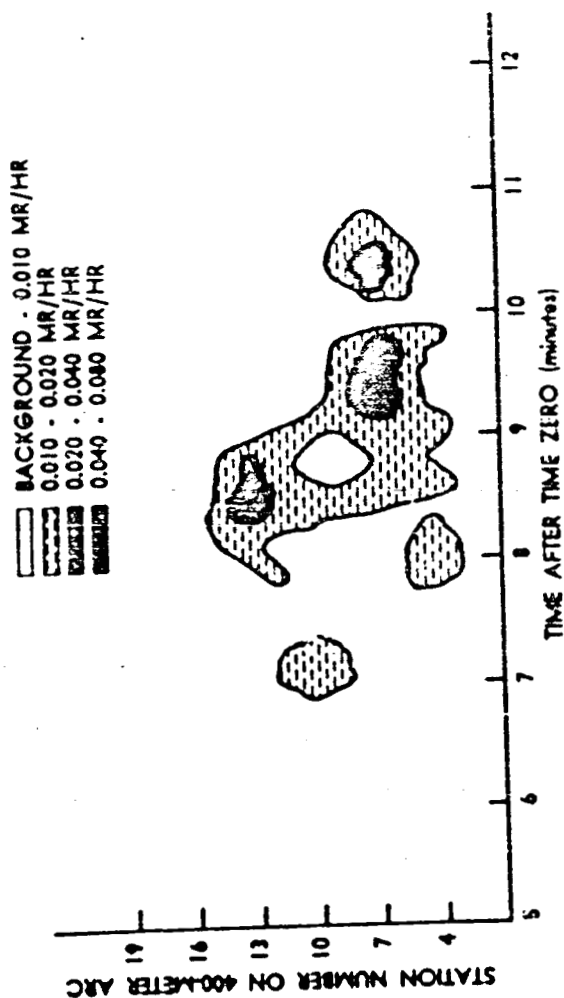


FIGURE NL11 GAMMA DOSE RATE FROM CLOUD PASSAGE
(Activity Contours)

I.14 Radiobiology

Rats were placed four at a station at positions on the 100-meter arc. Whole body and tissue counts were obtained in disintegrations per minute using the counting efficiency for barium-137m. These data are presented in Figures M.I.12 and M.I.13.

Dogs were placed on the 100-, 200-, and 400-meter arcs. The tissue data from the dogs are presented in Table M.I.4.

I.15 Sand and Water Collection

No sand and water samples were collected for this release.

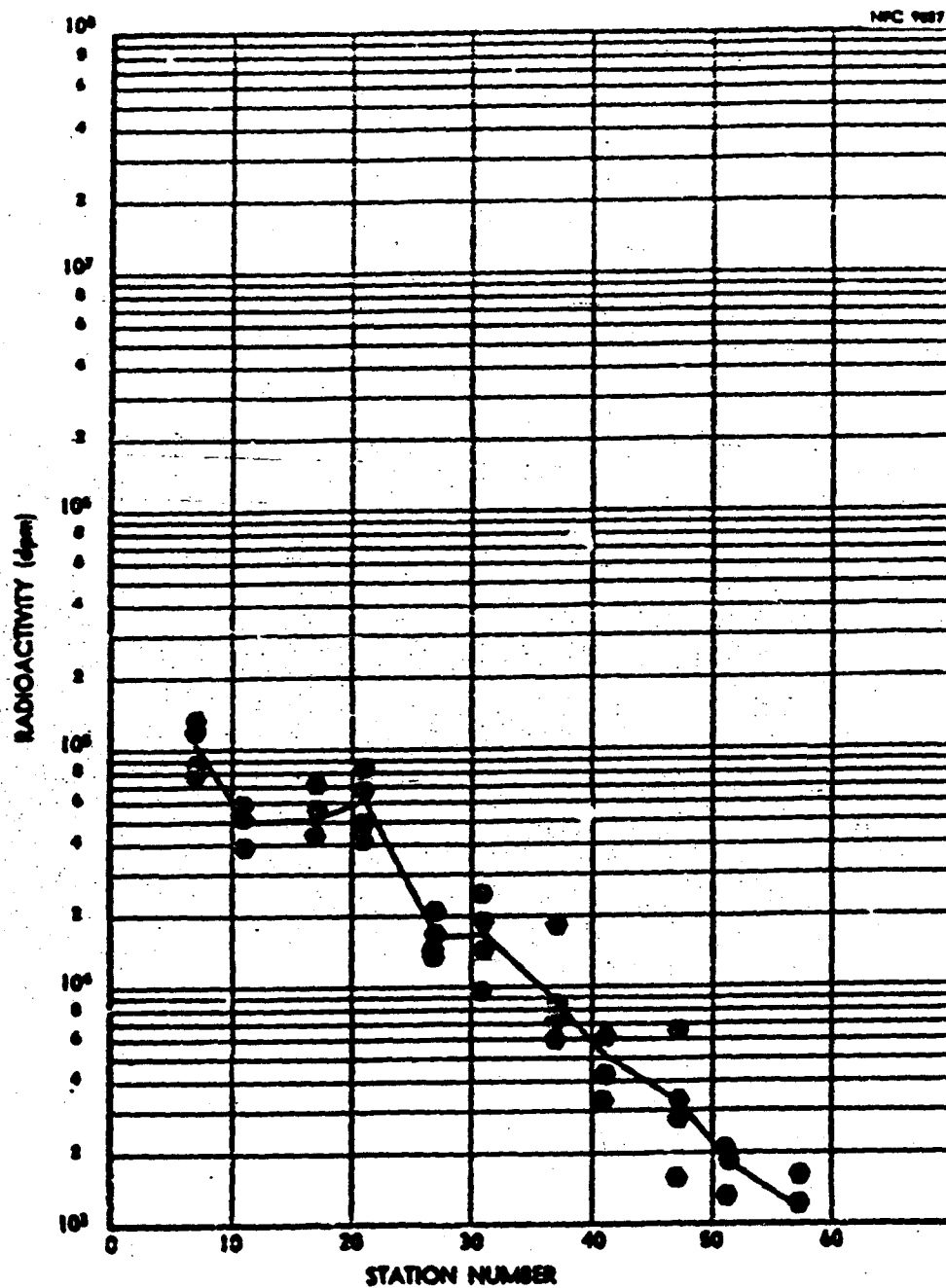


FIGURE N.1.12 RAY WHOLE-BODY EXPOSURE

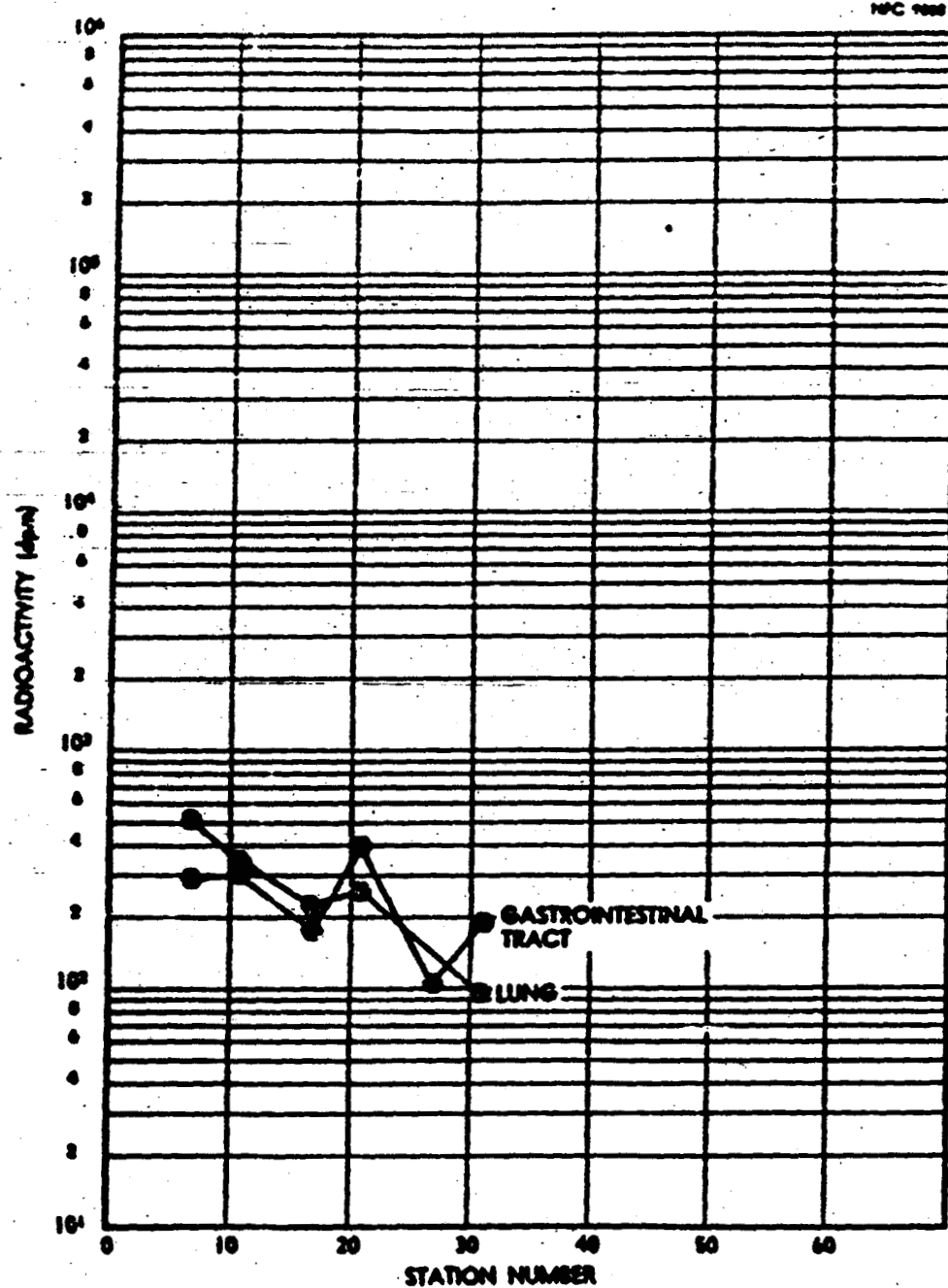


FIGURE N.L.13 - RAT TISSUE EXPOSURE

TABLE H.1.4

Radi. activity in (a)

Station location	Unit									
	100m-1P	100m-1P	100m-1P	100m-1P	100m-1P	100m-1P	100m-1P	100m-1P	100m-1P	100m-1P
Lung	1400	4220	4620	1100	1100	1100	1100	1100	1100	1100
Esophagus	1500	1410	--	--	600	600	600	600	600	600
Stomach	1500	7090	5000	1350	1460	740	740	740	740	740
Small Intestine (1)	1720	1660	1150	466	465	--	--	--	--	--
Small Intestine (2)	3880	9060	784	358	--	3/4	3/4	3/4	3/4	3/4
Large Intestine	1350	5110	416	342	--	1100	1100	1100	1100	1100
Kidneys	1630	520	875	358	--	--	--	--	--	--
Trachea	--	--	--	--	--	410	410	410	410	410
Urine	410	1110	none	--	--	none	none	none	none	none
Blood	--	751	--	--	--	--	--	--	--	--
Fecal	--	--	301	--	--	--	--	--	--	--
Muscle (100 gms)	--	--	--	--	--	--	--	--	--	--

• Small intestines were cut into two pieces

REFERENCES

C. E., Martin, W. J., Parker, G. W., "Experiments on Release of Fission Products from Molten Reactor Fuels," A. E. C. Report No. ORNL-2616 (22 July 1959).

_____, "Background Information for Nuclear Plant Safety Analysis Program," Convair Report No. 5-022 (22 Nov. 1957).

W. E. et al., "Radioactive Fallout," U. S. A. E. C., 528 (April 1959).

_____, H. E., "Engineering Estimates of Atmospheric Dispersion," Ind. Hyg. Jour. 20, 183-189 (June 1959).

_____, O. G., Micrometeorology, McGraw-Hill Book Co., Inc., (1953).

_____, Erlain, A. C., "Aspects of Travel and Deposition of Gases and Vapor Clouds," Atomic Energy Research Establishment (Br.) Report No. AERE HP/R 1261 (17 Sept. 1953).

_____, "Report of International Subcommittee II on Permissible Doses for Internal Radiation," Atomic Energy Commission Report ICRP 15414 (1954).

_____, "Design and Operational Summary of the APD Heat Transfer Reactor Experiment (HTRF) No. 1; Work Performed January thru December 1956," General Electric Co. Report No. APEX-398, Secret (15 Aug. 1958).

_____, G., "Preliminary Report of Fission Products Field Release Test-1," U. S. A. E. C. Report No. IDO-12006 (Feb. 1959).

_____, J. S., Rider, B. F., "High Level Dissolution and Chemical Analysis of Pre- and Post-Melt Samples from Air Field Release Test-1," General Electric Co., Scitons Atomic Laboratory Report XDC 59-5-48, Secret, Jan. 1959).

_____, G. H. et al., "Field Studies of Fission Product Inhalation. Part I Fission Product Inhalation Following An Experimental In-Pile Meltdown." University of Rochester Report 555 (Aug 12, 1959).

_____, "Theoretical Possibilities and Sequences of Major Accidents in Large Nuclear Power Plants," A. E. C. Report No. WASH-740 (Mar. 1957).

REFERENCES (Con't)

13. Barad, M. L., "Project Prairie Grass, A Field Program in Diffusion," 1, Geophysical Research Papers No. 59, Project 7657, U. S. Air Force (July 1958).
14. _____, "Meteorology and Atomic Energy, U. S. A. E. C. A. E. C. C. Report No. 3000 (July 1955).
15. Burnet, T. J., "Reactor Hazards vs. Power Level," Nuclear Science and Engineering, 2, 382-393 (1957).
16. _____, "Beckman-Whitley Anemometer Calibration," National Bureau of Standards Report No. 6.3/140c58.
17. _____, "Reviews of Modern Physics", American Physical Society, 30, 2, Part II (April 1958).

UNCLASSIFIED

UNCLASSIFIED

UNCLASSIFIED/LIMITED

Policy on the Redistribution of DTIC-Supplied Information

As a condition for obtaining DTIC services, all information received from DTIC that is not clearly marked for public release will be used only to bid or perform work under a U.S. Government contract or grant or for purposes specifically authorized by the U.S. Government agency that is sponsoring access. Further, the information will not be published for profit or in any manner offered for sale.

Non-compliance may result in termination of access and a requirement to return all information obtained from DTIC.

NOTICE

We are pleased to supply this document in response to your request.

The acquisition of technical reports, notes, memorandums, etc., is an active, ongoing program at the Defense Technical Information Center (DTIC) that depends, in part, on the efforts and interest of users and contributors.

Therefore, if you know of the existence of any significant reports, etc., that are not in the DTIC collection, we would appreciate receiving copies or information related to their sources and availability.

The appropriate regulations are Department of Defense Directive 3200.12, DoD Scientific and Technical Information Program; Department of Defense Directive 5230.24, Distribution Statements on Technical Documents; American National Standard Institute (ANSI) Standard Z39.18-1987, Scientific and Technical Reports- Organization, Preparation, and Production; Department of Defense 5200.1-R, Information Security Program Regulation.

Our Programs Management Branch, DTIC-OCP, will assist in resolving any questions you may have concerning documents to be submitted. Telephone numbers for that office are (703) 274-6847, or DSN 284-6847. The Reference Services Branch, DTIC-BCR, will assist in document identification, ordering and related questions. Telephone numbers for that office are (703) 274-7633 or DSN 284-7633.

DO NOT RETURN THIS DOCUMENT TO DTIC

**EACH ACTIVITY IS RESPONSIBLE FOR DESTRUCTION OF THIS
DOCUMENT ACCORDING TO APPLICABLE REGULATIONS.**